STANFORD
SCHOOL OF MEDICINE
Stanford University Medical Center

Lucas Center Annual Report 2011

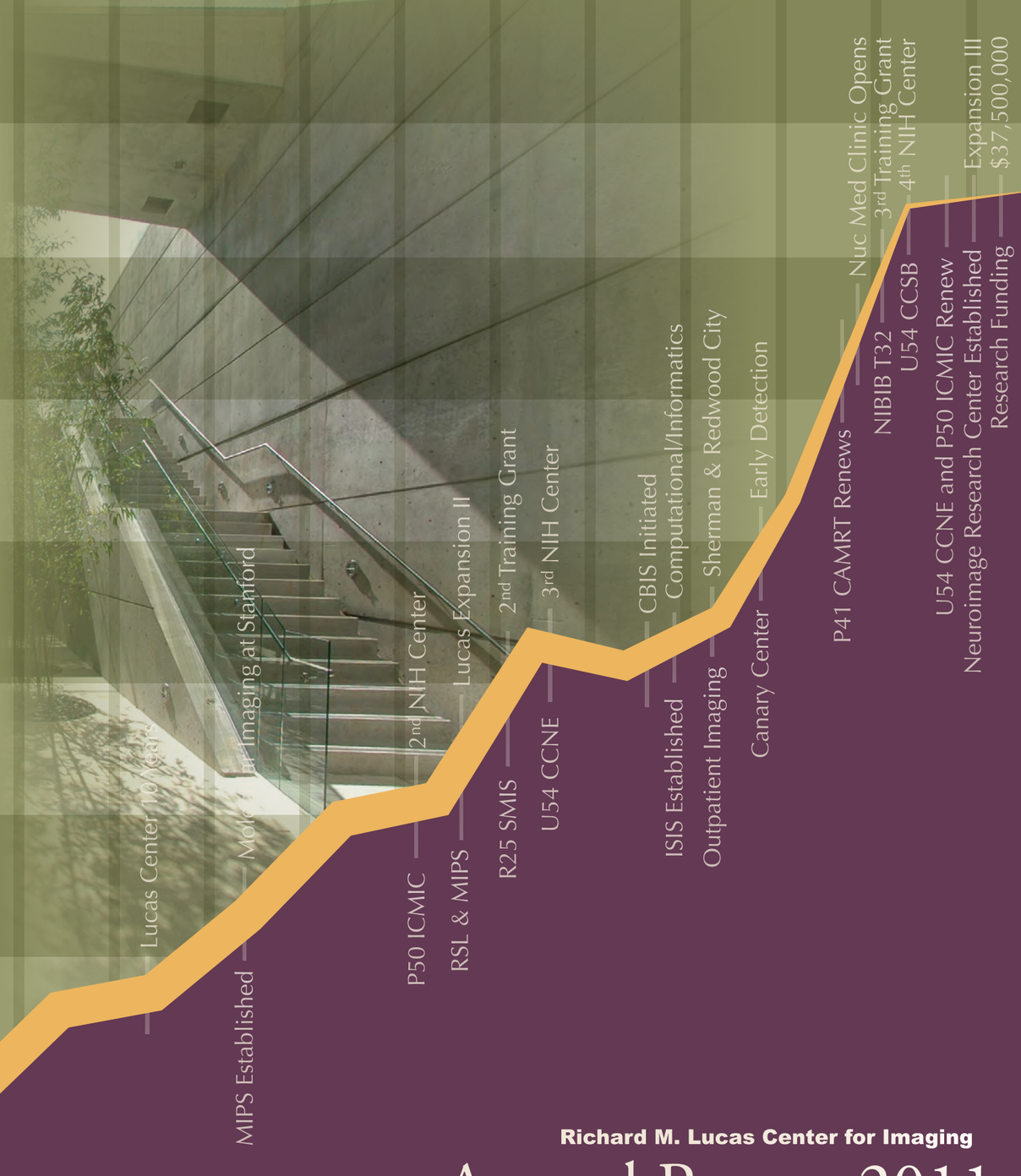

Richard M. Lucas Center for Imaging

Annual Report 2011

Richard M. Lucas Center for Imaging

Annual Report 2011

Cover Image:

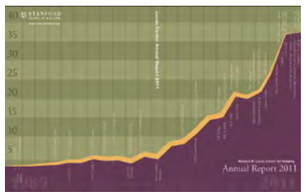

The cover image illustrates the dramatic increase in research funding for the Department of Radiology during Gary Glazer's Chairmanship (1989-2011).

2011 Lucas Report Team:

Editor: Susan Kopiwoda
Design: Amy Morris
Production: Joe Hubbard, Amy Morris
Photography: Mark Riesenberger
Archiving: Joe Hubbard
Printing: Lahlouh, Inc.

STANFORD
SCHOOL OF MEDICINE
Stanford University Medical Center

Contents

Forward

The Richard M. Lucas Center was dedicated in June 1992 with a keynote address by Nobel Laureate Richard Ernst, a chemist credited with pioneering developments including Fourier Transform Nuclear Magnetic Resonance. With the Center now in its nineteenth year as a world-class focus of biomedical imaging research, and on the occasion of Gary M. Glazer stepping down as department Chair, it is appropriate to review some of the achievements of the Center over this period. It is entirely because of Gary's vision, passion, and excitement for research that the Center was created and has become home for hundreds of scientists for periods of a few months to more than 19 years. During this time, thousands of research papers, books, and abstracts have been written, dozens of trainees have graduated, and many faculty careers have begun and flourished. A historical review as seen through Prof. Glazer's Foreword comments in previous Annual reports is, therefore, especially timely. This year's report is dedicated to Gary in grateful thanks for all that he has given to the Lucas Center, the Department, and the international biomedical imaging community. Following are edited snippets from selected annual reports.

1994
- Our proposal for the Center for Advanced MR Technology (CAMRT) is expected to be funded. This honor will bring substantial recognition and funding to the Lucas Center
- In three years, the number of NIH-funded grants based at the Lucas Center has doubled

1995
The research environment in the coming year will become even more exciting as two major programs are developed:
- An R&D program in interventional MRI that is a collaboration between Stanford and GE
- An R&D program with Siemens using electron-beam CT, which is ten times faster than routine

1996
We have developed the following new programs and investigations:
- A 3D laboratory in conjunction with several industrial partners and Stanford collaborators
- fMRI applications move into the clinical environment
- Advances in breast cancer imaging using MRI

1997
Expansion of the Center to include:
- A high field MR program with the siting of a 3 Tesla magnet as an R&D effort was developed with GE
- A 5-year program in advanced imaging of children is funded by the Packard Foundation

1999
Imaging studies now achieve a spatial resolution of 1 mm anywhere in the body and can be acquired very rapidly
- A new program: We will be studying cost effectiveness and impact of our work on disease outcomes

2001
As we look forward to celebrating the Center's 10-year anniversary, we have much to be proud of and tremendous enthusiasm for the next decade. We have created the intellectual and physical resources that have helped to transform medical imaging.

2002
During my recruitment to Stanford I spent a great deal of time dreaming about how we might achieve important innovations in medical imaging. Some ten years later, as I travel to different universities and hospitals, it gives me a great deal of pride to see techniques originally developed at the Lucas Center being used to improve health around the world.
- Stanford approved our request for a major expansion, to include a very high field (7 Tesla) magnet and a cyclotron

Thank you *Gary*, and
Thank you, members of the
Lucas Foundation Board
from all of us

2003
- Molecular imaging program founded with recruitment of Sam Gambhir

2005
- Lucas expansion completed, more than doubling the size of the Lucas Center
- NIH funding received for the in-vivo Cellular and Molecular Imaging Center (ICMIC)

2006
NIH funding received for the Center of Cancer Nanotechnology Excellence Focused on Therapy Response (CCNE-TR)

2007
The span of 15 years is an eternity in rapidly moving scientific disciplines such as imaging… What I can report is that the term "Lucas Center" is synonymous with excellence and innovation in imaging throughout the world.

2008
- Information Sciences in Imaging@Stanford (ISIS) section created
- Canary Center at Stanford for Cancer Early Detection created

2010
- Renovation plans begun for replacement of 2 end-of-life scanners and siting of new program in PET/MR/13C Hyperpolarization
- NIH-funded Center for Cancer Systems Biology (CCSB) created, augmenting existing centers CAMRT, ICMIC and the CCNE-TR

In summary, the Lucas Center has always been, and remains, an exciting, lively and dynamic nexus for fundamental and applied imaging research. All members of the RSL, MIPS, and ISIS programs with studies housed in the Center are deeply indebted to Gary Glazer for having his audacious dreams and making them come true. We are also deeply grateful to the Lucas Foundation for their generous and steadfast support over these nearly two decades.

Dr. Sanjiv Sam Gambhir is Appointed Chair

of the Department of Radiology

Sanjiv Sam Gambhir, MD, PhD

Please welcome Dr. Sam Gambhir, MD, PhD, as the next chair of the Department of Radiology. Dr. Gambhir was recruited to Stanford in 2003 to serve as Director of the then newly created Molecular Imaging Program at Stanford (MIPS) as well as Chief of the Division of Nuclear Medicine in the Department of Radiology.

Dr. Gambhir graduated from the Medical Scientist Training Program at UCLA, where he obtained his PhD in Biomathematics and MD in 1993. He trained in Nuclear Medicine at UCLA and is a Diplomate of the American Board of Nuclear Medicine. At UCLA he quickly rose from trainee to being Director of the Crump Institute for Molecular Imaging, Vice Chair of the Department of Molecular and Medical Pharmacology, and Professor of Molecular and Medical Pharmacology. He directed the activity of over 100 scientists at UCLA and was internationally recognized as a pioneer in helping to develop the field of molecular imaging. He moved over 35 scientists with him from UCLA to Stanford to build a multi-Departmental effort in molecular imaging. His laboratory has developed fundamental strategies to image cellular and molecular events for cancer detection and treatment with a focus on gene and cell therapies.

Since joining Stanford in 2003, Dr. Gambhir has developed a leading program in molecular imaging that developed unique collaborations and interactions across Stanford University and the world. He also designed and opened the new Nuclear Medicine & Molecular Imaging Clinic in late 2010 that brings state-of-art clinical care to adult and pediatric patients. He has recruited over 12 faculty to Stanford including 9 to the Department of Radiology. He successfully competed as PI for the NIH center grants In Vivo Cellular and Molecular Imaging Center (ICMIC) P50, Center for Cancer Nanotechnology Excellence (CCNE) U54, Early Detection Research Network (EDRN) U01, and Stanford Molecular Imaging Scholars (SMIS) R25T training grant. He also grew the Molecular imaging program from 35 to over 150 scientists.

Dr. Gambhir's honors and awards for his work include the Taplin Award (2002), Holst Medal (2003), AMI Distinguished Basic Scientist of the Year Award (2004), SMI Achievement Award (2004), Doris Duke Distinguished Clinical Scientist Award (2004), Hounsfield Medal from Imperial College London (2006), Election as a fellow to the American Institute for American and Biomedical Engineering (2006), The Society of Nuclear Medicine Paul C. Aebersold Award (2006), Organized and Co-Chaired a Nobel Symposium in Stockholm (2007), Elected to the American Society of Clinical Investigation (2007), Tesla Medal from UK Royal College of Radiologists (2008), RSNA Outstanding Researcher Award (2009), Virginia and D.K. Ludwig Endowed Professorship (2009), and The Society of Nuclear Medicine George Charles de Hevesy Nuclear Pioneer Award (2011). He was also elected to the Institute of Medicine (IOM) of the US National Academy of Sciences as one of its youngest members, the highest honor possible for a physician.

Since 2004, he has served on the National Cancer Institute Scientific Advisory Board. He has over 400 publications including over 20 publications in the Nature series. He has edited several leading textbooks in the field, has 35 patents granted or pending, and has received over $75 million in NIH funding as a principal investigator. He has given over 100 keynote talks including major international meetings and leading academic centers. He continues to actively engage the local community, and he raised significant gift funds to open the Canary Center at Stanford for Cancer Early Detection in 2009. Dr. Gambhir has significant experience with Industry and serves as an advisor for many companies including General Electric and Bayer. He serves on the scientific advisory boards of several companies including Visualsonics, MagArray, Spectrum Dynamics, Enlight, ImaginAB, and NinePoint Medical. He has also founded several new biotechnology companies including Endra and CellSight.

Dr. Gambhir is internationally recognized for his scientific contributions and for training and educating the new generation of physicians and scientists focusing on molecular imaging. While there is also no doubt that the field of radiology and imaging will change dramatically in the years ahead, Stanford will have Dr. Gambhir carrying on the tradition of excellence in radiology and imaging science.

We welcome Dr. Gambhir as our new Chair of the Stanford Radiology Department and wish him the best of success.

Welcome

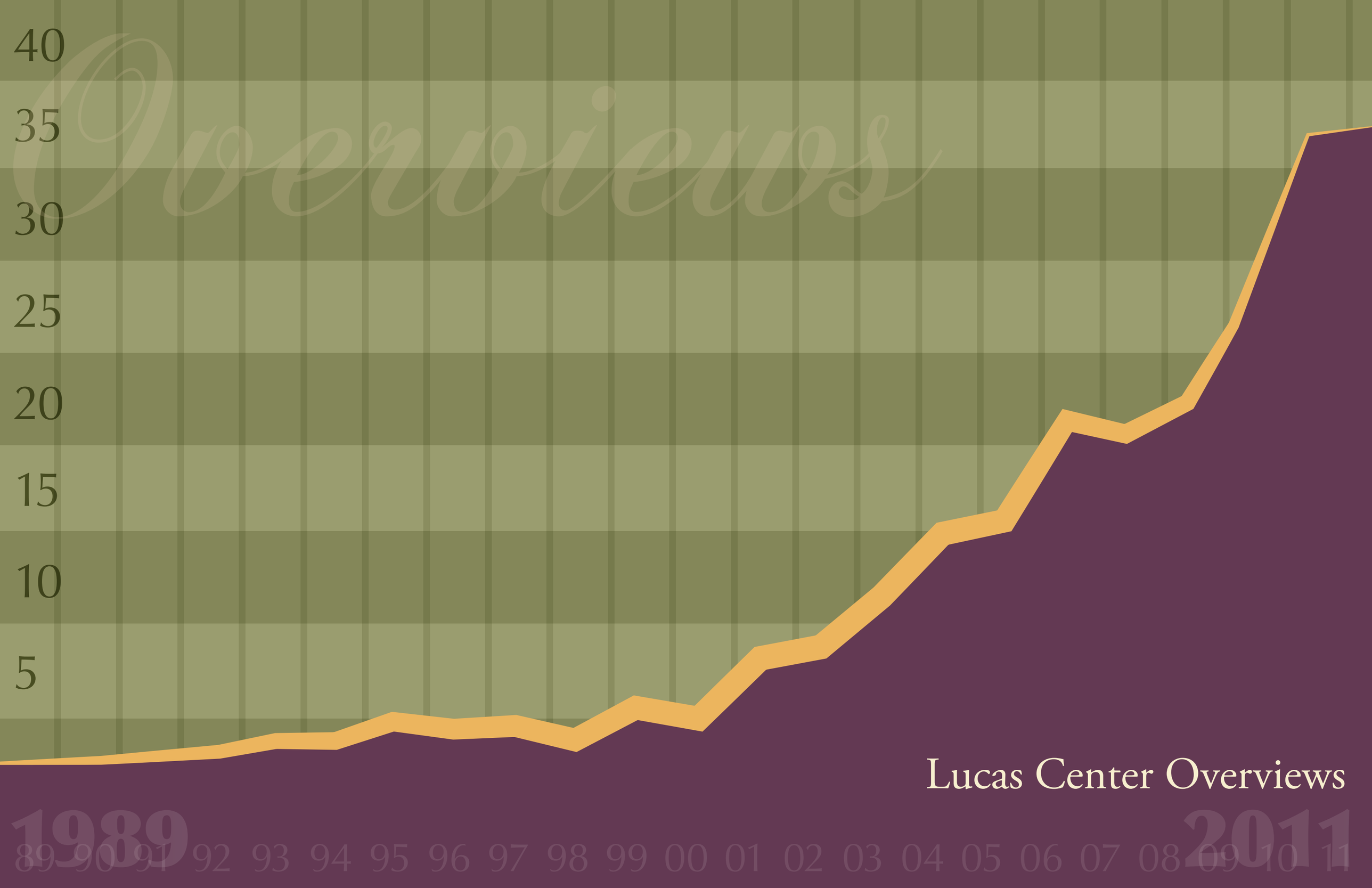
Overviews
40
35
30
25
20
15
10
5
Lucas Center Overviews
1989
2011
89 90 91 92 93 94 95 96 97 98 99 00 01 02 03 04 05 06 07 08 09 10 11

NIH Centers of Excellence

The Stanford Department of Radiology is home to four National Institutes of Health (NIH)-funded Centers of Excellence that contribute significant advances to improve health care for patients worldwide. In addition to technological, computational, biochemical, and biological innovation in the imaging sciences, we have trained more than 500 individuals since our first center was established in 1995. The following provides a short synopsis of each of these programs.

The National Center for Advanced Magnetic Resonance Technology at Stanford (CAMRT - P41)

The Center for Advanced Magnetic Resonance Technology at Stanford (CAMRT), led by Gary Glover, PhD, was established as a National Research Resource in 1995 and in 2010 began its 17th year as an NIH-funded center. This Center brings together the expertise and talent of individuals from the Radiology Department's Richard M. Lucas Center for Imaging and the Electrical Engineering Department's Magnetic Resonance Systems Research Laboratory. This multidisciplinary group shares the common goals of developing innovative Magnetic Resonance Imaging and Spectroscopy (MRI/MRS) techniques for fundamental anatomic, physiologic and pathophysiologic studies, and serving the academic and scientific community through collaborations, education, and access to Center facilities and resources. In addition to development of technology projects, the CAMRT provides support for collaborations and use of the facilities with users in the Radiology Department as well as more than 75 faculty and more than 200 other users from at least 14 departments. In addition, the innovative developments that emerge from this group are also shared across the U.S. and internationally. For further details, please see http://rsl.stanford.edu/research/camrt.html and the CAMRT/RSL Overview (page 6).

The In Vivo Cellular and Molecular Imaging Center at Stanford (ICMIC@Stanford - P50)

The ICMIC, directed by Sam Gambhir, MD, PhD, established in 2005 recently began its second cycle (2010) with an overall vision that emphasizes the application and extension of molecular imaging to translational research and clinical applications. While the ICMIC continues with its original goals to i) exploit molecular imaging by extracting basic information from animal models and pre-clinical studies, ii) provide new information on tumor diagnosis, initiation, progression, and responses to therapy, and iii) develop new imaging technologies, it now expands into clinical applications. The major goal for this new cycle is to provide the groundwork to integrate molecular imaging into translational studies that will move into clinical cancer applications. We will accomplish these goals by ensuring that basic scientists and clinician scientists are collaborating on ICMIC projects with well-defined end goals of clinical application. Additionally, ICMIC investigators form important scientific links to our NCI Funded CCNE U54 (Center for Cancer Nanotechnology Excellence) and NTR U54 (Network for Translational Research in Optical Imaging) programs through use of in vitro nanosensors and intraoperative microscopy, respectively. This will help to further accelerate our ability to bring important state-of-the-art solutions to cancer research and cancer patient care. For further details, please see http://mips.stanford.edu/public/grants/icmic/ and the MIPS Overview (page 11).

The Center for Cancer Nanotechnology Excellence and Translation (CCNE-T - U54)

The Center for Cancer Nanotechnology Excellence and Translation (CCNE-T), led by Sam Gambhir MD, PhD, was approved for funding in 2010 and builds on the success of the CCNE-TR that was established in 2006. This new CCNE-T brings together scientists and physicians from Stanford University, University of California Berkeley/Lawrence Berkeley National Lab, University of California Los Angeles, University of Southern California, and the Massachusetts Institute of Technology. Our goals with the CCNE-T build on our vision that in vitro diagnostics, used in conjunction with in vivo diagnostics, can markedly impact cancer patient management. Through the use of nanotechnology we will significantly advance both in vitro diagnostics through proteomic nanosensors and in vivo diagnostics through nanoparticles for molecular imaging. The CCNE-T focuses markedly on bringing nanotechnology into clinical use. For further details of the CCNE, please see http://mips.stanford.edu/public/grants/ccne/ and the CCNE Overview (page 14).

Cancer Center for Systems Biology (CCSB - U54)

The Stanford Cancer Center for Systems Biology (CCSB), led by Sylvia Plevritis PhD, is one of twelve National Centers for Systems Biology funded by the NIH and the NCI. The Center, located at Stanford University School of Medicine, represents a multi-disciplinary collaboration Our Center represents a multi-disciplinary collaboration with its mission to promote the analysis of cancer as a complex system by merging experimental and computational methods. The Stanford CCSB aims to discover molecular mechanisms underlying cancer progression by studying cancer as a complex biological system that is driven, in part, by impaired differentiation. CCSB's overarching goal is to provide a better understanding of the differentiation and self-renewal properties of cancer that will enable us to identify molecular therapeutic targets and strategies to eradicate this disease, or at least, maintain it in a nonlethal state. Our approach integrates high-throughput experimental datasets at the genomic, transcriptomic and proteomic levels, with novel computational techniques, in order to reveal critical molecular networks that drive cancer progression. Our multidisciplinary Center brings together faculty from the Schools of Medicine, Engineering, and Human Sciences, with expertise ranging from molecular biology and oncology to mathematics, statistics, and computer science. For further details of the CCSB, please see http://ccsb.stanford.edu/ and the ISIS Overview (page 13).

Research Overview

Norbert Pelc, ScD, Associate Chair for Research
Susan Kopiwoda, MS, MPH, Director, Strategic Research Development

The Department of Radiology showed significant strength in the year 2011, maintaining its research programs in spite of a nationwide economic downturn and concerns over the NIH budget. Since 2004, NIH has averaged an approximate 2% increase in dollars budgeted/year not accounting for inflation; with a correction for inflation, NIH shows an average increase of 0% since 2004. To compound issues, while the NIH budget remains flat, the number of applications submitted to NIH steadily increases each year, thereby increasing competition and decreasing funding success rates. In spite of these odds, our progress this year has been excellent due to our researchers' ability to develop outstanding proposals to obtain resources to support their research.

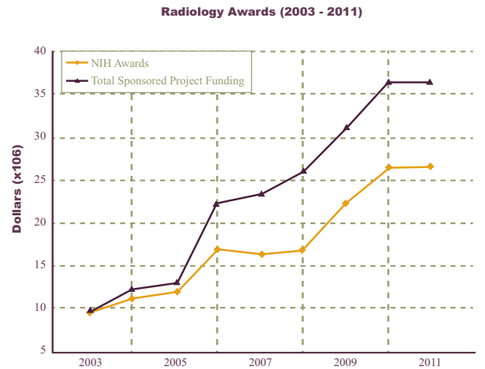

Fig 1. Funding for years 2003-11. The NIH total for 2011 is flat due to simultaneous funding of 2 CCNE Center grants in 2010. The CCNE awards overlap (one ending and one beginning) camouflages the outstanding success we are seeing for 2011 that includes awards for 11 new or competing NIH programs.

2011 Success: This year, our faculty, postdoctoral scholars, and research staff secured funding for 22 new or competitively renewed sponsored projects. Of these, 11 are new NIH funded projects, 5 of them R01/U01 programs. The awards include: 3 R01s (Bammer, Levin, Quon); 2 U01s (Gambhir, Plevritis) 2 R21s (Daniel, Daldrup-Link); 1 RC1 (Wu); 1 T32 (Pelc); 1 R25 (Gambhir); 1 S10 (Rutt); 2 DOE/DOA (Levin, Spielman); 1 CIRM (Rutt); 9 Industry or Foundation (Gambhir, Gold, Hoffman, Hovsepian, Marks). Our postdoctoral scholars have also been successful in recruiting funding. We are pleased to announce that two postdocs have been awarded K99 funding (Balchandani and Smith). It is also worth noting that Dr. Quon has achieved NIH investigator status with his first R01 awarded this year. We also have two other new investigators (Paulmurugan and Willmann) who are waiting for final funding decisions regarding their new NIH R01 programs.

A history of Stanford Radiology research funding from 2003 to 2011 is presented in Figure 1. In 2010 two large center grants, CCNE-TR and CCNE-T overlapped funding resulting in an unusually high awards total for 2010. If we correct for this unusual event we can demonstrate steady and strong growth in awarded research dollars from 2003 to 2011.

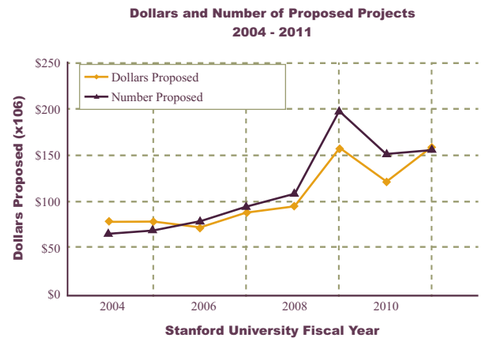

Fig 2. A steady increase in proposed funding from 2004 to 2011. The increase seen in 2009 was due to an unusual number of proposals submitted that year in response to US government stimulus dollars available.

Our research success relies heavily on a strong base of funding requests. Figure 2 tracks our proposal history from 2004-2011 showing a consistent increase in the number of funding requests each year. The 2009 peak was due to a bolus of proposals submitted under the American Recovery and Reinvestment Act (ARRA) during that year. Other than 2009, we have increased the number and dollars requested each year since 2006 and will continue that increase for the coming years due primarily to an increase in the number of faculty. There is on-going concern that the 2012 NIH budget will suffer significant cuts; this concern does not appear to have an effect on our proposal activity. We believe that in order to sustain and expand our programs, it is necessary to submit proposals of the highest quality, increase the number of grants submitted per year, explore sponsors other than NIH, and maintain and strengthen collaborations at all levels.

Personnel: This year we have added four new faculty and three new clinician-educators. See pages 20-21 for a short bio and photo of these faculty who already contribute to the clinical and research interests of the Department. Overall, our research group, including faculty, scientific staff, postdocs, graduate students, and administrative staff grew by 15% (from 250 to 287) this year.

Space: The Richard M. Lucas Center for Imaging is undergoing its third remodel to accommodate new and upgraded facilities, office space for new faculty, additional space for research, and space for students and staff associated with new programs. Our off-campus research site on California Avenue, the Canary Center at Stanford, is close to full capacity. As we hire new faculty and expand our research, we continue an active dialogue with the University and Hospital leadership for facilities and space to support our programs.

In the next few pages, you will read about advances made by our NIH-supported Centers of Excellence, and the three Stanford Radiology sections that make up our research effort. These include: 1) the Radiological Sciences Lab (RSL), led by Gary Glover, PhD; 2) the Molecular Imaging Program at Stanford (MIPS), led by Sanjiv (Sam) Gambhir, MD, PhD; and 3) ISIS (Information Sciences in Imaging @ Stanford), co-led by Sandy Napel, PhD and Sylvia Plevritis, PhD. You will also find a complete listing of all of our sponsored projects on pages 185-192.

It is with continued support of the Lucas Family Foundation and the Canary Foundation that we are able to maintain leadership in research, train the next generation of imaging clinicians and scientists, and, above all, deliver the most advanced diagnostic and therapeutic techniques to benefit our patients and patients worldwide.

RSL Overview

Radiological Sciences Laboratory and The Center for Advanced MR Technology (CAMRT)
Gary H. Glover, PhD, Director, Radiological Sciences Laboratory

The Lucas Center has been home to the Radiological Sciences Laboratory (RSL), a section of the Radiology Department, since the building's dedication in 1992. In conjunction with the Electrical Engineering Department the RSL has hosted the Center for Advanced MR Technology, an NIH-funded National Research Resource since 1995. The Center also houses a cyclotron and radiochemistry labs as well as other wet labs for the Molecular Imaging Program under Dr. Sanjiv Gambhir. The Center's state of the art imaging facilities support research of the RSL and others in the Radiology department as well as hundreds of on-campus and extramural researchers as a core facility. The Center has always been, and remains an exciting and lively nexus for fundamental imaging research.

THE RADIOLOGICAL SCIENCES LABORATORY

The RSL comprises 9 faculty, approximately 45 graduate and postdoctoral students, approximately 30 scientific staff and 6 administrative assistants, as well as the Lucas Center/RSL Administrative Services Director, Donna Cronister. These numbers represent a small increase in trainees over 2010.

The faculty serve in a wide variety of advisory roles to government and foundation agencies such as the NIH and in policy-making positions for international scientific societies such as the ISMRM and RSNA. Many of our faculty, scientific staff and students have garnered prestigious awards for their exceptional research achievements. Some of the faculty and their students' activities of the past year are noted here.

THE NATIONAL CENTER FOR ADVANCED MR TECHNOLOGY AT STANFORD (CAMRT)

The CAMRT is a National Biotechnology Research Resource, sponsored by the NIH's National Center for Research Resources (NCRR) with Dr. Glover as PI. The Center, initiated in 1995 as a close collaboration with Electrical Engineering, maintains the broad goal of developing and making available a spectrum of cutting edge MR imaging research tools for scientists who would otherwise not have access to such tools, as well as to train students and others in MRI. Over the years that goal has remained, as research projects have been introduced, matured and been replaced with new developments and opportunities. The grant is now in its 17th year of continuous funding. During its last 5 year renewal review in 2010 it received a perfect score (10) from the study section.

Outstanding progress has been made in all five of the core technology development areas that include RF pulse design, reconstruction methods (John Pauly, EE Department, core director), hardware (Brian Rutt, core director), body MRI techniques (Brian Hargreaves), neuro MRI (Gary Glover, with Mike Moseley and Roland Bammer contributing), and spectroscopic imaging development (Dan Spielman). Much of this exciting research is chronicled in the scientific reports that follow. These reports are acknowledged with funding from P41 RR009784.

Faculty and their Students' Activities

Roland Bammer:

- Invited as member of BMIT NIH study group
- Proposed, and is now director of the Center for Functional Quantitative Neuroimaging This center is focused on translation of innovative imaging methods into clinical practice.
- Member of AMPC, JMRI editorial board, Chair of Publications committee, Chair of Motion Correction study group
- Research Associate, Stefan Skare, accepted faculty position at Karolinska hospital in Sweden

Rebecca Fahrig

- Serves on the Physics Advisory Board for Siemens AX
- Axiom research lab renovation underway with placement of the NIH awarded zeego system
- Erin Girard successfully defended her PhD thesis; now a Siemens Collaborations Manager
- Jared Starman, PhD, graduated Dec, 2010; now an Associate with Exponent, Inc.
- Arundhuti Ganguly, PhD, now an Associate at Varian

Brian Hargreaves:

- Awards:
  - Brian Hargreaves: NIH Edward Nagy New Investigator Award
  - Kyung Sung (finalist) for ISMRM poster award for Quantitative MRI of Breast Cancer
  - Christina Chen: SCBT/MR for MRI near Metallic Implants
  - Brian Hargreaves: ISMRM HM poster award for Metal-Induced MRI Artifacts
- Student Highlights:
  - Misung Han, PhD, graduated
  - Ernesto Staroswiecki defended PhD successfully
- Research translation:
  - Manoj Saranathan's rapid DCE imaging being used clinically for Liver MRI
  - Imaging near Metallic Implants being used clinically for C-spine Neuroimaging

Faculty and their Students' Activities

Michael Moseley:

- Editorial Boards:
  - Journal of Magnetic Resonance Imaging (JMRI)
  - Cerebrovascular Diseases (CD)
  - Journal of Cerebral Blood Flow and Metabolism (JCBFM)
  - International Journal of Stroke (IJS)
- Advisory Boards:
  - American Heart Association. AHA/ASA Stroke Council Writing Committee
  - (Definition of Stroke)
- Study section service
  - NIH Center for Scientific Review - Service on 6 study sections
  - NIH Center for Scientific Review - NIBIB ARRA P30 Review.

Kim Butts Pauly:

- Serves on the board of ISTU (International Society for Therapeutic Ultrasound)
- Director of CBIS (Center for Biomedical Imaging at Stanford)
- Two grad students received PhDs: Lena Keye, Andrew Holbrook
- Two trainees accepted faculty positions: Viola Rieke at UCSF and Peji Ghanouni at Stanford
- Student Juan Plata received an NSF graduate fellowship

Norbert Pelc:

- We obtained the first images from the Inverse Geometry CT scanner constructed under support from NIH and collaboration with GE.
- Submitted and awarded T32 training grant for doctoral students interested in biomedical imaging technology - funds 2 new students each for 2 years

Brian Rutt:

- Study Section Service:
  - Cancer Prevention and Research Institute of Texas, Interfaces Review Committee (IRC): permanent study section member
- New NIH Grants Funded:
  - NIH 1 S10 RR026361 (Rutt): Next Generation 7T MRI Platform Upgrade with Parallel Transmit Capabilities
  - NIH R01 AR054458 (PI: Daldrup-Link): Monitoring of Stem Cell Engraftment in Arthritic Joints with MR Imaging
  - NIH R21 AR059861 (PI: Daldrup-Link): Novel Imaging Approach to Monitor Chondrogenic Differentiation of iPS Cells
- New non-NIH Grants Funded:
  - GE (PI: Gold): Advanced MR Applications Development, Year 4
  - CIRM (Rutt): Development of Single Cell MRI Technology using Genetically-Encoded Iron-Based Reporters
- Prachi Pandit: awarded Stanford Molecular Imaging Scholars postdoctoral fellowship
- Jonathan Liu: awarded NSF Graduate Research Fellowship
- Jonathan Liu: awarded Stanford Graduate Fellowship

Dan Spielman:

- Two new grants: NIH K99/R00 (Balchandani): High Resolution Magnetic Resonance Imaging and Spectroscopy of Epilepsy at 7T
- DOD grant (Spielman): In Vivo Imaging of Branched Chain Amino Acid Metabolism in Prostate Cancer

Gary Glover:

- Awarded University of Minnesota's Outstanding Achievement Award, 2nd highest UoM honor given.
- Grad student Catie Chang received PhD, will serve as postdoc at NIH (Jeff Duyn's group).
- Postdoc Priti Balchandani received K99/R00 NIH fellowship award.

ISIS Overview

Information Sciences in Imaging at Stanford
Sandy Napel, PhD and Sylvia Plevritis, PhD, Co-Directors

David Paik, Sandy Napel, Danae Barnes, Sylvia Plevritis, Daniel Rubin

The ISIS (Information Sciences in Imaging at Stanford) section of the Radiology Department is committed to harnessing the power that informatics can bring to imaging. This includes deriving new clinical and biological knowledge of normal and pathological processes, predicting clinical outcomes such as response to therapy and 5-year survival probability, and creating decision support applications. Researchers within ISIS collectively explore the full spectrum of information-intensive activities in imaging (e.g., image management, storage, retrieval, processing, analysis, understanding, visualization, navigation, interpretation, reporting, and communications) and in associated non-imaging domains (e.g., pathology, ophthalmology, oncology, molecular and genetic markers, family history, prior medical reports, and clinical outcomes). This is done by leveraging methods to extract computational and semantic features in images and integrate them with related clinical and molecular data.

The expertise of the ISIS faculty, staff, postdocs, and students spans image acquisition, image quantification, imaging informatics, knowledge engineering, bioinformatics, biocomputation, and systems biology. ISIS is co-led by Drs. Sandy Napel, Professor of Radiology, and Sylvia K. Plevritis, Associate Professor of Radiology, and includes core faculty David S. Paik, Assistant Professor of Radiology, and Daniel L. Rubin, Assistant Professor of Radiology. Our affiliate faculty member is Professor Robert J. Herfkens, whose expertise helps ISIS bridge between clinical imaging and information systems. ISIS, a highly collaborative group, has active projects with many of our Stanford faculty as well as around the world. ISIS administrative activities are handled by Administrative Program Manager Danae Barnes.

ISIS Core Resources

Critical to the ISIS mission is the development and application of new core resources to collect annotated imaging, clinical and molecular data, and to integrate them by creating databases and novel computational models that identify relationships among these data. In these areas, advancements over the past year include:

- **Electronic Physician Annotation Device (ePAD):** ePAD, led by Dr. Rubin, is an open source tool enabling researchers and clinicians to identify and extract quantitative and semantic features ("imaging biomarkers") from images, which include both "semantic annotations" on radiological images as well as quantitative features that algorithms extract from images (Figure 1). These metadata are stored in a standards-based syntax created by the cancer Biomedical Informatics Grid (caBIG) project. Semantic annotations enforce standardized terminologies such as RadLex and SNOMED. Currently, ePAD is being used in many ISIS projects where extracting semantic and quantitative features is required.
- **Computational Methods and Resource for CT Liver Lesion Diagnosis and Discovery**: This project, led by Drs. Rubin, Beaulieu, and Napel, aims to build tools and methods for creating and mining databases of CT scans of liver lesions for knowledge discovery and eventual use in decision support through content-based image retrieval (CBIR) methods. A translational component is being pursued in collaboration with (and funded by) GE.
- **Tools for Linking and Mining Image and Genomic Data:** Led by Drs. Napel and Plevritis, this collaborative effort with Radiology Department members Daniel Rubin, Ann Leung, and Andy Quon, and Cardiothoracic surgeon Chuong Hoang, has begun to develop a radiogenomic map of non-small cell lung carcinoma that links image features to tumor gene expression, which in turn can be linked to prognosis and, potentially therapy response. The tools developed for integrating this genomic and imaging data can then then be more broadly applied to other conditions where such data exists.
- **RadBank Data Warehouse: RadBank/RadTF**, led by Dr. Rubin, is an integrated data warehouse that brings together radiology reports with pathology and clinical information (and in the future, molecular data) to enable researchers, clinicians, and educators to find cases of particular imaging findings, diagnoses, modalities, and other information. To date, the RadTF component is being used extensively by all clinical faculty in the department to identify teaching cases, to perform retrospective research, and to identify cohorts for new research.
- **Imaging Biomarker Ontology (IBO):** The Paik Lab has developed an initial draft of the Imaging Biomarker Ontology and is working to refine and expand this knowledge resource to cover the domain of how quantitative imaging measurements are captured from imaging data, with an emphasis on molecular imaging. IBO is being used to enable intelligent and semantically-searchable warehousing of quantitative measurements from molecular imaging analogous to the way in which microarray data is currently captured in public databases, thereby enabling imaging to realize its potential in translational bioinformatics research. One collaboration for the deployment of IBO is with the FDA and NIST to create a system for benchmarking quantitative imaging biomarkers.
- **Standards for Interchange of Nanoparticle Data:** As part of a national working group in collaboration with the NCI's caBIG, ASTM, and Pacific Northwest National Labs, the Paik Lab has been developing computational standards for the leading nanoparticles used for diagnostic imaging and/or therapeutic delivery. These efforts have helped guide development of caNanoLab, the NCI's repository of nanoparticle characterization data, the adoption of the NanoParticle Ontology (NPO) as a standard and the development of Nano-TAB, a data exchange format for nanomaterial composition and characterization.

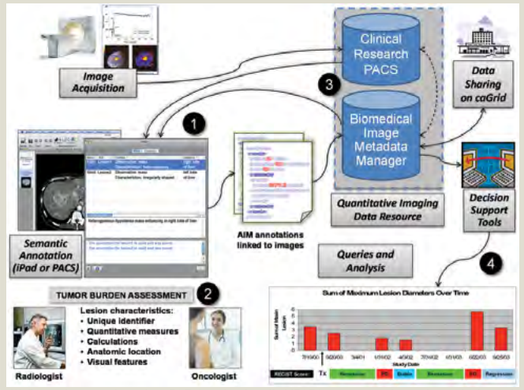

(1) Semantic annotation using ePAD (previously called iPAD) to extract and record quantitative and radiologist features seen on images, (2) both oncologists and radiologists view images and capture information, such as identifying target lesions and recording image features, respectively, (3) warehousing and integration of imaging features with clinical data, (4) automated decision support tools query the machine-accessible image data and clinical data to compactly summarize complex serial imaging data to enable decision support on patient response.

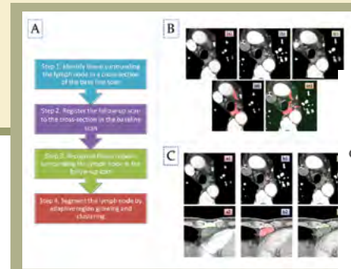

Figure 2: Algorithm (A) results (B, C) of automated quantitative imaging methods to detect and quantify cancer lesions on follow-up CT images of cancer patients.

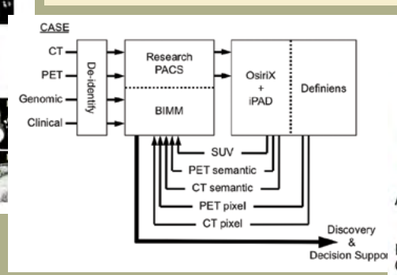

Figure 3: System diagram for "Tools for Linking and Mining Image and Genomic Data in Non-Small Cell Lung Cancer" project. All data gets stored in our database, including a research PACS for DICOM images, and BIMM for storage of metadata. Processing occurs using OsiriX and Definiens, platforms for image manipulation and quantitation, respectively. Results of processing go back to BIMM, from which they can be mined for discovery and decision support.

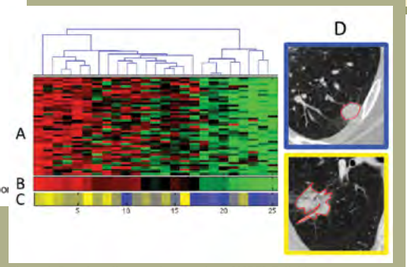

Figure 4: Sample radiogenomics mapping of NSCLC, linking gene expression to image features. (A) One particular gene cluster (genes along rows, samples along columns), with gene expression encoded high (red) vs. low (green), functionally annotated to represent molecular changes in the extracellular matrix, particularly TGF-beta regulated genes. (B) Metagene of cluster; (C) Computed "compactness" CT feature: low (yellow) vs. high (blue) compactness; (D) Example CT images of compactness: high (top) and low (bottom)

ISIS Research Grants

- **Modeling the Role of Differentiation in Cancer Progression:** In one of twelve national Centers for Cancer Systems Biology funded by the NIH, Dr. Sylvia Plevritis directs a $12.8 million dollar, 5-year multidisciplinary program to study the role of differentiation in hematologic malignancies. This program integrates a diversity of high-throughput data, including genomic, transcriptomic, and proteomic, to elucidate molecular networks driving cancer progression and treatment response. More information about CCSB can be found at http://ccsb.stanford.edu.
- **Computerized Quantitative Imaging Assessment of Tumor Burden:** Dr. Rubin is Principal Investigator of one of the centers in the newly established Quantitative Imaging Network (QIN), composed of researchers who will develop approaches to validate and standardize imaging data and related imaging metadata for quantitative measurements of responses to cancer therapies. Stanford's part of the QIN will be to create computer algorithms to measure tumor burden in patients, and to identify and quantify novel imaging biomarkers that can provide earlier indications of treatment response to cancer therapies (Figure 2).
- **Simulation Modeling of Breast Cancer Health Care Policies:** Dr. Plevritis has been a Principal Investigator of the NCI CISNET breast cancer program over the past ten years has received an additional 5 years of funding to mathematically model the impact of alternative cancer control policies on breast cancer incidence and mortality. Currently, her research program focuses on the role of MRI screening, particularly in the high risk population, the impact of postmenopausal hormone therapy on past breast cancer trends, and the impact of biomarker-specific screening and treatment interventions on future trends.
- **Simulation Modeling of Lung Cancer Health Care Policies:** Dr. Plevritis has been a Principal Investigator of the NCI CISNET lung cancer program, which over the past five years has received an additional 5 years of funding to mathematically model the impact of alternative CT screening policies on lung cancer incidence and mortality. Currently, her research program focuses on translating the results of the National Screening Trial (NLST) to the population level, in collaboration with investigators from CISNET and NLST.
- **Integration of Imaging and Molecular Phenotypes for Improved Management and Understanding of Lung Cancer:** This project, supported in part by a grant from General Electric Medical Systems and led by Drs. Napel and Plevritis, has made significant progress. With the goal of integrating medical imaging and molecular features from lung cancer patients who undergo surgical resection, we have curated and correlated databases containing features from cross-sectional imaging exams (CT and PET) and gene expression of the human tissue specimens (Figure 3) to create a radiogenomics map of NSCLC (Figure 4). By leveraging our radiogenomics map of NSCLC with public databases linking gene expression to survival, we have created the first results suggesting that survival can be predicted from imaging alone (Figure 5). These pilot data have been submitted to the National Cancer Institute and a larger project is now awaiting funding.
- **Computerized Quantitative Imaging Assessment of Age-Related Acute Macular Degeneration (AMD):** Dr. Rubin is Principal Investigator of a Bio-X Interdisciplinary Initiatives Program grant which fosters a new collaboration between Ophthalmology and Radiology (a novel intersection even outside Stanford) to exploit the expertise in imaging informatics in ISIS to tackling challenges and opportunities in the domain of retinal imaging (Figure 6). The specific goal of the project is to develop quantitative imaging methods to assess disease burden, prognosis, and treatment response in patients with

ISIS Overview (continued)

Information Sciences in Imaging at Stanford
Sandy Napel, PhD and Sylvia Plevritis, PhD, Co-Directors

AMD, and in the the future, with other retinal diseases. The methods being developed have mutual benefits to imaging analysis methods in both radiology and ophthalmology.

- **Quantitative imaging assessment of breast cancer:** Dr. Rubin is Principal Investigator of a Stanford Cancer Center Interactive Project Grant to develop quantitative imaging informatics methods to characterize patients with breast cancer. The project is developing tools and methods to analyze perfusion MRI data in breast cancer and to discover computational imaging biomarkers that differentiate patients who respond to treatment from those who fail to respond. The quantitative methods aim to be generalizable to other types of cancer and to be useful in other ISIS projects.
- **Cancer Nanotechnology Knowledgebase for Nanoparticle Analysis and Design:** Dr. Paik is Principal Investigator of a Driving Biological Project sub-contract from the National Center for Biomedical Ontology to build a powerful new toolset for information retrieval for cancer nanotechnology-related information using biomedical ontologies. This project aims to develop computational representations of nanoparticle structure that will be used to develop search queries across a variety of relevant nanomedicine online resources.

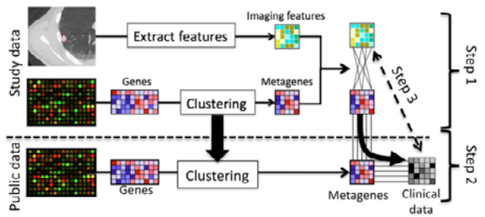

Strategy for the creation and application of the NSCLC radiogenomics map. Step 1 integrates the CT and PET/CT image and the gene microarray data from our study cohort. Step 2 maps the metagenes to publicly available microarray data with survival. Step 3 links image features expressed in terms of metagenes to public gene expression data.

Summary

Through the efforts described above, we believe that ISIS has made progress that will enable the realization of its three main goals: (1) an evidenced-based diagnostic decision support system, whereby patient-specific images, clinical data and, if available, molecular data, can be compared to the database to suggest the most likely diagnoses, prognoses, and most relevant treatments, (2) biological discovery, i.e., synthesis and potential testing of hypotheses regarding the underlying biology in the development, progression and hopeful eradication of specific diseases, and (3) the translation of these developments into clinical practice using computers and image storage systems that are ubiquitous in healthcare enterprises today.

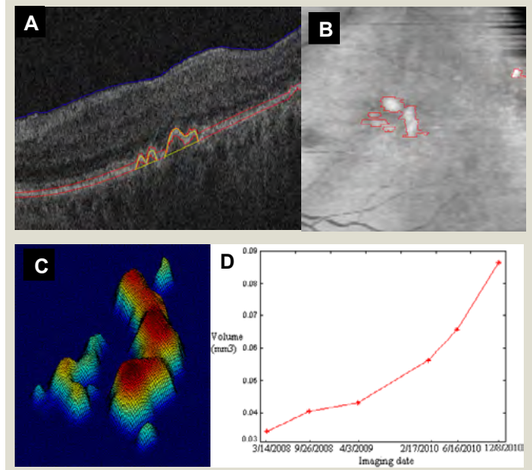

(A) Cross sectional optical coherence tomography (OCT) image of the retina in a patient with AMD showing distortion of the retinal pigment epithelium (bright band) by abnormal drusen which have been automatically segmented and quantified by our computational method. (B) Selective slab summed voxel projection image produces a novel visualization of drusen analogous to that seen by ophthalmologist when examining the eye, but with drusen enhancement through image processing. (c) quantitative analysis of drusen morphology from which numerous quantitative features about drusen are extracted, so that in (D) quantitative features such as volume of disease burden can be tracked and correlated with treatment response.

ISIS Affiliated Programs

ISIS is closed affiliated with the following two programs in the Department of Radiology:

- **3-Dimensional and Quantitative Imaging Laboratory (3DQ Lab):** The 3DQ Lab applies and delivers innovative techniques for efficient quantitative analysis and display of medical imaging data to the Stanford community. The co-directors are Drs. Sandy Napel and Brooke Jeffrey, both Professors of Radiology. More information about 3DQ Lab can be found at http://3dradiology.stanford.edu.
- **Systems Biology Discovery Lab:** ISIS has acquired a Systems Biology Discovery Lab that will enable experimental validation of computationally derived results; this lab is located in LUCAS P169 and is under the supervision of Dr. Plevritis. New work in the laboratory is focused on understanding the tumor microenvironment by integrating molecular and imaging data.

MIPS Overview

Molecular Imaging Program at Stanford
Sanjiv S. Gambhir, MD, PhD, Director, Molecular Imaging Program at Stanford

The Molecular Imaging Program at Stanford (MIPS) continues to experience significant growth. Many faculty within the Department of Radiology and from other Departments continue to help build the program. The MIPS structure is also supported by two recently renewed NCI programs, the In vivo Cellular Molecular Imaging Center (ICMIC) P50 and the Center for Cancer Nanotechnology Excellence (CCNE) U54, which help to advance projects in the Radiology Department, the School of Medicine, across the Stanford campus, and nationwide at a number of academic centers. Very recently we have learned that our NCI-funded R25 postdoctoral training program, the Stanford Molecular Imaging Scholars (SMIS), which was originally funded in 2006 to train the next generation of cancer molecular imaging post-doctoral scholars, will be funded for an additional 5 years. We also participate in an NIH postdoctoral training grant (T32) for cardiovascular molecular imaging, which is in its third year. In addition, all labs continue to grow with new faculty, new students, post-doctoral fellows, and outstanding research staff joining the program. Also, many visiting scientists from around the world visit our program to learn more about molecular imaging.

Regarding new projects funded during 2011, Dr. Gambhir has been awarded an NCI Early Detection Research Network (EDRN – U01) to conduct research on the early detection of prostate cancer. Dr. Gambhir has also been newly awarded by the Ben and Catherine Ivy Foundation to develop a research program in neuro-oncologic clinical imaging. On the positron emission tomography (PET) front, Dr. Levin leads a new program in preclinical translation of new scintillation light detection concepts for PET. Also on the PET front, Dr. Quon now leads an NIH R01that evaluates a PET tracer (18F-fluorothymidine (FLT)) for the purpose of therapy monitoring for lymphoma patients. Dr. Rutt, whose interests combine MRI and molecular nanotechnology, was awarded a CIRM technology grant and an NIH shared instrumentation grant. Dr. Daldrup-Link has received an R21 for her research in applying nanoparticles (ferumoxytol) to detect tumor associated macrophages in breast cancer. This year, we also have three investigators receiving their first NIH R01grants. Dr. Quon now leads a clinical trial study to evaluate a new PET tracer; Dr. Willmann will develop microbubble probes for breast cancer early detection; and Dr. Paulmurugan will study tamoxifen resistance in breast cancer. In addition, Dr. Bryan Smith, a graduate of our SMIS R25 program, has recently been awarded his first NIH award, a K99. All of these new projects, along with ongoing projects are listed in the Appendix (Funded Research Projects).

Through the Canary Foundation's efforts to develop a new center for early cancer detection, we continue to build bridges with many investigators on campus. Our off-campus space on California Avenue, acquired in 2010 and now at capacity, facilitates our cancer early detection efforts. We are convinced that more investments are needed in the earlier detection of all disease, including cancer. Detecting disease earlier allows a much better potential for cure. The Canary Center works on novel in vitro diagnostics (e.g., using patient blood samples) as well as new imaging strategies with high sensitivity to detect very low disease burden. It is hoped that in the next 3-5 years Stanford will become a world-leader in the important field of early cancer detection.

We continue to have several seminar series on campus to help educate scientists about molecular imaging. The molecular imaging seminar series (http://mips.stanford.edu/public/mi_seminar.adp) is now in its sixth year and has a large collection of videos available on-line of speakers from the last few years. Students from different MIPS labs now routinely present as well. The Nanobiotechnology seminar series (http://mips.stanford.edu/public/nanobiotech_seminar.adp), which focuses on new applications of nanotechnology to cancer, continues to draw attendance for faculty from all over campus. Several speakers from around the country have already presented in the series and all lectures are available on-line.

MIPS now has 55 faculty members with 24 full members and 31 associate members. While many MIPS members are from the Department of Radiology, overall our program attracts faculty from all over campus representing more than 25 different disciplines. The number of graduate students, MSTP students, post-doctoral fellows, research scientists, technicians, and administrative staff continues to grow and is currently approximately 175. Although we have experienced a significant increase in personnel with the Canary Center for Cancer Early Detection, with the addition of new faculty this year, we anticipate that number to continue increasing.

Our new Molecular Imaging/Nuclear Medicine clinic became fully operational late last year with a grand opening in September 2010. This advanced facility with its spectacular design and up to date equipment consolidates all of the PET-CT , SPECT-CT, and SPECT imaging systems with related equipment in one location. The new radiochemistry facility, also at this location, is currently pending design approval. Newer cardiac and optical imaging equipment will also be placed in this new clinic. And for our advanced pre-clinical research, we have designed the clinic so that large animal imaging experiments can be performed there. Research trials that combine state-of-art imaging with in vitro diagnostics (e.g., blood proteomics) are also now possible in this new facility.

An important link in the MIPS research chain focuses on industrial partnerships with key leaders in the molecular imaging community. Several projects to develop new imaging agents/strategies are underway with General Electric Global Research, General Electric Healthcare, Schering-Plough, Bayer-Schering, and GlaxoSmithKline. It is likely that additional industrial partners will enter into collaborative research relationships over the next several years. These relationships are key to our goals to translate discoveries at Stanford to the patient bedside. Several faculty are also involved in new startup-company efforts with intellectual property from their laboratories at Stanford. These include new efforts in diagnostics, small animal imaging and clinical imaging.

Canary Center Overview

Sanjiv Sam Gambhir, MD, PhD, Director
Daniela Starcevic, PhD, Deputy Director

The Canary Center at Stanford for Cancer Early Detection celebrated its second anniversary in June 2011. The mission of the Canary Center, which occupies ~30,000 square feet of the building at 1501 S. California Ave, is to lead and foster research programs leading to the development of blood and imaging tests for the early detection of lethal types of cancer. The Center represents a novel alliance between the Canary Foundation, the Department of Radiology, the Cancer Center, and the School of Medicine. The Center also actively fosters intellectual and programmatic alliances with the Schools of Engineering & Humanities and Sciences.

The Center's mission is based on the striking association between early cancer diagnosis and improved survival rates: the chances of survival are far greater when cancer is detected in its earliest stages, while still localized to the organ of origin and amenable to treatment. To optimize the detection of cancer at this stage, the Center is taking a binary approach including 1) identifying blood biomarkers that can be detected by simple blood screening tests and developing clinically translatable screens for these biomarkers, and 2) developing molecular imaging tests to confirm and localize early cancerous lesions. The extraordinary technical challenges associated with this dual strategy include the refinement of molecular imaging agents to specifically detect pre-invasive malignant tumors the size of a blueberry (< 5 mm). They also include the development of proteomic approaches that can reliably detect minute (< 0.1 ng/ml) quantities of cancer-specific proteins released into the bloodstream by these small lesions. Cost-effective solutions are expected by applying a relatively cheap blood test followed by a more expensive imaging study, although in some cases the blood test and the imaging test will be performed concurrently. Having both approaches will also likely lead to a greater overall accuracy.

To accomplish these goals, the Center was specifically designed to house state-of-the-art core facilities and collaborative research programs in molecular imaging, proteomics, chemistry, and bioinformatics. The Proteomics Core facility houses cutting-edge mass spectrometry platforms dedicated to the discovery and validation of blood and tissue protein biomarkers. The Chemistry Core is engaged in the specific design and refinement of molecular imaging agents for early detection, which then undergo preclinical testing using in vivo and ex vivo model systems, including patient blood and tissue samples. The Molecular and Cell Biology Core works closely with both the Proteomics and Chemistry Cores to screen and refine agents that can bind cancer-specific targets in tissues and thus complements the efforts of the Chemistry and Proteomics Cores to develop blood and imaging tests for cancer early detection. A significant effort has been put forward over the past year to equip the Center cores and laboratories with state-of-the-art instrumentation to promote and facilitate innovative research efforts. Three new mass spectrometers are already in place and the acquisition of additional ones is planned.

Collaborative research efforts fostered at the Center are made possible by creating a truly multidisciplinary team of faculty members. Current faculty members focus on imaging technologies, chemistry, and disease mechanisms/cell biology. Two new faculty members were recruited to the Center to fulfill two out of the 8 billets committed by the Stanford School of Medicine. Dr. Sharon Pitteri is particularly interested in breast and ovarian cancers and focuses on identifying and characterizing biomarkers for cancer risk, diagnosis, progression, and recurrence. Additionally, the Pitteri group is working toward identifying tissue biomarkers for imaging applications. Dr. Parag Mallick is interested in integrated computational and experimental systems-biology approaches to uncover circulating and cell-surface proteins useful for early cancer detection. Dr. Mallick's lab develops rigorous dynamic systems models of tumor and host behavior, and validates those models by large-scale measurements in both animal model systems and clinical samples.

Canary Center research programs are actively interfacing with other facilities and programs on campus, including MIPS and CCNE-TR, in order to leverage the latest developments in molecular imaging and nanotechnology into the early detection effort. Collectively, these initiatives form a direct pipeline for the translation of early cancer detection into clinical trials and practice.

A specific example of a novel molecular imaging strategy that is expected to help the goal of early cancer detection is ultrasound with targeted microbubbles. These gas filled microbubbles can be chemically coupled to targeting ligands that allow the bubbles to bind to tumor vasculature. This will allow molecular imaging using a conventional anatomical imaging strategy (ultrasound). This is expected to allow detection of tumors in the 3-5 mm range. A specific example of a novel strategy being pursued for blood biomarker detection is based on magnetonanoarrays being developed as part of the Stanford CCNE-TR. This novel technology allows the detection of many different biomarkers at levels that are 10-100 fold better than the most sensitive ELISA tests currently available.

The National Cancer Institute (NCI) Early Cancer Detection Network (EDRN) has recently awarded a major U01 grant to the Canary Center team. Under the leadership of Drs. Sam Gambhir and James Brooks (Department of Urology), this project will further examine the microbubble and magneto-nanoarray technologies as they apply to prostate cancer early detection and enable the first clinical trial using this technology. Many exciting new developments for early cancer detection are on the horizon and will be pioneered by the Center. The past year was marked by an aggressive effort to bring additional funding into the Center through both private foundations and government funding. Decisions regarding the outcome of several pending grant proposals are expected in the upcoming months.

As we head into the upcoming year, our goals include recruiting several new faculty members in the area of bioinformatics and in vitro and in vivo diagnostics, building up the Biorepository Core which will store and organize human samples for research efforts headed by the Center, and pursuing a number of other funding opportunities.

http://canarycenter.stanford.edu

CCSB Overview

Center for Cancer Systems Biology
Sylvia K. Plevritis, PhD, Director

The Stanford Center for Cancer Systems Biology (CCSB) is one of twelve Centers for Systems Biology funded by the NCI's Integrative Cancer Biology Program. The Stanford CCSB aims to discover molecular mechanisms underlying cancer progression by studying cancer as a complex biological system that is driven, in part, by impaired differentiation. Increasing evidence indicates that many cancers, like normal tissue, are composed of a hierarchy of cells at different stages of differentiation, and that the disease is maintained by a self-renewing subpopulation. Our overarching goal is to provide a better understanding of the self-renewing properties of cancer that will enable us to identify molecular therapeutic targets and strategies to eradicate this disease, or to maintain it in a nonlethal state.

Our biological projects are integrated with novel computational techniques, designed to dissect processes and causal factors underlying impaired differentiation as a driver of cancer progression in several hematologic malignancies. In order to identify mechanistic underpinnings of cancer progression, we believe that a network-based and multiscale viewpoint is needed Increasingly, diseases such as cancer are recognized as resulting from disruption in the coordinated performance of a complex biological system. This systems biology viewpoint necessitates the incorporation of high throughput, high dimensional data, and development of computational methods specifically geared to its analysis. We aim to develop three essential and interlocking requirements for a comprehensive systems analysis of cancer. First, powerful methods are required to infer molecular regulatory networks that drive phenotypic processes such as differentiation. Second, computational approaches are needed that can identify and isolate underlying patterns of progression in cancer, which can then be related to underlying regulatory networks. Third, executable models are desirable so that it is possible to pose hypothetical "what if" questions to predict how, for example, a targeted intervention might affect the subsequent course of disease. These computational approaches are applied to the study of differentiation in a range of hematological malignancies. In fact, our Research Plan is divided among 4 research projects (see Figure 1). Project 1 is dedicated to developing novel computational methods, whose applications are deeply integrated into our three complementary experimental projects in AML (Project 2), FL (Project 3), and T-ALL (Project 4). Taken as a whole, the four projects will provide a systems-level, network-focused view of the role of differentiation in cancer. Our integrative approach will enable us to ascertain differences between these hematologic malignancies, and commonalities, which may generalize to other cancers.

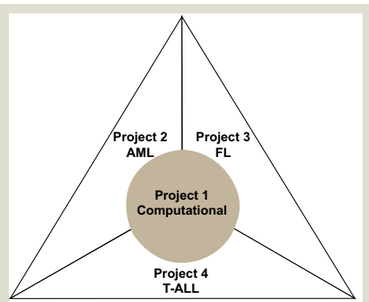

Figure 1. Organization of CCSB research projects.

The Stanford CCSB faculty brings clinical and basic cancer researchers together with researchers from mathematics, information technology, imaging sciences, and computer science to work on key questions in cancer biology. The CCSB core faculty includes PI Sylvia K. Plevritis, PhD, Associate Professor of Radiology, co-PI Garry Nolan, PhD, Professor of Microbiology & Immunology, Daphne Koller, PhD, Professor of Computer Science, David Dill, PhD, Professor of Computer Science, Ronald Levy, MD, Professor of Medicine (Oncology), Ravindra Majeti, MD, PhD, Associate Professor of Hematology, Dean Felsher, MD, PhD, Lead, Associate Professor of Medicine (Oncology) & Pathology.

Our CCSB also maintains a Core for Data Integration, which is lead by Andrew Gentles, PhD, CCSB Scientific Program Manager and includes Rob Tibshirani, PhD, Professor of Health Research and Policy (Biostatistics) and Ramesh Nair, PhD. The purpose of this Core is to facilitate interactions between computational projects and experimental projects, and to ensure timely dissemination of resources. The core also provides initial processing of complex data sets, and dissemination of them and computational tools developed in their analysis. We aim to make all data, software, and results generated by the Stanford CCSB readily available to all researchers. Our CCSB Data Portal is coming soon!

Our CCSB operations are lead by Anita Samantaray, MPH, Program Manager, who also coordinates our outreach and education efforts. The Stanford CCSB produces education and outreach programs for students at all levels. Public outreach activities and research experiences enhance CCSB's impact in the bay area. We continue to offer annual symposia and monthly seminar series on campus to help educate scientists about cancer systems biology. The CCSB seminar series (http://ccsb.stanford.edu/events/seminars.html) is now in its second year and its Video Gallery can be viewed online (http://ccsb.stanford.edu/events/video_gallery.html).

http://ccsb.stanford.edu

CCNE Overview

Center for Cancer Nanotechnology Excellence
Sanjiv Sam Gambhir, MD, PhD, Director, and Demir Akin, DVM, PhD, Deputy Director

Stanford University is home to two large consortia, the Center for Cancer Nanotechnology Excellence focused on Therapy Response (CCNE-TR, http://mips.stanford.edu/grants/ccne) and the Center for Cancer Nanotechnology Excellence and Translation (CCNE-T, http://mips.stanford.edu/grants/ccne-t). Both Centers are funded through the National Cancer Institute (NCI) and composed of prominent US universities, non-profit organizations, and for-profit groups. These two projects, collectively referred to as the CCNE, operate simultaneously and fall under the School of Medicine's larger parent program Molecular Imaging Program at Stanford (MIPS), which is led by Dr. Sanjiv Sam Gambhir. The original Center was funded in 2006 (CCNE-TR); the competing renewal (CCNE-T) was awarded in October 2010 for an additional 5 years. The CCNE brings together scientists, engineers, and physicians from different disciplines including chemistry, materials science, engineering, radiology, molecular biology, cancer biology, and oncology. The CCNE-TR consortium includes leading scientists and physicians from Stanford University, University of California Los Angeles (UCLA), University of Southern California (USC) and the Fred Hutchinson Cancer Research Center (FHCRC). The CCNE-T consortium includes Stanford University, University of California Berkeley (UCB), Lawrence Berkeley National Lab (LBNL), UCLA, USC, and the Massachusetts Institute of Technology (MIT). The names of a few of the CCNE members include Drs. Sanjiv Sam Gambhir (PI), David Agus, Demir Akin (CCNE Deputy Director), Paul Alivisatos, Jonathan Berek, Alice Fan, Dean Felsher, Samir Hanash, Luke Lee, Parag Mallick, Scott Manalis, Martin McIntosh, Ed Myers, David Paik, Steve Quake, Jianghong Rao, Brian Rutt, Robert Sinclair, Mark Stolowitz, Mary Tang, Shan Wang (Co-PI of CCNE-T), Irv Weissman, Robert Wilson and Anna Wu. These Centers leverage several activities in cancer biomarker discovery and validation efforts within the Canary Foundation and the Canary Cancer Early Detection Center at Stanford. The CCNEs and the Canary Center share the common assumptions that: 1) in vitro diagnostics used in conjunction with in vivo diagnostics can markedly impact medical care and management for cancer patients; and 2) nanotechnology can significantly advance in vitro diagnostics through proteomic nanosensors as well as in vivo diagnostics through nanoparticles for molecular imaging. Although we are broadly interested in all types of cancers, our primary cancer concentrations are on lung and ovarian and secondarily on brain, prostate and colorectal cancers. Our Centers highly leverage resources at the Stanford Bio-X and Nanoscale Science and Engineering Programs, the California Nanosystems Institute, and the Cancer Centers of Stanford, UCLA, USC and Fred Hutchinson. We also rely on resources at several small companies (most of these are CCNE outgrowths) and General Electric as well as other industrial partnerships to accelerate clinical translation of our technologies. We are also tightly connected with several long running Cancer trials and patient sample repositories so that our results are rapidly applicable to cancer patient use. Thanks to the significant investment in our center from Stanford University, the School of Medicine, the Department of Radiology, the Stanford Cancer Center, the Lucas Foundation, and the National Cancer Institute (NCI), our CCNEs are rapidly growing both in their research scope and physical boundaries. A brief summary of our exemplary success is shown in Figure 1. Twenty-nine provisional patents have been filed by our investigators and six spin-off companies were founded within the past 5 years. These companies are: MagArray Inc. (Dr. S. Wang, Magneto Nano Sensors), ImaginAB (Dr. A. Wu Engineered Antibodies for Diagnostics), Zymera Inc. (Dr. J. Rao/S.S. Gambhir, Self-Illuminating Quantum Dots for Diagnostics and in vivo imaging), Endra Inc. (Dr. S.S. Gambhir, Photoacoustic Imaging), Nine Point Medical (Dr. S.S. Gambhir, Raman imaging for the GI tract), CellSight (Dr. S.S. Gambhir, Small Molecule and Nanoparticle Strategies for imaging Cell Trafficking in Patients).

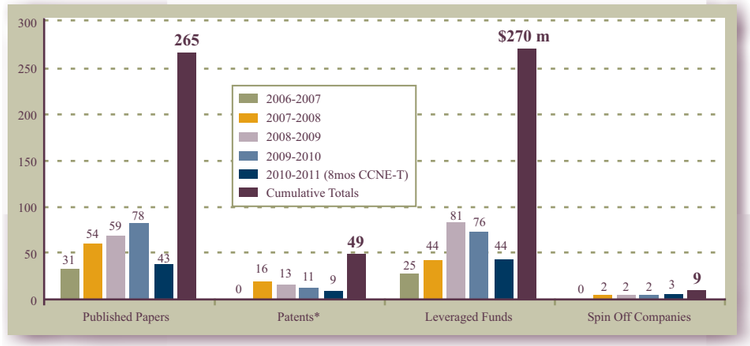

Image 1:A summary of the performance of the CCNE-TR and CCNE-T.

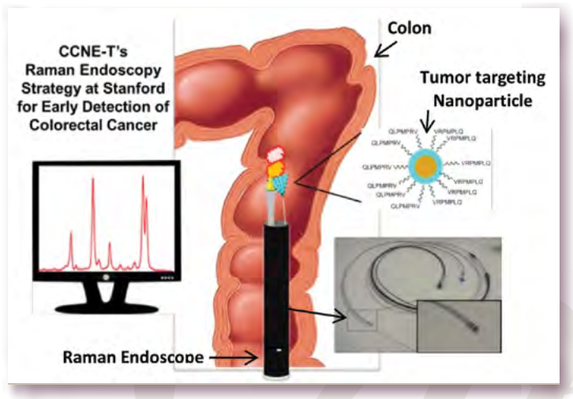

Image 2:An advanced clinical Raman endoscope being developed within the CCNE-TR and CCNE-T for colorectal cancer.

Our cancer and nanotechnology research not only results in high impact publications but also inspires and guides the entire relevant biomedical community. With our four research projects and four supportive cores within the CCNE-T, we are focusing on the development of novel next generation smart nanoparticles including Raman and self-assembling nanoparticles, the application of our maturing magneto-nanotechnology platform in blood proteomics and cell sorting, and the use of multiple other nano-platforms to interrogate single circulating tumor cells in a unique way that exists only at Stanford. We also focus on molecular imaging of ovarian cancer with photoacoustics and Raman nanoparticles, and monitoring response to therapy using imaging and magneto-nanosensors. Several of our nano-enabled research products are at an advanced development stage, thanks to the excellent staff, nanofabrication, and nanocharacterization infrastructure at Stanford. One such product is our clinical Raman Endoscope instrument being developed through the CCNE-T. Endoscopic imaging has proven to be an invaluable diagnostic tool with its ability to non-invasively assess deep tissues within the body and has played a key role in the screening of colon cancer and is credited with the decline in deaths due to prevention through the early removal of cancerous polyps. However, conventional white light endoscopy only offers physicians real time structural detail with little physiological information. We have developed an accessory Raman endoscopic probe that has the potential to provide real time functional information during routine endoscopy at unsurpassed sensitivity levels and multiplexing capabilities that did not exist until now. This novel approach would allow endoscopists to distinguish between normal and cancerous tissues instantly, as well as to identify flat lesions that are easily missed during conventional screening endoscopy.

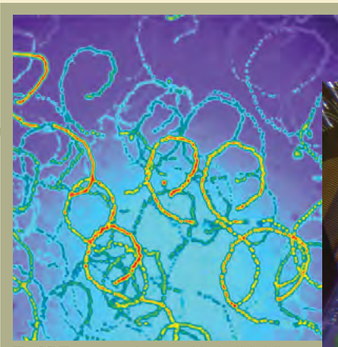

The CCNE uses magnetic nanoparticles in clinical diagnostics and therapy. This image reveals the trajectories of flurophore labeled magnetic naoparticles under a rotating magnetic field gradient.
Aihua Fu, PhD and Shan X Wang, PhD

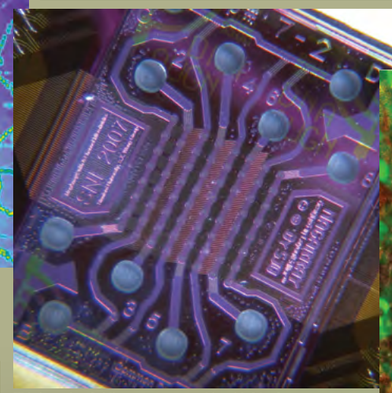

This is a microfluidic magneto-nano chip with 8 by 8 sensors arrays and 8 microfluidic channels. These chips are being developed to monitor protein profiles in blood samples from cancer patients to improve therapeutic effectiveness.
Sebastian J. Osterfeld, PhD and Shan X. Wang, PhD

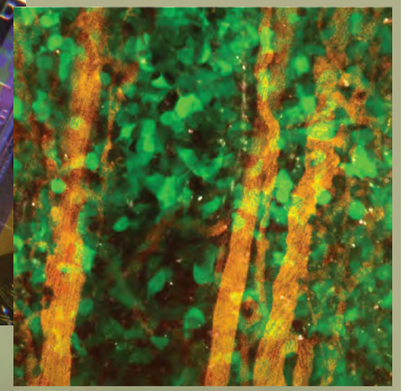

The CCNE uses special microscopes to study the targeting of nanoparticles to tumor blood vessels and to individual tumor cells (red). In this image, the white spots are single-walled carbon nanotubes that have been chemically linked to molecules that selectively target the cancer cells (green). These nanotubes can be used to diagnose and kill tumors.
Bryan R Smith, PhD and Sanjiv Sam Gambhir, MD, PhD

In the CCNE-T program, our multidisciplinary scientists and physicians use nanotechnology to create the tiniest of devices (one billionth of a meter in size) that will enable us to eventually screen individuals by a simple blood test. By then performing an analysis and using imaging, we will be able to find problem cells and simultaneously eradicate or treat those cells successfully before they have grown out of control. Through use of today's advanced nanotechnology materials and molecular biology techniques for earlier detection and treatment monitoring, we expect to dramatically improve cancer survival rates and provide reassurance to patients that their treatment is effective. With our highly interactive and cohesive program focused on developing and validating nanotechnology for anti-cancer therapy response and earlier cancer detection, **we will continue to imagine, invent, and innovate for the benefit of cancer patients.**

http://mips.stanford.edu/grants/ccne
http://mips.stanford.edu/grants/ccne-t

Personnel

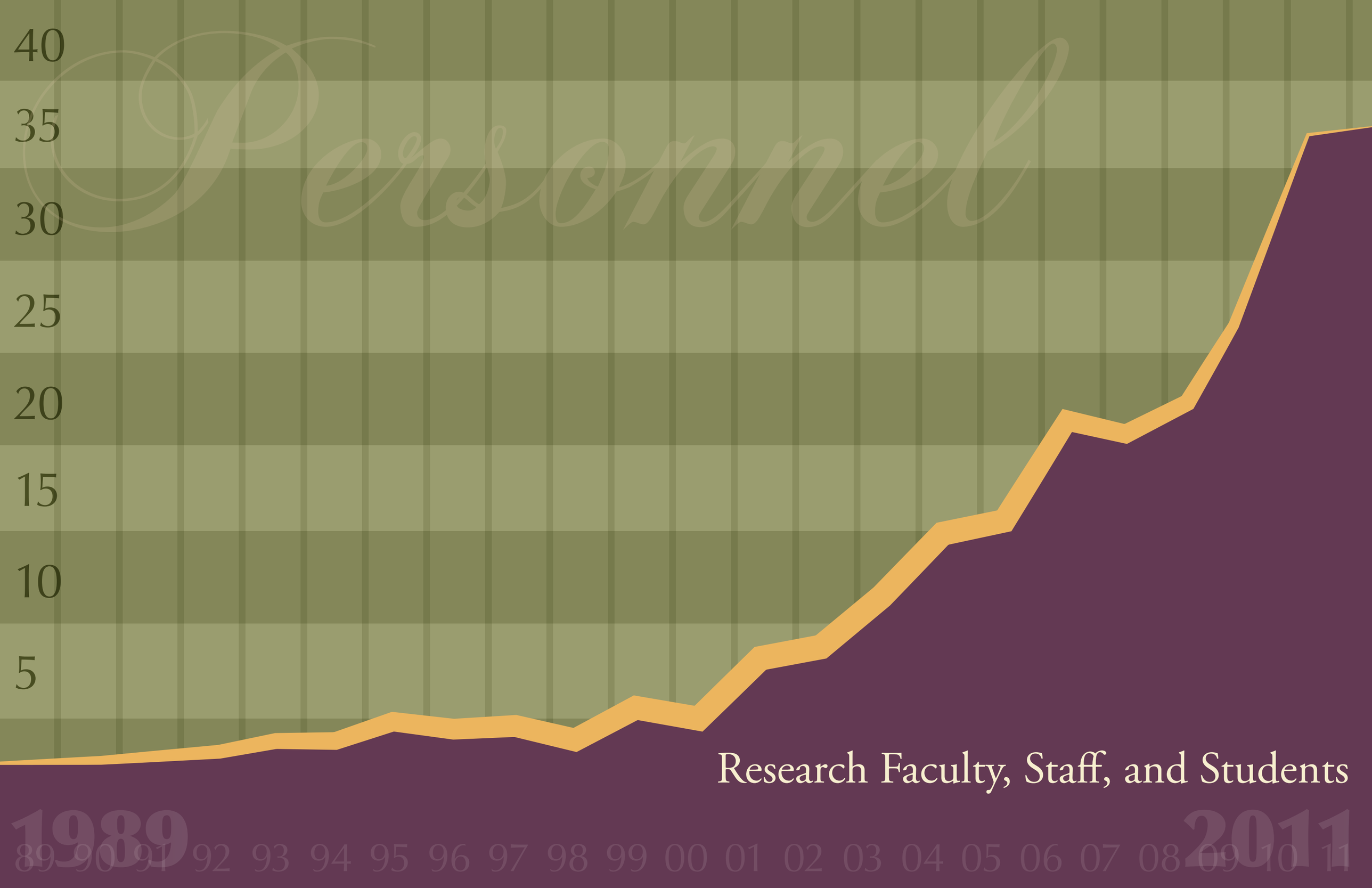
40
35
30
25
20
15
10
5
Research Faculty, Staff, and Students
1989
2011
89 90 91 92 93 94 95 96 97 98 99 00 01 02 03 04 05 06 07 08 09 10 11

Radiology Research Faculty, Staff, and Students

Faculty & Staff

Faculty

Roland Bammer, PhD
Sandip Biswal, MD
Kim Butts Pauly, PhD
Zhen Cheng, PhD
Heike Daldrup-Link, MD
Rebecca Fahrig, PhD
Sanjiv Sam Gambhir, MD, PhD
Gary M. Glazer, MD
Gary H. Glover, PhD
Garry Gold, MD
Brian Hargreaves, PhD
Robert J. Herfkens, MD
Andrei Iagaru, MD
Craig Levin, PhD
Amelie Lutz, MD
Parag Mallick, PhD
Michael E. Moseley, PhD
Sandy Napel, PhD
David Paik, PhD
Ramasamy Paulmurugan, PhD
Norbert J. Pelc, ScD
Sharon Pitteri, PhD
Sylvia K. Plevritis, PhD
Jianghong Rao, PhD
Daniel Rubin, MD
Brian Rutt, PhD
Daniel M. Spielman, PhD
Shreyas Vasanawala, MD, PhD
Juergen Willmann, MD
Joseph Wu, MD, PhD
Greg Zaharchuk, MD, PhD

Administrative & Support Staff

Karen Aguilar, BS
Danae Barnes, MS
Mary Bobel, MA, MBA
Maggie Bos
Janet Checchi-Acosta
Michelle Christierson
Bonita Crabbe
Donna Cronister
Kelly Englese
Debra Frank
Elizabeth Gill
Sofia Gonzales, MS
Sondra Horn
Joe Hubbard, BA
Mandeep Kaur, BA
Susan Kopiwoda, MS, MPH
Marlys Lesene
John Mendoza
Amy Morris, BA
Teresa Newton, MA
Donna Nienberger, RN
KimChi Nguyen
Kala Raman, MS
John Reuling
Patricia Riley
Lanzie Rivera
Billie Robles, BS
David Russel
Anita Samantaray, MPH
Monique Schareck, MHA
Judy Schwimmer, MA
Susan Singh
Susie Spielman
Jean Stevens
Wei Xiong
Yun-Ting Yeh, MBA

Scientific Staff

Aaryani Tipirini, PhD
Andrew Holbrook, PhD
Demir Akin, DVM, PhD
Murat Aksoy, PhD
Marcus Alley, PhD
Eva Bajorek
Priti Balchandani, PhD
Sanjiv Bhandari, MS
Wendy Baumgardner, RVT, LATg
Thomas Brosnan, PhD
Carmel Chan, PhD
Edwin Chang, PhD
Danye Cheng
Frederick Chin, PhD
Garry Chinn, PhD
Aradhana Dhanabalan
David Dick, PhD
Diqiang Qiu, PhD
Aloma D'Souza, PhD
Aihua Fu, PhD
Andrew Gentles, PhD
Gayatri Gowrishankar, PhD
Meng Gu, MS
Frezghi Habte, PhD
Samantha Holdsworth, PhD
Derek Innes
Ken Ito, PhD
Fangjun Jia, PhD
Jesse Jokerst, PhD
Richard Kimura, PhD
Daniel Korenblum
Keshni Kumar, CRT
Ken Lau
Jelena Levi, PhD
Manoj Saranathan, PhD
Dirk Mayer, PhD
Melvin Ooi, PhD
Erik Mittra, MD
Ramesh Nair
Mohammed Namavari, PhD
Kazim Narsinh, MD
Arutselvan Natarajan, PhD, DVM
Laura Pisani, PhD
Rafael O'Halloran, PhD
Rachel Bitton, PhD
Robert Reeves, MA
Viola Rieke, PhD
Jarrett Rosenberg, PhD
Ataya Sathirachinda
Anne Marie Sawyer, BS, RT (R)(MR)
Greig Scott, PhD
Alan Snyder
Charles Stanley
Mark Stolowitz, PhD
Matus Straka, PhD
Murugesan Subbarayan, PhD
Kyung Sung, PhD
Robert Teed
Waldo Hinshaw, PhD
Sen Wang, PhD
Ron Watkins
Debra Willrett
Pauline Worters
Lingyun Xu, PhD
Xinrui Yan, PhD

Visitors

Visiting Researchers & Scholars

Hakan Bulu
Georges Hankov, MS
Russell Haynes
Jinbo Li
Hongguang Liu, PhD
Ermelinda Lucente
Tarik Massoud, PhD
Nicole Haazen, MS
Chang-Hyun Oh
Lior Weizman, PhS
Zhengming Xiong, MD, PhD
Meng Yang
Joon-Kee Yoon, MD, PhD
Ping Zhao

Undergraduate & High School Students

Aaron Abajian
Rohan Bansal
Sunil Bodapati
Luxi Chen
Martina de Geus
Varun Krishnamurthy
Elizabeth Li
Pooja Naik
Danielle Rasooly
Krithin Sitaram

Trainees

Post-Doctoral Fellows

Ahn Van, PhD
Jongduk Baek, PhD
Deepak Behera, PhD
Bhavya Shah, MD
Bousselham, Abdelkader PhD
Carpenter, Colin, PhD
Qiang Chen, PhD
Kai Cheng, PhD
Cahterine Moran, PhD
Ben Cosgrove, PhD
Helen D'Arcuil, PhD
Nirupama Deshpande, PhD
Constantin Dragos, PhD
Anca Dragulescu-Andrasi, PhD
Eddy Lee, PhD
Saadet Ayca Erdogan, PhD
Kira Foygel, PhD
Olivier Gevaert, PhD
Pejman, Ghanouni, MD, PhD
Zhumur Ghosh, PhD
Gonzalez, Eric, PhD
Grace Tye, MD
Benjamin Hackel, PhD
Feng Han, PhD
Aileen Hoehne, PhD
Hong Key Jo, PhD
Sharon Hori, PhD
Shijun Hu, PhD
Mei Huang, PhD
Michelle James, PhD
Sonal Josan, PhD
Andreas Keil, PhD
Kim, Ealgoo PhD
Kelvin, Billngsley, PhD
Uma Kota, PhD
Sri-Rajasekhar Kothapali, PhD
Masakatsu Kotsuma, PhD
Majlinda Kullolli, PhD
Feng Lan, PhD
Joo Hyun Lee, PhD
Zongjin Li, PhD
Yang Liu, PhD
Zhe Liu, PhD
Emily McWalter, PhD
Zheng Miao, PhD
Gang Niu, PhD
Natesh Parashurama, MD, PhD
Kyeongsoon Park, PhD
Prachi Pandit, PhD
MaryBeth Pysz, PhD
Qingfei Luo, PhD
Gang Ren, PhD, MD
Hongjun Ren, PhD
Ying Ren, PhD
John Ronald, PhD
Narayana Murthy Sekar, PhD
Bryan Smith, PhD
Virginia Spanoudaki, PhD
Ning Sun, PhD
Taghibakhsh, Farhad PhD
Thomas Christen, PhD
Urvi Vyas, PhD
Domonique Van de Sompel, PhD
Stephanie van de Ven, MD
Arne Vandenbroucke, PhD
Thillai Sekar Veerapazham, PhD
Thillai Sekar Veerapazham, PhD
Vinke, Ruud, PhD
Hui Wang, PhD
Yun Wu, PhD
Zuyong Xia, PhD
Yung Xing, PhD
Yeom, Jung Yeol, PhD
Cristina Zavaleta, PhD
Keren Ziv, PhD
Wesley Zun, PhD

Graduate Students

Rahul Argawal
Aravind Babu
Bieniosek, Matthew MS
Brady Quist, MS
Bragi Sveinsson, MS
Catie Chang, MS
Cui, Jingyu MS
Erin Girard, MS
Eun So Choi, MS
Jessica Faruque, MS
Charles Feng, MS
Shangping Feng, MS
Francisco Gimenez
Kristi Granlund, MS
Alex Grant
Yi Gu, MS
Yihan Guan
Scott Hsieh
Hye-Seon Yoon, MS
JaeMo Park, M.S.
Jang Hwan Choi, MS
Caroline Jordan, MS
Juan Plata, MS
Elena Kaye, MS
Kranthi Kode, BS
Daniel Kopeinigg, MS
Frances Lau, MS
Andrew Lee, BS
Prasheel Lillaney, MS
Ray Lin, MS
Tiffany Liu
Mihye Shin, MS
Michael Marx, MS
Diego Munoz
Andy Nnewihe, MS
Chinyere Nwabugwu
Peter Olcott, MS
Jeremy Pearl, BS
Rebecca Rakow-Penner, MD
Julia Rasooly, BS
Paul Reynolds, MS
Randy King, M.S.
Witi Sachchamarga
Debashis Sahoo, MS
Laura Sasportas
Heiko Schmiedeskamp, MS
Florian Schmitzberger
Harpeet Singh
Vanessa Sochat
Ernesto Staroswiecki. MS
Jason Su, MS
Uche Monu, MS
Wang, Zhiguang MS
Adam Wang, MS
Kitch Wilson, MD
Wendy Ni, MS
Jiajing Xu
Tao Xu, MS
Yuan Yao, MS
Jinjian Zhai

2011 Graduates

Murat Aksoy, PhD	Research Associate, RSL	Stanford University
Catie Chang, PhD	Postdoctoral Fellow	NIH
Misung Han, PhD	Postdoctoral Fellow	UCSF
Andrew Holbrook, PhD	Research Associate, RSL	Stanford University
Jared Starman, PhD	Associate	Exponent Engineering & Scientific Consulting
Adam de la Zerda, PhD	Postdoctoral Fellow, Chemistry	UC Berkeley

2011 Transitions

Didem Aksoy, PhD	Staff Scientist, RSL	Stanford University
Anca Dragulescu-Andrasi, PhD	LSRA	Stanford University
Arun Ganguly, PhD	Senior Scientist	Varian Medical Systems
Pejman Ghanouni, MD, PhD	Assistant Professor, Radiology	Stanford University
Erin Girard	Collaborations Manager	Siemens Corporate Research
Ben Hackel, PhD	Assistant Professor	University of Minnesota
Sam Mazin, PhD	President	RefleXion Medical
Jennifer Prescher, PhD	Assistant Professor, Chemistry	UC Irvine
Viola Rieke, PhD	Assistant Professor	UCSF
Stefan Skare, PhD	Faculty	Karolinska Institute
Bryan Smith, PhD	Staff Scientist, MIPS	Stanford University
Matus Straka, PhD	Senior Research Associate, RSL	Stanford University
Tau Xu, PhD	Associate	Citadel Investment Group

New Clinical and Research Faculty

Pejman Ghanouni, MD, PhD, Body MRI Section

Dr. Pejman Ghanouni will join the Department of Radiology as an Assistant Professor in the Body MRI Section on January 1, 2012. Following completion of his undergraduate training at Harvard, Dr. Ghanouni acquired his MD and PhD in the Medical Scientist Training Program (MSTP) at Stanford. For his PhD research he used biophysical techniques to investigate the mechanism of activation of the beta-2 adrenergic receptor, a model G protein coupled receptor. Dr. Ghanouni served as Chief Resident while at Stanford, and also was awarded a Radiological Society of North America (RSNA) Trainee Prize in 2009 for his research using MRI to monitor the role of macrophages in the development of chronic pain behavior. As a National Cancer Institute Fellow, Dr. Ghanouni is studying clinical and preclinical applications of MR-guided focused ultrasound surgery. Dr. Ghanouni is a co-Principal Investigator on two human clinical trials using focused ultrasound to palliate painful bone metastases.

Amelie Lutz, MD, PD, Musculoskeletal Section

Amelie M. Lutz, MD, PD, was appointed as an Assistant Professor in the Department of Radiology in the Musculoskeletal (MSK) section on May 2, 2011. Dr. Lutz has been a clinical instructor and clinician researcher in radiology and molecular imaging since 2009. After completing medical school and internship in Internal Medicine/Endocrinology at the Albert-Ludwigs-University in Freiburg, Germany, Dr. Lutz did her residency in Diagnostic Radiology at the University Hospital in Zurich, Switzerland and a fellowship in Body Imaging/Musculoskeletal Imaging at the Kantonal Hospital in Frauenfeld, Switzerland. In 2008 she received the venia legendi (member of the academic faculty, PD) in Diagnostic Radiology for her work in the field of kinematic and cellular-targeted MR imaging at the University of Zurich. Her research interests include the development of novel diagnostic strategies for early detection of cancer, especially of ovarian cancer. She is currently working on preclinical and translational studies including multimodality strategies using blood biomarker tests and molecular imaging for ovarian cancer early detection as well as on the translation of these strategies into clinical pilot studies.

Parag Mallick, PhD, Molecular Imaging Program at Stanford (MIPS)

Dr. Mallick joined the department of Radiology as an Assistant Professor of Radiology in the MIPS section on January 1, 2011. He completed his undergraduate degree in Computer Science and Biochemistry at Washington University (St. Louis, MO), after which he obtained his PhD in Chemistry & Biochemistry at UCLA. For his doctoral research, Dr. Mallick performed whole-proteome structure and function studies and investigated protein networks. Dr. Mallick then joined Dr. Ruedi Aebersold's group at the Institute for Systems Biology where he performed fundamental studies of proteomics technologies and developed clinical proteomics workflows to study cancer and neurodegenerative diseases. Dr. Mallick was also faculty at USC and UCLA where he focused on experimental and computational systems biology and proteomics. In his current role as a member of the Canary Center at Stanford for Cancer Early Detection, he focuses on 1) systems-based studies to develop quantitative models of the states and trajectories of cancer cells, and 2) remote-sensing models that describe how to infer those states and trajectories via measurements of the circulation. By combining these two areas of inquiry, the Mallick lab hopes to develop a strategy to rationally identify molecular indicators for lung cancer, prostate cancer, and lymphoma.

Sharon Pitteri, PhD, Molecular Imaging Program at Stanford (MIPS)

Dr. Pitteri joined the Department of Radiology as an Assistant Professor of Radiology in the MIPS section on November 1, 2010. After completing her undergraduate degree in chemistry at Carleton College (Northfield, MN), she obtained her PhD in chemistry from Purdue University (West Lafayette, IN). Dr. Pitteri joined Dr. Sam Hanash's laboratory as a post-doctoral research fellow in the Public Health Sciences division at the Fred Hutchinson Cancer Research Center (Seattle, WA), where she applied advanced proteomic technologies to molecular diagnostics. As a member of the Canary Center at Stanford for Cancer Early Detection, the Pitteri Lab is focused on discovering and validating novel molecular indicators for breast cancer and ovarian cancer and looks forward to opportunities for collaborations.

New Clinical Educators

We also welcome new Clinical Instructors whose primary and critical role is to provide excellence in radiological clinical care, teaching, and institutional service appropriate to their training and clinical interest areas. Please welcome our new clinical instructors whose commitment and dedication to patient care are highly valued and provide critical service and discipline in all clinical areas of the Department of Radiology.

Bao Do, MD, Musculoskeletal Radiology Section

Dr. Bao Do joined the faculty in July 2011 as a Clinical Instructor after completing his subspecialty fellowship in Musculoskeletal Radiology at Stanford. He received his BS/BA in Biochemistry and Economics with honors at UC Davis as a University of California Regents Scholar and his MD at the University of Illinois. He began his training at the University of Iowa and completed his Diagnostic Radiology Residency at Stanford. His clinical interests include musculoskeletal mri, natural language processing, and designing information retrieval and computer decision support systems in Radiology. Dr. Do is a co-developer of rad TF, a Radiology domain semantic search engine, with Dr Andrew Wu, MD and Dr Daniel Rubin, MD.

Rajesh Shah, MD, Interventional Radiology Section

Dr. Rajesh Shah joined the Radiology faculty as a Clinical Assistant Professor in August 2011. He received his BS (magna cum laude) in Electrical Engineering from the University of Illinois at Urbana-Champaign. He worked in web development before going to medical school at The University of Chicago. He completed his internship at California Pacific Medical Center followed by a residency in diagnostic radiology at the University of Illinois at Chicago Medical Center. He did a fellowship in Vascular and Interventional Radiology at Stanford. Dr. Shah worked at Memorial Sloan Kettering Cancer Center before joining the faculty at Stanford as Chief of Interventional Radiology at the Palo Alto Veterans Administration Health Care System. His interests include chemoembolization, bland embolization, selective internal radiation therapy, lung and liver ablation, and arterial and venous interventions.

David Wang, MD, Interventional Radiology Section

Dr. David Wang joined the faculty in 2011 as a Clinical Instructor. He completed fellowship training in Vascular and Interventional Radiology at the University of Pennsylvania Medical Center as the Constantin Cope-Cook Medical Fellow preceded by residency training in Diagnostic Radiology at Stanford. He received his medical degree from Stanford University School of Medicine, where he was an HHMI research fellow and the lead founder of Stanford's Pacific Free Clinic. Dr. Wang earned his undergraduate degrees at Stanford University, graduating with honors and distinction in Biological Sciences and Economics. His clinical interests include interventional oncology, minimally invasive treatment of arterial and venous diseases, and endovascular management of dialysis accesses. His research interests include therapeutic applications of molecular imaging, use of interventional techniques to advance molecular and cell-based therapies, targeted gene and drug delivery, tissue engineering, and device design and development.

Faculty Awards

For additional awards, see
Sponsored Project Awards pages 186 - 192

For additional awards, see
Sponsored Project Awards pages 186 - 192

Recipient	Award
Scott Atlas, MD	2011 University of Chicago Distinguished Alumni Achievement Award nominee
Scott Atlas, MD	2011 University of Illinois Alumni Achievement Award Distinguished Alumni
Scott Atlas, MD	2011 University of Illinois Liberal Arts and Sciences Distinguished Alumni
Scott Atlas, MD	Member, Nominating Committee, Nobel Prize in Medicine and Physiology; 2004 – 2010
Roland Bammer, PhD	Senior Fellow, Freiburg Institute of Advanced Studies (FRIAS), University of Freiburg, Germany
Sandip Biswal, MD	2010 Resident Teaching Award: Junior Faculty of the Year
Zhen Cheng, PhD	Certificate of Recognition: Siemens Competition Mentor
Zhen Cheng, PhD	Cover page article of Bioconjugate Chemistry 22(3)
Zhen Cheng, PhD	Cover page article of Small 6(10)
Heike Daldrup-Link, MD	Editor's Recognition Award with special distinction for reviews for the journal Radiology
Heike Daldrup-Link, MD	Elected member of the Board of Directors of the Society for Pediatric Radiology
Bruce Daniel, MD	Finalist, Young Investigator Award competition. 2010 International Society for Magnetic Resonance in Medicine. “A Pilot Study Comparing Blood Oxygen Level Dependent (BOLD) Contrast in the Human Healthy and Malignant Breast”
Dominik Fleischmann, MD	2011 Society of Gastrointestinal Radiologists Wyle J. Dodds Research Award: "Prognostic Value of Early Changes in Liver Metastases Treated with Bevacizumab determined with Dynamic Contrast Enhanced CT"
Sanjiv Sam Gambhir, MD, PhD	Society of Nuclear Medicine's 2011 Georg Charles de Hevesy Nuclear Pioneer Award for "extraordinary contributions to the field of molecular imaging"
Garry Gold, MD	2011 Allan V. Cox Medal for Faculty Excellence in Fostering Undergraduate Research
Garry Gold, MD	Fellow, International Society of Magnetic Resonance in Medicine
Garry Gold, MD (Chen, Christina)	SCBT/MR Young Investigator Award: "Improved Methods for MR Imaging Around Metallic Implants: Artifact Assessment and Clinical Impact"
Garry Gold, MD	SNM Correlative Imaging Council Walter Wolf Award: "Correlation Between MRI and NaF PET/CT in Patients with Patellofemoral Knee Pain"
Garry Gold, MD (Lauren Shapiro)	Stanford Firestone Medal for Excellence in Undergraduate Research - mentor to Ms. Lauren Shapiro
Brian Hargreaves, PhD	General Electric “Thought Leader” Award, May 2010 for “Reducing Metal Artifacts”
Brian Hargreaves, PhD	ISMRM HM Poster Award for "Metal-Induced MRI Artifacts"
Brian Hargreaves, PhD	NIH Edward Nagy New Investigator Award, April 2011
Lawrence Hofmann, MD (Stefanie Carr)	2010 Dr. Constantin Cope Medical Student Society of Interventional Radiology Annual Scientific Meeting Research Award – Mentor for Stephanie Carr.
Lawrence Hofmann, MD (Keith Chan)	2011 Dr. Constantin Cope Medical Student Society of Interventional Radiology Annual Scientific Meeting Research Award – Mentor for Keith Chan
Lawrence Hofmann, MD	Ohio State School of Medicine Early Career Achievement Award
Lawrence Hofmann, MD	The Society of Interventional Radiology elected fellow
Andrei Iagaru, MD	Best Essay Award, ACNM Annual Meeting: “Classical Hodgkin Lymphoma in First Complete Remission: Is There a Role for 18F FDG PET/CT Surveillance?”
Andrei Iagaru, MD	Research featured on AuntMinnie.com and SNM News Highlights
Andrei Iagaru, MD	Winner – Young Professionals Tournament, 1st Sino-American Conference on Nuclear Medicine
Aya Kamaya, MD	2011 Society of Gastrointestinal Radiologists Wyle J. Dodds Research Award: "Prognostic Value of Early Changes in Liver Metastases Treated with Bevacizumab determined with Dynamic Contrast Enhanced CT"
Aya Kamaya, MD	2011 SUR Research Award. Society of Uroradiology for grant application: "Photoacoustic Imaging of Bladder Cancer"
Nishita Kothary, MD	Committee member, Interventional Radiology (VIR) board certification for Exam of the Future (EOF), American Board of Radiology
Nishita Kothary, MD	Elected to the Society of Interventional Radiology Fellowship (FSIR) for Outstanding Contribution to the Field of Interventional Radiology
Nishita Kothary, MD	Invited member to the American Association of Physicists in Medicine Task Group 199 - Implanted Target Surrogates for Radiation Treatment Verification
William Kuo, MD	Dr. Gary J. Becker Young Investigator Award – Society of Interventional Radiology Foundation.
William Kuo, MD	Outstanding Faculty Award – Society of Interventional Radiology.
William Kuo, MD	SIR Dr. Gary J. Becker Young Investigator Award for Most Outstanding Clinical Science Research Paper
William Kuo, MD	Society of Interventional Radiology elected fellow
Craig Levin, PhD	Physics in Medicine and Biology Featured Article by Editors of Institute of Physics, selected for "novelty, high level of interest and potential impact on future research"
Margaret Lin, MD	2010 Stanford Radiology Clinician Educator of the Year
Andrew Quon, MD	2011 Image of the Year - Society of Nuclear Medicine
Hans Ringertz, MD, PhD	RSNA Special Presidential Award: "Significant Contributions to the Field of Radiology or the Radiologic Sciences"
Daniel Rubin, MD, MS	2010 caBIG Connecting Collaborators Award, National Cancer Institute
Daniel Rubin, MD, MS	AMIA Distinguished Paper Award: "Natural Language Processing for Lines and Devices in Portable Chest X-Rays"
Daniel Rubin, MD, MS	caBIG® Connecting Collaborators Award
Daniel Rubin, MD, MS	RSNA Cum Laude Award: "Natural Language Processing in Radiology"

Faculty Awards

For additional awards, see
Sponsored Project Awards pages 186 - 192

Recipient	Award
Juergen Willmann, MD	2011 Society of Gastrointestinal Radiology Roscoe E. Miller Award: Best Paper presentation
Joseph Wu, MD, PhD	Receives the CIRM Basic Biology Award
Joseph Wu, MD, PhD	2010 White House Presidential Early Career Award for Scientists & Engineers (PECASE)

Postdoctoral and Trainee Awards

Recipient	Award
Priti Balchandani, PhD	K99/R00 Pathway to Independence Award: High Resolution Magnetic Resonance Imaging and Spectroscopy of Epilepsy at 7T
Keith Chan, MS	SIR Constantin Cope Medical Student Award: Common Iliac Vein Stenosis: A Risk Factor for Oral Contraceptive-induced Deep Vein Thrombosis
Christina Chen	SCBT/MR Young Investigator Award: Improved Methods for MR Imaging Around Metallic Implants: Artifact Assessment and Clinical Impact
Nick Conley, PhD	BioX Interdisciplinary Initiatives Program grant
Nick Conley, PhD	Awarded the Cardiovascular Institute's Younger Fellowship Award for: High-Throughput Mutagenesis of Neuropilins to Elucidate Domains Required for Hedgehog Signaling
Jing-yu Cui	Awarded an HHMI Fellowship
Jing-yu Cui	Received the Pan Wen-Yuan Foundation Scholarship for outstanding academic performance
Aloma D'Souza, PhD	AACR Poster Award for: A Novel Method of Tumor Characterization by Protein and microRNA Biomarker Release Using Ultrasound
Jessica Faruque, MS	SIIM research grant: Developing a Scalable Similarity Reference Standard for a Content-based Image Retrieval (CBIR) System
Eugene Gu	Awarded an HHMI Fellowship
Aileen Hoehne, PhD	Wiley Award for the International Symposium on Radiopharmaceutical Sciences (ISRS) in Amsterdam for best submitted abstract
Aileen Hoehne, PhD	Received the Wiley Award from International Symposium for: Radiolabeling of a Saxitoxin derivative for PET/MRI imaging of pain
Susan Koppmann, PhD	SNM Poster Award in Oncology for: Characterization of 177Lu-Affibody-HSA bioconjugate for radionuclide therapy of EGFR-expressing head and neck carcinomas
Albert Hsiao, MD, PhD	ARRS Residents in Radiology President's Award: Fast Pediatric Cardiac MR Flow and Ventricular Volume Assessment
Shijun Hu, PhD	2010-12 American Heart Association Postdoctoral Fellowship
Frances Lau, PhD	Selected as Institute of Physics Journal's Featured Article for: Analog signal multiplexing for PSAPD-based PET detectors: simulation and experimental validation
Andrew Lee	2010-13 Bio-X Graduate Student Research Fellowship
Jonathan Lu	NSF Graduate Research Fellowship

Postdoctoral and Trainee Awards

For additional awards, see
Sponsored Project Awards pages 186 - 192

Recipient	Award
Jonathan Lu	Stanford Graduate Fellowship
Hua Fan-Minogue, MD, PhD	Cover Article PNAS for: Noninvasive molecular imaging of c-Myc activation in living mice (PNAS, 2010)
Divya Nag	2010 American Heart Association Summer Fellowship
Kazim Narsinh	RSNA Research Medical Student Grant: Imaging Human Induced Puripotent Stem Cell-derived Cardiomyocyte Transplants
Patricia Nguyen, MD	2010-12 ACC/GE Healthcare Career Development Award
Juan Plata	NSF Graduate Fellowship
Prachi Prandit, PhD	Stanford Molecular Imaging Scholars Postdoctoral Fellowship
Guillem Pratx, PhD	BCRP Fellowship Award
Laura Sasportas, MS	Awarded an HHMI Fellowship
Conroy Sun, PhD	BCRP Fellowship Award: X-ray Luminescent Nanophosphors for Breast Tumor Detection and Treatment
Kyung Sung, PhD	Finalist for ISMRM Post Award for Quantitative MRI of Breast Cancer
Li Wang, PhD	2011-13 American Heart Association Postdoctoral Fellowship
Huaijun (Morgan) Wang, MD, PhD	Stanford Dean's Fellowship Award
Yanmei Yang, PhD	Cover Picture/Article: Enzyme-Responsive Multifunctional Magnetic Nanoparticles for Tumor Intracellular Drug Delivery and Imaging (Chem. Asian J. 6/2011)

Our group photo represents approximately half of the Radiology research personnel found in various locations on the medical school campus.

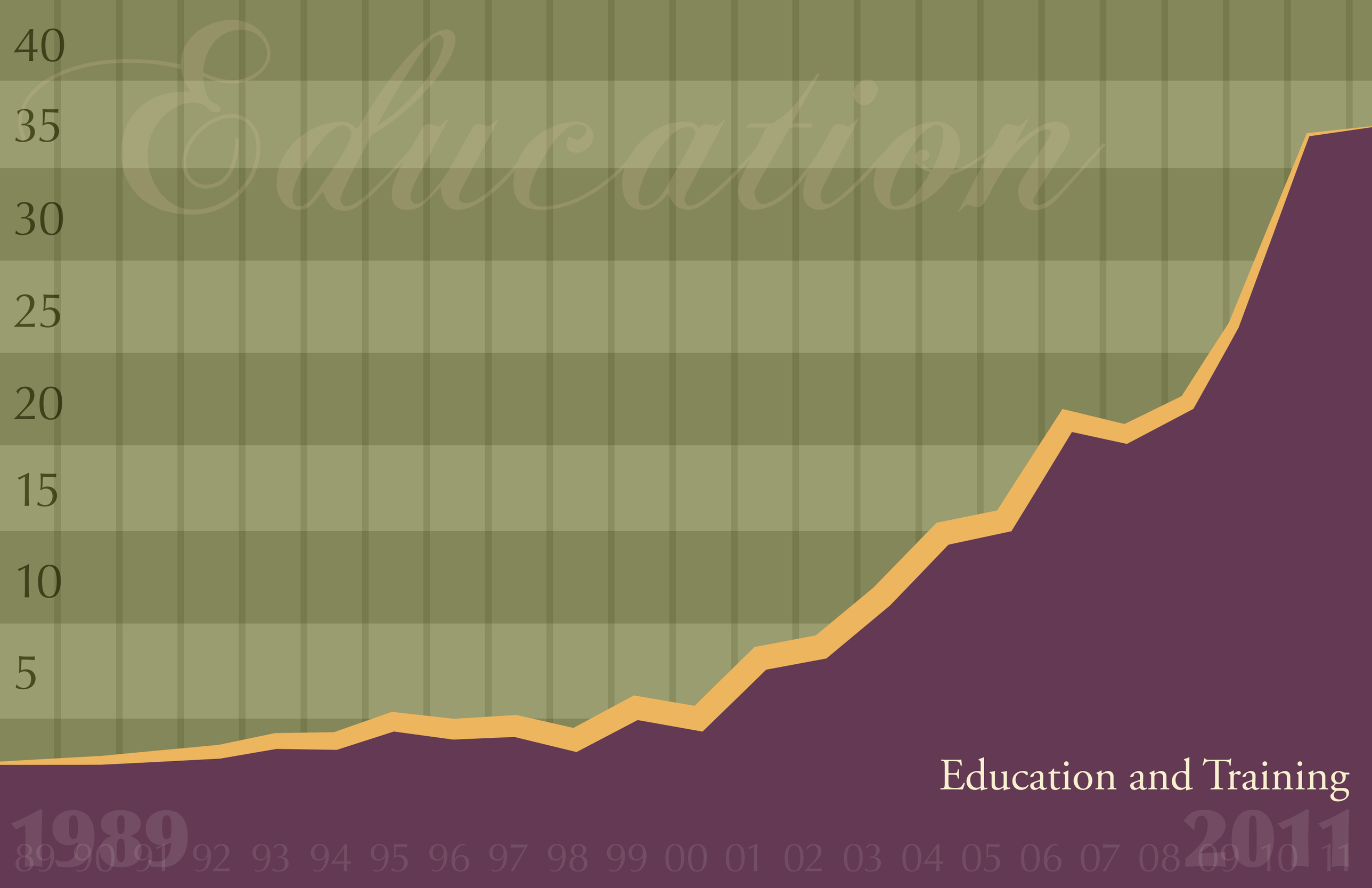
Education
40
35
30
25
20
15
10
5
Education and Training
1989
2011
89 90 91 92 93 94 95 96 97 98 99 00 01 02 03 04 05 06 07 08 09 10 11

NIH/NCI T32 CA 09695

Advanced Techniques for Cancer Imaging and Detection - T32

PI: Gary M. Glazer, MD
Program Manager: Donna Cronister/Lanzie Rivera

The Department of Radiology at Stanford University offers qualified individuals a unique research opportunity through our Advanced Techniques for Cancer Imaging and Detection Program, which began its 19th year of training on March 1, 2011. The goal of our program is to provide MD and PhD research fellows training in cancer-related imaging research. Fellows have the opportunity to work with our world-renowned faculty who are committed to sharing their knowledge and mentoring future leaders in radiology. Our program allows basic scientists in medical imaging (PhD) and clinical scientists (MD post-residency) to collaborate in an unparalleled environment that combines medical imaging sciences, clinical sciences, a strong cancer focus, and an institutional commitment to training academic radiologists and basic scientists in imaging science. We are preparing a competing renewal application for this program in January 2012 as our current funding will end on February 28, 2013.

A specific aim of our training program is to position our trainees for a career in academic radiology. To date, we have graduated 32 trainees from our program. Of these 32 alumni, 23 have taken positions in academia; 3 in industry and 6 are in private practice. Our trainees continue to be extremely productive. We often collaborate with them in their new positions both locally and throughout the country. We are grateful to the National Institutes of Health for its recognition of the strength and success of our training program.

Currently we have 5 trainees in the program: Drs. Dragos Constantin, Sarah Geneser, Pejman Ghanouni, Catherine Moran, and Bhayva Shah. Dr. Grace Tye ended her two year fellowship on June 30, 2011 and joined a private practice radiology firm in La Jolla, California. On July 1, 2012, two clinical fellows will join the program, both specialize in body imaging. Current trainees and their research interests are summarized briefly below.

Current NCI T32 Postdoctoral Trainee Research Interests

Dragos Constantin, PhD joined RSL as an NCI fellow in 2009. His research interests involve theoretical and experimental investigation of the magnetic resonance imaging integration with a medical linear accelerator to provide real-time image guidance to target temporally changing tumor anatomy, particularly for cancers in the thorax and abdomen. Dr. Constatin began his second year of training with Dr. Rebecca Fahrig in February 2010 and is working closely with faculty in the Department of Radiation Oncology.

Sarah Geneser, PhD, joined the RSL group as an NCI fellow in 2011. In 2010 Dr. Geneser was awarded the highly competitive Dean's Postdoctoral Fellowship award from the Stanford School of Medicine. During this fellowship year, her goals focused modeling the impact of hormone replacement therapy on breast cancer risk and progression to better understand the physiological effects on breast tumor development. She continues her research breast cancer with Dr. Sylvia Plevritis to investigate the impact of mammography screening and treatment on breast cancer incidence and survival. Dr. Geneser received her PhD in computer science from the University of Utah in 2008.

Pejman Ghanouni, MD, PhD, joined the NCI program on July 1, 2010 after completing the Stanford Radiology residency program. Pejman has a very keen interest in research and as an NCI fellow is studying clinical and preclinical applications of MR-guided focused ultrasound surgery. Dr. Ghanouni is a co-Principal Investigator on two human clinical trials using focused ultrasound to palliate painful bone metastases. In January, 2012, Dr. Ghanouni will join the Stanford Radiology Department as an Assistant Professor.

Catherine Moran, PhD, joined the NCI program in April 2011. Her primary research interest is improving lesion characterization in breast MRI through the use of novel contrast mechanisms, with specific application of these techniques in women at a high risk for breast cancer. Training with Dr. Daniel and Dr. Hargreaves, her work encompasses both basic science and clinical translational aspects of breast MRI. Dr. Moran received her PhD in medical physics from the University of Wisconsin in 2009.

Bhayva Shah, MD, began his two year traineeship on August 1, 2011. Dr. Shah will be working with Dr. Sandip Biswal in the Department of Radiology Musculoskeletal Section. He has been busy studying for his Radiology Boards which he will take in September. After completion of his boards, Dr. Shah will decide on an initial research project. In addition to studying, Dr. Shah has been attending the weekly RSL meetings and the residents' AM and Noon conferences.

T32 Program Graduates

NCI Fellow	Completed	Current Position	Current Institution	Primary Mentor
John Strang, MD	1995	Assistant Professor	University of Rochester, Rochester, NY	Herfkens
Ian Chen, MD	1996	Radiologist	Southwest Washington Medical Center, Vancouver, WA	Li
Susan Lemieux, PhD	1996	Assistant Professor	Diagnostic Imaging Western Virginia Univ., Morgantown, WV	Glover
Bruce Daniel, MD	1997	Associate Professor	Radiology, Stanford University, Stanford, CA	Herfkens
Garry Gold, MD	1997	Associate Professor	Radiology, Stanford University, Stanford, CA	Macovski
Yi-Fen Yen, PhD	1997	Research Scientist	GE Advanced Health Care	Glover
Esther Yuh, PhD	1998	Clinical Fellow	Radiology (Neuroradiology), UCSF, CA	Li & Napel
Roger Shifrin, MD	1998	Assistant Professor	University of Florida, FL	Pelc & Herfkens
Steven Heiss, MD	1999	Radiologist	Radiology Imaging Associates, Denver, CO	Li
Martin Blum, MD	2000	Researcher	PET/Nuclear Medicine, Palo Alto VA, CA	Jeffrey
Curtis Coulam, MD	2001	Radiologist	Gem State Radiology Group, Boise, ID	Sommer
Lawrence Chow, MD	2002	Assistant Professor	University of Oregon, Eugene, OR	Sommer
Samira Guccione, PhD	2002	Assistant Professor	Radiology, Stanford University, Stanford, CA	Bednarski
Yishan Yang, PhD	2002	Research Associate	Radiology, Stanford University, Stanford, CA	Bednarski
Charles Liu, MD	2003	Radiologist	La Jolla Radiology, La Jolla, CA	Herfkens & Sommer
Karl Vigen, PhD	2003	Research Scientist	University of Wisconsin-Madison, Madison, WI	Butts Pauly
Susan Hobbs, MD, PhD	2003	Radiologist	CT Section Chief, Kaiser Permanente, Walnut Creek, CA	Bednarski
John Levin, MD	2004	Radiologist	St. Luke's Medical Center & Clinic, Minneapolis, MN	Herfkens & Sommer
Laura Pisani, PhD	2004	Postdoctoral Fellow	Radiology, Stanford University, Stanford, CA	Glover
Daniel Margolis, MD	2005	Assistant Professor	Dept. of Radiology, UCLA, Los Angeles, CA	Jeffrey
Daniel Ennis, PhD	2006	Postdoctoral Fellow	University of Washington, Seattle, WA	Pelc
Anthony Faranesh, PhD	2007	Research Scientist	NIH, Washington, DC	Pelc & Hargreaves
Lewis Shin, MD	2007	Assistant Professor	Radiology, Stanford University, Stanford, CA	Herfkens
Michael McDonald, PhD	2007	Research Scientist	NIH, Washington, DC	Guccione
Byard Edwards, MD, PhD	2008	Scientific Researcher	Vanderbilt University	Jeffrey
Cristina Zavaleta, PhD	2008	Scientific Researcher	MIPS, Radiology, Stanford University, Stanford, CA	Gambhir
Jinha Park, MD, PhD	2008	Assistant Professor	University of Southern California, Los Angeles, CA	Gambhir
Stephanie Bailey, PhD	2009	Scientific Researcher	Comprehensive SDSU/UCSD Cancer Center	Plevritis
Moses Darpolor, PhD	2010	Postdoctoral Fellow	Radiation Oncology, Stanford University, Stanford, CA	Spielman
Rachel Bitton, PhD	2010	Postdoctoral Fellow	RSL, Stanford University, Stanford, CA	Butts-Pauly
Grace Tye, MD	2011	Radiologist	Alvarado Breast Center, La Jolla, CA	Jeffrey, Napel

NIH/NCI R25 CA 118681

Stanford Molecular Imaging Scholars - SMIS R25

PI: Sanjiv Sam Gambhir, MD, PhD
Program Manager: Sofia Gonzales, MS

The Stanford Molecular Imaging Scholars (SMIS) program is a cross-disciplinary post-doctoral training program at Stanford University that brings together 45 faculty mentors from 15 departments in the Schools of Medicine, Engineering, and Humanities and Sciences. Faculty mentors provide a diverse training environment spanning biology, physics, mathematics/biocomputation/biomedical informatics, engineering, chemistry, biochemistry, cancer biology, immunology, and medical sciences. The centerpiece of the SMIS program is the opportunity for trainees (PhD or MD with an emphasis on PhD) to conduct innovative molecular imaging research that is co-mentored by faculty in complementary disciplines. SMIS trainees also engage in specialized coursework, seminars, national conferences, clinical rounds, ethics training, and the responsible conduct of research. The three-year program culminates with the preparation and review of a mock grant in support of trainee transition to an independent career in cancer molecular imaging with the ultimate goal of training them to become leaders in the field. Thus far, 16 trainees have entered the SMIS program and 8 have completed the program.

We have just received notification that our program, submitted for a competing renewal in 2010, will be funded for an additional five years (to 2016).

SMIS R25 Program Graduates

SMIS Fellow	Completed	Current Position	Institution	Primary Mentor
Ted Chu, PhD	2008	Research Scientist	Regeneron	Kuo
Jill Lin, PhD	2009	Consultant	Beghou Consulting,	Paik
Keith Hartman, PhD	2009	Senior Analyst	Boston Consulting Group	Gambhir
Bryan Smith, PhD	2010	Postdoctoral Scholar	Stanford University (MIPS)	Gambhir
Henry Haeberle, PhD	2010	Senior Scientific Officer	University of New South Wales, Australia	Contag
Hua Fan-Minogue, MD, PhD	2010	Graduate Student, BMI Program	Stanford University	Gambhir
Jennifer Prescher, PhD	2010	Assistant Professor of Chemistry	University of California, Irvine	Contag
Richard Kimura, PhD	2010	Senior Research Scientist	Canary Center at Stanford for Cancer Early Detection	Cochran

Current SMIS R25 Trainee Research Interests

Rehan Ali, PhD, joined the SMIS program in 2010 under the joint supervision of Drs. Edward Graves and Ramasamy Paulmurugan, after completing his PhD in biomedical image analysis at the University of Oxford. His research focus is the development of non-invasive in vivo techniques for detecting and predicting tumor resistance to radiation therapy, using a combination of experimental and modeling techniques.

Prachi Pandit, PhD, began her SMIS fellowship in 2010 after completing her PhD in Biomedical Engineering at Duke University. Her primary mentor in the program is Dr. Brian Rutt. Prachi, in collaboration with Dr. Jianghong Rao's group, is working on developing magnetic resonance imaging based molecular imaging systems to image cancer-specific enzymatic activity of protease in vivo. This work focuses on "smart" Gd-based probes, which upon encountering a specific molecular target aggregate to form nanoparticles, thereby increasing the detection sensitivity of the system.

Nicholas Conley, PhD, joined the SMIS program in 2009 after completing his PhD in Chemistry at Stanford. He is working with Drs. Matthew Scott and Jennifer Cochran on projects related to the Hedgehog signaling pathway. Hedgehog (Hh) signaling is responsible for controlling cell fates in most developing tissues and organs, as well as during many regeneration events. Unregulated activation of the Hh signaling pathway leads to birth defects and cancer.

Eric Gonzalez, PhD, began his SMIS fellowship in 2009 after completing a PhD in Physics at Texas Christian University in Fort Worth, Texas. His research interests include the development of algorithms for Positron Emission Tomography (PET). He works with Dr. Craig Levin as his primary mentor to develop a methodology of detecting and processing multiple-photon events that are typically discarded in standard PET imaging.

Jesse Jokerst, PhD, joined the SMIS program in 2009 after completing his PhD in chemistry at University of Texas, Austin. With a background in graduate school that emphasized Raman fluorescent nanoparticles for biomarker measurement in vitro, Dr. Jokerst has found the SMIS program an opportunity to expand his experience in nanotechnology a perfect fit. His primary mentor in the program is Dr. Sam Gambhir.

Benjamin Cosgrove, PhD, joined the SMIS program in 2008 after completing a PhD in bioengineering at MIT. He is working with Dr. Helen Blau to develop molecular imaging approaches, primarily using bioluminescence imaging, to evaluate muscle stem cell behaviors following transplantation. He is testing muscle stem cell therapies by ex vivo perturbation of signaling pathways dysregulated in muscle diseases and validation by transplantation of treated stem-cell populations.

Sharon Hori, PhD, joined the SMIS program 2008. She is integrating mathematical modeling and in vivo experimental techniques to identify ways of accelerating early cancer detection, based on the use of cancer blood biomarker assays to predict tumor volume. Dr. Hori has developed a novel mathematical model relating cancer biomarker secretion kinetics and tumor growth, which is currently being used to identify key factors and processes involved in cancer biomarker secretion and detectability. To test these mathematical predictions, she is also establishing a novel mouse model which links blood biomarker detection and in vivo tumor imaging. She is working with Drs. Sam Gambhir and Ramasamy Paulmurugan.

Marybeth Psyz, PhD, joined Dr. Juergen Willmann's lab in October 2008. She is interested in multi-modality imaging of pancreatic cancer and identifying new molecular targets for early detection using molecular ultrasound and/or PET-CT imaging. She also investigates other methods for sensitive quantitation of vascular map profiles of microbubble contrast agent signals with real-time ultrasound imaging in mice using a clinical ultrasound scanner and a high-resolution ultrasound scanner for small animals. Mentors for Dr. Psyz include Drs. Juergen Willmann and Sam Gambhir.

NIH/NCI P50 CA 114747

In Vivo Cellular and Molecular Imaging Center at Stanford - ICMIC P50

PI: Sanjiv Sam Gambhir, MD, PhD
Program Manager: Billie Robles, BS

Current ICMIC P50 Postdoctoral Trainee Research Interests

Dominique van de Sompel, PhD, joined the ICMIC program in 2010. Dr. Van de Sompel completed his PhD training at the University of Oxford in Medical Image Processing prior to coming to Stanford and joining Dr. Sam Gambhir's research lab in multimodality molecular imaging. Dr. Van de Sompel is particularly interested in algorithm development for quantitative in vivo cancer imaging, and would like to learn more about the underlying molecular biology that prompts the need for research in the first place. His current work is focused on Raman spectroscopy and photoacoustic tomography.

Thillai Sekar Veerapazham, PhD, also joined the ICMIC program in 2010. His interests in nanoscale synthesis and assembly for biomedical applications make him a good fit for the labs of Dr. Jianghong Rao and Dr. Heike Daldrup-Link. Dr. Veerapazham will acquire hands-on experience with cell cultures, collecting image data, small animal handling, as well as strengthening his organic and nanoparticle synthetic skills, as well as gaining experience with clinical work. His clinical interests focus on applying his basic science knowledge and experience in areas of breast cancer research.

Yang Liu, PhD, very recently joined the ICMIC program as a postdoctoral trainee in Dr. Zhen Cheng's lab, the Cancer Molecular Imaging Chemistry Laboratory (CMICL). Dr. Yang received his PhD at the Zhejiang University in Hangzhou, China (2009), where he focused on fluorescent probe development as a graduate student and a postdoctoral fellow. Dr. Yang will continue to explore his interests and apply his expertise in probe development as a postdoctoral trainee in the ICMIC program. His interests in novel probe development for non-invasive detection of cancer are a perfect fit for the ICMIC and the Cheng lab.

ICMIC P50 GRADUATES (NCI P50CA114747)

The following table lists all graduates from our NIH/NCI funded ICMIC program (P50CA114747):

ICMIC Fellow	Completed	Current Position	Institution	Primary Mentor
Sheen-Woo Lee, MD	2005	Assistant Professor	Gachon University Medical School, Inchon, Korea	Biswal
Gayatri Gowrishankar, PhD	2006	Research Scientist	Stanford University	Rao
Ehran Yenilmez, PhD	2007	Research Scientist	Nanomix, Inc.	Melosh
Meike Schipper,MD	2007	Chief Resident, Nuclear Medicine	Stanford University	Gambhir
Weibo Cai, PhD	2007	Assistant Professor	Univ of Wisconsin, Madison, WI.	Chen
Arne Vandenbroucke, PhD	2008	Research Scientist	Cenix BioScience	Levin
Frank Cochran, PhD	2008	Postdoctoral Fellow	Bioengineering, Stanford Univ	Cochran
Michael Helms, PhD	2008	Research Scientist	Cenix BioScience	Contag
Phuoc Tran, MD, PhD	2008	Assistant Professor	Johns Hopkins	Felsher
Zibo Li, PhD	2008	Assistant Professor	Univ of Southern California	Chen
Gang Ren, PhD	2009	Research Scientist	Stanford University	Cheng
Michael Benoit, PhD	2009	Research Scientist	Stanford University	Matin
Priti Balchandani, PhD	2009	Post-doctoral fellow	Stanford University	Spielman
Zheng Miao, PhD	2009	Research Scientist	Stanford University	Cheng
John Ronald, PhD	2010	Postdoctoral Fellow	Stanford University	Gambhir/Rutt
Pascale Kallasi, PhD	2011	Postdoctoral Fellow	Stanford University	Harris

Current ICMIC Fellow				
Dominique van de Sompel, PhD	2011	Postdoctoral Fellow	Stanford University	Gambhir
Yang Liu, PhD	2011	Postdoctoral Fellow	Stanford University	Cheng
Thillai SekarVeerapazham, PhD	2011	Postdoctoral Fellow	Stanford University	Ramasamy

Introducing a new Training Program: NIH NIBIB T32 EB009653-01

Predoctoral Training in Biomedical Imaging at Stanford – T32

PI: Norbert Pelc, ScD
Program Manager: Teresa Newton, BA

This new multidisciplinary pre-doctoral training program at Stanford University in biomedical imaging technology is approaching the end of year 1 during which time we have successfully recruited two trainees as proposed. Our mission is to train the next generation of researchers in and inventors of biomedical imaging technology. Imaging technology continues to evolve at a rapid pace generating new techniques in research today that will become the standard of care for tomorrow. There is a high need for trained researchers in this field to fill positions in academia, industry, and government. Stanford University has a unique multidisciplinary research effort in biomedical imaging, spanning magnetic resonance, computed tomography and radiography, radionuclide and optical methods for molecular imaging, ultrasound, and hybrid imaging such as Xray/ MR and PET/MR, as well as image processing and analysis for diagnosis, radiation therapy, and science.

Our program attracts students from six different degree granting programs to train in biomedical imaging technology with faculty from 8 different departments and Interdepartmental Programs. In keeping with the program goals to recruit two trainees during our first, planning and recruiting year, we are pleased to introduce two outstanding trainees who have joined our program. Michael Marx is an Electrical Engineering graduate student at Stanford and completed his undergraduate training in electrical and mechanical engineering at Penn State University. Juan Plata is a Bioengineering student who completed his undergraduate training at University of Nevada, Las Vegas, Nevada. We are pleased to welcome these two outstanding students to our training program.

Lucas Center MR Systems Training and Support

1.5T, 3T1, 3T2, and 7T Whole Body Magnets

Anne Marie Sawyer, BS, RT (R)(MR), FSMRT

MRI Safety Training and System Operation Instruction 2010 - 2011

MRI safety training and system instruction have been provided to 285 new researchers including scientists and clinicians conducting experimental MRI studies at the Lucas Center over the last twelve months (Figure 1). Initial MRI safety training and the annual refresher course are required for all researchers assisting or conducting studies on any of the MRI systems at the Lucas Center. The annual MRI safety refresher course is required as an on-line tutorial and will provide renewal instruction to 296 researchers (Figure 2). This ensures that all users and assistants are qualified to operate the MRI systems and satisfies Lucas Center and University requirements for safety. MRI system and safety support is provided to the researchers 7 days a week, 24 hours a day to ensure that research endeavors are successful, generate valuable data, and, above all, are safe for the researchers, the human subjects and the MRI systems and components. MRI safety is an on-going concern as the MRI environment can be a potentially lethal setting without continuing education and persevering support.

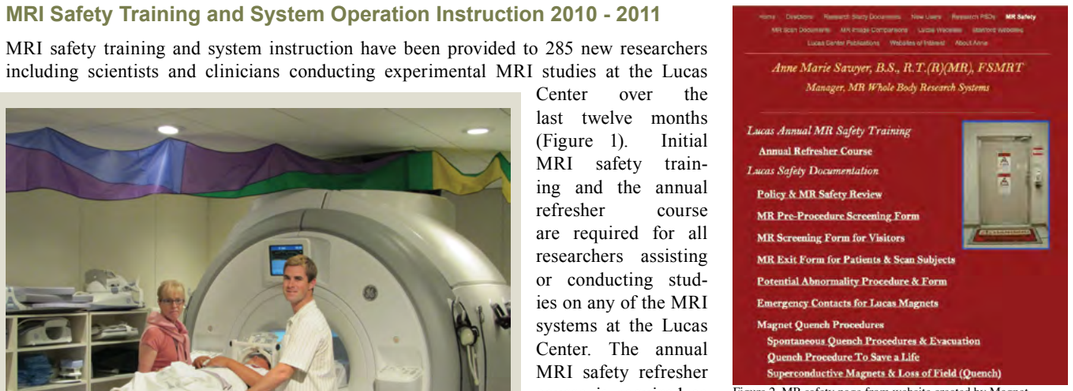

Figure 2. MR safety page from website created by Magnet Manager, Annemarie Sawyer, which includes the annual required safety and policy online training.

Figure 1. Magnet Manager Annemarie Sawyer assists researcher Ryan Kelley from Department of Psychiatry (Allan Reiss, M.D.), Stanford University School of Medicine, with scan subject preparation.

The research environment generates many new yet prototype designs in RF imaging coils, imaging accessories, monitoring and response devices such as button boxes, eye trackers, and electroencephalogram (EEG) recorders (Figure 3), and sensory devices. Evaluation of these new devices is on-going to ensure that neither the image data, the safety of the human subject, nor the integrity of the MRI systems are compromised by the presence of these devices in the magnet room, in the bore of the magnet, or in the presence of an RF coil.

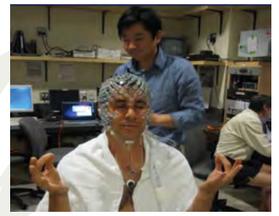
Figure 3. A scan subject is being prepared for a functional MRI scan (fMRI) that includes the MR safe EEG (electroencephalography) system (www.egi.com). Functional MRI is a type of specialized MRI scan used to measure the hemodynamic response (change in blood flow) related to neural activity in the brain or spinal cord. EEG is the recording of electrical activity along the scalp. EEG measures voltage fluctuations resulting from ionic current flows within the neurons of the brain.

Groups

40
35
30
25
20
15
10
5

Research Group Updates

1989 2011

89 90 91 92 93 94 95 96 97 98 99 00 01 02 03 04 05 06 07 08 09 10 11

Inverse Geometry CT and Conventional CT

Norbert Pelc, ScD

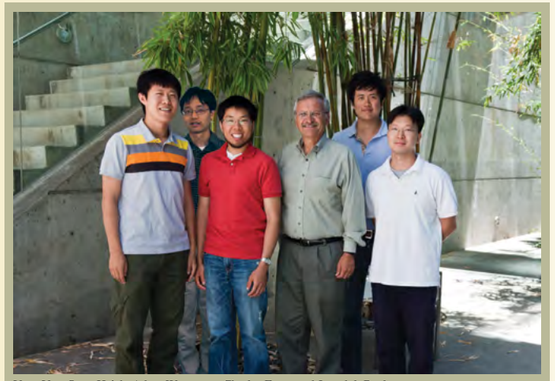

Yuan Yao, Scott Hsieh, Adam Wang, me, Charles Feng, and Jongduk Baek

Our research is directed toward the development of technology and applications of computed tomography (CT). The long-term aim of this work is to push the limits of CT performance, to improve dose efficiency, and to aid in the development of new applications. Intrinsic in these goals is the need to understand the basic limitations in current systems and, when physically possible, to develop solutions to effectively address them.

For many years, we have been working on a project to develop a system that can image an arbitrarily thick section of anatomy (e.g. an entire organ) in a single fast rotation while producing uncompromised image quality and outstanding dose efficiency using an inverted geometry (therefore the term Inverse Geometry CT). In collaboration with GE Global Research, we completed assembly of the first-ever gantry mounted IGCT system and Jongduk Baek reconstructed initial images using an array of 8 sources. The initial images are excellent. We are now completing expansion of the source to 32 elements and expect to test this system in the coming months. One of the limitations of the current system is mechanical complexity. To address this Scott Hsieh is working on concepts for stationary source array systems.

Uncompromised image quality and Dose efficiency

We are also working on a number of problems relevant to all CT configurations. Charles Feng is extending the previous work of Adam Wang, developing an interactive tool for synthetic CT that will allow radiologists to optimize clinical protocols and also allow the creation of realistic images expected from systems that don't yet exist (Feng abstract). One of the challenges of volumetric CT systems is how to measure the spatial resolution (Modulation Transfer Function). Jongduk Baek found that the method described in the literature can be misleading and developed a new technique (Baek abstract). Dual energy CT imaging offers important tissue information by measuring x-ray transmission with two x-ray spectra. One system achieves this by rapidly modulating the x-ray tube voltage. We know that, in the ideal world, each of the resulting spectra would be modified by an optimized filter. However, it is not possible currently to have mechanical filters that switch as fast as the tube voltage. Yuan Yao studied the possibility of using a single fixed filter in these rapid kVp-switching systems. We found that gadolinium can lead to noise performance comparable to that of the commercial systems with significant reductions in dose. One technology with significant potential to improve CT performance is photon-counting detectors. Instead of the currently used technology which measures the total energy of all the x-ray photons that strike the detector in a particular small time period, photon counting detectors sense and process individual photons. However, their response is imperfect and it is important to understand the level of performance that is needed. Adam Wang studied the impact of different types of performance limitations of these detectors and showed that further improvements are needed before system benefits would be obtained (Wang abstract). One particular challenge for photon counting detectors is handling high count rates. When the intensity is too high the detectors miscount photons and make errors in measuring their energy. Scott Hsieh developed an idea for a dynamic bowtie filter that can, among other things, protect the detector from seeing exceedingly high intensities. The dynamic bowtie can lead to performance improvement additional to those through photon counting detectors (Hsieh abstract).

Sam Mazin, a postdoctoral fellow, left this year to pursue his entrepreneurial dream. We wish him well.

X-Ray Guidance of Interventional Procedures

Rebecca Fahrig, PhD

Top row - Geoff Nelson, Erin Girard, Mi Hye Shin, Jared Starman, Andreas Keil; Middle row - Jang Hwan Choi and son, Dragos Constantin, Rebecca Fahrig, Andreas Maier, Prasheel Lillaney; Bottom row - Arun Ganguly, Marlys Lesene, Waldo Hinshaw

Our group conducts research with the broad goal of improving the x-ray guidance of minimally invasive procedures, including guidance of radiation therapy. The Axiom Lab houses a clinical C-arm fluoroscopy system, which can also be used for high-resolution, high-contrast CT imaging. This lab is scheduled to be renovated including an upgrade to the new, state-of-the-art, robotic system (Siemens zeego®), which was purchased with American Recovery and Reinvestment Act (ARRA) funding through an NIH Shared Instrumentation Program. The renovation installation is scheduled to begin in the fall of 2012. The current C-arm CT system (Siemens Artis dTA) has been used for a number of in vivo investigations. The Advanced X-Ray Imaging Lab is used for hardware and software development (table-top digital x-ray imaging, cone beam CT, new detector development and X-ray/MR system development).

High resolution, High contrast, No artifacts

Software investigations have the primary goal of improving the image quality of C-arm CT reconstructions. Our flexible, open-source JAVA-based framework for C-arm CT reconstruction, including CUDA-accelerated forward and back-projection, has been used to simulate patient motion while acquiring images in a weight-bearing geometry (abstract by Choi, collaboration with University of Erlangen-Nurnberg and Dept. of Mechanical Engineering at Stanford). The weight-bearing imaging project recently received seed funding from the Center for Biomedical Imaging at Stanford (CBIS).

Clinical imaging protocols developed in the Axiom lab include a new investigation into early biomarkers of pancreatitis (abstract by K. Blum), liver blood volume and liver perfusion imaging (abstract by Ganguly, collaboration with University of Erlangen-Nurnberg) and imaging of fresh and chronic myocardial infarct using ECG-gated C-arm CT (abstract by Girard, NIH ARRA R01 Cardiac C-arm CT). All three projects were also in collaboration with Siemens AX.

In hardware developments, design and optimization of an MR-compatible rotating anode x-ray tube continues (abstracts by Lillaney and Shin, NIH R01 X-ray Tube and ARRA supplement), as do our simulations of new designs for an MR-compatible linear accelerator (abstract by Constantin, NIH NCI fellow). The Stanford-Varian collaboration (NIH NCI R01 kV-MV Imaging) continues, with work on detector crystal design optimization using Monte Carlo simulation (abstract by Constantin) and on combined kV and MV reconstruction algorithms (abstract by Keil). This project has the overall goal of removing artifacts due to high-density materials such as fillings and hip implants in radiation therapy treatment planning.

Research

Laboratory of Imaging Informatics (LII)

Daniel L. Rubin, MD

top row from left: Francisco Gimenez, Hakan Bulu, Lior Weizman, Rohan Bansal, bottom row from left: Hayit Greenspan, Alan Snyder, Jiajing Xu, Daniel Rubin, Vanessa Sochat, Pooja Naik. Missing: Jessica Faruque, Debra Willrett, Tiffany Ting Liu, Mustafa Safdari, Raghav Pasari, Kelly Englese

Our research group uses computational methods to leverage detailed information about disease that is depicted in images ("imaging phenotypes") to enable biomedical discovery and to guide physicians in providing personalized care. Our work spans a broad gamut, from basic science discovery (using image phenotypes to define molecular characteristics of diseases) to clinical practice through translational research (decision support, disease profiling, treatment response assessment, and personalized treatment selection).

Basic science activities: Just as biology has been revolutionized by online genetic data, our goal is to advance radiology by developing computational methods to extract quantitative and semantic content from images ("image biomarkers") and to use them in conjunction with clinical, pathology, and molecular data to discover image-based predictors of disease and treatment response. Our ultimate goal is to "profile" patients based on image-based characteristics to enable personalized care and to detect whether disease is responding to treatment earlier than currently possible. Our laboratory is one of the sites in the National Cancer Institute's Quantitative Imaging Network (QIN), a national research consortium which is advancing the science of quantitative methods of imaging to understand cancer and improve its treatment. We are developing a national informatics infrastructure to define a new paradigm for acquiring, mining, and using a broad range of quantitative imaging data in cancer research, and to provide decision support to physicians based on quantitative imaging assessments of patients with cancer. We are also developing innovative imaging informatics methods to enable this work, including (1) tools to efficiently and thoroughly capture the semantic terms radiologists use to describe lesions; (2) standardized terminologies and ontologies to enable radiologists to describe lesions comprehensively and consistently; (3) novel image processing methods to extract quantitative features from images that are informative of the underlying biology of lesions; and (4) a large database of annotated quantitative imaging cancer studies as a resource for discovering new biomarkers that will improve the sensitivity of detecting cancer treatment response.

Personalized medicine through Computational methods

Translational and clinical activities: We are developing and translating our biomedical informatics methods into clinical workflow to improve radiology practice. Projects include (1) content-based image retrieval to improve radiologist diagnostic accuracy; (2) automated segmentation of lesions in serial imaging studies, enabling physicians to objectively and reproducibly assess lesions in images and to monitor the response to treatment; (3) quantitative image analysis of retinal images to detect and monitor progression of eye diseases, (4) natural language techniques to enable uniform indexing, searching, and retrieval of radiology information resources such as radiology reports; and (5) decision support applications integrated into the reporting workflow to improve diagnosis and reporting clarity and completeness.

We collaborate with a variety of investigators at Stanford, in Radiology, Oncology, and Ophthalmology, as well as with investigators outside Stanford. We also participate in a national working group that is developing imaging informatics infrastructure for the cancer Biomedical Informatics Grid program at NCI. Our ultimate goal is to bring cutting-edge radiological knowledge into practice and to guide care of individual patients based on the most robust evidence acquired from imaging.

Cancer Systems Laboratory (CSL)

Sylvia K. Plevritis, PhD

Front row, left to right: Cathy Shachaf, (Saadet) Ayca Erdogan, Anita Samantaray, Maggie Bos Sylvia Plevritis, Andrew Gentles, Yihan Guan, Allison Kurian, Back row: Wenshuai Wan, Aravindakshan Babu, Olivier Gevaert, Ramesh Nair, Diego Muñoz, Missing: Emily Tsai, Peng Qiu

Cancer Systems Laboratory (CSL) views cancer as a complex system whose components can be reverse-engineered for the purposes of understanding the underlying mechanisms of cancer progression and identifying approaches for more effective cancer control strategies. Currently, our laboratory infers complex features of cancer progression through a variety of approaches that include: (1) reconstructing molecular networks of cancer, (2) integrating a diversity of molecular, pathological, imaging and clinical cancer data, and (3) mathematically modeling the progression of primary disease to metastatic stages in patients. Ultimately, our goal is to develop a comprehensive, multiscale view of cancer progression that merges these various approaches.

(1) Reconstructing molecular networks: We apply a wide range of computational and statistical techniques to infer molecular networks underlying cancer using genomic, transcriptomic and proteomic data. These networks often represent interactions between genes or sets of genes, mediated by a diversity of molecular regulators. We use these networks to generate new hypotheses about cancer initiation and progression. Recently, we have been funded by the NCI Integrative Cancer Biology Program as a national Center for Cancer Systems Biology to promote this research with a grant entitled "Modeling the Role of Differentiation in Cancer Progression," which focus on hematologic malignancies with a multi-disciplinary team across the Stanford campus. We have established a "wet-lab" in LUCAS P169 to experimentally validate our computationally-derived findings. With this new experimental laboratory, we are now expanding our molecular-network-based research to the analysis of solid tumors, specifically the microenvironment of breast cancer.

Molecular networks, Data integration, Mathematical modeling

(2) Integrating a diversity of molecular, imaging and clinical data: We have embarked on numerous projects that involve the integration of multi-platform cancer datasets through probabilistic modeling. In a recent collaborative effort through ISIS, with investigators from the Stanford Departments of Radiology and Surgery, we are creating an association map between CT and PET image features and gene expression microarrays of human non-small cell lung carcinoma. This map provides a molecular characterization of imaging features of lung cancer. It also enables us to identify prognostic significance image biomarkers by leveraging on a vast amount of clinically annotated, publically available lung cancer gene expression microarray. This effort is being supported by pilot funds from GE Medical Systems.

(3) Mathematically modeling clinical cancer progression and cancer control health policies: We develop multi-scale models of the natural history of cancer that describe the stochastic behavior of tumor growth and metastatic spread. We have used these models to address important health policy questions related to early detection, such as: how do screening mammography and MRI impact breast cancer mortality; and how would CT screening for lung cancer impact lung cancer mortality rates? This effort has been funded for over 10 years and has been renewed for an additional 5 years of funding through the NCI Cancer Intervention and Surveillance Network (CISNET).

In summary, CSL brings together computational and biomathematical modelers, engineers, biological experimentalists and clinical researchers to ensure the biological and clinical relevance and translation of our work.

Research

Research Group Updates

Image Analysis, Bioinformatics, and Computational Modeling

Imaging Bioinformatics Laboratory

David Paik, PhD

Our group is primarily interested in how biological information is extracted and quantified from both anatomic and molecular imaging, how it is represented, how it is modeled and how it is disseminated with an outlook toward combining imaging-derived information with other sources of biological and clinical information. We are particularly interested in applying computational techniques toward a better understanding of cancer. While most computational models and analyses focus on a single source or modality of data, it is becoming increasingly clear that models must integrate across a wide variety of data types as well as spatial and temporal scales. Our focus is on developing these types of models.

Front row (left to right): Danielle Rasooly, Tiffany Liu, Chinyere Nwabugwu, Frezghi Habte. Back row (left to right): David Paik, Kranthi Hode, Rahul Agrawal.

In the area of molecular imaging, we are working on a variety of projects to improve and standardize the quantitation derived from molecular imaging. While this type of imaging is producing breakthrough biological results, better quantitation and mathematical models will lead to a more detailed understanding of specific biological mechanisms. Examples include statistical analysis of ROI methods, knowledge representations of quantitative imaging, and improving software for quantitative imaging. In the area of nanomedicine, we are working on computational methods for representing the structure of nanoparticles in order to enable structure-based queries of online nanomedicine resources and algorithms for hyperspectral unmixing. And finally, in the area of clinical imaging, we are working on methods to better understand the perceptual factors that influence diagnostic accuracy.

Our long-term goal is to enable and simplify the problem of information extraction and information flow from medical/molecular imaging to be on par with that of genomic and proteomic profiling technologies so that these very different types of information may be treated as siblings computationally. Our philosophy is that for an integrative approach to imaging and non-imaging information to come to fruition, a major pre-requisite is to be able to maximally extract and represent information from imaging, with an emphasis on the specificity of molecular imaging.

Radiology 3D Visualization and Analysis Laboratory

Sandy Napel, PhD

Our group addresses the field of medical image analysis, focusing on volumetric visualization, structure segmentation, quantitative analysis, computer-aided detection of lesions, and the capture and use of imaging phenotype and integration with other clinical data, including those from high throughput technologies such as gene arrays, for knowledge discovery and decision support.

L-R: Sandy Napel, Hayit Greenspan, Alan Snynder, Jiajing Xu, Francisco Gimenex (sitting in front of Jiajing), Jessica Faruque, Inseong Kim

Advances here have impact in many technical and clinical areas. Examples are: automated visualization and quantitation of vascular image data, virtual colonoscopy, intra-procedural registration of 2D fluoroscopic images of instruments with 3D volume data, automated computation of peak flow velocity using a novel ultrasound transducer for reproducible determinations of carotid stenosis, automatic generation of curved-planar images through blood vessels, determination of likely neuronal connections of the visual tracts in the brain. More recent work includes visualization of dual energy CT data from the head and neck, and cardiac CT segmentation and visualization. Our group is highly collaborative, working with many radiology department investigators (including Chris Beaulieu, Dominik Fleischmann, Rusty Hoffmann, Brooke Jeffrey Jr., Nishita Kothary, David Paik, Sylvia K. Plevritis, and Daniel L. Rubin) as well as many other Stanford (e.g., Pierre Khuri-Yakub, electrical engineering) and non-Stanford (Justus Roos: University Hospital Zurich, Geoffrey D. Rubin: Duke University) faculty. This year we have focused on automated feature extraction from liver and lung CT images, efficient methods for the creation of a visual similarity standard for content-based image retrieval and decision support, correlation of image features to molecular profiles of excised tissue in lung cancer, evaluation of CAD of lung nodule data, evaluation methods for CAD in the absence of ground truth, and gaze tracking for improving interpretations. We are also starting new projects aimed at prediction of survival and response to therapy in liver and lung cancer as a function of imaging features. Based on our work this past year, 7 new manuscripts have been accepted for publication, 8 presentations were given at international meetings, and 4 grant proposals, all related to our ISIS initiative, were submitted to the NIH.

Research Group Updates

Magnetic Resonance Research

Interventional and Open MRI

Kim Butts Pauly, PhD

Ultrasound energy can be focused to a point deep within the body without damage to overlying tissues. MRI provides a means to target the treatment, monitor the temperature during treatment, and evaluate the tissue after the treatment. This year, led by collaborators Peji Ghanouni and David Hovsepian, we joined a multicenter trial in the palliation of painful bone metastases with MR-guided focused ultrasound. In addition, we continue our development of advanced guidance techniques for focused ultrasound treatment of diseases in the liver, bone, prostate, breast, heart, and brain.

Pejman Ghanouni, Andrew Holbrook, Urvi Vyas, Viola Rieke, Patrick Ye, Rachelle Bitton (in front of Patrick), Ronnie Instrella, Ron Watkins, Randy King, Juan Plata, Elena Kaye, Hyo-Seon Yoon (in front of Elena), Mike Marx, and Kim Butts Pauly

In the liver application, we demonstrated real-time steering of the ultrasound beam under MR-guidance to targets in the liver during free breathing. We also demonstrated that acoustic radiation force MR imaging can provide a picture of the focus for focal spot calibration in a fraction of the energy that a low temperature test spot would require. Our collaborative project with Graham Sommer and Chris Diederich on MR-guided high intensity ultrasound ablation in the prostate with transurethral ultrasound applicators tested our methods for feedback and control of the treatment. In addition, we are developing a real-time integrated thermometry/diffusion acquisition for monitoring thermal ablation in the prostate. In our cardiac project, in collaboration with Mike McConnell, our hybrid multibaseline-referenceless cardiac thermometry method has been implemented with real-time spiral imaging. In collaboration with Bruce Daniel, we investigated the visibility and palpability of focused ultrasound lesions in breast tissue.

In the brain, we extended the hybrid multibaseline-referenceless processing to MR thermometry and demonstrated a significant reduction in temperature errors. We demonstrated methods for MR-guided focusing in the presence of phase aberrations based on acoustic radiation force imaging. In collaboration with Bill Newsome in Neurobiology, we have been investigating neuromodulation with focused ultrasound. See these abstracts on pages 88-91.

Functional MR Imaging

Gary Glover, PhD

The functional MRI group continues to develop and optimize methods for the acquisition of functional MR imaging data. Projects include the development of fMRI methods that reduce signal dropout and/or improve efficiency, real-time biofeedback for training brains and reduction of physiological noise in fMRI signals and investigation of brain network dynamics. In addition, we continue to play an active role in the NCRR-funded FIRST BIRN schizophrenia test bed project, with Gary Glover as the chair of the calibration working group.

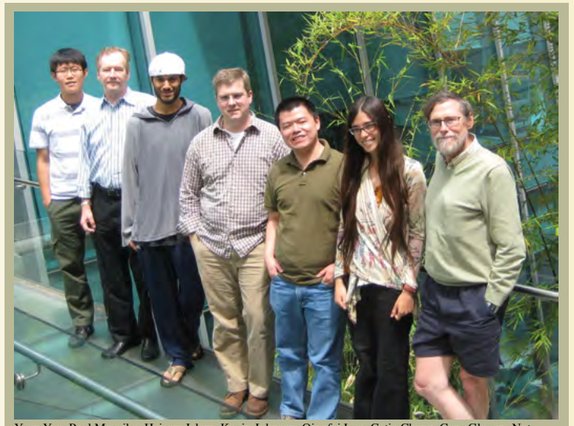

Yuan Yao, Paul Mazaika, Haisam Islam, Kevin Johnson, Qingfei Luo, Catie Chang, Gary Glover. Not shown: Fumiko Hoeft, Allyson Rosen, Elizabeth Stringer.

The following are only a few of the highlights of scientific progress; see abstracts for further details.

Grad student Catie Chang received her PhD in EE with her thesis focused on dynamic properties of intrinsic brain networks. During her defense presentation, it was noted that Catie has published an astonishing 18 papers during her 5 years, with ten authored by her. She was the first to discover that the brain's resting state networks are highly variable in their inter-region activity, and her publication on this work has been cited an exceptional 20 times in only the past year. This suggests high scientific acceptance of this exciting finding.

Postdoc Qingfei Luo has found that when a high-density (256 channels) EEG cap is used during concurrent EEG/fMRI experiments, the large mass of wires that exit the head coil under the subject's head cause a large amount of signal dropout. However, his measurements and theory demonstrate that, amazingly, this signal loss does not lead to loss of fMRI signal. This is very good news for the users of this technology in our group and the Lucas Center.

High Field MR

Brian Rutt, PhD

Michael Zeineh, Priti Balchandani, Jonathan Lu, Jason Su, Prachi Pandit, Manoj Sananathan, Mohammad Khaligi, Brian Rutt.

The long-term objective of the high field MR group is to develop a next-generation 7 Tesla whole-body magnetic resonance imaging (MRI) facility at Stanford to serve as a platform for cutting-edge imaging research and development, as well as for radiological and neuroscience research. The scientific scope of the projects that will use this new facility will span the range from fundamental biology to patient-based clinical imaging research. The group approach is interdisciplinary, bringing together researchers from the specialties of physics, engineering, bioengineering, biology, physiology, radiology, neurology, psychiatry, and psychology. The 7T MR facility will act as a catalyst and common platform for this broad group to create, refine, implement, validate and utilize the most advanced forms of magnetic resonance imaging. Major patient-based imaging research applications of the next-generation 7T MRI platform will include studies of brain development, psychopathology, drug dependence, alcohol-induced brain damage and its functional consequences, neurodegenerative processes, brain injury, musculoskeletal disorders, and therapeutic interventions associated with some or all of the above.

Major technology development directions that will be enabled by this next-generation 7T MRI platform include MR spectroscopic imaging (MRSI) of the proton (1H) nucleus as well as non-proton nuclei in both brain and musculoskeletal systems, advanced perfusion and diffusion tensor imaging in brain, and, importantly, parallel transmit technology for mitigating B1 inhomogeneities that limit the use of high magnetic field MRI in any organ system. The initial goals of the high field MR group are to develop software and hardware methods to allow 7T MRI to have a much greater impact on clinical research than possible before, as well as to extend the capabilities of high field MRI to unprecedented levels of spatial resolution, metabolite and iron sensitivity, and tissue characterization. Major users are expected to come from interdisciplinary laboratories directed by international leaders in imaging research. Projects and research foci have already been established in the following areas: high field and high sensitivity MRI methodology development, developmental disorders and clinical neuroscience, DTI methodology development, musculoskeletal and breast MRI methodology development, parallel transmit and RF pulse technology development, psychiatric disorders and neuroimaging, MR spectroscopic imaging methodology development, psychiatric disorders and clinical neuroscience, cognitive neuroscience and neurovascular imaging.

Translational Tumor and Stem Cell Imaging lab

Heike Daldrup-Link, MD

Upper row - left to right: Rosalinda Castaneda, John Martin, Olga Lenkov, SungMin Lee. Lower row - left to right: Heike Daldrup-Link, Rakhee Gawande, Celina Ansari, Nooshin Aflakian, Hossein Nejadnik, Aman Khurana, Qiaoyun Shi

Our team develops MR imaging techniques for cancer imaging and stem cell imaging, which can generate detailed information about specific cells in the body. The ultimate goal of our research is to detect specific cells in the tumor environment that are linked to poor prognosis, to monitor tumor cell-targeted therapies, and to monitor stem cell engraftment outcomes in vivo. We utilize iron oxide nanoparticles to specifically target tumor-associated macrophages (TAM), which are associated with tumor progression and an unfavorable prognosis. We investigate novel therapeutics that improve tumor delivery of diagnostic and therapeutic macromolecules and we are developing combined diagnostic and therapeutic ("theranostic") nanoparticle compounds in this context. We just started a first clinical trial to investigate the value of the nanoparticle-based contrast agent ferumoxytol for the detection and characterization of bone sarcomas in patients. We also utilize nanoparticle based MR contrast agents to investigate stem cell engraftment outcomes in vivo. We label stem cells with clinically applicable cell markers and investigate the imaging characteristics of successful versus unsuccessful stem cell transplants with MR imaging. We currently focus these investigations on in vivo monitoring of nanoparticle labeled stem cell transplants in osteochondral defects of knee joints for the purpose of cartilage regeneration. We recently added evaluations of novel, activatable, MR contrast agents for non-invasive diagnoses of stem cell death or successful differentiation outcomes in this context. More info can be found on our lab's website: http://daldrup-link-lab.stanford.edu/

Body MR Imaging

Brian A. Hargreaves, PhD

Back L to R: Catherine Moran, Brian Hargreaves, Brady Quist, Kyung Sung, Marcus Alley, Bragi Sveinsson, Haisam Islam, Manoj Saranathan, Anderson Nnewihe; Front L to R: Uche Monu, Kristin Granlund, Pauline Worters, Emily McWalter, Ernesto Staroswiecki, Caroline Jordan

The body MR imaging group focuses on applications of MRI including abdominal imaging, musculoskeletal imaging, breast imaging, and cardiovascular imaging. Our collaborators include numerous clinicians at Stanford Hospital as well as scientists at GE Healthcare and Electrical Engineering. More information is at http://bmr.group.stanford.edu.

Over the past year, Misung Han received her PhD, specializing in rapid MRI techniques for breast imaging. Manoj Saranathan and Pauline Worters presented extensive work in non-contrast vascular imaging techniques at the Magnetic Resonance Angiography Club annual meeting. Catherine (Kitty) Moran received funding as a NCI fellow in our Department. Caroline Jordan received an honorable mention for her efforts as a TA in BioEngineering 220, while Kyung Sung was a finalist in the ISMRM poster contest. Brian Hargreaves was invited to present our work on high resolution breast MRI at the NIH Edward Nagy New Investigator Symposium. Finally, our work on imaging near metallic artifacts won awards at the SCBT/MR and ISMRM this year.

New students Bragi Sveinsson, Uche Monu, and Brady Quist have joined our group and are working on 3D diffusion imaging and characterization of metallic implants. Our group continues to support clinical scanning in Breast MRI, vascular imaging and body imaging at Stanford Hospital and Lucille Packard Children's Hospital in collaboration with Bruce Daniel and Shreyas Vasanawala, while our MRI methods for imaging near implants are also being used routinely.

In Vivo Magnetic Resonance Spectroscopy and Multinuclear Imaging

Daniel Spielman, PhD

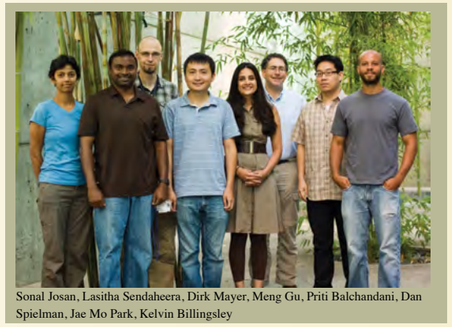

Sonal Josan, Lasitha Sendaheera, Dirk Mayer, Meng Gu, Priti Balchandani, Dan Spielman, Jae Mo Park, Kelvin Billingsley

Our multinuclear magnetic resonance spectroscopy (MRS) research investigations continue along three distinct directions. First, research on the technical development of ultrahigh field (7T) proton spectroscopy of the brain continues to focus on the design and evaluation of novel adiabatic RF excitation pulses for addressing the magnetic field inhomogeneities encountered at 7T and the development of new pulse sequences to exploit novel contrast mechanisms. Highlights of this work include an innovative adiabatic B1 shimming algorithm for multiple channel transmit, the design and evaluation of a self-refocused adiabatic pulse for 7T spin echo imaging, a new approach for designing adiabatic RF pulses using the Shinnar-Le Roux algorithm. In addition to multiple publications, two US patents, #7,821,263 and #7,966,053, resulted from this work. Furthermore, based on her high field imaging and spectroscopy research, Dr. Priti Balchandani was awarded an NIH K99/R00 grant entitled "High Resolution Magnetic Resonance Imaging and Spectroscopy of Epilepsy at 7T". Congratulations to Priti, and best of luck to her as she makes the transition from post-doctoral fellow to faculty! Second, under an ongoing program in the development of volumetric 1H MRSI at 1.5 T and 3.0 T, funded through an NIBIB Bioengineering Partnership grant (EB000822), we have begun a multi-site evaluation of a volumetric echo-planar 1H spectroscopic imaging sequence and associated automated data reconstruction software. Third, our efforts in the area of hyperpolarized 13C MRS and MRSI continues to move rapidly forward. Hyperpolarized 13C is a highly promising technology capable of directly probing key metabolic pathways by providing unprecedented increases in signal-to-noise ratio for these in vivo measurements. Over the past year we have successfully developed several novel MRSI protocols and associated metabolic modeling tools including the use of hyperpolarized [1-13C]-lactate to investigation cardiac metabolism, hyperpolarized 13C-labeled α-keto-isocaproate for the evaluation of prostate cancer, metabolic studies of a rat C6 glioma model, imaging of ethanol metabolism in the rat liver, and novel pulse sequences for optimum detection of in vivo pyruvate metabolism. We are currently applying these techniques to the study of multiple pathologies including liver metabolic disorders, brain tumors, prostate cancer, and alcoholism. This work is funded under NIH grants EB009070 "Dynamic Metabolic Imaging of Hyperpolarized Substrates", AA018681 "Metabolic Imaging of the Cardioprotective Effects of Alcohol and ALDH2 Activators", and RR09784 "Center for Advanced Magnetic Resonance Technology at Stanford", in addition to a new DOD award "In Vivo Imaging of Branched Chain Amino Acid Metabolism in Prostate Cancer".

Research Group Updates

Magnetic Resonance Research

Clinical Center for Advanced Neuroimaging (CFAN)

Greg Zaharchuk, PhD, MD
Michael Moseley, PhD

State-of-the-art advances in magnetic resonance imaging (MRI) continue to improve neuroimaging. With advanced neuroimaging MR methods, we now routinely map and measure brain tissue water diffusion rates and direction, the perfusion of blood, and the brain's ability to develop and maintain functional-structural integrity. To develop and apply our expertise in advanced imaging in a large number of diseases in patients, the Clinical Center For Advanced Neuro Imaging (CFAN) is built upon a large framework of funded NIH grants from the RSL, Lucas Center, and Stanford Stroke Center faculty dedicated to bringing the best MRI techniques into everyday clinical use.

First Row (Left to Right), Wesley Hun, Ryan Spilker, Greg Zaharchuk, Second Row: Tom Brosnan, Thomas Christen, Mike Moseley. Third Row: Jordan Michael Nechvatal, Deqiang Qiu Bottom Row: Georges Hankov, Shangpeng Feng, Caleb Folkes.

We continue to develop and advance imaging technologies in several key clinical areas including diffusion and perfusion techniques for the imaging of acute stroke and of white matter structure and integrity. The 7 tesla MRI scanner is now routinely used to improve higher-resolution tools at high-field and high-speed MRI, focusing on disease processes in stroke, brain tumors, and cerebrovascular diseases using diffusion MRI (DWI), tissue perfusion mapping (PWI), as well as the new field of mapping the brain connectivity, DTI, and susceptibility-weighted MRI (SWI). CFAN also develops and uses high-resolution diffusion tensors to explore and map hippocampus structure and function in active mental tasking to reveal new key findings in the developing and aging brain function, which can be used to separate short-term from long-term structural changes in the brain. The same high-resolution methods are also used in cholesteatomas, trigeminal nerve palsy, and to assess patients with demyelinating diseases such as MS.

State-of-the-art MR imaging sequences pioneered at the Lucas Center, in particular for stroke imaging, are now used worldwide and provides unlimited opportunities for local and international collaborations. Clinical decisions on treatment and therapy are made from our methods even while the patient is still in the MRI for the initial acute event. With two clinical 3T MRIs now housed at Lucas and six installed in our out-patient facilities, we will further advance our MR imaging tools and sharpen our focus on the critical clinical issues with new experimental and clinical MR methods to predict brain injury; to detect diffuse abnormalities in the brain occult to conventional imaging; to further map how the brain and spine are "wired"; to understand the complex physiological stresses and changes that the brain experiences during ischemia and other pathologic processes; and to extend these tools to to improve therapy monitoring.

Under the CFAN umbrella, Professors Greg Albers, Christine Wijman, Martin Lansberg, and Jean-Marc Olivot of the Stanford Stroke Center conduct work on clinical functional neuroimaging for acute stroke and the field of functional imaging of coma patients. Jean-Marc, stroke neurologist, collaborates with Professors Zaharchuk and Moseley on a clinical evaluation of Xenon-enhanced CT perfusion and MR perfusion for transient ischemic attacks. Jian Zhang is a fourth-year graduate student now graduated and working at the NIH. Jian, Deqiang Qiu, and Shangping Feng are involved in 3D volume spiral imaging for diffusion and functional imaging applications in mapping hippocampus and cortical connections in the aging brain and in stroke patients. Jordan Michael Nechvatal (Psychiatry) joins this group to gain an understanding of how short-term memories are converted into long-term cortical pathways.

Many of our highly qualified CFAN members interact daily with Dr. Scott Atlas, head of our clinical neuroradiology section, or with Greg Zaharchuk who is an Associate Professor and also a member of the Neuroradiology Section. Greg is PI on an NIH-funded R01, which quantifies collateral blood flow in cerebrovascular disease; he also heads the Neuro Tiger team, a joint effort with GE Healthcare; and collaborates on several projects with Neurology and Neurosurgery to clinically evaluate CFAN methods in patients with altered CNS blood flow in MS, Moyamoya, TIA, stroke, and cerebral vascular diseases of the aging brain. The CFAN team also extends its expertise to imaging children from the newborn to the developing adolescent with their unique needs for advanced MRI of the brain. Dr. Zaharchuk's mentee, Albert Hsiao, received the Young Investigator Award for best paper at this year's SPR meeting.

Dr. Moseley is a past president and Gold Medal winner of the International Society of Magnetic Resonance in Medicine (ISMRM) and was elected as a Lifetime Member of the Society of Magnetic Resonance Technologists (SMRT). As a leading expert and pioneer of stroke imaging, Dr. Moseley also sits on many NIH study sections and journal editorial boards. This year, Dr. Moseley received a highly competitive S10 award from the NIH through stimulus (ARRA) funds. This award provides a major hardware upgrade for our 7T animal system in the Clark Center, which will expand research capabilities for many investigators and their pre-clinical MR work.

Thomas Christen, Wesley Hun, Ryan Spilker, Georges Hankov, and Greg Zaharchuk have developed a battery of clinical imaging methods mapping brain oxygenation utilization and reserve for patients with compromised vascular systems. This has been tied to the magnetic susceptibility brain mapping work of Shangpeng Feng and Deqiang Qiu. This work is being added to the clinical stroke workup protocol in an effort to predict whether acute stroke therapy can be extended in patients receiving early MRI scans at Stanford and Lucile Packard. New CFAN members inlcude Dr. Helen D'Arceuil and Caleb Folkes, a summer student from Oklahoma.

Elemental to the CFAN team and to the Lucas Center, is Thomas Brosnan, Senior Research Staff, who directs the RSL and Lucas IT infrastructure. Tom adapts the novel MR sequences to the clinics where the imaging data is fed in real time to the RSL servers for rapid processing and feedback to the clinicians. Lanzie Rivera provides the administrative support for us and is an instrumental resource when it comes to institutional review boards, grants management, and financial matters.

Research Group Updates

Magnetic Resonance Research

Bammer Lab

Roland Bammer, PhD

The general research focus of the Bammer lab is to develop novel MRI acquisition and reconstruction methods for clinical neuroimaging. Currently, our research program is primarily concentrated around improving pediatric neuroimaging as well as various studies on the adult side. Our lab also provides support for users of the Lucas Center for Imaging who are interested in all sorts of diffusion imaging.

From left to right: Lanzie Rivera, Roland Bammer, Murat Aksoy, Rafael O'Halloran, Lily, Eric Gibbons, Melvyn Ooi, Heiko Schmiedeskamp, Matus Straka, Anh Tu Van, Aaryani Tipirneni. Not pictured: EunSoo Choi, Daniel Kopeinigg and Samantha Holdsworth

A major goal in our laboratory is to reduce motion- and distortion-sensitivity of MRI by means of various sophisticated methods, such as stereo-vision and RF tracking in concert with real-time MRI. Motion correction can improve the diagnostic quality of MR images, reduce the number of repeat studies, and the need for sedation/anesthesia.

Another major focus of our lab is the development of high-resolution MRI methods for diffusion-weighted and susceptibility-weighted imaging of the brain and spine, which find utility in the diagnostic work-up of traumatic, oncologic, psychiatric, developmental, or neurovascular abnormalities.

Our lab also continues to develop MR imaging sequences and analysis tools to study vasculature on the macroscopic (angiography) and microscopic (perfusion) level. For example, with our collaborators from the Stanford Stroke Center we have developed software tools that can identify, out of a large number of patients, those who might benefit from advanced stroke therapy.

Thanks mostly to the generous support by the NIH, the Bammer Lab continues to grow. Last fall Melvyn Ooi (Columbia University) joined us as Research Associate working on motion correction. Anh Tu Van (Univ. of Illinois) also joined in the fall as a Postdoctoral Fellow. Also in late 2010, Arryani Tipirneni (St. Jude's Hospital Memphis) started as Staff Scientist. Lastly, this summer Eric Gibbons (Univ. of Salt Lake City) joined us as a BioE graduate student and has already made fantastic progress.

We had also a couple of promotions this year. Matus Straka was promoted to Senior Research Associate. In addition, both Matus Straka and Samantha Holdsworth have become parents for the second time. Congratulations! Murat Aksoy – our hitstar EE student – graduated and was immediately promoted to Research Associate. Just recently, Didem Aksoy was promoted to Staff Scientist. Congrats to both!

Last fall was also the time when a strong pillar of our lab moved on to new endeavors. Stefan Skare, our long-time RA and friend, went back to Stockholm where he is now junior faculty at the renowned Karolinska hospital.

Musculoskeletal MR Imaging (MMR)

Garry Gold, MD

Dr. Gold, who is PI on an NIH-funded R01 for the study of osteoarthritis, an Arthritis Foundation grant, and a multi-investigator industry funded project to develop advanced MR applications, collaborates daily through his research with Lucas Center faculty. Through his research and basic science collaborations, Dr. Gold has been able to introduce a number of new solutions for musculoskeletal imaging into clinical use. These include improved MR imaging around metallic implants, isotropic 3D imaging, and sodium MRI for detection and characterization of osteoarthritis. Dr. Gold's background and training in Electrical Engineering and as a practicing radiologist makes him an ideal collaborator for faculty, postdocs, graduate students, and undergraduates who are interested in discussing and understanding biomedical imaging limitations and requirements for clinical applications. We have strong collaborative ties with the Departments of Electrical Engineering, Mechanical Engineering, Human Biology, Orthopaedic Surgery, and Bioengineering, contributing to the success and evolution of our primary research goals. We actively seek to further educate and train our research team members through various means including clinical scanning, translational hardware development, abstract and peer-reviewed publications, presentations at major conference venues, and in-house didactics. We believe that a diversely educated and experienced team will translate into further advances in musculoskeletal imaging.

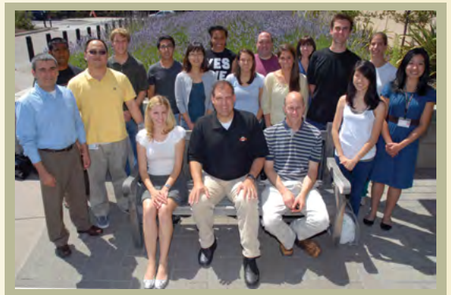

Front Row: Caroline Jordan, Garry Gold, Brian Hargreaves, Kambiz Ansari, Joe Hubbard, Min-Sun Son, Lauren Shapiro, Hillary Middle L to R: Braun, Bragi Sveinsson, Mai Nguyen, Pauline Worters, Saikat Pal, Stephen Matzat, Eric Davalos, Uche Monu, Back Row L to R: Ernesto Staroswiecki, Emily McWalter, Melissa Vogelsong

Multimodality Molecular Imaging Lab (MMIL)

Sanjiv Sam Gambhir, MD, PhD

Multimodality Molecular Imaging Lab

We are developing imaging assays to monitor fundamental cellular events in living subjects. We are actively investigating technologies such as micro-positron emission tomography (micro-PET); bioluminescence optical imaging with a charge coupled-device (CCD) camera; fluorescence optical imaging; micro-computerized axial tomography (microCAT); ultrasound; photoacoustics; intravital microscopy; and Raman spectroscopy in small animal models. Our goals are to marry fundamental advances in molecular/cell biology with those in biomedical imaging to advance the field of molecular imaging. We have a particular focus on cancer biology. We have developed several reporter genes/reporter probes compatible with all of the above imaging modalities. These reporter genes are being used in cell trafficking models, gene therapy models, as well as in transgenic models for studying cancer biology. We are developing novel nanoparticle for Photoacoustics, Raman, and multimodality imaging strategies. Imaging of biologics with engineered proteins for cancer cell surface targets are being pursued. Assays to interrogate cells for mRNA levels, cell surface antigens, protein-protein interactions, protein phosphorylation, and intramolecular folding are also under active development. We are also extending many of these approaches for human clinical applications. New patient trials for PET imaging of T-cell trafficking in patients are being performed with our reporter gene strategies. We are also developing several new PET agents for cell surface targets based on new protein scaffolds.

Cancer Molecular Imaging Chemistry Lab (CMICL)

Zhen Cheng, PhD

(l-r), Ermelina Lucente, Susan Hoppmann, Meng Yang, Qizhen Cao, Han Jiang, Zhen Cheng, Gang Ren, Jinbo Li, Shuanglong Liu

The main research of our group is to develop novel multimodality imaging probes and techniques for cancer early detection. Our multidisciplinary team is composed of members with expertise in organic chemistry, radiochemistry, bionanotechnology, biochemistry, molecular and cell biology, radiological science, medicine, and molecular imaging.

Currently, we are actively studying several important problems in the molecular imaging field. First, we are investigating a variety of novel platform molecules (peptides, proteins, nanoparticles) as universal strategies for cancer imaging. Second, we are establishing new methodologies for site-specific labeling these platform molecules for multimodality imaging. Third, by applying the knowledge obtained from the above research, we are optimizing PET and optical imaging probes for imaging of melanoma, breast cancer, prostate cancer, and ovarian cancer, and we hope to quickly translate two molecular probes into clinical PET imaging in near future.

The research is supported by National Institute of Health, Department of Defense, Melanoma Research Alliance and Radiology Department at Stanford.

Trainee fellowships are supported by China Scholarship Council.

Cellular and Molecular Imaging Lab (CMIL)

Jianghong Rao, PhD

Jianghong Rao; 2nd row from left: Hexin Xie, Jodie Chen, Liqin Xiong; 3rd row from left: Kyung Hyun Lee, Deju Ye, Jeongho Jeon, Jessica Gall; 4th row: Jocelyn Barker; Not present: Lina Cui, Grigory A. Tikhomirov, Kanyi Pu, Adam Shuhendler

The general research interest in the Rao lab is to develop novel molecular probes and imaging strategies for in vivo imaging by combining chemical synthesis and macromolecular engineering with imaging technology. Current projects are broadly defined in the following areas:

1) Multimodality imaging of enzyme activity in vivo: As a unique class of protein molecules, enzymes catalyze biochemical transformations and are widely implicated in biological processes and diseases. We are developing "smart" activatable probes for imaging and detection of beta-lactamase activity from Mycobacterium tuberculosis (TB) in vivo to study TB biology and to evaluate the efficacy of therapeutics in preclinical animal models. The second class of enzyme target we are interested in is proteases, many of which display aberrant activity in diseases such as cancers and arthritis. We are employing both small molecule probes and nanoparticles-based nanosensors for in vitro detection and in vivo imaging of the activity of proteases such as matrix metalloproteinases and furin in cancer cells. Toward imaging these enzyme targets, different imaging modalities have been employed including optical imaging, magnetic resonance imaging, and positron emission tomography.

2) Developing general strategies to label proteins and RNAs in living cells: Our approach is to design small organic dye molecules that are not fluorescent initially but that become fluorescent after binding to a receptor or tag fused to either a protein or RNA molecule of interest. We are combining rational design and library selection methods, such as SELEX and phage display, to discover such novel molecular tags for super high-resolution single-molecule imaging in living cells.

3) The third area is nanotechnology: We are applying both protein engineering and nano engineering to create novel nanoparticles for imaging and sensing applications. We invented the QD-BRET technology widely applicable for in vitro biosensing and in vivo imaging. We are currently synthesizing novel multiple functional nanoparticles for multi-modality cancer imaging and theranostic applications. One example is fluorescent magnetic nanoparticles with tumor-specific prodrug conjugated for breast cancer imaging and treatment in a collaborative effort with Dr. Heike Daldrup-Link's lab.

Molecular Imaging Instrumentation Laboratory (MIIL)

Craig Levin, PhD

Back row, left to right: Frances Lau, Eric Gonzalez, Paul Reynolds, Alex Grant, Octoavio Viramontes, Ruud Vinke, Peter Olcott, Derek Innes; Next row, left to right: Garry Chinn, KeyJo Hong, Yi Gu, Jung-Yeol Yeom, Arne Vandenbroucke, Farhad Taghibakhsh; Next row, left to right: Jing-yu Cui, Matthew Bieniosek; Front row, left to right: Virginia Spanoudaki, Craig Levin, Ealgoo Kim, Abdelkader

Our research interests are to advance instrumentation and algorithms for the non-invasive imaging of basic cellular and molecular signatures associated with disease. These new "cameras" image photon emissions from molecular probes designed to target specific molecular processes associated with disease in cells located deep within the tissues of living subjects. The technical goals of the instrumentation projects are to advance the photon detection efficiency and spatial, spectral, and temporal resolutions. The algorithmic goals are to understand the physical system comprising the subject tissues, photon transport, and camera, and to realize the best available reconstructed image quality and quantitative accuracy. The work involves the design, development, and testing of novel position sensitive photon sensors and systems; low-noise readout electronics; data acquisition electronics; computer modeling; computer graphics; tomographic image reconstruction algorithms; signal/image processing algorithms; and data/image analysis. Key goals of our research are to incorporate these innovations into practical imaging devices and introduce new in vivo imaging tools to advance studies of molecular mechanisms and aid discovery of novel treatments of disease in the clinic as well as in preclinical research. If successful, these novel systems will substantially enhance the visualization and quantification of subtle molecular signatures associated with disease with the hope that molecular imaging can play a role in earlier disease management. The research is supported by grants from the National Cancer Institute, National Institute of Biomedical Imaging and Bioengineering, Department of Energy, GE Healthcare and Philips Healthcare. Trainee fellowships are supported by Stanford's Bio-X Program, School of Medicine Deans Fellowship Program, Stanford Molecular Imaging Scholars Program, Stanford REU Program, US Department of Defense, Society of Nuclear Medicine, Swedish Research Council, National Science and Engineering Research Council of Canada, China Scholarship Council, AXA Research Fund, and TLI Inc.

Cardiovascular Cellular & Molecular Imaging Laboratory

Joseph Wu, MD, PhD

Ischemic heart disease is the number one cause of morbidity and mortality in the United States. The repeated ischemic insults can lead to congestive heart failure, which is the leading cause of hospital admissions for people aged 65 years and over. In the next decade, cardiovascular diseases will likely be targeted at the basic cellular and molecular levels. The Cardiovascular Cellular & Molecular Imaging lab (http://wulab.stanford.edu) combines expertise in molecular and cell biology, cardiovascular physiology, and molecular imaging. We work on the biological mechanisms of adult stem cells, embryonic stem cells, and induced pluripotent stem cells. We use a combination of gene profiling, tissue engineering, physiological testing, and molecular imaging technologies to better understand stem cell biology in vitro and in vivo. For adult stem cells, we are interested in monitoring stem cell survival, proliferation, and differentiation. For ESC, we are currently studying their tumorigenicity, immunogenicity, and differentiation. For iPSC, we are working on novel derivation techniques. We also work on development of novel vectors and therapeutic genes for cardiovascular gene therapy applications. The eventual goal is to establish molecular imaging as a platform for translational research in cellular and gene therapies for ischemic heart disease in the 21st century.

Members of the Wu Lab.

Molecular Imaging of Nocieption and Inflammation Lab (MINIL)

Sandip Biswal, MD

Chronic pain sufferers are unfortunately limited by poor diagnostic tests and therapies. The lab is interested in using multimodality molecular imaging techniques to study nociception and neuronal inflammation as a means of improving objective, image-guided diagnosis and treatment of chronic pain generators. Deepak Behera, DNB continues to admirably lead and manage the lab, juggling a number of projects, collaborations and students. This past year has brought some new additions to the lab including MedScholar Eric Davalos, and new collaborations with Garry Gold and Brian Hargreaves (as part of the Tiger Team) to help develop improved isotropic MR approaches for MR Neurography. Another MedScholar, David Attarzadeh, has been studying platelet-rich plasma therapy and whether or not it helps heal tendons. Preeti Borgohain and Supradha Nagineni have also recently joined the lab and will be studying the role of various neuronal mediators in chronic pain models using PET-MRI. We continue our exciting collaborations with Justin Du Bois, PhD, William Parsons, BS, John Mulcahy, PhD, Frederick Chin, PhD, Aileen Hoehne, PhD, Bin Shen, PhD, and David Yeomans, PhD, studying the role of voltage-gated sodium channels in neuropathic pain using PET-MRI and radiolabeled guanidinium toxins. Important collaborations with the Stuart Goodman Lab continue to thrive as we continue to examine the role of mesenchymal stem cells and macrophages in the prosthetic-induced osteolysis and in fracture models. A new collaboration with Pankaj Jay Pasricha, MD, Chief of the Division of Gastroenterology has formed in hope of finding better PET-based methods to study abdominal pain syndromes.

(From Left) Sandip Biswal, Bao Do, Deepak Behera, Preeti Borgohain, Supradha Nagineni and Eric Davalos. (Missing) David Attarzadeh

Cellular Pathway Imaging Laboratory (CPIL)

Ramasamy Paulmurugan, PhD

The current foci of our lab are 1) to develop new molecularly targeted therapy for triple negative breast cancer (TNBC), 2) to study the molecular mechanisms involved in tamoxifen resistance in breast cancer, and 3) to explore the use of non-invasive molecular imaging of histone methylations in living animals. Breast cancer is a highly heterogeneous disease, and there is a growing body of evidence that this heterogeneity occurs at both genetic and phenotypic levels. Although breast cancer research has improved the efficacy of therapies, especially for the treatment of a sub-type of breast cancer that is estrogen receptor positive (endocrine therapy), the increase in the incidence of the receptor negative phenotype and the presence of the receptor positive anti-estrogen non-responsive (tamoxifen resistant) phenotype have contributed to a continual increase in the mortality rates of breast cancer. Two common subtypes of breast cancer, the triple negative phenotype and receptor positive phenotype that develops tamoxifen resistance during treatment, are hard to treat clinically. We mainly target microRNAs', the global regulators of gene expression, which are deregulated in cells under different pathological conditions. Similarly, we study the biological role of ERβ-, the second sub-type of ER, whose role in different types of breast cancers has largely been ignored thus far, and which is over-expressed in breast cancers of TNBC phenotypes. Specifically, we are interested in developing a combinatorial therapeutic approach in that we will combine ERβ-specific ligands with the down-regulation of some specific microRNAs, which are over-expressed in receptor negative breast cancers. Lastly, we are also interested in developing new in vivo imaging assays to monitor different epigenetic processes, especially histone methylation, which are critical for maintaining cellular homeostasis, and may be potential therapeutic targets for treating many cellular diseases with altered cellular homeostasis, including different cancers.

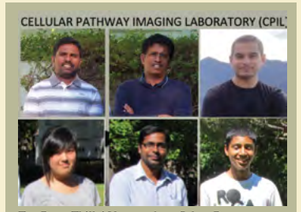

Top Row: Thillai Veerapazham Sekar, Ramasamy Paulmurugan, Rehan Ali ; Bottom Row: Elizabeth Lee, Narayana Murthy Sekar, Varun Krishnamurthy

Translational Molecular Imaging Lab (TMIL)

Jürgen K. Willmann, MD

In the United States, cancer continues to be the leading cause of death in patients between 25 and 64 years of age, and the second leading cause of death in patients older than 65 and between 1 and 14 years. Prognosis and survival of patients with cancer depends on tumor stage of the cancer at the time of diagnosis, therefore, early cancer detection holds great promise in prolonging survival and improving quality of life in cancer patients. Novel imaging strategies that allow detection of cancer at early, still curable stages are thus highly desirable. With the advent of novel therapeutic options for cancer patients, there is an increasing demand for non-invasive imaging biomarkers to identify those patients early on that benefit most from a given treatment or to terminate or modify treatment for those patients not responding to a certain treatment.

In our Lab, we focus on the development and clinical translation of novel molecular and functional imaging biomarkers. We have a special focus on imaging abdominal and pelvic cancer including pancreatic, liver, renal, ovarian, and prostate cancers. We further advance clinically available radiological imaging modalities such as ultrasound, magnetic resonance imaging (MRI), and positron emission tomography (PET) as promising imaging tools for early detection and treatment monitoring of abdominal and pelvic cancer.

Our mission is to translate these novel molecular and functional imaging strategies into clinical protocols for improved patient care in the shortest possible time frame.

Left to Right: Hak Jong Lee, Alice Gardner, Ying Ren, Juergen Willmann, Kira Foygel, Sunitha Bachawal, Marybeth Pysz, Huaijun Wang (Morgan)

Cancer Molecular Diagnostics Laboratory

Sharon Pitteri, PhD

Our group is focused on the discovery and validation of blood-based molecular diagnostic markers for cancer early detection. We are interested in defining novel protein signatures for breast and ovarian cancers, including sub-types of these diseases. These protein signatures have potential applications such as molecular indicators of cancer risk, diagnosis, progression, and recurrence. Our primary tools are liquid chromatography and mass spectrometry, which are used to perform in-depth quantitative proteomics, and to characterize post-translational modifications associated with disease state. Using human plasma samples, tumor tissue, cancer cell lines, and genetically engineered mouse models, the origins of these proteins are being investigated. This laboratory is also focused on the identification of proteins with expression restricted to the surface of cancer cells, which can be used as novel targets for molecular imaging technologies. This year has been dedicated to building our lab and establishing collaborations with Stanford investigators and investigators outside Stanford.

Sharon Pitteri and Majlinda Kullolli

Facilities

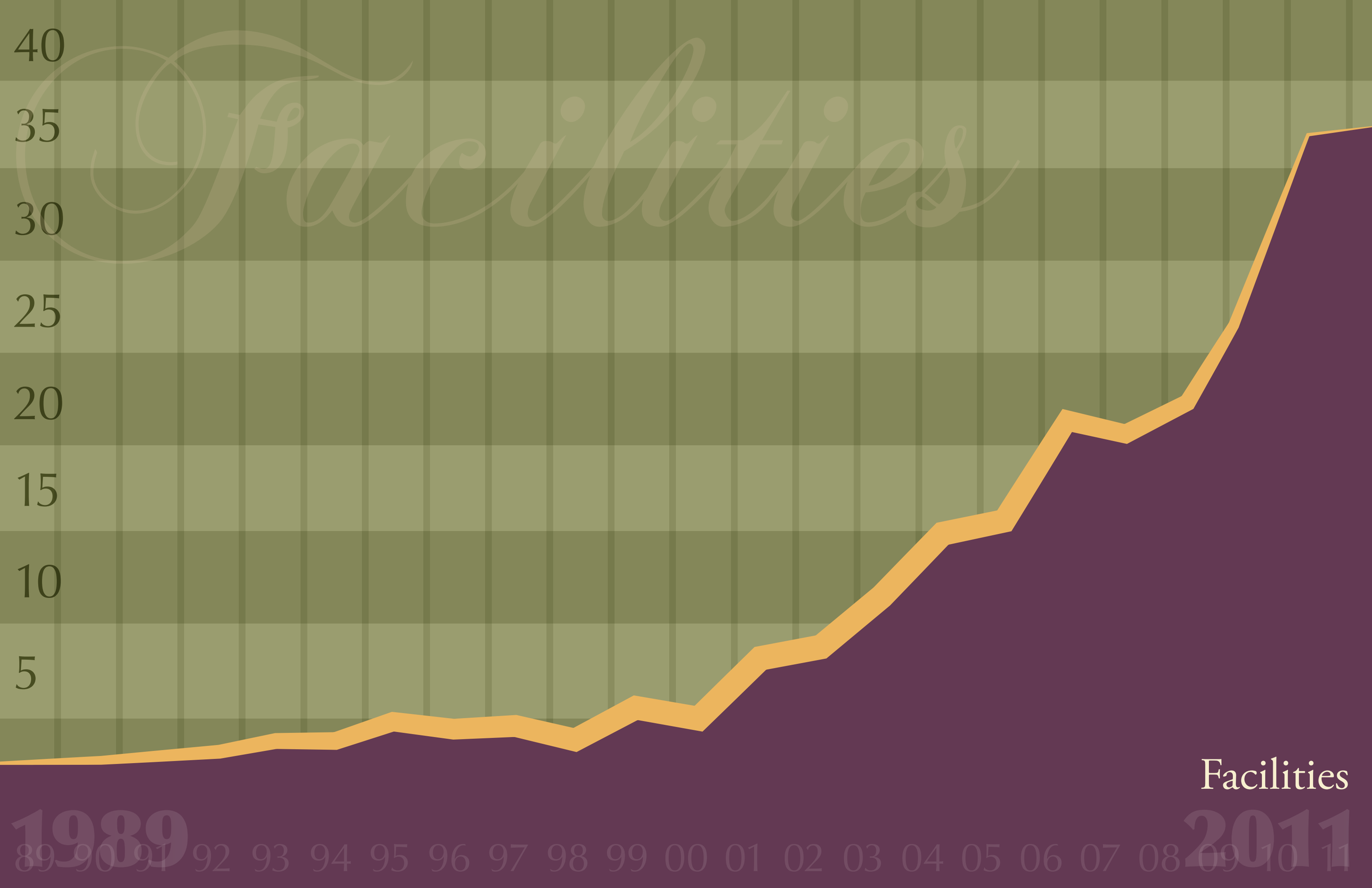
40
35
30
25
20
15
10
5
Facilities
1989
2011
89 90 91 92 93 94 95 96 97 98 99 00 01 02 03 04 05 06 07 08 09 10 11

Stanford Radiology 3D and Quantitative Imaging Laboratory (3DQ Lab)

Sandy Napel, PhD, Lab Director
R. Brooke Jeffrey, Jr., MD, Lab Director
Charles Stanley, RT(R)(CT)(MR), Lab Manager

The Stanford Radiology 3D and Quantitative Imaging Laboratory is guided by the mission of developing and applying innovative techniques for efficient analysis and display of medical imaging data through interdisciplinary collaboration. Since 1996, our clinical goal has been to deliver 3D imaging advances to the Stanford and surrounding communities as rapidly as possible for the swift and accurate diagnosis, tracking, and treatment of disease; our educational goal is to disseminate knowledge to replicate our 3D services at other institutions; we continue to facilitate cutting edge research through our collaborations with faculty in Radiology and other Departments. In early 2011 we changed our name to "Stanford Radiology 3D and Quantitative Imaging Lab (the 3DQ Lab)." This was done to reflect the Lab's increasing involvement in quantitative imaging, as our resources are being sought out and have expanded our scope beyond the traditional "images as pictures" paradigm.

Progress

Clinical: Over the past year, the 3DQ Laboratory has continued its operations simultaneously in the Lucas Center as well as the James H. Clark Center, a building dedicated to interdisciplinary science. Our average monthly 3DQ volume has held steady at approximately 950 examinations, and we have processed over 89,000 examinations overall since our inception. The majority of our referrals continue to come from vascular surgery, cardiothoracic surgery, gastroenterology, cardiology, urology, reconstructive surgery, orthopedics, neurology, and neurosurgery. 3DQ clinical procedures now offered by the Lab include Volumetric rendering of liver volumes to aid in tumor quantification(fig 1), Volume rendered view of vascular structures to assess stent placement (fig 2), and musculoskeletal exams to aid in surgical planning (fig 3).

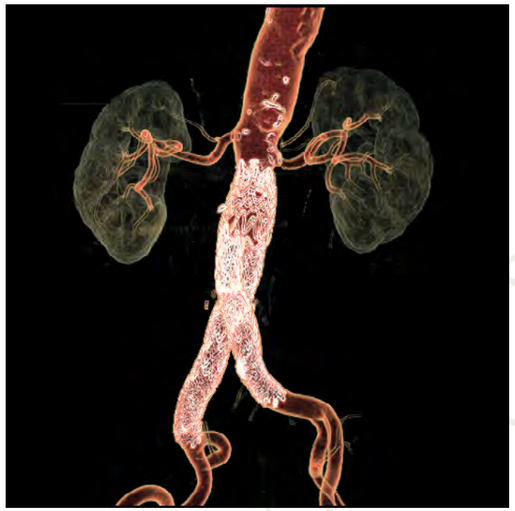

Volume rendered view with edge enhancement of post stent placement in the distal aorta and proximal iliac. Renal anatomy is also visualized. Vascular imaging remains the highest clinical volume of work done in the 3DQ lab.

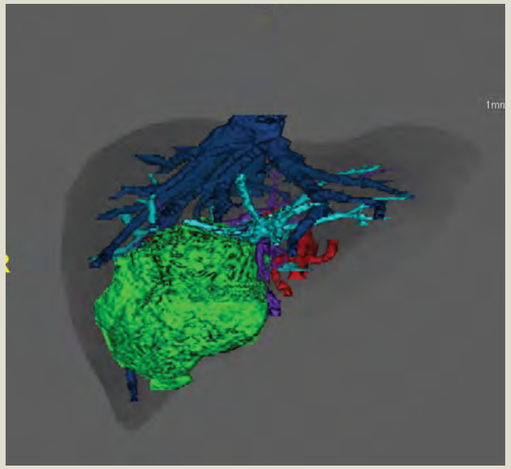

Composite view of liver showing biliary tree (purple), portal veins (teal), hepatic veins (blue), hepatic arteries (red), and large hepatic mass (green). These images and quantification measurements are provided for use in surgical planning techniques and tumor tracking. Volumetric and Quantitative imaging is a fast growing segment of the work done in the 3DQ lab.

Education: This year the 3DQ Laboratory has been attended by international visiting scholars from Japan, China, and Kazakhstan as well as Stanford Radiology fellows, residents, and medical students who acquire skills in 3D processing and interpretation as part of their medical training. Stanford researchers from engineering and medical departments have also been trained in processing and acquiring 3D images and data for research projects, including measurements of craniofacial deformities for reconstructive surgery, pulmonary vasculature volumes for 3D model fluid flow simulations for vascular surgery, and 3D modeling for multimodality small animal imagers.

Research: The research arm of the lab hosts an annual average of 8 graduate students and post-doctoral scholars from several departments of the university, as well as 2 clinical MD researchers. This year, projects included investigations by visiting physicians from Japan of the utility and limitations of cardiac CT angiography, and use of eye gaze-tracking to understand and improve the detection of pulmonary nodules in volumetric CT scans.

Finally, reflective of the envisioned growth in quantitative imaging, Dr. Daniel L. Rubin, MD, MS, has joined the 3DQ Lab to lead our research and translational efforts in this area; we have already begun to offer core lab services for clinical trials that use imaging as surrogate biomarkers.

Infrastructure

The last 12 months have been a time of transition for the Lab as 2 of its pioneers have departed to continue their careers at Duke University. Lab co-Director Dr. Geoffrey D. Rubin left to assume the position of Chairman of Radiology at Duke University, and Lab Manager Laura Pierce left to manage the nascent 3D Lab at Duke. Current Stanford 3DQ Lab personnel include: Charles Stanley, 3DQ Laboratory manager; senior 3DQ technologists Linda Horst and Marc Sofilos; 3DQ technologists Kristen Bogart, Caryn Damits, Keshni Kumar, Rhea Lang, Nancy Ware, and Shannon Walters. Support staff includes administrative assistants Debra Frank and Lakeesha Winston, and database administrator, Kala Raman.

On flat panel: Nancy Ware, Marc Sofilos, Lakeesha Winston; Back Row L-R: Shannon Walters, Debra Frank, Linda Horst, Rhea Liang, Kristy Bogart, Keshni Kumar, Caryn Damits, Kala Raman; Front Row L-R: Daniel Rubin, Sandy Napel, R. Brooke Jeffrey Jr., Charles Stanley

In the Clark Center, a central area table invites professional collaboration, and student desks with moveable workspaces provide areas for independent research. The Lucas Center 3DQ Laboratory also houses equipment on a central area table, surrounded by student carrels. The lab equipment consists of 12 advanced 3D workstations, two research and development servers for image and data storage, and three TeraRecon servers, which also provide remote 3D rendering to other parts of the Stanford medical community.

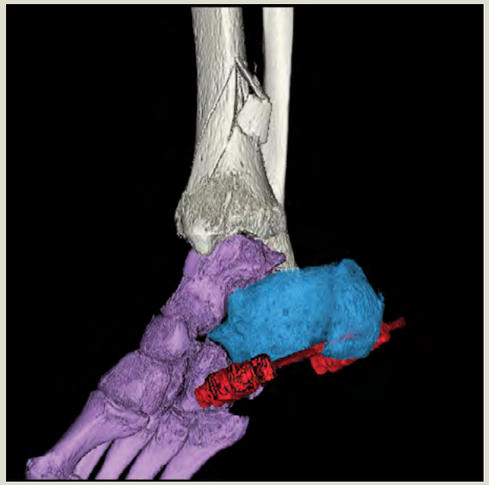

Volume rendered view of the ankle showing an external fixator (red) attached thru the os calcus (blue). Musculoskeletal imaging remains an important part of the work done in the 3DQ Lab.

Three remote PACS workstations allow access to all Stanford medical imaging and reporting. This past year the 3DQ Lab acquired servers from GE Healthcare and Vital Images; this is reflective of the entire industry moving away from standalone workstations to server/thin client models. These servers are currently being integrated into the lab workflow and will further enable us to expedite the processing and sharing of data throughout the lab. These upgrades will also allow for flexible workspaces utilizing generic PC workstations while accessing all 3D applications from these centrally located servers. During this evolution, we continue our excellent relationships with corporate developers of 3D workstations/servers (e.g., GE Healthcare, TeraRecon, and Vital Images) who site their hardware and software in the 3DQ lab in anticipation of our feedback. These relationships continue to ensure that we maintain the most advanced multi-dimensional analytical technologies available. The lab continues to support the use of the MEDIS QMass® and QFlow® analysis software, which allow for enterprise collaboration when measuring cardiac output and analyzing muscle mass.

Conclusion

During this time of transition with regards to mission and resources, the 3DQ Medical Imaging Laboratory continues to function as an international leader in clinical care, teaching, and research in medical imaging analysis and quantitation. The confluence of talented medical and engineering expertise with the most up-to-date equipment has been a consistent source of innovation in diagnostic, monitoring, and treatment planning approaches.

3D and Quantitative Imaging Lab

Animal Model Management

Wendy Baumgardner, RVT, LATg
Pam Hertz, RVT

In our continuing efforts to provide support research in the Department of Radiology, we are entrusted with the responsibility of overseeing all animal model protocols within our department and all other departments carrying on research studies at the Lucas Center. Two-experienced California Licensed Veterinary Nurses (RVT), with over 33 years in the field, support all animal model studies with the health and welfare of the animal always our most important priority. Diligent care is taken during all procedures involving animal subjects; they are treated with the utmost respect, compassion, and professional care. Animal studies improve both treatment and diagnostic capabilities for humans, and are managed with the same level of compassion that is extended for our clinical patients.

All personnel working with animal models under approved Institutional Animal Care and Use Committee (IACUC) protocols have completed required training from the Stanford University Department of Comparative Medicine. In addition, specifically tailored "one on one" training for more advanced techniques are taught by the veterinary technicians at the Lucas Center.

We realize that living subjects are needed to advance our knowledge, and to that end we ensure that proper respect for life is part of all research studies. Research conducted at the Lucas Center improves and develops new invasive and non-invasive procedures that utilize Magnetic Resonance Imaging (MRI), High Intensity Focused Ultrasound (HIFU), Computed Tomography (CT), CT/fluoroscopy, and Positron Emission Tomography (PET) to guide them. Clinical studies currently conducted include the study of cardiac and liver radio frequency (RF) ablation, myocardial infarction, liver and prostate cancers, neuromodulation with ultrasound, and structural neuroimaging of the brain. The techniques currently being explored at the Lucas Center contribute to more efficient and effective medical treatment for human illness and disease.

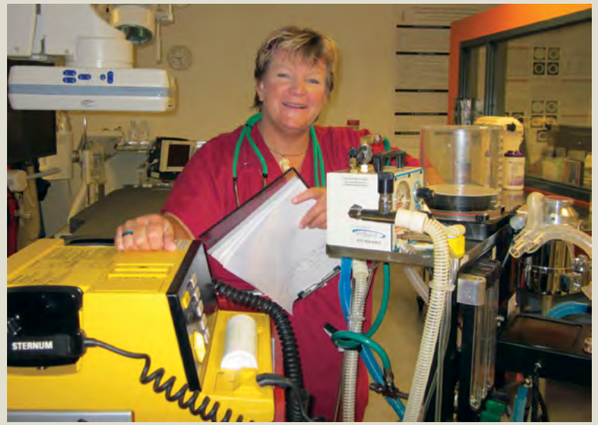

Licensed Veterinary Technicians Wendy Baumgardner

Small Animal Imaging Center - SCi3

Tim Doyle, PhD, Head, Small Animal Imaging Facility, MIPS

With demand for small animal imaging by groups in the School of Medicine continuing to increase, the imaging core has responded by upgrading instruments available for use. Dr. Michael Moseley was successful in obtaining an NIH shared instrumentation grant in 2010, which has allowed us to upgrade the 7 Tesla MRI scanner with new gradient inserts and electronics. This upgrade will allow the instrument to be used for animals larger than rats and will provide for overall improvement in imaging protocols. The 7T MRI upgrade is due to be completed at the end of August, 2011. Drs. Christopher Contag and Brian Rutt were instrumental in obtaining a demonstration of a small 1 Tesla MRI system from Aspect Imaging. This system uses permanent magnets that do not require active cooling to operate, and thus functions as a room-temperature bench-top instrument. Extensive use of this magnet for the development of novel MR contrast agents has been made.

Using funds obtained from the School of Medicine, the University, the Stanford Cancer Institute, and the Department of Radiation Oncology, we were able to purchase a new Siemens Inveon MicroPET-CT scanner, which was installed at the end of 2010. This instrument is now available for all users and has resulted in an increase in MicroPET studies, and nicely complements the older Siemens R4 MicroPET scanner. A bioluminescence microscope was installed in the imaging core, with the LV200 microscope provided by Olympus with funds from the Stanford Cancer Institute used to purchase the Hamamatsu CCD camera. In addition to imaging luciferase-generated photons from cells and tissues, this system has been used to image Cerenkov radiation, a phenomenon in which certain radionuclides emit photons in visible spectrum. In the near future, we hope to install two new photo-acoustic scanners for mouse imaging. Photo-acoustic imaging has recently garnered a lot of interest with Dr. Sam Gambhir's group pioneering the development of new imaging agents for this modality.

The new small animal imaging facility space in the Larry I. Lokey Stem Cell Research Building (SIM1) opened this year and currently offers access to a Caliper Life Sciences IVIS Spectrum imaging system. This new imaging facility is located within the new Stanford barrier mouse facility and offers imaging capability to animals housed there. We hope that other modalities, such as PET, CT, ultrasound and MR will also soon be available in this new facility.

Lucas Center MR Systems

Anne Marie Sawyer, BS, RT (R)(MR), FSMRT

1.5T, 3T1, 3T2 AND 7T Whole Body Magnets

MRI Systems and Support 2010 - 2011

The 3.0 Tesla #1 G.E. Healthcare MRI system is currently operating at 15.x systems revision; and the 3.0 Tesla #2 GE Healthcare Discovery 750 at 21.x software (Figure 1). The systems operate at a maximum slew rate of 150 Tesla per meter per second and maximum gradient amplitudes of 40 milliTesla per meter at 3T1 and 50 milliTesla per meter at 3T2. The hardware currently allows the use of 16 channels at 3T1 and 32 channels at 3T2.

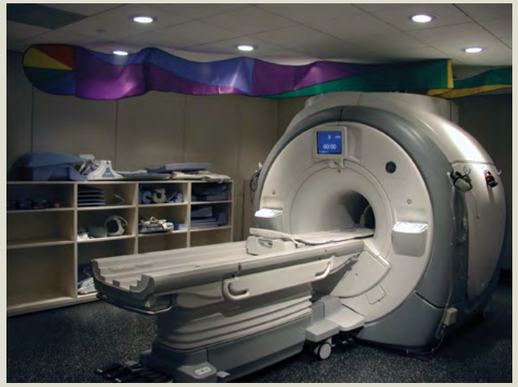

Figure 1. The '3T2' at the Lucas Center is a G.E. Healthcare Discovery 750 MRI system

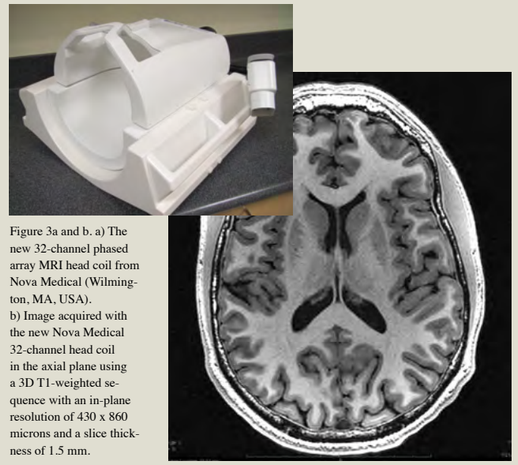

Figure 3a and b. a) The new 32-channel phased array MRI head coil from Nova Medical (Wilmington, MA, USA). b) Image acquired with the new Nova Medical 32-channel head coil in the axial plane using a 3D T1-weighted sequence with an in-plane resolution of 430 x 860 microns and a slice thickness of 1.5 mm.

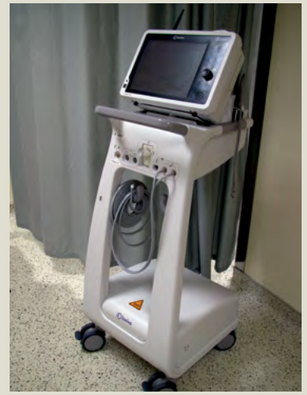

Figure 4. The new Invivo Expression physiologic monitor that includes the following options: wireless ECG (electrocardiogram), wireless SPO2 (heart rate and saturated oxygen), body temperature, invasive blood pressure, NIBP (non-invasive blood pressure), EtCO2 (end-tidal CO2), sedation and anesthesia.

Figure 2. The 1.5T magnet upon being removed from the Lucas Center. The suite is currently under renovation with a planned installation of a G.E. Healthcare 3T Discovery 750 MRI system in September.

The 1.5T MRI system has been removed and renovations of the suite are underway for a new GE Healthcare Discovery 750 at 22.x software with 32 channels to be installed in September of 2011 (Figure 2). The 7.0T MRI system is undergoing a hardware and software upgrade to the GE Healthcare Discovery 950 at 22.x software with 32 channels.

New additions to the MRI systems for use in research studies include a new Nova Medical head coil with 32 channels (Figure 3a and 3b), a new Invivo Expression physiologic monitoring system (Figure 4), and a new EGI 256-channel EEG (electroencephalography) system to be used in the bore of the MRI to simultaneously collect functional MRI data and EEG data.

Daily support in MR system operation and screening and safety is provided to all researchers including faculty, post-doctoral fellows, graduate students, and visiting scholars in the Lucas Center and Department of Radiology; researchers from other University departments such as Psychology, Psychiatry, Neurology, Neurosurgery, and Nephrology; and service center users from outside of the University.

Cyclotron Suite Update

Frederick Chin, PhD
David Dick, PhD

The Radiochemistry Facility (RF) develops and offers radiotracers for early detection and therapeutic monitoring of disease in both preclinical and clinical imaging settings. Our radiochemistry personnel (faculty, staff, and postdocs) continues to number around 30 people including recently hired Amit Hetsron, MS, So-Hee Kim, MS, and Zheng "Ben" Miao, PhD. Additional instruments that were installed in 2010-2011 include two GE radiosynthesis modules (TRACERlab FX-N Pro and FX-FN), two Agilent HPLC with autosampler systems, and a prototype miniature microwave system (CEM PETwave). A clinical radiochemistry laboratory is in the final stages of completion in the new Nuclear Medicine and Molecular Imaging Clinic, which opened in October 2010. This extra lab space will provide clinical-grade radiopharmaceuticals to meet essential clinical radiochemistry demands while abiding by current regulatory policies. The existing radiochemistry labs continue to provide tracers for pre-clinical investigations and maintain our [C-11]carbon dioxide and [F-18] fluorine gas radiochemistries for all our research needs.

Front row (left to right): Amit Hetsron, Frederick Chin, Zheng "Ben" Miao, Michelle James; Back row (left to right): Aileen Hoehne, Bin Shen, David Dick, George Montoya, Mohammed Namavari, So-Hee Kim; Missing from picture: Murugesan Subbarayan

Our staff continues to provide routine clinical tracers for use at the Stanford Hospital. Fluorine-18 labeled fluorodeoxyglucose (FDG) is still produced daily (6-days/week) and is made using the new FASTlab FDG system with much higher yields relative to the MX-FDG module. Nitrogen-13 ammonia (myocardial perfusion assessment) and fluorine-18 sodium fluoride (bone imaging) are also synthesized for the clinic as needed.

Pre-clinical and Clinical Investigations

GE TRACERlab modules are the workhorses in the lab and perform the syntheses of our ^{18}F and ^{11}C-labeled radiotracers for our many collaborations at Stanford and pharma. These modules have enabled us to perform new radiochemistries such as [^{18}F] FSPG (imaging cystine/glutamate exchanging in tumors) for human studies. Additional PET radiotracers that study the mechanisms and treatment of cancer as well as neurological disorders will soon become available to meet the increasing needs for performing preclinical ([^{11}C]raclopride, [^{18}F]saxitoxin, [^{18}F]FBR, [^{18}F] FTC-146, [^{18}F]FA-YF_3) and clinical ([^{64}Cu]rituximab, [^{18}F]Avid/Bayer/GE compounds, [^{18}F]FSPA-RQ, [^{18}F]AraG) research studies with PET.

Radiolabeled Compounds

The following table presents a summary of radiolabeled compounds that are made in the research radiochemistry lab, excluding research compounds protected under confidentiality agreements (**Bolded tracers** = preclinical and clinical use).

Tracer	Use	Application
[^{11}C]Raclopride	Imaging dopamine-2 receptors (D2R)	Monitoring D2R-related neurological disorders (i.e. Parkinson's Disease)
[^{11}C]PIB	**Imaging αβ amyloid in brain**	**Monitoring progression of Alzheimer disease in brain**
[^{18}F]CBT	Prosthetic labeling group	Radiolabeling peptides with specific cysteine moiety
[^{18}F]AraG	Imaging agent for T-cells	Detection of disease of T-cell origin
[^{18}F]FA-YF_3	Imaging folate receptors	Imaging tumors
[^{18}F] FAZA	Hypoxia imaging agent	Evaluating clinical-relevant hypoxia-directed cancer therapies
[^{18}F]MISO	Hypoxia imaging agent	Evaluating clinical-relevant hypoxia-directed cancer therapies
[^{18}F]EF-5	**Hypoxia imaging agent**	**Evaluating clinical-relevant hypoxia-directed cancer therapies**
[^{18}F]Fluorouracil	**Tumor imaging agent**	**Evaluating clinical-relevant cancer therapies**
[^{18}F]fluorobenzaldehyde	Prosthetic labeling group	1) Radiolabeling peptides for potential clinical use 2) Radiolabeled affibody for imaging of NER2neu
[^{18}F]fluorobenzoic acid	Prosthetic labeling group	Radiolabeling peptides for potential clinical use
[^{18}F]Fluoropropionic Acid	Prosthetic labeling group	Radiolabeling peptides for potential clinical use
[^{18}F]SFB	Prosthetic labeling group	Radiolabeling peptides for clinical use
[^{18}F]FBR	Imaging agent for TSPO receptors (formerly known as peripheral benzodiazepine receptors)	Monitoring neuroinflammation induced by stroke or radiotherapy
[^{18}F]FEAU	Imaging substrates expressing mutant HSV1-sr39tk	1) Monitoring gene therapies targeting cancer 2) Monitoring cell therapies
[^{18}F]FHBG	**Imaging agent for tumors expressing HSV1-tk**	**Monitoring various cancer therapies**
[^{18}F]FLT	**Imaging agent for tumor cell proliferation**	**Monitoring various cancer therapies**
[^{18}F]FPPRGD2	**$\alpha_v\beta_3$ integrin imaging agent**	**Imaging tumor integrin expression**
[^{18}F]FSPA-RQ	Imaging neurokin-1 receptors	Imaging pain and anxiety
[^{18}F]FSPG	**Imaging agent for cystine/glutamate exchanger**	**Imaging tumors**
[^{18}F]FTC-146	Imaging agent for sigma-1 receptor	Imaging agent for studying depression, Schizophrenia, Alzheimer's Disease, drug addiction, pain, and certain cancers (e.g., prostate, breast)
[^{18}F]Saxitoxin	Imaging agent for sodium channels	Imaging agent for sodium channels linked to pain
Other ^{18}F-labeled RGD peptides	$\alpha_v\beta_3$ integrin imaging agent	Imaging tumor integrin expression

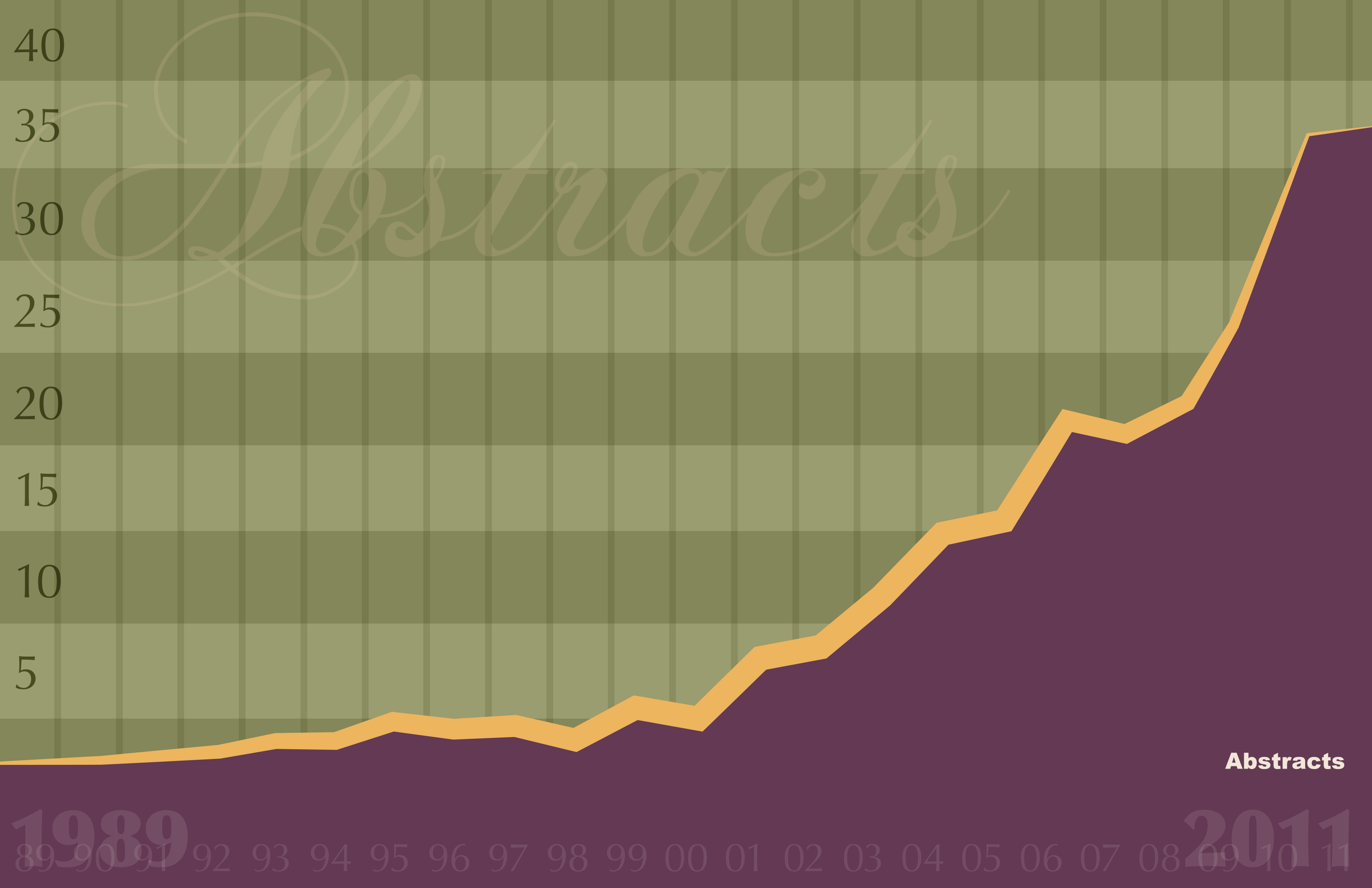
Abstracts
40
35
30
25
20
15
10
5
Abstracts
1989
2011
89 90 91 92 93 94 95 96 97 98 99 00 01 02 03 04 05 06 07 08 09 10 11

Abstracts in this section describe research that is conducted using sophisticated x-ray and Computed Tomography (CT) techniques to improve image quality, decrease the amount of radiation exposure, or reduce the amount of time required to complete an exam. The overall goal of these projects is to improve our ability to detect and monitor disease using these x-ray based methods.

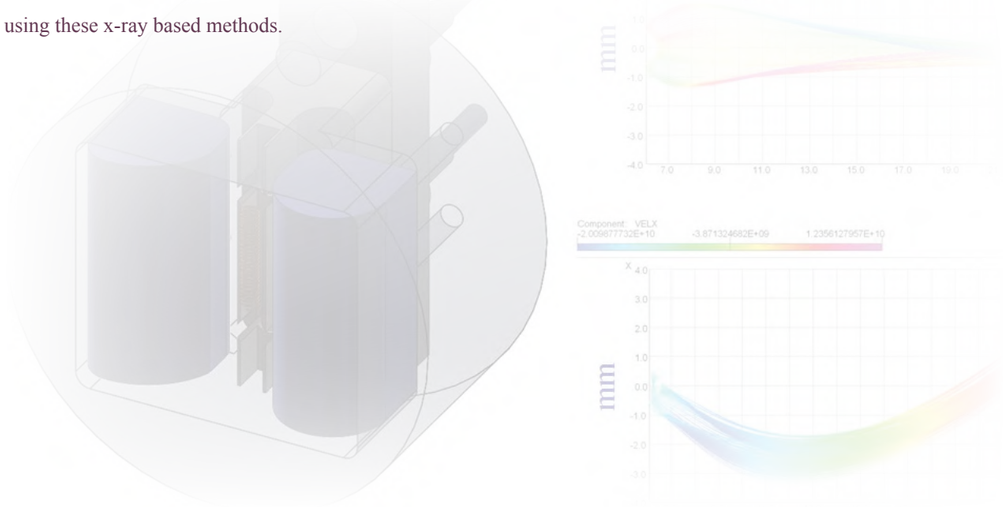

Synthetic CT: Simulating arbitrary CT protocols from a single dual-energy scan

C Feng[1], A Wang[2,3], NJ Pelc[1,2,3]
Departments of [1]Bioengineering, [2]Radiology, [3]Electrical Engineering, Stanford University, CA

One major goal in CT is achieving adequate visualization of relevant tissue structures at the lowest possible dose. This requires choosing an optimal imaging protocol (kVp, mAs, filtration) in addition to an optimal reconstruction kernel, which is oftentimes difficult to ascertain prospectively due to large variances in patient body structure. Accordingly, we have developed a rapid method and user interface for synthesizing CT images at arbitrary protocols using data from a single dual-energy scan to allow for simulated protocol switching and comparison.

We performed two-material decomposition on axial scans of a phantom acquired on a GE CT750 HD system at 80 kVp and at 140 kVp. By applying estimated source spectra and detector gains to the decompositions, then adjusting the final data to match the expected noise from each synthesized scan, we were able to create realistic images which were indistinguishable from the corresponding actual scans. Furthermore, using the same decomposition data, we were able to estimate dose distribution maps that were very similar to those generated by Monte Carlo simulations.

The clinical utility of our method would be greatly enhanced by rapid interactivity. This requires rapid synthesis of images corresponding to many protocols, and so our algorithms were constrained to a maximum runtime of a few seconds. We were able to accomplish this by using vector calculations and parallel processing, and a dose algorithm estimating the image pixels intersected by each incident ray using both back and forward projection.

Ultimately, our synthetic CT method allows for the rapid determination of optimal scan protocols in addition to allowing users to see how changes in protocol affect visualization. It is our hope that scanning at these optimal protocols in the future will minimize patient dose while maximizing diagnostic efficacy. Our method also allows the simulation of systems that don't yet exist, enabling a prediction of the appearance of clinical images with the new systems.

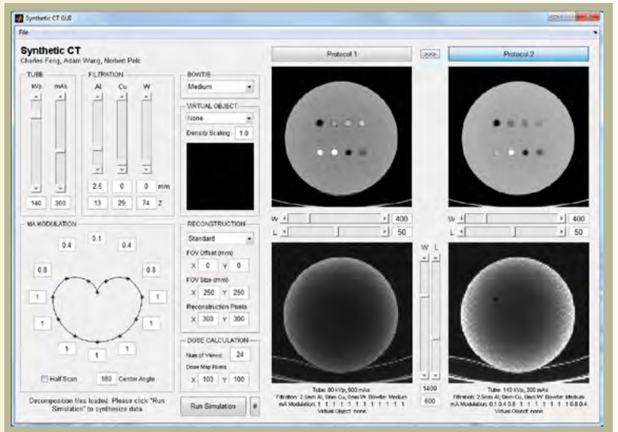

Our synthetic CT graphical user interface. The left side allows the user to select the imaging protocol and reconstruction parameters, while the right side has two simulated CT scans: an 80 kVp scan (left), and a 140 kVp scan with mA modulation applied (right). On the right side, on top are the reconstructed CT images, while on bottom are the estimated dose maps.

References/Funding Source C Feng, NJ Pelc. Synthetic CT: Simulating arbitrary CT protocols from a single dual-energy scan (in preparation). GE Healthcare, the Lucas Foundation.

Efficacy of Fixed Filtration for Rapid kVp-Switching Dual Energy X-ray Systems

Y Yao[1], AS Wang[3], NJ Pelc[1,2,3]
Departments of [1]Bioengineering, [2]Radiology, [3]Electrical Engineering, Stanford University, CA

Purpose: The dose efficiency of dual kVp imaging can be improved if the beams are filtered to increase spectral separation. Since it may not be feasible to have differential filtering for rapid kVp-switching dual energy x-ray systems, we are interested in whether a fixed added filter can improve the dose efficiency of these systems.

Methods: We hypothesized that a K-edge filter would work. Preliminary simulations were done for objects comprised of varying amounts of aluminum and water using 80/ 140 kVp x-ray spectra. The precision of the decomposition based on the propagation of the Poisson noise in the detected intensities through the decomposition function showed that lanthanide elements offer benefit. Considering availability and cost, we finally chose a commercial Gd2O2S screen as our filter for experimental validation.

To gain a more comprehensive understanding of our selected filter on different thickness objects, we made an acrylic-copper step wedge phantom with various combinations of each basis material. We used 70/125 kVp x-ray spectra during the experiment and kept the phantom exposure roughly the same with and without filtration by adjusting the tube current. The variance of the decomposition was measured and the variance reduction ratio of filtered and unfiltered beams was calculated. Simulations were performed with the same experimental settings for validation and to aid in data interpretation.

Results: Simulations showed that the variance reduction monotonically improved as the object becomes more attenuating and the spectra are more separated. The experimental result agreed with this finding, although the measured improvement was somewhat smaller than expected. At more clinical relevant thickness regions, the experiment shows a promising precision improvement with the tested filter.

Conclusions: This study demonstrates the potential of fixed Gd filtration to improve the dose efficiency and material decomposition precision for rapid kVp-switching dual energy systems.

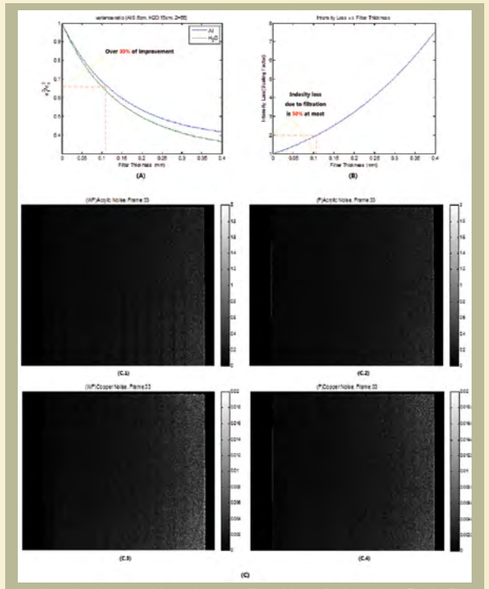

(A) Normalized decomposition variance vs. filter thickness for dysprosium (Z=66). (B) X-ray intensity loss vs. filter thickness for dysprosium (Z=66). (C) Material decomposition noise images: (C.1) Acrylic, without filtration; (C.2) Acrylic, with Gd2O2S filtration; (C.3) Copper, without filtration; (C.4) Copper, with Gd2O2S filtration.

References/Funding Source 1. NJ Pelc, "Improved dose efficiency in rapid switching dual kVp CT using a single x-ray filter," International Society for Computed Tomography: MDCT Symposia in San Francisco, 2011. 2. Y Yao, "Efficacy of Fixed Filtration for Rapid kVp-Switching Dual Energy X-ray Systems," 2011 Joint AAPM/COMP Meeting in Vancouver. 3. Y Yao, AS Wang, NJ Pelc, Efficacy of Fixed Filtration for Rapid kVp-Switching Dual Energy X-ray Systems (in preparation).

Use of sphere phantoms to measure the 3D MTF of FDK reconstructions

J Baek[1], NJ Pelc[1,2,3]
[1]Department of Radiology, RSL, [2]Bioengineering, [3]Electrical Enginnering, Stanford University, CA

To assess the resolution performance of modern CT scanners, a method to measure the 3D Modulation Transfer Function (MTF) is needed. Ideally, a point object would be used as a test phantom but this is difficult to accomplish experimentally. Recently, Thornton et al. described a method to measure the directional MTF using a sphere phantom [1]. We tested this method for cone-beam CT systems using the well-known Feldkamp (FDK) reconstruction by simulating a sphere and a point object located near the center (0.01 cm , 0.01 cm, 0.01 cm) and off center in the axial direction (0.01 cm, 0.01 cm, 10.01 cm) and compared the directional MTF estimated from the reconstructed sphere with that measured from an ideal point object. While the estimated MTF from the sphere near the isocenter showed excellent agreement with that from the point object, the estimated MTF from a sphere offset in the axial direction had significant errors, especially along the fz axis (shown in Figure 1 (a)). We found that this is caused by the long tails of the impulse response of the FDK reconstruction far off the central plane. We developed and tested a new method to estimate the directional MTF using the sphere data. As shown in Figure 1 (b), the new method showed excellent agreement with the MTF from an ideal point object. Caution should be used when applying the original method in cases where the impulse response may be wide.

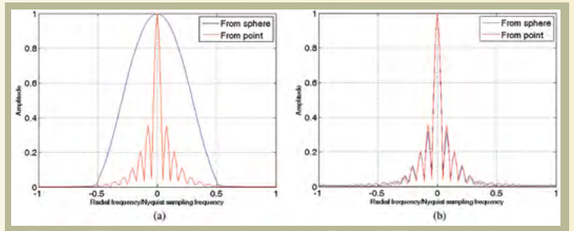

(a) Estimated MTF along fz axis using a previous method. (b) Estimated MTF along fz axis using a new method.

References/Funding Source GE Healthcare, Lucas Foundation, and NIH grant EB006837. [1] MM Thornton, MJ Flynn. "Measurement of the spatial resolution of a clinical volumetric computed tomography scanner using a sphere phantom," Medical Imaging 2006: Physics of Medical Imaging, Proc. SPIE, 6142, p. 61421Z-1 - 61421Z-10, 2006.

Comparison of dual kV and photon counting for diagnostic dual energy x-ray imaging

AS Wang[1,2], NJ Pelc[1,2,3]
Departments of [1]Electrical Engineering, [2]Radiology, RSL, [3]Bioengineering, Stanford University, CA

Dual energy x-ray and CT imaging enable the decomposition of an object into two basis materials. In addition to allowing material specific images, dual energy imaging can allow for contrast enhancement or material subtraction, which can be useful for clinical diagnoses. Dual energy imaging requires measuring the attenuation of the object with at least two different energies. Today's clinically available implementations use two separate exposures, at a low and high tube voltage (dual kV). Photon counting x-ray detectors (PCXDs) are an alternative technology that take advantage of an x-ray source's broad spectrum by counting the number of transmitted photons at each energy from a single exposure. The richness of the information contained in these measurements can depend heavily on the detector's energy resolution and count rate. Therefore, we seek to compare the material decomposition precision of dual kV with energy integrating detectors to that of realistic PCXDs.

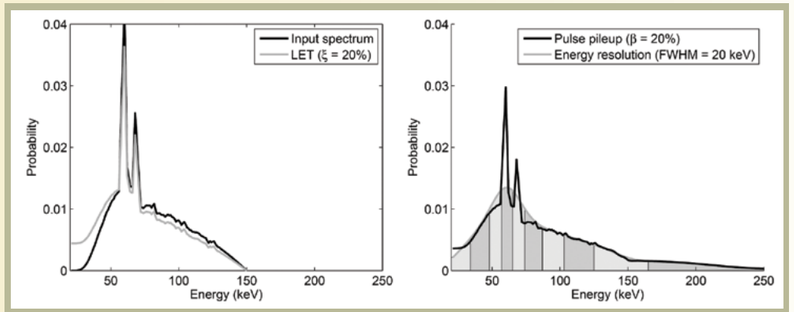

On the left, a 150 kVp spectrum is incident on a PCXD, where it is degraded by low energy spectrum tailing (LET). The spectrum then suffers from pulse pileup (right), before the electronics cause a finite energy resolution during readout. The alternating shaded regions indicate the final output counts into 10 bins.

We study the three primary effects that degrade PCXD performance: count rate limitations, energy resolution, and spectrum tailing. The high flux rates required for clinical imaging pose a serious challenge for PCXDs, which suffer from count rate losses and pulse pileup if they cannot operate as fast as the transmitted flux. Smaller pixels can reduce the flux per pixel, but increase the effect of charge sharing and cross-talk, which increases spectrum tailing. Given these constraints, we found that a well-optimized dual kV protocol performs on par with today's PCXDs. For dual kV protocols, it is important to increase the energy separation between the spectra by increasing the kV separation and adding filtration. For PCXDs, we found it most important to increase the detector's count rate capability and reduce the spectrum tailing. In conclusion, material decomposition precision can be further improved by either increasing the tube load for dual kV or by using more ideal PCXDs.

References/Funding Source AS Wang, NJ Pelc. "A comparison of dual energy x-ray imaging between dual kVp energy integrating and energy discriminating photon counting detectors," in preparation. GE Healthcare and The Lucas Foundation.

A piecewise-linear dynamic bowtie filter for photon-counting detectors

SS Hsieh, NJ Pelc
Department of Radiology, Stanford University, CA

The bowtie filter in computed tomography systems shapes the intensity distribution across the fan beam of the x-ray beam incident on the patient. Rays that are expected to be highly attenuated by the patient are minimally attenuated by the bowtie, and vice versa, so that ideally the total attenuation for any ray would be as close to constant as possible. This serves to minimize the dynamic range on the detector, to increase the radiation dose efficiency, and to improve image quality by decreasing the harmful effects of scatter. While traditional bowtie filters are helpful, they are designed for a nominal circularly symmetric object and cannot adapt to a specific patient. This limits the achievable dynamic range reduction. We developed a concept that could lead to a dynamic bowtie filter that can morph throughout the course of the scan. It produces a different piecewise-linear attenuation profile at any given time thereby achieving a much larger reduction in dynamic range. This additional reduction of dynamic range would be especially welcome in enabling photon-counting detectors. Photon-counting detectors have recently emerged as a potential technology for lowering radiation dose, providing spectral information, and eliminating electronic noise. However, these detectors do not function well when the dynamic range is large due to count rate limitations. Initial studies suggest that the dynamic bowtie is able to reduce the dynamic range beyond that of a conventional bowtie by a factor of five or more depending on the body section studied. Thus, the dynamic bowtie could lead to a relatively simple approach to significantly improve the performance of CT systems.

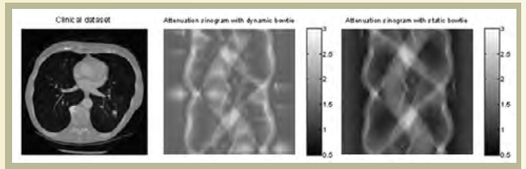

Orders of magnitude of attenuation for an example clinical dataset using both the dynamic bowtie and the traditional bowtie. The system with the static bowtie has a dynamic range of 59.3, whereas the dynamic bowtie is able to reduce the dynamic range to 11.8, which translates to a fivefold reduction.

References/Funding Source NDSEG Fellowship, NIH Grant R01EB006837

Early Diagnosis of Pancreatitis in Swine Pilot Study

R Fahrig[1], G Hwang[1], R Hofmann[1] , G Glazer[1], T Moore[2], K Blum[1]
[1]Dept of Radiology, Stanford University, CA; [2]Dept of Comptuer Science, Siemens AG, Healthcare Sector, Forchheim, Germany

Pancreatic Cancer is among the deadliest forms of cancer, accounting for the fourth lowest survival rate in individuals affected in the United States. A minimally invasive procedure for the possible depletion of pancreatic cancer is controlled tissue ablation within the region of cancerous cells. In particular, Irreversible Electroporation has been successfully demonstrated as a method for non-thermal controlled tissue ablation within the pancreas of swine. However, while successful in the induction of cellular death within well-defined regions of pancreatic tissue, a potential limitation of controlled tissue ablation is the effect on the entity of the pancreas, beyond the focal region. More specifically, alternative methods of controlled tissue ablation--such as injection of ethanol within the pancreas of swine-- have been associated with complications of pancreatitis signaled by an elevation in levels of serum amylase and lipase.

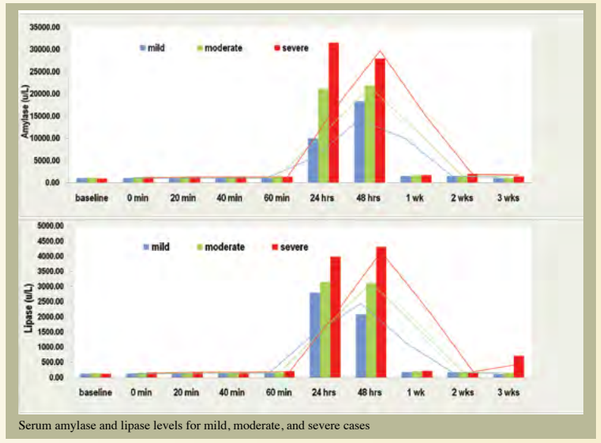

Serum amylase and lipase levels for mild, moderate, and severe cases

We hypothesize that an increase in the concentration of enzymes or other blood markers could be used as an early marker for pancreatic stress, and therefore could provide a stopping criteria for therapeutic ablation. Specifically, our aim is to evaluate blood serum levels with respect to different stages of pancreatic ablation, in order to investigate Irreversible Electroporation as a possible therapy for pancreatic cancer.

Under institutional approval, Irreversible Electroporation was performed within the tail of the pancreas across 3 Yorkshire pigs mean weight: (43.4 kg +2.3 kg).Using C-Arm CT imaging and Ultrasound guidance, 1 lesion (1.0x1.5x1.0 +1 cm) was created within the mild case, 3 lesions (1.0x 1.0x 1.0 + 1 cm) within the moderate case, and 3 lesions (0.5x 0.5x 0.5 + 0.5 cm) within the severe case. Throughout each case, serum was obtained in accordance with the following design: prior to the creation of each lesion (for baseline measurements), immediately following the creation of each lesion, 20 minutes, 40 minutes, and 60 minutes following the creation of the final lesion. As displayed within the corresponding graphs, levels of serum amylase and lipase were sharply elevated at 24 and 48 hours, and normalized by day 7 in all three cases.

References/Funding Source 1. Jernal, et al. CA Cancer J Clin. 2010 Sep-Oct; 60 (5):277-300. Epub 2010 Jul 7. 2. K Charpentier, et al. Irreversible electroporation of the pancreas in swine: a pilot study. HPB: Journal of the International Hepato Pancreato Biliary Association 2010, 12, 348–351 3. Aslanian, H, et al. EUS-guided ethanol injection of normal porcine pancreas: a pilot study. Gastrointestinal Endoscopy.2005; 62:723-7) Siemens AG, Healthcare, Germany. and the Lucas Foundation

Realistic Monte Carlo based simulation of mega voltage computed tomography detectors

D Constantin[1], J Star-Lack[2], R Fahrig[1]
[1]Department of Radiology, Stanford University, CA; [2]Varian Medical Systems, Palo Alto, CA

It is possible to greatly reduce the incidence of metal artifacts produced in kV-CT images by using megavoltage (MV) photons that penetrate high-Z objects with much less differential absorption than kilovoltage (kV) photons, thus providing a measurable signal. In this sense we propose to develop a greatly improved MV CT detector with high spatial resolution and very high detective quantum efficiency (DQE) that can be integrated with the Electronic Portal Imaging Device (EPID) on a radiotherapy system, to selectively compensate for missing projections and/or rays in images provided by Planning CT or by the on-board kV cone beam CT (CBCT).

The main hypothesis is that the combination of kV-CT imaging with limited MV-CT data acquisition, can largely eliminate the severe image and treatment planning artifacts caused by high-Z objects that are frequently encountered in patients, using a cost effective and low added dose approach, based on a novel, high DQE, thin strip of focused scintillator integrated on a standard EPID.

Schematic view of a single scintillating crystal with optical photons trajectories (Geant4)

The first step in developing an MV-CT detector was to model different scintillator materials (BGO, CaWO4, CsI) and inter-septa materials (white plastic or Vikuity ESR) for a 6 MV spectrum. In this sense we have used existing experimental data for BGO and CsI crystals and we have simulated the active matrixes flat-panel imagers using the Geant4 toolkit. We have determined that the agreement between experimental data, e.g. the presampled modulation transfer function (MTF) or the optical Swank noise factor, is below 2%.

We had to modify the Geant4 toolkit to permit optical photons to cross the inter-septa material thus increasing the optical cross-talk between neighboring pixels. This allowed us to calibrate the optical Monte Carlo based simulations against experimental data, thus providing realistic models for future optimization studies.

References/Funding Source This work was supported in part by NIH Grant T32-CA09695, the Stanford-Varian grant R01CA138426, and the Lucas Foundation

Advanced X-Ray and Computed Tomography (CT) Techniques

Robotic linac adaptation (RLA) with a novel electron gun design for the in-line MRI-linac configuration

D Constantin[1], L Holloway[2] , PJ Keall[3] , R Fahrig[1]
[1]Department of Radiology, Stanford University, CA; [2]Liverpool and Macarthur Cancer Therapy Centres, Liverpool, NSW, AU; [3]University of Sydney, Sydney, NSW, AU

The emergence of MRI based guidance systems in radiation therapy has the potential for real-time volumetric imaging and targeting. This work investigates a continuous delivery technique for an in-line MRI-linac system with a non-MR-shielded linac. Similar to the CyberKnife™ system the linac tracks the tumour motion and adapts its orientation in the fringe field of the magnet.

An electron gun model resembling a plane capacitor is proposed to function with an unmodified Varian 600C linac. Space charge and electron transport simulations were used to characterize the electron gun-linac system in the fringe field of a 0.5T open bore MRI scanner (GE Signa SP) at 0.18T. The assembly was displaced off the axis of symmetry and moved along the magnetic field lines to account for tumour motion and the beam characteristics of the systems were determined.

The minimum transverse rms emittance of the beam is ~6.4 π-mm-mrad 4.4mm away from the electron gun cathode with a current of 360mA. This compares favourably with the performance of a standard Pierce-type gun placed at the same location in the magnet, which demonstrates significant reduction of current and/or emittance as high as 25 π-mm-mrad. We show that the linac can be displaced off axis with minimal reduction in capture efficiency while maintaining low emittance if the linac is aligned with the field lines. The linac capture efficiency, the beam current at the gun exit, and the beam current at the linac exit were computed within the domain of linac motion.

A specially designed electron gun-linac assembly can function in the fringe field of a MRI magnet for various relative orientations of the linac with respect to the MR scanner. This technique allows the linac to simultaneously deliver dose and continuously track and adapt its position based on tumour motion.

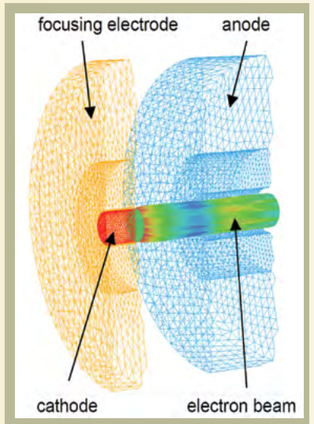

Modified electron gun geometry with simulated electron beam trajectories at 0.18T magnetic field.

References/Funding Source D. Constantin, P. Keall and R. Fahrig. "Robotic linac adaptation (RLA) with a novel electron gun design for the in-line MRI-linac configuration", Med. Phys., 38, 2011. This work was supported in part by NIH Grant T32-CA09695 and the Lucas Foundation.

Quantifying the size of a myocardial infarction during an interventional procedure using cardiac C-arm CT imaging

E Girard[1], A Al-Ahmad[2], D Lee[2], F Chan[3], J Rosenberg[3], R Luong[4], T Moore[5], G Lauritsch[6], J Boese[6], R Fahrig[3]
Departments of [1]Bioengineering, [2]Cardiovascular Medicine, [3]Radiology, [4]Comparative Medicine, Stanford University, CA; [5]Siemens Medical Solutions Incorporation, Malvern, PA; [6]Siemens AG Healthcare Sector, Forchheim, Germany

Cardiac C-arm CT is a valuable imaging modality that can provide three-dimensional images of the heart during an interventional procedure. As the technology advances to provide better image quality and faster acquisition times, the potential clinical uses increase. The size and extent of infarcted tissue after an acute myocardial infarction(MI) (heart attack) could furnish early prognostic information for risk stratification and predict functional recovery.

In 12 swine, a coronary artery was occluded with an angioplasty balloon for 60 minutes to create a model of reperfused MI. Iodine contrast-enhanced C-arm CT imaging was performed the day of infarct creation (acute, n=6) or 4 weeks after infarct creation (subacute, n = 6) and the volume of the infarct was compared against pathology to validate the visualization of infarction. Acute MI is best visualized at 1 minute after contrast injection as a region of combined hyper- and hypoenhancement (mean ± 95% confidence interval: hyperenhancement 36 ± 22 HU; hypoenhancement -65 ± 38 HU) whereas subacute MI appears as a region of hyperenhancement with peak contrast enhancement at 5 minutes post contrast injection (47 ± 14 HU). C-arm CT infarct volumes compared well with TTC staining (acute: range 4.0 – 25.0 cm3, mean 13.1 cm3, mean difference -0.5 cm3; subacute: range 6.2 – 13.4 cm3, mean 9.0 cm3, mean difference -0.7cm3).

In conclusion, cardiac C-arm CT has been established as a consistent and reliable technique for imaging myocardial infarction in the interventional suite. This imaging technique has immediate clinical value providing early information for prognosis and risk stratification. In the future, 3D images of MI could be used for guidance of stem cell and regenerative therapies as well as during the guidance of ablation therapies for ventricular arrhythmias.

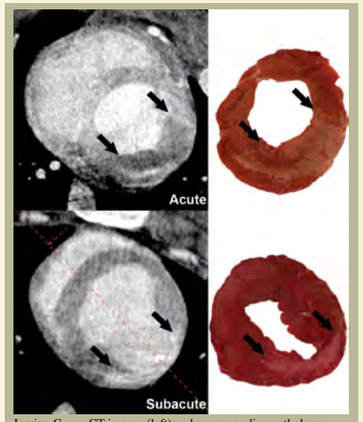

In vivo C-arm CT images (left) and corresponding pathology images (right) of a myocardial infarction (black arrows) in the left ventricle. C-arm CT images of acute MI (top) are characterized by hypo- and hyper-enhanced regions whereas subacute MI (bottom) is hyperenhanced.

References/Funding Source NIH grant R01 HL087917 and EB003524, Siemens Healthcare (Forchheim Germany), Medtron AG (Saarbruecken, Germany), Lucas Foundation.

C-arm cone-beam CT for liver perfusion imaging

A Ganguly[1], A Fieselmann[2,3], Y Duerling-Zen[2], J Boese[2], N Kothari[1], T Moore[2], K Blum[1], R Fahrig[1]
[1]Dept of Radiology, Stanford University, CA; [2]Siemens AG, Healthcare Sector, Forchheim, Germany, Dept of Computer Science, [3]Erlangen Graduate School in Advanced Optical Technologies (SAOT), Friedrich-Alexander University Erlangen-Nuremberg, Germany

Perfusion CT (PCT) imaging of the liver can be a useful tool in the diagnosis and treatment of hepatic carcinoma1. Availability of intra-procedural PCT imaging can provide valuable information regarding procedural progress and end point determination. Most commonly image-guided interventional treatments use fluoroscopic and angiographic images obtained from C-arm based x-ray systems. Recent systems are also capable of providing cone-beam CT (CBCT) images. However the rotation speed of such systems is slow (~4s) compared to clinical CT (~0.5s). This makes PCT imaging with a C-arm CBCT systems difficult. We have tested a recently reported technique2 for imaging following injection of a constant bolus of iodinated contrast and have obtained liver perfusion blood volume (PBV) maps from corresponding CBCT data.

Four anesthetized pigs (52.75±5.27 kg) were imaged using a C-arm CBCT system (Axiom Artis dTA and DynaCT, Siemens AG). The C-arm rotates in 4.3s with 1.25s for turn-around. We used an 8s mask run followed by a continuous injection of iodinated contrast (Omnipaque, GE Healthcare) for 14s at 3ml/s during which the C-arm rewinds and then scans for the 8s. A baseline scan of the liver was first obtained in all 4 animals. In 3 of the animals, the left lobe of the liver was embolized using 200-400m Embospheres™ (Biosphere Medical, UT).

Figure 1 shows the PBV map for the baseline and post embolization of the left lobe. The changes in the left lobe perfusion values are fairly consistent at 91.6±0.7% while the average right lobe value change is 29.5±33.1%. Obtaining liver PBV maps appears feasible using a C-arm CT system. Ongoing studies involve further optimization of the injection and scanning parameters as well as perfusion flow measurements.

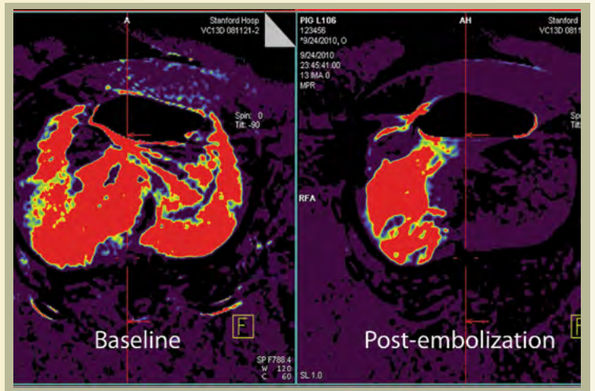

Liver perfusion blood volume maps of the liver pre and post embolization of the left lobe.

References/Funding Source 1. KA Miles. "Perfusion CT for the assessment of tumour vascularity: which protocol?", BJR, 76 (2003), S36–S42. 2. AS Ahmed, et al, "C-Arm CT Measurement of Cerebral Blood Volume: An Experimental Study in Canines", AJNR 30:917–22, 2009. K99 EB007676-01A2 and research grant from Siemens AG, Healthcare, Germany and the Lucas Foundation.

3D Knee Geometry under Weight-Bearing Conditions using a C-Arm CT Scanner

J-H Choi[3], A Keil[1], A Maier[1], C Niebler[6], M Sarmiento[7], A Fieselmann[6], S Pal[5], T Besier[7], GE Gold[1], S Delp[2,3,4], R Fahrig[1,2]
Departments of [1]Radiology, [2]Bioengineering, [3]Mechanical Engineering, [4]Orthopaedic Surgery, [5]Computational Biomechanics Lab, Stanford University, CA; [6]University of Erlangen-Nuremberg, [7]Siemens AG, Healthcare Division, Forchheim, Germany; [7]Auckland Bioengineering Institute, The University of Auckland, Auckland, New Zealand

Recent developments in C-Arm CT provide a promising technique to characterize the knee joint under loaded conditions. We were able to acquire data in a horizontal scan plane for the first time using our C-Arm system. The remaining challenge is compensation for the involuntary tremor of the standing subject during a weight-bearing acquisition. We constructed the 4D Digital Extended Cardiac-Torso (XCAT)-based knee model, and controlled it to behave as a human patient does. Computationally efficient methods for generating 2D projections and volume reconstruction are presented.

We used an 8-camera optical tracking system to capture 9 volunteers' motion at a rate of 120 Hz while standing with 60 degree of knee flexion. We scaled and transformed the knee model to a subject so that its motion with a 6 DOF subject-specific knee joint was synthesized to the subject. The model was tessellated to triangles and 191 projections were generated based on ray casting. Reconstruction was performed using filtered back projection accelerated using graphics hardware.

Average motion of 2.4 mm (+/- 1.6 mm) was seen at both knees which is about 7 times larger than the detector resolution in 2×2 binning (0.316 mm pixel size). As a comparison, the left leg volumes with and without a subject's tremor were reconstructed. The motion corrupted volume's deviation from the static volume, defined as the root mean square deviation normalized to the mean of each voxel value, is calculated as 41.1%.

From the study, we can estimate potential motion artifacts before actually scanning a human patient. We expect artifacts in reconstructions to be significant for squat positions if no motion correction is applied; the effect will be even worse in patients with knee pain. Recently, we developed marker-based motion correction algorithm which effectively reduces motion artifacts.

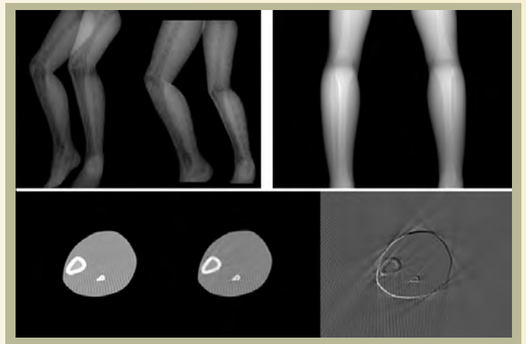

(Top) Left: The XCAT-based lower body model were scaled and transformed based on the positions of VICON markers. Right: The first 2D projection. The model was forward-projected and 191 projections were generated. (Bottom) The 2D projections were backward-projected and a 512×512×512 volume was reconstructed. Left: the central slice of the left leg volume image. Middle: the center slice of the left leg volume image motion-corrupted. Right: the difference between the left and middle images.

References/Funding Source This work was supported by National Institute of Health (NIH, grant 1R01HL087917), by Siemens Health Care, and by the Lucas Foundation.

Adapted Iterative Methods for Specialized Cone Beam Reconstructions

A Keil[1], J Star-Lack[2], R Fahrig[1]
[1]Department of Radiology, RSL, Stanford University, CA; [2]Varian Medical Systems, Mountain View, CA

Modern radiotherapy systems rely on the accurate delineation of lesions and critical structures in diagnostic CT images for generating an optimized treatment plan. But the segmentation of these anatomical structures is hampered by reconstruction artifacts. One of the most severe of these artifacts is streaking caused by "photon starvation", i.e., metal implants attenuating almost all of the incident X-ray photons. This problem is especially relevant in neurology applications in the presence of tooth fillings and for the pelvic region in the case of hip implants. Since this highly non-linear attenuation process is not modeled in standard filtered back projection algorithms, the resulting images are reconstructed based on false assumptions, resulting in the aforementioned streaking artifacts.

Several methods have been proposed to iteratively cope with these artifacts (mostly by interpolating the missing projection data). But the underlying problem of not having reliable data along rays intersecting high-density material cannot be solved without additional measurements for obtaining better attenuation statistics.

Luckily, such measurements are available in modern radiotherapy systems offering to capture images from the high-energy treatment beam. The MeV treatment photons easier penetrate high-density objects thus generating valuable measurement data where the low-voltage diagnostic photons are blocked. The downside of reconstructions purely based on MV photon data is the lower soft tissue contrast resolution. A combination of both input data therefore has the potential to yield reconstructions with improved, artifact-less reconstructions. This should result in better treatment plans with a better effective dose rate and thus improved treatment outcome for cancer patients with metal implants.

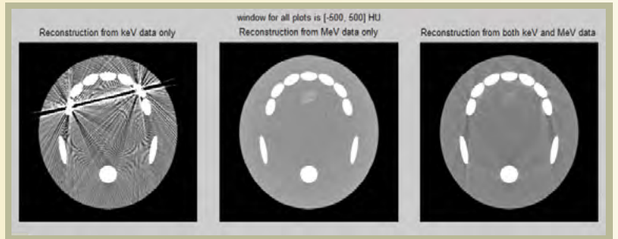

Reconstruction from low and high energy photon data as well as a combination thereof.

Among the questions to be addressed over the course of this project are an optimization of the MV detector, different approaches of combining the two input data sets, and a better modeling of the physical processes during the image acquisition. Preliminary results already show that a combination of kV and MV data results in drastically reduced artifacts but image quality heavily depends on the spectrum of high-energy photons from the treatment head.

References/Funding Source NIH grant no. 1R01CA138426-01A1 and the Lucas Foundation

X-ray tube cathode design for operation in the magnetic field of an MR imaging system

P Lillaney[1,2], R Fahrig[1]
Departments of [1]Radiology, [2]Bioengineering, Stanford University, CA

The purpose of this study is to evaluate the effectiveness of electrostatic mechanisms for controlling electron trajectories in X-ray tubes operating in the fringe field of an MR bore, and to determine a cathode design to implement the correction mechanism while not compromising normal X-ray tube operation.

Using a combination of theoretical calculations and high voltage vacuum standoff constraints, a cathode design is derived that is practical for standard X-ray tube geometry. The crucial part of the design consists of two voltage-biased deflection electrodes placed adjacent to the cathode. Space charge beam simulations are performed for the design to determine current density changes and beam deflection in the presence of a magnetic field. Phase space information from the beam simulation is input into a Monte Carlo engine to determine the effect of the cathode design on the X-ray photon energy spectrum.

For a 0.07T magnetic field, a 120 kV cathode-anode potential, a 14.4 mm cathode-anode separation distance, and a 35 kV electrode bias potential, the deflection of the X-ray tube focal spot is within 2 mm of the original position with slight distortions to focal spot shape. However, the increased curvature of the electron trajectories results in a tangential velocity 10 times larger than the control case. The electron velocity changes coupled with slightly lower current density on the anode reduces the total number of photons generated by 7.5% without significantly altering the energy spectrum of the X-ray photons.

In conclusion, the electron beam simulations demonstrate that focal spot deflection can be controlled to within reasonable values. The generated spectrum is not significantly different from that of a standard X-ray tube, with only a moderate decrease in overall photon fluence. Work is underway to evaluate the cathode design in an experimental setting.

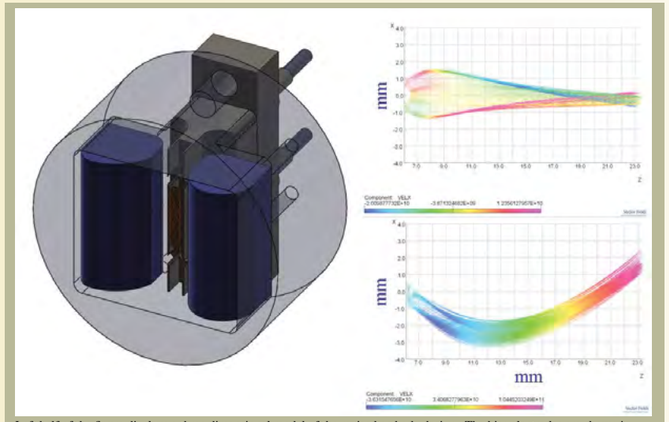

Left half of the figure displays a three dimensional model of the revised cathode design. The bias electrodes are shown in blue with the filament positioned in between. The electrodes are held in position by a ceramic backing. Right half of the figure displays two sets of simulated electron trajectories. The top is the control simulation, while the bottom is the simulation with a 0.07T magnetic field and a 35 kV electrode bias potential.

References/Funding Source NIH R01 EB 007627, Bio-X Fellowship, Lucas foundation

Modal analysis of both conventional and modified MR compatible x-ray tubes

M Shin[1,2], R Fahrig[1]
Departments of [1]Radiology, RSL, [2]Mechanical Engineering, Stanford University, CA

A rotating anode x-ray tube design consisting of a 3-phase MR compatible motor was developed and the mechanical resonance frequencies of the structure were analyzed. Qualitatively speaking, it is better to have a higher fundamental resonance frequency, since it allows for a larger range in stable rotation speeds.

Based on our finite-element analysis it was determined that a conventional x-ray tube has a fundamental resonance frequency of 87.75Hz (5265rpm); which agrees with literature values. While the conventional tube is mostly made out of steel, our new x-ray tube is mainly composed of ceramic (MACOR). Overall diameters of the structures are also different: 1.47 in for the conventional tube and 2.9 in for the new tube design. Our new rotating anode x-ray tube design has a resonance frequency of 40.76Hz (2445.6rpm). Since we plan to operate the tube at speeds higher than 2500 rpm we must revise the design in order to increase the fundamental resonance frequency. We can change several factors such as cross-sectional area, stress concentration, and distribution of materials. An improved design with a larger anode shaft and chamfers yields a resonance frequency of 57.14Hz (3428.4rpm).

Based on FEA thermal analysis, we know that a larger diameter of the anode shaft conducts more heat from the anode to the other parts of the structure. When the anode reaches steady state, the highest temperature of the rotor is about 100°C. The resultant temperature needs to be decreased to reduce mechanical stress on the brittle ceramic material. Future work will focus on balancing the resonant frequency and temperature trade-off.

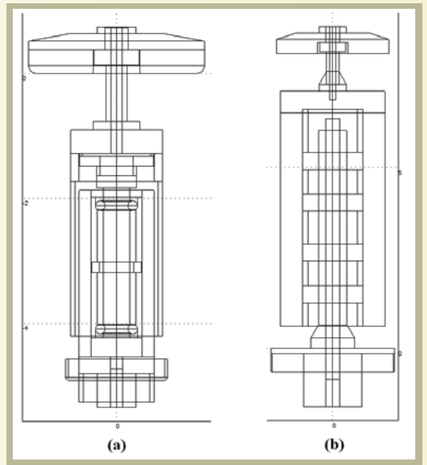

Modal analysis for x-ray tubes. (a) 2D view of COMSOL 3D model for a conventional x-ray tube, (b) 2D view of COMSOL 3D model for an improved 3-phase MR compatible x-ray tube.

References/Funding Source NIHR01 EB 007627 and the Lucas Foundation

Image Analysis, Bioinformatics, and Computational Modeling

In this section, you will read about innovations in display and interaction, feature extraction, and computer simulation and modeling techniques. These projects aim to improve the accuracy and efficiency of human interpretation of medical imagery, as well as predict patient prognosis, the molecular subtypes of their disease, and their response to treatment options in a way that is highly personalized for each patient. These efforts share the common goal of developing decision-making tools that assist with patient diagnosis, treatment, and disease monitoring.

Topological analysis of ARACNE networks on Acute Myeloid Leukemia data

A Babu[1], G Carlsson[2], A Gentles[3], S Plevritis[3]
[1]Institute for Computational and Mathematical Engineering, Departments of [2]Mathematics, [3]Radiology, Stanford University, CA.

We analyze the structure of gene interaction networks using the MAPPER algorithm. MAPPER visualizes large, high-dimensional geometric objects as small networks(graphs) that capture the overall structure of the original object. The visualization is done with respect to a certain orientation of the geometric object (i.e. a height function). Different orientations of the object reveal different structural information. We apply MAPPER to visualize gene expression (ARACNE) networks after first converting them into geometric objects via a kernel embedding technique.

This process summarizes the original network by collapsing all the non-hub genes into a single node in the summary network. Hub genes are collapsed into sets of 'nearby' hub genes, each set being represented by a node. The hub-ness or the centrality of a gene is not determined solely by the number of genes connected to it(degree), but also by the centrality of the nodes it connects to. The summary network retains the information about the interrelationship (the network connectivity structure) between the hub genes, which is the high-level topology of the original network.

The above process being run on three AML public gene expression datasets, generated by Metzeler et al., Tomasson et al. and Wouters et al., reveals common structure and some differences. Five sets of hub genes that repeatedly occur across these datasets were identified. While not all five sets occur in every dataset, the genes that make up each set are well-preserved and have well-defined & relevant biological function (e.g. erythrocyte homeostasis). It is also observed that each set of hub genes has the same z-score across its constituent genes, further highlighting the significance of these sets. The interconnectivity between the hubs is simple and is preserved across datasets. Currently we are attempting to combine the above analysis with the notion of intramodular hub genes, which are of high biological significance.

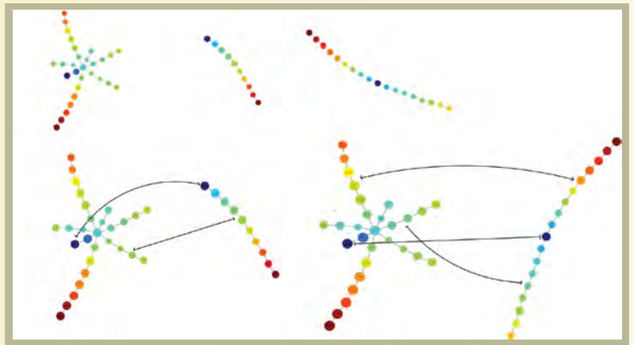

First row: Summary networks for the Metzeler et al., Tomasson et al. and Wouters et al. AML gene expression datasets (left to right). The individual flares are sets of hub genes. Metzeler et al. has five such sets, Tomasson et al. one and Wouters et al. two. The dark blue node in each summary network represents all the collapsed non-hub genes. Second row: Correspondences between the summary networks; first Metzeler et al. vs. Tomasson et al., second Metzeler et al. vs. Wouters et al. The dark blue node is essentially the same across the networks this correspondence is indicated by an arrow between the dark blue nodes. The other arrows show the correspondences between the sets of hub genes.

References/Funding Source We gratefully acknowledge funding from the NCI/NIH (U54 CA149145).

Simulation modeling of the impact of prophylactic surgery on life expectancy in BRCA1/2 mutation carriers

DF Munoz[1], BM Sigal[1], AW Kurian[2,3], SK Plevritis[1]
Departments of [1]Radiology, [2]Health Research and Policy, [3]Medicine, Stanford University, CA

Women with BRCA1/2 mutations cancer susceptibility genes are recommended a number of intensive risk-reducing strategies to manage their high risks of breast and ovarian cancer, including prophylactic surgery and screening. However, there remains significant controversy about the overall health benefits of these procedures. Building upon previous work, we report the methodology developed to build a Monte Carlo simulation model that computes the life expectancy of women at different ages, who choose to undergo prophylactic mastectomy (PM) and/or prophylactic oophorectomy (PO) immediately, or delaying the procedure 5, 10 or 15 years after their BRCA1/2 mutation is detected.

The benefits of the evaluated alternatives are measured in terms of life years gained with respect to the case in which no intervention is performed. The largest gains in life expectancy are achieved by performing PM and PO immediately after carrier status is determined; these vary according to age at carrier status determination and range between 7.3-10.7 years for BRCA1, and 3.6-4.6 years for BRCA2 carriers. Delaying prophylactic surgery can still provide valuable gains in life expectancy, which are also dependent on age of carrier status determination and choice of intervention; these gains range between 1-9.9 years for BRCA1, and 0.9-4.3 years for BRCA2 carriers. Our sensitivity analysis shows that, despite the uncertainties associated to BRCA1/2 cancer incidence and risk-reducing strategy effectiveness, prophylactic surgery provides relevant gains in life expectancy, even when the intervention is delayed after carrier status is determined.

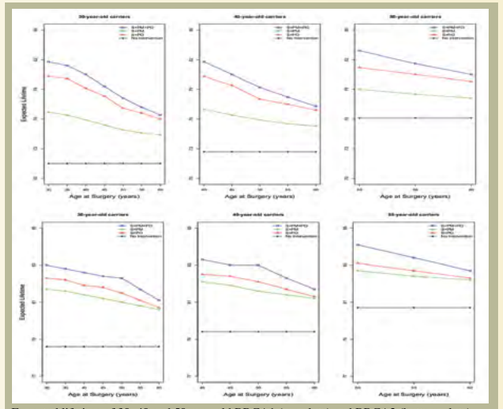

Expected lifetime of 30, 40 and 50 year-old BRCA1 (top plots) and BRCA2 (bottom plots) mutation carriers under different strategies, including prophylactic mastectomy (PM), prophylactic oophorectomy (PO) and screening with mammography and magnetic resonance imaging (S). All scenarios include screening, performed from the moment of BRCA status determination until age at PM or at age 70, whichever comes first. For all 3-carrier ages, the "No Intervention" scenario (black line with solid dots) shows the baseline expected lifetime where no intervention is pursued.

References/Funding Source We gratefully acknowledge funding from the NCI (U01CA088248).

A leukemic stem cell signature predicts outcome in Acute Myeloid Leukemia

AJ Gentles[1], SK Plevritis[1], R Majeti[2], AA Alizadeh[2]
Departments of [1]Radiology, [2]Internal Medicine, and Institute for Stem Cell Biology and Regenerative Medicine, Stanford University, CA.

In many cancers, specific subpopulations of cells appear to be uniquely capable of initiating and maintaining tumors. The strongest support for this cancer stem cell model comes from transplantation assays in immune-deficient mice indicating that human acute myeloid leukemia (AML) is organized as a cellular hierarchy driven by self-renewing leukemia stem cells (LSC). This model has significant implications for the development of novel therapies, but its clinical significance remains unclear. We defined a gene expression signature of LSC-enriched subpopulations from primary AML patient samples and xenografts, based on a functional definition in transplantation assays. Using previously published gene expression data of bulk AML from four independent cohorts totaling 1047 patients, we defined an LSC score and evaluated it for associations with known predictors of risk including cytogenetic subtype and molecular mutations, and as an independent prognostic factor. The LSC score was similar across most AML subtypes, but was lower in promyelocytic leukemia, and prognostically favorable cases harboring NPM1 or CEBPA mutations. Strikingly, high scores predicted inferior overall (OS), event-free (EFS), and relapse-free survival (RFS) in these independent cohorts, whether considering patients with a normal karyotype, or those with cytogenetic anomalies (HR range for OS 1.07-1.15, p<0.01 in all cases). In multivariate analysis, the LSC score predicted poor outcomes independently of age, FLT3 or NPM1 mutations, and cytogenetic risk group, and added to their prognostic value.

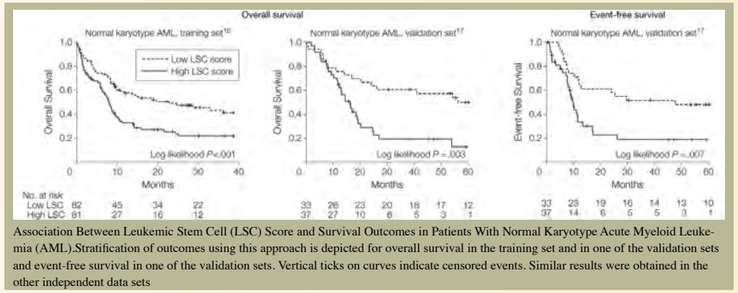

Association Between Leukemic Stem Cell (LSC) Score and Survival Outcomes in Patients With Normal Karyotype Acute Myeloid Leukemia (AML).Stratification of outcomes using this approach is depicted for overall survival in the training set and in one of the validation sets and event-free survival in one of the validation sets. Vertical ticks on curves indicate censored events. Similar results were obtained in the other independent data sets

References/Funding Source We gratefully acknowledge funding from the NCI/NIH (U54 CA149145).

Global cancer map of associations between gene expression and survival outcomes

AJ Gentles[1], S Smits[1], AA Alizadeh[2], SK Plevritis[1]
Departments of [1]Radiology, [2]Internal Medicine, and Institute for Stem Cell Biology and Regenerative Medicine, Stanford University, CA

A common use of high-throughput cancer datasets is to identify genes whose expression or mutational status is prognostic of patient survival. However, such "gene signatures" are often difficult to interpret in terms of the underlying biology. Moreover, lack of reproducibility often arises due to differences in patient populations, treatments, and technological platforms. In recent work we found that expression of a group of genes defined by their expression in purified leukemic stem cell (LSC) populations is reproducibly associated with patient survival across multiple studies in acute myeloid leukemia (AML). I will describe how meta-analysis of hundreds of public datasets can be applied to implicate which biological processes and cell sub-populations drive clinical outcomes in cancer. Both cancer-wide and cancer-specific robust patterns emerge. Induction of pluripotency and blocks in differentiation are implicated in poor outcomes across a range of malignancies. Conversely, infiltration of particular immune cell populations, and activation of specific pathways within them, predict good outcomes.

Association of gene expression levels with cancer clinical outcomes across multiple cancer datasets. Each row represents a gene, and each column a study. Red indicates that high expression of a gene is associated with poor outcome (shorter survival). Green indicates that high gene expression associates with better outcome. ALL=acute lymphocytic leukemia, AML=acute myeloid leukemia, CNS=central nervous system tumors, Mel=melanoma, Ova=ovarian cancer.

Application of this approach to AML identifies a DNA damage response that, when over-expressed in LSC, is associated with worse patient survival. The same pathway is utilized in protecting normal hematopoietic stem cells from damage induced by reactive oxygen species. This suggests that its over-expression in LSC may confer them with the ability to resist death due to therapy-induced DNA damage, leading to treatment failure and disease relapse.

References/Funding Source We gratefully acknowledge funding from the NCI/NIH (U54 CA149145).

The regulatory network of T cell acute lymphoblastic leukemia

O Gevaert[1], A Gentles[1], J Meijerinck[2], SK Plevritis[1]
[1]Department of Radiology, RSL, Stanford University, CA; [2]Department Pediatric Oncology/Hematology, ErasmusMC Hospital, Netherlands

Pediatric T cell acute lymphoblastic leukemia (T-ALL) is an aggressive hematological malignancy of thymocytes that amounts to 10-13% of all ALL cases and is often fatal without therapy. A number of genetic abnormalities have been identified that transform normal T-cells to a malignant phenotype in a mutually exclusive way. These abnormalities include translocations, duplications, deletions, amplifications and mutations that results in expression of TAL1, TAL2, LMO1, LMO2, HOXA, TLX1 or TLX3 genes which arrest T-cell differentiation at different stages of T-cell development. Microarray studies have confirmed that these abnormalities direct T-ALL to different subgroups with the same transcriptional response, e.g. TAL1, TAL2, LMO1 and LMO2 form the TALLMO group with a similar transcriptional response while HOXA, TLX1 and TLX3 form other subgroups with distinct transcriptional profiles.

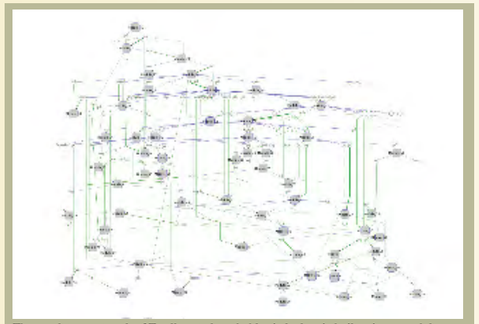

The regulatory network of T cell acute lymphoblastic leukemia built using a module network approach based on elastic net regularized linear regression.

Treatment depends heavily on the subgroups classification, therefore it is important to understand what makes these subgroups differ on a transcriptional level and which mechanisms are driving T-cells to a malignant phenotype. Currently however not much is yet known about the regulatory network that is responsible for these mutually exclusive subgroups. Much of the previous research has focused upon defining subgroups and developing classification models based on a small subset of genes to classify T-ALL patients into the subgroups.

We have used a module network approach in combination with regularized linear regression to model the transcriptional program of T-ALL. More specifically we have used a previously developed approach that uses elastic net regularized linear regression to model the regulatory program. This regularization approach allows accommodating for correlated regulators while still forcing the regulatory program to be sparse. In addition we used the same methodology to model the relationship between the modules and the genetic subgroups. We applied this method on a set of 117 patients that were profiled with microarray technology. Our results show that modules were identified related to the different subtypes of T-ALL which are regulated by T-ALL genes such as TLX1, TLX3. In addition our analysis enables us to make several hypothesis about regulatory interactions in different T-ALL subtypes and are in the process of validating them both computationally and experimentally.

References/Funding Source U54 CA149145

Evaluating the Impact of Hormone Therapy on Breast Cancer Incidence

Y Guan[1], SK Plevritis[2]
Departments of [1]Management Science and Engineering, [2]Radiology, Stanford University, CA

Postmenopausal hormone therapy (PHT) is now widely recognized as a risk factor of breast cancer, however its effect on the pathogenesis and progression of the disease is not fully understood. We hypothesize that changes in US breast cancer incidence and mortality rates following changes in PHT use may provide insights. After the release of the 2002 report of the Women's Health Initiative (WHI) trial of estrogen plus progestin, the use of PHT in the U.S. reduced remarkably. Subsequently, a reduction in breast cancer incidence was observed in the Surveillance, Epidemiology and End Results (SEER) program of the NCI for the year 2000-2005, further implicating a cause-and-effect relation between HT and breast cancer. Our study aims to quantify the effect of PHT on breast cancer incidence using a stochastic simulation model of the impact of PHT on the natural history of breast cancer. We assume that PHT only effect the progression of breast cancer and does not initiate new cancers. Under these assumptions, we estimate the relative impact of PHT use on the mean tumor volume doubling time and the median tumor size detectable on a mammogram. The estimates of PHT's effect are calculated by calibrating the predicted breast cancer incidence and mortality rates to actual rates from SEER database. We find that the discontinuation of PHT use causes a rapid drop in breast cancer incidence, consistent with the SEER data. Our preliminary results support the hypothesis that PHT use increases breast cancer incidence through accelerating tumor growth and affecting mammographic tumor detectability.

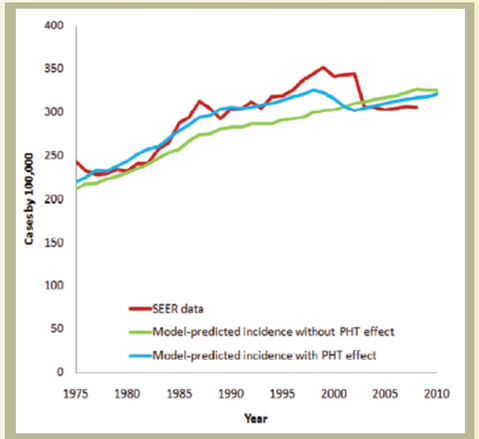

Comparison of SEER data and model-predicted age-adjusted breast cancer incidence (top panel) rates of age group 50-69, with two scenarios considered: with PHT effect and without PHT effect.

References/Funding Source We gratefully acknowledge funding from the NCI (U01CA088248).

Application of Stochastic Modeling to Simulation and Analysis of Mayo CT Lung Cancer Screening Trial

SA Erdogan, W Wan, RS Lin, EB Tsai, SK Plevritis
Department of Radiology, Stanford University, CA

Lung cancer is the leading cause of cancer-related deaths among both men and women, for which the 5-year survival rate is only 3.5%. Screening has only recently been shown to provide benefits in mortality reduction through repeated low-dose CT imaging; however, this benefit has not been fully explored in the Mayo CT lung cancer clinical trial, which lacked an unscreened control arm. We aim to simulate the results of the Mayo CT trial using a natural history model to analyze effects of CT screening on incidence and mortality.

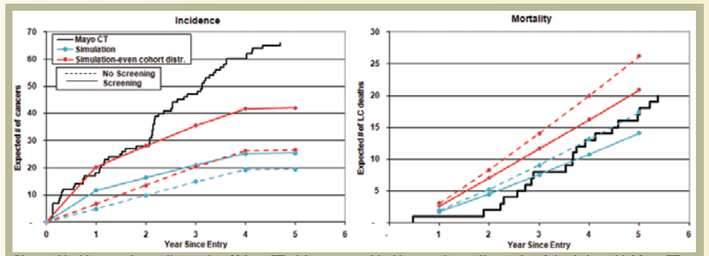

Observed incidence and mortality results of Mayo CT trial vs. expected incidence and mortality results of simulation with Mayo CT cohort distribution and compliance (blue) and even cohort distribution and perfect compliance (red), both in presence and absence of screening.

A stochastic model of the natural history of lung cancer was used to estimate the likelihood of cure as a function of tumor size. Parameters were estimated based on the Surveillance, Epidemiology and End Results (SEER) cancer registry. Results were first externally validated against the control arm of the Mayo Lung Project. For this simulation, screening, follow-up, and treatment components were implemented into the model based on published protocols matching those used in Mayo CT diagnosis and treatment.

Our simulation models show adjusted incidence rates of 26-42 cases over the 5-yr duration of the trial (compared to 68 actual cases in Mayo CT) depending on 1) age distribution of trial participants, and 2) level of adherence to scheduled screening. Annual interval screening increased detection of lung cancer by 80% and reduced 5-yr mortality by 23% compared to the simulated, unscreened cohort. Further efforts in model refinement will clarify the exact benefits and the impact of screening on overdiagnosis and false positives.

References/Funding Source U01 CA152956

TreeViz: A graphical tool for tree visualization

P Qiu, SK Plevritis
Department of Radiology, Stanford University, CA

Network-based analyses of high-dimensional biological data often produce results in the form of tree structures. Generating easily interpretable layouts to visualize these tree structures is a non-trivial task. We present a new visualization algorithm, TreeViz, to generate two-dimensional layouts for complex tree structures.

TreeViz emphasizes the longest path and major branches of a tree structure. Given the adjacency matrix of a tree structure, TreeViz first identifies the longest path, and rearranges the nodes along it into an arch-like shape. Then, the remaining nodes are ordered and sequentially appended. The ordering of the tree nodes is derived as follows: TreeViz breaks the tree into chains of nodes. The longest chain is defined as the main chain. Chains that are directly connected to the main chain are defined as the side chains . For complex tree structures, each side chain can also have its own lower level side chains. Tree nodes are arranged in an order such that nodes in the main chain come first, followed by nodes in the side chains, and then the lower level side chains.

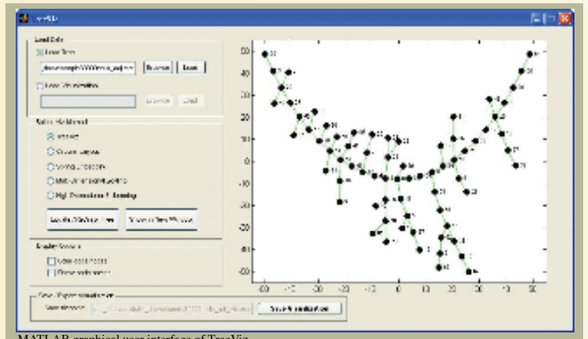

MATLAB graphical user interface of TreeViz.

After ordering the tree nodes, TreeViz rearranges nodes in the main chain on an arch-like curve, with unit distance between adjacent nodes. The remaining nodes are appended one at a time, according to the ordering defined above. Between the new node and each existing node, we assume a repelling force, which is inversely proportional to their distance. Each edge is assumed to be a string whose length is less than or equal to unit distance. Since the new node is attached to one of the nodes that are already visualized, the position of the new node is within a unit radius disk of its visualized neighbor. TreeViz exhaustively examines all positions within this unit disk, and places the new node at the position where it is under balanced forces.

References/Funding Source P Qiu, SK Plevritis. “TreeViz: A MATLAB-based Tool for Tree Visualization”, submitted to Bioinformatics. U54 CA149145

SPADE: Spanning-tree Progression Analysis of Density-normalized Events

P Qiu[1], EF Simonds[2], SC Bendall[2], K Gibbs[2], MD Linderman[3], K Sachs[2], GP Nolan[2], SK Plevritis[1]
Departments of [1]Radiology, [2]Microbiology and Immunology, [3]Computer Systems Laboratory, Stanford University, CA

Flow cytometry captures the heterogeneity of biological systems by providing multiparametric measurements of individual cells. Traditional analysis of cytometry datasets is a subjective process that requires extensive familiarity with the biological system. We present a novel computational approach, Spanning-tree Progression Analysis of Density-normalized Events (SPADE), to identify and visualize branched differentiation hierarchies in multidimensional flow data, without requiring prior knowledge about the developmental hierarchy in the data. SPADE enables several novel approaches for cytometric analysis, including merging of overlapping reagent panels and direct comparison of marker intensities across multiple datasets. We applied SPADE to conventional (8-parameter) and next-generation (31-parameter) cytometry data of mouse and human bone marrow. In both datasets, SPADE detected a differentiation heirarchy which recapitulates well-described patterns of hematopoiesis. From the conventional flow dataset, SPADE identified major cell types of mouse bone marrow, and the findings were confirmed using a traditional analysis method, namely gating (results shown in figure). By exploiting the high dimensionality of next-generation cytometry data, SPADE defined a functionally distinct cell population in human bone marrow, using subtle differences in marker expression, even in the absence of a population-specific marker. This population was then inferred to be NK cells based on additional surface markers from an automatically merged second staining panel. By reserving a set of functional markers in the tree-building step, we used SPADE to map intracellular signal activation across the landscape of human hematopoietic development. SPADE is a versatile tool for analysis of multidimensional flow cytometry, facilitating de novo discovery of developmental transitions, automated comparison of functional markers, and identification of rare or malignant cell populations.

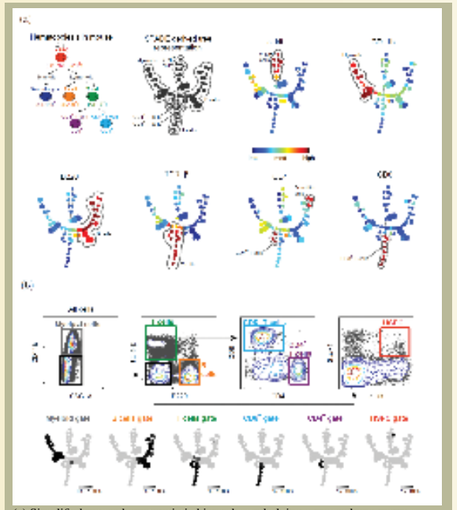

(a) Simplified mouse hematopoietic hierarchy underlying a mouse bone marrow flow dataset, and the tree structure derived by SPADE. The tree was color-coded by median intensities of one individual marker, to show how markers behave across the tree. (b) Traditional gating analysis of the mouse bone marrow data. To illustrate the concordance between SPADE and gating, for each gated population, the SPADE-derived tree was drawn, where each node was color-coded by the percentage of gated cells in that node.

References/Funding Source U54CA149145

RED-SIGN: REconstructing Directed SIgned Gene regulatory Network from microarray data

P Qiu, SK Plevritis
Department of Radiology, Stanford University, CA

Great efforts have been made to develop both algorithms that reconstruct gene regulatory networks, and systems that simulate gene networks and expression data for the purpose of benchmarking network reconstruction algorithms. An interesting observation is that although many simulation systems chose to use Hill kinetics to generate data, none of the reconstruction algorithms were developed based on the Hill kinetics. One possible explanation is that, in Hill kinetics, activation and inhibition interactions take different mathematical forms, which brings additional combinatorial complexity into the reconstruction problem.

We propose a new model that qualitatively behaves similar as the Hill kinetics, but has the same mathematical form for both activation and inhibition. Based on our new model, we tailored an algorithm RED-SIGN to reconstruct gene regulatory networks, where we can predict the directions, signs and weights of the reconstructed edges. Extensive simulations demonstrated the superior performance of RED-SIGN. Simulation results suggested that in gene knockout experiments, repressing protein synthesis to a certain extent may lead to better expression data and higher network reconstruction accuracy.

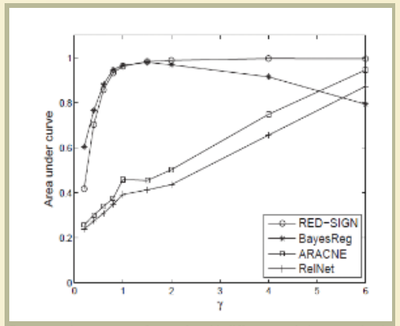

Reconstruction accuracy of networks with different regulation strength. r is inversely related to the regulation strength.

References/Funding Source U54 CA149145

Rapid identification of prognostic imaging biomarkers by leveraging public gene expression data

O Gevaert[1], J Xu[2], C Hoang[3,4], A Leung[1], Y Xu[3], A Quon[1], DL Rubin[1], S Napel[1], SK Plevritis[1]
Departments of [1]Radiology, [2]Electrical Engineering, [3]Cardiothoracic Surgery, Stanford University, CA; [4]Veteran’s Affairs Palo Alto Healthcare System, Palo Alto, CA

Personalized medicine aims to tailor medical care to an individual’s need through recognition of biological heterogeneity in patients. Current technologies however require invasive biopsies that are not necessary representative of the disease. Medical imaging is non-invasive and also gives anatomical, morphological and physiological information. We propose to harness this information by creating a radiogenomic map that associates medical imaging data with publicly available high-throughput molecular data with clinical outcome. This allows to link imaging data with clinical outcome without the need for follow-up data.

We demonstrate our approach on non-small cell lung carcinoma patients for whom CT, PET/CT and gene expression data were obtained. We extracted 149 computational features, 30 semantic features and PET-SUV from the imaging data. The microarray data was processed using an advanced clustering algorithm and 56 high quality clusters were represented using metagenes. We found several though provoking associations between imaging features and metagenes. 115 of 180 image features were predicted by a sparse regression on 56 metagenes with an accuracy of 65-86%. After mapping the predicted image features to a public gene expression dataset, we found 26 image features were significantly associated with recurrence-free survival and 22 with overall survival. A multivariate survival analysis identified prognostic image features independent of clinical covariates.

Our results show that we have developed a method that can be used as a non-invasive way for rapid prognostic assessment of imaging. This motivates investing in larger studies that collect and store medical images and tissue of the same patients in NSCLC and other diseases such that our method can be used to assess immediately the prognostic relationship of new imaging biomarkers or technologies without the need for follow-up data. Our bioinformatics strategy for identifying imaging biomarkers may be most relevant to the clinical evaluation of emerging and evolving imaging modalities, thereby promising to accelerate the translation of novel imaging technologies.

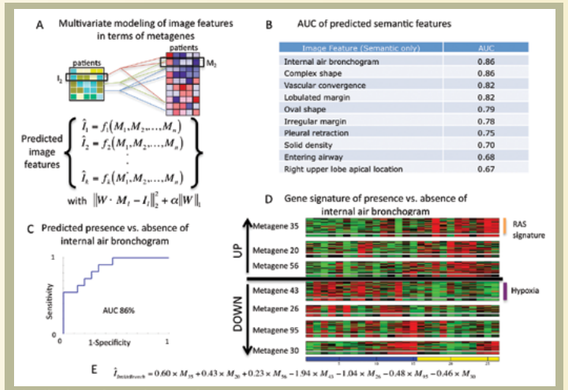

Modeling image features in terms of metagenes.
(A) Strategy for multivariate modeling of image features in terms of metagenes. Each image feature is modeled as a linear combination of metagenes using L1-regularization to induce sparsity in the number of metagenes that are selected. Ii represents the i-th image features, Mj represents the j-th metagene, fi represents linear regression for the i-th image feature, α is the regularization parameter, Wj (not shown) represents the weight for each metagene Mi, and W represents the matrix with all weights. (B) Semantic features predicted by metagenes with an AUC of 65% or greater, based on leave-one-out cross-validation (LOO-CV) analysis. AUC stands for Area Under Curve for the Receiver Operating Characteristic (ROC) curve. (C) ROC curve for the predicted presence vs. absence of internal air bronchogram on CT, when expression in terms of metagenes. (D) Multivariate metagene prediction model for the presence vs. absence of internal air bronchogram on CT. The top 7 metagenes are shown representing 95% of the weight of the multivariate model; the top 3 metagenes are up-regulated when an air bronchogram is present, and the bottom 4 metagenes are down-regulated. The down-regulated metagenes are enriched in hypoxia related pathways; the up-regulated metagenes contain a RAS signature and genes up-regulated by RAS. (E) Multivariate model for internal air bronchogram corresponding to (D). For gene expression, red represents over-expression and green represents under-expression; for image features, blue denotes absence of feature and yellow presence of image feature.

References/Funding Source O Gevaert, J Xu, C Hoang, A Leung, Y Xu, A Quon, D Rubin, S Napel, S Plevritis. Rapid identification of prognostic imaging biomarkers for non-small cell lung cancer by leveraging public gene expression microarray data. Submitted 2011. This research was supported by Information Sciences in Imaging at Stanford (ISIS), the Center for Cancer Systems Biology (CCSB) at Stanford (U54 CA149145), and GE Healthcare.

Estimating Breast Cancer Survival by ER Molecular Subtype in the Absence of Screening and Treatment

DF Munoz, SK Plevritis
Department of Radiology, Stanford University, CA

The relative contributions of screening and treatment on biomarker-specific breast cancer survival curves is not well characterized because many of the biomarkers that are of interest today were not routinely collected in the absence of screening. Estimates of breast cancer survival in the absence of screening may be found from SEER data from the years 1975 to 1979, but a limitation of this data is that biomarkers, such as ER-status, were not registered at that time. ER-status is being collected by SEER starting 1990 hence, ER-specific survival curves are confounded by screening and treatment effects. We present a modeling approach to back-calculate ER-specific survival curves in the absence of screening and treatment, then compute the relative contributions of screening and treatment on the ER-specific survival curves. Our approach makes use of a previously developed Monte Carlo simulation model that generates the life and screening histories of individual level patients, and determines ER-status by matching screening and tumor characteristics with estimates calculated from clinically observed BC patients. Running the simulation long enough provides us with a simulated database of BC patients tagged with ER-status, from where it is possible to back-calculate ER-specific survival in the absence of screening and treatment. Subsequently, these survival curves are then used to validate our model when run in the presence of screening and treatment. Knowledge of ER-specific survival curves in the absence of screening and treatment is not only valuable to determine the underlying differences between disease subtypes, but also form to fundamental inputs to models which aim to predict future US breast cancer trends with changes and advances in screening and adjuvant therapy.

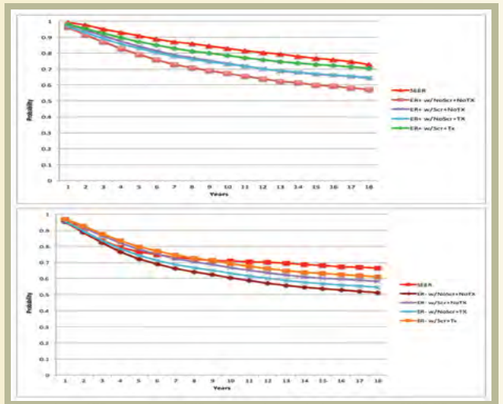

Comparison of ER+ (top plot) and ER- (bottom plot) survival curves versus SEER ER-specific survival curves from years 1990-2006. Our model's ER-specific survival curves are given under 4 different scenarios: in the absence of both screening and treatment, in the presence of screening and the absence of treatment, in the absence of screening and the presence of treatment and the presence of both screening and treatment.

References/Funding Source We gratefully acknowledge funding from the NCI (U01CA088248, U01CA152958).

A Web-based Method to Disseminate Radiology Appropriateness Criteria for Decision Support

DL Rubin[1], A Walvekar[2]
[1]Department of Radiology, Stanford University, CA; [2]The Harker School, San Jose, CA

Purpose: With the explosion in radiology imaging, there is pressing need to ensure it is ordered appropriately. Radiology appropriateness criteria are being developed, but it is challenging to ensure physicians are aware of them when ordering imaging. Our goal was to develop a Web-based mechanism to disseminate, operationalize, and evaluate radiology appropriateness criteria in clinical practice.

Method and Materials: We encoded portions of a subset of the ACR appropriateness criteria for a variety of clinical conditions in the Semantic Mediawiki (a semantic implementation of the wiki used to host Wikipedia). We created 100 clinical case scenarios for which these appropriateness criteria would guide physician practice. We matched each case to the appropriateness criteria such so that the Web application could provide decision support on exam appropriateness for each case. We recruited 4 medical residents and asked each to select the single most appropriate test for each clinical case (each resident did the task independently). Two months later the residents repeated the task on the same cases, in random order from previously, with our web-based decision support system. The rating of the appropriateness the exams they ordered was evaluated against the ACR criteria and compared with and without decision support using Student's t-test.

Results: Without decision support (baseline performance), the average resident appropriateness of exams ordered was 5.26 (SD 3.18), significantly lower than optimum ordering appropriateness by ACR criteria (mean 8.04, SD 1.68). However, the appropriateness of their ordering increased significantly with the Web-based support (mean 5.75, SD 3.21, $p < 0.03$). All residents reported that the Web-based decision support was highly intuitive to use and they reported that using it would not hinder their workflow.

Conclusion: A Web-based wik methodology facilitates electronic encoding and distribution of radiology appropriateness criteria, and resulted in significantly increased practitioner radiology order appropriateness.

Wiki-based automated decision support application shows the user the potential radiology exams that may be ordered in the given clinical context, with the appropriateness rating ("Rating") and relative radiation level ("RRL").

References/Funding Source RSNA 2011

Radiological Assessment of Cancer Lesion Response and Comparison of Alternative Metrics Using Web-based Tool

AC Abajian[1], DL Rubin[2]
[1]Department of Medicine, Yale Medical School, New Haven, CT; [2]Department of Radiology, Stanford University, CA

Background: A crucial challenge for radiologists is to determine whether cancers are responding to treatment and to be able to compare alternative measures (e.g., linear dimensions of RECIST against area/volume, etc). Our goal was to develop a tool to facilitate radiologist assessment of cancer lesions response as well as comparison of alternative quantitative tumor response metrics.

Evaluation: Our system adopts the Annotation and Image Markup (AIM) standard of caBIG. We created an XML database and a PACS database. In our paradigm, the radiologist annotates images using an AIM-compliant image viewing workstation. Our system reads the AIM files, extracts the quantitative image information, and overlays it on the corresponding images retrieved from the PACS archive (Figure). We evaluated our system in a CT imaging study of a patient who had one baseline and two follow up scans and it successfully produced an automated summary of response.

Discussion: Our system may provide a better mechanism for radiologists to evaluate temporal imaging studies in cancer patients than the current practice which lacks summarization of the quantitative measurements. Our approach provides a streamlined mechanism for radiologists to interpret oncology studies and provides researchers with a tool to identify better quantitative measures of response than RECIST.

Conclusion: We developed a system to generate a graphical summary of cancer lesion measurements from radiology images which may enhance radiology interpretation, clinician interpretability, and clinical care.

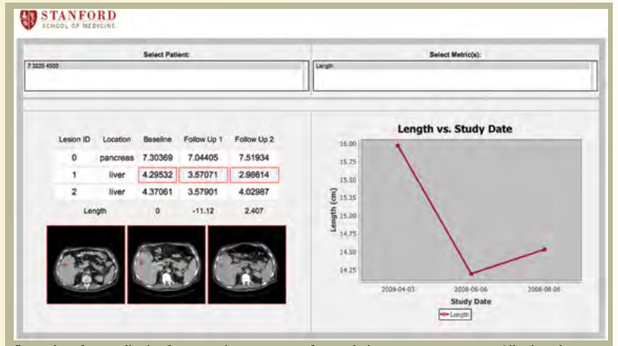

Screenshot of our application for automating assessment of cancer lesion response to treatment. All values shown are automatically generated based on query to machine-accessible semantic annotations (in AIM format) on images. The user has selected a patient and evaluation metric (top) and a table summarizing lesions and measurements is provided (left). A graph showing treatment response based on summed length is also shown (right). This type of automated display will likely greatly facilitate summarizing of large serial imaging studies and enable rapid comparison of alternative quantitative image metrics of cancer response.

References/Funding Source RSNA 2011. NCI U01 grant, U01-CA-142555

ePAD: A Cross-Platform Semantic Image Annotation Tool

DL Rubin, A Snyder
Department of Radiology, Stanford University, CA

Background: The cancer Biomedical Informatics Grid (caBIG) Annotation and Image Markup (AIM) standard can empower the radiologist by enabling image metadata access, exchange, and usage; however, AIM is generally not accessible in clinical practice since vendor adoption in clinical workstations is slow and variable. Our goal is to provide a freely-accessible method of universal radiologist access to AIM benefits in a cross-platform tool that can be integrated into all radiology workstations.

Evaluation: We have created ePAD (the electronic Physician Annotation Device), an implementation of AIM in a rich Web client architecture. ePad a freely-available tool that runs on modern Web browsers and provides semantic image annotation on any platform and within any image workstation environment, including the Apple iPAD. The ePAD tool consumes images within any image viewing workstation, it extracts the quantitative information from radiologist annotations on the images, and it and saves these image metadata in AIM. Communication of ePAD and the workstation occurs via a proxy; we are also developing vendor-specific API calls where available to make the integration even more seamless. This exhibit will show the features and operation of ePAD and potential benefits to radiologists.

Discussion: Developments in quantitative imaging are occurring rapidly, but improved radiology practice is thwarted by slow and variable vendor adoption of cutting-edge advancements. Our rich Web-based image viewing architecture enables new tools such as AIM to be executed on any platform, including vendor workstations, provided they run a Web browser. Ultimately, we foresee a paradigm where semantic image annotation and capture of machine-accessible image content via AIM will be as seamless as DICOM implementations currently provide with image data.

Conclusion: We developed a cross-platform Web-based image viewing/semantic annotation tool to enable radiologists to access the benefits of image metadata collection/exchange in clinical practice. We believe this approach will catalyze adoption and dissemination of the AIM standard and empower radiologists with the benefits of image metadata sharing and interoperability.

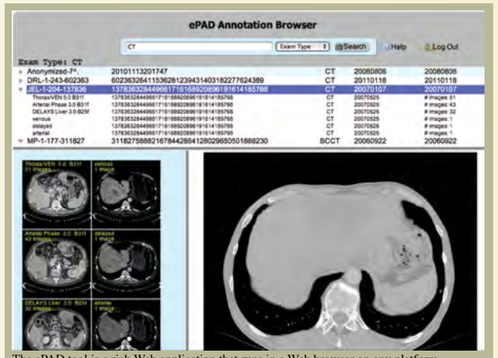

The ePAD tool is a rich Web application that runs in a Web browser on any platform. Radiologists can access, view, and annotate image obtained from their PACS, save the image metadata in the standard AIM image metadata format, and access the benefits of AIM metadata interoperability.

References/Funding Source RSNA 2011. NCI U01 grant, U01-CA-142555

Active Feature Acquisition Using Sensitivity Analysis to Classify Mammography Reports

F Gimenez[1], DL Rubin[2]
[1]Biomedical Informatics Training Program, [2]Department of Radiology, Stanford University, CA

Purpose: We present a method to automatically select a subset of BI-RADS observations for use in prediction of diagnostic codes in mammography reports. This method is optimized to rapidly converge to high classification accuracy with a small number of radiological annotations.

Method and Materials: 7,468 unilateral diagnostic mammography reports containing BI-RADS codes between 1-6 were obtained from the Stanford RADTF database. BI-RADS observations were extracted from free text reports using natural language processing techniques that account for misspellings, ambiguous term usage, and negation. There are 48 possible observations which were concatenated into a binary feature vector to indicate their presence in a report. Reports were stratified into 3 classes: Class 1 containing reports with ratings 1 and 2, Class 2 containing reports with ratings 3 and 4, and Class 3 containing reports with ratings 5 and 6. Under this categorization, classes can be interpreted as benign, abnormal, and at risk. A Naïve-Bayes classifier was trained to predict the BI-RADS diagnostic code from the feature vectors. Single features were progressively selected maximize the first-order Sobel (FOS) score of the output class. Reports were classified using this smaller subset of features.

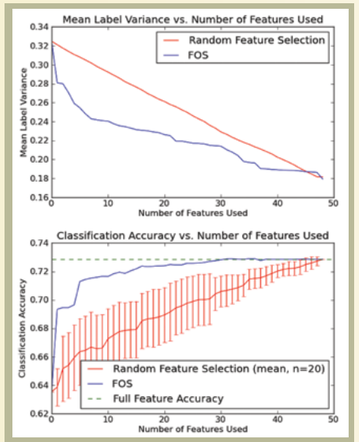

Figure A shows the reduction in Bi-Rads variance as a function of features selected. Figure B shows the convergence of classification accuracy with respect to features selected.

Results: First-order Sobel indices are meant to reduce variance in the output class rapidly. We plotted the variance with respect to the number of features selected. Results show an exponential drop in variance compared with the linear decrease of random feature selection. A signed rank confirmed that the difference was statistically significant (p=7.8E-260). We then plotted the classification accuracy with respect to features used. Once again, the plot shows the classification improving as a function of features selected.

Conclusion: We have demonstrated a method to automatically select BI-RADS observations with relation to their importance in classification accuracy. Such a method can be used to reduce workload on radiologists while ensuring unambiguous reporting.

References/Funding Source RSNA 2011. NLM Training Grant, NCI U01 grant, U01-CA-142555

Using the Semantic Web for Radiology Decision Support of Focal Liver Disease

I Djomehri, DL Rubin
Department of Radiology, Stanford University, CA

Objective: Our goal is to develop a system leveraging Semantic Web technologies to deliver knowledge to radiologists "just-in-time" as they are interpreting images to help them tackle the challenge of accessing the vast amounts of radiology knowledge. Our system may reduce variation in radiological practice by providing radiologists the knowledge they need.

Methods: We developed an ontological representation of radiological knowledge of focal liver disease diagnosis, encoding the information in two independent knowledge sources (Dahnert's textbook and STATdx from Amirsys Inc.). The model encodes diagnoses, clinical contexts, radiology image features of liver lesions, and probabilistic relationships among entities. We built a computer reasoning application that accesses this knowledge resource (ultimately to be deployed on the Semantic Web), receives input about the clinical context and image features, and outputs the most likely diagnoses and qualitative probability rankings. We evaluated the system by providing it several cases of known diagnosis.

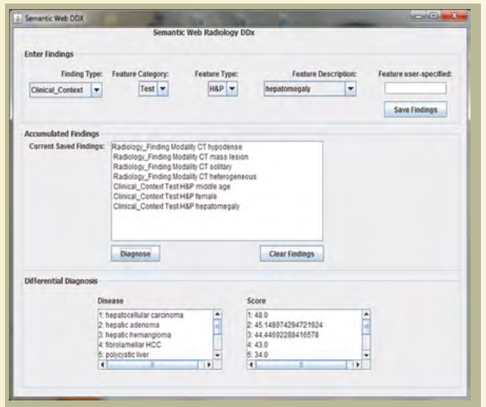

Screen-shot of decision support application showing radiologist-entered imaging findings and resulting differential diagnosis.

Results: Our ontological model of radiology successfully captured all the major pieces of information in the knowledge sources. Our decision support application generated a correct differential diagnosis based on observed imaging features in each of the test cases. We are now conducting a study to evaluate the ability of our tool to reduce variation in performance of radiologists interpreting cases of focal liver disease.

Conclusion: We have demonstrated the feasibility of encoding radiological knowledge in a human-readable, machine-accessible ontological form. We also showed the feasibility of using this knowledge to deliver decision support. Our methods may help to improve radiologist diagnostic performance.

References/Funding Source RSNA 2011. MedScholars fellowship, Department of Radiology – Stanford University

An Automated Approach to Analyzing, Reporting, and Communicating Quantitative Imaging

DL Rubin[1], A Snyder[1], M Levy[2]
[1]Department of Radiology, Stanford University, CA; [2]Department of Biomedical Informatics, Vanderbilt University, Nashville, TN

Background: A major challenge for quantitative imaging is consistent and reproducible measurement and reporting of cancer lesion measurements over serial imaging. Many different tools to improve lesion measurement and tracking have been developed, but they do not interoperate and thus have not been implemented in clinical practice. We describe an informatics framework that will permit radiologists to "plug together" the various quantitative imaging tools to provide seamless collection, reporting, and communication quantitative imaging studies, focusing on oncology, but generalizable to all of quantitative radiology.

Evaluation: We used the Annotation and Image Markup (AIM) standard of caBIG as the "glue" to tie together different components of quantitative imaging functionality into a cohesive system that automates collection, analysis, and reporting of quantitative imaging studies in cancer. In our framework, the radiologist views the images and annotates the measurable disease in an AIM-compliant workstation (perform linear measure at baseline and each follow up exam). We added a commercial system that consumes the AIM, and uses the radiologist annotations as seed points to automatically segment the lesions and derive additional quantitative measures such as volume and area. We also created an analytic application that consumes all AIM-encoded image results to provide a graphical summary of the lesions and various quantitative measures (linear dimension, area, volume) over time, providing decision support to the oncologist and a discovery platform to explore novel biomarkers to the clinical researcher.

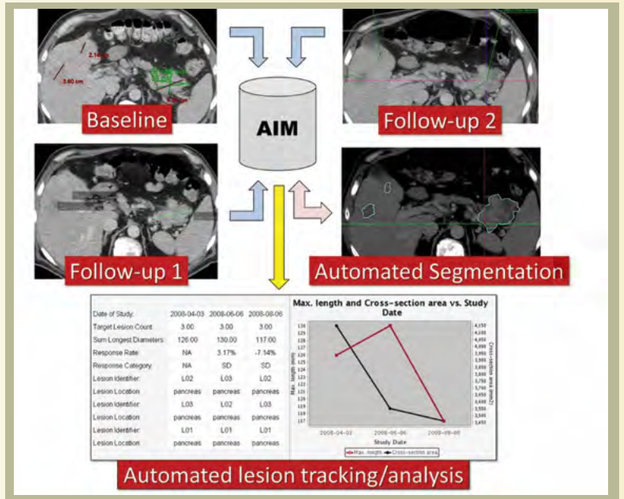

Three types of quantitative imaging components plugged together using AIM: (1) Annotation: lesions in a cancer patient were measured on 3 different AIM-compliant PACS workstations to annotate/measure lesions at each time point; (2) Segmentation: The annotations extracted from AIM provided seed points to automated segmentation routine, outputting its segmentation results in AIM; (3) Analysis/reporting: The AIM-encoded metadata from each time point was consumed and summarized by a tool providing tabular/graphical summary of lesion response, as well as providing comparisons of alternate quantitative imaging biomarkers (lines measure vs. area).

Discussion: Our exhibit shows how radiologists can plug together AIM-enabled quantitative imaging tools into a powerful platform to streamline quantitative image analysis and reporting. By collecting and exchanging image metadata in AIM, we can automate and improve image-based analysis of disease status and response to treatment. The approach, however, is applicable to all of quantitative radiology.

Conclusion: Tools that save image metadata in standard formats (AIM) can be plugged together to build a powerful system to automate quantitative imaging practice and enable research.

References/Funding Source RSNA 2011. NCI U01 grant, U01-CA-142555

Automatic Extraction of Breast Density Information from Mammography Reports

B Perhcha[1], H Nassif[2], JA Lipson[3], ES Burnside[2], DL Rubin[3]
[1]Biomedical Informatics Training Program, [3]Radiology, Stanford University, CA; [2]Department of Radiology, University of Wisconsin Madison, Madison, WI

Purpose: Breast tissue composition is an important risk factor for susceptibility to breast cancer, and information on breast density could play an important role in the development of classification systems for the early and accurate diagnosis of malignancy. Our goal was to develop an automated method to detect and extract the breast density assessments from free-text mammography reports.

Method and Materials: We studied many different mammography reports to understand the variety of ways breast density is reported. We developed an algorithm, based on pattern matching and regular expressions in free text, to automatically detect and extract BI-RADS breast density classes. Using radiologists' unstructured descriptions of mammograms as its input, the algorithm classifies each report into one of four density classes: fatty (1), fibroglandular (2), heterogeneously dense (3), or extremely dense (4). We evaluated the algorithm's performance on a total of 600 reports from two different institutions. Two different radiologists reviewed the reports to establish the gold standard.

Results: The algorithm achieved 100% and 99% classification accuracy on the reports from the two institutions,
respectively.

Conclusion: Our automated method to extract breast density composition from unstructured mammography reports has high accuracy in our testing, and appears promising. This method could enable epidemiological research by facilitating data-mining of large-scale data sets to correlate breast density with other covariates.

References/Funding Source RSNA 2011. NLM Training Grant

Automated drusen segmentation and quantitation in SD-OCT images

Q Chen[1,2], T Leng[3], DL Rubin[1]
[1]Department of Radiology, [3]Byers Eye Institute, Stanford University, CA; [2]School of Computer Science and Technology, Nanjing University of Science and Technology, Nanjing, China

Objective: Spectral domain optical coherence tomography (SD-OCT) is a useful tool for the efficient measurement of drusen in patients with age-related macular degeneration (AMD), however, objective assessment of drusen is thwarted by the lack of a method to robustly quantify these lesions on serial OCT images. Here, we describe an automatic drusen segmentation method and quantitative measurement for SD-OCT retinal images.

Methods: Our method leverages a priori knowledge of normal retinal morphology and histological features. The highly reflective and locally connected pixels located below the retinal nerve fiber layer (RNFL) are taken as the initial estimate of the retinal pigment epithelium (RPE) layer location. The potentially abnormal and normal RPE layers are obtained by interpolating and fitting the estimated RPE layer, respectively. The areas located between the fitted normal and interpolated RPE layers are marked as drusen. We also developed a novel method of fundus projection to generate an en face fundus image based on the RPE extraction, which improves the efficiency of drusen visualization over the current approach to producing this projection based on a summed-voxel projection (SVP), and it provides a means of obtaining quantitative features of drusen in the en face projection. The segmented drusen are refined through several post-processing steps: drusen judgment with consecutive slices, drusen refinement with projection image and drusen smoothing.

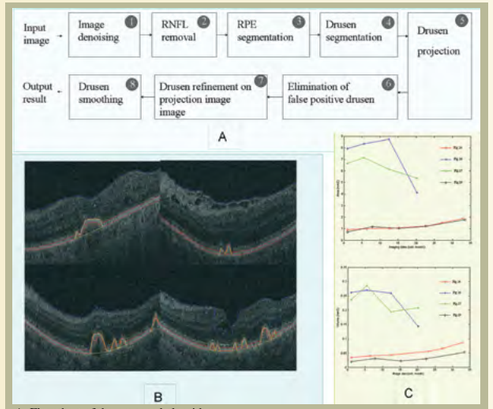

A. Flowchart of the proposed algorithm
B. Drusen segmentation results (yellow lines)
C. Change of drusen area (up) and volume (down).

Results: In a preliminary analysis, quantitative drusen measurements, such as area and volume, correlate with the drusen progression in non-exudative AMD, suggesting that our approach may produce useful quantitative imaging biomarkers to follow this disease and predict patient outcome.

Conclusion: We have developed a novel automated drusen segmentation algorithm for SD-OCT images, which incorporates the 3D spatial information in retinal structures and information in drusen projection images. The qualitative and quantitative evaluations may be clinically useful for evaluating the progress of drusen.

References/Funding Source Bio-X Interdisciplinary Initiatives Program of Stanford University and NCI U01 grant, U01-CA-142555

Fundus projection image for drusen visualization

Q Chen[1,2], T Leng[3], DL Rubin[1]
[1]Department of Radiology, [3]Byers Eye Institute, Stanford University, CA; [2]School of Computer Science and Technology, Nanjing University of Science and Technology, Nanjing, China

Objective: Three-dimensional optical coherence tomography (3D OCT) produces cross sectional images of the retina, providing detailed display of the shape of sub-retinal abnormalities such as drusen. The purpose is to generate en face fundus image based on 3D OCT images and visualize drusen.

Methods: We describe a novel approach, the improved summed-voxel projection (SVP), to generate en face projection images of the retinal surface. The approach can generate en face fundus images and visualize very small drusen, because the method is enhanced by restricting the projection to the retinal pigment epithelium (RPE) layer neighborhood, and the substance regions of drusen are filled with bright pixels.

Results: Comparative results demonstrate that our method is more effective to display drusen and retinal vessels than conventional SVP.

Conclusion: This paper presents a RPE based projection method for 3D OCT retinal images. By comparing the traditional SVP and two improved projection methods, our method is more effective for the drusen visualization in fundus images, which is important for ophthalmologists to directly and rapidly assess the drusen.

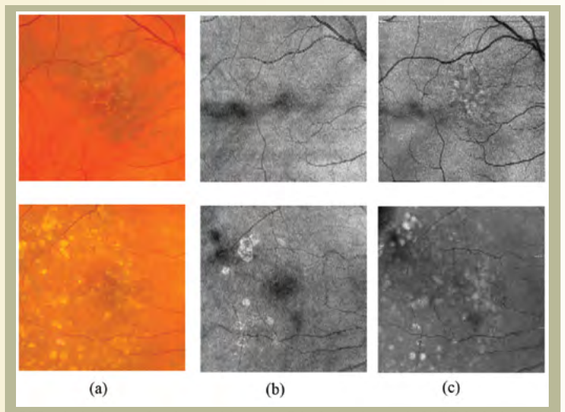

OCT projection images of another two right eyes (a) Color fundus photograph. (b) SVP fundus image. (c) RPE based fundus image.

References/Funding Source Bio-X Interdisciplinary Initiatives Program of Stanford University and NCI U01 grant, U01-CA-142555

Automated Temporal Tracking and Segmentation of Lymphoma on serial CT Examinations

J Xu[1], H Greenspan[3], S Napel[1,2], DL Rubin[2]
Departments of [1]Electrical Engineering, [2]Radiology, Stanford University, CA; [3]Department of Biomedical Engineering, Tel Aviv University, Tel Aviv, Israel

Purpose: It is challenging to reproducibly measure cancer lesions on numerous follow up studies; the process is time-consuming and error-prone. Our goal was to develop a method to automatically and reproducibly identify and segment abnormal lymph nodes in serial CT exams.

Materials and Methods: Our method leverages radiologist-circumscription of cancerous lymph nodes in the baseline scan. We then identify an approximate region for the node in the follow-up scans using non-rigid image registration. The baseline scan is also used to locate regions of normal, non-nodal tissue surrounding the lymph node and to map them onto the follow-up scans, in order to reduce the search space to locate the lymph node on the follow-up scans. Adaptive region growing and clustering algorithms are then used to obtain the final contours for segmentation. We applied our method to 24 distinct enlarged lymph nodes at 3 or 4 time points from 14 patients. The scan at the earlier time point was used as the baseline scan to be used in evaluating each follow-up scan, resulting in 70 total test cases (e.g. a series of scans obtained at 4 time points results in 3 test cases). For each of the 70 test cases, a "reference standard" was obtained using manual segmentation by a radiologist. We assessed the performance of our method using Response Evaluation Criteria in Solid Tumors (RECIST), and by calculating node overlap ratio (NOR) and Hausdorff distance (HD) between the computer and radiologist-generated contours.

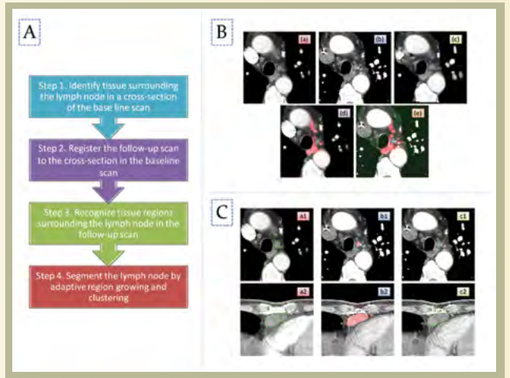

A. Overview of the proposed algorithm
B. (a) Baseline CT scan; (b) Follow-up CT scan; (c) Deformed baseline CT scan (applying non-rigid trans-formation on the baseline CT scan); (d) the identified regions (in pink) in baseline CT scan; (e) the follow-up CT scan with overlays of region mask (in pink) and intensity mask(in green).
C. Automated segmentation example. (a1-a2) Baseline scan (lymph node outlined in green by radiologist); (b1-b2) Automated segmentation results using proposed method (highlighted in pink); (c1-c2) Radiologist's "reference standard" in the follow-up scan.

Results: Compared to the reference standard, our method made the correct RECIST assessment 67/70 (95.7%) times. The average NOR was 80.6% +/- 10.2% s.d., and the average HD was 3.2 mm +/- 1.8 mm s.d.

Conclusion: Our automated method achieves excellent overall segmentation performance and provides equivalent RECIST assessment. It potentially will be useful to streamline and improve cancer lesion measurement and tracking and to improve assessment of cancer treatment response.

References/Funding Source RSNA 2011. NCI U01 grant, U01-CA-142555

Geographic atrophy segmentation for SD-OCT images

Q Chen[1,2], T Leng[3], DL Rubin[1]
[1]Department of Radiology, [3]Byers Eye Institute, Stanford University, CA; [2]School of Computer Science and Technology, Nanjing University of Science and Technology, Nanjing, China

Objective: Age-related macular degeneration (AMD) is a leading cause of irreversible vision loss among the elderly. The advanced form of AMD associated with severe vision loss is characterized by the development of macular neovascularization and geographic atrophy (GA). Automatic quantification of GA is important for determining disease progression and facilitating clinical diagnosis of AMD.

Methods: This paper presents an automatic GA segmentation method for spectral domain optical coherence tomography (SD-OCT) images. Firstly, the retinal pigment epithelium (RPE) layer is estimated according to the reflection property of different retinal layers. Then, three-dimensional (3D) OCT images are transformed to 2D fundus projection images by restricting the projection to the region underneath the RPE layer. Finally, an adaptive edge-based level set method is adopted to segment the GA based on the projection image.

Results: Experimental results demonstrate that the proposed method is effective for the GA segmentation. The segmentation accuracy is approximately 97%.

Conclusion: We have developed a novel automated GA segmentation algorithm for SD-OCT images, which transforms the 3D OCT image segmentation into 2D fundus projection image segmentation. The quantitative evaluations indicate that our method can achieve high segmentation accuracy.

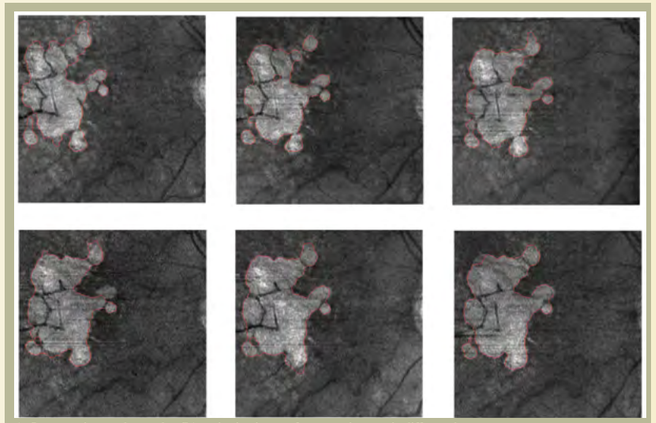
A. Segmentation results overlay GA projection images for one patient on six different dates

References/Funding Source Bio-X Interdisciplinary Initiatives Program of Stanford University and NCI U01 grant, U01-CA-142555

Lesion Classification using Dictionary of Words Approach

R Pasari[1], H Greenspan[2], DL Rubin[1]
[1]Department of Radiology, Stanford University, CA; [2]IBM Almaden Research Laboratories

PURPOSE: A challenge in developing automated image analysis for diagnosis in radiology is variation in appearances of disease. Our goal was to develop a method for automated lesion diagnosis that learns from actual case data by leveraging image patch methodology.

METHOD AND MATERIALS: We obtained 73 CT images of liver lesions (25 cysts, 24 metastasis and 24 hemangiomas). A radiologist circumscribed each lesion, and we extracted uniform-sized patches such that the entire lesion and its margins were included. We extracted features in the patches using principal components analysis, selected of the highest energy components, and clustered them to build a "visual dictionary" where the cluster centroids represent the distinct "words" in the images. We built a feature vector for each image that records the fraction of its patches that are closest to each cluster centroid (length of the vector is the number of cluster centroids). These feature vectors were used to train a multi-class SVM classifier (LibSVM) to predict the diagnosis for each image. We used leave-one-out cross-validation to measure the accuracy. We optimized the number of PCA components, clusters in K-means, and size of a patch. We created separate dictionaries for the interior and for the boundary of a lesion to improve system performance.

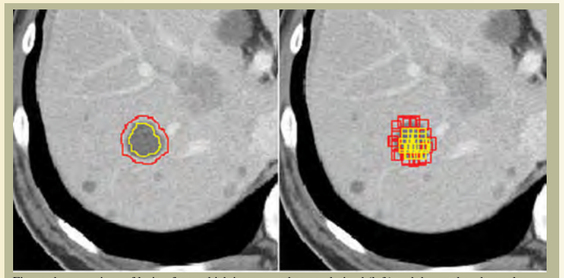

Figure shows regions of lesion from which image patches are derived (left) and the patches themselves (right). Patches are derived by centering them on pixels within the substance of the lesion (yellow) and in proximity to the boundary of the lesion (red).

RESULTS: Our method predicted the correct diagnosis for the lesions with an accuracy of 95%. The few errors in classification which occurred are due to the hemangioma being confused as metastasis. The benefit of the image patch-based method is that it uses the raw image itself as features, and its performance may generalize beyond the three types of lesions tested in this study.

CONCLUSION: We developed an automated method to analyze and classify three types of focal liver lesions based on image patches and a visual dictionary of words derived from them. The classification accuracy appears promising, and the results may generalize to a wider range of lesion diagnoses as we accrue a larger database of liver lesions.

References/Funding Source RSNA 2011. NCI U01 grant, U01-CA-142555

Lesion Detection using Dictionary of Words Approach

R Pasari[1], H Greenspan[2], DL Rubin[1]
[1]Department of Radiology, Stanford University, CA; [2]IBM Almaden Research Laboratories

PURPOSE: Our goal was to develop an automated tool which can detect and segment lesions in a liver CT scan image.

METHOD AND MATERIALS: We obtained 73 CT images of liver lesions. A radiologist circumscribed one lesion in each image. Also we had the radiologist mark areas of normal liver in the images. We extracted image patches from the lesion and normal liver and we performed PCA analysis on them and clustered the results using k-means clustering. Then we built a feature vector for each image of lesion and normal liver that records the fraction of its patches that are closest to each cluster centroid (length of the vector is the number of cluster centroids). These feature vectors were used to train a binary SVM classifier (LibSVM) to predict lesion or normal liver. Then given a query image we divide it into sub-windows and classify each sub-window as either normal liver or lesion.

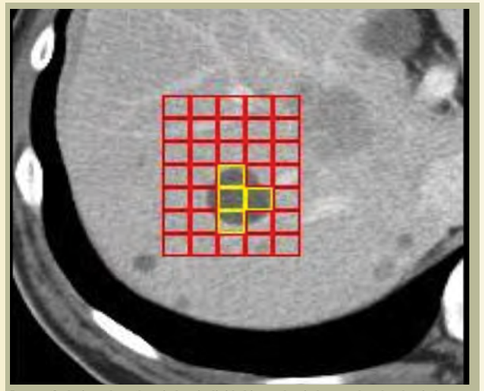

Image of a lesion where the window is divided into sub-windows and each sub-window classified as either lesion (yellow box) or normal liver (red box).

RESULTS: Lesion detection using this dictionary based approach is giving very good preliminary results without using any post processing. It is mostly correctly identifying the lesions. However, the method also identifies the liver boundary as lesion. This is a case of false positives and will reduce our precision.

CONCLUSION: We developed an automated method to segment lesions from a liver image using image patches and a visual dictionary of words derived from them. The results appear promising and the case of false positives described above can be tackled by using some liver segmentation algorithm which demarcates the margin of the liver.

References/Funding Source RSNA 2011. NCI U01 grant, U01-CA-142555

Extension and Application of RadLex to Annotation of Neuroimaging Data

J Turner[1], JV Mejino[2], T Detwiler[2], M Martone[3], J Brinkley[2], DL Rubin[4]
[1]The MIND Research Network, Phoenix, AZ; [2]Department of Biological Structure, University of Washington, WA; [3]Department of Neurosciences, UC San Diego, CA; [4]Department of Radiology, Stanford University, CA

PURPOSE: There are several different terminologies available for annotating functional neuroimaging results to enable data sharing and reuse. Our goal was to address this challenge by harmonizing the major neuroanatomy terminologies which we then incorporated into RadLex, a standard ontology for radiology.

METHOD AND MATERIALS: We used a reference ontology, the Foundational Model of Anatomy Ontology (FMA), to include and correlate information on cytoarchitectonics (Brodmann area labels), and morphological cortical ontologic schemes (e.g., the part of Brodmann area 6 located in the left precentral gyrus) that are represented in the different terminologies. This representation was used to augment the neuroanatomical axis of RadLex, the ontology for clinical imaging. To evaluate our work, we annotated a large functional neuroimaging dataset with terms from the expanded RadLex ontology. We applied a reasoning engine to the annotated images to analyze them in conjunction with the ontology to answer the research questions associated with this dataset.

RESULTS: Our neuroanatomy ontology declares the explicit representation of structural relationships such as parthood and connectivity between neuroanatomical entities which allows for relating ontologically the neuroanatomical entities referenced by the different labeling schemas. This therefore provides RadLex an ontology that can harmonize and unify image datasets that are annotated with disparate neuroanatomical terminologies. The analyses we performed on the RadLex-annotated images achieved successful inferences from the most granular level (e.g., how many subjects showed activation in a sub-part of the middle frontal gyrus) to the most general level (e.g., how many activation sites were found in either right or left frontal cortex).

CONCLUSION: We have augmented RadLex to harmonize the major terminologies and cortical parcellation schemes used in neuroimaging. Our work can be exploited by computer reasoning engines to make inferences about neuroanatomical relationships in imaging datasets that use the different terminologies, and could enable

knowledge discovery from large distributed fMRI studies.

References/Funding Source RSNA 2011. Grants from NIBIB and RSNA

High-throughput multiple mouse imaging on MicroPET and MicroPET-CT scanners: Effect on Quantitation

F Habte[1,2], G Ren[1,2], TC Doyle[1,3], Z Cheng[1,2], D Paik[1,2]
Departments of [2]Radiology, [1]MIPS, [3]Pediatrics, Stanford University, CA

Small animal microPET imaging is becoming an increasingly important modality, currently commonly used in the development of novel imaging agents, drug treatments and animal disease models. This increased demand has lead the use of a three- or four-mouse "hotel" to simultaneously image multiple anesthetized animals. This significantly reduces the scan time, while also allowing experiments to be designed with significantly larger cohorts of animals, as well as decreasing the data processing time, storage requirements and post-acquisition analysis required. In this study, we assessed the quantitative impact of scanning four animals, relative to single animals on a multi-modality MicroPET-CT scanner and on a dedicated MicroPET scanner. Mice were injected with a 64Cu-labeled radiotracer (with a relatively long half-life to minimize decay variance between imaging studies), and then sequentially scanned either in a four-mouse "hotel" or individually on both MicroPET-CT and MicroPET scanners. For validation purposes, we also scanned cylindrical phantoms using both single and multiple animal techniques. A semi-automatic threshold-based Region of Interest (ROI) tool was used to minimize operator variability during image analysis. Ex vivo bio-distribution studies were performed on all animals as a gold standard to compare with image quantitation. Our results indicate that there is minimal difference in the quantification of radionuclide uptake in selected major organs between conventional single mouse scans and multi-animal scans in our mouse "hotel" on either the MicroPET or MicroPET-CT scanners. We obtained less than 7% relative error difference with respect to %ID/gram between the multi-mouse and single mouse scans, and a 4% relative error difference with the cylinder phantom studies. These results confirmed that there is little no significant difference in uptake quantification of small animal PET images compared to the near 20% variability seen in repeat scans, and that use of the mouse "hotel" is a valid aid to increasing instrument throughput on small animal scanners.

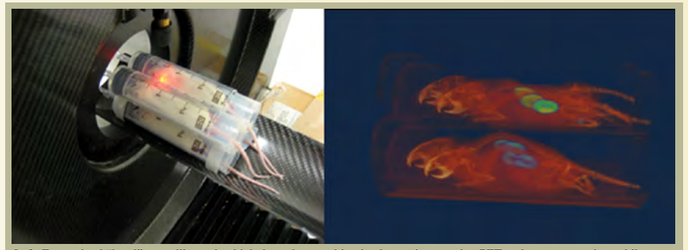

Left: Four animal "hotel" setup illustrating high throughput multi-animal scanning on microPET to decrease scan time while decreasing data storage and processing demands. Right: Corresponding volume rendered microPET/CT data.

References/Funding Source Abstract accepted for WMIC 2011 Poster presentation (Control ID: 1124585). ICMIC@Stanford (NIH P50 CA114747) and CCNE-T (NIH U54 CA151459)

Narrow Peak Spectral Algorithm: Improved Method for Unmixing of Raman Labeled Nanoparticles

K Kode[1,3], C Shachaf[1,2], S Elchuri[2], G Nolan[2], DS Paik[1]
Departments of [1]Radiology, [2]Microbiology and Immunology, [3]Computational and Mathematical Engineering, Stanford University, CA

Raman spectroscopy can differentiate the spectral fingerprints of many molecules, resulting in potentially high multiplexing capabilities of Raman-tagged nanoparticles. However, accurate quantitative unmixing of Raman spectra is challenging because of potential overlaps between Raman peaks from each molecule as well as slight variations in the location, height and width of the very narrow peaks. If not accounted for, even minor fluctuations in the spectra may produce significant error which will ultimately result in poor unmixing accuracy.

We developed and evaluated an algorithm named Narrow Peak Spectral Algorithm (NPSA) for unmixing the contributions from each nanoparticle allowing simultaneous quantitation of several nanoparticle concentrations during sample characterization. The Carbon Organic-inorganic Nanoparticles (COINs) used in this study were prepared by reduction of silver nitrate with sodium borohydride and then were aggregated with organic Raman labels in the presence of sodium chloride. The COINs were then encapsulated with bovine serum and cross-linked with glutaraldehyde.

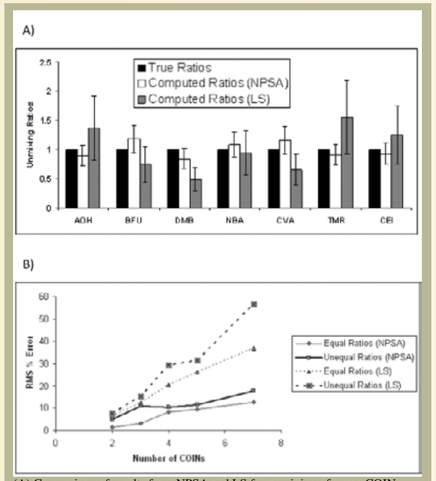

(A) Comparison of results from NPSA and LS for unmixing of seven COINs. (B) RMS % Error of unmixing results for NPSA and LS. The performance of NPSA compared to LS is much better particularly as the number of COINS unmixed increases.

Using NPSA, we were able to successfully unmix Raman spectra from up to 7 Raman nanoparticles after correcting for the spectral variations of 30% in intensity and shifts in peak locations of up to 10 cm-1 which is equivalent to 50% of the full width at half maximum (FWHM). We compared the performance of NPSA to the conventional least squares analysis (LS), error in NPSA is approximately 50% lower than LS. The error in estimating the relative contributions of each nanoparticle using NPSA are in the range of 10-19% for unmixing of 7 COINs whereas the errors using the traditional least squares approach were in the range of 25-68%.

Our results demonstrate that accounting for variability in the spectra can lead to better and more reliable performance in quantitative unmixing thereby enabling Raman spectroscopic imaging in living subjects.

References/Funding Source CCNE-TR NIH (U54-CA119367) and FAMRI YSCA grant (CS)

Characterization of Variability across SERS spectra of Raman Labeled Nanoparticles

K Kode[1,3], C Shachaf[1,2], S Elchuri[2], G Nolan[2], DS Paik[1]
Departments of [1]Radiology, [2]Microbiology and Immunology, [3]Computational and Mathematical Engineering, Stanford University, CA.

The potential of Raman spectroscopy in multiplexing of Raman-tagged nanoparticles which is crucial in immuno-detection is limited by the variability associated with the SERS spectra of these nanoparticles. If not accounted for properly, even minor fluctuations in the spectra may produce significant error which will ultimately result in poor unmixing accuracy. The objective of our study was to characterize the variability across SERS spectra of different Carbon Organic-inorganic Nanoparticles (COINs).

To study the variability in the SERS spectra of different COINs, spectra were collected from 289 (17x17) spots for each sample. A peak detection algorithm was developed to extract features from each spectra. The approximate peak location, height and full width at half maximum (FWHM) of the Raman peaks obtained from peak detection algorithm were refined by fitting Gaussian functions to the peaks using an optimization routine.

The variation in center location of peaks was quite significant in some of the spectra with the peaks being shifted by as much as 14 cm-1 with respect to the mean location. Similarly, variations in the peak intensity as well as FWHM were significant enough to render quantitative unmixing erroneous. Also, the variations observed in different peaks of the spectra were highly uncorrelated suggesting that each peak should be corrected for independently.

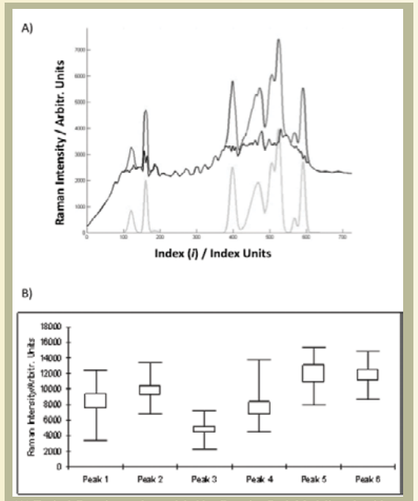

(A) Typical Gaussian peaks modeled by Gaussian Peak Modeling algorithm. (B) The variations in peak intensity observed in different peaks of SERS spectra of NBA COIN.

While the narrow peaks of the Raman spectra provide specificity of each nanoparticle's spectrum, their steep slopes can lead to large errors in the presence of very minor spectral shifts or changes in width. Our results demonstrated that the SERS spectra of COINs have significant variation and accounting for this is necessary to achieve reliable performance in quantitative unmixing thereby enabling Raman spectroscopic imaging in living subjects. We developed an efficient unmixing algorithm that accounts for the observed variability which is discussed in our Lucas report 'Narrow Peak Spectral Algorithm: Improved Method for Unmixing of Raman Labeled Nanoparticles'.

References/Funding Source CCNE-TR NIH (U54-CA119367) and FAMRI YSCA grant (CS).

A systems approach to characterize molecular targets for imaging agents

TT Liu[1,2], D Paik[1,2]
Departments of [1]Radiology, MIPS, ISIS, [2]Biomedical Informatics, Stanford University, CA

The development of novel imaging agents and the identification of their molecular targets are areas of intense research and have a wide range of applications in both biomedical research and in clinic. Here we show we can use a computational approach to characterizing the molecular target of an imaging agent. We hierarchically clustered targets based on the molecular features of their corresponding imaging agents. Although previous studies have applied and validated this approach on pharmacological data, to our knowledge, this is the first study that this approach is applied to imaging agent data. Our dataset consists of 400 small molecular imaging agents annotated into sets for over 80 protein targets. First, we demonstrated the feasibility of this computational approach on imaging agents by performing unsupervised clustering based on topology of imaging agents.

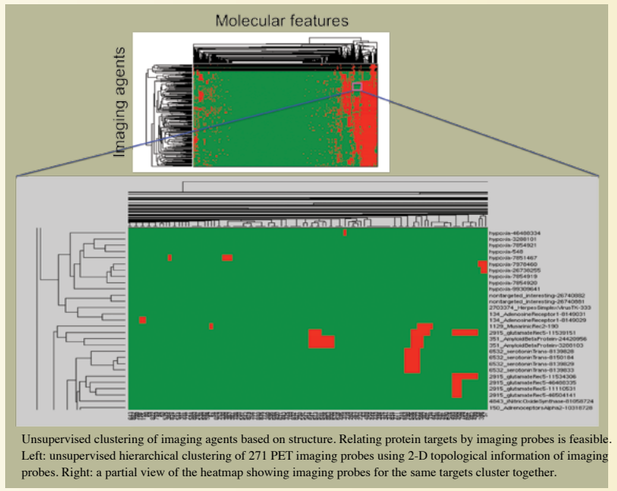

Unsupervised clustering of imaging agents based on structure. Relating protein targets by imaging probes is feasible. Left: unsupervised hierarchical clustering of 271 PET imaging probes using 2-D topological information of imaging probes. Right: a partial view of the heatmap showing imaging probes for the same targets cluster together.

Our result shows that imaging agents for the same biological target cluster together based on chemical structure features. We calculated a pairwise similarity score between every two sets of imaging agents. The similarity scores were expressed in a network with nodes being the targets. We further tested the model on an external set of EGFR imaging agents, and EGFR was returned as the top hit of a ranked list of molecular protein targets. Although experimental validation is needed, this systems approach to molecular imaging agents across multiple targets is effective for characterization and identification molecular targets for imaging agents.

References/Funding Source T Liu, DS Paik. A systems approach to characterize molecular targets of imaging probes. The 19th annual international conference on Intelligent Systems for Molecular Biology (ISMB), March 2011, accepted conference poster

The Imaging Biomarker Ontology: ontology-based support for imaging biomarker research

TT Liu[1,2], E Savig[3], DL Rubin[1,2], D Paik[1,2]
Departments of [1]Radiology, MIPS, ISIS, [2]Biomedical Informatics, [3]Cancer Biology Program, Stanford University, CA

The purpose of this project is to develop an ontology to represent and integrate the heterogeneous knowledge in the domain of imaging biomarkers, for the purpose of enabling the storage and retrieval of desired imaging biomarker measurements, mining the expanding imaging literature, and discovery of novel imaging biomarkers.

We have developed the Imaging Biomarker Ontology to support imaging biomarker research. It integrates heterogeneous knowledge in the field of imaging biomarker research, and bridges pre-clinical and clinical imaging biomarker research. The Imaging Biomarker Ontology we have developed integrates knowledge in different fields represented by 9 upper classes, including image technique (imaging agent, imaging instrument), method of quantitation (image processing and analysis algorithm), and biology of interest (biological target, indicated biology, and biomarker application). The ontology also includes both clinical terms (e.g. DISEASE) and terms used in basic biological research (e.g. BIOLOGICAL PROCESS). Integration of these different fields will facilitate biomarker discovery and accelerate translation of imaging biomarker from research to clinical use. In addition, we reuse existing ontologies whenever possible. To our knowledge, this is the first ontological representation of knowledge in imaging biomarker research. The complete Imaging Biomarker Ontology will soon be made available to the public domain. Following the ontology development, we will validate the ontology using published imaging biomarker data and demonstrate its utility in various applications, such as data retrieval, mining new information from the literature, and discovering novel imaging biomarkers.

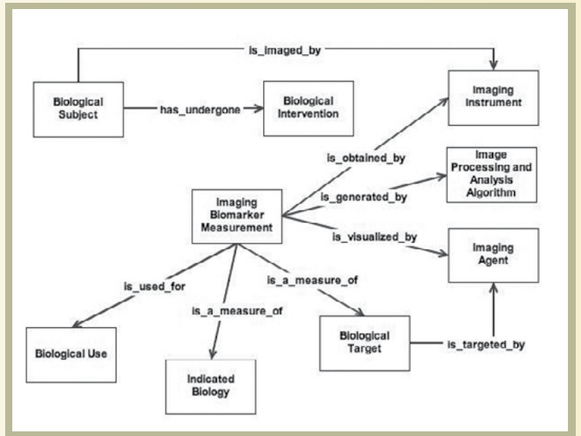

Top level classes and their relationships

References/Funding Source TT Liu, E Savig, DL Rubin, DS Paik. The Imaging Biomarker Ontology: Ontology-based Support for Imaging Biomarker Research. The Society for Imaging Informatics in Medicine 2011 Annual Meeting, 2011, accepted conference abstract

Software Only Method for QC of Monitor Quality and Reading Conditions in Multisite Image Reading Trials

D Rasooly, F Schmitzberger, TJ Kim, M Tall, J Roos, S Napel, G Rubin, D Paik
Department of Radiology, Stanford University, CA

Purpose: Quality control (QC) of display monitors and reading environment in a multisite image reading trial is difficult to maintain. We have validated a simple psychoperceptual software-only test that eliminates the need to send a photometer to each site for QC.

Methods: Characteristic luminance curves were measured using a photometer on 24 displays (18 LCD, 6 CRT). 6 readers incremented grayscale intensity differences (ΔI) between text and background until able to correctly read a 4 digit code in an 8-bit image on white, gray, and black backgrounds. Tests were done with indoor lighting both on and off, with the controls done in a closed office (no windows) and the experimental measurements in a suboptimal, non-clinical reading environment (windows with significant ambient light). As a gold standard of reader contrast detectability, just noticeable difference in contrast (C_JND) was calculated. Acceptable performance under the various lighting conditions was set at C_JND<7.5%.

Results: ΔI scores obtained with indoor lighting were on average 0.08-0.86 grayscale units higher than corresponding ΔI scores obtained with no ambient lighting, indicating that ambient light has minimal influence on perceptual ability compared to inter-reader variability. Of the 18 different monitor and monitor setting tested, 9 had maximum luminance values less than 173 cd/m2, the AAPM recommended minimum value. ΔI scores obtained from the 9 monitors below the 173 cd/m2 threshold averaged at 6.5-10.6 grayscale units, while those over the threshold averaged at 7.6-11.4 grayscale units leading to a difference of 0.1-1.1 grayscale units between the two groups, indicating that poor monitor luminance also has minimal influence on perceptual ability. Out of 256 grayscale values on a typical 8-bit display of window-leveled images, these differences in grayscale perception are minimal and in fact, well below inter-reader variation.

Conclusion: Somewhat counter-intuitively, ambient lighting and poor monitor quality have minimal influence on perceptual ability, especially when compared to inter-reader variability. This effect can be modeled using either the Weber-Fechner law of perception or the DICOM Grayscale Standard Display Function (GSDF).

A Computational Representation of Nanoparticle Structure to Enable Structure-Based Queries of Nanomedicine Resources

C Nwabugwu[1,2], K Kode[1,3], S Gaheen[4], N Baker[5], D Paik[1]
Departments of [1]Radiology, [2]Electrical Engineering, [3]iCME, Stanford University, CA; [4]National Institutes of Health; [5]Pacific Northwest National Laboratory

The data being generated from experiments in cancer nanotechnology research–an intrinsically interdisciplinary research field devoted to the development and application of nanotechnology-based methods in the treatment, diagnosis and detection of cancer–is growing at an exponential pace. It is vital to keep up with the flood of new information about the biological properties of nanoparticles used for both imaging and therapy. We are devising a method for graphically specifying database queries based on the structure of nanoparticles. This includes developing a computational representation of the modular structure of engineered nanoparticles.

The NanoParticle Ontology (NPO) is an ontology–a formal, explicit representation of knowledge belonging to a subject area–which has been developed within the framework of the Basic Formal Ontology (BFO), and implemented in the Ontology Web Language (OWL) using established ontology design principles. It was developed to represent knowledge underlying the preparation, chemical composition, and characterization of nanomaterials involved in cancer research. nano-TAB is a tab-delimited spreadsheet type of format facilitating the submission and exchange of data pertaining to nanomaterials and their characterizations (physico-chemical, in vitro, and in vivo). It is based on existing standards developed by the European Bioinformatics Institute (EBI) and the Investigation/Study/Assay (ISA-TAB) file format, which represents a variety of assays and technology types. The nano-TAB specification leverages ISA-TAB files describing investigations, studies, and assays and provides extensions to support nanomaterial structural information and concepts on nanotechnology assay measurements defined in the NPO. We have developed and object-oriented design for representing nano-TAB materials files using the Java programming language and we are currently implementing a graphical user interface for creating these files from a palette of nanostructures. Future work will involve creating a similarity metric for nanoparticle structures, searching multiple online resources and eventually using this tool for novel nanoparticle design.

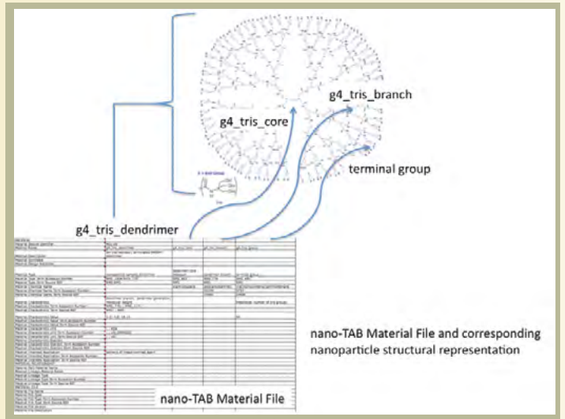

Figure 1. The G4 tris(hydroxyl) terminated PAMAM dendrimer structure and its corresponding nano-TAB material file. Structure comes from caNanoLab NCL-20 (Hall, et al).

References/Funding Source DG Thomas, et al. NanoParticle Ontology for cancer nanotechnology research, J Biomed Inform (2010), doi:10.1016/ j.jbi.2010.03.001. NCBO (NIH U54 HG004028) and CCNE-T (NIH U54 CA151459)

A Gold Standard for Visual Similarity of Lesions on CT Liver Images: Inter-reader Variability

JS Faruque[1], DL Rubin[2], CF Beaulieu[2], J Rosenberg[2], RM Summers[3], A Kamaya[2], G Tye[2], S Napel[2]
Departments of [1]Electrical Engineering, [2]Radiology, Stanford University, CA; [3]National Institutes of Health Clinical Research Center, Bethesda, MD

Purpose: We are creating a perceptual gold standard for visual similarity in medical images that may be used for training and validating a content-based image retrieval system. In this study, we evaluated inter-reader variability when assessing visual similarity of liver lesions seen at portal venous CT.

Methods and Materials: We displayed 19 portal venous CT images containing liver lesions individually (phase 1) and in all 171 pair-wise combinations (phase 2) to 3 radiologists in random order. For phase 1, each image was rated for 6 visual attributes ((1) number of different compartments and (2) densities, (3) average density, (4) margin definition and (5) contour, and (6) rim density) on a 9-point scale. For phase 2, each pair of images was rated for similarity in the same 6 attributes as well as for overall similarity. We calculated inter-reader variability between each set of ratings and each pair of readers using the Cohen's Kappa metric.

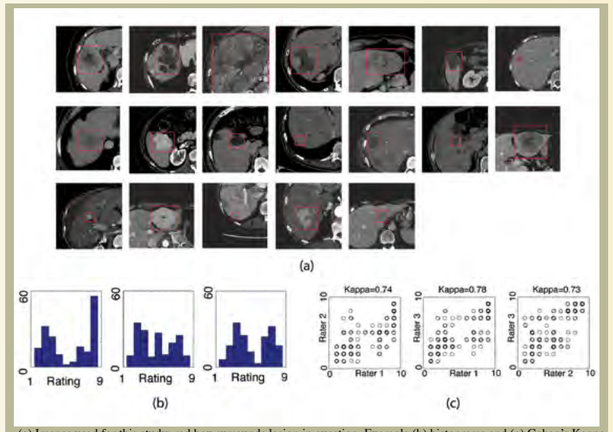

(a) Images used for this study; red box surrounds lesion in question. Example (b) histograms and (c) Cohen's Kappa scores for Phase 2 ratings of the similarity of average density between image pairs.

Results: For Phase 1, the Kappa scores ranged from 0.49-0.53, 0.29-0.73, 0.88-0.92, 0.61-0.67, 0.56-0.64, and 0.41-0.79 for attributes (1) through (6), respectively. For Phase 2, the Kappa scores ranged from 0.29-0.54, 0.39-0.51, 0.73-0.78, 0.47-0.54, 0.38-0.62, 0.29-0.39, and 0.42-0.72 for attributes (1) through (6) and overall similarity, respectively.

Conclusion: Inter-reader agreement varied in a wide range depending on attributes. Inter-reader agreement is better when rating attributes of single images as opposed to rating similarity (attribute-wise or overall) between pairs. The attributes of Average Density, Margin Definition, and Margin Contour had greater inter-reader agreement and may thus be more valuable when creating a reference standard.

References/Funding Source J Faruque, D Rubin, C Beaulieu, J Rosenberg, R Summers, A Kamaya, G Tye, S Napel. A Scalable Reference Standard for Visual Similarity for a Content-Based Image Retrieval System. IEEE Healthcare, Informatics, and Systems Biology Conference, 2011.NIH NIGMS Training Grant T32 GM063495, Stanford Bio-X Program, NIH Clinical Center Intramural Research Program

Prediction of radiologist observations using computational image features

F Gimenez[1], J Xu[2], Y Liu[1], T Liu[1], CF Beaulieu[3], DL Rubin[3], S Napel[3]
Departments of [1]Medicine (Biomedical Informatics Research), [2]Electrical Engineering, [3]Radiology, Stanford University, CA

PURPOSE: We propose that radiological annotations can be predicted using quantitative features derived from image data.

METHOD AND MATERIALS: We utilized 79 portal-venous phase CT studies containing liver lesions. A radiologist selected a representative slice from each study, circumscribed the lesion, and annotated it using a controlled vocabulary of 76 terms. The annotations were performed using OsiriX and the Electronic Physician's Annotation Device (ePad) plug-in. Annotations were concatenated into a binary feature vector referred to as the "semantic features." Computationally derived features were then extracted from the images that describe lesion intensity, texture, shape, and edge sharpness of lesions. These features were used to train a logistic regression classifier with L1-regularization to predict each semantic feature. Leave-one-out cross-validation was used to calculate the probability of a feature's presence given the computationally-derived features. These probabilities were used to create receiver operating characteristic (ROC) curves. Area under the curve, optimal classification threshold, and misclassification rate were computed to analyze the effectiveness of classification.

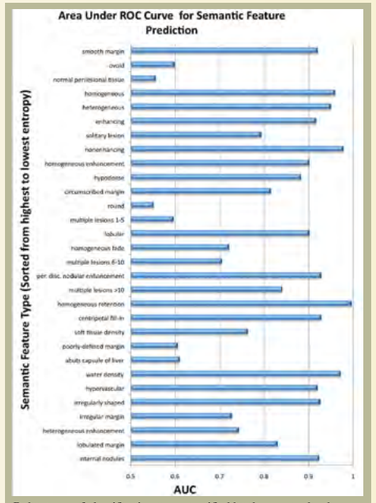

Robustness of classification was quantified by the area under the ROC curve. 1 indicates perfect classification, 0.5 indicates random classification.

RESULTS: The AUC for the semantic features indicated good performance (mean 0.82 +/- 0.14). The mean misclassification rate using the optimal classification thresholds was 0.14 +/- 0.09. Several annotations were predicted particularly well, including water density, homogeneous retention, non-enhancing, heterogenous, and homogenous, all of which had an AUC over 0.95. A few semantic features were difficult to predict, including normal perilesional tissue, round, and ovoid (AUC < 0.6).

CONCLUSION: We used a statistical machine learning classifier to predict radiological annotations of liver lesions using computationally derived quantitative imaging features. Results showed that prediction of such features is feasible and may potentially be used in conjunction with radiologists to verify their observations in real-time. Further work may be done to extract more relevant image features, to improve classification accuracy, and to verify this system using a larger data set.

References/Funding Source submitted to Radiological Society of North America 97th Scientific Sessions, November 2011. accepted for presentation at the First IEEE Conference on Healthcare Informatics, Imaging, and Systems Biology (HISB2011), July 2011. NIH Bioinformatics Training Grant T15 LM007033-27.

Quantitative analysis of 4-d gaze tracks through lung CT data during nodule search

K Roychoudhury[1], M Tall[1], JE Roos[3], GD Rubin[1], S Napel[2]
Departments of [1]Radiology, Duke University, NC; [2]Radiology, Stanford University, CA; [3]Radiology, University Hospital Zurich, Switzerland

PURPOSE: Gaze tracking is a promising tool to enhance our understanding of the search for and detection of lung nodules. We have developed a platform for recording four-dimensional (x, y, z, t) gaze data while radiologists search and identify lung nodules in CT scans. Our goal is to develop an analysis of these data that characterizes the relationship between the gaze path and nodule detection.

METHOD AND MATERIALS: Two radiologists performed unrestricted search on sets of contiguous transverse sections from 38 lung CT scans implanted with between 3 and 6 simulated nodules per scan. The gaze path over the computer display (x, y, t) was associated with variations in longitudinal position (z, t) controlled by the readers using a computer mouse. The speed of eye movement was estimated from smoothed time derivatives of x and y movement obtained using a short window smoothing spline. Locations of rapid eye movement (saccades) were estimated by applying a speed threshold. Saccadic epochs (time intervals) were identified using a zero crossing algorithm applied to the speed function. Fixation (dwell time) epochs are identified as complementary to saccadic ones. Variations in saccadic and fixation durations were identified using analysis of variance (ANOVA).

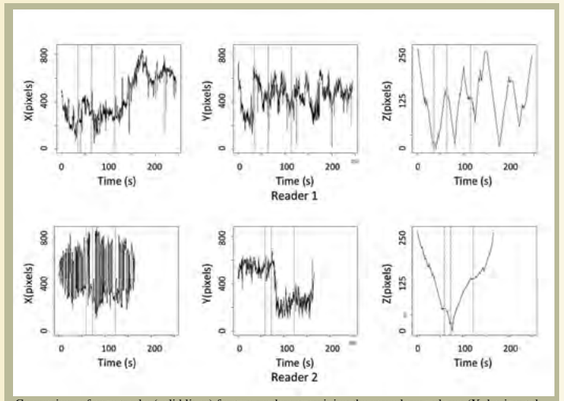

Comparison of gaze tracks (solid lines) for two readers examining the same lung volume (X=horizontal; Y=vertical; Z=slice number) implanted with 4 simulated nodules. The dotted lines mark times of detection. Note different search strategies. Both readers missed one nodule, but not the same one.

RESULTS: Spatial analysis revealed significant differences in scanning patterns for the same task across readers. Typically movement in the Z direction is much slower than in the XY plane, hence Z movement did not contribute to the identification of transient features like saccades. The saccade identification algorithm was validated across different readers and cases. For nodule detection, median durations were 0.12 seconds for saccades and 0.55 seconds for fixations, but with significant differences across readers. The distributions of saccades and fixations are positively skewed but can be approximately normalized using a log transform.

CONCLUSION: The recording and subsequent analysis of four dimensional gaze paths during lung CT interpretation reveal unique aspects of radiologist's search strategies, thus offering the potential for directing readers toward improved accuaracy and consistency of performance when searching for lung nodules.

References/Funding Source Submitted to RSNA 2011. NIH R01 CA109089

Annotation and integration of CT and PET images with gene expression in NSCLC for decision support and discovery

S Napel[1], CD Hoang[2], J Xu[3], O Gevaert[1], DL Rubin[1], Y Xu[2], ANC Leung[1], A Quon[1], SK Plevritis[1]
Departments of [1]Radiology, [2]Cardiothoracic Surgery, [3]Electrical Engineering, Stanford University, CA

PURPOSE: Use of images for data-driven discovery and decision support requires their annotation with machine accessible features. We show methods and preliminary results in 26 NSCLC patients (18 male; 8 female; aged 50-86, mean 68) who had imaging and gene expression microarrays of the excised tumor.

METHOD AND MATERIALS: CT parameters: slice thickness ≤1.5 mm, 120 kVP, tube current 100-700 mA, pitch 0.9-1.0. FDG-PET/CT parameters: FDG 10-17 mCi (.21 mCi/kg), slice thicknesses 3.75-5 mm. We annotated an NSCLC nodule in each CT study by choosing from among 71 controlled terms from each of 19 categories (e.g., location, density, calcification status) and in each PET scan using SUV. We also computed 153 pixel-based features (e.g., Gabor texture, margin sharpness and shape) of the nodule in the CT scans. We processed gene expression from Illumina Whole Genome Bead Chips (Human HT-12) by k-means clustering into 56 co- expressed clusters. We performed univariate and multivariate analyses to integrate image features and metagenes using Significance Analysis of Microarrays, and sparse linear regression, respectively.

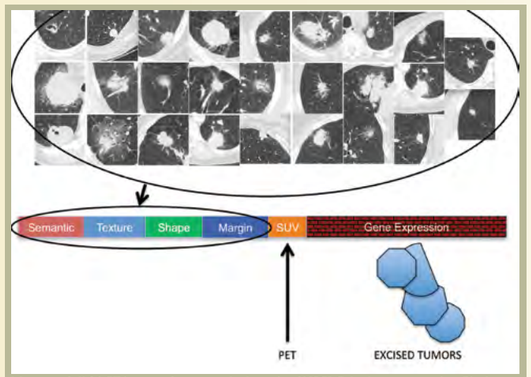

Montage of all 26 CT images of tumors and schematic of NSCLC database construction: Pixel-based image features of identified tumors from thin-section CT images, SUV from FDG-PET images (not shown), and gene expression from excised tumors are combined into a single feature vector for each tumor. Collection of feature vectors from cohort can then be analyzed for relationships between image features and gene expression data.

RESULTS: We observed diverse features in this small cohort: 31% of the semantic and 39% of the computational features have entropy > 0.8 and variance > 10%, respectively. Univariate analysis found 243 significant associations between image features and metagenes; e.g., a metagene implicated in focal and cell adhesion, extracellular matrix receptor interaction, and TGF-beta signaling pathways was associated with image features indicating pleural and blood vessel displacement towards the tumor. Multivariate analysis showed that all 56 metagenes could be modeled by the image features with a mean accuracy of 72% (59%-83%), and that the top 10 predicted computational image features (predominately associated with lesion size, edge shape and edge sharpness), could be predicted with an average accuracy of 85%.

CONCLUSION: It is possible to derive a machine-accessible image phenotype based on semantic and pixel-based features, which can in turn be linked to molecular features. Continued evaluation in a larger database is warranted.

References/Funding Source Submitted to RSNA 2011. General Electric Medical Systems

Developing Image Features for Characterizing Non-small Cell Lung Cancer

J Xu[1], CD Hoang[2], ANC Leung[3], A Quon[3], DL Rubin[3], O Gevaert[3], SK Plevritis[3], S Napel[3]
Departments of [1]Electrical Engineering, [2]Cardiothoracic Surgery, [3]Radiology, Stanford University, CA

Purpose: The ability to use images for data-driven discovery and decision support requires their annotation with machine accessible features. Accordingly, we aim to accomplish this for Non-small Cell Lung Cancer (NSCLC), and have begun with a database of 26 patients who each had a thin-section CT as well as a PET study.

Materials and Methods: For each case, a thoracic radiologist identified and annotated a pulmonary nodule in the CT study using a controlled vocabulary of 71 semantic terms, a nuclear medicine physician determined the Standard Uptake Value (SUV) from the PET scan, and we applied computer algorithms to the nodule area identified in the CT scans to extract pixel-based imaging features. Each nodule was represented by a 178-element feature vector composed of 71-element binary semantic descriptor, 1-element SUV, and a 106-element computational feature vector, including Gabor texture features, margin sharpness features, and a generalized shape descriptor.

A

Location Segmental	20 locations, e.g., left lower lobe posterobasal, left upper lobe apical
Location Axial	central, peripheral
Shape	complex, oval, polygonal, round
Margins	5 choices e.g., concave, spiculated
Density	ground glass, part solid, solid
Calcification	6 descriptions, e.g., none, eccentric
Cavitation	Absent, Present
Necrosis	Absent, Present
Pleural Retraction	Absent, Present
Entering Airway	Absent, Present
Internal Air Bronchogram	Absent, Present
Lesion Periphery	5 choices, e.g., emphysema, fibrosis
Satellite Nodules in Primary Tumor Lobe	Absent, Present
Nodules in non-Tumor Lobe	Absent, Present
Thickened Adjacent Bronchovascular Bundle	Absent, Present
Intralobular Septal Thickening	Absent, Present
Centrilobular Nodules	Absent, Present
Vascular Convergence	Absent, Present
Lesion Attachment	4 choices, e.g., none, fissure

B

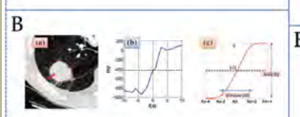

C

Semantic Term	Entropy
Complex shape	1.00
Internal Air Bronchogram Absent	0.99
Internal Air Bronchogram Present	0.99
No attachment	0.99
Entering Airway Absent	0.98
Entering Airway Present	0.98
Pleural Retraction Absent	0.98
Pleural Retraction Present	0.98
Lobulated margin	0.98
Normal periphery	0.98

D

Feature Name	Variance
Edge Sharpness - window skewness	0.15
Gabor-10	0.11
Gabor-6	0.11
Edge Sharpness - scale stdev	0.10
LAH Mean r=1.10R	0.10
LAH stdev r=1.2R	0.09
Edge Sharpness - scale mean	0.09
LAH stdev r=1.5R	0.08
LAH Mean r=1.8R	0.07
LAH stdev r=1.3R	0.06

E

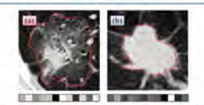

A. Table of semantic term categories and example terms for lung tumors in thin section chest CT images.
B. (a) Cropped CT image containing lung nodule, with one normal drawn at boundary. (b) Pixel values along the normal line (c) sample sigmoid fit showing the scale and window parameters. Scale (S) measures the difference in intensities outside and inside the nodule; window (W) characterizes the transition from the lung nodule to the normal lung tissue at the boundary.
C. Table showing 10 semantic terms with the highest entropy.
D. Table showing quantitative features with highest variance.
E. Cropped CT images containing 2 example lung nodules (ROI highlighted in red), and the mean Gabor energy in 12 bands normalized between 0 (black) and 1 (white) for a lung nodule characterized as (a) 'part solid density,' and (b) 'solid density.'

Results: We examined the features extracted for our database. Table 2 lists the top 10 semantic terms with the highest entropy. Table 3 lists the top 10 quantitative features with the highest variance (each of 106 quantitative features is normalized between 0 and 1). These features with high variance or high entropy may be used to differentiate amongst tumor types. The features that are relatively constant across tumors might be not useful for this dataset.

Conclusion: These feature vectors can potentially be used to retrieve similar appearing images for decision support and, combined with gene expression, may reveal molecular characteristics underlying medical image features and find use as predictive markers for molecularly-targeted therapeutics.

References/Funding Source General Electric Medical Systems

A Software Framework for Extracting Computational Imaging Features from Medical Imaging Data

J Xu[1], CF Beaulieu[2], DL Rubin[2], S Napel[2]
Departments of [1]Electrical Engineering, [2]Radiology, Stanford University, CA

Purpose: We are in the process of building large databases linking image features to other data, e.g., clinical, gene expression, pathology. To this end, we are developing a software platform for rapid and complete characterization of imaging features from medical imaging data.

Materials and Methods: Regions of interest (ROI) in representative cross-sections of volumetric imaging data were defined and stored in a set of XML-format Annotation and Image Markup (AIM) files, along with pointers to the relevant DICOM image files. In addition to the coordinates of the ROIs, each AIM file contained semantic annotations, described by radiologists. To this sematic description of the each ROI, our software added pixel-based features computed from pixels within the ROI, resulting in rich feature vectors describing each image in the database.

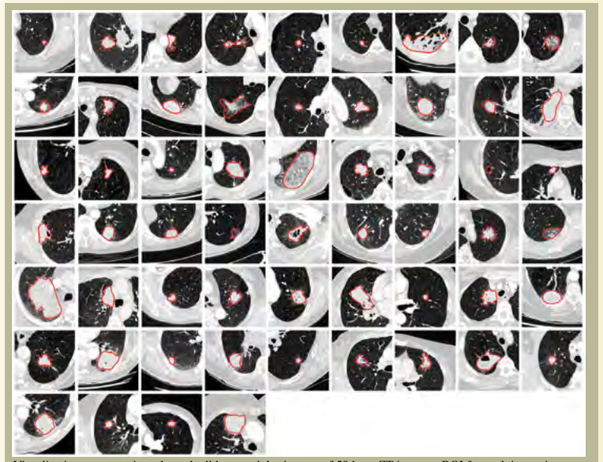

Visualization cross-sections through all lung nodules in a set of 58 lung CT images. ROI for each image is shown in red.

Results: The software has been tested using a set of 79 portal venous liver CT images containing various types of lesions, and a set of 58 lung CT images containing various types of nodules. Each computational feature vector contained 178 scalars, describing such attributes as shape, texture, boundary edge sharpness, and semantic annotation.

Conclusions: Our Matlab-based platform allows researchers to conveniently build a database of computational feature vectors describing each image in a set of medical images. The feature vectors can potentially be used in data mining applications for radiological discovery, to retrieve similar appearing images for decision support and, combined with gene expression, may reveal molecular characteristics underlying medical image features and find use as markers for molecularly-targeted therapeutics.

References/Funding Source General Electric Medical Systems

Magnetic Resonance Research

This MRI section will explore and highlight new and novel accomplishments made over the last year in the critical areas of MRI instrumentation and applications. These new advances provide improved capabilities to detect pathologies in clinical applications as well as to inform basic science understanding of the human body's physiology, function, and biology.

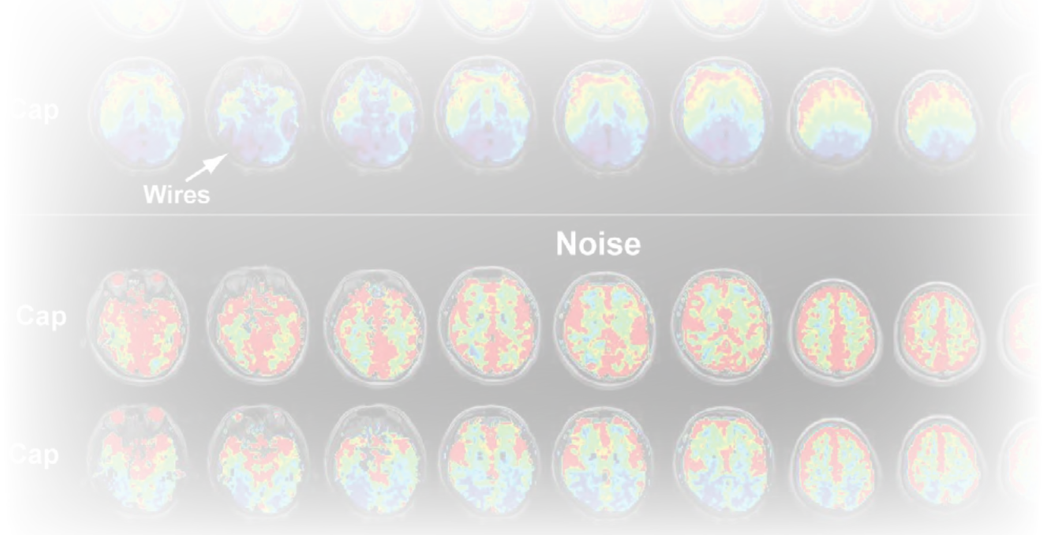

MR-guided High Intensity Focused Ultrasound for Pre-surgical Localization of Occult Breast Tumors

R Bitton[1], E Kaye[2], F Dirbas[3], B Daniel[1], K Butts-Pauly[1]
Departments of [1]Radiology, [2]Electrical Engineering, [3]Surgery, Stanford University, CA

Breast conservation surgery (BCS) has become a standard of care as an accepted alternative to mastectomy in patients suffering from limited stage breast cancer 1. Non-palpable tumors present a challenge for surgeons, as palpability often locates the tumor in the breast. The most clinically accepted standard is image-guided single needle wire localization2. Wire localization has several downsides, including wire dislocation between placement and surgery, wire entry site conflicting with ideal surgical site, and the inability to delineate non-palpable tumor boundaries of irregular shape3. As an alternative to wire localization, we propose using MR-guided High Intensity Focused Ultrasound (MR-HIFU) to create thermal lesions that circumscribe a non-palpable breast tumor, providing an excision guide during breast conservation surgery. We use an elastography technique called MR Acoustic Radiation Force Imaging (MR-ARFI) to "remotely palpate" ablations and test lesion stiffness in ex vivo cadaveric breast.

MR-HIFU ablations spaced 5mm apart were made in 18 locations using the ExAblate2000® system. Ablations were formed a square perimeter in mixed adipose and fibroglandular tissue. Ablation was monitored using T1wFSE images. MR-ARFI was used to remotely palpate each ablation location, measuring tissue displacement before and after thermal sonications. Profiles centered at each ablation spot were plotted for comparison. The cadaveric breast was manually palpated to assess stiffness of ablated lesions and dissected for gross examination. This study was repeated on three cadaveric breasts.

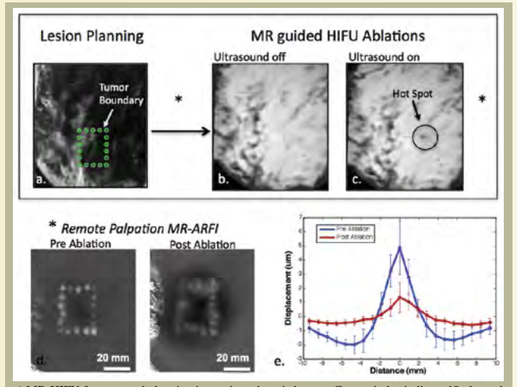

a) MR-HIFU fat saturated planning image in cadaveric breast. Green circles indicate 18 planned ablation lesions representing a tumor boundary. b,c) Treatment monitoring during breast tissue ablation. T1wFSE images b) before ablation with US off and c) during ablation with US on, showing the location of the focal spot. d)* Indicates MR-ARFI remote palpation. MR-ARFI phase maps show baseline displacement before MR-HIFU ablation (left), and after ablation (right). e) MR-ARFI displacement profiles (mean ± std) where post ablation profiles (red) show a reduction in tissue displacement, indicating increase in tissue stiffness.

MR-ARFI showed a collective post ablation reduction in displacement of 54.8%, indicating the tissue became stiffer after the ablation. Manual palpation and dissection of the breast confirmed increased palpability, a darkening of ablation perimeter, and individual ablations visible in fibroglandular tissue.

The results of this preliminary study show MR-HIFU has the ability to create palpable lesions in ex vivo cadaveric breast tissue, and may potentially be used to pre-operatively localize non-palpable breast tumors.

References/Funding Source R Bitton, E Kaye, F Dirbas, B Daniel, K Butts-Pauly. Toward MR-guided High Intensity Focused Ultrasound for Pre-surgical Localization: Focused Ultrasound Lesions in Cadaveric Breast Tissue. J Magn Reson Imaging (in press). 1. M Morrow, E Strom, L Bassett, et al. Standard for breast conservation therapy in the management of invasive breast carcinoma. CA: a cancer journal for clinicians 2002;52(5):277-300. 2. R Bigelow, R Smith, PA Goodman, GS Wilson. Needle localization of nonpalpable breast masses. Arch Surg 1985;120(5):565-569. 3. RJ Gray, C Salud, K Nguyen, et al. Randomized prospective evaluation of a novel technique for biopsy or lumpectomy of nonpalpable breast lesions: radioactive seed versus wire localization. Annals of Surgical Oncology 2001;8(9):711-715. Support: California Breast Cancer Research Program of the University of California, Grant Number 16FB-0090, and the Lucas Foundation.

Real Time Respiration Based Steering for High Intensity Focused Ultrasound in the Liver

AB Holbrook[1], C Dumoulin, JM Santos, Y Medan, K Butts-Pauly[1]
Department of [1]Radiology, RSL, [2]Bioengineering, Stanford University, CA; [3]Department of Radiology, Cincinnati Children's Hospital Medical Center, Cincinnati, OH; [4]HeartVista, Inc, Palo Alto, CA; [5]InSightec, Ltd, Tirat Carmel, Israel

Free breathing HIFU liver treatment requires maintenance of the target focus, requiring tracking of both target and transducer. We developed an MR-guided system for guiding liver ablation, with key elements being target tracking and steering through correlation with respiratory bellows and temperature monitoring. The purpose of this work was quantifying steering accuracy with this approach. A phantom was immersed in water and placed above a fixed phased-array transducer. The setup was positioned inside a 3T scanner. A servo-motor moved the phantom sinusoidally, with an attached respiratory belt measuring motion. The phantom's edge was marked on pre-heating images and tracked throughout motion, and built-in tracking coils determined transducer position. Upon target selection, a lookup table relating transducer phases to respiration was created. MR-ARFI was performed throughout the motion for calibration. Thermal images were collected with a thermometry sequence with hybrid multibaseline/ referenceless reconstruction. Stationary, non-steered, and steered ablations were performed until each ablation reached 15 degrees C. Steered ablations required slightly higher more energy (118 J, 12.8% more energy) to reach this target compared to a static ablation, while unsteered ablations required 6559 J (812%) more energy to achieve this. The spot dimensions of the steered ablations were very similar to static ablations.

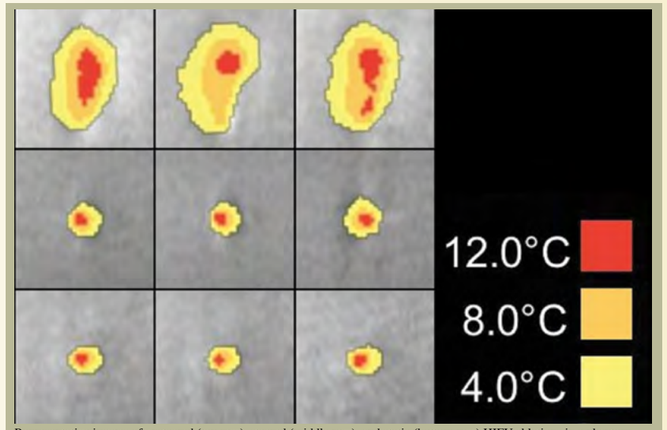

Representative images of unsteered (top row), steered (middle row), and static (bottom row) HIFU ablations in a phantom. Note that the steered ablations very closely resemble the static examples.

References/Funding Source AB Holbrook, CL Dumoulin, JM Santos, Y Medan, K Butts-Pauly. Real Time Respiration Based Steering for High Intensity Focused Ultrasound in the Liver. ISMRM 19th Scientific Meeting, 525, 2011. AB Holbrook, JM Santos, Y Medan, K Butts-Pauly. Real Time Respiration Based Steering for High Intensity Focused Ultrasound in the Liver. 11th International Symposium on Therapeutic Ultrasound in New York, NY. April 10-13, 2011. R01-CA121163, P41-RR09784

Fabrication of CMUT 2D arrays using Thick-BOX process for HIFU liver ablation

HS Yoon[1], S Vaithilingam[1], F Sarioglu[1], M Kupnik[1], K Butts-Pauly[2], BT Khuri-Yakub[1]
Departments of [1]Electrical Engineering, [2]Radiology, Stanford University, CA

Recently, we have developed capacitive micromachined ultrasonic transducer (CMUT) for high intensity focused ultrasound (HIFU) liver ablation. To meet the challenging demands of the large area arrays, we are using a new fabrication process named "Thick-BOX process" as it allows the top silicon surface to be ground resulting in good shielding for human safety and better signal quality. The "Thick BOX" layer in the substrate wafer is a robust cell structure with immunity to breakdown voltage. Starting with SOI wafer, 0.4-µm of gap height is defined using double oxidation method. Deep trenches around the gap are then etched down to the BOX layer to isolate the center silicon electrode. 0.4-µm of thermal oxide is grown as an insulation layer, followed by direct wafer bonding using chemical surface activation. For the backside electrical access, via holes are etched from the backside and filled with poly silicon. Under bump metallization is stacked with Al, Ti, Ni and Au, then electrically isolated by trenches on the backside. Handle layer is removed by isotropic dry etching also by wet etching for oxide layer. Top exposed plate is patterned and etched to connect the top plate to the ground. Finally, thin aluminum layer is evaporated with 45 ° angle to connect the sidewalls of the top silicon plate of the ground cells. Electrical impedance is measured with 1mm single-element transducers, resonant frequency are around 2.5 MHz 3 MHz in air. As next tasks, the small transducers will be tiled to 2D arrays, tuned with inductors and output pressure will be measured in immersion.

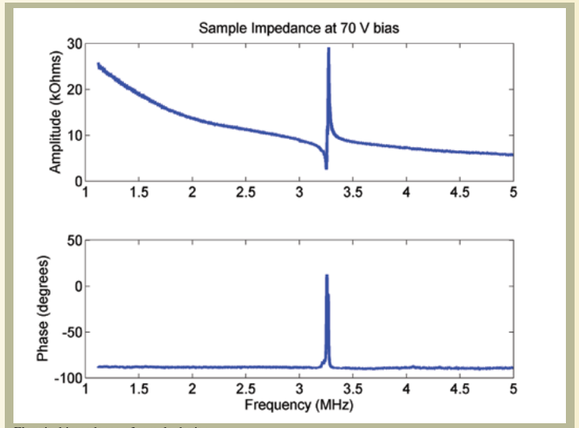

Electrical impedance of sample device

References/Funding Source NIH

Measuring temperature rise during spin echo MR-ARFI acquisition

E Kaye[1,2], K Butts-Pauly[2]
Departments of [1]Electrical Engineering, [2]Radiology, RSL, Stanford University, CA

MR-guided Focused Ultrasound (FUS) is a promising minimally invasive treatment for various pathologies [1-2]. During the targeting stage of the treatment, the transducer is calibrated to insure the accurate position of the focal spot based on small temperature rise sonications, and visualized with MR using PRF thermometry. MR Acoustic Radiation Force Imaging (MR-ARFI) has been recently demonstrated [3-4] as an alternative tool for focal spot localization that is not expected to produce a temperature rise. To ensure safe use of such sequences in this work we show how temperature and displacement can be monitored simultaneously using a modified spin echo MR-ARFI pulse sequence (Figure 1).

A spin echo MR-ARFI pulse sequence was modified to acquire a gradient echo after 90º RF pulse. The sequence was tested in ex vivo porcine brain tissue using a planar FUS transducer. The duration of the FUS pulse was 18 ms. The acoustic power was varied from 37W to 185W in step of 18W and at each power level a temperature map and a displacement map were acquired simultaneously using a 3T GE MRI scanner. GRE TE was 10 ms and SE TE was 47 ms.

The temperature and displacement images are shown in Figure 2. The mean temperature and mean displacement calculated in the 4 pixel region of interest in the center of focal spot are plotted as a function of power. Both quantities linearly increase with power. The results show that 1 to 2 degree temperature rise is anticipated for the lowest acoustic power necessary to produce measurable displacement. This temperature rise should be negligible in perfused tissue, however, if the MR-ARFI is going to be performed repeatedly, temperature monitoring could be still beneficial.

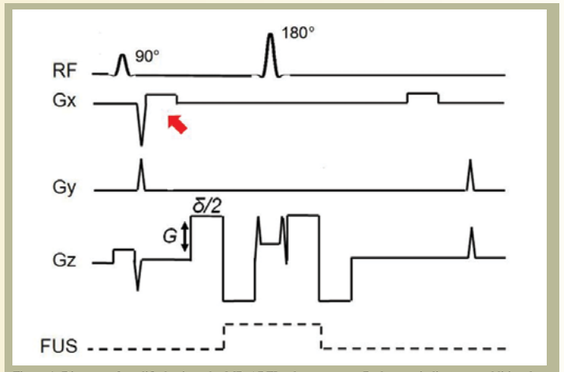

Figure 1. Diagram of modified spin echo MR-ARFI pulse sequence. Red arrow indicates an additional echo incorporated for temperature measurements.

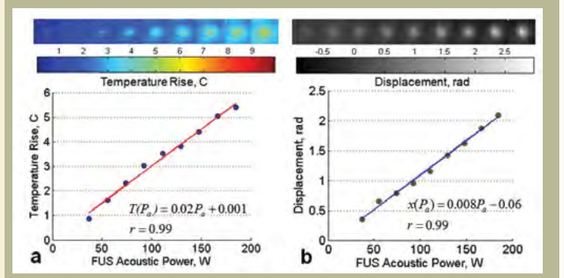

Figure 2. Top: cropped 2.6 cm2 a) temperature rise images and b) displacement images obtained for varying acoustic power. Bottom: mean a) temperature and b) displacement calculated in the focal spot at each power level. Data and linear fits are displayed.

References/Funding Source Proceedings of ISMRM 2011, Montreal, Canada [1] K. Hynynen et al., Radiology (219) 2001. [2] E Martin, et al., Ann Neurol (66) 2009. [3] N.McDannold, et al., Med Phys, 35(8):3748–58, 2008. [4] J Chen, et al, MRM (63), 2010. NIH R21 EB011559.

Real-time Monitoring of Tissue ADC During High Intensity Ultrasound Ablation of the Prostate

J Plata[1], A Holbrook[1], P Prakash[2], V Salgaonkar[2], P Jones[2], C Diederich[2], G Sommer[1], K Butts-Pauly[1]
[1]Department of Radiology, Stanford University, CA; [2]University of California San Francisco, CA

Introduction Diffusion weighted MRI (DWI) has demonstrated a 36% reduction in ADC following high intensity ultrasound (HIU) induced tissue damage of the prostate. Unlike contrast-enhanced MRI (CE-MRI), the current "gold standard" for assessing tissue viability, DWI can be used repeatedly because it is not affected by contrast material present in the tissue. In addition, real-time DWI can potentially provide insight as to how tissue properties are changing during the procedure, allowing for a physiological measure of treatment completion.

Methods A real-time DWI tool was developed based on EPI with b values <= 1000s/mm^2, in 3 directions, for a scan time of 6 s for each ADC map. Real-time ADC monitoring during ex vivo tissue ablation was performed with an Insightec Conformal Bone System (37 acoustic Watts for 100 s). Accuracy of the tool was verified by demonstrating the known ADC drop in vivo after transurethral ultrasound ablation of the canine prostate.

Results and Discussion Real time ADC monitoring of ex vivo tissue demonstrated increased ADC values from 0.912x10^{-3}mm^2/s to 1.153x10^{-3}mm^2/s at the peak of heating (p=2.6x10^{-4} , N=4), returning to 0.992x10^{-3}mm^2/s (p=0.045, N=4) five minutes after ablation. In vivo ADC values changed from 1.93x10^{-3} mm^2/s (preablation) to 1.23x10^{-3} mm^2/s (80 minutes post-ablation), verifying the known 36% ADC drop seen after in vivo ablation of the prostate.

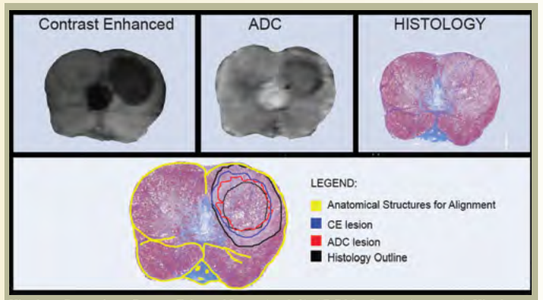

Histology Comparison: Contrast Enhanced Image (top left), ADC Map Image, (top center), Histology (top right), Outlines of lesion superimposed over the histology (bottom) where yellow lines represent anatomical structures that were used for image registration.

References/Funding Source JC Plata, AB Holbrook, P Prakash, V Salgaonkar, P Jones, C Diederich, G Sommer, K Butts-Pauly. Realtime Monitoring of Tissue Viability HIU Treatment with DWI. Poster session presented at International Society of Therapeutic Ultrasound; 2011 April 11-13; New York City, NY. NIH RO1 CA111981, NIH T32 EB009653

Hybrid PRF-Thermometry for MRgFUS Brain Applications

V Rieke[1], B Werner[2], N McDannold[3], W Grissom[4], E Martin[2], K Butts-Pauly[1]
[1]Department of Radiology, RSL, Stanford University, CA; [2]MR-Center, University Children's Hospital Zurich, Switzerland; [3]Department of Radiology, Brigham and Women's Hospital, MA; [4]Imaging Technologies Laboratory, GE Global Research, Munich, Germany

Objective: Clinical applications for MR-guided focused ultrasound in the brain have included tumor ablation and neuropathic pain management, and may include the treatment of Parkinson's disease, tremor, and epilepsy. MRI has the ability to provide tissue temperature, but the phase subtraction process for PRF thermometry is hampered by motion artifacts. Here we investigate if a hybrid multibaseline/referenceless temperature reconstruction method can reduce these errors compared to the conventional single baseline subtraction method.

Material and Methods: Sagittal brain images from five patients acquired during FUS treatment were reconstructed with the two different methods and temperature uncertainties were compared. We also reconstructed images from normal volunteers without heating. The volunteers were instructed to remain as motionless as possible for the first part of the MR scan, then to purposefully perform tongue or jaw movement, or to take a deep breath.

Results: Temperature maps of one patient undergoing FUS ablation are shown in Fig. 1. The hybrid method shows a clear depiction of the heating spot, almost completely removing the severe errors present when using baseline subtraction (~1ºC) in all areas.

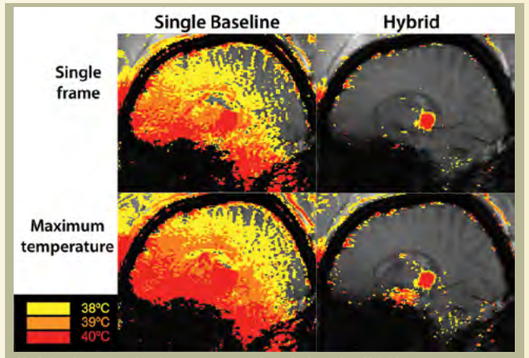

Single baseline subtraction shows severe errors due to brain motion. Hybrid reconstruction shows a clear depiction of the heating spot, almost completely removing the severe errors present when using baseline subtraction.

The volunteer images showed temperature fluctuations over time with baseline subtraction possibly caused by pulsation of the brain. These fluctuations were much reduced and hardly noticeable with the hybrid method. Tongue and jaw movement as well as taking a deep breath caused severe errors in baseline subtraction, whereas hybrid reconstruction showed only a minimal increase in temperature errors.

Conclusion: These results show that the hybrid method is beneficial to monitor FUS ablation in the brain. It is robust to spontaneous events such as swallowing, jaw or tongue movement, or changes in respiration. Hybrid thermometry accurately measures temperature in the brain with less artifacts and errors than baseline subtraction.

References/Funding Source V Rieke, B Werner, N McDannold, W Grissom, E Martin, K Butts-Pauly. Hybrid referenceless and multi-baseline thermometry for MRgFUS brain applications. 19th ISMRM, Montreal, Canada, 2011, #1771. NIH K99 HL09703, NIH R21 EB011559, NIH P41 RR009784, Lucas Foundation.

Prospective Motion Correction for Diffusion-weighted Breast Imaging

KL Granlund[1,2], CJ Moran[1], E Staroswiecki[1,2], MT Alley[1], BL Daniel[1], BA Hargreaves[1]
Departments of [1]Radiology, RSL, [2]Electrical Engineering, Stanford University, CA

The Double Echo Steady State (DESS) sequence [1,2] has been shown to provide high-resolution T2- and diffusion-weighted images in short scan times and with low distortion [3,4]. Such image contrast is useful for improving the specificity of breast MRI [5,6] without the need for an exogenous contrast agent. This steady-state sequence can also be used to quantify T2 and ADC [7,8]. However, the DESS sequence, like all diffusion-weighted sequences, is sensitive to motion, and breast imaging is affected by cardiac, respiratory, and bulk patient motion. We evaluated different techniques for reducing the motion artifact in DESS imaging of the breast including breath holding, physiological gating, and non-sequential phase encode ordering.

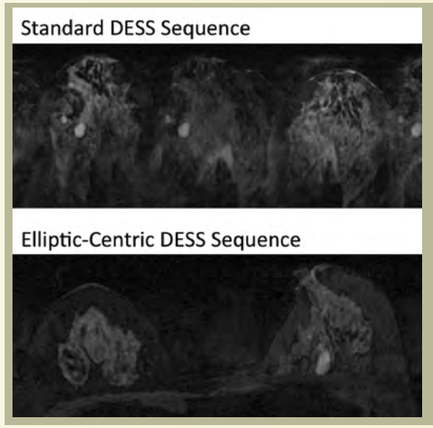

Top image shows a patient scanned with the standard DESS sequence. Motion artifact causes signal to appear in the center of the image, where there is no tissue. The motion artifact obscures the anatomy, impeding diagnosis. Bottom image shows a patient scanned with elliptic-centric phase-encode ordered DESS sequence. The motion artifact is visually suppressed, and a cyst is clearly seen on the right side of the image.

We compared a standard DESS scan to a breath-held scan, a cardiac-gated scan, a respiratory-gated scan, a cardiac- and respiratory-gated scan, and an elliptic-centric phase-encoded scan. The breath-held scan slightly reduced the motion artifact, but limited the resolution and field of view that we could acquire in the limited scan time (~30s). The physiological gating did not sufficiently reduce the artifact and the resulting scan times were prohibitively long: the cardiac-gated scan and respiratory gated scans were twice as long as the standard scan, and the cardiac- and respiratory-gated scan was four times as long as the standard scan. Using elliptic-centric phase encode ordering (phase encodes near the center of k-space are acquired first [9]) visually suppressed the motion artifact without affecting the scan time.

The DESS sequence results in images with much lower distortion than the standard DWI sequence, though it is still sensitive to motion. We found that using an elliptic-centric phase encoding order results in the best improvement in image quality and does not increase the scan time or limit resolution. Further improvements in image quality may be possible with retrospective correction.

References/Funding Source KL Granlund, CJ Moran, E Staroswiecki, MT Alley, BL Daniel, BA Hargreaves. Prospective Motion Correction for Diffusion-weighted Breast Imaging. Proc. of 19th ISMRM, Montreal, 2011. p. 1017. [1] T Redpath, et al. MRM 1988; 6:224-34. [2] Bruder H, et al. MRM 1988; 7:35-42. [3] K Granlund, et al. ISMRM 2010; 366. [4] E Staroswiecki, et al. ISMRM 2010. [5] CK Kuhl, et al. JMRI 1999; 9(2):187-96. [6] Y Guo, et al. JMRI 2002; 16:172-8. [7] Welsh, et al. MRM 2009; 62:544-9. [8] E Staroswiecki, et al. ISMRM 2011. NIH Grant EB009055; NIH Grant EB012591; NIH Grant RR009784; Richard M. Lucas Foundation; GE Healthcare; NSF Graduate Research Fellowship Program

Musculoskeletal MRI at 7.0T: Relaxation Times and Image Contrast

CD Jordan[1,2], M Saranathan[1], E Starosweicki[1,3], N Bangerter[4], BA Hargreaves[1], GE Gold[1]
Departments of [1]Radiology, [2]Bioengineering, [3]Electrical Engineering, Stanford University, CA; [4]Electrical & Computer Engineering, Brigham Young University, Provo, UT

The purpose of our study was to measure the relaxation times of musculoskeletal tissues at 7.0T, to compare them with 3.0T, and to optimize musculoskeletal MRI methods at 7.0T. In the knees of five healthy volunteers for each measurement, we measured the T1 and T2 relaxation times of cartilage, muscle, synovial fluid, bone marrow and subcutaneous fat at 7.0T. The T1 relaxation times were measured using a Spin-Echo Inversion Recovery Sequence at six inversion times. The T2 relaxation times were measured using a Spin-Echo sequence with seven echo times. Accuracy of the T1 and T2 measurements was verified in phantoms. The measurements of T1 and T2 were compared with the same volunteers at both 3.0T and 7.0T. The relaxation times will be used to develop high resolution protocols for proton density fast spin echo sequences, T2-weighted fast spin echo sequences, and 3D CUBE sequences at 7.0T that had similar fluid-cartilage contrast as the standard clinical protocols at 3.0T. MRI at 7.0T can ultimately be used to improve resolution in musculoskeletal imaging.

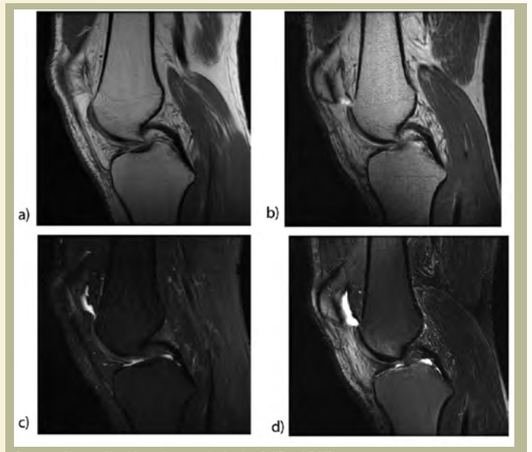

Images of knee of healthy volunteer obtained at 3.0T and 7.0T:
a) Sagittal Proton Density-FSE at 3.0T with an in-plane resolution of 0.11mm^2 b) Sagittal Proton Density-FSE at 7.0T with an in-plane resolution of 0.028 mm^2 c) Sagittal T2-weighted-FSE at 3.0T with an in-plane resolution of 0.159 mm^2 d) Sagittal T2-weighted-FSE at 7.0T with an in-plane resolution of 0.057 mm^2

References/Funding Source Lucas Foundation, Arthritis Foundation Grant.

High-Resolution 3D T2-Weighted Imaging for Improved Lesion Characterization in Breast MRI

CJ Moran[1], AN Nnewihe[1,2], BL Daniel[1], KL Granlund[1,3], BA Hargreaves[1]
Departments of [1]Radiology, [2]Bioengineering, [3]Electrical Engineering, Stanford University, CA

Breast MRI has emerged as a promising adjunct to mammography for the detection and diagnosis of breast cancer. In particular, MRI has shown promise in women that have a high risk of developing breast cancer based on genetic predisposition or family history [1]. The strength of breast MRI is that most malignant lesions are detected, however, distinguishing benign from malignant lesions can be challenging. The inability to clearly determine that a lesion is benign can lead to unnecessary biopsies and follow-up exams.

The Body MRI group at Stanford has been working on multiple techniques to improve the diagnostic capabilities of breast MRI. The purpose of this specific project is to provide high-resolution, high-SNR T2-weighted breast images by combining a new GE 3D T2-weighted sequence (FSE-Cube) [2] with a prototype breast coil [3]. T2-weighted images have been shown to help in the characterization of benign lesions, but inherent limitations of conventional T2-weighted methods restrict this information. The GE FSE-Cube sequence that we utilize addresses some of these limitations and thus provides high-resolution T2-weighted images in clinically feasible scan times. The prototype breast coil developed by our group achieves 3-4 times improvement in SNR in comparison to a clinically available breast coil, further facilitating the acquisition of very high-resolution images.

Signal-to-noise and resolution comparisons were performed with the FSE-Cube sequence in volunteers and demonstrated a 4 times improvement in SNR in the T2-weighted GE FSE-Cube images using the prototype coil and a 65% reduction in voxel size. In asymptomatic volunteers, the improved resolution allows for clear depiction of fine tissue structure in the T2-weighted images (Figure) thus potentially expanding the diagnostic utility of these images as clear depiction of fine tissue structure can help in the characterization of benign lesions. Studies of this method in patients with biopsy-proven lesions are ongoing.

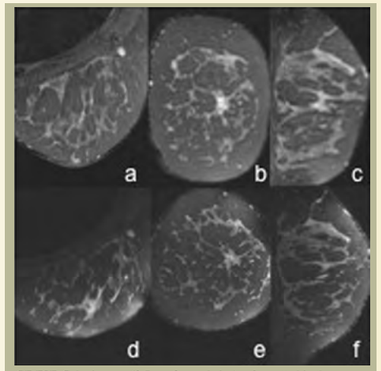

GE FSE-Cube images (0.7 mm3 voxel size) reformatted in three orthogonal planes (a,d: axial, b,e: coronal, c,f: sagittal) demonstrate the improved depiction of fine structural detail available with the prototype breast coil (d-f) in comparison to the reformatted images (2.25 mm3 voxel size) from a commercially available 8-channel coil (a-c). The improved depiction of fine structural detail in all reformats may impact the diagnostic utility of T2-weighted images in the breast as certain structural lesion characteristics differ between benign and malignant lesions.

References/Funding Source 1. D Saslow, et al., CA Cancer J Clin 2007; 57:75–89. 2. RF Busse, et al., MRM 2006; 55:1030-37. 3. A Nnewihe, et al., MRM, 2011. Support provided by NIH EB009055, GE Healthcare

RF Induced Heating On or Near Passive Metallic Implants

U Monu[1], P Worters[2], GE Gold[2], BA Hargreaves[2]
Departments of [1]Electrical Engineering, [2]Radiology, Stanford University, CA

As MRI is a key imaging modality used for orthopedic patient care, the safety of commonly used metallic implants in an MRI environment is important. Metallic implants can cause elevated energy deposition near the implant and induce local tissue heating. This, combined with reported cases of pain, heating and burns [1], means there is a need to thoroughly evaluate and quantify the RF power on the tissue surrounding metallic implants.

This study addresses this issue by measuring temperature changes at points of possible maximum SAR deposition, on three common metallic implants: shoulder (180mm long), hip (205mm long) and spinal pedicles (150mm long). Temperature measurements were obtained with and without the metallic implant at 1.5T and 3T in a 30kg rectangular shaped gel phantom that simulates the electrical and thermal properties of the human body. Measured temperature differences for three consecutive runs over a 15min scan period were obtained.

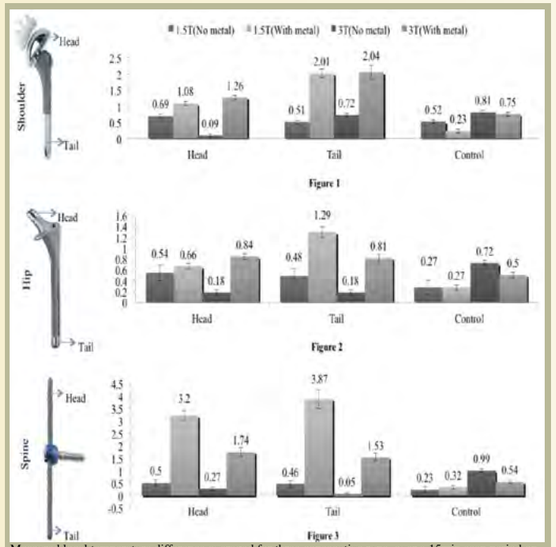

Measured local temperature difference averaged for three consecutive runs, over a 15min scan period on the shoulder implant (Figure1), hip implant (Figure 2) and spinal implant (Figure 3)

The highest temperature changes were observed on the spinal implant with temperature increases at the head and tail of the implant of up to 3.8 o C at 1.5T and 1.7 o C at 3T (Figure 3). Both the shoulder implant and hip prosthesis recorded a lower temperature rise at both 1.5T and 3T than the spinal implant (Figure 1, 2). For the spinal implant, RF heating [2] may account for the higher temperature values of the thinner construct as opposed to the larger surface area of the hip and shoulder implant.

Factors such as phantom geometry, metallic material and perfusion expected in a heterogeneous human body have been excluded and should be taken into consideration when analyzing the results demonstrated. Spinal fixation devices up to 40cm in length are currently used in patients with scoliosis and may produce more heating, so further investigation of these and other devices is needed.

References/Funding Source [1] FDA-Medical-Device-Reporting Database, Access Number:M375292. [4] MK Konings, et al. Catheters and Guidewires in interventional MRI:problems and solutions. Medica Mundi 2001; 45: 31–39. GE Healthcare, EB 008190, NIH EB002524.

Novel Variable Voxel Intensity Correction Scheme and Application to Breast Imaging

A Nnewihe[1,2], K Sung[1], BL Daniel[1], BA Hargreaves[1]
Departments of [1]Radiology, RSL, [2]Bioengineering, Stanford University, CA

High-density surface coil arrays have been used for attaining highly accelerated, high-resolution images for brain, breast and cardiac MRI studies. Due to the layout and size of the coil elements, these arrays usually exhibit sensitivity variations across the field of view. Several intensity-correction schemes have been investigated in literature, and many of these algorithms significantly change the spatial noise profile. Especially, in cases with large coil sensitivity variations, these corrections can obscure the overall image quality. In this study, we introduce a novel variable voxel size intensity correction method that reduces intensity variations across the image while keeping the desired noise profile. This is a new approach for intensity correction as it involves lowering spatial resolution in low sensitivity areas in order to gain SNR. For in vivo breast imaging, we compare this novel technique to two commercially available techniques: PURE (Phased array UnifoRmity Enhancement) and SCIC (Surface Coil Intensity Correction) [GE Healthcare]. PURE corrects field inhomogeneities using a low-resolution proton density weighted calibration scan. SCIC utilizes statistics from the actual image for inhomogeneity correction and does not require a calibration scan. Each technique shows improved signal uniformity in the breasts. Using the correction techniques, the glandular structures at the posterior of the breast become more isointense with the anterior of the breast. However, the PURE algorithm shows noise amplification at the background and between the breasts (see zoomed portion), while the variable voxel technique minimizes this added noise at the expense of spatial resolution in these areas. The SCIC image is less noisy when compared to PURE, but SCIC has poorer visualization of some areas of the chest wall (see arrow) in comparison to the other two techniques. Figure 1(bottom) shows the increase in voxel volume with reference to the original image.

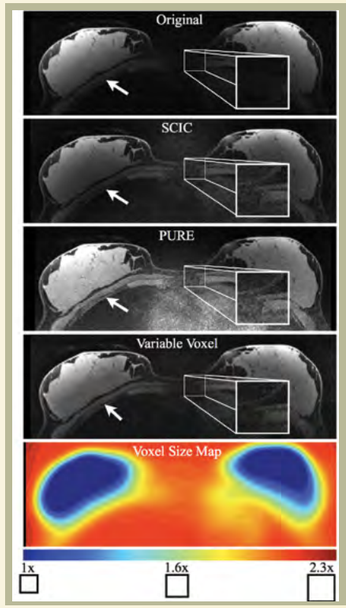

T1W Axial Images of Healthy Volunteer. We windowed images a) - d) at the same level relative to the brightest voxel in each image. SCIC shows subpar visualization of the chest wall in some areas (see arrow), and there is noticeable noise amplification between the breasts using PURE (see zoomed-in portion). The variable voxel approach provides clear visualization of the chest wall and breast, while minimizes the noise at the expense of reduced spatial resolution in peripheral areas.

References/Funding Source A Nnewihe, K Sung, B Daniel, B Hargreaves. “Novel Variable Voxel Intensity Correction Scheme and Application to Breast Imaging.” 19th ISMRM Meeting, May 2011. P41RR009784, R01-EB009055, and GE Healthcare.

Simultaneous Fat Suppression and Band Reduction with Large-Angle Multiple-Acquisition bSSFP

B Quist[1], BA Hargreaves[1], T Cukur[2], GR Morrell[3], GE Gold[1], NK Bangerter[3,4]
Departments of [1]Radiology, [2]Electrical Engineering, Stanford University, CA; [3]Department of Radiology, University of Utah, Salt Lake City, UT; [4]Department of Electrical & Computer Engineering, Brigham Young University, Provo, UT

Balanced steady-state free precession (bSSFP) MRI is a rapid and SNR-efficient imaging method, but suffers from characteristic bands of signal loss in regions of large field inhomogeneity. Several methods have been developed to reduce the severity of these banding artifacts, typically involving the acquisition of multiple bSSFP data sets. Fat suppression with bSSFP is also challenging; most existing methods require an additional increase in scan time, and some are incompatible with bSSFP band-reduction techniques.

This work was motivated by the need for both robust fat suppression and band reduction in the presence of field inhomogeneity when using bSSFP for flow-independent peripheral angiography. The large flip angles used in this application to improve vessel conspicuity and contrast lead to SAR considerations, longer TR, and increased severity of banding artifacts. In this work, a novel method that simultaneously suppresses fat and reduces bSSFP banding artifact with the acquisition of only two phase-cycled bSSFP data sets is presented. The technique exploits the near-sinusoidal shape of the bSSFP off-resonance spectrum for many tissues at large (>50 degrees) flip angles. The spectral profiles can be shifted to approximate a sine and cosine by incrementing the phase of the RF pulse by some $\Delta\varphi = 0°$ and $\Delta\varphi = 180°$, respectively, from excitation to excitation. A dataset with spectral profile shifted by an arbitrary Δf can then be synthesized from the two acquisitions using the relationship $\sin(f+\Delta f) = \cos(\Delta f)\sin(f) + \sin(\Delta f)\cos(f)$. This relationship is exploited on a voxel-by-voxel basis, where Δf is chosen so that the fat signal is in the stop band while keeping water signal in the pass band.

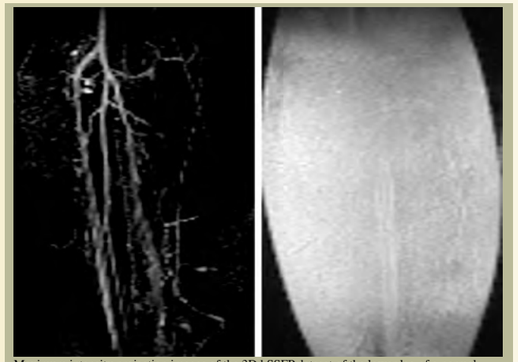

Maximum intensity projection images of the 3D bSSFP dataset of the lower leg of a normal volunteer at 1.5T with the proposed Large-Angle Multiple-Acquisition (LAMA) bSSFP reconstruction with fat suppression (left), and standard root sum-of-squares reconstruction without fat suppression (right). The LAMA bSSFP effectively suppresses fat while eliminating banding.

A maximum intensity projection (MIP) image of the 3D dataset before and after fat-suppression with our new technique is shown in Figure 1. Our new technique performs quite well, effectively eliminating banding artifact and accurately suppressing much of the fat.

References/Funding Source B Quist, BA Hargreaves, T Cukur, GR Morrell, GE Gold, NK Bangerter. Simultaneous Fat Suppression and Band Reduction with Large-Angle Multiple-Acquisition bSSFP. Magnetic Resonance in Medicine 2011 (in press). This work was supported by NIH 1 R01 HL075803-01, NIH R01 EB002524-01, NIH 5 K08 CA112449, The Ben B. and Iris M. Margolis Foundation, and Brigham Young University.

Simultaneous Estimation of T_2 and ADC in Cartilage with a Modified 3D DESS Sequence

E Staroswiecki[1,2], KL Granlund[1,2], MT Alley[1], GE Gold[1], BA Hargreaves[1]
Departments of [1]Radiology, RSL, [2]Electrical Engineering, Stanford University, CA

Osteoarthritis is a degenerative joint disease that involves functional, structural, morphological, and biochemical changes to the cartilage. Assessing articular cartilage in the early stages of disease with MRI requires techniques that are sensitive to both cartilage morphology and matrix changes. T2 mapping and diffusion-weighted imaging complement morphological imaging for assessing cartilage disease and injury. The double echo steady state (DESS) sequence has been used for morphological imaging and generates two echoes with markedly different T2 and diffusion weighting. Modifying the spoiler gradient area and flip angle in DESS allows greater control of the diffusion weighting of both echoes. Data from two acquisitions with different spoiler gradient areas and flip angles are used to simultaneously estimate the T2 and apparent diffusion coefficient (ADC) of each voxel. This method is verified in phantoms and validated in vivo in the knee; estimates from different regions of interest in the phantoms and cartilage are compared to those obtained using standard spin-echo methods. Both phantom and in vivo validation show remarkable agreement between our new method and the standard methods. However, our method achieves full-knee T2 maps faster and with fewer limitations than the standard method, and ADC maps without distortions that are typical of standard methods. High accuracy, both for simultaneous 3D T2 and apparent diffusion coefficient measurements, is demonstrated, while also providing morphologic 3D images without blurring or distortion in reasonable scan times of around 12 min.

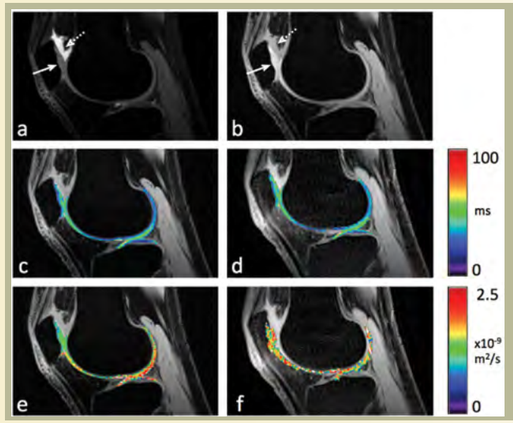

Detail of sagittal modified 3D DESS images, ADC and T2 maps of the knee in vivo. Sum-of-squares image from the modified 3D DESS acquisition with lower diffusion weighting (a) and with higher diffusion weighting (b). The different diffusion weightings clearly result in different contrasts between cartilage (solid arrow) and fluid (dashed arrow) in (a) and (b). Both the DESS T2 map (c) overlaid on (b) and the standard FSE T2 map (d) overlaid on a source FSE T2-weighted image exhibit the expected variation within cartilage, including magic angle effects. The DESS ADC map (e) overlaid on (b) does not show any distortion or blurring, while the standard SE-DWI ADC map (f) overlaid on a source FSE T2-weighted image is clearly distorted.

References/Funding Source E Staroswiecki, KL Granlund, MT Alley, GE Gold, BA Hargreaves, Simultaneous Estimation of T2 and ADC in Human Articular Cartilage In Vivo with a Modified 3D DESS Sequence at 3 T. Proc. of the 19th ISMRM, Montreal, Canada, p. 500. E Staroswiecki, KL Granlund, MT Alley, GE Gold, BA Hargreaves, Simultaneous Estimation of T2 and Apparent Diffusion Coefficient in Human Articular Cartilage In Vivo with a Modified Three-Dimensional Double Echo Steady State (DESS) Sequence at 3 T. Magn. Reson. Med., in press.Arthritis Foundation, GE Healthcare, NIH grants: EB002524, EB009055, EB012591, RR009784

Mapping of T2 and ADC in Articular Cartilage Using DESS with B1 Correction

B Sveinsson[1,2], BA Hargreaves[1]
Departments of [1]Radiology, [2]Electrical Engineering, Stanford University, CA

Measurements of T2 and diffusion in articular cartilage can provide a valuable indication of potential damage or degenerative disease such as osteoarthritis. The Double-Echo-Steady-State (DESS) method, a variant of steady state magnetic resonance imaging, has been shown to provide fast and reliable estimates of both parameters[1]. This is achieved by running two DESS acquisitions with different flip angles and spoiler gradients and comparing the resulting four acquired echoes to mathematical signal models relating the echo strengths to the parameters of the tissue. This method, however, is sensitive to unwanted deviations in the applied flip angle during the scan.

We have increased the accuracy of using DESS for estimation of T2 and diffusion by acquiring a B1 map along with the DESS acquisitions and incorporating the flip angle deviations into the fitting of the measurements to the signal models. The method has been tested on standard phantoms with the results showing greatly increased robustness to flip angle variations. We plan to further improve this method by increasing the quality and speed of the B1 map acquired and tuning the sensitivity of the signal model fit, as well as increasing the speed of the fit. The method will also be extended to in vivo measurements.

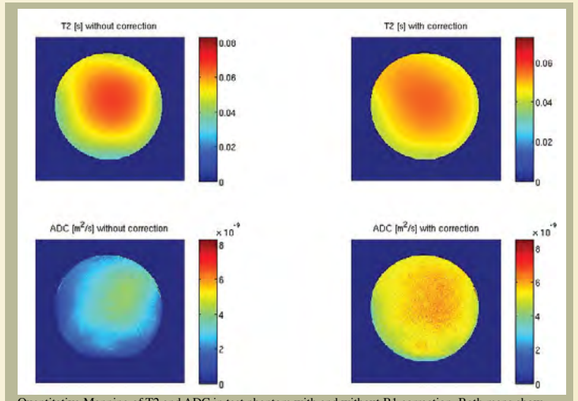

Quantitative Mapping of T2 and ADC in test phantom with and without B1 correction. Both maps show improved homogeneity with B1 mapping.

References/Funding Source [1] E Staroswiecki. Simultaneous Estimation of T2 and ADC in Human Articular Cartilage In Vivo with a Modified 3D DESS Sequence at 3 T. Magnetic Resonance in Medicine. In press. NIH: R01-EB002524

Abdominal MRA using Breath-hold, IR-prep, Dixon bSSFP

PW Worters, M Saranathan, SS Vasanawala, BA Hargreaves
Department of Radiology, Stanford University, CA

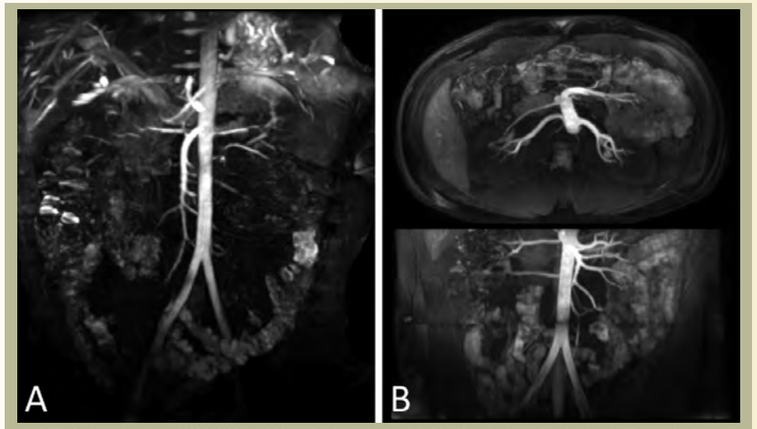

(A) MIP of a three-slab, coronal NORISKS acquisition using three 18-s breath-holds. Note the decreasing signal in the iliac arteries due to reduced arterial inflow. (B) Axial and reformatted coronal MIPs of a two-slab, axial acquisition using two 24-s breath-holds, showing the renal and mesenteric arteries.

Inflow-based MR angiography methods without administration of an intravenous contrast agent have been used successfully in recent years to provide bright-blood angiograms of the abdominal arteries [1]. However, these methods typically use free-breathing acquisitions (3-6 minutes) that rely on respiratory-bellows or navigator-gated schemes. In our experience, subjects often fall asleep in these free-breathing acquisitions, leading to irregular breathing patterns and resulting in non-diagnostic images. We have developed a breath-hold MR acquisition strategy to avoid the afore-mentioned pitfalls and improve robustness to breath-hold failure. This new method, which we call Non-contrast Outer Radial Inner Square k-space Scheme or NORISKS, has shown promising initial results in recent clinical experience [2].

Although NORISKS requires slightly more effort than free-breathing acquisitions to prepare the subject, it avoids respiratory compensation failure (which costs minutes of time) and acquires important information in a shorter time.

Also, NORISKS can be extended to a multiple breath-hold acquisition for larger spatial coverage of the entire abdominal vasculature using both axial and coronal acquisitions.

All acquisitions were made on a 3.0 T system (MR750, GE Healthcare) with an 8-channel phased array coil. NORISKS is based on a dual-echo Dixon balanced SSFP sequence with IR preparation to enable inflow sensitivity and suppress background and venous signal. The figure shows maximum intensity projection (MIP) reformats of two NORISKS acquisitions from two subjects, clearly depicting the aorta, mesenteric and renal arteries.

In conclusion, NORISKS enables breath-hold acquisitions for abdominal MRA and avoids scan time penalties when respiratory-triggered schemes fail. The method can be used in axial and coronal planes to allow increased flexibility.

References/Funding Source [1] Miyazaki and Isoda. Non-contrast-enhanced MR angiography of the abdomen. Eur J Radiol, 2011. [2] Worters, Saranathan, Xu, Vasanawala. Robust Renal MRA using Breath-hold, IR-prep, Dixon bSSFP at 3T. ISMRM, 2011. Richard M. Lucas Foundation, P41-RR009784, GE Healthcare.

Flexible Multislice Interleave Ordering for Efficient Acquisition

BA Hargreaves, PW Worters
Department of Radiology, Stanford University, CA

INTRODUCTION: Interleaved multislice imaging is efficient and is widely used in MR. However, particularly for T1-weighted imaging, the number of slices that can be interleaved within the desired repetition time (TR) is often limited. This leads to suboptimal contrast if TR is increased to accommodate all slices, or increased scan time if multiple acquisitions are needed. We present and demonstrate a very simple method that guarantees maximally efficient interleaving of an arbitrary number of slices without the need to change the TR.

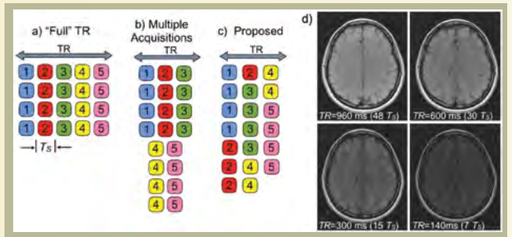

Multislice acquisition schemes with 5 slices, each requiring 4 excitations. (a) TR=5TS to encompass all slices, with a total time of 20TS. (b) The desired TR of 3TS results in 2 acquisitions and possibly loss of efficiency (8 TRs or 24TS). (c) Filling the required excitations for each slice vertically allows near-perfect efficiency (7 TRs or 21TS). In most cases the efficiency gain over (b) is even greater. (d) Images show different contrast with identical scan times but arbitrary TR choices.

METHODS AND RESULTS: Figure 1a-c show the typical interleaving schemes (a,b) and the more efficient approach (c). The key difference is that in the proposed approach, the slices that are excited in a particular TR can vary, and while this may require one extra TR (total) to achieve smooth equilibrium, the overall effect is that any TR less than the TR for full-interleaving can be used, without changing scan time significantly. We demonstrated this method in human scans where 48 slices were interleaved in different ways with completely arbitrary TR choices and no change in overall scan time, but substantial changes in image contrast, as shown in Fig. 1d.

DISCUSSION: The key strategy for flexible and efficient interleaving is to allow arbitrary slice numbers to be excited at different positions within the repetition. This method is compatible with all standard imaging methods such as parallel imaging and partial-Fourier imaging, and different interleave orders. Additionally, the method completely supports many schemes where different slices may require a different number of excitations, such as using a varying field-of-view or matrix size is for different slices. Overall, this flexible interleaving scheme is trivial to implement, and allows complete flexibility of TR selection for applications including T1-weighted multislice MRI.

References/Funding Source NIH R21-008190.

Ultra high spatio-temporal resolution liver imaging using a new view ordering scheme and a 2-point Dixon acquisition

M Saranathan, B Daniel, S Vasanawala, BA Hargreaves
Department of Radiology, Stanford University, CA

Both Dynamic contrast enhanced MRI (DCEMRI) and MR angiography (MRA) are challenged by the conflicting requirements of spatial and temporal resolution. Various solutions have been proposed involving combinations of partial Fourier imaging, undersampling, view sharing and parallel imaging. We propose DISCO (DIfferential Subsampling with Cartesian Ordering), a pseudorandom k-space segmented view-sharing scheme that minimizes sensitivity to eddy currents and motion for dynamic imaging while dispersing artifacts and residual ghosting. DISCO uses a variable density Cartesian undersampling scheme. Elliptical ky-kz is segmented into N annular regions, each sub-sampled by a factor of i with the central region fully sampled and the outer regions progressively under-sampled. Note that k-space points are confined to a Cartesian grid, enabling an FFT-based image reconstruction. Temporal footprint was minimized by nearest neighbor view sharing of the under-sampled views, to generate fully sampled k-space at each temporal phase. View sharing was restricted to within a breath-hold, minimizing temporal blurring and motion misregistration. DISCO was implemented on a 3D SPGR sequence with a bipolar readout for 2-point Dixon fat-water separation. After a 12s breath-hold, a pre-contrast mask phase is generated. Following injection of Gadolinium contrast, 6-7 phases were acquired in a 25-28s breath-hold with a temporal resolution of ~4s and a 320x224x60 matrix with 3-3.4 mm section thickness. We have demonstrated the use of DISCO in fast multi-phasic contrast enhanced liver imaging with a 32-channel torso-phased array coil, with no compromise in spatial resolution or coverage. The high spatio-temporal resolution enables robust visualization of the peak arterial phase in the liver, critical for diagnosis of fast enhancing tumors like hepato-cellular carcinoma and neuro-endocrine metastases. It also eliminates the need to precise contrast bolus timing schemes. The method can also be applied to other areas like breast and prostate DCEMRI.

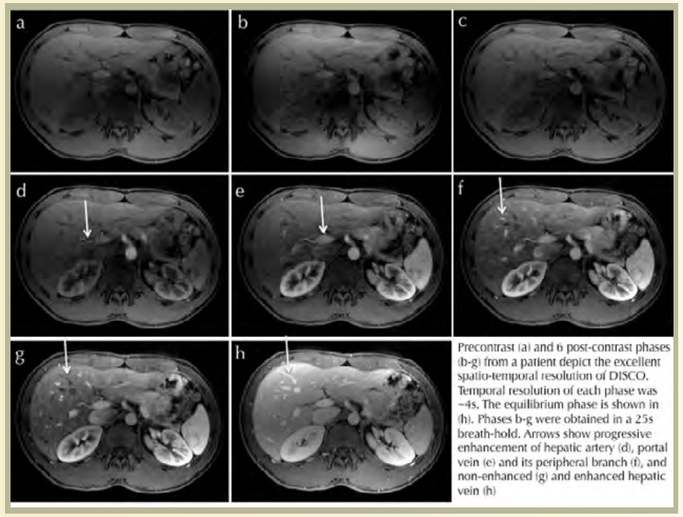

Precontrast (a) and 6 post-contrast phases (b-g) from a patient depict the excellent spatio-temporal resolution of DISCO. Temporal resolution of each phase was ~4s. The equilibrium phase is shown in (h). Phases b-g were obtained in a 25s breath-hold. Arrows show progressive enhancement of hepatic artery (d), portal vein (e) and its peripheral branch (f), and non-enhanced (g) and enhanced hepatic vein (h)

Very high spatio-temporal resolution breast imaging using a pseudo-random variable density view ordering scheme and 2-point Dixon fat-water separation

M Saranathan, S Vasanawala, BA Hargreaves, BL Daniel.
Department of Radiology, Stanford University, CA

Breast dynamic contrast enhanced MRI (DCEMRI) is challenged by the conflicting requirements of spatial and temporal resolution, leading to poor specificity of breast DCEMRI despite a high sensitivity. We propose DISCO (DIfferential Subsampling with Cartesian Ordering) for ultra fast dynamic breast imaging. DISCO uses a pseudo-random variable density k-space segmentation scheme that minimizes sensitivity to eddy currents while dispersing artifacts and residual ghosting. Elliptical ky-kz is segmented into N annular regions, each sub-sampled by a factor of i with the central region fully sampled and the outer regions progressively under-sampled. Note that k-space points are confined to a Cartesian grid, enabling an FFT-based image reconstruction. Nearest neighbor view sharing of the under-sampled view was used to generate fully sampled k-space at each temporal phase. Keyhole imaging was used to further increase the temporal resolution of the dynamic phases immediately following Gadolinium injection (~2-3 min). DISCO was implemented with a 3D SPGR sequence with a bipolar readout for 2-point Dixon fat-water separation. A fully sampled 90s pre-contrast mask phase was first acquired. Following injection of Gadolinium contrast, 16-20 dynamic wash-in phases were acquired using the DISCO view sharing and keyhole at a temporal resolution of ~10s. Following this, 4 fully sampled wash-out phases were acquired with a temporal resolution of ~90s. An acquisition matrix of 256x256x160 over a 28 cm FOV and 1.2 mm section thickness was maintained throughout. The ability to switch seamlessly between moderate spatial resolution, high temporal resolution (~10s) dynamic wash-in imaging and high spatial resolution wash-out imaging allows simultaneous visualization of breast tumors and enhancing structures with high spatial resolution for characterization and pharmacokinetic modeling for quantitative parametric characterization of tumor permeability.

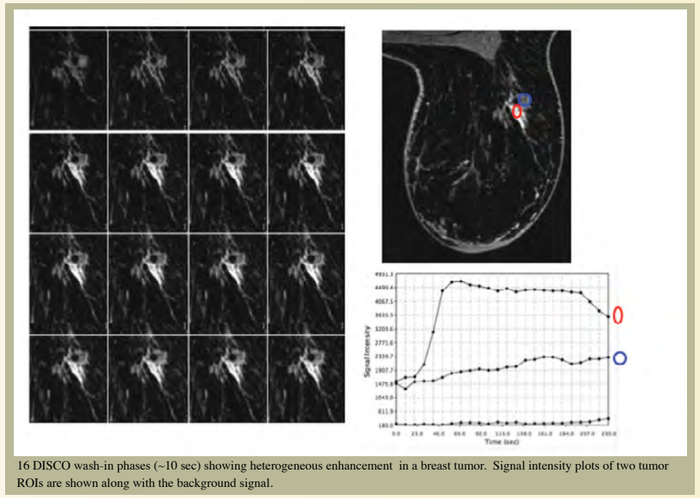

16 DISCO wash-in phases (~10 sec) showing heterogeneous enhancement in a breast tumor. Signal intensity plots of two tumor ROIs are shown along with the background signal.

Improved Time-Resolved, 3D PC Imaging with Variable Poisson Sampling and Partial Respiratory Triggering

MT Alley[1], MJ Murphy[2], K Keutzer[2], M Lustig[2], SS Vasanawala[1]
[1]Department of Radiology, Stanford University, CA; [2]Department of Electrical Engineering and Computer Science, UC Berkeley, CA

Time-resolved 3-dimensional phase-contrast MR imaging (4D-PC MRI) has been shown to be an important tool in a wide variety of research applications, such as wall shear stress measurements [1], aortic pulse wave velocity measurements [2], and the investigation of flow patterns in the heart [3]. The adoption of this technique in routine clinical imaging is primarily hampered by two issues: The long scan time inherent in the acquisition and the resulting respiratory artifacts that come from free breathing during the study. Parallel imaging can be used to significantly reduce scan time [4], but undersampling patterns suitable for GRAPPA-like reconstructions often result in coherent artifacts in the final images. We have demonstrated the use of variable density Poisson-disc/ellipse pseudorandom sampling [5] in conjunction with the compressed sensing L1-SPIRiT [6,7] parallel imaging reconstruction implemented on general purpose graphics processors (GPGPU) [8]. In addition, we have implemented a partial respiratory triggering approach to further reduce breathing artifacts with a minimal increase in scan time. This combined approach provides improved image quality and better artifact reduction within clinically viable acquisition and reconstruction times.

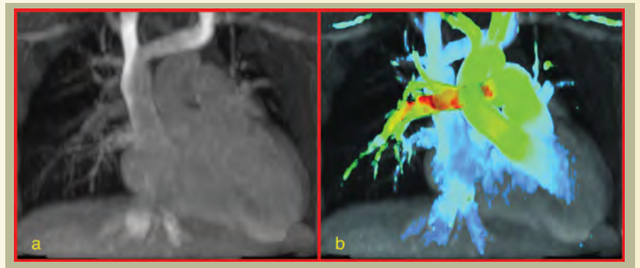

Images from a 3 year old female with right upper lobe partial anomalous pulmonary venous return to the superior vena cava. This protocol consisted of 52 slices and an in-plane matrix of 256 x 192 for a final resolution of 0.94 x 1.25 x 2.4 mm3. The variable Poisson disc sampling pattern used reduction factors of 2 in both directions, leading to an overall scan time of 11.9 minutes. The first 30% of the acquisition was done using respiratory gating over 30% of the respiratory cycle. Gadofosveset was given intravenously as a blood-pool contrast agent.

[1]: M. Markl et al., Circ Cardiovasc Imaging. doi: 10.1161/CIRCIMAGING.110.958504 [2]: M. Markl et al., Magn Reson Med. 2010; 63:1575-82. [3]: M. Hope et al., Radiology. 2010; 255:53-61. [4]: M. Alley et al., ISMRM-ESMRMB, 2010; Stockholm, p. 1343. [5]: H. Tulleken et al., Poisson Disk Sampling Tutorial, Dev. Mag. Magazine 2008; 21:21-25 (devmag.org.za). [6]: M. Lustig et al., ISMRM, 2009; Honolulu, p. 379. [7]: S. Vasanawala et al., Radiology. 2010; 256:607-616. [8]: M. Murphy et al., ISMRM-ESMRMB, 2010; Stockholm, p. 4854.

References/Funding Source MT Alley, MJ Murphy, K Keutzer, M Lustig, SS Vasanawala, Improved Time-Resolved, 3D Phase Contrast Imaging through Variable Poisson Sampling and Partial Respiratory Triggering, in Proc., ISMRM, 19th Annual Meeting, Montreal, page 1218, 2011. Research funded in part by NIH, Tashia & John Morgridge Foundation, and GE Healthcare

Transmit B1 Field Inhomogeneity and T1 Estimation Errors in Breast DCE MRI at 3T

K Sung, BL Daniel, BA Hargreaves
Department of Radiology, Stanford University, CA

A measurement of T1 is important to monitor contrast agent concentration using signal intensity in quantitative dynamic contrast enhanced (DCE) MRI [1]. Variable flip angle acquisitions, called DESPOT1, are a common choice to measure T1 since they can provide a fast 3D volumetric T1 mapping [2]. DESPOT1, however, heavily depends on the set of flip angles used, and therefore is sensitive to any flip angle variation. Transmit B1 field (B1) inhomogeneity creates flip angle variations of 30 - 50% across the breast at 3T [3].

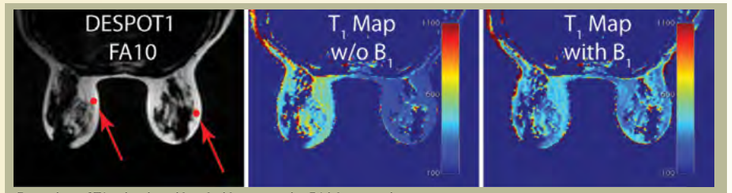

Comparison of T1 estimation with and without correcting B1 inhomogeneity

We validate the T1 estimation correction by including B1 mapping in our breast DCE imaging protocol. We then compare T1 relaxation in fat (as a validation) with and without compensating B1 variation in a total of 25 patients at 3T.

The image shows T1 maps with and without compensating for B1 inhomogeneity in one subject. The fat only image is displayed for anatomical reference. The T1 map has a substantial T1 difference between the left and right breast while the compensated one shows more uniform T1 across the whole breast. In 25 patients, the average B1 variations were 115.4% (on the left breast) and 82.4% (on the right breast), which conforms to the literature [3]. The average T1 difference between the left and right ROIs was 52% from uncorrected maps, and was reduced to 7% by including B1 variation. More importantly, the estimated T1 values (374.4 ms and 346.5 ms) were close to the literature-reported values (T1 = 366 ms) [4].

We have shown that severe B1 variations over the breast can cause a substantial error in T1 estimation using DESPOT1 and compensated the error by measuring the actual B1 variation. This improvement in T1 calculation can benefit quantitative breast DCE MRI.

References/Funding Source K Sung, BL Daniel, BA Hargreaves. Transmit B1 Field Inhomogeneity and T1 Estimation Errors in Breast DCE MRI at 3T, Proceedings ISMRM Nineteenth Scientific Sessions, May 2011, p3086. [1] Larsson, et al., MRM 1990;16:117 [2] Deoni, et al., MRM 2003;49:515 [3] Azian, et al., JMRI 2010;31-234 [4] Rakow-Penner et al., JMRI 2006;23:87.
Supported by NIH R01-EB009055, P41 RR 009784 and GE Healthcare

Delta Relaxation Enhanced Magnetic Resonance Imaging

E Lee, BK Rutt
Department of Radiology, Stanford University, CA

A goal of MR molecular imaging is to closely mimic the PET imaging paradigm (high sensitivity, low background) without sacrificing the spatial resolution advantages of MRI. Delta relaxation enhanced MRI (dreMR) aims to accomplish this with dispersive contrast agents that exhibit T1 relaxivity that varies as a function of field. As dreMR requires field-cycling hardware to enable imaging at different fields, a feasible implementation of dreMR is the insertion of a small resistive magnet into a whole body MR system. This setup has achieved dreMR imaging of up to +/- 0.15T, albeit with some image specificity and artifact issues. We aim to develop the next generation of dreMR imaging hardware to cover a significantly wider field strength range; this should markedly improve image contrast and eliminate image artifacts.

We have partnered with Stelar (Mede, Italy) for the development of a next generation magnet capable of producing +/- 0.5T, with an inner diameter of 30mm suitable for imaging of mice. Two important characteristics of the prototype magnet have been measured to date: eddy current (EC) due to dreMR field switching, and interface performance with clinical scanners. The magnet generates scanner-dependent, quantifiable EC that arises from coupling between the pulsed field magnet and the main magnet. In a GE 1.5T Signa, initial EC measurements showed 250Hz field offset per 0.1T dreMR field decaying with a time constant of 20ms, while in a Philips 1.5T, initial EC was 500Hz per 0.1T and the time constant was 100ms. The scanner and the dreMR magnet controller were synchronized via a programmable digital board, with negligible jitter. Proof-of-principle phantom images were acquired showing that our system is capable of producing dreMR images at field of up to +/- 0.36T, which is the highest dreMR field reported to date. We are now developing EC-compensating dreMR field hardware and image processing methods to remove image artifacts.

References/Funding Source ICMIC

RF Coil Design for 7 Tesla MRI

J Lu[1], BK Rutt[1,2]
Depts of [1]Electrical Engineering, [2]Radiology, Stanford University, CA

We are currently studying coil design for improving B1+ field uniformity and signal and examining specific absorption rate (SAR) for high field (7T) magnetic resonance imaging (MRI). Among our methods for studying such designs is the use of the finite element (FEM) and finite-difference time domain (FDTD) methods. Such simulation methods allow the solution of Maxwell's equations to generate electric and magnetic fields in and around coils and sample. Accurate calculation and visualization of such fields would allow us to optimize the coil parameters to increase B1+ signal and uniformity and reduce SAR (absorbed power: proportional to E field squared). We have also performed studies of the Butler matrix, which is essentially a hardware implementation of a Fourier transform. Using such a stage before a degenerate birdcage provides intrinsic decoupling between coils allowing for use in parallel excitation.

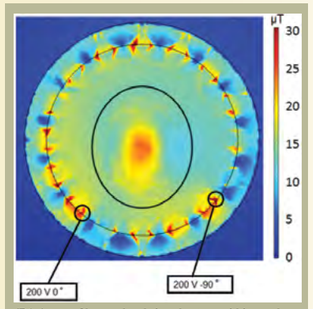

|B1+| map of human head size phantom within quadrature driven birdcage coil

References/Funding Source P41, NSF

Gd-based "smart" MRI probes for molecular imaging

P Pandit[1], D Ye[1], J Ronald[1], J Rao[1,2], BK Rutt[1]
Departments of [1]Radiology, [2]Chemistry, Stanford University, CA

Our group has devised a novel platform for the development of "smart" probes based on biocompatible chemical reactions where Gd-containing molecules, under the control of pH, disulfide reduction and/or enzymatic cleavage, get activated to form magnetic nanoparticles with enhanced relaxivity (Figure a). Two separate condensation schemes are being tested; one based on intramolecular polymerization (GL scheme)[1], and the other on intermolecular cyclization (DJ scheme) [2]. We have assessed the MR properties of these two smart probe schemes in living cells (breast carcinoma cell line MDA-MB-468) and compared the results with the commercially available cell-labeling agent, GdF-M.

Activatable and non-activatable forms of the probes for both GL (GL62 and GL141) and DJ (DJ137 and GJ171) schemes were prepared as previously described [1,2]. 4 million cells were incubated with GdF-M, GL62, GL141, DJ137, DJ171 (~250 uM) for 2, 4, 8, and 24 hours respectively. Following incubation, the cells were washed, fixed and centrifuged to form pellets. Cell pellets were then imaged at 0.5T, 1.5T and 3T at 35 °C and T1 measurements made from these images. Relaxation rates (R1) were determined as 1/T1. Longitudinal relaxivities, r1 (mM-1s-1) were calculated as the slope of R1 vs [Gd] after the determination of true Gd concentration of each cell pellet by ICP-MS measurement.

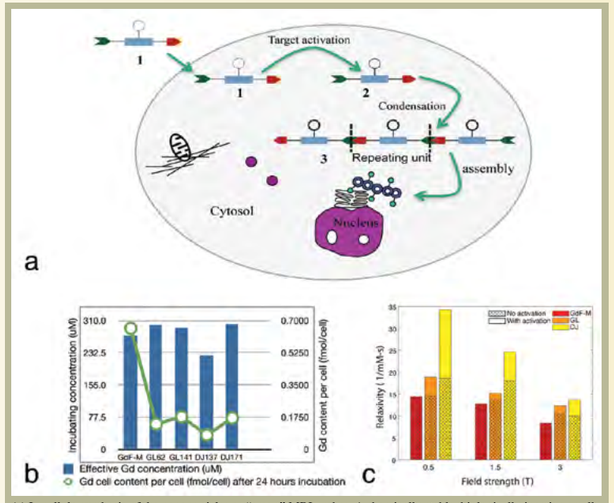

(a) In cellulo synthesis of the nanoparticles as "smart" MRI probes. A chemically stable, biologically inactive small molecular (monomer 1) enters cells and is converted by reduction and/or enzymatic processing into an intermediate 2, which quickly undergoes condensation reaction to generate oligomer 3. The self-assembly of 3 leads to the formation of nanoparticles accumulated locally at or near the enzyme location in cells. For the GL scheme, intermediate 2 undergoes intra-molecular polymerization and self-assembly to form Gd-nanoparticles, whereas for the DJ scheme, intermediate 2 undergoes inter-molecular macro-cyclization and self-assembly to form the Gd-nanoparticles. (b) Gd concentration of the incubation medium for the 5 probes (left) and the cellular uptake after the 24-hour incubation period (right). Gd content in both cases was measured with ICP-MS. (c) Comparison of MR relaxivity of GdF-M with the the non-activatable and activatable form of the "smart" probes synthesized for the GL scheme (polymerization) and DJ scheme (macro-cyclization). Relaxivity measurements were carried out at 0.5T, 1.5T and 3T.

For the same incubation concentration, the cellular uptake of the "smart" probes was lower than that for GdF-M (Figure b). Nonetheless, both non-activated forms of the "smart" probes showed similar or higher MR relaxivity than GdF-M, with an additional increase after activation, particularly at lower field strengths (80% for DJ, 30% for GL at 0.5T) as can be seen in Figure c. We hypothesize that the increased rotational correlation time (τR) due to nanoparticle formation results in relaxivity amplification after activation. These results successfully demonstrate the in cellulo behavior of our "smart" MRI probes.

References/Funding Source [1] Liang, et al., Nature Chemistry (2010) 2: 54-60.[2] Ye, et al., Angew Chem. Int. Ed. (2011) 50: 2275-2279. SMIS, CCNE

Fast B_1^+ Mapping using an Optimized, Asymmetric Bloch-Siegert Method

M Saranathan[1], M Khalighi[2], BK Rutt[1]
[1]Department of Radiology, Stanford University, CA; [2]Global Applied Science Lab, GE Healthcare, Menlo Park, CA

B_1^+ mapping is important in a number of high-field imaging applications including multi-transmit rf pulse design and accurate MR relaxometry. The recently proposed Bloch-Siegert (BS) B_1^+ mapping method [1] circumvents spoiling and saturation issues faced by magnitude-based methods such as Actual Flip-angle Imaging (AFI) [2] and the Double Angle Method [3] and its variants. While the BS method is relatively fast due to its T1 insensitivity, its accuracy depends on the power of the BS pulse, which is SAR limiting, especially at 7T. This SAR limit can prolong acquisition times, especially for multiple transmit channel B_1^+ mapping applications. We have developed a novel, fast whole brain 3D Bloch-Siegert B_1^+ mapping method that is optimized for very short scan times and/or low SAR and demonstrate isotropic whole human brain B_1^+mapping in scan times on the order of 30 seconds at 3T and less than a minute at 7T. The main features include: a. elliptical k-space ordering with elimination of the corners of k-space (70% reduction in scan time); b. use of optimized Bloch-Siegert pulse with 4 ms width and 2000 Hz offset compared to the 6 ms 4000 Hz offset conventional (Fermi) pulse resulting in SAR reduction by ½ or ANR increase by 2; c. acquisition of the second scan on-resonance with no BS pulse or using the Bo map data for phase correction, reducing the scan time and SAR.

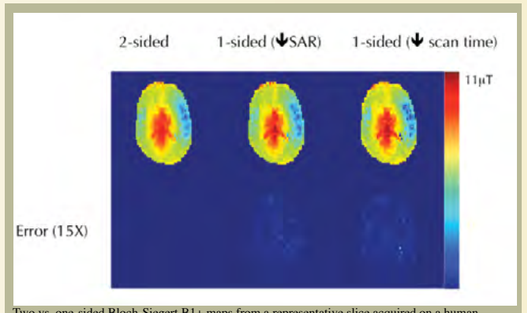

Two vs. one-sided Bloch-Siegert B1+ maps from a representative slice acquired on a human volunteer at 7T.

References/Funding Source GE Healthcare Tiger Team

mcDESPOT in Longitudinal Multiple Sclerosis Studies

J Su[1], H Kitzler[2], M Zeineh[1], C Harper-Little[3], A Leung[4], M Kremenchutzky[5], S Deoni[6], BK Rutt[1]
Departments of [1]Radiology and Electrical Engineering, Stanford University, CA; [2]Neuroradiology, Technische Universitaet Dresden, Dresden, Germany; [3]Robarts Research Institute, [4]Diagnostic Radiology and Nuclear Medicine, [5]Clinical Neurological Sciences, University of Western Ontario, London, Ontario, Canada; [6]Engineering, Brown University, Providence, RI

Using the whole-brain, myelin-selective MR method, multi-component Driven Equilibrium Single Pulse Observation of T1 and T2 (mcDESPOT), we examined the development of disease in a cohort of patients and controls at baseline and 1 year; the first longitudinal application of this new MR methodology. The baseline cross-sectional study revealed that measures derived from a voxel-wise comparison of myelin water fraction (MWF) in standard space between a subject and the normal control population was highly sensitive to abnormalities in early MS cases. Continuing with the longitudinal follow-up, this measure has also demonstrated statistically significant changes in definite MS patients compared to controls, while the coarse EDSS clinical disability score was unable to detect any change. These measures are promising new markers for assessing the progression of disease. Further study is being conducted with the pre-MS and relapsing-remitting subtypes. These patients have the best chance of having successful disease course-altering treatment and are being tracked carefully with scans every month for half a year or longer. These studies represent a major litmus test for mcDESPOT and its future application to MS.

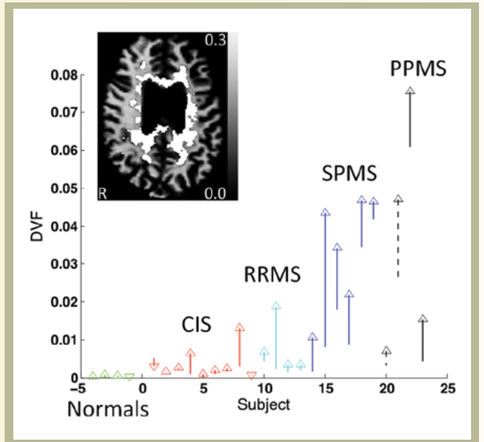

A plot of the change in demyelinated volume fraction for each subject. Colors denote the MS course: controls (green), CIS (red), RRMS (light blue), SPMS (dark blue), PPMS (black). Arrowheads indicate the direction of change and the DVF at 1-year. Dashed lines show subjects who also had a change in EDSS. The inset picture shows an image of MWF with demyelinated voxels in white.

References/Funding Source Hagen Kitzler, Jason Su, Michael Zeineh, Cynthia Harper-Little, Andrew Leung, Marcelo Kremenchutzky, Sean Deoni, Brian Rutt. Deficient MWF Mapping In Multiple Sclerosis Using 3D Whole-Brain Multi-Component Relaxometric MRI. NeuroImage (2011) submitted. Lucas Foundation

Metabolic Kinetics of a Glioma Model using Hyperpolarized 13C MRSI

JM Park[1,2], S Josan[2,3], T Jang[4], M Merchant[4], Y-F Yen[5], R Hurd[5], L Recht[4], D Spielman[1,2], D Mayer[2,3]
Departments of [1]Electrical Engineering, [2]Radiology, [4]Neurology and Neurological Sciences, Stanford University, CA; [3]SRI International, Neuroscience Program, Menlo Park, CA; [5]Applied Science Laboratory GE Healthcare, Menlo Park, CA

13C Magnetic Resonance Spectroscopy (MRS) has been used to study in vivo tumor metabolism in brain tumor models, and the altered energy metabolism was confirmed by the elevated production of 13C-labeled lactate (Lac) in tumor tissue. DNP (Dynamic Nuclear Polarization) and the recent development of a dissolution process that retains polarization into the liquid state enables the real-time investigation of in vivo metabolism with more than 10,000-fold signal increase over conventional 13C methods. Recently, a study showed the feasibility of using hyperpolarized [1-13C]-pyruvate (Pyr) for evaluating in vivo metabolism of a human glioblastoma xenograft in a rat brain at a single time point. In this work, we measured the kinetics of pyruvate metabolism in a glioma brain tumor model using the hyperpolarized 13C technique with the fast spiral CSI (Chemical Shift Imaging) sequence, and compared the metabolism kinetics from three different ROIs (Region of Interests): brain tumor, normal brain, and vasculature. In vivo results clearly demonstrated the kinetics of the brain tumor metabolism with comparison to those of normal brain and vasculature. The Pyr signal also provided an estimate of tissue perfusion in which blood-brain barrier breakdown results in the Pyr curve from the tumor ROI approaching that from the vascular ROI in some animals. Robust dynamic curves of Pyr and Lac were achievable repeatedly with 3 seconds of temporal resolution using the variable RF excitation angle on a single slice, whereas bicarbonate signal detection was limited by the SNR. We also scanned with a recently developed dynamic volumetric spiral CSI sequence covering the entire brain (n=1), with and without additional 12C-Lac in the dissolution buffer. Lac peak, SNR, and CNR were improved by 15.8 %, 4.68 %, and 6.92 % compared to those obtained with a normal NaOH buffer, identifying isotopic exchange as an important process in 13C-Lac labeling.

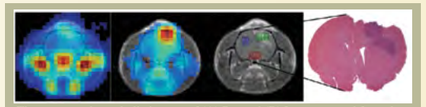

Time-averaged metabolic images of (A) Pyr and (B) Lac computed from three 2D dynamics studies on the same rat (RatC6_2). (C) Voxels selected for ROI analysis: Tumor (Green), Normal brain (Blue), Vasculature (Red). (D) The histology image of the scanned slice.

References/Funding Source NIH: RR09784, AA05965, AA018681, AA13521-INIA, and EB009070, The Lucas Foundation, and GE Healthcare

CT-PRESS Spiral MRSI with Multiple Dualband Frequency-Selective RF Pulses

M Gu[1], DM Spielman[1], NM Zahr[2], A Pfefferbaum[2], EV Sullivan[2,3], D Mayer[1,2]
Departments of [1]Radiology, [3]Psychiatry & Behavioral Sciences, Stanford University, CA; [2]Neuroscience Program, SRI International, Menlo Park, CA

Using effective homonuclear decoupling, constant-time point-resolved spectroscopy, CT-PRESS, has been proposed for the detection of coupled resonances such as glutamate (Glu) and myo-insitol (mI). As a 2D spectroscopy technique, it requires long minimum scan times for multivoxel applications, prohibiting wide spread use in clinical settings. To shorten the minimum scan time, CT-PRESS has been combined with fast spiral spatial encoding. To avoid lipid contamination, however, the method usually employs either the excitation of a restricted brain region using PRESS volume pre-selection, losing metabolite signals from subcortical regions, or applies inversion recovert, resulting in reduced SNR. Recently, a robust suppression scheme using multiple dualband frequency-selective RF pulses has been proposed to suppress both water and lipids and thus provide whole-brain coverage without metabolite signal loss. Here, we combine this suppression technique with the CT-PRESS based spiral spectroscopic imaging sequence for improved detection of metabolites of Cho, Cre, mI, Glu, Gln and NAA with whole-brain coverage. The effectiveness of the multiple dualband RF pulses was demonstrated in an in vivo human study within an acquisition time suitable for clinical study. Results demonstrate effective water and lipid suppression and undisturbed metabolite spectra.

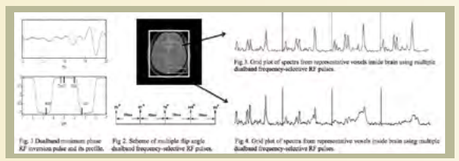

References/Funding Source Gu, et al, CT-PRESS Based Spiral Spectroscopic Imaging with Robust Water and Lipid Suppression Using Multiple Dualband Frequency-Selective RF Pulses, Annual Scientific Meeting of the ISMRM, Monteal, CA, May 2011, p 3420. Lucas foundation, GE Health Care, NIH RR09784, MH080913, AA005965, AA013521-INIA, AA017347 and AA017168.

Adiabatic B1 Shimming Algorithm for Multiple Channel Transmit at 7T

P Balchandani[1], MM Khalighi[2], SS Hsieh[1,3], K Setsompop[4], J Pauly[3], D Spielman[1]
Departments of [1]Radiology, [3]Electrical Engineering, Stanford University, CA; [2]Global Applied Science Laboratory, GE Healthcare, Menlo Park, CA; [4]A.A. Martinos Center for Biomedical Imaging, Harvard Medical School, Massachusetts General Hospital, Charlestown, MA

Adiabatic B1 shimming is a hybrid high-field imaging approach that combines the flexibility offered by multiple transmit RF channels with the B1-immunity of custom adiabatic RF pulses. In this work, a simulated annealing (SA) optimization algorithm was developed to determine the RF amplitude and phase adjustments to adiabatic RF pulses played on individual transmit channels. The amplitude and phase of the pulses are chosen to maximize the percentage of the final B1 field over the region of interest (ROI) that exceeds the adiabatic threshold for the applied RF pulses. The adiabatic B1 shimming algorithm was applied to 2-channel and 8-channel 7T B1 transmit maps and the resultant shim values were tested in simulation. Greater than 95% uniformity was achieved for the simulated flip angle in phantoms and in vivo, when applying the B1 shim values obtained using our optimization algorithm. Input amplitudes are within hardware limits and worst case SAR is lowest when using a simulated annealing approach to minimization. We plan to insert the adiabatic 180° pulse used in simulations into a standard GRE sequence as an inversion pulse and test the efficacy of inversion over the ROI when compared to conventional and adiabatic 180° inversion without B1 shimming. Values registered on the SAR monitor will also be compared. Future work will be focused on optimizing the loss function for the minimization algorithm to more accurately reflect global SAR.

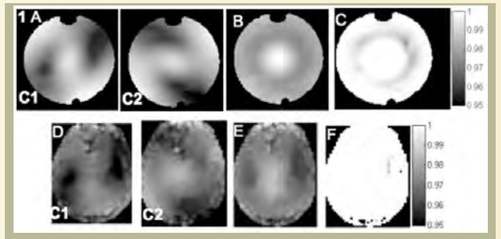

Figure 1: (A) B1 maps for a spherical water phantom obtained from a 2-channel (C1, C2) 7T transmit setup. (B) RF amplitude achieved when adiabatic B1 shimming algorithm is applied. (C) Simulated magnitude of slice profile for 180° adiabatic SLR pulse when using B1 shim values from (B). Results from the same experiment and simulations performed in vivo are shown in (D-F). High uniformity in the flip angle is achieved over the entire slice by ensuring RF amplitudes remain above the adiabatic threshold.

References/Funding Source Balchandani, et al, Adiabatic B1 Shimming Algorithm for Multiple Channel Transmit at 7T, Annual Scientific Meeting of the ISMRM, Monteal, CA, May 2011, p. 3517. Lucas Foundation, NIH R01 MH080913 and GE Healthcare.

RF excitation scheme effects in dynamic volumetric imaging of hyperpolarized [1-13C]-pyruvate

S Josan[1,2], R Hurd[3], AB Kerr[4], Y-F Yen[3], PE Larson[5], A Pfefferbaum[1,6], D Spielman[2], D Mayer[1,2]
[1]SRI International, Menlo Park, CA; Departments of [2]Radiology, [4]Electrical Engineering, [6]Psychiatry and Behavioral Sciences, Stanford University, CA; [3]GE Healthcare Applied Science Laboratory, Menlo Park, CA; [5]Dept of Radiology and Biomedical Imaging, UC San Francisco, CA

Recent studies have demonstrated dynamic metabolic imaging of hyperpolarized pyruvate (Pyr) and its metabolic products for a wide variety of applications. While 3D techniques permit the largest volumetric coverage, they require a large number of RF excitations, which can have a substantial impact on the shape of the dynamic response, the calculation of apparent rate constants, and signal to noise ratio (SNR) averaged over the response. Multiband spectral-spatial RF pulses provide an efficient use of hyperpolarized magnetization for dynamic imaging by using a low excitation flip angle for the injected substrate to preserve its magnetization for subsequent conversion and a higher flip angle for the metabolic products to increase their SNR. However, due to different tissue perfusion, i.e., in- and outflow rates, and metabolic activities, the optimal excitation scheme might depend on the specific organ. This work investigates the performance of different flip angle schemes in multiple organs. Dynamic 3D 13C data were acquired for kidney and liver using the 1º/4º, 2º/8º, 5º/20º multiband or 5º/5º flip angle schemes, and for brain using the 2º/8º and 5º/20º schemes. Comparing the Lac SNR from the weighted average images, the average ratio of SNR of 2º/8º to SNR of 5º/20º was: brain=1.44±0.08; kidney=1.27±0.24; liver=1.11±0.07. The relative SNR ratios of 1º/4º:2º/8º:5º/20º were 0.74:1:0.84 in kidney and 0.74:1:0.9 in liver (in 1 animal). The SNR of 2º/8º relative to 5º/5º was 1.13 in kidney and 1.26 in liver (in 1 animal). Overall, the 2º/8º excitation scheme for dynamic 3D imaging provides good SNR for a wide range of transport kinetics and metabolic activity allowing estimation of tissue specific apparent rate constants.

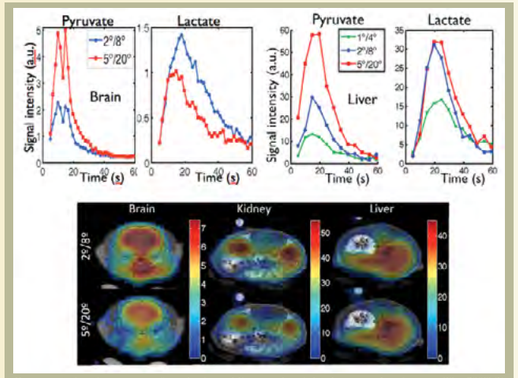

Representative time courses from brain and liver, and weighted average Lac images. The 2º/8º flip angle scheme provided higher Lac SNR in brain and equal SNR in kidney/liver vs. the 5º/20º.

References/Funding Source S Josan, et al, Effects of RF excitation scheme on signal-to-noise-ratio and apparent rate constant estimation in dynamic volumetric imaging of hyperpolarized [1-13C]-pyruvate, Annual Scientific Meeting of the ISMRM, Montreal, Canada, May 2011, p. 3528. NIH RR09784, AA05965, AA018681, AA13521-INIA, EB009070and EB007588

Fast Volumetric Imaging of Ethanol Metabolism in Rat with Hyperpolarized [1-13C]-Pyruvate

S Josan[1,2], D Spielman[2], Y-F Yen[3], R Hurd[3], A Pfefferbaum[1,4], D Mayer[1,2]
[1]SRI International, Menlo Park, CA; Departments of [2]Radiology, [4]Psychiatry and Behavioral Sciences, Stanford University, CA; [3]GE Healthcare Applied Science Laboratory, Menlo Park, CA

Rapid, time-resolved, volumetric imaging of hyperpolarized pyruvate (Pyr) and its metabolic products lactate (Lac) and alanine (Ala) allows the measurement of metabolic activity in different tissues and can be useful to distinguish between normal and diseased tissues. This work applies dynamic 3D magnetic resonance spectroscopic imaging (MRSI) to investigate Pyr metabolism modulated by ethanol. Ethanol is metabolized in the liver via the breakdown of ethanol to acetaldehyde and acetaldehyde to acetate. Both of these reactions reduce the coenzyme nicotinamide adenine dinucleotide (NAD+) to NADH. Thus, ethanol consumption leads to accumulation of NADH in the liver. Because NADH is also a coenzyme in Pyr-to-Lac conversion, this altered liver metabolic state created by ethanol can be interrogated by hyperpolarized Pyr measurements. Spielman et al have previously reported MRS measurements of hyperpolarized Pyr to study rat liver metabolism modulated by ethanol. Dynamic 13C MRS was used to measure the conversion rates of Pyr to Lac and Ala in the presence and absence of ethanol. However, the MRS data were not spatially localized within a slice, which contained vascular and other structures in addition to the targeted organs. Dynamic 3D 13C MRSI can provide improved rate-constant estimates by allowing the analysis of spectra from organ-specific regions-of-interest (ROIs). This work extends the 2D spiral MRSI sequence to provide volumetric coverage and applies it to ethanol metabolism. We demonstrate time-resolved volumetric metabolic imaging of hyperpolarized 13C Pyr and its metabolic products using an undersampled spiral CSI sequence, with an acquisition time of 4.5 s for a nominal 5mm isotropic resolution. The dynamic 3D acquisition allows the analysis of spectra from organ-specific ROIs, thus providing improved rate-constant estimates.

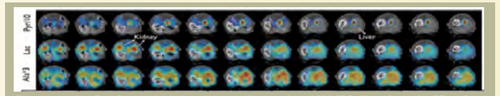

Representative Pyr, Lac and Ala images superimposed on 1H MRI slices from the 3D volume covering kidneys and liver. 13C images are averaged over all 16 time-points acquired.

References/Funding Source S Josan, et al, Fast Volumetric Imaging of Ethanol Metabolism in Rat with Hyperpolarized [1-13C]-Pyruvate, Annual Scientific Meeting of the ISMRM, Monteal, Canada, May 2011, p. 3519. NIH grants RR09784, AA05965, AA018681, AA13521-INIA, and EB009070

Quantitative Positive Contrast MRI of Magnetotactic Bacteria

S Josan[1,2], A Hamilton[3], M Benoit[3], C Cunningham[4], D Spielman[2], A Matin[3], D Mayer[1,2]
[1]SRI International, Menlo Park, CA; Departments of [2]Radiology, [3]Microbiology and Immunology, Stanford University, CA; [4]Sunnybrook Health Sciences Center, Toronto, ON, Canada

Contrast agents incorporating superparamagnetic iron-oxide (SPIO) nanoparticles have shown great promise in visualizing labeled cells using MRI. The objective of this work is to explore techniques for improvements in MRI of cancer using genetically encoded magnetite as a contrast agent. The magnetotactic bacteria Magnetospirillum magneticum AMB-1 endogenously produce magnetite particles, and have been shown to generate positive MRI contrast in mouse xenograft tumors using T1-weighted MRI [1]. However, as the T2 shortening effect of the magnetite on the signal intensity surpasses the T1 effect, the enhanced contrast peaks within a certain range of magnetite concentration, preventing quantitative assessment. Several techniques exist for visualization of the magnetite particles, but accurate quantitation remains challenging. In this work, two positive contrast imaging techniques were implemented on a 7T small-animal scanner and evaluated for quantitative detection of the magnetite particles. Figure 1 shows a GRE image as well as positive contrast images of the phantom. Both the off-resonance excitation and the SGM post-processing techniques visualize the magnetite spots well, with good background suppression. Figure 1d shows that a linear correlation exists between the iron concentration and the sum of the signal intensity of all "positive contrast voxels" within a region-of-interest at the spot location. A voxel was considered "positive contrast" if its signal intensity was >3 times the standard deviation above the background signal level. The two methods showed different slopes for the signal dependence on concentration highlighting their different sensitivities. Future work will involve further investigating the sensitivity of the two methods and the minimum detection limit of Fe concentration for both techniques and applying these in an in vivo tumor model.

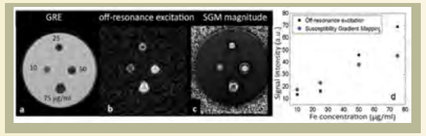

References/Funding Source S Josan, et al., Comparison of Susceptibility Gradient Mapping and Off-Resonance Excitation for Quantitative Positive Contrast MRI of Magnetotactic Bacteria, Annual Scientific Meeting of the ISMRM, Monteal, Canada, May 2011, p. 2659. R21 CA140903, P41 RR009784, P50 CA114747

Hyperpolarized [1-13C]-Lactate as a Tool for the In Vivo Investigation of Cardiac Metabolism

D Mayer[1,2], Y-F Yen[3], RE Hurd[3], S Josan[1,2], JM Park[2], A Pfefferbaum[1,4], DM Spielman[2]
[1]Neuroscience Program, SRI International, Menlo Park, CA; Departments of [2]Radiology, [4]Psychiatry and Behavioral Sciences, Stanford University, CA; [3]GE Healthcare, CA

Among its many applications, hyperpolarized [1-13C]-pyruvate is used to study cardiac metabolism in healthy and diseased states. The fact that lactate has low toxicity and serves as an important energy source for the heart suggests that hyperpolarized lactate might be an alternative substrate for probing heart metabolism. Chen et al. demonstrated the feasibility of both polarizing [1-13C]-lactate and detecting its metabolic conversion in vivo. The aim of this work was to apply hyperpolarized [1-13C]-lactate to the measurement of cardiac metabolism and compare it to [1-13C]-pyruvate as a substrate. Comparing the time courses of Pyr, Lac, and Bic acquired with FID after injections of hyperpolarized [1-13C]-pyruvate and [1-13C]-lactate, both isotopic exchange and metabolic flux contribute to the conversion between Pyr and Lac as the lactate dehydrogenase (LDH) catalyzed reaction is readily reversible. By contrast, the appearance of Bic reflects flux through pyruvate dehydrogenase (PDH) when Pyr is converted to acetyl coenzyme A via decarboxylation [1]. When lactate was injected, Bic was detected at similar levels as Pyr. With both substrates, the time course of Bic reaches a maximum at around 20 s. However, its subsequent decay appears to be faster with lactate as the substrate. With half of the substrate concentration, the maximum Bic signal after lactate injection was approximately 40-45% of the Bic level after pyruvate injection despite the fact that Lac had to be converted first to Pyr. The presented data demonstrate that bicarbonate as a secondary product of hyperpolarized [1-13C]-lactate can be detected in the heart. Therefore, hyperpolarized lactate can be used as an alternative substrate to probe cardiac metabolism.

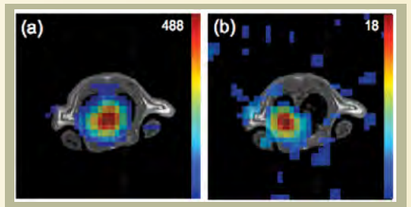

Metabolic images of (a) Lac and (b) Bic from a slice through the heart acquired with dynamic spCSI after injection of hyperpolarized [1-13C]-lactate. The images were averaged over 4 time points (10 to 25 s).

References/Funding Source Mayer, et al, Hyperpolarized [1-13C]-Lactate as a Tool for the In Vivo Investigation of Cardiac Metabolism, Annual Scientific Meeting of the ISMRM, Montreal, Canada, May 2011, p. 1507. NIH grants RR09784, AA05965, AA13521-INIA, EB009070, AA018681, and Lucas Foundation

Reduced Field of View Imaging for Twice-Refocused Diffusion EPI using a Perpendicular Refocusing Slab

RL O'Halloran, M Aksoy, ES Choi, R Bammer
Department of Radiology, Stanford University, CA

Introduction: The single-refocused spin echo, requires a large percentage of the TR reducing scan time efficiency. The Diffusion-Weighted Steady State Free Precession sequence (DW-SSFP), however, can have high diffusion sensitivity with short diffusion gradients [1,2]. Here, spiral projection imaging (SPI) readout is used to achieve whole brain coverage and to allow phase navigation by batching interleaves acquired in similar cardiac phases [3].

Methods: MRI: DW-SSFP SPI was performed on a volunteer using a 1.5T scanner. The k-space trajectory was a spiral-in, rotated in 3D to cover the full 3D k-space sphere. Sequence parameters included: isotropic 1.4 mm3 resolution, 280 mm3 FOV, scan time 2 min per direction for 3 diffusion directions, 5000 spiral interleaves per volume, diffusion gradient width 5.5 ms with 1ms ramps, and diffusion gradient strengths 5, 2.5, 1, and 0.5 G/cm

• Recon: Reconstruction was done by binning the data into 10 cardiac phases and performing iterative SENSE algorithm [3, 4]. Gridding was performed for comparison.

Results and Discussion: SENSE-reconstructed images are given in Fig 1. In the higher diffusion-weightings (Fig 1a last column) there are residual phase errors. Figure 1b shows 3 orthogonal slices through the volume using the maximum gradient strength, demonstrating the isotropic 3D full brain coverage. Figure 2 shows the improvement achieved by using cardiac binning and SENSE (arrow, b) compared to gridding (arrow, a).

Conclusion: A 3D isotropic high-resolution DW-SSFP technique is demonstrated that covers the whole brain. Cardiac gated SENSE reconstruction was able correct much of the phase errors and led to better image quality than gridding reconstruction.

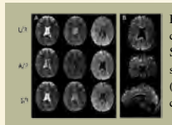

Fig. 1 - (a) Central axial slices of each 3D scan (a, columns) and each diffusion direction (a, rows). Scans were performed with a diffusion gradient strength of 0.5, 1, and 2.5 G/cm (from left-to-right); (b) axial, sagittal, and coronal views from the 5 G/cm scan with A/P diffusion encoding.

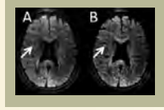

Fig. 2 - Standard gridding (a) compared to the SENSE reconstruction (b). The SENSE reconstruction restores signal around the ventricles (white arrows).

References: [1] Mcnab et al. MRM 2010. [2] Jung et al JMRI 2009. [3] Miller and Pauly. MRM 2003. [4] Liu et al MRM 2005

References/Funding Source Isotropic High-Resolution 3D Diffusion Weighted SSFP Imaging with Spiral Projection Imaging. RL O'Halloran, M Aksoy, ES Choi, R Bammer. In Proceedings of the 19th Annual Meeting of the ISMRM. 1 R01 EB008706, 1 R01 EB008706 S1, 5 R01 EB002711, 1 R01 EB006526, 1 R21 EB006860, Center of Advanced MR Technology at Stanford (P41RR09784), Lucas Foundation, Oak Foundation. GE Healthcare

Benefits of Optical Prospective Motion Correction for Single-Shot DTI

M Aksoy[1], C Forman[2], D Kopeinigg[1], M Straka[1], R O'Halloran[1], S Holdsworth[1], S Skare[3], R Bammer[1]
[1]Department of Radiology, Stanford University, CA; [2]Computer Science, Friedrich-Alexander-University Erlangen-Nuremberg, Erlangen, Germany; [3]Clinical Neuroscience, Karolinska Institute, Stockholm, Sweden

Introduction: Involuntary patient motion causes pixel misregistration and changes the effective diffusion-encoding, which, in turn, results in erroneous estimation of diffusion tensors or higher-order variants (1-3). The most common method of motion correction for DTI is retrospective coregistration of diffusion-weighted volumes to a reference volume. However, retrospective correction methods cannot repair incomplete diffusion-weighted volumes, spin history effects, or non-equidistant sampling of the diffusion-encoding direction space. In this study, we propose to use an adaptive optical tracking system (4) to correct for motion artifacts in single-shot EPI DTI and aim to demonstrate the advantages of this prospective approach over retrospective volume-to-volume realignment.

Methods: Prospective Optical Motion Correction – A small camera was mounted on an 8-channel head coil and acquired images of a self-encoded marker attached to the subject's forehead [5]. The video frames were processed on an external computer. The patient's pose was determined at a rate of 25Hz and the geometry update was sent back to the sequencer in real-time so that the scan volume followed the subject's head with minimum delay.

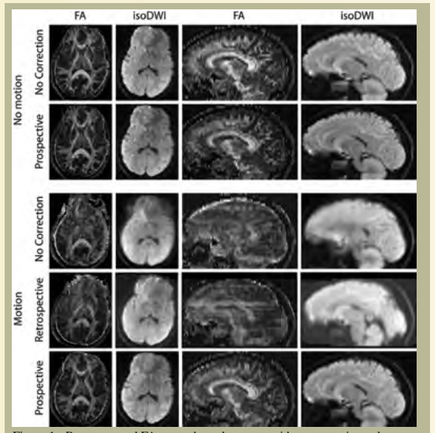

Figure 1 - Reconstructed FA maps show that, even with retrospective volume-to-volume realignment, motion-related image artifacts remain because of intra-volume motion and spin history effects. Prospectively corrected FA maps show the most similarity with the reference dataset.

Experiments – A single-shot DTI-EPI sequence was used (TR/TE=10sec/75msec, FOV=24cm, 96x96 matrix, 36 3mm slices @ 1mm gap, b=1000 sec/mm2, # diffusion directions = 25 (+3 b=0)). The volunteer was asked to perform mixed (in-plane) shaking and (through-plane) nodding motion throughout the scan, once every ~15 seconds. This scan was repeated with & without prospective motion correction. The data without adaptive motion correction was also reconstructed after retrospective volume-to-volume realignment with SPM8. For reference, two additional datasets were obtained where the subject was asked to stay still and prospective motion correction was turned off and on.

Results and Discussion: Figure 1 shows FA and mean diffusivity maps for DTI experiments using single-shot EPI with 96x96 resolution. The non-corrected FA maps show detrimental motion artifacts. Retrospective correction using volume-to-volume realignment improved the image quality, but artifacts still remain mainly due to intra-volume motion and spin history effects. The dataset with prospective motion correction shows the highest degree of similarity with the data with no motion.

References: [1] Rohde, MRM, 2004 [2] Aksoy, MRM, 2008 [3] Leemans, MRM, 2009 [4] Aksoy, MRM, 2011 [5] Forman, MICCAI, 2010

References/Funding Source M Aksoy, C Forman, D Kopeinigg, M Straka, R O'Halloran, SJ Holdsworth, ST Skare, R Bammer. Benefits of Optical Prospective Motion Correction for Single-Shot DTI. Proceedings of the 19th Scientific Meeting of ISMRM; 2011; Montreal, Canada. p 171. This work was supported in part by the NIH (1R01EB008706, 5R01EB002711, 1R01EB006526, 1R21EB006860, P41RR09784), Lucas Foundation, Oak Foundation, and GE Healthcare.

Effect of Blood Pressure Reduction on Perihematomal Perfusion in Acute Intracerebral Hemorrhage

DB Aksoy[1], JT Kleinman[2], RW Snider[1], M Mlynash[1,3], I Eyngorn[1], M Straka[4], R Bammer[4], CAC Wijman[1,3]
[1]Stanford Neurocritical Care Program, Stanford Stroke Center, [2]Stanford University Medical Center, Departments of [3]Neurology and Neurological Sciences, [4]Radiology, Stanford University, CA

Introduction: Optimal blood pressure control following acute intracerebral hemorrhage (ICH) remains poorly defined. Blood pressure control may prevent hematoma expansion, while aggressive blood pressure reduction may cause perfusion deficits and subsequent perihematomal ischemia. We investigated perihematomal perfusion in relation to blood pressure reduction using magnetic resonance imaging (MRI) within 24 hours of ICH onset.

Methods: Consecutive prospectively enrolled ICH patients were included if they had an MRI within 24 hours of ICH symptom onset. FLAIR, GRE and perfusion weighted images were acquired and co-registered. T_{max} maps were generated using RApid processing of PerfusIon and Diffusion (RAPID) software. The perihematomal region was defined by outlining the perihematomal edema on FLAIR images and subtracting the inner surface of blood products on the GRE to generate a rim around the hematoma. A $T_{max}\geq 6s$ was defined as abnormal. Image processing was done using Medical Image Processing Analysis and Visualization software.

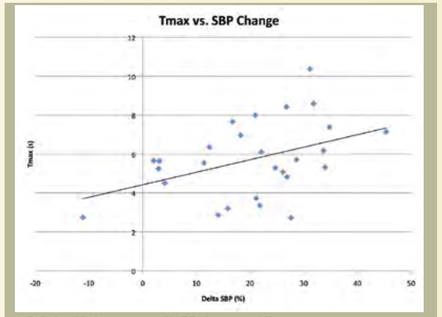

1. Relationship between systolic BP changes and T_{max}
2. Systolic BP drops more than 30% are associated with significantly delayed bolus arrival

Hourly systolic blood pressures (SBP) were recorded from hospital presentation to MRI acquisition. Statistical analyses were done using MATLAB.

Results: Twenty-seven patients were included (age: 62.7±17.9; ICH volume: 25.6±25.7cc). 41% percent of patients had a mean $T_{max}\geq 6s$ in the perihematomal region. Delayed bolus arrival (high T_{max}) in the perihematomal region was associated with larger absolute and percent change in SBP from presentation. Patients whose SBP was lowered >30% had significantly higher T_{max} values, 5.3s (3.6-6.2), than those whose SBP was lowered <30%, 7.3s (6.2 – 8.6), (p=0.014).

Discussion and Conclusion: In this cohort, regional cerebral perfusion in the perihematomal area was commonly impaired and manifest as increased T_{max}. Reductions in SBP of >30% were associated with regional T_{max} values concerning for ischemia. Perihematomal perfusion by MRI may have a role in determining safe thresholds for BP lowering in individual patients. The interaction between regional cerebral perfusion, perihematomal ischemia and neurological status requires further study.

Rapid Diffusion Spectrum Imaging with Partial Q-Spce Encoding

AT Van, RL O'Halloran, S Holdsworth, R Bammer
Department of Radiology, Stanford University, CA

Introduction: Diffusion spectrum imaging (DSI) [1] is a variant of q-space imaging which allows one to measure and interpret the complex diffusion process in microstructures without the necessity of limiting signal models. Despite its great potential, applications of DSI to in in vivo studies have been hindered by DSI's long total acquisition time to sample q-space. Many studies have tried to speed up DSI, either by using compressed sensing [2], by multiplexing slices in acquisitions [3, 4], or by using signal models and/or signal decomposition [5-7] at the cost of a loss of generality and sometimes a loss of information. The current approach proposes to reduce the total acquisition time of DSI by employing a partial q-space encoding scheme, similar to the partial Fourier encoding in traditional k-space imaging. The method does not require any signal modeling and is compatible with previously proposed acquisition-based speed-up techniques [2-4].

Methods: The measured DSI signal and the probability distribution function (pdf) of the diffusion process in imaged tissues are related through the Fourier relationship. Since all pdfs are real, from the property of the Fourier transform, the measured q-space data are Hermitian symmetric, meaning $S(q) = S^*(-q)$ where $S(.)$ is the measure q-space signal and * represents the complex conjugate operation. This Hermitian symmetry property of the q-space signal allows the acquisition of only half of the q-space signal; the other half can be filled in using the above equation, resulting in 50% speed-up. Data Acquisition: Single-shot DSI of the brain at the corpus callosum level was performed on a healthy volunteer using a 1.5T MRI scanner with a 8-channel head coil. Q-space matrix size was 9 x 9 x 9 with a maximum b-value of 15,000 s/mm2. The obtained resolution for the diffusion propagator was 11 μm with 44 μm FOV.

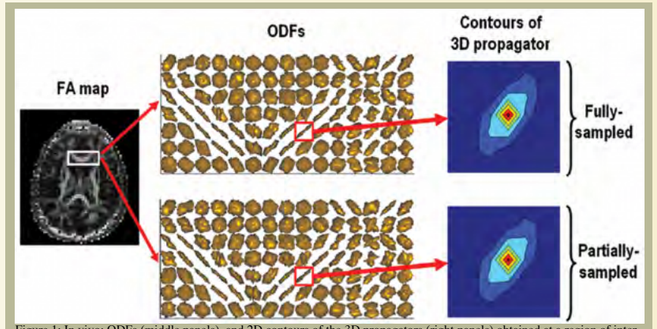

Figure 1: In vivo: ODFs (middle panels), and 2D contours of the 3D propagators (right panels) obtained at a region of interest within the corpus callosum using fully-sampled, and partially-sampled q-space data.

Results and Discussion: The middle panels of Fig. 1 show the obtained ODFs in the region of interest pointed out by the white square box on the FA map. No difference was observed between the ODFs generated by partially-sampled q-space data and the ODFs generated by fully-sampled q-space data. The right panels of Fig. 2 compares the 3D propagators reconstructed from fully-sampled and partially-sampled q-space data. The structure of the propagator is well-preserved in the partially-sampled case. By using partial q-space encoding, the total acquisition time was reduced by 44.4%.

Conclusion: We have shown that partial q-space encoding is an efficient acquisition method for diffusion spectrum imaging. The method is proposed based on the intrinsic property of the diffusion propagator and does not require any signal modeling.

References: [1] Wedeen et al., MRM. 54, p. 1377-1386, 2005; [2] Menzel et al., ISMRM, p. 1698, 2010; [3] Reese et al., JMRI. 29, p. 517-522, 2009; [4] Setsompop et al., ISMRM, p. 187, 2010; [5] Tuch, MRM. 52, p. 1358-1372, 2004; [6] Assaf et al., NeuroImage. 27, p. 48-58, 2005; [7] Wu et al., NeuroImage. 36, p.617-629.

References/Funding Source Rapid Diffusion Spectrum Imaging with Partial Q-Space Encoding. AT Van, RL O'Halloran, S Holdsworth, R Bammer. In Proceedings of the 19th Annual Meeting of the ISMRM. 1913 1 R01 EB008706, 1 R01 EB008706 S1, 5 R01 EB002711, 1 R01 EB006526, 1 R21 EB006860, Center of Advanced MR Technology at Stanford (P41RR09784), Lucas Foundation, Oak Foundation. GE Healthcare

A Geometric Distortion Correction Algorithm to Augment Prospectively Corrected EPI Data

MB Ooi[1], TR Brown[2], R Bammer[1]
[1]Department of Radiology, RSL, Stanford University, CA; [2]Department of Radiology, Medical University of South Carolina, SC

While prospective rigid-body motion correction can be performed very accurately[1], a secondary effect of head motion is non-rigid image distortion in echo-planar imaging (EPI) caused by changes in the effective shim within the brain[2]. We implemented an approach that uses prospective motion correction in combination with retrospective distortion correction to obtain single-shot EPI scans that are compensated for both rigid motions and susceptibility-induced non-rigid deformations.

Complex EPI-data from the prospectively corrected images[3] was saved to generate field-maps for additional retrospective distortion correction. Phase images Φ_n of the nth diffusion scan were unwrapped, and the field variation map ΔB_n calculated: $\Delta B_n = (\Phi_n - \Phi_1)/(2\pi TE)$. ΔB_n thus yields a frequency-difference map (Hz) of the relative field inhomogeneity deviation between the nth and first (reference) time-frame due to the different head positions relative to B_0. Since field inhomogeneities cause negligible pixel mislocation in the readout direction for EPI, the distortion correction then simplifies into a series of 1D pixel-shifts in the phase-encode direction which – due to the prospective scan-plane tracking – remains "locked" to the patient orientation. To calculate the necessary pixel-shifts, the local ΔB_n is converted into a pixel-shift map $r_n = \Delta B_n / BW_{PE}$, where BW_{PE} is the bandwidth per pixel in the phase-encode direction. A shifting algorithm4 was implemented where each pixel at location r_n was used to shift the corresponding image pixel. In this manner every nth time-frame was undistorted back to the reference. This (non-rigid-body) distortion correction was retrospectively applied to the (rigid-body) prospectively corrected dataset and yielded considerable improvement over prospective motion correction alone (see figure). Achieving better congruence between individual images is key for applications where multiple volumes are acquired, such as diffusion, perfusion, and functional MRI. The proposed distortion correction algorithm can effectively augment any prospective correction method, as long as the complex EPI data is saved.

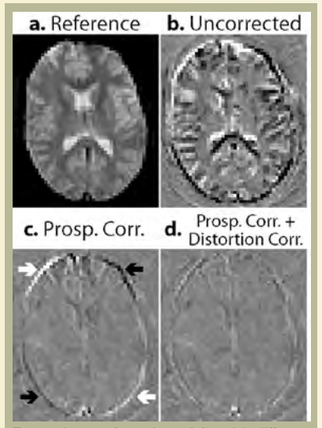

Top row shows a reference image (left), and the difference between an image in the time-series acquired after 5° of head rotation without any correction (right). Bottom row shows that prospective motion correction mitigates the misregistration (left) but geometric distortions still remain (highlighted by arrows). Combined prospective and retrospective correction leaves only minor differences (right).

References/Funding Source [1] MB Ooi, et al.,MRM 2009;62(4):943-54. [2] P Jezzard, et al.,HBM 1999;8(2-3):80-85. [3] MB Ooi, et al.,MRM 2011;66(1):73-81. [4] P Jezzard, et al., MRM 1995;34(1):65-73. NIH R21EB006877, NIH/NCRR UL1RR024156, NIH 5R21EB006860, NIH 1R01EB011654

Spin- and Gradient-Echo EPI for Imaging of Brain Perfusion with MRI

H Schmiedeskamp[1], M Straka[1], G Zaharchuk[1], NJ Fischbein[1], MG Lansberg[2], J-M Olivot[2], GW Albers[2], ME Moseley[1], R Bammer[1]
Departments of [1]Radiology, [2]Neurology, Stanford University, CA

A spin and gradient echo (SAGE) EPI sequence that is capable of simultaneously measuring spin- (SE) and gradient-echo (GE) perfusion-weighted imaging (PWI) data was previously introduced). This sequence was adopted from recent work on PWI by merging multi-GE EPI with a combined GE and SE EPI acquisition. Boxerman et al. found a difference in sensitivity to the underlying microvasculature in brain tissue, depending on whether GE or SE images were acquired. The great advantage of SAGE-EPI is that it acquires GE and SE perfusion maps simultaneously, and allows one to relate changes in R2 to changes in R2* for vessel size imaging (VSI) . Here, we refined the SAGE-EPI pulse sequence to facilitate the simultaneous acquisition of 5 EPI readout trains, all with echo times TE < 100 ms. Furthermore, the PWI processing pipeline was adjusted such that cerebral blood volume (CBV) and cerebral blood flow (CBF) were calculated from R2 and R2* estimates, rather than relative changes in signal intensity, with the goal to produce T1-independent, more quantitative PWI maps. Fig. 1 shows results in case of subacute left posterior MCA infarct. While single-echo based GE and SE PWI maps reflect little to no increase in CBV, PWI maps produced with the help of R2 and R2* resulted in considerably increased CBV in the left temporal lobe (red arrows). Increased mean transit time (MTT) was associated with higher CBV, a common finding in subacute stroke lesions. VSI resulted in a small, but notable drop in vessel size within the area in question, more pronounced on the maps created with the multi-echo ΔR2*/ΔR2 approach. In summary, the calculation of PWI parameters could be enhanced by correcting for T1-shortening effects based on the estimates of the transversal relaxation times R2 and R2*.

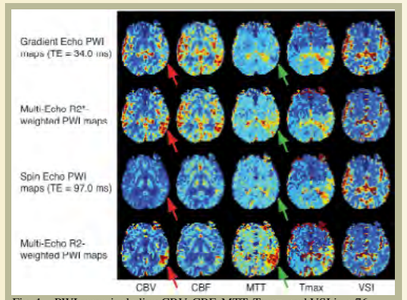

Fig. 1 – PWI maps including CBV, CBF, MTT, Tmax, and VSI in a 76-year old patient with subacute infarct in left posterior MCA territory with enhanced CBV visible on R2 and R2*-weighted CBV maps, suppressed on single echo GE and SE CBV maps (red arrows). Associated increase in MTT, particularly well defined in R2-weighted maps. Single echo MTT maps even show a decreased MTT in questioned area (green arrows).

References/Funding Source H Schmiedeskamp, M Straka, G Zaharchuk, NJ Fischbein, MG Lansberg, J-M Olivot, GW Albers, ME Moseley, R Bammer. Spin- & Gradient-Echo EPI for Imaging of Brain Perfusion with MRI. Proc ISMRM 2011, Montréal, Canada. p 788. NIH(5R01EB002711,5R01EB008706,5R01EB006526,5R21EB006860,5R01NS047607,2P41RR009784), Lucas & Oak Foundation.

Behavioral correlates of temporal variations in brain network connectivity

C Chang[1,2], X Shen[1], GH Glover[1,2]
Departments of [1]Electrical Engineering, [2]Radiology, Stanford University, CA

Functional connectivity among brain networks, as averaged across a several-minute fMRI scan, has been found to reflect conditions such as neurological disorders and behavioral state. It was recently demonstrated that the coherence between brain networks can display marked variations in magnitude and phase across a resting-state scan, suggesting that connectivity variability, as well as mean strength, may be a relevant index of cognitive state. Here, we used sustained task manipulations (continuous 1-back and 2-back working memory tasks) to probe the causes and potential significance of temporal variability in low-frequency BOLD signal connectivity. After filtering out task-related frequencies (>0.12 Hz), we examined whether variability in connectivity between the default-mode network (DMN) and other brain regions can be modulated by cognitive load, and quantified the degree to which variability can explain individual differences in behavior (reaction time).

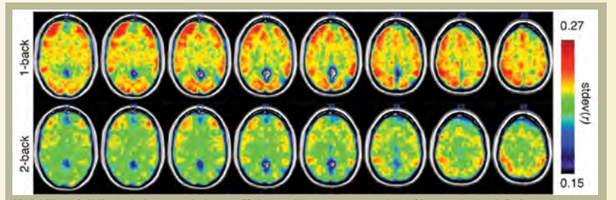

Variability of sliding-window correlation coefficients with respect to a region of interest in the default-mode network, averaged across subjects, for both 1-back (top row) and 2-back (bottom row) working memory tasks.

Temporal variability in connectivity with the DMN was modulated by task load (Fig. 1); overall, greater variability was observed in the 1-back task, compared to the 2-back task. Across subjects, functional connectivity between the DMN and both the anterior cingulate cortex and caudate was predictive of mean reaction times in both 1- and 2-back tasks. Within subjects, a sliding-window analysis (window size = 1 min) revealed that changes in mean reaction time across the scan were correlated with changes in functional connectivity between the DMN and a cluster in the dorsolateral prefrontal cortex (DLPFC) for both 1- and 2-back tasks, and with clusters in the DLPFC and hippocampus for the 2-back task. These findings contribute evidence that dynamics of network connectivity may relate to inter- and intra-individual differences in behavioral performance, and hence may serve as a meaningful index of cognitive or attentional state.

References/Funding Source C Chang, X Shen, GH Glover. (2011) Behavioral correlates of temporal variations in brain network connectivity. Proceedings of the Organization for Human Brain Mapping, 17th Annual Meeting, Quebec City. NIH F31-AG032168 to CC, NIH P41-RR09784 to GHG

Influence of Dense Array EEG Cap on fMRI Signal

Q Luo, GH Glover
Departments of Radiology, RSL, Stanford University, CA

Dense-array (>64 channel) EEG systems are increasingly being used in simultaneous EEG-fMRI studies. However, with increasing channel count, dense-array EEG caps can induce more severe signal dropout in the MRI images than conventional systems due to the radio frequency (RF) shielding effect of the denser conducting wire bundle. This study investigates the influence of a 256 channel EEG cap on MRI image quality and detection sensitivity of BOLD fMRI signal. A theoretical model is first established to describe the impact of the EEG cap on anatomic signal, noise, signal-to-noise ratio (SNR) and contrast-to-noise ratio of BOLD signal. Seven subjects were scanned to measure and compare the T2*-weighted image quality and fMRI detection sensitivity with and without the EEG cap using an auditory/visual/sensorimotor task. As shown in the figure, the experimental results indicated that the dense-array EEG cap can substantially reduce the anatomic signal in the brain areas (visual cortex) near the conducting wires (average percent decrease ≈ 38%). However, the noise is also reduced by the EEG cap, and the percent decrease in the noise is about the same as in the signal at a given position. Hence, the image SNR with the EEG cap remains approximately unchanged compared to that without the EEG cap. From the seven subjects, it is found that the average percent decrease of SNR induced by the EEG cap is less than 8% in all the brain regions, and there was no statistically significant difference in the average t-value and activation volume of BOLD activation. This suggests that the ability to detect fMRI signal is nearly unaffected by dense-array EEG caps in simultaneous EEG-fMRI experiments.

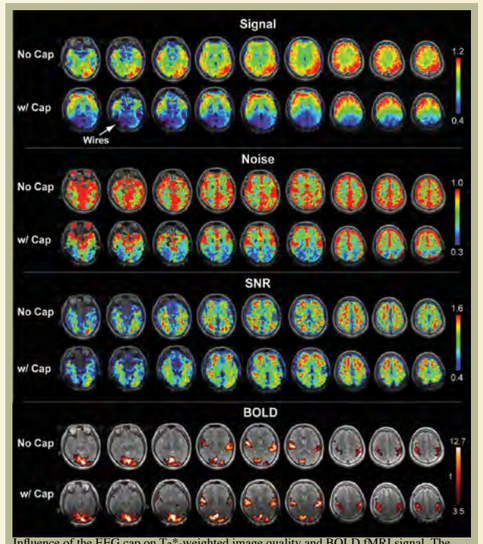

Influence of the EEG cap on T_2*-weighted image quality and BOLD fMRI signal. The maps of image quality parameters (anatomic signal, noise and SNR) and BOLD activation without and with the EEG cap are obtained from a single subject and overlaid on the corresponding high-resolution structural images to facilitate visual inspection. The signal, noise, and SNR values are normalized to the corresponding average values in the prefrontal brain region, where the shielding effect on the signal and noise is negligible.

References/Funding Source Q Luo, GH Glover. Influence of Dense Array EEG Cap on fMRI Signal. Magn Reson Med (submitted). This work was supported by an NIH grant, P41 RR009784.

Rapid Motions in Pediatric and Clinical Populations

PK Mazaika[1], GH Glover[2], AL Reiss[1]
Departments of [1]Psychiatry and Behavioral Sciences, [2]Radiology, RSL, Stanford University, CA

The analysis of neuroimaging data from children with developmental disorders is key to understanding the neural correlates of impaired cognitive development. However, these subjects may not tolerate tight head padding, and rapid head motions may introduce artifacts in fMRI data that can degrade the accuracy of the results. The goal of this study was to quantify the density of rapid motion artifacts for several pediatric and clinical populations. All subjects were prepared before the real scan by practice in a mock MRI scanner in an effort to desensitize them to the sights and sounds of an actual MRI environment. We counted the fraction of scans with rapid motions of more than 0.5 mm/TR using existing fMRI data (254 scan sessions) from a variety of healthy and high motion subject populations. The populations included healthy adults, adolescents, and young children, and subjects with fragile X syndrome, Williams syndrome, Turner syndrome, and bipolar disorder. The rapid motion characteristics are shown as a quartile plot in the figure. Among the healthy subjects, adolescents have more rapid motions than adults, and young children have the most rapid motions. For all the populations (except healthy adults, and females with Fragile X syndrome), there are rapid motion artifacts in the fMRI data for more than half of the data sets. Artifact suppression algorithms must be able to process data with 10% or more artifacts in order to be successful in these populations. The ArtRepair software toolbox is one method that will automatically suppress the residual motion effects and artifacts that occur in fMRI data from these populations. (http://cibsr.stanford.edu/tools/ArtRepair).

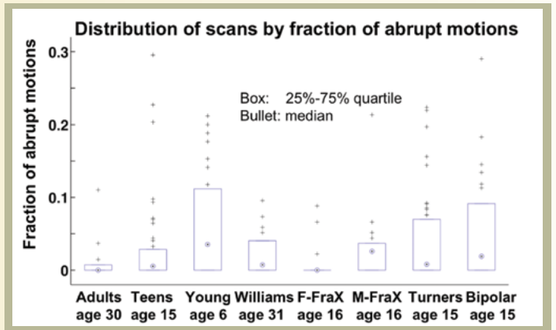

Distribution of scan sessions by the fraction of artifacts in the data for healthy and clinical populations.

References/Funding Source Organization of Human Brain Mapping Conference, Quebec City, Canada, June 28, 2011. K25MH077309 National Institute of Mental Health

Pseudocontinuous and Velocity Selective Arterial Spin Labeling vs. Gold Standard Xenon CT

D Qiu, ME Moseley, G Zaharchuk
Department of Radiology, RSL, Stanford University, CA

In standard arterial spin labeling (ASL), differences in arterial transit arrival time can be a major source of error in the quantification of cerebral blood flow (CBF). This problem becomes worse in some pathologies, such as stroke, where blood flow is slow and/or there is collateral flow. Recently, velocity-selective ASL (VSASL) has been proposed and is expected to overcome this limitation. However, clinical data on VSASL is rare. In this study, we compared the performance of a 3D-FSE pseudocontinuous ASL (pcASL) with different post-label delay (PLD) times and VSASL, using xenon CT CBF as gold standard. High-quality pcASL, pcASL-VS, and xeCT CBF maps were obtained. VSASL CBF maps, however, have relatively lower SNR due to the use of a saturation rather than inversion labeling pulse. Visually, PLD dependence of pcASL and pcASL-VS CBF measurement was obvious in slow-flow regions, though these were somewhat mitigated at longer PLD's, such as 3s. Overestimation of CBF for pcASL studies with long PLD was seen in regions with delayed arrival, and may reflect differences in the true and assumed T1 decay of the label. Correlation analysis showed that among different PLD times, the strongest correlation with xeCT CBF measurement was found in CBF maps acquired with PLD=1.5s for both pcASL and pcASL-VS. VSASL had moderate correlation with xeCT measurement, largely attributable to lower SNR in VSASL CBF measurement. In general, differences between VSASL and xeCT CBF values were among the smallest for all ASL sequences, and importantly the standard deviations of these differences were also small, suggesting that VSASL may provide a quantitatively more accurate measurement of CBF in these patients.

To our knowledge, these are the first reports of VSASL in clinical patients with severe prolongations in arterial arrival times. pcASL CBF maps with long PLD more closely approximated xenon CT CBF maps, but required long scan times (8 min) and had relatively poor SNR. The expected PLD dependence of pcASL and pcASL-VS CBF measurements was observed. VSASL provided more accurate absolute CBF measurement, though correlation with xeCT was lower, largely owing to lower SNR. Further development of VSASL techniques may enable accurate CBF measurements in patients with cerebrovascular disease.

References/Funding Source D Qiu, ME Moseley, G Zaharchuk. Comparison of Pseudocontinuous and Velocity Selective Arterial Spin Labeling with Gold Standard Xenon CT: a Study in Patients with Moyamoya Disease. Proceedings of the ISMRM, 2010, Stockholm Sweden. NIH R01-NS066506; Lucas and Oak Foundation; GE Healthcare; and EC Wong for providing the VSASL sequence and post-processing tools.

Consequences of Multi-echo Fits in Perfusion MRI for the Determination of MTT in Presence of T1-Effects.

M Straka[1], H Schmiedeskamp[1], G Zaharchuk[1], JB Andre[1], J-M Olivot[2], NJ Fischbein[1], MG Lansberg[2], ME Moseley[1], GW Albers[2], R Bammer[1]
[1]Department of Radiology, Stanford University, CA; [2]Stanford Stroke Center, Stanford University, CA

Although it was already pointed out that T1-shortening can be a considerable confounder in DSC-PWI, it has been heavily underestimated so far by the community. While practitioners are aware of potential CBV underestimation due to T1-shortening, time-based perfusion parameters are widely deemed to be immune against confounding effects that primarily influence the calculation of the time course of contrast concentration. In this study, we demonstrate in simulations and on clinical data that current DSC-PWI approaches can also lead to incorrect estimates of MTT, specifically in areas of contrast agent (CA) leakage due to a compromised blood-brain barrier. This can be seen as a confirmatory study for the predictions. With the current trend of neuroimaging migrating towards higher fields and shorter sampling rates, T1 shortening warrants even more attention as these effects will be increased. Here, we show that T1-effects can have considerable consequences for the estimation of MTT, whereas Tmax is more robust against this confounder.

Estimated values of MTT in presence of T1-effects were 50% higher compared to situations in which T1-effects were removed, however, Tmax values did not show any significant differences (data not shown). A very similar behavior was observed in the scanned data. Presence of T1-shortening in a scan performed at 3T and at high temporal resolution (TR = 1.8sec) resulted in considerable differences between multi-echo T2 and T2* DSC-PWI maps and those derived from conventional single-echo GE or SE methods. Specifically, both single-echo GE and SE derived MTT maps did not show significant increase in the region of the subacute stroke (accompanied by noticeable T1 extravasation), whereas Tmax maps derived from these methods clearly showed alterations in hemodynamics.

In assessment of stroke, the T1-shortening can severely limit the veracity of MTT maps (derived using bolus tracking methods) when not accounted for. This is due to errors in the estimation of contrast agent concentration; to some degree immediately before and during the first pass of the bolus, but to a much greater extent after the first pass. The results shown here might be exaggerated because the GEs were acquired with a 90° flip angle, which could be adjusted towards lower flip angles to reduce the T1 sensitivity. To eliminate this T1 sensitivity entirely and to leverage higher SNR from more optimal flip angles, a SAGE approach as described in this work should be used, ultimately leading to more accurate estimates of tracer concentration and therefore MTT. On the other hand, Tmax appears not to be affected by T1 effects. This is mostly because it is an AIF-corrected bolus arrival map; Tmax is not sensitive to erroneous signal changes predominantly occurring at the tail end of the bolus, but these signal changes are mainly responsible for MTT estimation errors. In summary, when reporting clinical MTT values in addition to Tmax, caution should be exercised, as regions with prolonged MTT might be severely underestimated.

References/Funding Source Consequences of Multi-echo Fits in Perfusion MRI for the Determination of MTT in Presence of T1-Effects. M Straka, H Schmiedeskamp, G Zaharchuk, JB Andre, J-M Olivot, NJ Fischbein, MG Lansberg, ME Moseley, GW Albers, R Bammer. Proceedings of the ISMRM, 2010, Stockholm Sweden. NIH (5R01EB002711, 5R01EB008706, 5R01EB006526, 5R21EB006860, 5R01NS047607, 2P41RR009784, 2R01NS047607), Lucas & Oak Foundation

Quantitative Susceptibility Imaging using L1 regularized reConstruction with Sparsity Promoting Transformation: SILC

D Qiu, G Zaharchuk, S Feng, T Christen, K Sung, ME Moseley
Department of Radiology, RSL, Stanford University, CA

The phase image has been shown to provide superb tissue contrast at high imaging field, and reveals anatomical details that cannot be easily identified in magnitude images. Reconstruction of the susceptibility distribution from phase images provides a quantitative measure of tissue properties, but faces many difficulties, including zero points in the convolution kernel. Methods have been proposed to solve the problem. Here we develop a novel method of reconstructing susceptibility distribution from phase images, which borrows ideas from compressed sensing.

Simulation analysis showed that there were residual streaking artifacts in the KM reconstructed susceptibility image while SILC nearly perfectly reconstructed the susceptibility image. For the KM method, the mean estimated susceptibility value inside the tube was found to depend on the truncation level and largely underestimated the true value (0.02ppm). In contrast, for the SILC method, the mean estimated susceptibility value closely approached the true value for a range of values of ρ.

The SILC method successfully reconstructed susceptibility distributions from the in-vivo human brain data, and the contrast matches known distribution of susceptibility in the brain. The susceptibility image reconstructed using KM method showed lower resolution, possibly due to modification of the kernel; and the values were lower than that in SILC reconstructed image, consistent with simulation results.

We have proposed a novel method (SILC) for reconstructing susceptibility image from field map using L1 regularization with sparsity-promoting transformation. Simulations showed high fidelity of the reconstructed image using SILC to the gold truth for a range of the data consistency penalty parameter ρ. This quantitative susceptibility imaging technique has many potential applications, including measurement of blood oxygenation level in the vessels, quantification of iron loading in the brain, definition of arterial input function in dynamic susceptibility contrast imaging.

References/Funding Source Quantitative Susceptibility Imaging using L1 regularized reConstruction with Sparsity Promoting Transformation: SILC. D Qiu, G Zaharchuk, S Feng, T Christen, K Sung, ME Moseley. Proceedings of the ISMRM, 2010, Stockholm Sweden. NIH (2P41RR009784 and 2R01NS047607-05), Lucas Foundation, Oak Foundation.

Prescription opioid analgesics rapidly change the human brain.

J Younger, L Chu, N D'Arcy, K Trott, L Jastrzab, S Mackey
Department of Anesthesia, Stanford University, CA

Long-term opioid abuse has been associated with neuroplastic changes in the human brain; however, it is unknown if opioids used over short periods of time and at analgesic dosages can similarly change brain structure. Ten individuals with low-back pain were administered oral morphine for one month (mean daily dosage = 72 mg). Nine other individuals were administered a placebo substance for the same period of time. High-resolution anatomical images of the brain were acquired from participants before and after the one-month morphine or placebo administration. Individuals receiving morphine reported a significant decrease in low-back pain, as well as a significant increase of anxiety and non-significant increase of depression. Grey matter volumetric changes were assessed using tensor-based morphometry. Regional areas of atrophy and hypertrophy were examined on the whole brain, and regions exhibiting a significant change over time were subsequently tested for correlations with morphine dosage. Dosage-correlated grey matter atrophy was observed in the amygdala, and dosage-correlated hypertrophy was seen in the posterior cingulate, hypothalamus, inferior pons, inferior frontal gyrus, superior temporal gyrus, and cerebellar tonsil. No regions of atrophy or hypertrophy were observed in the placebo group. In order to differentiate neural mechanisms of desirable morphine outcomes (analgesia) from the mechanisms of adverse outcomes, a series of post-hoc correlation tests were performed on the regions evidencing significant neuroplasticity. Self-reported changes in pain intensity, anxiety, and depression were used in the post-hoc correlations. Individuals reporting the greatest pain reduction also showed the most grey matter volume reduction in the hippocampus, and the most volume increase in the posterior cingulate. Increases in anxiety over time were associated with hypertrophy in the posterior cingulate and posterior insula. Increased reports of depression corresponded to atrophy in the oribtofrontal gyrus, and hypertrophy in the dorsal posterior cingulate and mid-cingulate. Prescription opioid analgesics can cause morphologic changes in the human brain after one month of daily administration. Furthermore, the neuroplastic mechanisms underlying the desirable consequences of opioid use may be distinct from the mechanisms of unwanted consequences.

References/Funding Source K99DA023609, K23GM071400).

Spin-echo and Gradient-echo PWI CBF vs. ASL CBF: An Initial Comparison

M Straka[1], H Schmiedeskamp[1], G Zaharchuk[1], JB Andre[1], J-M Olivot[2], NJ Fischbein[1], MG Lansberg[2], ME Moseley[1], GW Albers[2], R Bammer[1]
Departments of [1]Radiology, [2]Neurology, Stanford University, CA

The SAGE PWI sequence [1, 2] leverages on both gradient-echo (GRE) and spin-echo (SE) data for advanced perfusion-weighted imaging (PWI). It also allows quantification of the baseline R2 and R2*, as well as true ΔR2 and ΔR2* changes during the passage of the gadolinium tracer. This sequence allows one to quantify perfusion parameters from both capillaries (via SE data) and arterioles/venules (via GRE data) at high temporal resolution and without T1 contamination. Although current routine PWI scans use primarily the GRE data, it has been long suggested that cerebral blood flow (CBF) values derived from GRE are overestimated due to excessive sensitivity to larger vessels. Here, we compared CBF values from by GRE- and SE-based SAGE CBF to reference arterial-spin labeling (ASL) CBF data.Ten clinical cases were acquired using a 3T GE Discovery MR750 scanner. The study was IRB approved and written informed consent was obtained from each subject.

Our initial results show that CBF derived from SE based maps was approx. 4.8-times smaller than CBF derived from GRE-based maps, and hence the SE CBF must be corrected with this factor to match GRE CBF values. The 4.8-fold difference was very similar between gray and white matter, and could be considered in future studies. Results also show that SE- and ΔR2-based CBF maps correlate with ASL CBF better than GRE or ΔR2*-based maps as the large vessel contribution present on GRE-based maps tend to obfuscate tissue microperfusion. Our results also manifest that the slope of SE CBF vs. ASL CBF is less than 1.0, and the intercept is non-zero. Specifically, the relation between ASL CBF and SE CBF was different in both gray and white matter, which is most likely caused by sensitivity of ASL to label delay and variable label efficiency in gray and white matter. Based on the correlation coefficient R and visual impression, we conclude that SEbased/ΔR2-based PWI CBF maps are more similar to ASL than those obtained from single-GRE/ΔR2*-based data. However, differences between single-SE and ΔR2-based CBF values require further analysis.

References/Funding Source Spin-echo and Gradient-echo PWI CBF vs. ASL CBF: An Initial Comparison. M Straka[1], H Schmiedeskamp[1], G Zaharchuk[1], JB Andre[1], J-M Olivot[2], NJ Fischbein[1], MG Lansberg[2], ME Moseley[1], GW Albers[2], R Bammer[1]. Proceedings of the ISMRM, 2010, Stockholm Sweden. NIH(5R01EB002711,5R01EB008706,5R01EB006526,5R21EB006860,5R01 NS047607,2P41RR009784), Lucas & Oak Foundation.

Evaluating an Intensive Behavioral Intervention for Children and Adolescents with Fragile X Syndrome

SS Hall, JL Hammond, KM Hustyi, AL Reiss
Department of Psychiatry and Behavioral Sciences, Stanford University, CA

This study will attempt to overcome putative specific learning dysfunction in children and adolescents diagnosed with Fragile X syndrome (FXS) using a stimulus equivalence (SE) teaching paradigm. Mathematical performance and brain activation prior to and following SE training will be examined. The efficacy of the intervention will be studied in comparison to a control group of gender, verbal IQ, and age-matched individuals diagnosed with non-specific developmental delay (DD) in order to understand the specificity of mathematical dysfunction exhibited by individuals with FXS. Performance in the targeted skill areas (fraction, pie chart, and decimal conversion) will be compared prior to and following SE training, using functional magnetic resonance imaging (fMRI) and behavioral metrics. It is hypothesized that following SE training, individuals with FXS will show gains in their discrimination of both trained and untrained mathematical relations, and will show increased activation in posterior parietal (PPC) and dorsolateral prefrontal cortex (DLPFC). In addition, we hypothesize that these regions will show increased functional connectivity compared to pre-test measures.

References/Funding Source National Institute of Mental Health (K08)

Stress Coping and Brain Development: A Longitudinal MRI Study

JM Nechvatal[1], D Qiu[2], CL Buckmaster[1], AF Schatzberg[1], ME Moseley[2], DM Lyons[1]
Departments of [1]Psychiatry, [2]Radiology, RSL, Stanford University, CA

Coping with early intermittent stress changes the developing brain. Here we describe how these neuroadaptations arise in a longitudinal study of adolescent squirrel monkeys (Saimiri sciureus).

T1-weighted anatomical brain images were acquired once each year over the first 3 years of life from monkeys previously exposed to either an intermittent stress coping condition (IS, n = 11) or a no-stress control condition (NS, n = 9). Total gray and white matter brain volumes were determined and voxel-based morphometry (VBM) was used to localize specific regions of volumetric expansion or contraction.

From 1 to 3 years of age, both IS and NS animals exhibited reductions in total gray matter volumes along with white matter increases. Total gray matter reductions were smaller and white matter increases greater in IS than NS animals. VBM analysis revealed prefrontal gray matter contraction in both IS and NS animals, with additional contraction in anterior cingulate observed only in NS animals. Prefrontal gray matter expansion was observed only in IS animals late in adolescent development. White matter expansion was observed in prefrontal regions for both groups and was greater in IS than NS animals.

These data suggest that larger prefrontal volumes previously reported [1, 2] for two different samples of adolescent IS compared to NS monkeys arise from smaller reductions and not just increased expansion of gray matter tissue. Changes in the density of synaptic connections, dendrites, neurons or glial cells may play a role in refining stress coping-dependent neural circuitry.

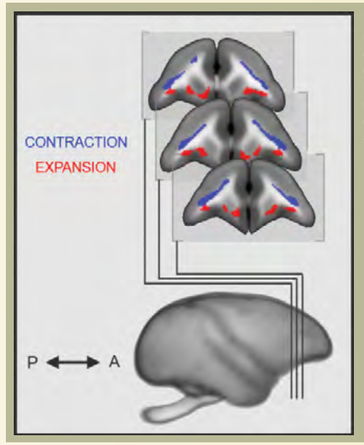

VBM-determined regions of gray matter expansion (red) and contraction (blue) in monkeys exposed to the stress coping condition. P=posterior and A=anterior.

References/Funding Source 1. M Katz, et al. 2009. Dev Neurosci; 31: 293–299. 2. DM Lyons, et al. 2002. Behav Brain Res; 136: 51–59. [Supported by NIMH4753, NIMH77884, and NSF Gradute Research Fellowship]

MRI guides diagnostic approach for ischaemic stroke

M A Kumar,[1,2,3] H Vangala,[4] D C Tong,[5] D M Campbell,[6] A Balgude,[7] I Eyngorn,[8,9] A S Beraud,[10] J M Olivot,[8,9] A W Hsia,[11] R A Bernstein,[12] C A Wijman,[8,9,13] M G Lansberg,[8,9] M Mlynash,[8,9] S Hamilton,[8,9] M E Moseley,[14] G W Albers[8,9]
Departments of [1]Neurology, [2]Neurosurgery, [3]Anesthesiology and Critical Care, University of Pennsylvania Medical Center, Philadelphia, PA; [4]Department of Internal Medicine, Oroville Hospital, Oroville, CA; [5]Department of Neurology, California Pacific Medical Center, San Francisco, CA; [6]Department of Neurosurgery, Wake Forest University Baptist Medical Center, Wake Forest, NC; [7]Department of Radiology, University Hospitals Case Medical Center, Cleveland, OH; Departments of [8]Neurology, Stanford Stroke Center, [9]Neurology, [10]Medicine, Division of Cardiovascular Medicine, [13]Neurocritical Care Program, [14]Radiology, Stanford University, CA; [11]Department of Neurology, Stroke Center, Washington Hospital Center, Washington, DC; [12]Department of Neurology, Feinberg School of Medicine of Northwestern University, Chicago, IL

Identification of ischaemic stroke subtype currently relies on clinical evaluation supported by various diagnostic studies. The authors sought to determine whether specific diffusion-weighted MRI (DWI) patterns could reliably guide the subsequent work-up for patients presenting with acute ischaemic stroke symptoms. 273 consecutive patients with acute ischaemic stroke symptoms were enrolled in this prospective, observational, single-centre NIH-sponsored study.

Among patients with a thromboembolic DWI pattern, transoesophageal echocardiography was the principal determinant of diagnostic change in 8.8% versus 0% for the small vessel group and 1.7% for the other group ($p<0.01$). Among patients with the combination of a thromboembolic pattern on MRI and a negative cervical MRA, transoesophageal echocardiography led to a change in diagnosis in 12.1%. There was no significant difference between groups using a CT-based scheme. Conclusions DWI patterns appear to predict stroke aetiologies better than conventional methods.

The study data suggest an MRI-based diagnostic algorithm that can potentially obviate the need for echocardiography in one- third of stroke patients and may limit the number of secondary extracranial vascular imaging studies to approximately 10%.

References/Funding Source MRI guides diagnostic approach for ischaemic stroke. M A Kumar, H Vangala, D C Tong, D M Campbell, A Balgude, I Eyngorn, A S Beraud, J M Olivot, A W Hsia, R A Bernstein, C A Wijman, M G Lansberg, M Mlynash, S Hamilton, M E Moseley, G W Albers. Study was funded by National Institutes of Health (NIH) grant no. 2R01 NS34866-04 (MEM).

Resting state functional connectivity in adolescents with bipolar I disorder

M Singh[1], R Kelley[1], L Bararpour[1], E Sanders[1], R Shoemaker[1], S Li[1], M Howe[1], A Reiss[1], K Chang[1]
[1]Department of Psychiatry and Behavioral Sciences, Stanford University, CA

Background: Neuroimaging studies of youth with bipolar disorder (BD) have demonstrated dysfunction in frontotemporal regions involved in emotion regulation. The goal of this study was to examine resting state functional connectivity in adolescents with BD I as compared to controls.

Methods: Adolescents (13-18 years old) with BD I (N=18) and adolescents without any personal or parental history of DSM-IV Axis I disorders (N=20) were scanned with fMRI at 3T, at rest. Group differences in resting state functional connectivity were analyzed using a Functional Connectivity Toolbox, after band-pass filtering (0.005 – 0.10 Hz) and correcting for physiological noise and motion. Regions of interest (ROIs) were defined as 10mm spheres of medial prefrontal cortex (MPFC), posterior cingulate cortex, lateral parietal cortices and 5mm spheres of nucleus accumbens. Bilateral amygdala ROIs were derived from the Automated Anatomical Labeling Atlas. ROI-to-whole-brain analyses were performed with statistical thresholds of p=0.01 for voxel height and p=0.05 Family-Wise Error (FWE) corrected for cluster extent.

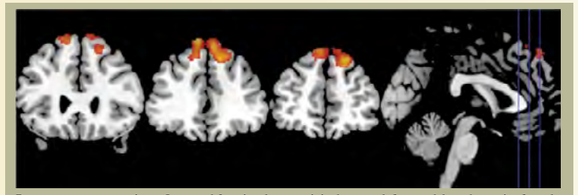

Between-group comparison: Increased functional connectivity between left amygdala and superior frontal gyrus in the BD group compared to HC

Results: Relative to controls, adolescents with BD showed increased network connections between the left amygdala and superior frontal gyrus (SFG) (p=0.01 uncorrected signal and p=0.01 FWE extent). Exploratory analyses investigating medication effects of BD subjects exposed to Lithium or Valproate treatment (N=9) compared to those without exposure (N=9) displayed increased network connections from the nucleus accumbens and right amygdala with visual cortex and left parietal cortex, along with decreased connectivity between left lateral parietal (LLP) and right amygdala and nucleus accumbens (p=0.01 uncorrected signal and p=0.05 FWE extent).

Conclusions: Altered frontotemporal resting state functional connectivity in adolescents with recent onset BD suggests aberrant neural circuitry that may contribute to the pathophysiology of BD. Further studies are needed to understand how altered resting state functional connectivity in adolescents with BD-I impacts long-term clinical outcome.

References/Funding Source Presented at the 66th Annual Meeting of the Society for Biological Psychiatry, San Francisco, CA, May 12-14, 2011. The authors gratefully acknowledge the Klingenstein Third Generation Foundation and the American Psychiatric Association

Language and Reading Skills in School-Aged Children and Adolescents Born Preterm are Associated With White Matter Properties on Diffusion Tensor Imaging

HM Feldman[1], ES Lee[1], JD Yeatman[2], R Bammer[3]
Departments of [1]Pediatrics, [2]Psychology, [3]Radiology, Stanford University, CA

Children born preterm are at risk for deficits in language and reading and also for white matter injuries to periventricular regions of the brain. The goal of this study was to determine whether performance on language and reading measures would be associated with white matter properties in children born preterm and in full-term controls. Children born before 36 weeks gestation (n=23, mean +/- SD age 12.5 +/- 2.0 years, gestational age 28.7 +/- 2.5 weeks, birth weight 1184 +/- 431 grams) and controls born after 37 weeks gestation (n=19, 13.1 +/- 2.1 years, 39.3 +/- 1.0 weeks, 3178 +/- 413 grams) underwent a battery of language and reading tests and Diffusion Tensor Imaging (DTI). DTI scans were processed using Tract-Based Spatial Statistics to generate a core white matter skeleton that was anatomically equivalent across participants. Fractional anisotropy (FA) was the main diffusion property used in these analyses. Results showed that in the preterm group only regions of the entire skeleton were significantly associated with four tasks: verbal IQ, linguistic processing speed, syntactic comprehension, and decoding. Twenty-two clusters on 15 tracts from both the left and right hemispheres were associated language and reading measures. Exploratory multiple regression analysis found that for each task, a single brain region significantly predicted each measure, accounting between 27 and 44% of the variance in that measure. For four tasks, the region was in the right hemisphere. These findings suggest that the white matter network that serves language and reading in children born preterm is widely distributed and that performance in language and reading is associated with microstructural properties of the network.

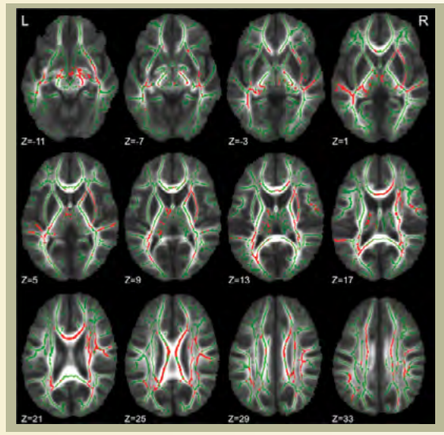

White Matter Language and Reading Network. White matter regions (red) on the FA-skeleton (green), overlaid on axial slices of mean FA image (grayscale), associated with at least one behavioral measure, $p < .05$, in the preterm group (n=23). Regions located on 15 tracts: corpus callosum (z = 4 – 34), forceps major (z = 4 – 16), forceps minor (z = 7 – 22), bilateral anterior thalamic radiation (z = 4 – 19), bilateral corticospinal tract (z = 4 – 37), bilateral inferior fronto-occipital fasciculus (z = 4 – 22), bilateral inferior longitudinal fasciculus (z = 4 – 7), bilateral superior longitudinal fasciculus (z = 16 – 37), and bilateral uncinate fasciculus (z = -25 – -7).

References/Funding Source This work was supported by a grant from the National Institutes of Health, Eunice Kennedy Shriver National Institute of Child Health and Human Development, RO1 HD046500 to HM Feldman; RO1 EB8706, RO1 EB11654, and RO1 EB006526 to R Bammer; NIH Pediatric Research Loan Repayment Program Award to I Loe; and by the Clinical and Translational Science Award 1UL1 RR025744 for the Stanford Center for Clinical and Translational Education and Research (Spectrum) from the National Center for Research Resources, National Institutes of Health.

The Brain Basis of the Phonological Deficit in Dyslexia is Independent of IQ

H Tanaka[1,2], JM Black[1,3,4], C Hulme[5], LM Stanley[1,2], SR Kesler[1,3], S Whitfield-Gabrieli[6], AL Reiss[1,3], JDE Gabrieli[6], F Hoeft[1,3]
[1]Center for Interdisciplinary Brain Sciences Research (CIBSR), [3]Department of Psychiatry and Behavioral Sciences, Stanford University, CA; [2]Pacific Graduate School of Psychology, Palo Alto University, CA; [4]Graduate School of Social Work, Boston College, Chestnut Hill, MA; [5]Department of Psychology, York University, York UK; [6]Department of Brain and Cognitive Sciences, Massachusetts Institute of Technology, Cambridge, MA

Although the role of IQ in the diagnosis of developmental dyslexia remains controversial, the dominant clinical and research approaches rely on a discrepancy definition requiring reading skill to be below the level expected by an individual's IQ. Here, with functional magnetic resonance imaging (fMRI), we examined whether differences in brain activation during phonological processing that are characteristic of dyslexia are similar or dissimilar in children with poor reading ability who had either high (discrepant) or low (non-discrepant) IQ scores. In two independent samples of 131 children, using univariate and multivariate pattern analyses, poor readers with discrepant or non-discrepant IQ scores exhibited similar patterns of reduced brain activation in brain regions including left parieto-temporal and occipito-temporal regions. These results converge with behavioral evidence that poor readers have similar kinds of reading difficulties in relation to phonological processing regardless of IQ.

References/Funding Source H Tanaka[1,2], JM Black[1,3,4], C Hulme[5], LM Stanley[1,2], SR Kesler[1,3], S Whitfield-Gabrieli[6], AL Reiss[1,3], JDE Gabrieli[6], F Hoeft[1,3]. The Brain Basis of the Phonological Deficit in Dyslexia is Independent of IQ. Psychological Science (in press) National Institute of Child Health and Human Development Grant HD054720, Stanford University Lucile Packard Children's Hospital Child Health Research Program, National Center for Research Resources Grant P41RR009874, William and Flora Hewlett Foundation, Richard King Mellon Foundation, National Alliance for Research on Schizophrenia and Depression Young Investigator Award, Ellison Medical Foundation, Massachusetts Institute of Technology Class of 1976 Funds for Dyslexia Research, Bard and Julie Richmond through the Martin Richmond Memorial Fund

Neural Systems Predicting Long-Term Outcome in Dyslexia

F Hoeft[1], B McCandliss[2], JM Black[1], A Gantman[1], N Zakerani[1], C Hulme[3], H Lyytinen[4], S Whitfield-Gabrieli[5], GH Glover[6], AL Reiss[1], JDE Gabrieli[5]
Departments of [1]Psychiatry and Behavioral Sciences, Center for Interdisciplinary Brain Sciences Research (CIBSR), [6]Radiology, Stanford University, CA; [2]Vanderbilt University, Nashville, TN; [3]University of York, York UK; [4]University of Jyväskylä, Jyväskylä Finland; [5]Massachusetts Institute of Technology, Cambridge, MA

Individuals with developmental dyslexia vary in their ability to improve reading skills, but the brain basis for improvement remains largely unknown. We performed a prospective, longitudinal study over 2.5 years in children with dyslexia (N=25) or without dyslexia (N=20) to discover whether initial behavioral or brain measures, including functional MRI (fMRI) and diffusion tensor imaging (DTI), can predict future long-term reading gains in dyslexia. No behavioral measure, including widely used and standardized reading and language tests, reliably predicted future reading gains in dyslexia. Greater right prefrontal activation during a reading task that demanded phonological awareness and right superior longitudinal fasciculus (including arcuate fasciculus) white-matter organization significantly predicted future reading gains in dyslexia. Multivariate pattern analysis (MVPA) of these two brain measures, using linear support vector machine (SVM) and cross-validation, predicted significantly above chance (72% accuracy) which particular child would or would not improve reading skills (behavioral measures were at chance). MVPA of whole-brain activation pattern during phonological processing predicted which children with dyslexia would improve reading skills 2.5 years later with over 90% accuracy. These findings identify right prefrontal brain mechanisms that may be critical for reading improvement in dyslexia and that may differ from typical reading development. Brain measures that predict future behavioral outcomes (neuroprognosis) may be more accurate, in some cases, than currently available behavioral measures.

References/Funding Source F Hoeft, B McCandliss, JM Black, A Gantman, N Zakerani, C Hulme, H Lyytinen, S Whitfield-Gabrieli, GH Glover, AL Reiss, JDE Gabrieli. Neural systems predicting long-term compensation in dyslexia. Proc Natl Acad Sci USA. 2011; 108(1):361-6. PMID: 21173250. PMCID: PMC3017159. National Institute of Child Health and Human Development Grant HD054720, Stanford University Lucile Packard Children's Hospital Child Health Research Program, National Center for Research Resources Grant P41RR009874, William and Flora Hewlett Foundation, Richard King Mellon Foundation, National Alliance for Research on Schizophrenia and Depression Young Investigator Award, Ellison Medical Foundation, Massachusetts Institute of Technology Class of 1976 Funds for Dyslexia Research, Bard and Julie Richmond through the Martin Richmond Memorial Fund

The Use of Diffusion Tensor Imaging (DTI) in Young Children with Type 1 Diabetes

T. Aye[1], N. Barnea-Goraly[2], C. Ambler[3], Y. Park[2], D. Wilson[1], A. Reiss[2,4,5], B. Buckingham[1]
Departments of [1]Pediatrics, Division of Pediatric Endocrinology and Diabetes, [2]Center for Interdisciplinary Brain Sciences Research, Psychiatry, [4]Radiology, [5]Department of Pediatrics, Stanford University, CA; [3]Hospital Educational Advocacy Liaisons Program, Lucile Packard Children's Hospital, Stanford, CA

DTI is used to investigate white matter (WM) structure in the brain. DTI has shown deficits in WM structure in adult subjects with T1DM that correlated with reduced neurocognitive function. However, there are no published DTI studies in children with T1DM. Young children, ages 3 to 10 years, with T1DM and matched healthy controls (HC) completed age appropriate batteries of neuropsychological tests and MRI scans of the brain. Twenty-one DTI scans from children with T1DM (mean age 7.9 ± 1.6) and 12 scans from HC (mean age 7.3 ± 1.6) were analyzed using Tract-Based Spatial Statistics (TBSS). Voxel-wise between-group comparisons of Fractional Anisotropy (FA, degree of diffusion anisotropy), Radial Diffusivity (RD, representing diffusion perpendicular to the fiber axis) and Axial Diffusivity (AD, representing diffusion along the fiber axis) were performed using Threshold-Free Cluster Enhancement in a fully corrected analysis. We used TBSS to conduct correlation analysis between WM structure and HbA1C levels, duration of T1DM, and neuropsychological test scores. Using a whole-brain analysis, there were no significant differences between T1DM and HC. Negative correlations of FA ($p = 0.053$) and RD ($p = 0.055$) with increased HbA1c in the internal capsule and splenium of the corpus callosum approached significance. A negative trend was seen between FA and NEPSY attention scores (0.09) in the fronto-striatal tracts which are known to be related to attention. These tracts were used in a post-hoc analysis as a region of interest to investigate whether attention-related circuits are affected in T1DM. In this analysis, significantly reduced AD was seen in T1DM when compared to HC ($p = 0.04$). This is the first study to suggest early signs of WM variation in children with T1DM. Larger studies of WM structure are needed to define the impact of T1DM on the developing brain.

Effects of duloxetine and placebo in patients with chronic low back pain

KA Johnson, N Chatterjee, N Noor, A Crowell, R McCue, S Mackey
Department of Anesthesia, Stanford University, CA

Chronic low back pain has a tremendous impact and is difficult to treat. Duloxetine is a serotonin-norepinephrine reuptake inhibitor used for a variety of indications, including depression, diabetic peripheral neuropathy, and fibromyalgia. Recent studies suggest that duloxetine may have efficacy in treating chronic lower back pain. In a randomized, double-blind, placebo-controlled crossover study, we used clinical assessments to examine the effects of duloxetine and placebo. Additionally, we used MRI to detect possible brain effects of duloxetine and placebo. Patients with at least 6 months of back pain (no radicular symptoms), a minimum 4/10 pain rating for two weeks prior to enrollment, and no current pain medication use (except acetaminophen) were eligible to enter the study. Duloxetine administration was 30mg/day for one week, followed by 60mg/day for five weeks. Placebo administration and assessment were identical to duloxetine administration. Clinical assessments occurred at baseline, and at weeks 1, 2, and 6 into each medication period. Week 6 was the crossover point, where patients were switched to duloxetine or placebo. Additional at-home measures were collected. Clinical measures included basic medical assessments, a battery of pain related questionnaires, and mood and depression ratings. Data collection was completed in 18 patients. Preliminary analysis indicates a significant change in pain ratings at the end of the duloxetine period, particularly for patients who received placebo first. Most patients had minimal to mild depression (BDI < 19) upon study enrollment. A few patients entered the study with moderate or severe depression, which decreased with duloxetine and placebo treatment. Preliminary structural MRI indicated changes in gray matter with both duloxetine and placebo, including increases in frontal cortex regions. Initial analysis indicates that duloxetine has brain and behavioral effects for chronic low back pain patients.

References/Funding Source American Pain Society Conference, 2011, Austin Texas. Supported by a research grant from Eli Lilly

Central sensitization in the human spinal cord as measured with functional magnetic resonance imaging

PG Nash, JE Brown, SC Mackey
Department of Anesthesia, Stanford University, CA

Central sensitization, which involves an increased gain in the nociceptive system, has received growing support as a possible mechanism underlying chronic pain conditions. The heat-capsaicin model has been shown to reliably evoke symptoms of chronic pain such as secondary mechanical hyperalgesia (SMH). In experimental animals, SMH has been shown to result from central sensitization within the dorsal horn of the spinal cord, however the difficulties associated with imaging the spinal cord has mean that this is yet to be confirmed in humans. The aims of this study are to determine the activation patterns in the spinal cord due to mechanical stimuli in an experimentally induced model of central sensitization. Following the establishment of heat-capsaicin model on the volar forearm, a continuous series of fMRI brain images (212 spiral in out, gradient echo volumes, voxel size=1.25x1.25x4mm, TR=2.5seconds) were collected over a 9minute period. The scan began with a 40 second baseline followed by 30 seconds of mechanical stimulation the site of SMH, this was repeated 7 times. The contralateral-untreated side was stimulated identically in the same location to serve as a control. Images were converted and retrospectively corrected for heart rate and respiratory motion using RETROICor software. Additional motion correction was made using Art_Repair software. Images were realigned, normalized and smoothed (3mm full width half maximum (FWHM)) using SPM8. Changes in signal intensity were determined using a box-car model convolved with a haemodynamic response function (random-effects procedure; uncorrected) Results revealed an increase in spinal BOLD activation on the side ipsilateral to painful allodynic brushing. Furthermore this was found to be anatomically appropriate to the dermatome stimulated. These results demonstrate our ability to image the effects SMH as generated by the heat-capsaicin model. This indicates the possibility of imaging central sensitization in the spinal cord in pathological pain conditions.

References/Funding Source American Pain Society Conference, 2011, Austin Texas . RO1 NS053961-01

Neural Effects of Systemic Lidocaine on Chronic Neuropathic Pain Patients

H Ung, S Mackey, N Chatterjee, M Tieu, R Moericke, I Carroll
Department of Anesthesia, Stanford University, CA

Millions of Americans with neuropathic pain also present with mechanical allodynia, in which normally innocuous stimuli elicits pain. Sodium channel blockers such as lidocaine have shown efficacy in attenuating the painful sensation, though the specific changes that occur within the central nervous system remain ambiguous. This study aims to elucidate the mechanism of analgesic response prompted by systemic lidocaine through the use of functional magnetic resonance imaging (fMRI). Chronic pain patients (N = 8) with mechanical allodynia provided written and informed consent according to protocols approved by the Stanford Institutional Review Board. Functional MRI scans were conducted at a Stanford University 3 Tesla GE scanner using a standard block design where the stimulus was brushing of the allodynic area under 3 conditions: baseline, saline placebo, and lidocaine. Brushing of an unaffected area under baseline conditions was used as a control. A fixed effects, general linear model analysis was performed using SPM8. We found increased activity in prefrontal areas and decreased activity in the amygdala and hippocampal regions in conditions of lidocaine versus placebo. In addition, systemic lidocaine reduced activity in the primary sensory cortex, supplemental motor area, and putamen. Although lidocaine is a nonspecific sodium channel blocker and sodium channels are ubiquitous throughout the nervous system, these results indicate that lidocaine influences specific regions of the brain. The exact mechanism remains unclear, and further analysis and data are required to improve our understanding of the analgesic effects of lidocaine.

References/Funding Source American Pain Society Conference, 2011, Austin Texas. This study was supported by a Mentored Research Training grant from the Foundation for Anesthesia Education and Research (FAER), the Chris Redlich Pain Research Endowment, and NIH K24 DA

White Matter Characteristics Associated with Attention, Anxiety, & Executive Function in Preterm Adolescents

ES Lee[1], IM Loe[1], JD Yeatman[2], R Bammer[3], HM Feldman[1]
Departments of [1]Pediatrics, Division of Neonatal and Developmental Medicine, [2]Psychology, [3]Radiology, Stanford University, CA

Adverse outcomes of children born preterm include increased rates of inattention and anxiety and poor executive function skills. Prematurity is associated with injury to the white matter tracts of the brain. Diffusion Tensor Imaging (DTI) is a magnetic resonance imaging technique that provides quantitative characterization of white matter tracts. This study used DTI to compare white matter characteristics in children and adolescents born preterm and full-term and to examine the degree of association between fractional anisotropy of white matter and three outcomes: attention problems, anxiety symptoms, and executive-function impairment. Participants were 9 to 16 years of age; 23 were born at less than 36 weeks gestation (mean = 28.7 weeks, birth weight = 1184 grams) and 19 were full-term. Outcome measures included parent-rated attention problems and anxiety symptoms and objective measures of executive function. We analyzed the results using Tract-Based Spatial Statistics, a technique that generates a skeleton representing the core of white matter tracts for the brain. We found no statistical differences in any of the diffusion parameters comparing preterm and control groups. However, in the combined group, attention problems, anxiety symptoms, and measures of executive function were each associated with fractional anisotropy (FA); unfavorable scores were consistently associated with lower FA. Thirty-four regions on 10 tracts were associated with all three outcomes, indicative of distributed and shared mapping. However, for each of the functions, only one to three tracts and age accounted for 35 to 52% of the variance in scores. For each function, at least one of these tracts coursed into the frontal lobes. DTI contributes to understanding individual differences in attention, anxiety, and executive function in children and adolescents born preterm and full-term.

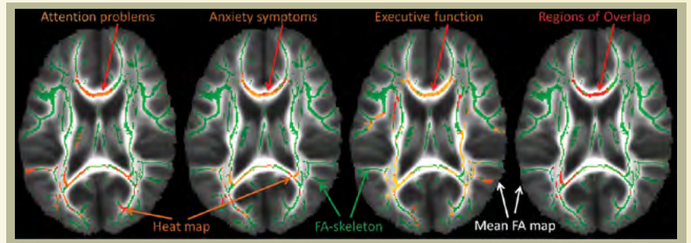

White matter regions (red-yellow heat map) on the FA-skeleton (green) that were associated withAttention-Problems (p < .05), Anxiety-Symptoms (p < .05), and Strategy-Score (p < .05), overlaid on axial slices (z axis = 18) of the mean FA image (grayscale). The regions of overlap among all three functional outcomes is also shown. L = left. R = right

References/Funding Source Submitted for publication NeuroImage. This work was supported by a grant from the National Institutes of Health, Eunice Kennedy Shriver National Institute of Child Health and Human Development, RO1 HD046500 to HM Feldman; RO1 EB8706, RO1 EB11654, and RO1 EB006526 to R Bammer; NIH Pediatric Research Loan Repayment Program Award to I Loe; and by the Clinical and Translational Science Award 1UL1 RR025744 for the Stanford Center for Clinical and Translational Education and Research (Spectrum) from the National Center for Research Resources, National Institutes of Health.

Fractional anisotropy along the trajectory of selected white matter tracts in adolescents born preterm with ventricular dilatation

NJ Myall[1], KW Yeom[2], JD Yeatman[3], S Gaman-Bean[4], R Bammer[2], HM Feldman[4]
Departments of [1]School of Medicine, [2]Radiology, [3]Psychology, [4]Pediatrics, Stanford University, CA

The aim of this study was to assess the microstructural characteristics of white matter tracts in adolescents born preterm with non-shunted ventricular dilatation secondary to intraventricular hemorrhage. Three adolescents born preterm with ventricular dilatation (ages 12-17 years, gestational age [GA] 26-29 weeks, birth weight [BW] 825-1624 grams) were compared to three full-term controls (ages 14-17 years, GA 39-40 weeks, BW 3147-3345 grams) and three adolescents born preterm without ventricular dilatation (ages 10-13 years, GA 26-29 weeks, BW 630-1673 grams). Tractography was performed using a two region-of-interest method for the following white matter tracts: superior longitudinal fasciculus/arcuate fasciculus, inferior longitudinal fasciculus, inferior fronto-occipital fasciculus, uncinate fasciculus and corticospinal tract. The mean fractional anisotropy, axial diffusivity and radial diffusivity of each fiber tract were calculated. Fractional anisotropy was also calculated at 30 equidistant segments along each tract. Subjects with moderate ventricular dilatation showed increased fractional anisotropy compared to the other two groups in multiple bilateral tracts. The pattern of fractional anisotropy along the trajectory of tracts adjacent to the lateral ventricles distinguished preterms with ventricular dilatation from full-term controls and preterm comparisons. By contrast, the pattern of fractional anisotropy along the uncinate fasciculus did not vary between groups. Prematurity is often associated with decreased fractional anisotropy. Our findings suggest that concomitant ventricular dilatation may have opposing effects on fractional anisotropy possibly secondary to increased packing density of axons.

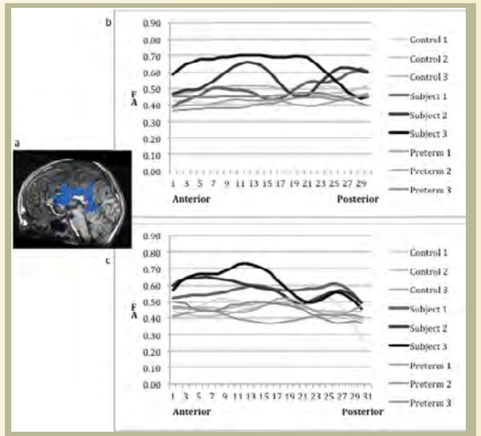

(a) The superior longitudinal fasciculus/arcuate fasciculus in a full-term control. Red markers represent the location of the two ROIs used for tractography. FA along the tract at 30 equidistant points is shown for the left (b) and right (c) hemispheres. Subjects with ventricular dilatation showed elevated FA at various points across the trajectory of the tract compared to full-term controls and preterm comparisons.

References/Funding Source Submitted to Human Brain Mapping. This work was supported by grants from the Stanford Medical Scholars Research Program and the National Institutes of Health, Eunice Kennedy Shriver National Institute of Child Health and Human Development, RO1 HD046500 to HM Feldman; RO1 EB8706, RO1 EB11654, and RO1 EB006526 to R Bammer; and by the Clinical and Translational Science Award 1UL1 RR025744 for the Stanford Center for Clinical and Translational Education and Research (Spectrum) from the National Center for Research Resources, National Institutes of Health. We thank the children and families who participated in our study.

Anticipatory hippocampal responses predict individual differences in reward-based modulation of memory

SM Wolosin, D Zeithamova, AR Preston
The University of Texas at Austin, Austin, TX

Emerging evidence suggests that medial temporal lobe (MTL) memory processing is modulated by reward, resulting in enhanced encoding of episodic information—long-term memory for events. Recent neuroimaging research has further revealed activation in hippocampus prior to stimulus presentation that predicts later memory performance, suggesting that modulatory processes such as reward may influence encoding processes in anticipation of upcoming events. Moreover, individual differences in neural responses to reward predict performance in reinforcement learning paradigms. Such individual differences in reward sensitivity may similarly influence the degree to which reward impacts MTL encoding. Using high-resolution functional magnetic resonance imaging (fMRI), the present study examines (1) how cues indicating future rewards influence MTL subregional activation prior to associative encoding and (2) how individual differences in reward sensitivity are reflected in MTL subregional activation. A high-value or low-value monetary cue preceded a pair of objects indicating potential reward for successful retrieval of the association. Memory was tested using a two-alternative forced-choice paradigm. Behaviorally, memory was superior for high-value associations relative to low-value associations. fMRI analysis revealed anticipatory responses within the hippocampus predicting memory formation that were further modulated by reward. Importantly, the observed enhancement of anticipatory activation for high-value compared to low-value pairs correlated with individual differences in behavioral reward sensitivity (hit rate for high-value pairs – hit rate for low-value pairs). The results suggest that reward-based motivation influences memory by facilitating hippocampal encoding processes prior to stimulus presentation, and that increased behavioral sensitivity to reward is reflected by increases in reward effects within the hippocampus.

Motivation during associative encoding influences subsequent recall responses in medial temporal subregions

SM Wolosin, D Zeithamova, AR Preston
The University of Texas at Austin, Austin, TX

Emerging evidence suggests that hippocampal memory processing is modulated by reward, resulting in enhanced encoding of episodic information—long-term memory for events. Current theories further propose that memory processing in hippocampal subregions may be differentially influenced by reward. While previous research has examined reward influences on episodic encoding, no study to date has examined how motivation during encoding influences hippocampal responses at retrieval. Using high-resolution functional magnetic resonance imaging (fMRI), the present study investigated the function of medial temporal lobe (MTL) subregions, including hippocampal subfields, midbrain, and nucleus accumbens during cued recall of associations learned under varying conditions of reward. During encoding, high-value or low-value monetary cues preceded object pairs indicating potential reward for successful retrieval of the associations. At retrieval, participants were presented with a cue object (a single object from a studied pair) and were asked to recall and imagine the associated object during a delay period. At the end of the trial, participants viewed a probe object and judged whether the probe was the correct object (a "match") or another object viewed at encoding, but as part of a different pair (a "mismatch"). Behaviorally, cued recall performance was superior for high-value compared to low-value pairs. fMRI analysis revealed regions in hippocampus, including dentate gyrus/CA2,3, CA1, and subiculum, as well as parahippocampal cortex and nucleus accumbens that demonstrated greater cue and delay period activation for high-value compared to low-value associations. Importantly, such reward-based modulation of cue and delay period activation was observed in the absence of explicit reward cues. Of these regions, left CA1 uniquely showed an interaction between reward status and retrieval based success effects where activation differed for correct and incorrect trials only for high-value associations. At probe, several MTL regions demonstrated match responses with greater activation for correct match probes relative to correct mismatch probes. In these probe-sensitive regions, match effects in left CA1 and left dentate gyrus/CA2,3 were limited to high-value trials. Together these findings suggest that motivation during encoding affects subsequent associative retrieval processing in MTL subregions, and highlight that within the hippocampus CA1 may play an important role incorporating motivational salience into episodic retrieval processes.

Population receptive fields in human visual cortex measured with subdural electrodes

J Winawer[1], AM Rauschecker[1], KN Kay[1], J Parvizi[2], BA Wandell[1]
Departments of [1]Psychology, [2]Neurology & Neurological Sciences, Stanford University, CA

PURPOSE. Population receptive fields (pRFs) in human visual cortex have been measured with fMRI (Dumoulin and Wandell, 2008; Kay et al., 2008) and with electrocorticography (ECoG) in pre-surgical clinical subjects (Yoshor et al, 2007). We present an efficient method for pRF measurements using ECoG, closely matched to the fMRI methods developed by Dumoulin and Wandell (2008), and we compare the results to those obtained with fMRI.

METHODS. Three patients with intracranial electrodes (2-mm diameter) viewed flickering contrast patterns through a bar aperture that swept across the visual field 8 times (96 seconds). For one subject, bar width varied across experiments to test response linearity. The contrast pattern reversed 15 times / s, creating a steady-state ECoG response at this frequency. Time-series were extracted in the steady-state (15-Hz) and gamma-band (30 Hz - 180 Hz) to estimate the spatial pRF, modeled as an isotropic 2D-Gaussian.

RESULTS. The pRF model provided good fits to the steady-state and gamma-band time-series of V1, V2, and V3 electrodes. The position and size parameters of the pRFs were similar to those obtained from fMRI in the same subjects. However the steady-state ECoG data differed markedly from the gamma-band and fMRI data in one respect: as bar width increased, the steady-state signal amplitude systematically increased, whereas the gamma-band and fMRI signals saturated. Consequently, the steady-state data were well fit by a linear model whereas the fMRI and gamma-band data were better fit by a model with a saturating non-linearity.

CONCLUSION. There is good agreement between fMRI and ECoG pRFs despite significant differences in their physiological bases. The agreement is best in the gamma band, which, like the fMRI measures, contains a saturating non-linearity. ECoG provides a valuable complement to fMRI for probing population-level spatiotemporal properties of receptive fields in human visual cortex.

References/Funding Source J Winawer, A Rauschecker, J Parvizi, BA Wandell (2011). Population receptive fields in human visual cortex measured with subdural electrodes. Vision Sciences Society Annual Meeting (2011). NIH Grant EY19224 (BW), NIH Grant EY03164 (JW), Stanford NeuroVentures Program (JP).

Thalamo-cortical connectivity distinguishes painful from non-painful stimulation in humans

J Brown, N Chatterjee, S Mackey
Department of Anesthesia, Stanford University, CA

Neuroimaging studies reveal a distributed network of brain regions activated by painful stimulation, suggesting that the subjective experience of pain depends not only on the activity within individual brain regions, but also on their interactions. A recent study showed pre-stimulus interactions among pain-related brain areas were associated with pain perception in humans. However, it remains largely unknown how interactions among brain regions during pain perception are related to subjective aspects of the pain experience. We address this issue using fMRI to correlate activity among several brain regions during the perception of painful and non-painful thermal stimulation. We hypothesized that brain regions previously implicated in pain interact with each other differently during the perception of pain than during the perception of non-painful thermal stimulation. We presented painful and non-painful stimuli to the left forearm and recorded BOLD signal change from each region of the canonical pain matrix: primary and secondary sensory cortices (S1 and S2), thalamus, prefrontal cortex (PFC), insular cortex (IC), and anterior cingulate cortex (ACC). For each stimulus presented we computed the average BOLD signal change that resulted as a percentage of the preceding baseline period. We then computed pair-wise correlations of the BOLD signal change in each region during each stimulus presentation. A stronger correlation between two regions during painful than non-painful stimulation might indicate that the two regions are each receiving more similar inputs during painful stimulation or that one is influencing the other in a more consistent manner during periods painful than non-painful stimulation We found that pair-wise correlations including thalamus-S1, thalamus-S2, thalamus-IC, and thalamus-ACC were significantly greater during painful stimulation than during non-painful stimulation. Our findings demonstrate that pain processing is associated with strong thalamo-cortical interactions. It is important to determine how these interactions relate to pain ratings, fear of pain, and anxiety.

References/Funding Source Society for Neuroscience Conference, 2010. NRSA: 1F31GM08361-01 and RO1 NS053961-01

Differences in neural activation between preterm and full term born adolescents on a sentence comprehension task: Implications for educational accommodations

LHF Barde[1], JD Yeatman[2], ES Lee[1], G Glover[3], HM Feldman[1]
Departments of [1]Pediatrics, [2]Psychology, [3]Radiology, Stanford University, CA

This fMRI study compared patterns of neural activation during a sentence comprehension task in children born preterm (n = 18) and full-term (n = 14), and described patterns associated with individual differences. Participants (approximately 10-16 years) were matched across group for verbal IQ and receptive vocabulary. Both groups showed bilateral activation in superior and middle temporal gyri comparing sentence comprehension to fixation during the initial Auditory phase of the task. The preterm group showed greater activation in the precuneus when processing syntactically difficult sentences. Patterns of activation shifted for both groups in the Verification/Response phase of the task. There, the preterm group showed greater activation in the left middle frontal gyrus than did the full-term group when processing syntactically difficult sentences, controlling for receptive language ability. The results suggest that in comparison to full-term peers, the preterm group showed greater activation in an area associated with cognitive control when processing difficult material despite comparable performance. These findings, in conjunction with other features of children born preterm, such as weak executive function skills, high rates of inattention, and elevated anxiety symptoms, suggest the importance of considering the child's early medical history and neurological status in education.

References/Funding Source This work was supported by a grant from the National Institutes of Health, Eunice Kennedy Shriver National Institute of Child Health and Human Development, RO1 HD046500 to HM Feldman and by the Clinical and Translational Science Award 1UL1 RR025744 for the Stanford Center for Clinical and Translational Education and Research (Spectrum) from the National Center for Research Resources, National Institutes of Health. We also acknowledge support from the Lucile Packard Children's Hospital Foundation and a Pediatric Research Fellowship grant to LHF Barde.

Default-mode and task-positive network activity in Major Depressive Disorder: Implications for adaptive and maladaptive rumination

JP Hamilton[1], D Furman[1], C Chang[2], M Thomason[3], E Dennis[3], I Gotlib[3]
Departments of [1]Psychology, [2]Radiology, [3]Psychology, Stanford University, CA

Background. Major Depressive Disorder (MDD) has been associated reliably with ruminative responding, which can involve both maladaptive and adaptive components. Levels of activity in the default-mode network (DMN) relative to the task-positive network (TPN), as well as activity in structures that influence DMN and TPN functioning, may represent important neural substrates of maladaptive and adaptive rumination in MDD.

Methods. We used a unique metric to estimate DMN dominance over TPN from blood-oxygen-level dependent (BOLD) data collected during eyes-closed rest in 17 currently depressed and 17 never-disordered adults. We calculated correlations between this metric of DMN dominance over TPN and the depressive, brooding, and reflective subscales of the Ruminative Responses Scale, controlling for associations both among these measures and between these measures and severity of depression. Finally, we estimated and compared between groups right fronto-insular cortex (RFIC) response during initiations of ascent in DMN and TPN activity.

Results. In the MDD participants, increasing levels of DMN dominance were associated with higher levels of maladaptive, depressive rumination and lower levels of adaptive, reflective rumination (see Figure 1). Moreover, the RFIC state-change analysis showed increased RFIC activation in the MDD participants at the onset of increases in TPN activity and, conversely, increased RFIC activation in the healthy control participants at the onset of increases in DMN activity.

Conclusions. These findings provide empirical evidence for a formulation in which the DMN supports the representation of negative, self-referential information in MDD, and the RFIC, when prompted by increased levels of DMN activity, initiates an adaptive engagement of the TPN.

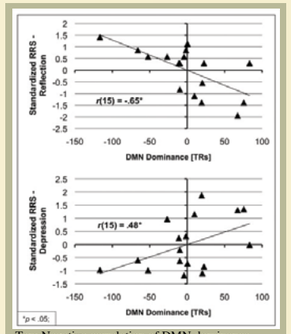

Top: Negative correlation of DMN dominance with RRS-Reflection in the MDD group; Bottom: positive correlation of DMN dominance with RRS-Depression.

References/Funding Source JP Hamilton, DJ Furman, C Chang, ME Thomason, E Dennis, IH Gotlib (in press). Task-positive and default-mode network activity in Major Depressive Disorder: Implications for adaptive and maladaptive rumination. Biological Psychiatry.

Fast Susceptibility Weighted Imaging (SWI) using Readout-Segmented (RS)-EPI

SJ Holdsworth[1], RL O'Halloran[1], S Skare[2], R Bammer[1]
[1]Department of Radiology, Stanford University, CA; [2]Clinical Neuroscience, Karolinska Institute, Stockholm, Sweden

Introduction: Susceptibility-weighted imaging (SWI) is an MRI technique that has been used to provide improved conspicuity of venous blood vessels and other sources of susceptibility effects. The most commonly used SWI acquisition uses a 3D gradient echo (GRE) sequence, however due to the inefficient coverage of k-space per TR, 3D GRE is hampered by a long scan time. In addition, even subtle motion in 3D GRE can considerably hamper the quality of final processed SWI image. Here we explore the use of 3D Readout-Segmented (RS)-EPI as a fast alternative to 3D GRE for SWI. In RS-EPI, a 'brick' made up of several adjacent (and slightly) overlapping EPI segments are acquired.

Methods: 3D RS-EPI and 3D GRE data were acquired on a healthy volunteer using a 3T GE system and an 8-channel head coil. The SWI images were produced by generating a phase mask using a 2D Hanning window for each individual coil, a multiplication of the phase mask by the magnitude coil by 5 times, followed by the sum of squares over coils.

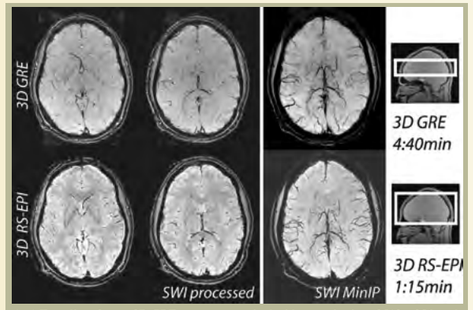

(a,c) Two slices from a 3D GRE sequence acquired with a matrix size of 512 x 256, and (b,d) two slices from a 3D RS-EPI sequence acquired at 288 x 288. Both sequences used a partition thickness = 2mm and FOV = 23cm. As shown schematically on the far right, 3D RS-EPI acquired full brain coverage (twice the coverage compared with 3D GRE) in a significantly reduced scan time.

Results: A comparison between the SWI images acquired with 3D GRE and 3D RS-EPI is shown in the figure. Although the resolution and SNR is highest for the 3D GRE, the 3D RS-EPI images show it is possible to acquire good quality SWI images with twice the brain coverage in about a third of the scan time.

Conclusion: The acquisition of 3D RS-EPI SWI images in 1:15min makes this technique applicable for routine use in the clinics and a fast alterative to 3D GRE. The inherent motion robustness of 3D RS-EPI is another major advantage of RS-EPI over both GRE and interleaved EPI. As long as the brick frame rate in 3D RS-EPI is fast enough and there is enough overlap between bricks, it should be possible to correct for motion between bricks in k-space in 3D.

References/Funding Source SJ Holdsworth, R O'Halloran, S Skare, R Bammer. Fast Susceptibility Weighted Imaging (SWI) using Readout-Segmented (RS)-EPI. " In: 19th Annual Meeting of the ISMRM, Montreal, Canada, #4363, 2011. NIH (5R01EB002711, 5R01EB008706, 3R01EB008706, 5R01EB006526, 5R21EB006860, 2P41RR009784), the Center of Advanced MR Technology at Stanford (P41RR09784), Lucas Foundation, Oak Foundation, and the Swedish Research Council (K2007-53P-20322-01-4).

Evaluating airfoil trailing edge film cooling geometries based on 3D velocity and scalar field measurements

M Benson, C Elkins, J Eaton
Department of Mechanical Engineering, Stanford University, CA

The high temperature blades and vanes in gas turbine engines are cooled by passing cooler air through their interiors and venting it through holes in their surfaces. The effectiveness of this approach is governed by the rate of mixing of the coolant with the mainstream flow. One important region of interest is the thin trailing edge of a blade or vane airfoil which is particularly vulnerable to melting. Ideal cooling results in a uniform distribution of 100% coolant over the entire trailing edge surface. In this study, several different trailing edge cooling geometries were evaluated for cooling effectiveness. Coolant concentration was measured using the Magnetic Resonance Concentration (MRC) technique which uses a T1 weighted imaging sequence to measure the mixing of a contrast solution with plain water. The scans measured the concentration distribution with a spatial resolution of 0.5 mm3 and an uncertainty near 5%. 3D phase contrast measurements were made to provide 3D, mean velocity measurements in the identical flow. The coupled concentration and velocity measurements were used to understand the relationship between geometrical features, flow structures, and cooling effectiveness. Improved geometries increased the spanwise averaged coolant concentration at the trailing edge by as much as 15% and improved the spanwise distribution uniformity.

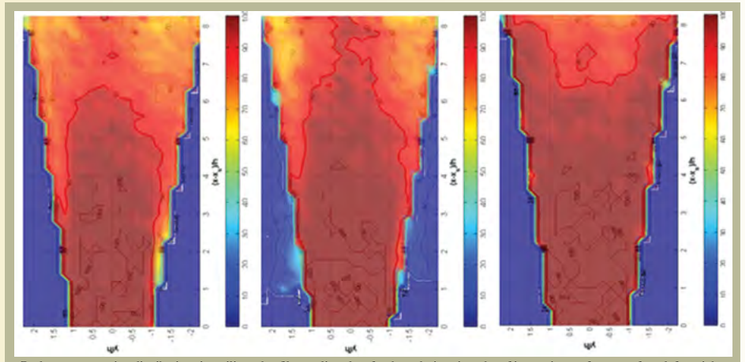

Coolant concentration distributions in trailing edge film cooling slots for three designs in order of improving performance from left to right.

References/Funding Source Army Research Office, General Electric, Lucas Center

Flow separation control in a conical diffuser with an annular inlet

K Lo, C Elkins, J Eaton
Department of Mechanical Engineering, Stanford University, CA

In a combined cycle power plant, the high velocity exhaust from the power turbine has to be slowed down before reaching the steam generator. A conical diffuser is commonly used behind the turbine to slow down the flow and recover pressure. The inlet to the diffuser is an annulus due to the annular flow passage of the turbine. A large central separation bubble forms if the central hub ends abruptly because the flow is incapable of negotiating around a sharp corner. Previous experiments demonstrate that a Coanda jet at the end of the hub can strongly reduce or completely eliminate the central separation bubble, depending on the jet blowing ratio. However this can cause flow separation along the conical diffuser walls in some cases. A backward facing step in the outer diffuser wall acts to fix the location of separation making it more amenable to control. A single circumferential separation bubble forms downstream of the step. Experiments were performed in scaled down diffuser models to investigate a geometric perturbation approach for reducing the size of the step separation bubble. The Reynolds number is 64000 based on the annulus bulk velocity and hydraulic diameter. Full-field, three-component velocity data were measured in a series of diffuser models using phase contrast magnetic resonance velocimetry. The step separation bubble is around eight step-heights long when no control is present. A wavy step edge design, where the separating edge of the step is a sinusoid, significantly reduces the size of the bubble by almost 50%. The single circumferential bubble is broken down into a series of smaller bubbles. Velocity data reveal pairs of counter-rotating in-plane vortices, which are responsible for the bubble size reduction by enhanced momentum mixing.

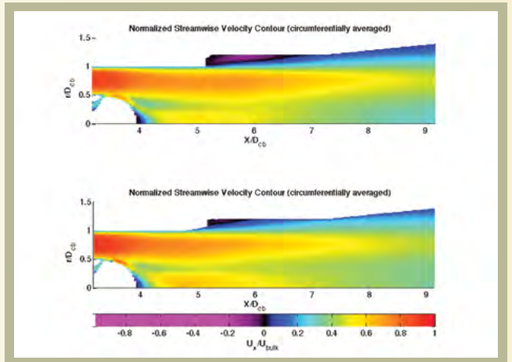

Velocity contour of the flow in a step diffuser. Flow direction is from left to right. Purple indicates reverse flow with negative velocity. The purple region between X/Dcb=5.1 and X/Dcb=7 (top) indicates a long step separation bubble without the wavy step edge. The purple region between X/Dcb=5.1 and X/Dcb=6 (bottom) indicates a significant shortening of the step separation bubble with the wavy step edge design.

References/Funding Source Study funded by Siemens Energy

Common abnormalities and disorder-specific compensation in anxiety versus depression

A Etkin[1,2], AF Schatzberg[1]
[1]Department of Psychiatry and Behavioral Sciences, Stanford University, CA; [2]Sierra-Pacific Mental Illness Research, Education, and Clinical Center (MIRECC) Veterans Affairs Palo Alto Health Care System

Objective: Anxiety and depressive disorders are both associated with abnormalities in the processing and regulation of emotion. Despite this, little is known about the similarities and differences between anxiety and depression at the neural level. Such research is essential, however, for understanding the organization and structure of mental illness, informing ideas about vulnerability, and defining opportunities for intervention.

Methods: 32 healthy controls, 18 generalized anxiety disorder only patients, 14 major depression only patients, and 25 comorbid patients were studied using functional magnetic resonance imaging while they performed an emotional conflict task, which involved categorizing facial affect while ignoring overlaid affect label words. We compared trial-by-trial changes in conflict regulation, a test of implicit regulation of emotional processing, using behavioral and neural measures.

Results: Behavioral data indicated that only patients with generalized anxiety (i.e. anxiety only and comorbids) failed to implicitly regulate emotional conflict. By contrast, deficits in activation and connectivity of the ventral anterior cingulate and amygdala – areas previously implicated in regulating emotional conflict – were found in all patient groups. Depression only patients, however, compensated for this deficit by also activating bilateral anterior lateral prefrontal cortices, wherein activity correlated with behavioral evidence of successful implicit regulation, thus mediating the disorder-specificity of the behavioral phenotype.

Conclusions: These data support the existence of a common anxiety/depression ventral cingulate-amygdalar abnormality, which may relate to a shared genetic etiology. Compensatory engagement of cognitive control circuitry in depression illustrates how the complex nature of psychopathology arises from the interaction of deficits and compensation, all of which can occur at an implicit level.

fMRI Imaging of Opioid Withdrawal in Healthy Human Volunteers

LF Chu[1], D Hoang[1], X Cui[2], A Clemenson[1]
Departments of [1]Anesthesia, [2]Center for Interdisciplinary Brain Sciences Research, Stanford University, CA

Background: Opioid medications are commonly prescribed for pain relief. When given over an extended period, physical dependence can develop. If opioid medications are suddenly stopped, opioid withdrawal occurs with unpleasant side effects, such as agitation and nausea. A medication named ondansetron can help ease or prevent these symptoms. Though the physical symptoms and treatment of opioid withdrawal have been extensively studied, it is still unknown how withdrawal affects brain activity. Through imaging of the brain by fMRI, we hope to see how opioid withdrawal, with and without the administration of ondansetron, affects brain activity.

Methods: Healthy male volunteers were randomized to receive ondansetron on one of two study days and placebo on the other. After the administration of placebo or ondansetron, patients received an infusion of morphine. Patients were transported to the Lucas Center, where they underwent a 24-minute fMRI scan. After 9 minutes of baseline scanning, patients were given an injection of Naloxone to precipitate withdrawal. Patients remained in the scanner for 15 minutes and were then transported back to the hospital.

Results: Our research is still in progress, but preliminary data has shown that there were significant positive and negative changes in brain activity during opioid withdrawal when the patients had only placebo treatment. When patients received ondansetron, there was very little positive or negative change.

Conclusion: Our research is still ongoing, but preliminary data suggests that ondansetron has a dampening effect on the positive and negative changes in brain activity. We are currently researching and analyzing these brain areas of interest.

Altered frontostriatal functional connectivity in Major Depressive Disorder

DJ Furman, JP Hamilton, IH Gotlib
Department of Psychology, Stanford University, CA

Dysfunction of the striatum and frontal cortex has been reported consistently in studies of neural structure and function in Major Depressive Disorder (MDD). Despite speculation that compromised connectivity between these regions may underlie symptoms of MDD, little work has investigated the integrity of frontostriatal circuits in this disorder. In this study we compared patterns of resting state frontostriatal functional connectivity in currently depressed and never-disordered women. Blood-oxygen-level dependent (BOLD) data were acquired from 21 currently depressed individuals and 19 healthy controls during eyes-closed, wakeful rest in a 3T GE scanner. Using four predefined regions of interest, we computed seed-to-whole brain correlations. We found that, compared to controls, depressed participants exhibited attenuated functional connectivity between the ventral striatum and both ventromedial prefrontal cortex and subgenual cingulate cortex. Depressed participants also exhibited a relative increase in the strength of connectivity between the dorsal caudate and dorsal prefrontal cortex. These results suggest that currently depressed individuals are characterized by altered connectivity in frontostriatal circuits posited to support affective and cognitive processing. Further work is required to examine the link between patterns of disrupted connectivity and specific symptoms of depression, and the extent to which these patterns normalize with remission of depressive illness.

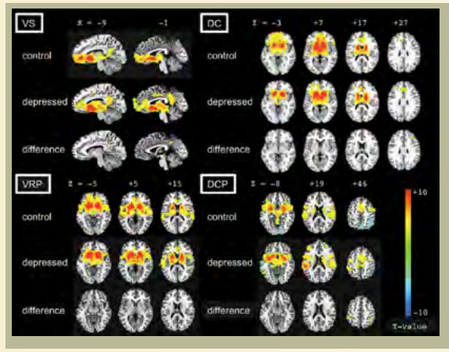

Statistical maps depicting regions of positive and negative functional connectivity with the ventral striatum (VS), dorsal caudate (DC), ventral rostral putamen (VRP), and dorsal caudal putamen (DCP) in depressed and control samples, and between-group differences in functional connectivity with these regions (control > depressed: blue, depressed > control: yellow). Voxel-wise $p < 0.005$, minimum cluster size = 26 voxels.

References/Funding Source DJ Furman, JP Hamilton, IH Gotlib. (under review). Altered frontostriatal functional connectivity in Major Depressive Disorder.

Functional connectivity tracks clinical deterioration in Alzheimer's disease

JS Damoiseaux[1], K Prater[2], BL Miller[3], MD Greicius[1]
[1]Functional Imaging in Neuropsychiatric Disorders (FIND) Lab, Department of Neurology and Neurological Sciences, Stanford University, CA; [2]Neuroscience Graduate Program, University of Michigan, MI; [3]Memory and Aging Center, Department of Neurology, University of California, San Francisco, CA

While resting state functional connectivity has been shown to decrease in patients with mild/moderate Alzheimer's disease, it is not yet known how functional connectivity changes in patients as the disease progresses. Furthermore, it has been noted that the default mode network is not as homogenous as previously assumed and several fractionations of the network have been proposed. Here, we separately investigated the modulation of three default mode sub-networks, as identified with group ICA, by comparing Alzheimer's disease patients to healthy controls and by assessing connectivity changes over time. Our results showed decreased connectivity at baseline in patients versus controls in the posterior default mode network, and increased connectivity in the anterior and ventral default mode networks (see figure). At follow-up, functional connectivity decreased across all default mode systems in patients. Our results suggest that earlier in the disease, regions of the posterior default mode network start to disengage whereas regions within the anterior and ventral networks enhance their connectivity. However, as the disease progresses connectivity within all systems eventually deteriorates.

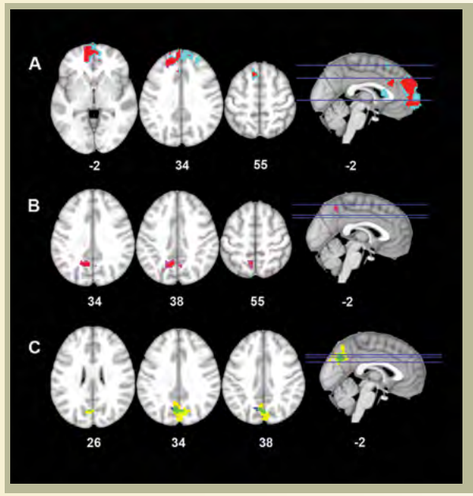

Functional connectivity difference maps of Alzheimer's patients versus healthy elderly controls at baseline. Functional connectivity differences between Alzheimer's patients and healthy elderly controls in the A) anterior; (B) ventral; and (C) posterior default mode network. The different colors represent the results with and without grey matter correction and the overlap between the two. Functional connectivity in the anterior and ventral default mode networks (A & B) is increased in Alzheimer's patients compared to controls (displayed in violet for results with grey matter correction; in cyan for results without correction; and in red for the overlap). Functional connectivity in the posterior default mode network (C) is decreased (displayed in blue for results with grey matter correction (only visible for a few voxels here); in yellow for results without correction; and in green for the overlap). The statistical maps, thresholded using TFCE and $p<0.05$ family wise error corrected, are overlaid on the MNI152 brain; MNI coordinates (in mm) of the slices are displayed.

References/Funding Source This work was supported by a grant from the John Douglas French Foundation and the following NIH grants: RO1NS073498; P01AG019724; and P50AG023501.

Compressive spatial summation improves models of extrastriate responses

KN Kay[1], J Winawer[1], A Mezer[1], BA Wandell[1]
[1]Department of Psychology, Stanford University, CA

Integrating image features across space is fundamental to visual function. Previous fMRI studies investigating retinotopy and related spatial properties have assumed implicitly or explicitly that responses to spatial contrast patterns sum linearly over the visual field. To test this assumption, we measured BOLD activity in human visual cortex while subjects viewed brief presentations of contrast patterns seen through horizontal and vertical apertures. A variety of different apertures were presented in random order in an event-related design. Throughout visual cortex the response to a large aperture was less than the sum of the responses to two parts of the aperture shown in separate trials. This sub-additive effect was larger in extrastriate areas than in V1. We modeled the sub-additivity by incorporating a compressive power-law nonlinearity into a basic linear model of population receptive fields (Dumoulin and Wandell, 2008; Kay et al., 2008). Using cross-validation to obtain unbiased measures of model accuracy, we found that the nonlinear model systematically outperforms the linear model, explaining up to 98% of the variance in the amplitudes of the responses to the various apertures. Moreover, the nonlinearity of the model was more pronounced in extrastriate areas, consistent with the larger degree of sub-additivity in these areas (for instance, in LO-1 the median exponent was 0.05 whereas in V1 the median exponent was 0.35). An important prediction of compressive spatial summation is reduced sensitivity to changes in the position and size of a viewed object. Indeed, in an independent dataset we measured responses to objects varying in position and size and confirmed that the nonlinear model (but not the linear model) accurately predicts the pattern of responses from each voxel. We speculate that compressive spatial summation is a key computation used by extrastriate cortex to achieve position and size tolerance.

References/Funding Source NIH grant EY019244, NEI grant RO1-EY03164

Detection of sequence violations in the medial temporal lobe: Subregional contributions to memory-based prediction through high-resolution fMRI

JC Liang, D Zeithamova, AR Preston
The University of Texas at Austin, Austin, TX

Current research proposes that medial temporal lobe (MTL) subregions perform distinct computations to enable comparison between past and present experience. Hippocampus is thought to play a unique role in the detection of sequence novelty, wherein associated items appear in a new order. However, it is unclear how hippocampal subregions and surrounding MTL cortex differentially contribute to novelty detection, and whether content-sensitive networks are differentially engaged when novelty is restricted to a certain class of content. Here, we used high-resolution fMRI to measure MTL responses to temporal sequence violations while subjects performed an incidental 1-back detection task. Trials consisted of two consecutive sequence presentations. In the first, participants observed a sequence of four object-scene pairs. In the second presentation, the same set of object-scene pairs were presented again in one of six conditions. In the repeated condition, the initial sequence was repeated in the same order. In the half condition (H), the order of the third and fourth object-scene pairs was switched. In the object-half (OH) condition, the order of objects in the third and fourth pair was switched. In the scene-half (SH) condition, the order of scenes was switched. In the novel (N) condition, the order of all four objects and scenes was scrambled. Finally, a familiar condition consisted of pre-exposed sequences seen repeatedly throughout the experiment. By comparing activation during the half conditions with novel sequences, we isolated responses that reflect novelty responses cued by a violation of expectation based on temporal order (a mismatch) from novelty responses that reflect novel associations per se. Furthermore, comparison of OH, SH, and novel sequences sought to reveal MTL regions that signal content-based mismatch responding. Preliminary analyses identified distinct populations of voxels that were sensitive to violations of object order (OH > N) and violations of scene order (SH > N) as well as voxels that were sensitive to violations based solely on overall temporal order (H > N). These associative mismatch responses were primarily restricted to hippocampal subfields. By contrast, MTL cortical regions showed sensitivity to novelty that was predominantly related to the amount of previous exposure when comparing novel to highly familiar sequences. These results expand on previous findings to suggest that hippocampal responses to associative novelty can be distinguished by the class of content being violated, and that MTL cortical regions show sensitivity to the familiarity status of stimulus configurations based on the amount of exposure.

Reduced hippocampal activity during encoding in cognitively normal adults carrying the APOE ε4 allele

M Adamson[1,2], JB Hutchinson[3], A Shelton[4], AD Wagner[3], JL Taylor[1,2]
[1]Department of Veterans Affairs, Sierra-Pacific MIRECC and WRIISC Palo Alto, CA; Departments of [2]Psychiatry and Behavioral Sciences, [3]Psychology, Stanford University, CA; [4]Department of Psychological and Brain Sciences, John Hopkins University, Baltimore, MD

Apolipoprotein (APOE) ε4-related differences in memory performance have been detected before age 65. The hippocampus and the surrounding medial temporal lobe (MTL) structures are the first site affected by Alzheimer's disease (AD) and the MTL is the seat of episodic memory, including visuo-spatial memory. While reports of APOE ε4-related differences in these brain structures are not consistent in either cross-sectional or longitudinal structural and functional magnetic resonance imaging (fMRI) studies, there is increasing evidence that brain activity at baseline (defined as activity during fixation or rest) may differ in APOE ε4 carriers compared to non-carriers. In this fMRI study, cognitively normal APOE ε4 carriers and non-carriers engaged in a perspective-dependent spatial learning task (Shelton and Gabrieli, 2002) previously shown to activate MTL structures in older participants (Borghesani et al., 2008). A low-level, visually engaging dot-control task was used for comparison, in addition to fixation. APOE ε4 carriers showed less activation than non-carriers in the hippocampus proper during encoding. Specifically, when spatial encoding was contrasted against the dot-control task, encoding-related activation was significantly lower in carriers than non-carriers. By contrast, no ε4-related differences in the hippocampus were found when spatial encoding was compared with fixation. Lower activation, however, was not global since encoding-related activation in early visual cortex (left lingual gyrus) was not different between APOE ε4 carriers and non-carriers. The present data document APOE ε4-related differences in the hippocampus proper during encoding and underscore the role of low-level control contrasts for complex encoding tasks. These results have implications for fMRI studies that investigate the default-mode network (DMN) in middle-aged to older APOE ε4 carriers to help evaluate AD risk in this otherwise cognitively normal population.

The impact of age-related brain changes on flight simulator performance and decision-making

M Adamson[1,2], D Heraldez[2], M Farrell[1], Q Kennedy[2], J Yesavage[1,2], JL Taylor[1,2]
[1]Department of Veterans Affairs, Sierra-Pacific MIRECC and WRIISC, Palo Alto, CA; [2]Department of Psychiatry and Behavioral Sciences, Stanford University, CA

Age-related decline in cognitive abilities and brain structures, crucial for aircraft navigation and decision making, may lead older pilots to perform poorly in a flight simulator task and can also influence their decision-making abilities. Studies also report the compensatory role of expertise in cognitive decline. We previously reported an interaction of brain size with aviation expertise in predicting flight simulator performance. We also reported that older pilots were more likely than younger pilots to take risks during landing in bad weather. These findings led to our current study that evaluates the role of age-related changes in the brain during the decision-making network during performance of a real-world skilled task: a pilot's crucial decision to land or not under difficult weather conditions. Understanding how older adults make crucial time-pressured real-world decisions, in relation to acquired expertise and age-related brain changes, have implications for their assessment of risk and safety in every-day life.

High-resolution fMRI reveals distinct forms of associative novelty responding in hippocampus

C Manthuruthil, D Zeithamova, A Preston
The University of Texas at Austin, Austin, TX

Hippocampal responding is greater when encountering novel relative to repeated events. Novelty, however, can take several forms, e.g., discrimination of never-before-seen stimulus combinations (associative novelty per se) or stimulus configurations that violate existing memories (associative mismatch novelty), to support distinct learning processes. Previous research suggests that signals reflecting associative novelty per se predict binding of information within individual events, whereas associative mismatch responses have been implicated in integrative encoding where information is bound across discrete episodes. By comparing hippocampal activation across repetitions of non-overlapping object associations (XY) with those elicited by overlapping associations (AB, BC), we aimed to isolate distinct forms of associative novelty responding within hippocampus using high-resolution fMRI. We hypothesized that hippocampal activation would differ for non-overlapping and overlapping associations, with decreasing hippocampal activation across repetition of non-overlapping pairs, reflecting decreasing novelty of the associations, and increasing hippocampal activation across repetition of overlapping associations, reflecting enhanced associative mismatch detection as memories are established. Consistent with these predictions, we observed two distinct novelty signatures within hippocampus. Bilateral hippocampus, inclusive of all subfields, showed decreased activation across repetition of non-overlapping associations, consistent with a signature of associative novelty per se. In contrast, a left hippocampal region, peak in subiculum, showed increased activation across repetition of overlapping events relative to non-overlapping events, consistent with an associative mismatch response. These results reveal distinct forms of associative novelty detection within the hippocampus, and further suggest that a hippocampally-mediated associative mismatch response enables integration of related memories to support the flexible use of experience.

Dopaminergic Modulation of Resting State Networks in Parkinson's disease

K Poston[1], W Shirer[1], F Tayim[1], V Menon[2], M Greicius[1]
Departments of [1]Neurology and Neurological Sciences, [2]Psychiatry and Behavioral Sciences, Stanford University, CA

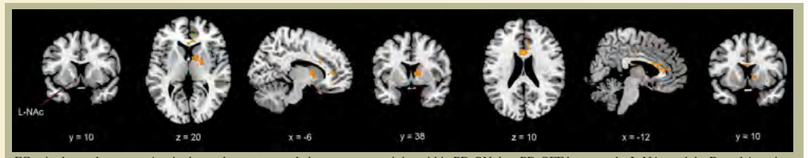

FC paired-samples t-tests. A paired-samples t-test revealed greater connectivity within PD-ON than PD-OFF between the L-NAc and the Dorsal Anterior Cingulate Cortex, the right Nucleus Accumbens, the right Putamen, and the right Globus Pallidius.

Introduction: Resting state fMRI studies can be used to explore the functional connectivity of complex organized resting state networks (RSNs). Multiple canonical RSNs have been described corresponding to critical brain functions; however, modulation of these RSNs with dopamine replacement in PD has not been studied. In the present study we identified changes in striato-cortical network connectivity in Parkinson's disease (PD) OFF and ON medications using resting state fMRI.

Methods: We acquired resting state fMRI data on 9 participants: 5 early PD (MDS-UPDRS-III 26.4±10.5) and 4 age-matched controls. PD patients were scanned both OFF and ON medications (PD-OFF and PD-ON). We applied independent component analysis (ICA) to the fMRI timeseries and used a template matching algorithm to identify the Motor Network (MN), Basal Ganglia Network (BGN), and a control network (Auditory Network (AN)). We conducted paired-sample t-tests and two-sample t-tests for each network to identify significant connectivity differences in PD-ON versus PD-OFF and PD versus controls, respectively. We confirmed these ICA findings with region-of-interest (ROI) analyses.

Results: For the ICA of the MN, controls and PD-ON had increased connectivity within the motor cortex compared to PD-OFF. In the BGN, PD-ON had increased connectivity in the putamen and caudate compared to both PD-OFF and controls. We then selected the following ROIs for analysis: MN-right motor cortex, BGN-right caudate/putamen, and AU-right primary auditory cortex. MN connectivity was reduced in PD-OFF compared to controls (p=0.019). Connectivity increased in PD-ON compared to PD-OFF (p=0.006), and there was no difference between PD-ON and controls (p=0.446). BGN connectivity was also increased in PD-ON compared to PD-OFF (p=0.03). By contrast, no comparisons for ICA or ROI analyses in the control network (AN) reached significance.

Conclusions: PD-OFF showed reduced connectivity in RSNs associated with motor function with strengthened connectivity when patients were ON medication. These findings suggest RSNs could serve as objective biomarkers of PD motor function.

References/Funding Source K Poston, WR Shirer, V Menon, MD Greicius (2011). Dopaminergic Modulation of Resting State Networks in Parkinson's disease. Organization for Human Brain Mapping. Quebec City, QC. NIH-NINDS (R01NS073498)

Decoding Subject-Driven Cognitive States with Whole-Brain Connectivity Patterns

W Shirer[1], S Ryali[2], E Rykhlevskaia[2], V Menon[2], MD Greicius[1]
Departments of [1]Neurology and Neurological Sciences, [2]Psychiatry and Behavioral Sciences, Stanford University, CA

Decoding specific cognitive states from brain activity constitutes a major goal of neuroscience. Previous studies of brain-state classification have focused largely on decoding brief discrete events and have required the timing of these events to be known. To date, methods for decoding more continuous and purely subject-driven cognitive states have not been available. Here, we demonstrate that free-streaming subject-driven cognitive states can be decoded using a novel whole-brain functional connectivity analysis. Ninety functional regions of interest (ROIs) were defined across 14 large-scale resting-state brain networks to generate a 3960 cell matrix reflecting whole-brain connectivity. We trained a classifier to identify specific patterns of whole-brain connectivity as subjects rested quietly, remembered the events of their day, subtracted numbers, or (silently) sang lyrics. In a leave-one-out cross-validation, the classifier identified these 4 cognitive states with 84% accuracy. More critically, the classifier achieved 85% accuracy when identifying these states in a second independent cohort of subjects. Classification accuracy remained high with imaging runs as short as 30--60 s. At all temporal intervals assessed, the 90 functionally defined ROIs outperformed a set of 112 commonly used structural ROIs in classifying cognitive states. This approach should enable decoding a myriad of subject-driven cognitive states from brief imaging data samples.

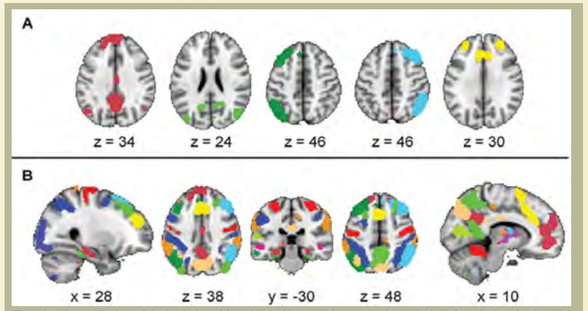

Functional parcellation of the brain into 90 regions of interest that cover the majority of cortical and subcortical gray matter. Group ICA applied to the resting-state data of 15 subjects yielded 14 ICNs of which 5 are shown in A (for all 14 ICNs, see Supplementary Fig. S2). Each ICN is thresholded to generate between 2 and 12 ROIs per ICN. When all 90 ROIs across the 14 ICNs are overlaid on a single brain image (B) the majority of cortical and subcortical gray matter is covered.

References/Funding Source WR Shirer, S Ryali, E Rykhlevskaia, V Menon, MD Greicius (2011). Decoding Subject-Driven Cognitive States with Whole- Brain Connectivity Patterns. Cereb Cortex. Dana Foundation; John Douglas French Alzheimer's Foundation; National Institutes of Health (AT005733, HD059205, HD057610, NS073498, NS058899).

Digital Map of Emboli From Carotid Procedures

AC Rosen[1,2], J Stephens[1,2], AR Laird[3], SB Eickhoff[4], PM Fox[3], G Chan[1], D Dinishak[5], M Ortega[1], B Lane[1,6], W Zhou[1]
[1]Palo Alto Veterans Affairs Health Care System, Palo Alto, CA; Departments of [2]Psychiatry, [6]Radiology, [7]Surgery, Stanford University, CA; [3]Research Imaging Institute, University of Texas Health Science Center at San Antonio, TX; [4]Department of Psychiatry and Psychotherapy, RWTH Aachen University, Aachen, Germany; [5]Pacific Graduate School of Psychology, Redwood City, CA

Background— Although carotid revascularization has a low rate of neurologic complications, subclinical microembolization visualized on postoperative diffusion weighted imaging MRI (DWI) is common. This study provides normative volumetric data on emboli to serve as a metric for lesion severity. We also characterize the regions vulnerable to procedure-associated emboli through a novel application of anatomic likelihood analysis (ALE).

Methods— DWI from 129 patients following carotid interventions were examined and embolic lesions were defined manually. Descriptive, image based analyses were performed characterizing the variability of lesion size, number, and location. Images were normalized and submitted to ALE.

Results— .. Forty five patients displayed post-procedure emboli. The frequency was higher for CAS (56.14% than CEA (18.06%), but the total volume of the lesions did not differ. Normative results were provided on lesion numbers, volume, and total lesion volume for a given patient. Patients with postoperative neurological symptoms were rare (8) but more common in those with a total lesion volumes greater than the 75th percentile (1128 mL). The areas with a high degree of convergence across embolic lesions included the anterior and posterior cingulate, white matter deep to the sensorimotor strip, parietal, and middle frontal gyrus, insula, basal ganglia, and temporoparietal junction.

Conclusions— Regions vulnerable to emboli include those implicated in memory (posterior cingulate), executive control and motor planning/speeded responses (anterior cingulate, middle frontal gyrus, basal ganglia), functions commonly affected in Alzheimer's and vascular dementias. The overall distribution is consistent with what is traditionally termed the "border zone". By identifying neural systems vulnerable to disruption, this study forms a basis for selecting a targeted neuropsychological battery for postoperative assessment.

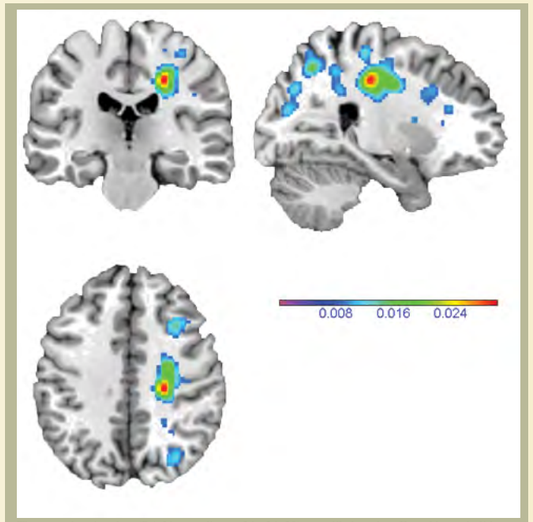

The posterior cingulate (BA 31: coordinates 24, -24, 38) most likely to be affected by emboli is displayed in red.

References/Funding Source This work was supported by grants from the NIA (AG12995), NIMH (MH59940), and AHA (Zhou10CRP2610312). ACR was supported by a K award (K01AG025157).

Molecular Imaging

Molecular imaging is the art of looking inside of a living organism or cell to evaluate biological processes, observe normal cell behavior, identify aberrant behaviors, and develop interventions to halt or rectify such abnormalities. Through molecular and functional imaging we have made huge strides in bridging many other disciplines such as, biology, chemistry, physics, and computer science and ultimately changing and improving how we use imaging in medicine.

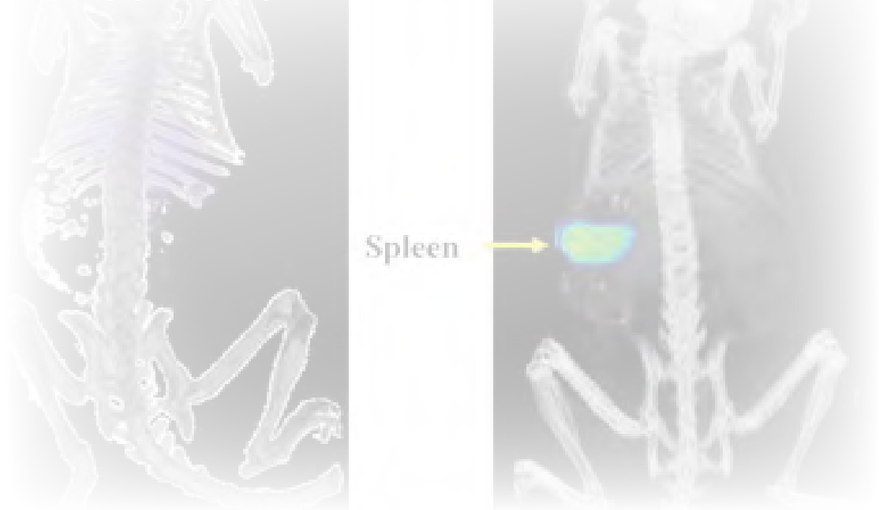

An 18F-FBEM labeled Affibody for PET imaging of tumor EGFR expression

Z Miao, G Ren, H Liu, S Qi, S Wu, Z Cheng
Departments of Radiology, MIPS, BioX Program, Stanford University, CA

Objectives: Previously, a 64Cu labeled anti-epidermal growth factor receptor (EGFR) Affibody (DOTA-ZEGFR:1907) was found to show excellent in vivo stability and good tumor-to-normal organ imaging contrast in xenograft mice model. The objective of this study was to further prepare and evaluate a radiofluorinated ZEGFR:1907 (termed as 18F-FBEM-ZEGFR:1907) for positron emission tomography (PET) imaging of tumor EGFR expression in living subjects.

Methods: The radiofluorination was accomplished through site-specific conjugation of the Ac-Cys-ZEGFR:1907 with N-2-(4-18F-fluorobenzamido)ethyl]maleimide (18F-FBEM). Binding affinity assay and in vivo biodistribution study was conducted with EGFR over-expression A431 cells and A431 xenograft tumor model. Correlation study of in vivo 18F-FBEM-ZEGFR:1907 PET imaging and in vitro Western blot analysis was then conducted in various EGFR over-expression tumors.

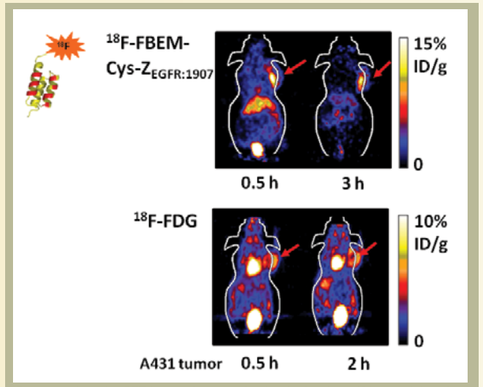

Representative microPET images (bottom) of nude mice bearing A431 tumor injected with 18F-FBEM-ZEGFR:1907 or 18F-FDG at 0.5 and 2 h post-injection. Arrow indicates the location of tumor.

Results: The resulting probe, 18F-FBEM-ZEGFR:1907, showed moderate specific activity (ca 10 GBq/μmol) and low nanomolar affinity (KD = 37nM) to A431 cancer cells. Biodistribution studies in A431 xenograft model demonstrated that 18F-FBEM-ZEGFR:1907 displayed high tumor uptake at 3 h post injection (p.i.), and co-injection of a large excess of the unlabeled Ac-Cys-ZEGFR:1907 as a blocking agent significantly reduced tumor uptake (3.9 vs. 1.0 %ID/g, at 3 h p.i., 75% inhibition, $P < 0.05$). In vivo microPET imaging showed that 18F-FBEM-ZEGFR:1907 rapidly accumulated in the tumor and quickly cleared from the normal organs except liver and kidney, allowing excellent tumor-to-normal tissue contrast to be obtained. It was found that the tumor uptakes at 3 h p.i. quantified by 18F-FBEM-ZEGFR:1907 PET were in good correlation with the EGFR expression levels measured by Western assay ($P = 0.007$, $r = 0.60$).

Conclusions: 18F-FBEM-ZEGFR:1907 is a promising PET probe for imaging EGFR positive tumors and EGFR expression level

References/Funding Source Z Miao, G Ren, H Liu, S Qi, S Wu, Z Cheng. An 18F-FBEM labeled Affibody for PET imaging of tumor EGFR expression. Oral presentation at the 57th Annual Meeting of the Society of Nuclear Medicine, San Antonio, TX, June 4-8, 2011. This work was supported by National Cancer Institute In Vivo Cellular Molecular Imaging Center (ICMIC) grant P50 CA114747 (SSG) and 5R01CA119053 (Z.C.).

In vivo PET imaging to track mesenchymal stem cells labeled with 64Cu-PTSM

K Chen, Z Miao, Z Cheng
Departments of Radiology, MIPS, BioX Program, Stanford University, CA

Objectives: With advancement of application of mesenchymal stem cells (MSCs) in biomedicine, in vivo tracking of MSCs in noninvasive, sensitive, quantitative, tomographic, and cell-non-hazardous ways is highly desired. Our study is to explore the advantages and disadvantages of tracking MSCs by uPET imaging using ex vivo 64Cu - pyruvaldehyde-bis (N4-methylthiosemicarbazone) (PTSM) cell labeling.

Methods: Murine bone marrow derived-MSCs were isolated and labeled with 64Cu -PTSM. In vivo uPET imaging was conducted after injection of MSCs into Bab/c mice. Biodistribution of labeled MSCs at early and late time point were measured. Also, cell uptake and efflux assay were conducted. Finally, the impact of 64Cu -PTSM labeling on MSCs growth, differentiation were evaluated by cell counting and staining.

Results: 64Cu -PTSM labeling efficiency of MSCs was around 75%. Labeling has no impact on MSCs viability. In vivo uPET imaging of 64Cu -PTSM labeled MSCs demonstrated quick lung accumulation at early time point (4 h) after tail vein injection of MSCs and showed decreased lung signal with time. Cell uptake of 64Cu -PTSM by MSCs already reached plateau as early as 1 h (94.3%). Cell retention of 64Cu -PTSM decreased over time and the value were 94.4% and 18.7% at 0.5 and 24 hr, respectively. Biodistribution result showed that lung uptake of 64Cu-PTSM was 70.7% at 4 h, which indicated that MSCs could be quantitatively assessed at early time point by uPET imaging based on uptake and efflux assay results, however, late time point uPET imaging cannot reflect real distribution of labeled MSCs due to quick efflux of 64Cu -PTSM. In addition, radiation of 64Cu -PTSM had no significant impact on MSCs growth and differentiation measured by cell counting and staining.

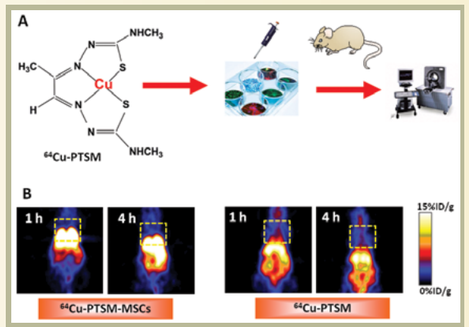

(A) 64Cu-PTSM labeling of MSCs for in vivo trafficking. (B) Representative microPET images of scid mice injected with 64Cu-PTSM labeled MSCs (left) or 64Cu-PTSM (right) at 1 and 4 h post-injection. The rectangle highlights the lung region.

Conclusions: This study demonstrates the feasibility of tracking MSCs by uPET imaging using ex vivo 64Cu -PTSM cell labeling

References/Funding Source K Chen, Z Miao, Z Cheng. In vivo PET imaging to track mesenchymal stem cells labelled with copper-64-pyruvaldehyde-bis (N4-methylthiosemicarbazone). Oral presentation at the 57th Annual Meeting of the Society of Nuclear Medicine, San Antonio, TX, June 4-8, 2011. This work was supported by the DOD-BCRP-Idea BC061781 (Z.C.).

64Cu-Labeled Fibronectin Domain for PET Imaging of EGFR+ Tumors

BJ Hackel, R Kimura, SS Gambhir
Department of Radiology, Stanford University, CA

The fibronectin domain (Fn) is a beta-sandwich protein that has been utilized as a scaffold for engineering molecular recognition domains but has yet to be demonstrated for use in molecular imaging. A 98-amino acid Fn, engineered with picomolar affinity for epidermal growth factor receptor (EGFR), is site-specifically conjugated to 1,4,7,10-tetraazadodecane-N,N′,N″,N‴-tetraacetic acid and labeled with 64Cu with modest specific activity (36 mCi/mg). The 64Cu-Fn tracer exhibits EGFR-specific binding to A431 epidermoid carcinoma cells in culture. The tracer is stable as it exhibits an unchanged HPLC chromatogram after 24h in 50% mouse serum at 37°. The 64Cu-Fn (~50 μCi injected via tail-vein) was used for positron emission tomography of EGFR-overexpressing A431 xenografts (~5-10 mm diameter) in mice (n=5). The tracer exhibits good tumor localization (2.6±0.8 %ID/g at 1h), retention (2.1±0.5 %ID/g at 24h), and specificity (5.1±1.2 tumor:muscle at 2h). Specific targeting is statistically significant as verified by low localization to a tumor with low EGFR expression (0.7±0.1%ID/g, $P<0.005$); specificity is further demonstrated as a non-binding wild-type control fibronectin has low localization to the EGFR-overexpressing A431 xenograft (0.7±0.1 %ID/g at 1h, $P<0.005$). These results are corroborated by ex vivo gamma counting analysis of dissected tissues. These data represent the first reported use of the fibronectin domain for in vivo imaging and demonstrate the potential for this domain to serve as a robust scaffold for the development of other molecular imaging agents.

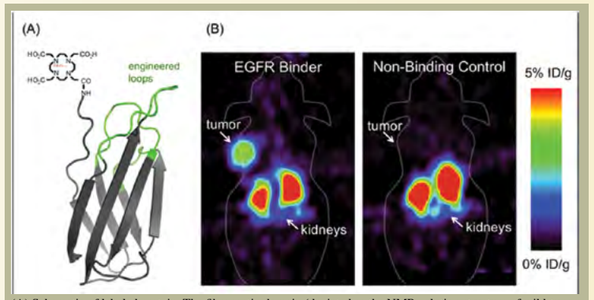

(A) Schematic of labeled protein. The fibronectin domain (depicted as the NMR solution structure of wild-type fibronectin domain (PDB code: 1TTG)) was engineered (mutated residues in green) for binding to EGFR. DOTA was conjugated to the sole primary amine (the N-terminus) and used to chelate 64Cu. (B) PET imaging. A431 epidermoid carcinoma cells were xenografted into nude mice. 64Cu-Fn3 (EGFR binder D' or non-binding control WT') was injected via the tail vein. 5 min. static scans were acquired at 1h post-injection.

References/Funding Source Presentation Number 0166 Scientific Session 21: Probes for Imaging the Tumor Microenvironment September 11, 2010 / 09:15-09:30 / Room: Main Hall. NCI: ICMIC P50CA114747, RO1 CA082214, CCNE-TR U54 CA119367, Canary Foundation, Ben & Katherine Ivy Foundation, Sir Peter Michael Foundation, American Cancer Society Postdoctoral Fellowship (BJH)

An 18F-labeled Agouti-related protein for PET imaging of integrin positive tumor

H Jiang[1,2], S Moore[3], S Liu[1], H Liu[1], Z Miao[1], F Cochran[3], J Cochran[3], H Zhang[2] , Z Cheng[1]
[1]Departments of Radiology, MIPS, BioX Program, [3]Bioengineering, Stanford University, CA; [2]Nuclear Medicine, Zhejiang University, Hangzhou, China

Objectives: A novel protein scaffold, agouti-related protein (AgRP) has been used to engineer mutants that bound to αvβ3 integrin with high affinity and specificity. In this study, for further clinical translation and applications, an 18F-labeled AgRP mutant(7C)was prepared and evaluated as a tumor imaging agent in vitro and in vivo.

Methods: AgRP-7C was synthesized by solid phase peptide synthesis. It was site-specifically conjugated with 4-nitrophenyl 2-18/19F-fluoropropionate to produce fluorinated peptide, 18/19F-FP-AgRP-7C.Competition binding assay of AgRP-7C and 19F-FP-AgRP-7C was performed using human glioblastoma U87MG cells that overexpress αvβ3 integrin.The biodistribution,metabolic stability and micro-positron emission tomography(PET)imaging studies of 18F-FP-AgRP-7C were conducted on U87MG tumor-bearing mice.

Results: Both AgRP-7C and 19F-FP-AgRP-7C specifically competed with 125I-echistatin for binding to U87MG cells. They showed high binding affinities (half maximal inhibitory concentration values were 9.40 and 8.37 nM,respectively).In vivo micro-PET imaging demonstrated that 18F-FP-AgRP-7C accumulated rapidly in tumors (3.24 percentage injected dose per gram at 0.5 h post injection).It was quickly cleared from blood, resulting excellent tumor-to-normal tissue contrast.The biodistribution study further demonstrated its high tumor uptake and rapid clearance. Furthermore,coinjection with a large molar excess of blocking peptide c(RGDyK) into U87MG tumor-bearing mice proved the integrin-binding specificity of 18F-FP-AgRP-7C in biodistribution and micro PET imaging studies. Serum stability and in vivo metabolite assays revealed that 18F-FP-AgRP-7C are sufficiently stable and suitable for in vivo molecular imaging.

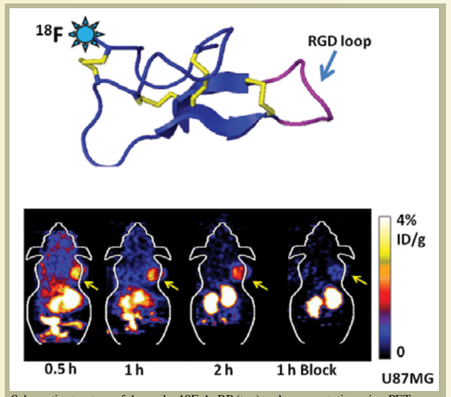

Schematic structure of the probe 18F-AgRP (top) and representative microPET images (bottom) of nude mice bearing U87MG tumor injected with the probe at 0.5, 1 and 2 h post-injection. Arrow indicates the location of tumor.

Conclusions: 18F-FP-AgRP-7C exhibits promising in vivo properties such as rapid tumor targeting and good tumor-to-normal tissue ratios.AgRP is an excellent scaffold for protein engineering and could be used to develop other targeting peptides for tumor imaging

References/Funding Source H Jiang, S Moore, S Liu, H Liu, Z Miao, FV Cochran, JR Cochran, H Zhang, Z Cheng. An 18F-labeled Agouti-Related Protein for PET Imaging of Integrin Positive Tumor. Poster presentation at the 57th Annual Meeting of the Society of Nuclear Medicine, San Antonio, TX, June 4-8, 2011. This work was supported by National Cancer Institute In Vivo Cellular Molecular Imaging Center (ICMIC) grant P50 CA114747 (SSG) and 5R01CA119053 (Z.C.).

A novel probe with dual targeting mechanisms for tumor imaging using positron emission tomography

S Liu, H Liu, Z Miao, Z Cheng
Departments of Radiology, MIPS, BioX Program, Stanford University, CA

Objectives: Lipophilic cations, such as tetraphenylphosphonium analogs have been explored for tumor targeting because of their high accumulation in tumor cells which possess elevated mitochondria membrane potential than normal cells. Cyclic arginine-glycine-aspartic acid (RGD) peptides have also been extensively used for cancer imaging based on their intergin receptors targeting ability. In this study, we designed, synthesized and radiofluorinated a novel ligand (TPP-RGD) which contains both RGD and cationic phenylphosphonium moieties for tumor targeting through dual mechanisms. It is expected that the resulting probe could be advantageous such as high and specific tumor uptake ability due to its dual-targeting mechanisms.

Methods: The TPP-RGD heterodimer was synthesized by conjugation of triphenylphosphonium (TPP) and RGD through a lysine linker, then it was site specifically labeled with 18F via the p-nitrophenyl 2-18F-fluoropropionate (18F-NFP) prosthetic group. The receptor-binding affinity of 19F-FP-TPP-RGD was evaluated in vitro by competition binding assay with 125I-echistatin using human glioblastoma U87MG cells. In vivo tumor-targeting efficacy of 18F-FP-TPP-RGD was evaluated by biodistribution and microPET studies.

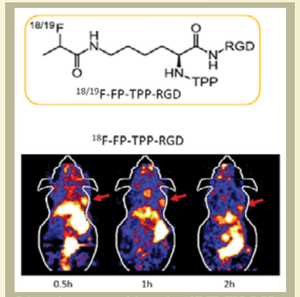

Schematic structure of the probe 18F-FP-TPP-RGD and representative microPET images (right) of nude mice bearing U87MG tumor injected with the probe at 0.5, 1 and 2 h post-injection. Arrow indicates the location of tumor.

Results: The receptor-binding affinities of RGD and 19F-FP-TPP-RGD were determined. 19F-FP-TPP-RGD displayed higher integrin αvβ3-binding affinity than RGD. In the microPET imaging study using U87MG-tumor bearing mice, 18F-FP-TPP-RGD had significantly higher tumor uptake compared with 18F-FP-RGD at all time points examined. The U87MG tumor uptake of 18F-FP-TPP-RGD was partially inhibited in the presence of an excess amount of unlabeled RGD.

Conclusions: Dual targets recognition of cell membrane receptor and mitochondria membrane potential showed significantly improved tumor-targeting efficacy. The same principle for designing other heterodimeric ligands could be applied to other receptor systems and imaging modalities in future studies

References/Funding Source S Liu, H Liu, Z Miao, Z Cheng. A novel probe with dual targeting mechanisms for tumor imaging using positron emission tomography. Oral presentation at the 57th Annual Meeting of the Society of Nuclear Medicine, San Antonio, TX, June 4-8, 2011. This work was supported by NIH R01 CA119053 (Z.C.).

Imaging Painful Neuropathic Nerves Using A Novel Sigma-1 Receptor (S1R) Radioligand With PET-MRI.

D Behera, B Shen, S Biswal, FT Chin
Department of Radiology, Stanford University, CA

Purpose: Sigma-1 receptors (S1R) modulate NMDA receptors and Ca2+-dependent processes, and therefore play a significant role in pain sensitization. S1R is upregulated in the nervous system in chronic pain and can potentially be used to highlight areas of increased nociceptive activity. We used 18F-FTC-146, a marker for S1R, and PET-MRI to detect increased S1R density in an injured nerve of a neuropathic pain model.

Materials and Methods: 18F-FTC-146 was synthesized via aliphatic nucleophilic fluorination using an automated module. Animal experiments were approved by Stanford IACUC. Adult male Sprague-Dawley rats were divided into 3 experimental groups (n=3): 1) Left Spared-Nerve Injury (SNI), a sciatic neuropathic pain model, 2) Sham surgery without nerve injury, and 3) control group without any surgery. The rats were allowed 4 weeks to heal and develop pain. Presence of pain in SNI was ascertained by testing for allodynia using von-Frey's filaments. Each rat was given approximately 500 μCi of 18F-FTC-146 IV followed by an immediate dynamic scan of the thighs for 20 minutes using a microPET, followed by T1-weighted FSE images obtained using a 7T microMRI.

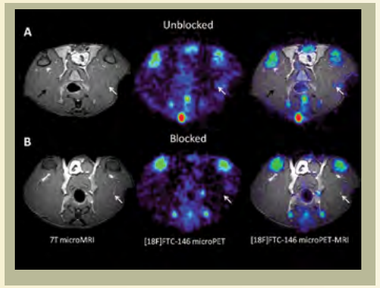

For blocking studies, Haloperidol (16 mg/kg IV) was given 20 min before tracer injection. PET and MRI images were fused (Amide image analysis software), and ROIs were placed on 5 mm segments of sciatic nerves, proximal to the level of injury in both hindlimbs of each rat using MR images. Signal was recorded from the fused PET images and normalized to background.

Results: Presence of allodynia only in the operated limb of SNI rats was confirmed ($p<0.03$). Higher 18F-FTC-146 signal was seen in the operated left sciatic nerve in the SNI group but not in the Sham or control groups (12.3, 5.2, 7.6 respectively). This difference disappears when blocked with haloperidol, demonstrating that the increased uptake in the sciatic nerve is due to specific binding with S1R.

Conclusion: Rats with neuropathic pain show increased 18F-FTC-146 uptake in the affected nerve. PET-MRI can be effectively used to study 18F-FTC-146 uptake in peripheral nerves.

Clinical Relevance: Combining the high sensitivity of PET with the excellent tissue contrast of MRI to locate nerve, 18F-FTC-146 PET-MRI can quantify neural S1R density and potentially identify chronic pain generators.

Novel 18F-labeled aliphatic probe for melanoma imaging

S Liu, H Liu, Z Miao, H Jiang, Z Cheng
Departments of Radiology, MIPS, BioX Program, Stanford University, CA

Objectives: Radiofluorinated benzamide and nicotinamide analogs have been demonstrated to be promising probes for melanoma PET imaging. The aim of this study was to explore the feasibility of using aliphatic compounds for development of new generation melanoma PET probes.

Methods: An aliphatic N,N-diethylethylenediamine precursor was directly labeled with a radiofluorination synthon, p-nitrophenyl 18F-fluoropropionate (18F-NFP), to produce a probe18F-FPDA. MicroPET imaging using 18F-FPDA was performed in melanoma murine models. The specificity of 18F-FPDA to melanoma was evaluated in vivo by biodistribution studies and micro-positron emission tomography (microPET) imaging in C57BL/6 mice bearing B16F10 murine melanoma tumors.

Results: Starting with precursor 18F-NFP, the total reaction time for 18F-FPDA, including final high-performance liquid chromatography purification, is about 30 min, with decay-corrected radiochemical yield of 79.8%. The B16F10 cell study demonstrated by significant different uptake in tyrosine-treated and untreated B16F10 cells in vitro. In pigmented-enriched B16F10 xenografts, tumor uptakes reached 5.41 %ID/g at 0.5 h post injection and the sustained tumor uptake at 2 h post injection was 3.05 %ID/g, while in the non-pigmented U87MG and PC3 models, the tumor uptakes were only the background levels. Due to the high selectivity between targeted and non-targeted organs for 18F-FPDA, the animal PET imaging study yielded a high tumor-to-muscle ratio of approximately 8:1 at 1 h and 14:1 at 2 h post injection.

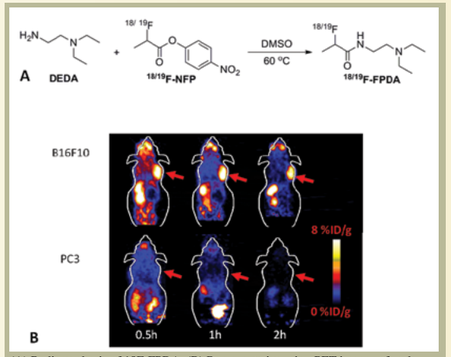

(A) Radiosynthesis of 18F-FPDA. (B) Representative microPET images of nude mice bearing melanoma B16F10 (top) or prostate cancer PC3 (bottom) injected with 18F-FPDA at 0.5, 1 and 2 h post-injection. Arrow indicates the location of tumor.

Conclusions: The new tracer 18F-FPDA was synthesized with high yield via 18F-NFP and the tracer exhibited high B16F10 tumor-targeting efficacy, and favorable in vivo pharmacokinetics. Further testing and clinical translation of 18F-FPDA for noninvasive clinical evaluation of suspected malignant melanoma are warranted

References/Funding Source S Liu, H Liu, Z Miao, H Jiang, Z Cheng. Novel 18F-labeled aliphatic probe for melanoma imaging. Oral presentation at the 57th Annual Meeting of the Society of Nuclear Medicine, San Antonio, TX, June 4-8, 2011. This work was supported by National Cancer Institute In Vivo Cellular Molecular Imaging Center (ICMIC) grant P50 CA114747 (SSG) and Melanoma Research Alliance (Z.C.).

Development of 18F-labeled picolinamide probes for melanoma PET imaging

S Liu, H Liu, Z Miao, Z Cheng
Departments of Radiology, MIPS, BioX Program, Stanford University, CA

Objectives: The aim of this study was to synthesize and evaluate the 18F-picolinamide probes (18F-P3BZA and 18F-P4BZA) for the imaging of malignant melanoma.

Methods: 18F-fluoropicolinamides were prepared by radiofluorination reactions using no-carrier-added 18F-fluoride and evaluated in vivo by biodistribution studies and micro-positron emission tomography (microPET) imaging in C57BL/6 mice bearing B16F10 murine melanoma tumors.

Results: 18F-fluorination of the corresponding bromopicolinamide precursors was achieved in yields of 10-20% (decay corrected on the basis of 18F-fluoride). The total synthesis time was less than 1 hour. The radiochemical purity of the 18F-labeled probes was more than 98% and the specific activity was 100-150 GBq/μmol. Noninvasive microPET and direct tissue sampling experiments demonstrated that the probes had melanin-specific tumor targeting in subcutaneous B16F10 melanoma xenografts, which yielded a tumor-to-blood ratio of approximately 20:1 at 1 h and greater than 30:1 at 2 h. Quantitative microPET imaging studies showed that 18F-P3BZA had tumor uptake of 11.8 ± 2.2, 13.2 ± 2.4, and 14.6 ± 3.2 %ID/g at 0.5h, 1 h, and 2 h postinjection, respectively. Of note, the 18F-P3BZA demonstrated good in vivo stability as evidenced by the low bone uptake in biodistribution studies.

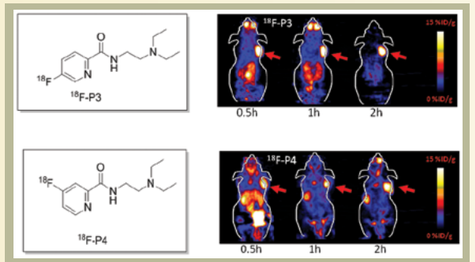

Schematic structure of the probes 18F-P3 and 18F-P4 (left) and representative microPET images (right) of nude mice bearing melanoma B16F10 injected with the probe at 0.5, 1 and 2 h post-injection. Arrow indicates the location of tumor.

Conclusions: The new 18F-picolinamide probes were synthesized with high specific activity via one-step 18F-fluorination within a short time frame. The probes exhibited high tumor uptake and metabolic stability, as well as favorable in vivo pharmacokinetics. These findings suggest that 18F-fluoropicolinamides could be promising imaging agents for the detection of melanoma

References/Funding Source Liu S, Liu H, Miao Z, Cheng Z. Development of 18F-labeled picolinamide probes for melanoma PET imaging. Oral presentation at the 57th Annual Meeting of the Society of Nuclear Medicine, San Antonio, TX, June 4-8, 2011. This work was supported by National Cancer Institute In Vivo Cellular Molecular Imaging Center (ICMIC) grant P50 CA114747 (SSG) and Melanoma Research Alliance (Z.C.).

Development of [18F]AlF-NOTA-RGD2 probe for microPET imaging in U87MG-tumor bearing mice

S Liu, H Liu, H Jiang, Z Cheng
Departments of Radiology, MIPS, BioX Program, Stanford University, CA

Objectives: Clinical translation of 18F-labeled arginine-glycine-aspartate (RGD) peptides is partially hindered by the multi-step and laborious radiosynthesis. The goal of this study was to investigate the feasibility of one-step 18F-labeling of a dimeric RGD peptide for microPET imaging via a simple chelation reaction between Al18F and NOTA-RGD2.

Methods: Cyclic peptide E[c(RGDyK)]2 (RGD2) was conjugated with macrocyclic chelator 1,4,7-triazacyclononane-1,4,7-triacetic acid (NOTA) and labeled with Al18F to synthesize [18F]AlF-NOTA-RGD2. The peptide conjugate's affinity and specificity to integrin were assessed by cell-based receptor binding assay, and the tumor targeting efficacy of [18F]AlF-NOTA-RGD2 was evaluated in a subcutaneous U87MG glioblastoma xenograft mouse model.

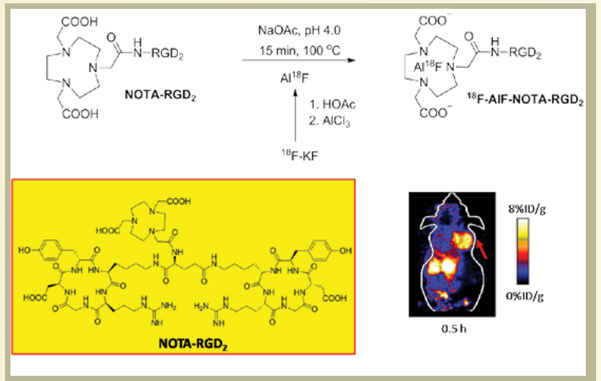

Radiosynthesis of [18F]AlF-NOTA-RGD2 and a representative microPET image of nude mice bearing U87MG injected with the probe at 0.5 h post-injection. Arrow indicates the location of tumor.

Results: The NOTA-RGD2 conjugate could be radiofluorinated in good yield within 40 min via Al18F intermediate. The IC50 of [19F]AlF-NOTA-RGD2 determined by U87MG cell-based receptor binding assay was 46 ± 4.4 nM using 125I-echistatin as radioligand. Quantitative microPET imaging studies using [18F]AlF-NOTA-RGD2 demonstrated the high tumor uptake, fast clearance from body, and good tumor to normal organ ratios.

Conclusions: The NOTA-RGD2 conjugate has been successfully labeled with Al18F in one single step. The good in vivo behavior plus the short synthesis route for [18F]AlF-NOTA-RGD2 warrant further exploration for kit-like production of 18F-labeled RGD PET radiopharmaceutical for integrin αvβ3 imaging and potential clinical translation

References/Funding Source S Liu, H Liu, H Jiang, Z Cheng. Development of [18F]AlF-NOTA-RGD2 probe for microPET imaging in U87MG-tumor bearing mice. Oral presentation at the 57th Annual Meeting of the Society of Nuclear Medicine, San Antonio, TX, June 4-8, 2011. S Liu, H Liu, H Jiang, H Zhang, Z Cheng. One-Step Radiosynthesis of 18F-AlF-NOTA-RGD2 for Tumor Angiogenesis PET imaging. European Journal of Nuclear and Medicine Molecular Imaging. 2011 May 27. [Epub ahead of print] PMID: 21617974. This work was supported by NIH R01 CA119053 (Z.C.).

Profiling EGFR in triple negative breast tumors using PET

G Ren, Y Xu, Z Miao, S Qi, H Liu, Z Cheng
Departments of Radiology, MIPS, BioX Program, Stanford University, CA

Objectives: Triple Negative Breast Cancer (TNBC) represents a group of refractory breast cancer with aggressive clinical manifestations as well as poor prognosis. Epidermal growth factor receptor (EGFR) expression is strongly associated with TNBC progression and it may serve as a therapeutic target for TNBC. We aimed to use EGFR Affibody based PET imaging to profile EGFR expression and to evaluate the response from anti-EGFR treatment in TNBC tumor bearing mice.

Methods: Ac-Cys-ZEGFR:1907 was chemically synthesized using a solid phase peptide synthesizer and then site-specifically conjugated with 1,4,7,10-tetraazacyclododecane-1,4,7,10-tetraacetic acid (DOTA) for radiolabeling or N-2-(4-18F-fluorobenzamido)-ethyl]-maleimide (18F-FBEM). The in vitro cell uptake study was performed using TNBC SUM159 cells. The biodistribution and microPET imaging using 64Cu-DOTA-ZEGFR:1907 or 18F-FBEM- ZEGFR:1907 were evaluated in nude mice bearing subcutaneous SUM159 tumors.

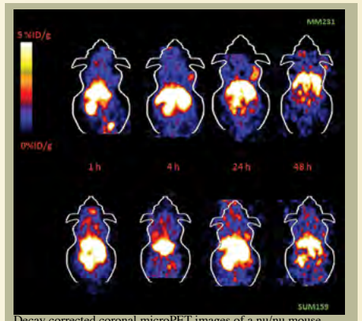

Decay corrected coronal microPET images of a nu/nu mouse bearing TNBC MDA-MB-231 (top) or SUM159 (bottom) after tail vein injection of 64Cu-DOTA- ZEGFR:1907

Results: Ac-Cys-ZEGFR:1907 was successfully synthesized and radiolabeled with 64Cu. Biodistribution study showed that tumor uptake value of 64Cu-Ac-Cys-ZEGFR:1907 remained at 4.07 ± 0.93 %ID/g at 24 h in nude mice (n = 4) bearing SUM159 xenografts. Furthermore, microPET imaging study demonstrated that 64Cu-DOTA-Ac-Cys-ZEGFR:1907 and 18F-FBEM-ZEGFR:1907 could both specifically delineate the EGFR positive TNBC tumor in vivo (Figure).

Conclusions: The study successfully demonstrated that 64Cu-DOTA-Ac-Cys-ZEGFR:1907 and 18F-FBEM- ZEGFR:1907 are promising molecular probes for PET imaging of EGFR expression in TNBC. The anti-EGFR targeted therapy is currently undergoing in TNBC models and EGFR targeted imaging will be utilized for profiling the EGFR as an effective TNBC biomarker

References/Funding Source G Ren, Y Xu, Z Miao, S Qi, H Liu, Z Cheng. Profiling EGFR in Triple Negative Breast Tumors using PET. Poster presentation at the 57th Annual Meeting of the Society of Nuclear Medicine, San Antonio, TX, June 4-8, 2011. This work was supported by National Cancer Institute In Vivo Cellular Molecular Imaging Center (ICMIC) grant P50 CA114747 (SSG) and 5R01CA119053 (Z.C.).

Characterization of 177Lu-Affibody-HSA for cancer radionuclide therapy

G Ren, Y Xu, Z Miao, S Qi, H Liu, Z Cheng
Departments of Radiology, MIPS, BioX Program, Stanford University, CA

Objectives: The epidermal growth factor receptor (EGFR) is an attractive target for radionuclide therapy of disseminated head and neck carcinomas. EGFR specific Affibodies have shown excellent tumor localizations in PET and SPECT studies, but on the other hand, display extremely high kidney uptakes (>100%ID/g). This represents a critical concern for high doses to the radiation sensitive kidneys. We have recently demonstrated that a human serum albumin (HSA)-HER2 Affibody conjugate exhibits improved pharmacokinetics. The purpose of this study is to further explore whether radiolabeled EGFR-HSA bioconjugates could be suitable for radionuclide therapy of EGFR expressing tumors.

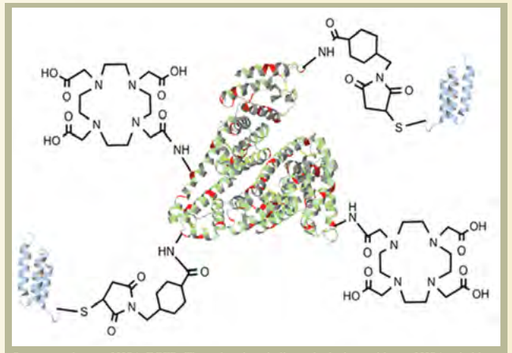

Structure scheme of HSA-EGFR. The red regions indicate the lysine residues of HSA suitable for the conjugation with DOTA and EGFR-Affibody molecules (violet structures). The radiolabeling occurs via complexiation of either 177Lu or 64Cu with DOTA chelators presented on the bioconjugates.

Methods: HSA was modified by a site-specific conjugation with DOTA-NHS and the bifunctional crosslinker Sulfo-SMCC. The EGFR Affibody analog Ac-Cys-ZEGFR:1907 was then covalently conjugated with the HSA through the sulfo-SMCC, and the resulting bioconjugate DOTA-HSA-ZEGFR:1907 was further radiolabeled with 64Cu and 177Lu. Radiometal labeled DOTA-HSA-ZEGFR:1907 was subjected to in vitro cell uptake and internalization studies using the human oral squamous carcinoma cell line SAS (n=5). PET, SPECT and biodistribution studies were examined using SAS tumor-bearing mice (n=4).

Results: Radiolabeling with 64Cu as well as with 177Lu resulted in high radiochemical yields (>70%). The in vitro stability of 177Lu-DOTA-HSA-ZEGFR:1907 in mouse serum was >80% at 168 h. Cell uptake studies displayed a significant (8.4% at 4 h) and specific uptake and the internalization of 177Lu-DOTA-HSA-ZEGFR:1907 could be verified. PET and SPECT using 64Cu-DOTA-HSA-ZEGFR:1907 and 177Lu-DOTA-HSA-ZEGFR:1907, respectively showed good tumor imaging contrasts. The imaging results were consistent with the biodistribution data: 177Lu-DOTA-HSA-ZEGFR:1907 displayed good tumor uptakes (5.1% ID/g) and high liver uptakes (31.5% ID/g) and relatively low kidney uptakes (8.5% ID/g) at 72 h p.i.

Conclusions: 177Lu-DOTA-HSA-ZEGFR:1907 is a promising agent for radionuclide therapy of EGFR expressing head and neck carcinomas

References/Funding Source S Hoppmann, S Qi, Z Miao, H Liu, H Jiang, Z Cheng. Characterization of 177Lu-Affibody-HSA bioconjugate for radionuclide therapy of EGFR-expressing head and neck carcinomas. Presentation at the 57th Annual Meeting of the Society of Nuclear Medicine, San Antonio, TX, June 4-8, 2011. This work was supported by National Cancer Institute In Vivo Cellular Molecular Imaging Center (ICMIC) grant P50 CA114747 (SSG) and 5R01CA119053 (Z.C.).

Signal Conditioning Technique for Position Sensitive Photodetectors

FWY Lau[1,2,3], P Reynolds[1,2,3], A Vandenbroucke[2,3], H Ho[1], CS Levin[1,2,3]
Departments of [1]Electrical Engineering, [2]Radiology, [3]MIPS, Stanford University, CA

When position sensitive photodetectors such as Position Sensitive Avalanche Photodiodes (PSAPDs) are used to read out pixelated scintillation crystal arrays, the flood histogram exhibits a non-linear, pin-cushion shape. This is due to the non-linear charge sharing occurring in the resistive sheet on the position sensitive detector. We present an electronic readout technique that allows the shape of the flood histogram and crystal identification capability to be manipulated while scaling the signal dynamic range to fit the dynamic range of the electronics. The technique involves adding a resistor on the four spatial channels of roughly the same resistance as the sheet resistance on the position sensitive detector. The technique also requires using an AC coupling capacitor in series with the preamplifier, where this AC coupling capacitor is selected to balance preamplifier noise and detector noise.

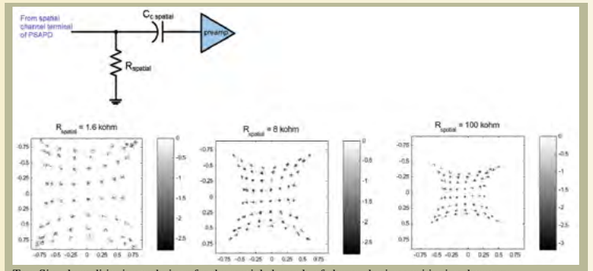

Top: Signal conditioning technique for the spatial channels of charge sharing positioning detectors.
Bottom: Experimental results. Flood histograms (in log scale) for different values of the extra resistor (Rspatial) added to scale the dynamic range. The Rspatial = 8 kohms case attenuated the signal without degrading the crystal identification ability.

This technique was verified and studied both experimentally and by simulation using PSAPDs coupled to 8x8 arrays of 1mm3 scintillation crystals. Results showed that the signal dynamic range could be scaled while controlling the pin-cushion distortion of the flood histogram and without degrading the crystal identification ability. The technique was implemented using digitally programmable circuits, resulting in a solution that facilitates dynamic adjustment of signal conditioning parameters based on process variations and real-time monitoring of variables, such as temperature and PSAPD gain.

References/Funding Source FWY Lau, PD Reynolds, A Vandenbroucke, H Ho, CS Levin, "Signal Conditioning Technique for Position Sensitive Photodetectors to Manipulate Pixelated Crystal Identification Capabilities," to be presented in IEEE Medical Imaging Conference and Nuclear Science Symposium, Oct 2011. Work funded by NIH grants R01 CA119056, R01 CA 119056-S1 (ARRA), R01 EB011552, DOD grant BC094158, the California Breast Cancer Research Program Dissertation Award 16GB-0060, and the Stanford Bio-X Fellowship.

Silicon Photomultiplier-based Detector Array for TOF-PET

JY Yeom[1], V Spandoudaki[1], CS Levin[1,2,3]
Departments of [1]Radiology, MIPS, [2]Physics, [3]Electrical Engineering, Stanford University, CA

Time-of-Flight (ToF) information in Positron Emission Tomography (PET) can contribute to a significant improvement in the reconstructed image signal to noise ratio, enabling image contrast improvement, a reduction in patient radiation dose, and/or shorter scan times

In this study, we propose a multi-element LSO-SiPM (Silicon photomultiplier) detector architecture, that reads out each element individually to maximize the time resolution performance. Two 4x4 SiPM detector modules were fabricated by tiling individual 3 mm SiPM elements (Hamamatsu MPPC). Each 4x4 SiPM array is readout with two edge-on preamplifier boards, each hosting 8 wideband 3 GHz bandwidth RF amplifiers (see figure). The temperature of each detector module is regulated by a Peltier cooler and all 32 SiPMs are individually biased through a 32-channel bias supply board. To assess the performance of these modules, single 3 x 3 x 5 mm3 and 3 x 3 x 20 mm3 LSO crystals were coupled to individual SiPMs of each detector module. The detectors were operated in coincidence and their signals were read out by a high speed oscilloscope. Measurements were performed in terms of linearity, energy and coincidence time resolution by irradiating the coincidence detectors with a 511 keV photon emitting Ge-68 source placed in-between.

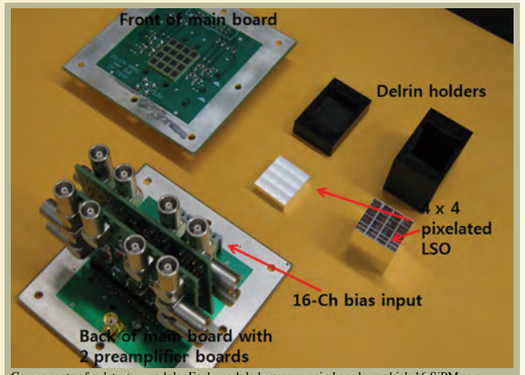

Components of a detector module. Each module houses a main board on which 16 SiPMs are mounted, two 8-ch preamplifier boards attached to the edge socket at the back of the main board to minimize trace distance, and the 5 and 20 mm length 4x4 crystal arrays that are covered with a light-tight Delrin holder.

A coincidence timing resolution of 240 +/- 2.3 ps (FWHM) was obtained at 71.5 V for the 5 mm length crystals and 350 +/- 3.1 ps (FWHM) at 71.7 V was achieved for the 20 mm length crystals.

These results verify that individual element readout for LSO-SiPM based detectors provides good timing performance for TOF-PET systems.

References/Funding Source Cygnus Fellowship

Algorithms for Multi-Interaction Photon Events in Sub-Millimeter CZT PET Detectors

G Chinn[1,2], CS Levin[1,2,3,4,5]
Departments of [1]Radiology, [2]MIPS, [3]Bioengineering, [4]Electrical Engineering, [5]Physics, Stanford University, CA

We are investigating a new cadmium zinc telluride (CZT) detector module with 0.5 mm^3 reconstructed spatial resolution for small animal PET and plant imaging. Inter-pixel scatter will occur in 75% of the detected events either degrading the spatial resolution or reducing the sensitivity if the events are discarded. CZT also has poor time resolution leading to reduced contrast because of a higher random coincidence rate. We will use the kinematics of Compton scattering to accurately position inter-pixel scatter events, so that these events can be used in the image reconstruction without degrading the spatial resolution. Further, we can estimate the incident photon direction from Compton kinematics to reject random coincidence photons. The performance of these Compton kinematic based algorithms are dependent on the geometric configuration of the detector. Therefore, we are investigating a new split-layer design and comparing it against a conventional detector geometry. We examined the contrast and contrast-to-noise ratio (CNR) of the reconstructed images and show up to a 64% improvement in contrast and 48% improvement in CNR over conventional energy weighted mean positioning and a time window for randoms rejection.

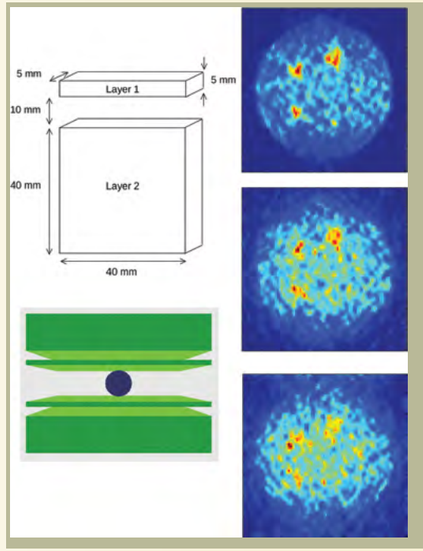

Left Column: (Top) A CZT detector module with two layers to increase the average distance between photon interactions in order to reduce geometric blurring. Each CZT crystal in a module is 5 mm width with the front layer 5 mm thick and back layer 40 mm thick; when arranged edge-on the module gives a 5 mm x 40 mm cross-section with respect to incoming photons and (Bottom) a 20 cm x 20 cm dual panel system comprising many dual-layer modules. Right Column: Reconstructed image slices for a simulated NEMA-2008 mouse phantom (30mm diameter) with a 2:1 activity ratio for the 1-5 mm dia. rods vs. the background and 5.2M total coincidence counts (83,000 counts per slice) (Top) Direction window to position and reject random coincidences with a contrast of 2.28±0.08 and a contrast/noise ratio of 2.13±0.14 vs. (Middle) Minimum photon distance positioning [1] and time window to reject random coincidences had a contrast of 1.64±0.11 and a CNR of 1.71±0.17 and (Bottom) Energy weighted mean positioning and time window to reject random coincidences had a contrast of 1.39±0.17 and a CNR of 1.44±.08.

References/Funding Source Submitted IEEE NSS-MIC 2011 This work was sponsored in part by Department of Energy grant DE SC0005290 and NIH grants R01 CA120474, R01 EB011552, and R01 CA119056

Single Ended Readout of Depth-of-Interaction in Scintillation Crystals for High Resolution PET

F Taghibakhsh[1], CS Levin[1,2]
Departments of [1]Radiology, MIPS [2]Electrical Engineering, Stanford University, CA

Incorporating photon depth-of-interaction (DOI) in PET image reconstruction improves image resolution,especially for high resolution applications such as organ specific or small animal imaging. We are investigating the performance of our novel DOI PET detector based on pulse height modulation with single-ended readout of scintillation crystals. The goal is to develop a less complex, cost-effective DOI detector technology. In the design under study, one end of each crystal element has a light absorbing coating to provide scintillation light absorption that varies with DOI; the other end has a sensor to measure the scintillation light. We experimented with a 4×4 array of 1×1×20 mm3 LYSO crystal elements, optically coupled to a position sensitive solid state photomultiplier (PS-SSPM). We observed that the DOI resolution varies from ~ 4.0 mm to ~ 8.0 mm (FWHM) along the crystals. The global energy and time resolution were measured to be 16.2% and 8ns (FWHM), respectively. Simulations of a PET system comprising 304 of these DOI detectors arranged on a 100 mm diameter detector ring were performed. We compared reconstructed images with and without DOI information based on the proposed single-ended light readout method. Results indicate that the proposed DOI detector improved spatial resolution such that, in contrast to non-DOI detectors, the single-ended readout DOI detector successfully resolved 20 µCi hot spheres of 2 mm diameter, placed 4 mm apart at 30 mm distance from the center of the FOV in the transversial direction. Compared to non-DOI and 2-layer DOI detectors, the proposed DOI detector achieved 110% and 31% better contrast resolution, respectively. The single-ended readout DOI detector based on pulse height modulation is compatible with standard PET detector configurations with photodetectors on only one end of the crystal array, and provides a cost effective DOI solution for high resolution PET applications.

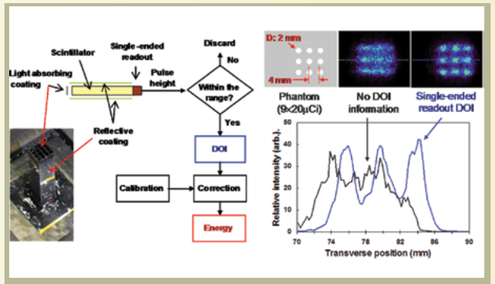

The light absorbing coating modulated pulse height based on DOI. Energy and DOI are extracted from pulse height & calibration data. (Bottom left) A 4x4 array of 1×1×20 mm3 LYSO crystals coupled to a position sensitive solid-state photomultiplier used for experiments. (Right) Simulated image reconstruction based on measured performance of single-ended readout DOI detectors indicated improved image resolution.

References/Funding Source 2011 World Molecular Imaging Congress & 2011 IEEE Medical Imaging conference. Natural Sciences and Engineering Research Council of Canada (NSERC).

Point Spread Function for PET Detectors Based on a Probability Density Function

E González[1,2], J-Y Cui[4], G Pratx[2] , PD Olcott[2,3], M Bieniosek[4], CS Levin[1,2,3,4,5]
[1]Stanford Molecular Imaging Scholars (SMIS) program, Departments of [2]Radiology, [3]BioEngineering, [4]Electrical Engineering, [5]Physics, Stanford University

We propose a new approach to calculate the Point Spread Function (PSF) for PET detectors based on the probability density function (PDF) of the line segment connecting two detector elements. Positron Emission Tomography (PET) events comprise the detection and positioning of pairs of oppositely directed 511 keV photons. The most significant blurring effect in PET is the considerable size of the detector elements, which causes uncertainty in the detected position of photons. Typically this physical blurring is modeled in the forward direction, following photons from the source to the detectors. This work presents an analytical framework for calculating this physical blurring, from the inverse approach, that is from the detector to the source. The kernel is derived from the parametrization of the line segment whose endpoints are random variables described by the intrinsic detector response function distribution. This kernel is calculated in a first order approximation, and when compared against a measured PSF profile yields less than 8% root mean square (RMS) differences. Also, from this kernel a PSF-FWHM function of the distance to the center of the scanner is derived. The ratio between the PSF-FWHM and the intrinsic detector resolution (FWHM0) agrees with the Monte Carlo simulations. For detectors whose intrinsic response functions are described by Gaussian profiles we calculated ratios 1/√2 and √5/8 at the center (R=0) and halfway from the center at (R=system-radius/2) respectively in agreement with published values of 1/√2 and 0.85; similarly for uniform (rectangular) profiles we get 1/2 and 3/4 which are equal to published values.

$$K(x) = \int_{-1}^{1}\int_{-\infty}^{\infty} w(t, x-\xi)\, p_{X_1}\left(\frac{\xi}{\frac{1}{2}(1-t)}\right) p_{X_2}\left(\frac{x-\xi}{\frac{1}{2}(1+t)}\right) d\xi\, dt \quad (1)$$

$$K(x) \approx \frac{1}{2}\int_{-1}^{1} w^{(0)}(t)\int_{-\infty}^{\infty} p_{X_1}\left(\frac{\xi}{\frac{1}{2}(1-t)}\right) p_{X_2}\left(\frac{x-\xi}{\frac{1}{2}(1+t)}\right) d\xi\, dt \quad (2)$$

(1) Probability Density Function (PDF) of the line segment with parameterization, X=1/2(1-t)X1+1/2(1+t)X2, pX1 and pX2 are the PDFs describing the intrinsic detector response functions.
(2) Approximation of (1)

References/Funding Source E González, J-Y Cui, G Pratx, PD Olcott, M Bieniosek, CS Levin, 2011 IEEE Nuclear Science Symposium and Medical Imaging Conference, Valencia Spain, November2011, High resolution & pre-clinical imaging instrumentation, techniques and systems, accepted This work is supported by NIH training grant R25CA118681

A New Data Path Design for PET Data Acquisition System: A Packet Based Approach

E Kim[1,2], PD Olcott[1,3], CS Levin[1,2,3,4]
[1]Departments of Radiology, MIPS, [2]Electrical Engineering, [3]Bioengineering, [4]Physics, Stanford University, CA

We are proposing a new data path design for Position Emission Tomography (PET) Data Acquisition (DAQ) systems . The proposed design can transmit, receive, and process all PET data through a single data stream. Instead of using separate paths for data, clock and control signals individually, which is the general case for conventional DAQ systems, the proposed system uses a packet concept to identify and process the various data types in a single fast data stream.

The proposed design increases flexibility during the design phase and enables efficient debugging, which is essential for scaling up channels in a DAQ system. New packets can easily be defined without changing the hardware. Debugging a specific board or a channel in a large system can be done efficiently by sending a packet to that board or channel requesting information.

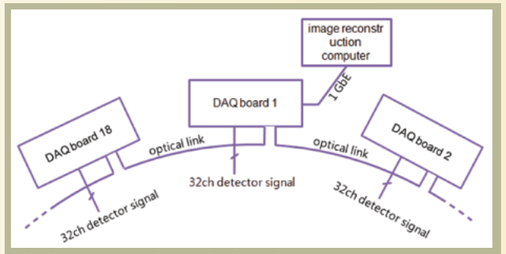

Daisy-chained data acquisition system (DAQ). DAQ board 1 to DAQ board 18, 18 boards are connected with single optical fiber each. This daisy chained system reduces interconnect problems during transmission of large positron emission tomography (PET) data.

We defined four different packet types to differentiate information in the data stream: singles packet, coincidence packet, configuration packet, and status packet. The length and overhead of these packets are optimized to increase overall throughput. We implemented the algorithm in a Xilinx FPGA board and partitioned the logic in a modular structure. The system consists of a high-speed network interface, a daisy-chain interface, an ADC interface, an ADC processor, a coincidence processor, an FSL interface, and an Ethernet interface. The coincidence processor can process single events up to 150M events/s and the ADC processor can receive new events locally up to 100M event/s. Coincidence events are sent to an image reconstruction PC with a throughput of more than 1M event/s.

References/Funding Source Part of the research is supported from the scholarship by TLi Inc.

Performance of an Electro-Optical-Coupled PET Detector for Time-of-Flight PET/MRI

MF Bieniosek[1,2], PD Olcott[2,3], CS Levin[1,2,3]
Departments of [1]Electrical Engineering, [2]Radiology, MIPS, [3]Bioengineering, Stanford University, CA

Combining PET with MRI in a single system provides clinicians with complementary anatomical and molecular information. However, current combined PET/MRI systems do not have time-of-flight (ToF)-PET capabilities due to certain design choices. We have developed an MRI-compatible front-end electronic system with fast timing capabilities for ToF-PET. Our approach employs a fast arrival time pickoff comparator to digitize the timing information and a laser diode to drive a fiber-optic cable to optically transmit timing information. The comparator and electo-optical link show 17ps +/- 0.2ps fwhm jitter in response to a fast digital pulse. When coupled with 3mmx3mmx5mm LYSO scintillation crystals and Hamamatsu MPPC silicon photomultipliers (SiPM), the comparator and electro-optical link achieved 283ps +/- 6.8ps fwhm coincidence time resolution using a Na-22 positron source, while maintaining detector energy resolutions of 15.0% +/- 1.7%, and 13.5% +/- 1.4% fwhm at 511keV

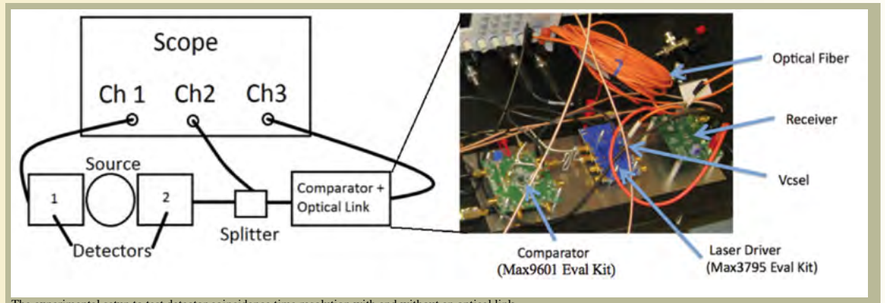

The experimental setup to test detector coincidence time resolution with and without an optical link.

References/Funding Source MF Bieniosek, PD Olcott, CS Levin, "Time Resolution Performance of an Electro-Optical-Coupled PET Detector for Time-of-Flight PET/MRI," to be presented in IEEE Medical Imaging Conference and Nuclear Science Symposium, Oct 2011. W. Noel Eldred Memorial Fellowship

Methods to enhance the sensitivity of simultaneous imaging of multiple PET isotopes

E González[1,2], PD Olcott[2,3], M Bieniosek[4], CS Levin[1,2,3,4,5]
[1]Stanford Molecular Imaging Scholars (SMIS) program, Departments of [2]Radiology, [3]BioEngineering, [4]Electrical Engineering, [5]Physics, Stanford University, CA

Multi-isotope PET (MIP) can distinguish the biodistributions of two simultaneously injected PET tracers,where one tracer has an isotope that is a pure positron emitter that generates two-photon coincidences,and the other emits a positron and a gamma ray in cascade yielding a triple coincidence. However triple coincidence detection suffers from very low sensitivity. This work presents a method to significantly enhance the sensitivity of triple coincidences for multi-isotope PET by adding an extra detector dedicated for the detection of the third prompt gamma in coincidence with the annihilation photons. We performed Monte Carlo simulations with Zr-89 and F-18 isotopes, and measurements with Na-22 and Ge-68. F-18 and Ge-68 are pure positron emitters; on the other hand, Zr-89 and Na-22 emit 909 keV and 1275 keV prompt gamma rays, respectively. For the simulations, a phantom was acquired in a simulated Siemens microPET R4 system with 8 cm diameter, 5 cm thick detector slab of BGO placed at one end of the system to increase detection efficiency of the third gamma ray. The simulations indicate a 3-fold increase in sensitivity with the extra detector added. For the measurements, we arranged two LYSO crystals coupled to Hamamatsu MMPC silicon photomultipliers (SiPM) s for the detection of 511 keV photons in coincidences and one large 8cm diameter, 2cm thick detector slab of LYSO coupled to a PMT dedicated for the detection of the 1275 keV gamma ray. The measured ratio of the triple-coincidence counts divided by the double-coincidence detection counts is 0.037±0.003, which compares well with the analytically calculated ratio of 0.042 estimated from intrinsic and geometric efficiency considerations. Furthermore, the 511 keV scintillation detectors were mounted on a linear stage that translated the detectors while acquiring double and triple coincidences counts simultaneously in order to generate one-dimensional profiles of the Na-22 and Ge-68 point sources. The triple-coincidence allows the distinction of the Na-22 point source profile from the standard 511 keV double-coincidence profile of the Ge 68 source.

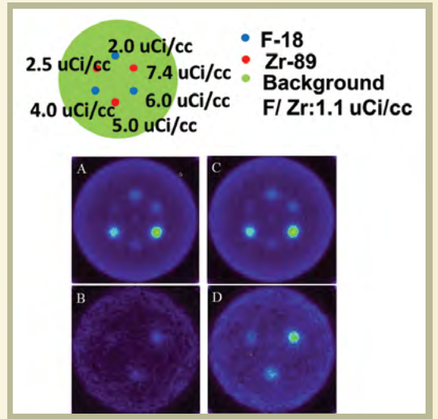

(A) Reconstructed image of annihilation photons only without the dedicated third gamma detector, (B) corresponding triple coincidence reconstructed image. (C) Annihilation photons reconstructed image with the dedicated third gamma detector, (B) corresponding triple coincidence reconstructed image. Notice the enhanced Zr-89 image quality when using the BGO dedicated third gamma detector.

References/Funding Source E González, PD Olcott, M Bieniosek, CS Levin, Society of Nuclear Medicine Annual Meeting, San Antonio Texas, June 2011, Scientific Poster Section: Instrumentation This work is supported by NIH training grant R25CA118681

Characterization of RF-transparent electro-optically coupled PET/MRI block detectors

PD Olcott[1,3], G Glover[2], CS Levin[1]
Department of Radiology, [1]MIPS, [2]RSL, [3]Bioengineering, Stanford University, CA

Objectives: We wish to make a MR compatible PET block detector that has little mutual effect between a PET and MRI system. The PET detector should use multiplexing to reduce the number of readout channels; finally, the MRI should be able to use a split transmit receive for MRI acquisition.

Methods: We fabricated two block detectors consisting of a 6 x 6 array of 2.1 mm x 2.1 mm x 20 mm LYSO crystals coupled to a 4 x 4 array of SiPM devices. The block detectors were Faraday shielded and powered using a battery. We characterized the coincidence flood histogram, energy resolution, and timing resolution for the block detectors in a 1.5T MRI. We designed the RF system to be able to transmit through the PET detector. We characterized the two detectors with and without RF body transmitter using split transmit and receive only coil for the MRI acquisition. We used a 3D gradient recalled echo (GRE) sequence to test for image artifacts, and a high duty cycle spin-echo pulse train to test for RF blanking and interference from the PET detector.

Results: We resolved all crystals in the 6x6 array with a 3.1:1 peak-sigma separation. We achieve a global delay corrected coincidence time resolution 2.55 +/- 0.051 ns FWHM and a per crystal gain corrected energy resolution of 15.5 +/- 0.7% FWHM @511 keV. There were no differences in spatial , energy or timing resolution when operating in the 1.5T field. The PET detectors did not saturate during RF transmit, and can be operated simultaneously with the RF transmitter. No MRI image artifacts were seen when transmitting using the RF body coils and receiving using a receive only 8-channel receive coil.

Conclusions: We have demonstrated a working PET/MRI block detector that is RF transparent, and has little mutual influence between MRI and PET.

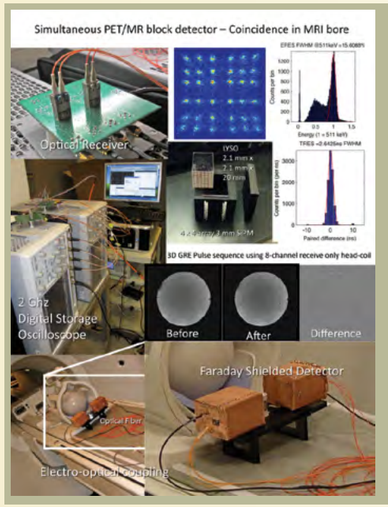

Characterization of a RF transparent PET/MRI compatible block detector that uses electro-optical coupling to couple the scintillation signals from a PET detector over multi-mode optical fibers. The PET detectors did not introduce and PET/MRI artifacts and had excellent energy , spatial, and timing resolution.

References/Funding Source Abstract #321, PD Olcott, et al, "Characterization of RF-transparent electro-optically coupled PET block detectors for simultaneous PET/MR imaging", Society of Nuclear Medicine, San Antonio, Texas, June 4 – 8, 2011 GE Industrial grant for PET/MRI SNM 2009 Pre-doctoral award

Studies of Electrode Design for a Sub-mm Resolution 3-D Position Sensitive CZT PET Detector

Y Gu, CS Levin
Deptartments of Electrical Engineering and Radiology, MIPS, Stanford University, CA

A 40×40×5 mm3 monolithic cadmium zinc telluride (CZT) crystal photon detector is being developed for a high-resolution small animal PET system with an 8×8×8 cm3 field-of-view (FOV). The detector employs a novel cross-strip electrode pattern capable of detecting the 3-D position of individual photon interactions to enable uniform 1 mm spatial resolution throughout the FOV as well as other advanced performance features. Through a series of 6 studies the CZT photon detector's charge collection efficiency and the spatial, time and energy resolution were experimentally determined as a function of the electrode pattern dimensions. This work presents generally applicable insights for all strip-electrode CZT photon detectors, and specifically the electrode dimensions and biasing details that optimize important PET performance parameters of the detector under development.

The detector studied employs a cross-strip electrode pattern with 100 μm wide anode strips on a 1 mm pitch, interspersed with steering electrodes of varying width that enhance anode charge collection. Cathode strips are oriented orthogonal to the anodes, with width and pitch of 3 mm or 5 mm. Because of the requirement of photon interaction positioning at sub-pitch resolution, 3 mm wide cathode strips were favored due to their finer structure. However, the higher charge sensitivity of 5 mm wide strips offered higher photon detection efficiency, and higher spatial resolution uniformity in the direction orthogonal to the electrode planes. 5 mm wide cathodes also offered a higher uniformity in coincidence time resolution (51.68 ± 19.53 ns), which varies with the photon interaction position. The detector charge collection efficiency is independent of the steering electrode width, but sensitive to the applied steering electrode bias. Complete charge collection occurred at -100 V relative to the anodes. Finally, for photon interactions depositing charge on two adjacent anode strips, steering electrodes of 400 μm width yielded the best photopeak energy resolution at 511 keV of 4.92 ± 0.31% FWHM.

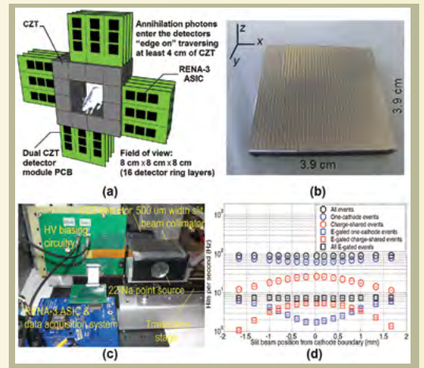

Subplots (a) to (d) show, respectively, (a) 3-D high-resolution small animal PET system with a 8×8×8cm3 field-of-view using CZT detectors, (b) anode face of the 40×40×5 mm3 cross-strip CZT detector, (c) collimated slit-beam experiment for characterizing the detector cathode response, and (d) photon detection efficiency (event count) of 5 mm wide cathodes as a function of collimated slit beam position.

References/Funding Source Submitted to Nuclear Science symposium and Medical Imaging Conference, 2011.This work was supported in part by NIH-NCI R01 CA120474.

All-optical encoding of PET detector signals

A Grant[1], P Olcott[1], CS Levin[1,2]
Departments of [1]Bioengineering, [2]Radiology, Stanford University, CA

Typical PET scanners use many electronic readout channels and dedicated electronic coincidence processing boards that contribute significantly to system complexity and costs. We have developed a method of optically encoding the position, energy, and arrival time of annihilation photon interactions in PET detectors with fast (150 ps FWHM) coherent optical pulse trains from telecommunications-grade lasers, and are developing a method of multiplexing all of the detector outputs in a PET scanner to a single optical fiber system output channel. This will allow the elimination of much of the currently used processing electronics, achieving coincidence time resolutions of <300 ps FWHM while decreasing system cost and complexity. We constructed a single channel proof-of-concept system using fast 10 Gbps off-the-shelf optical components and a silicon photomultiplier (SiPM) coupled to an LSO:Ce crystal. A custom PCB based on a fast comparator with adjustable threshold and hysteresis creates fast electronic pulses from the detector outputs. These electronic pulses are converted to optical pulses, and detector interaction information is encoded into precise delays between the pulses. Using this system, we demonstrated the encoding of photon position, energy, and arrival time into four coherent optical pulses. We measured extremely low timing jitter for the optical pulses (3 ps) and collected preliminary 22Na energy spectra (energy resolution 24.9% FWHM at 511 keV – not optimized yet) with all-optical pulse encoding. Optical encoding and multiplexing could greatly facilitate the construction of high resolution time-of-flight PET scanners with thousands of detector channels.

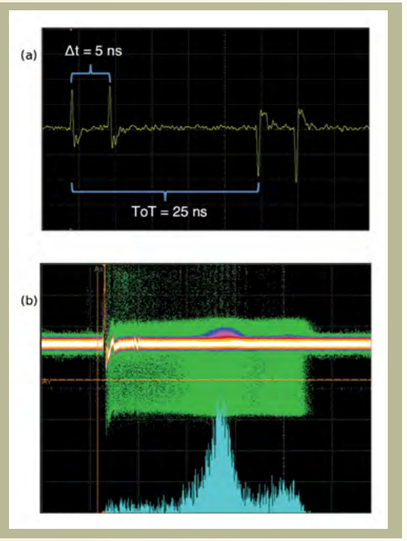

(a) Four-pulse train with characteristic channel identifying time Δt = 5 ns and ToT (time over threshold) of ~25 ns (x scale 5 ns/div). Each detector channel has a unique Δt value, allowing channel identification during data readout. Δt is created by splitting each optical channel into two arms, delaying one arm with a fiber loop, then recombining the two arms. Single event shown; ToT varies with pulse energy. The position of the first positive pulse gives the photon arrival time. (b) Energy spectrum (blue) of 22Na point source with LSO:Ce/SiPM, by measuring ToT from optically-encoded pulses. 511 keV peak visible in center. Green persistence plot shows the range of recorded ToT values between positive and negative pulses (x scale 10 ns/div). Energy resolution is 24.9% FWHM at 511 keV in preliminary (not optimized) system trials.

References/Funding Source NIH U54CA119367, Sub-Award; Stanford Bio-X

Data-Driven Spatially-Varying Point Spread Function for List-Mode PET Reconstruction on GPU

J Cui[1], G Pratx[2], S Prevrhal[5], B Zhang[5], L Shao[5], CS Levin[1,3,4]
Departments of [1]Electrical Engineering, [2]Radiation Oncology, [3]Radiology, [4]MIPS, Stanford University, CA; [5]Philips Healthcare, CA

We present a novel method to accurately model the spatially-varying point spread function (PSF) of a PET system reformulated for list-mode reconstruction on a graphics processing unit (GPU). The spatially-varying PSF for each LOR is modeled as an asymmetric Gaussian function whose variance changes asymmetrically according to the orientation of the line of response (LOR) and the voxel geometry. To fit the PSF parameters, a point source is imaged at twelve locations in a Philips Gemini TF PET system. To avoid tedious mechanical calibrations, the accurate point source location is estimated directly from the list-mode data. We introduce the "canonical sinogram" to enable reading out the sampled PSF directly from a stack of sinograms by exploring the rotational symmetry of the system matrix. The critical parameters for the PSF model are obtained by solving a convex optimization problem based on the measured point source data. The spatially-varying PSF is efficiently incorporated into the image reconstruction process on the GPU using the CUDA texture memory. The reconstruction algorithm incorporating the measurement-based shift-varying PSF takes 103 milliseconds per iteration to process a million LORs in a 75x75x26 image on a GeForce GTX 480 GPU, which is 190 times faster than a non-PSF implementation on a state-of-the-art central processing unit (CPU), and only 6.8% slower than a spatially-invariant fixed-width Gaussian kernel on the same GPU. Compared with reconstruction without PSF modeling, this shift-varying PSF reconstruction shows an average improvement of spatial resolution and contrast-to-noise ratio for point sources at the periphery of the field-of-view of 2.95±0.44% and 159.62±31.54%, respectively. Compared with reconstruction with a spatially-invariant PSF, the average improvements are 1.00±0.26% and 41.11±9.45%, respectively. These results indicate that the fast and accurate spatially-varying PSF reconstruction promises better resolution and contrast recovery with very small additional computational cost.

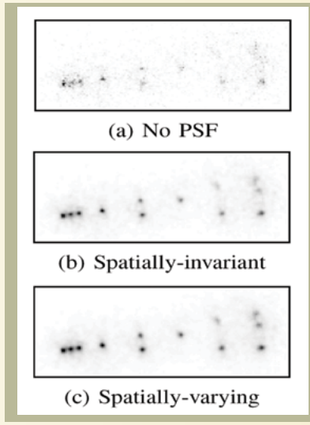

Reconstructed images from the whole point source data set with 10% true LORs and 90% randomly generated LORs artificially added to mimic background activity. Iteration 5 is chosen for all cases based on trade-off between contrast to noise ratio (CNR) and spatial resolution. Spatially-varying PSF yields an average improvement for spatial resolution and contrast to noise ratio (CNR) for the three point sources at the periphery of 2.95±0.44% and 159.62±31.54%, respectively. Compared with the spatially-invariant PSF case, the improvement is 1.00±0.26% and 41.11±9.45%, respectively, for the same parameters.

References/Funding Source This work was supported in part by a grant from Philips Healthcare and NIH grants R01 CA110956, ARRA R01CA119056-04S1, and R01 CA120474.

Evaluation of photon depth-of-interaction compensation for time-of-flight PET

V Spanoudaki[1], J-Y Cui[2], J-Y Yeom[1], CS Levin[1,2,3]
Departments of [1]Radiology, MIPS [2]Electrical Engineering, [3]Physics, Stanford University, CA

Time-of-flight (ToF) PET is a technique that reduces the positioning uncertainty of the emission point of 511 keV photons during PET data collection. The uncertainty is defined mathematically by a "kernel" or distribution of position along a system response line. Since photons are positioned more accurately along the system response lines, ToF information enhances the PET image signal-to-noise ratio (SNR), facilitating lesion detection and reduction of patient dose. 511 keV photons interact over a range of depths in the PET photon detectors (depth-of-interaction, DoI). We are currently developing a dual-head DoI-ToF prototype for experimental evaluation of the effects of DoI on ToF-PET performance. Two different DoI identification schemes, based on single-ended readout of one or multiple crystal layers, are under evaluation. We found from simulations and measurements that DoI information enables more accurate positioning of the ToF kernel and more precise estimation of the ToF kernel width. Experiments show the dependence of photon arrival time information on DoI. For variations in photon DoI over a 20 mm length scintillation crystal with rough surfaces, we experimentally observed a 15% degradation of the time resolution (ToF kernel width) and a 100% shift in the mean time difference (centroid of the ToF kernel) between coincident 511 keV photons along a given response line. These results were used to parameterize the ToF kernel information from every list-mode event using a second order polynomial of the DoI for each involved detector element. The effect on image quality is assessed by Monte Carlo simulations of a water phantom containing hot and cold spheres placed in a warm background with a 6:1 activity concentration ratio. We found that 2 iterations of the iterative image reconstruction algorithm optimizes the reconstructed image SNR for the various sphere sizes with and without DoI compensation.

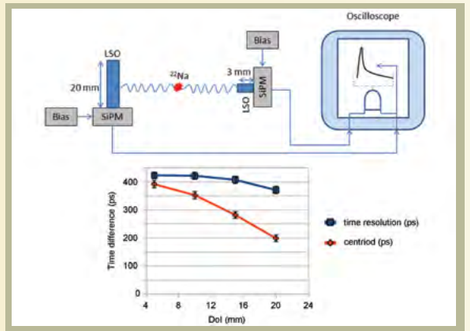

Top: Experimental setup to determine the dependence of time resolution on DoI for a 3x3x20 mm3 scintillation crystal. A 2x2x3 mm3 LSO crystal is used for electronic collimation of 511 keV photons emitted from the positron emitter (22Na). Bottom: Experimentally derived dependence of the coincidence time resolution FWHM (ToF kernel width) and the centroid of the coincidence time difference distribution (ToF kernel position) as a function of DoI along the 20 mm length scintillation crystal.

References/Funding Source AXA Research Fund Award

Study of Readout for Groups of PSAPDs Used in a 1 mm3 Resolution

PD Reynolds[1,2], A Vandenbroucke[2], F Lau[1,2], CS Levin[1,2]
Departments of [1]Electrical Engineering, [2]Radiology, MIPS, [3]Bioengineering, Stanford University, CA

We are developing a 1 mm3 resolution, high sensitivity PET system for breast cancer imaging. The system comprises two 16cm x 9cm x 2cm detector panels, each containing 2304 position sensitive avalanche photodiodes (PSAPDs) coupled to 8x8 arrays of 1mmx 1mm x 1mm LYSO scintillation crystal elements, for a total of 294,912 crystal elements. The LYSO-PSAPD detectors are multiplexed in pairs ("dual LYSO-PSAPD modules") to reduce the number of channels, resulting in 9216 channels per panel. The readout system has a modular data acquisition structure based on a 36-channel readout ASIC. This system design has multiple dual LYSO-PSAPD modules read out by a single ASIC, with each dual module having an adjustable high voltage bias and gain. This paper characterizes performance when small groups of dual LYSO-PSAPD modules are read out simultaneously.

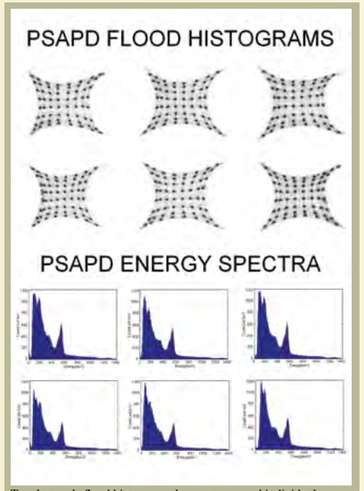

Top, log scale flood histograms demonstrate good individual crystal separation. Bottom, PSAPD energy spectra show the 511 keV peak and x-ray escape.

The multiple detector readout was tested with 3 dual modules connected to a single ASIC. The detectors are placed side by side, in a 3 x 2 array of position sensitive scintillation detectors. A Na-22 point source was used to generate 511 keV photons and irradiate the modules from a few centimeters above. List-mode single photon data was collected.

A similar setup was used to test the coincidence timing. Two independent data acquisition units were each used to read out 3 dual modules. A Na-22 point source was placed between two of the dual LYSO-PSAPD detectors to generate coincident 511 keV photons. The coincidence time difference was energy gated to be in the 511 keV peak and was corrected for per crystal position time delay and signal amplitude variations.

Data collected from 6 PSAPD detectors showed average global energy resolutions of 9.42±0.38% FWHM at 511 keV and a paired photon time resolution of 7.23±0.21 ns (4.74±0.02 ns unpaired) FWHM at 511 keV.

References/Funding Source Submitted for presentation at the 2011 IEEE Medical Imaging Conference, Valencia, Spain. NIH R01CA119056, R01CA119056-S1(ARRA), R33 EB003283, and R01CA120474.

Measuring 3D 511 keV Photon Interaction Locations in Position Sensitive Detectors

A Vandenbroucke[1], FWY Lau[2], PD Reynolds[2], CS Levin[1,2,3,4]
Departments of [1]Radiology, MIPS, [2]Electrical Engineering, [3]Bioengineering, [4]Physics, Stanford University, CA

Our objective is to construct high resolution PET cameras for breast and small animal imaging using a unique scintillation detector design that directly measures depth-of-interaction (DOI).

Our design employs detector modules comprising two 8x8 arrays of 1x1x1 mm3 LYSO crystals coupled to one Position Sensitive Avalanche Photo-diode (PSAPD) each, mounted on a common flexible circuit. Four of these modules were stacked together in a dedicated structure to form a 3-D positioning detector. Signals were routed over flexible cables to a discrete board housing signal conditioning electronics. The discrete board was connected to another board featuring a readout ASIC, ADCs and an FPGA. Data was collected using a 22-Na point source. The common signal of each PSAPD served as a trigger. When any module received a signal above a certain threshold, all 4 modules were read out.

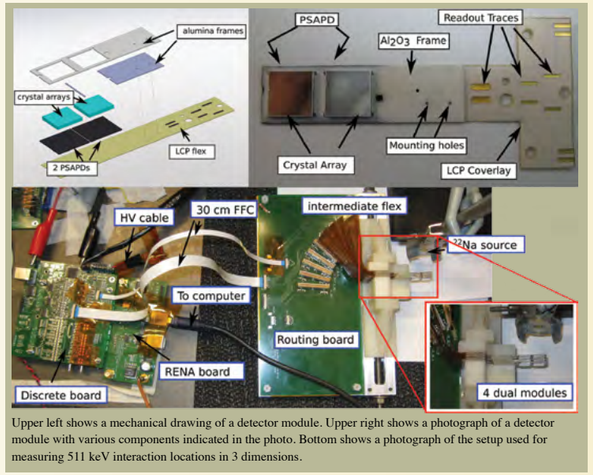

Upper left shows a mechanical drawing of a detector module. Upper right shows a photograph of a detector module with various components indicated in the photo. Bottom shows a photograph of the setup used for measuring 511 keV interaction locations in 3 dimensions.

Flood histograms show that all 64 crystal elements in each array are identified, with a global energy resolution of 18.1 +/- 0.1%. When limiting the data set to only contain hits with an energy falling within the photo-peak range in one particular module, and an open energy window in the other modules, we observed less than 2.5% hits in those other modules, indicating low electronic cross-talk and the ability to distinguish photo-electric interactions in different layers, thus enabling 3-D localization.

We also investigated multiple interaction events by considering events for which interactions occurred in multiple layers, with an energy deposition between 30 and 450 keV in each individual layer and a total deposited energy between 410 and 610 keV. We studied the occurrence of such events in different module layer combi-nations.

In conclusion, this paper presents the first experimental data from a scintillation detector capable of determin-ing the position of individual interactions in 3-D. The design shows low electronic cross-talk between layers and low noise per readout channel.

References/Funding Source Accepted for presentation at 2011 IEEE NSS-MIC Conference NIH Grants R01 CA119056, R01 CA119056-S1 (ARRA), DOD BC094158

Quantification of Inflammation in Inflammatory Bowel Disease by Molecular Ultrasound Imaging

N Deshpande[1], Y Ren[1], K Foygel[1], M Schneider[3], PJ Pasricha[2], JK Willmann[1]
Departments of [1]Radiology, [2]Gastroenterology, [2]Hepetology, Stanford University, CA; [3]Bracco Diagnostics

Inflammatory bowel disease (IBD) is a chronic relapsing and remitting inflammatory condition of the gastrointestinal tract that needs regular and accurate monitoring. The goal of our study was to assess the potential of molecular ultrasound (US) imaging using microbubbles (MB) targeted to the inflammation marker P-selectin (MBP-selectin) to quantify inflammation and to predict remission of inflammation following treatment in a chemically-induced colitis mouse model. Binding affinity and specificity of MBP-selectin was tested in a flow chamber under flow shear stress conditions (at 100 sec-1). In vivo binding specificity of MBP-selectin to P-selectin was tested in 10 mice with colitis (induced by rectal administration of TNBS) and in 10 control mice without colitis using non-linear in vivo US imaging (25 MHz). Furthermore, in vivo molecular US imaging signal in treated (n=6; prednisolone therapy) versus non-treated (n=6; saline only) mice was compared over 3 subsequent treatment days. Attachment of MBP-selectin was significantly (p=0.01) higher to P-selectin positive (stimulated by TNF-alpha) than unstimulated endothelial cells and compared to MBControl (p=0.003). Furthermore, attachment of MBP-selectin significantly (R2 >0.8, p=.01) correlated with expression levels of P-selectin on endothelial cells as quantified by flow cytometry. In vivo US signal of colitis was significantly higher (p=0.0003) with MBP-selectin compared with MBControl (Figure), and significantly (p=0.01) dropped by 53% following injection of blocking antibodies. In treated animals, in vivo US imaging signal significantly (p=.03) decreased during the course of treatment while in non-treated mice US signal in the colon wall remained elevated. In vivo US imaging signal significantly (R2 >0.6; p=.04) correlated with P-selectin expression levels as assess by ex vivo assays (WB and IF). In conclusion, molecular US using MBP-selectin allows non-invasive in vivo quantification and monitoring of inflammation at the molecular level in a chemically-induced colitis mouse model. This study lays the foundation for an eventual future clinical translation of molecular US imaging for monitoring inflammation in IBD.

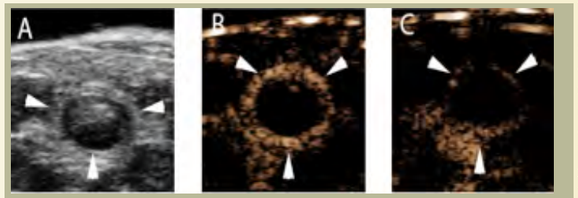

Figure. (A) Transverse B-mode image of the colon wall (white arrows) in a mouse with TNBS-induced colitis using a high-resolution US scanner. Molecular ultrasound imaging signal in colon wall (arrows) following injection of MBP-selectin (B) was significantly higher compared to control conditions following injection of MBControl (C), suggesting binding specificity of MBP-selectin to P-selectin in inflamed colon wall.

Longitudinal Assessment of Expression Levels of Tumor Angiogenic Markers with Molecular Ultrasound Imaging

N Deshpande, Y Ren, K Foygel, J Rosenberg, JK Willmann
Department of Radiology, Stanford University, CA

The purpose of this study was to evaluate molecular ultrasound (US) to non-invasively assess the temporal expression levels of three angiogenic markers, αvβ3 integrin, endoglin, and VEGFR2 on tumor vascular endothelial cells in vivo. Three types of targeted microbubbles (MBIntegrin, MBEndoglin, MBVEGFR2) were designed and the binding specificity of MB to their respective targets was tested on endothelial cells (positive and negative for angiogenic marker expression) under flow shear stress conditions (at 100 sec-1) in a flow chamber. In vivo molecular US imaging using the three different MB was performed at three different tumor stages (small, medium, large size) of three different subcutaneous tumor xenografts (breast, ovarian, pancreatic cancer) in mice (n=48) and was correlated with angiogenic marker expression levels as assessed by western blotting. Attachment of all three targeted MB was significantly (p=0.003) higher to positive than to negative cells and the attachment was significantly (p=0.026) decreased by blocking antibodies. The number of attached targeted MB significantly (R2>0.8, p=.0001) correlated with the expression levels of the angiogenic markers on cell lines as assessed by flow cytometry. For breast and ovarian cancer, endoglin expression was significantly higher than αvβ3 integrin (p=0.005) and VEGFR2 (p=0.0003) expression in small and medium tumors as assessed by in vivo US imaging. In contrast, in pancreatic cancer, αvβ3 integrin was highest in small tumors compared to endoglin and VEGFR2 (p=0.05) and endoglin expression peaked in medium and large tumors. In all tumors types, expression levels of all markers were lowest (p=0.005) in large tumors (Figure). In vivo US imaging signal significantly (R2>0.6; p<.05) correlated with ex vivo western blotting results for all three markers. In conclusion, molecular US imaging allows non-invasive assessment of the expression levels of different tumor angiogenic markers that vary during tumor growth in various subcutaneous human tumor xenografts. The results provide insights into tumor angiogenesis biology and may help in defining imaging targets for both early cancer detection and treatment monitoring using molecular US imaging.

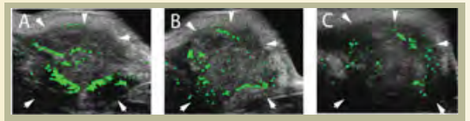

Transverse contrast-enhanced ultrasound images of a subcutaneous breast cancer tumor graft (arrows) in a nude mouse, imaged longitudinally at small (A), medium (B), and large (C) tumor sizes following intravenous administration of MBEndoglin. Endoglin expression (shown as green overlay on B-mode images) was highest at small tumor size and decreased at medium and large tumor sizes.

References/Funding Source 2010 World Molecular Imaging Congress, Kyoto, Japan. Oral presentation on Sept. 11, 2010. This work has been supported by the RSNA Seed grant RSD0809, the Howard S. Stern Research Grant of the Society of Gastrointestinal Radiologists, NCI ICMIC CA114747 P50 developmental grant, NIH R21 CA139279, the SMIS NIH fellowship program R25 CA11868, and the Canary Foundation.

A Novel Motion Correction Technique for Contrast-enhanced Ultrasound Imaging of Tumor Vascularity

MA Pysz[1], I Guracar[2], K Foygel[1], JK Willmann[1]
[1]Department of Radiology, MIPS, Stanford University, CA; [2]Siemens Medical Solutions, Mountain View, CA.

The purpose of our study was to develop and test a real-time adjustable motion correction algorithm for contrast-enhanced ultrasound (CEUS) imaging in human colon cancer xenografts in mice receiving vascular disruptive tumor treatment. A motion correction technique that measured horizontal and vertical B-mode pixel displacements using sum of absolute difference in a size- and location-adjustable tracking box, was incorporated into the software of a clinical US scanner (Sequoia Acuson 512, Siemens). Contrast-enhanced US imaging in the maximum intensity projection mode (14 MHz, MI=0.26) was performed on subcutaneous human colon cancer xenografts (implanted on backs of mice). Extent of tumor vascularity (expressed as % contrast area) was calculated in real-time with and without motion correction in tumors with different grades of vascularity (low, moderate, high; n=16), and in mice with (n=5) and without (n=5) treatment with a vascular disrupting agent (VDA). In moderately vascularized tumors, the effect of motion correction on the measured tumor vascularity was significantly (P<.001) higher (mean differences, 13.3% ± 2.3%) compared with tumors with low (mean differences, 3.2% ± 2.7%) or high (mean differences, 4.8% ± 2.5%) vascularity. The differences in tumor vascularity measurements with and without motion correction were also highest in animals taking a spontaneous deep breath when the tumors were moderately vascularized (mean differences, 25.4% ± 5.2%; Figure) compared to low (mean differences, 13.4% ± 7.2%) and highly (mean differences, 12.0% ± 10.0%) vascularized tumors. Following VDA treatment, tumor vascularity significantly (P=.003) decreased on motion-corrected images (51.7% ± 25.1% to 19.7% ± 11.4%), whereas vascularity minimally increased (P=.03) in non-treated mice (from 64.0% ± 15.4% to 70.7% ± 18.9%). In conclusion, the effects of real-time motion correction for CEUS imaging of tumor vascularity substantially depend on the grade of tumor vascularity and the extent of motion, and may improve CEUS imaging for treatment monitoring.

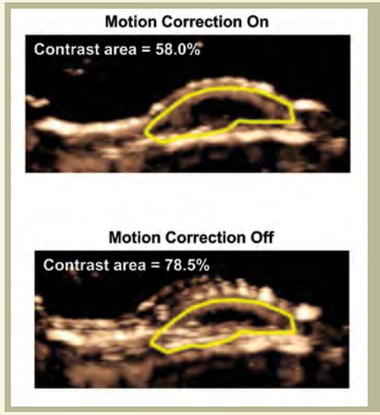

Subcutaneous human colon cancer xenograft imaged with contrast-enhanced ultrasound with (left) and without (right) novel real-time adjustable motion correction technique. Note substantial difference of measured tumor vascularity in mouse taking a spontaneous deep breath. A region of interest (yellow line) was placed to outline the tumor boundaries.

References/Funding Source 2010 World Molecular Imaging Congress, Kyoto, Japan. Poster presentation on Sept. 10, 2010. This work has been supported by the RSNA Seed grant RSD0809, the Howard S. Stern Research Grant of the Society of Gastrointestinal Radiologists, NCI ICMIC CA114747 P50 developmental grant, NIH R21 CA139279, the SMIS NIH fellowship program R25 CA11868, and the Canary Foundation.

Cationic and Neutral Microbubble and DNA Dose Effects on Ultrasound-mediated Gene Delivery In Vivo

C Panje[1], MA Pysz[1], DS Wang[1], Y Ren[1], M Schneider[2], JK Willmann[1]
[1]Department of Radiology, MIPS, Stanford University, CA; [2]Bracco Research, Geneva, Switzerland.

Ultrasound (US)-mediated sonoporation using contrast microbubbles (MB) is a promising strategy for therapeutic gene delivery. The purpose was to assess the influence of different MB and DNA doses on in vivo gene delivery to skeletal muscles in mice using novel cationic and neutral MB. Cationic and neutral MB were characterized for their charge and amount of bound plasmid DNA encoding Firefly luciferase (pFluc). Protective effects of cationic MB in binding DNA were tested by incubating pFluc-MB mixtures with DNase and assessing the extent of degraded DNA. US-mediated gene delivery of 4 μg pFluc to endothelial cells with 5E7 cationic or neutral MB was performed and quantified using the luciferase assay kit. US-mediated in vivo gene delivery to hindlimb skeletal muscle was performed with varying cationic and neutral MB (1E7, 5E7, 1E8, or 5E8 with 50 μg pFluc) or pFluc doses (10, 17.5, 25, 37.5, or 50 μg with 1E8 MB). Bioluminescence imaging was performed every 24h post-transfection to compare each dose and to negative control conditions (no MB or US). pFluc binding of cationic MB was significantly (P<0.01) higher and more protective to DNase degradation than neutral MB. Fluc activity using cationic MB was significantly higher both in cell culture (P<0.01) and in vivo (P<0.006) experiments and was significantly lower in negative controls (P<0.002). The magnitude of in vivo gene delivery using cationic compared to neutral MB increased linearly (R2=0.9) with the amount of bound pFluc (P<0.05). Cationic MBs bound with 10 μg pFluc (30% bound fraction) resulted in 3.4-fold higher gene delivery compared to neutral MB. In contrast, cationic MB mixed with 50 μg pFluc (6% bound fraction) resulted in only 1.3-fold higher gene delivery compared to neutral MB. US-mediated gene delivery is more efficient with cationic compared with neutral MBs when the fraction of bound DNA is maximized.

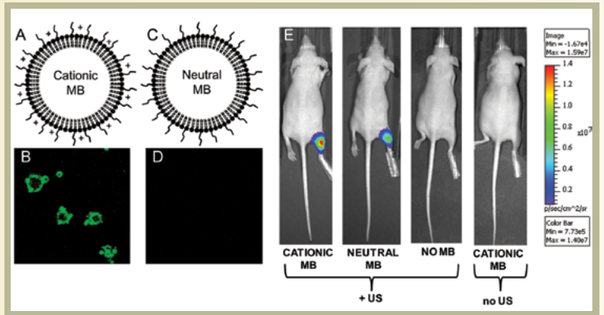

YOYO-1-labeled pFluc (green) binds to cationic (A) but not to neutral (C) microbubbles (MB) as evidenced by confocal microscopy (B, D). In vivo bioluminescence imaging of ultrasound-mediated delivery of 50 μg pFluc mixed with 1x108 MB demonstrates significantly higher imaging signal in skeletal muscles when using cationic versus neutral MB and compared to control conditions (no MB, no US). Differences between cationic and neutral MB was highest when the fraction of bound DNA was maximized.

References/Funding Source 2010 World Molecular Imaging Congress, Kyoto, Japan. Oral presentation on Sept. 11, 2010. This work has been supported by the RSNA Seed grant RSD0809, the Howard S. Stern Research Grant of the Society of Gastrointestinal Radiologists, NCI ICMIC CA114747 P50 developmental grant, NIH R21 CA139279, the SMIS NIH fellowship program R25 CA11868, and the Canary Foundation.

A Novel Paradigm to Markedly Enhance the Specificity of Gene Expression in Hepatocellular Carcinoma Using MicroRNAs

JA Ronald[1,2], RH Katzenberg[1,3], CH Nielsen[1,4], HJ Jae[1,3], LV Hofmann[1,3], SS Gambhir[1,2]
Department of [2]Radiology, [1]MIPS, [3]Interventional Radiology, Stanford University, CA; [4]Cluster for Molecular Imaging & Department of Clinical Physiology, Nuclear Medicine and PET, Rigshospitalet, University of Copenhagen, Copenhagen, Denmark.

In cancer gene therapy potent, tumor-specific expression is of utmost importance to improve outcome and ensure safety. Tumor-specific promoters may be used but often promote weak tumor and "leaky" non-tumor expression. Hence, novel strategies for specific, yet robust, expression are needed. MicroRNAs (miRNAs) are short, endogenous RNAs that inhibit translation by binding to complementary sequences (miRTs) in target mRNAs. Here we explore the ability to achieve the coveted tumor-on/liver-off expression profile in a rat hepatocellular carcinoma (HCC) model by engineering potent vectors regulated by miRNAs. The levels of 11 miRNAs downregulated in human HCC were compared in both rat HCC (n=5) and liver (n=8) by qRT-PCR. 7 miRNAs were reduced (p<0.05; range 3 to 16-fold) in rat HCC including, miR-26a, miR-101a, miR-122, miR-125a-5p, miR-125b, miR-139-5p and miR-150. The robustness of miRNA repression in vitro and in vivo was explored by constructing 3 vectors all expressing firefly luciferase (Fluc2) driven by the strong CMV promoter (pcDNA3.1) either with no miRTs (pCMV-Fluc2), or 4 tandem sense or 4 anti-sense miRTs (miRT and anti-miRT, respectively) for the liver-specific miR-122 inserted in the 3' untranslated region. HUH-7 (miR-122 +ve) cells were transfected and Fluc2 activity 24 hours later was decreased ~80% (p<0.05) for the miRT versus the 2 control vectors. Each vector was then hydrodynamically injected via the tail-vein of Balb/c mice (n=3 per group) to assess the degree of repression in liver. Importantly, average radiance (p/sec/cm2/sr) in bioluminescent images taken 48 hours post-injection was markedly reduced (~100-fold; p<0.05) with the miRT (4.7e6 ± 5.2e5) versus the control vectors (pCMV-Fluc2=4.1e8 ± 1.0e8; anti-miRT=3.2e8 ± 1.8e8) (Figure). Based on these exciting results current work focuses on generating additional vectors regulated by one or more miRNAs and expressing a reporter gene fused to a therapeutic gene for testing in tumor-bearing rats. This is the first work to explore the use of miRNAs to control transgene expression in HCC and should have broad applicability for other cancers and imaging across cell lineages.

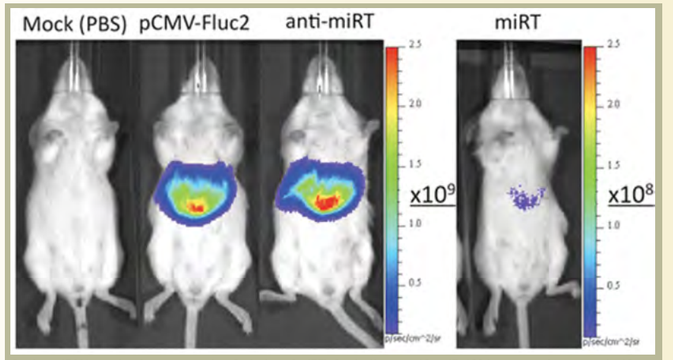

In vivo miRNA-regulated gene expression. Inclusion of miRTs for the liver-specific miR-122 into expression vector significant reduces (by approximately two log-orders) Fluc2 liver activity following hydrodynamic delivery in mice.

References/Funding Source Presentation Number 0193 Scientific Session 25: Gene Expression and Reporters September 11, 2010 / 10:00-10:15 / Room: D

Imaging of Vascular Progression Within a Lymph Node in a Lymphoma Mouse Model

K Ito[1], BR Smith[1], N Parashurama[1], C Miething[2], S Lowe[2], SS Gambhir[1]
[1]Department of Radiology, MIPS, Stanford University, CA; [2]Cold Spring Harbor Laboratory, Cold Spring Harbor, NY, USA.

Non-Hodgkin's Lymphoma is a heterogeneous disease with significant mortality. Data we have accumulated indicates that angiogenesis plays an important role in the genesis of lymphoma. We reasoned that intravital microscopy (IVM) could be used to assess the vascular progression of lymphoma in mouse models. We utilized a model of lymphoma in which tail vein-injected murine lymphoma cells undergo homing to the inguinal lymph node. Two types of murine lymphoma cell lines, p53 -/- (Doxorubicin (DOX) and Cyclophosphamide (CTX) resistant: IC50= 46.2nM and 84.1μM, respectively) and ARF -/- (DOX and CTX sensitive: IC50= 3.5nM and 10.0μM, respectively) were used. We tail-vain injected 1×106 cells of both groups and PBS as a control into C57BL/6 mice (p53-/- and ARF-/-: N=4, cont.: N=3). On the day of imaging, the inguinal lymph node was exposed by creating a tissue flap. IVM image stacks of blood vessels (using a near infrared intravascular dye) within the inguinal node were obtained and inguinal lymph node size was measured at days 0, 7, 14, and 21 after injection and analyzed using Image J software. We furthermore developed a lymph node window chamber in order to serially image vascularlization within the lymph node. We identified that micro vessel number and circulating dye intensity in the inguinal lymph node were significantly higher in p53-/- cell-injected mice compared to ARF-/- cells and control mice at day 7 ($p<0.01$). Mean vessel length was significantly longer in both p53-/- cells and ARF-/- cells-injected groups compared to control mice at day 7 (cont. vs. p53-/- $p<0.001$, cont. vs. ARF $p< 0.05$). At days 14 and 21, vessel growth was higher in both groups compared to control. There is no significant difference in inguinal lymph node size between p53-/- cells and ARF-/- cells-injected mice. These data indicate that inguinal lymph node imaging in an orthotopic murine lymphoma model using IVM is a powerful tool for elucidating unprecedented detail in lymphoma development.(KI and BS contributed equally.)

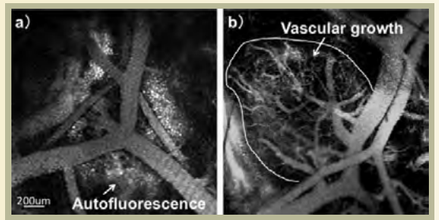

Intravital Microscope (IVM) Images in the Inguinal Lymph Node of a Living Mouse. a) Control mouse. Day7 after injection of PBS. b) Day 7 after injection of p53-/- lymphoma cells. Enhanced angiogenesis is significantly higher in panel b) as compared to panel a).

References/Funding Source Presentation Number 1001B Poster Session 3d: Imaging Disease/Organ Processes September 10, 2010 / 15:15-16:45 / Room: Exhibit Hall. PS-OC Grant

Affibody-Functionalized, Multimodal Raman/Fluorescence Nanoparticles for Biomarker Profiling and Tumor Imaging

JV Jokerst[1], Z Miao[1], C Zavaleta[1], CT Chan[1], Z Cheng[1,2], SS Gambhir[1,2]
Departments of [1]Radiology, MIPS, [2]Bioengineering, Bio-X, Stanford University, CA

Surface enhanced Raman spectroscopy (SERS) nanoparticles (NPs) offer picomolar sensitivity and extensive multiplexing in vivo. While these NPs' photo-physical properties are established, their use as biological probes requires further efforts. Here we report targeted hybrid NPs with tunable, multiplexed SERS signal, NIR fluorescence for high throughput cell assays, and selective binding to the cancer markers epidermal growth factor receptor (EGFR) and αvβ3 integrin. The NPs contain a gold core/silica shell functionalized with affibodies—an intriguing ligand for molecular imaging purposes due to its small size, high affinity, and capacity to be rapidly reprogrammed to different biomarkers. These affibodies coat NPs via a hetero-bifunctional, PEG-based linker with controlled synthesis resulting in ~200 ligands per NP. The SERS NPs are optimized in cell culture via the fluorescence mode. For NP with EGFR-specific affibodies incubated with A431 cells, 6.3-fold greater signal was observed by flow cytometry versus isotype control NPs and 55-fold greater signal than non-targeted NPs. Blocking studies with free affibody ("cold probe"), followed by the targeted NP, decreased signal by 7.3-fold. NP detection in vivo after sub-cutaneous injection yielded detection limits of 30 pM and 6 pM via fluorescence and Raman, respectively. Next, the bioconjugated NPs labeled EGFR on A431 tumors excised from Nu/Nu mice. The SERS signal via EGFR-targeted NPs was 11 times higher than unlabeled particles ($n = 3$; $p< 0.05$). Tumors blocked with unlabeled affibody produced signal 6 times lower ($n = 3$; $p< 0.08$). Alternatively, the αvβ3 integrins in U87MG cells were labeled via NPs with IgG antibody. Integrin signal (targeted NPs) to background (bare NPs) ratios of 25:1 and 13:1 were obtained for the particles via SERS and fluorescence, respectively. To the best of our knowledge, this is the first demonstration of affibody ligands deployed in tandem with multimodal SERS nanoparticles for biomarker identification. These results suggest that full utilization of SERS NPs will have significant potential for applications in living subjects.

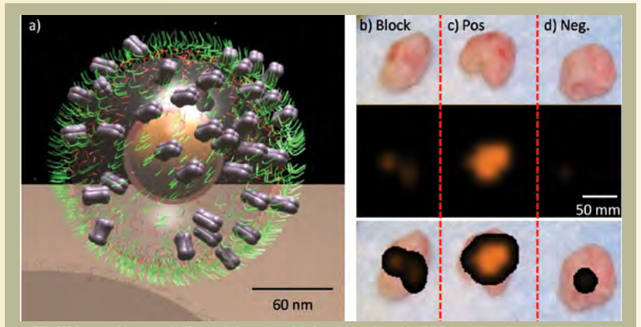

a) The NP has a gold core and silica clad, fluorescent label (red), passivated by PEG (green), and covalently coated with EGFR-specific affibody (purple). This probe labeled A431 tumors ex vivo: b) tumor is blocked with free affibody prior to staining, which decreases Raman signal; c) EGFR labeling by NPs as indicated by Raman signal; d) untargeted NPs producelow non-specific binding.

References/Funding Source Presentation Number 0928A Poster Session 2c: In Vivo Studies & Development/Novel Use of Imaging Probes September 9, 2010 / 15:15-16:45 / Room: E National Cancer Institute CCNE U54CA119367, In Vivo Cancer Molecular Imaging Centers ICMIC P50 CA114747, SMIS Program R25-T CA118681.

Evaluation of a PET Antibody Tracer for Monitoring Lymphoma Therapy in a Humanized Transgenic Mouse Model

A Natarajan[1], G Gowrishankar[1], CH Nielsen[1,3], S Wang[1], N van Bruggen[4], SS Gambhir[1,2]
Departments of [1]MIPS, Radiology, [2]Bioengineering, Bio-X, Stanford University, CA; [3]Cluster for Molecular Imaging & Department of Clinical Physiology, Nuclear Medicine and PET, University of Copenhagen, Rigshospitalet, Denmark; [4]Biomedical Imaging, Genentech, South San Francisco, CA

Positron emission tomography (PET) tracers offer a broad spectrum of clinical applications in oncology, including improved tumor diagnosis, staging, surveillance, monitoring of antitumor therapy, and tumor tissue characterization. Aim: To radiolabel and image in preclinical models an antibody based PET tracer, 64Cu-DOTA-Rituximab (Rmab). Method: The 64Cu was chelated to DOTA-NHS linked Rituximab. QA of the radiotracer was established by HPLC, sterility, and in vitro live cell uptake assay. To validate the study multiple radiolabeling and imaging experiments were carried out in three groups of mice; two groups of mice had huCD20 transgene (CD20TM) that expresses the human CD20 on their B cells. The study groups of mice are as follows; a) control (nude mice, n=2) received Rmab 200μCi/dose, b) negative (CD20TM, n=2): received 2mg/kg pre-dose of cold Rituximab prior to 2h of Rmab dose of 200μCi, and c) positive (CD20TM, n=2): Rmab alone 200μCi/dose. Small animal PET was used to image mice at various time points (0, 1, 2, 4, 24, 48, and 72h) after tracer injection. AMIDE software was used to analyze the images. Results: QA of the Rmab was: DOTA/antibody (>1), specific activity (75-125 μCi/μg), radiochemical yield (>80%), and purity (>98%). The Rmab immunoreactivity was >80% and sterile. At 24h, Rmab uptake (% ID/g) by spleen and liver of CD20TM were (mean ± STD): spleen uptake by negative and positive groups was 1.76 ± 0.006 % and 16.5 ± 0.713% (p value < 0.011); and liver uptake by negative and positive groups was 0.41 ± 0.088% and 0.55 ± 0.112% (p value < 0.153). Figure 1 μPET/CT image shows the specific uptake of Rmab in mice, compared to the liver the spleen specific uptake of Rmab is ~15 times high due to the expression of huCD20. Conclusion: We have optimized and validated Rmab radiochemistry and PET imaging in mice for clinical translation to applications in lymphoma patients.

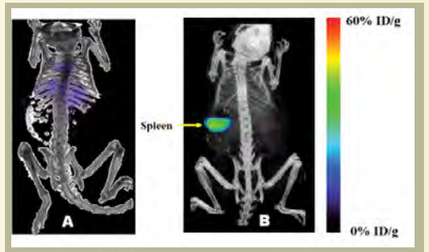

The small animal PET-CT transgenic mice images show after tracer injection of 64Cu-DOTA-rituximab (200μCi/2μg) at 24h: Figure A) received rituximab pre-dose of 2mg/kg 2h prior to tracer injection; B) mouse received only tracer no pre-dose. Figure B shows the specific uptake of tracer in the spleen where huCD20 expressing B cells.

References/Funding Source Presentation Number 1044A Poster Session 2d: Imaging Disease/Organ Processes September 9, 2010 / 15:15-16:45 / Room: Exhibit Hall. Genentech, South San Francisco, CA; ICMIC-P50 CA14474

Preliminary Intravital Microscopic Analysis Reveals Macrophage Uptake of Circulating Nanotubes and RGD-dependent Delivery into Tumor

BR Smith[1], H Rallapalli[1], J Prescher[1], C Zavaleta[1], J Rosenberg[1], Z Liu[2], H Dai[2], SS Gambhir[1]
Departments of [1]Radiology, MIPS, [2]Chemistry, Stanford University, CA

Molecular targeting of nanoparticles (nps) is known to increase tumor uptake, but is believed to do so via a direct np ligand-receptor binding mechanism. It is also well-known that macrophages (macs) tend to accumulate in tumor. The present work unexpectedly suggests that circulating macs can be programmed by molecularly-targeted nps to increase preferential deposition into tumor. We used intravital microscopy (IVM) to visualize U87MG tumor (EGFP) in a dorsal window chamber mouse model (n=25 mice) as we IV injected single-walled carbon nanotubes (SWNTs) conjugated to cy5.5 dye. In real time, we visualized uptake of SWNTs into circulating macrophages (identified via flow cytometry) and their behavior within tumor interstitium. We also used the intrinsic Raman signature of SWNTs to quantify overall tumor uptake. SWNTs were conjugated to RGD which binds integrin αvβ3 RAD peptide and unconjugated SWNTs (plain) were controls. We observed rapid uptake (< 1 min) of SWNTs into macs with plain SWNTs, compared with several hours for peptide-conjugated SWNT uptake. Macs observed in vasculature were categorized as 1) non-interacting (free-flowing) 2)interacting cells (crawling along the luminal surface). At one day p.i., we observed more non-interacting macs containing plain SWNTs than those with RAD, and more RAD than RGD ($p=0.0001$). However, interacting macs displayed the reverse trend (0.0057), suggesting that having peptides linked to SWNTs encouraged mac interaction with the endothelium. Last, across the first week p.i., we found more non-interacting macs in the plain condition than in the RGD-SWNT condition ($p<0.0001$), with no difference between RAD and plain SWNTs. We observed (1) SWNT-laden macs in tumor interstitium and (2) total SWNTs in tumor increased over the first week p.i. for RGD/RAD, but only for the first 3 days p.i. for Cy5.5. Together with the above results, the data imply SWNT delivery into tumor via the mac "Trojan Horse." Our data thus indicate that RGD may encourage not only typical np ligand-recptor binding routes, but also indirect uptake into (and perhaps on the surface of) macrophages. These RGD-SWNT laden macrophages appear to be preferentially taken up into tumor compared with SWNTs without RGD. In conclusion, these results could (1) lead to improved np design to increase mac delivery, (2) transform non-specific tumor macs into specific delivery vehicles, and (3) may explain the high tumor uptake displayed by SWNTs.

References/Funding Source Presentation Number 0091 Scientific Session 9: Tracking Immune Cells September 9, 2010 / 13:15-13:30 / Room: B-2

Dual Wavelength Imaging of a Novel Activatable Photoacoustic Probe

J Levi[1], SR Kothapalli[2], TJ Ma[3], B Khuri-Yakub[3], SS Gambhir[2,1]
Departments of [1]Radiology, Canary Center at Stanford; [2]MIPS; [3]Electrical Engineering, Stanford University, CA

Photoacoustic tomography has the capability of providing images of high spatial resolution and high contrast at depths up to 5 cm. As the breadth of application for this modality grows, so does the need for probes with high specificity. We report here the design, synthesis and evaluation of an activatable probe that shows great promise in providing highly specific photoacoustic images. Before the activation by its target, matrix metaloprotease MMP-2, the probe, an activatable cell penetrating peptide labeled with two different chromophores, shows photoacoustic signal of similar intensity at the two wavelengths corresponding to the absorption maxima of the chromophores. After the cleavage, the dye associated with the cell penetrating part of the probe accumulates in the cells, resulting in photoacoustic signal seen only at one of the wavelengths. The subtraction of the photoacoustic images at two wavelengths reveals the location of the cleaved probe only, as the signals at two wavelengths for the non-activated probe cancel out. To evaluate our approach towards smart photoacoustic probes, we have incubated human fibrosarcoma cells, HT 1080, with three probes: non-activated, MMP-2 specific probe, BHQ3-ACPP-Alexa750; non-activated, MMP-2 non-specific probe, BHQ3-CPP-Alexa750; and cleaved probe BHQ3-CPP. The uptake of the cleaved probe was clearly distinguished from the accumulation of both non-activated probes by subtracting the photoacoustic images taken at two wavelengths corresponding to the absorption maxima of the two chromophores used, BHQ3(675nm) and Alexa750(750nm) (Figure 1 d,e). A great utility of our probe in combination with dual wavelength imaging lies in the possibility of detection of the cleaved probe in the presence of the high levels of non-activated probe, a challenging task to attain in an absorbance-based modality. This method could prove useful in pre-clinical models, photoacoustic guided surgical interventions, treatment efficacy evaluations, as well as many other applications.

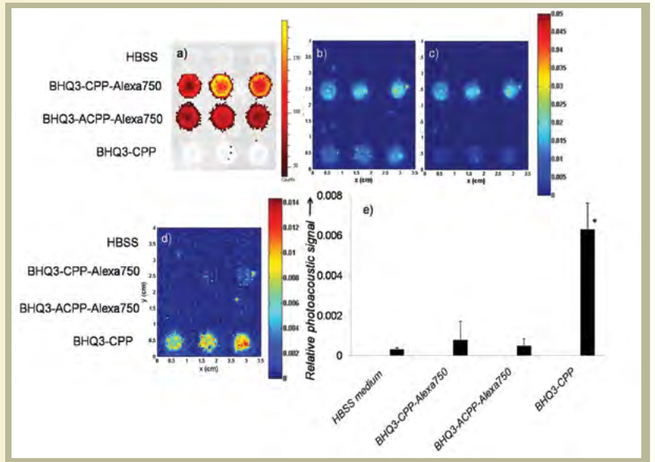

Photoacoustic imaging of the smart probe accumulation in cells. HT1080 cells were incubated with 150 µL of 10 µM solution of BHQ3-CPP-Alexa750, BHQ3-ACPP-Alexa750 or BHQ3-CPP for 10 minutes and embedded in triplicate in an agar phantom. (a) Fluorescence image (λα 675 nm, ICG emission filter) of the agar phantom shows location of the cells as well as the uptake of BHQ3-CPP-Alexa750 and BHQ3-ACPP-Alexa750. Photoacoustic images of the agar phantom with embedded cells taken at two wavelengths: 675 nm (b) and 750 nm (c). Subtraction of the images taken at 675 nm and 750 nm resulted in an image with distinct signal coming from the cells incubated with the cleaved probe, BHQ3-CPP (d). The accumulation of different probes in the cells was quantified from the subtraction image using mean photoacoustic values for each well (e). Errors bars represent the standard deviation of themean of triplicates. Accumulation of BHQ3-CPP probe was significantly different ($p<0.05$) from the accumulation of both BHQ3-ACPP-Alexa750 and BHQ3-CPP-Alexa750. Colors bars represent relative photoacoustic signal intensity.

References/Funding Source Presentation Number 0805B Poster Session 3c: In Vivo Studies & Development/Novel Use of Imaging Probes September 10, 2010 / 15:15-16:45 / Room: E

Comparison of 18F-FDG and 18F-FLT small-animal PET imaging in an orthotopic glioblastoma mouse model

E Mittra[1], H Fan-Minogue[1], FI Lin[1], V Sriram[2], S Medicherla[2], SS Gambhir[1,3]
Departments of [1]Radiology, Nuclear Medicine, [3]Bioengineering ,Stanford University, CA; [2]Merck Research Laboratories, Palo Alto, CA

Objectives: Pre-clinical orthotopic models of glioblastoma are important for the development of novel therapies. Non-invasive methods to assess response to therapy that can also be used in the clinic are favored, but currently limited. We investigate the utility of 18F-FDG and 18F-FLT small-animal PET in an orthotopic glioblastoma model in mice, using bioluminescence (BLI) as a reference. Methods: Fifteen 9 week-old nude mice (7 FDG; 8 FLT) were injected with 3x10^5 U87 MG-Luc2 cells directly into the right subcortical region. BLI and FDG or FLT PET were performed on these mice weekly for 5 weeks using dedicated small animal imaging apparatus. Region of interest (2D) analysis was used to calculate the photon flux per area (p/s/cm2/sr) and mean percent injected dose per gram (%ID/g), respectively. The BLI and PET signals were compared to assess their relative utility. Results: There was a steady increase in the BLI signal over the course of 5 weeks (Table). Both visually and quantitatively, FLT PET provided a better signal to background ratio than FDG PET within the brain ($P = 0.01$; Figure). The FLT signal was appreciable when the BLI signal reached ~3x10^7 which occurred 4 weeks post-implantation. The FDG signal never rose significantly above background levels in the brain. Conclusions: Orthotopic implantation of glioblastoma cells in the mouse brain is feasible and can be imaged non-invasively. BLI is much more sensitive than PET, but FLT PET can be successfully used for this application while FDG PET is not suitable. Subsequent work will evaluate the ability of these models to assess response to therapy.

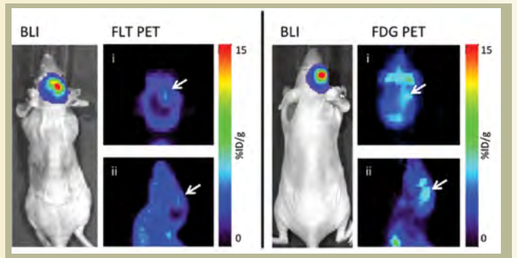

Whole-body BLI and small animal PET images of the head (coronal (i); sagittal (ii)) showing tumor (white arrows) visibility at 4 weeks. Both mice shown have similar luminescence of 4x10^7 p/s/cm2/sr. The FLT signal is clearly visible above background while the FDG signal is not. Average and standard deviation (SD) of BLI, FLT PET, and FDG PET signals among all mice over 5 weeks post-implantation.

References/Funding Source Presentation Number 1016B Poster Session 3d: Imaging Disease/Organ Processes September 10, 2010 / 15:15-16:45 / Room: Exhibit Hall

Use of Tumor Targeted Raman Nanoparticles for Early Detection of Colon Cancer in Conjunction with a Newly Developed Raman Endoscope

C Zavaleta[1], JV Jokerst[1], JT Liu[2], MJ Mandella[2], E Garai[1,2], J Hardy[2,4], C Contag[1,2], SS Gambhir[1,3]
Departments of [1]Radiology, [2]Pediatrics, [3]Bioengineering, [4]Microbiology and Immunology, Stanford University, CA

We have recently developed a new clinical imaging strategy utilizing a customized Raman endoscope in conjunction with locally administered tumor targeting Raman nanoparticles, to be applied during routine colonoscopy. This strategy could offer a new way to sensitively detect and characterize dysplastic flat lesions, which often go undetected within the colon using conventional white light endoscopy. In this study, we evaluated the ability of our surface enhanced Raman scattering (SERS) gold nanoparticles to effectively target fresh human colon cancer tissue after being covalently conjugated with a heptapeptide (VRPMPLQ) sequence previously shown by our group to bind to dysplastic colonocytes in humans. Fresh human colon tissue samples, both malignant and normal adjacent tissue (NAT), were provided to us through our hospital's tissue bank. Tissue sets (malignant and NAT) from each patient (n=4) were analyzed independently. Each of the malignant and NAT samples were cut into two pieces where one was exposed for 10 min to SERS nanoparticles (0.05 nM) conjugated with the tumor targeting (+) heptapeptide sequence and the other SERS nanoparticles (0.05 nM) conjugated with a (-) random heptapeptide sequence (control). The tissue samples were then rinsed with 3% bovine serum albumin for 5 sec and mapped luminal side up using Raman spectroscopy to evaluate binding. Raman imaging revealed a consistent trend where more binding of (+) heptapeptide SERS nanoparticles was seen in malignant versus NAT samples, with an average of 4 times more signal in malignant versus NAT samples of the (+) heptapeptide SERS conjugated nanoparticles. Within the malignant tissue samples themselves, there was also 2 times more signal of the (+) heptapeptide SERS nanoparticles versus the (-) random SERS nanoparticles. These results support the idea of using these heptapeptide labeled SERS nanoparticles as clinical tumor targeting beacons for the early detection of colon cancer in conjunction with our newly developed Raman endoscope.

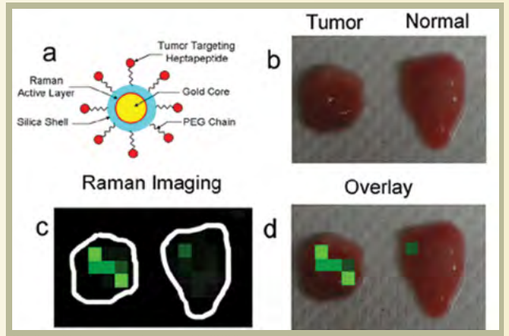

Binding efficiency of (+) heptapeptide SERS nanoparticles on tumor vs. normal human colon tissue. A) Schematic of SERS nanoparticles conjugated with tumor targeting heptapeptide. B) Digital photo of malignant tumor tissue and normal adjacent tissue. Each tissue was exposed to (+) heptapeptide SERS nanoparticles for 10 min. c) Raman image of the tissues using our Raman mapping system. D) Overlay of Raman intensity map over digital photo of fresh tissue samples. Notice the increased binding of the (+) heptapeptide SERS nanoparticles throughout the entire tumor tissue as opposed to the decreased localized non-specific binding seen in the normal adjacent tissue.

References/Funding Source Presentation Number 0829B Poster Session 4c: In Vivo Studies & Development/Novel Use of Imaging Probes September 11, 2010 / 15:15-16:45

The Mighty Mouse: Ubiquitous Expression of a Tri-Fusion (Bioluminescence, Fluorescence, PET) Reporter Gene in a Transgenic Mouse Model

X Yan[1], P Ray[1], R Tong[1], A Sathirachinda[1], SS Gambhir[1,2]
Departments of [1]Radiology, MIPS, [2]Bio-X Program, Stanford University, CA.

Reporter genes are extremely useful in following the gene expression and cellular behavior in development and disease studies in mice. We have created a transgenic mouse that expresses the tri-fusion reporter gene with pcAGGS-fluc2-tdTomato-ttk vector which is driven by the chicken β-actin promoter carrying an improved bioluminescent (fluc2), an improved red fluorescent protein (tdTomato) and a truncated herpes simplex virus type 1 sr39 thymidine kinase (ttk) reporter genes. This allows one to image any cell from the donor mouse using bioluminescent, fluorescent, and PET imaging (with [18F]FHBG) techniques. Mice (N=15) with different expression levels of the tri-fusion reporter were scanned, and multimodality imaging results show that the expression level of all three genes are correlated with each other (Figure 1). In vitro luciferase assay, fluorescent assay and TK assay were performed with cell lysates from the tail of those mice, the signal levels of fluc2 (8364-5,212,160 RLU/µg), tdTomato (0.2-20.5 FI/µg) and ttk (2055.6-281,836.5 dpm) are correlated to each other (R2=0.99), and the results from in vitro experiments are correlated to those from in vivo imaging. Organs from transgenic mice with high expression level of reporter gene were harvested and tested using in vitro assays. Muscle, heart, tail, pancreas and bladder have statistically higher expression ($P<0.05$) of reporter gene than other tissues, while the liver and intestine have less expression. To date, the signals from strong positive mice persist for 4 generations, and no developmental abnormalities/toxicity has been observed. To monitor MSC (mesenchymal stem cell) survival, FVB mice acute myocardial infarction were induced by coronary ligation with subsequent intramyocardial injection of MSC (mesenchymal stem cell) isolated from the bone marrow of the transgenic mice. Bioluminescence imaging results showed MSC signal decreased and became undetectable after 9 days . This mighty mouse will serve as an important tool in multiple fields such as stem cells and transplant biology.

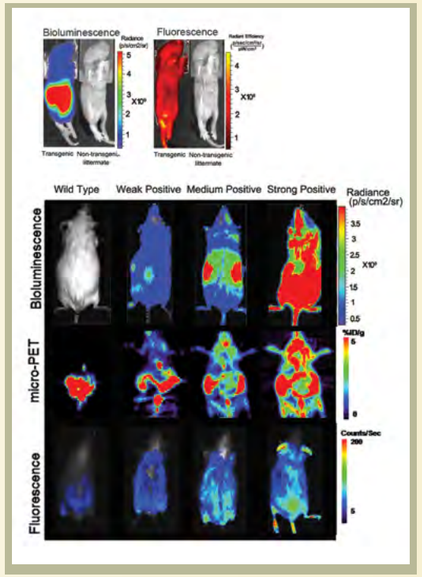

References/Funding Source Presentation Number 0172 Scientific Session 22: In Vivo Animal Models September 11, 2010 / 09:15-09:30 / Room: A

MR Imaging of Lumbar Spine using 3D FSE Cube and OsiriX: Initial Experience

EA Davalos, BH Do, GE Gold, S Biswal

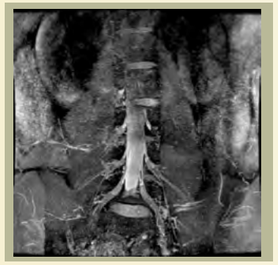

PURPOSE : A novel isotropic MRI sequence, 3D Fast Spin-Echo (FSE) Cube, has the potential to complement or perhaps even replace current conventional imaging sequences. We compared 3D-FSE-Cube to conventional 2D sequences for the investigation of the lumbar spine.

METHOD AND MATERIALS: IRB approval was attained. Twenty-two patients (13 men, 9 women; ages 27-81 yrs) were referred for low back or lower extremity pain. All patients were imaged on a 3.0-T MR unit). 3D FSE Cube protocol consists of coronal FSE T2-weighted pulse sequence with fat-saturation (TE/TR (3,000/35); 26-cm FOV; 288 x 256; bandwidth, 195; 90° flip angle. Post-processing techniques, including MIP and multiplanar reformation, were used to generate images of the lumbar spine with Osirix software. The images from both conventional and 3D FSE Cube scans were reviewed side by side for each case by two radiologists with experience in musculoskeletal MRI. Radiologists were blinded to each other. Each reviewer classified the relative degree of diagnostic confidence for the 3D FSE Cube images compared to the conventional images using a 3-point scale (were more confident, less confident, or equally confident) in their ability to assess for several spinal pathologies.

RESULTS: Images were reviewed for spinal canal stenosis, neural foraminal narrowing, pars defect, bone marrow edema, facet fluid, focal bone lesions, cord signal abnormality and annular fissure. The diagnostic confidence was higher or equal for the 3D FSE Cube images in the evaluation of spinal canal stenosis, lateral recess stenosis, pars defect, and facet fluid (22/22, 100% of patients). The diagnostic confidence was lower for the 3D FSE Cube images in the evaluation of neural foraminal narrowing, bone marrow edema, focal bone lesions, cord signal abnormality and annular fissure (22/22, 100% of patients).

CONCLUSION: 3D FSE Cube sequence improves the detection of pars defect, lateral recess stenosis and central canal stenosis. With further optimization of this sequence, it could potentially eliminate the need for 2D acquisitions in multiple planes, thus decreasing image time.

CLINICAL RELEVANCE/APPLICATION: Our preliminary experience has shown that the 3D FSE Cube sequence could improve diagnosis of certain spinal pathologies.

Imaging Pain Generators Using PET-labeled Sodium Channel Toxin Derivatives and PET-MRI

D Behera, A Hoehne, B Shen, W Parsons, D Yeomans, J Du Bois, F Chin, S Biswal

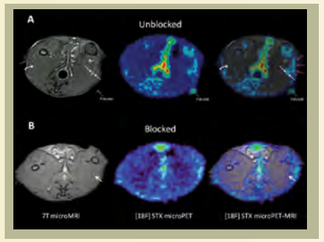

Purpose: Voltage gated sodium channel (NaV) play a critical role in the formation of action potentials. Its expression is enhanced in neuronal and inflamed tissues that promote nociceptive activity, and NaV can be targeted using a radiolabeled saxitoxin derivative ([18F]STX), which has nanomolar affinity for NaV. Using microPET-MRI we determined the localization of [18F]STX in a neuropathic pain model.

Materials and Methods: Conjugation of [18F]SFB with 6-aminohexylcarbamoyl-saxitoxin (6-AHC-STX) provided [18F]STX. Animal experiments were approved by Stanford IACUC. Spared-Nerve Injury (SNI) models (neuropathic pain model) were created in adult male Sprague-Dawley rats (n=5). The right hind limb was used as control. The rats were allowed 4 weeks to heal and develop pain. Presence of pain was ascertained by testing for allodynia using von-Frey's filaments. Each rat was given approximately 500 µCi of [18F]STX intravenously followed by an immediate dynamic scan of the thighs for 20 minutes using a microPET, followed by T1-weighted fast spin echo images obtained using a 7T small-animal MRI. The cold [19F]STX analog (0.08 mg/kg) was co-administered for blocking studies. PET-MRI fusion was performed using Amide image analysis software. For image analysis, ROIs were placed on 5 mm segments of sciatic nerves, proximal to the level of injury, in both hindlimbs of each rat using MR images and counts were recorded from the fused PET images. The maximum signal in each nerve was normalized to the average signal from adjacent muscle.

Results: Measured IC50 of [19F]STX against NaV was 10.6±0.8 nM in PC12 cells. Presence of allodynia in the operated limb was confirmed using von-Frey's filaments ($p<0.003$). Increased [18F]STX uptake was seen in the SNI nerve compared to control side between 10-15 minutes after injection (normalized PET signal on SNI side is 2.25 ± 0.43 while it is 1.6 ± 0.19 on control side; $p<0.05$), but not in the blocked studies (SNI side 1.82 ± 0.07; control side 2.09 ± 0.003; $p=0.17$).

Conclusion: Rats with neuropathic pain show increased [18F]STX uptake in the affected nerve. PET-MRI can be effectively used to study [18F]STX uptake in nerves.

Clinical Relevance: Combining the high sensitivity of PET with the excellent tissue contrast of MRI to locate nerves, PET-MRI with [18F]STX can quantify neural NaV channel density and potentially identify chronic pain generators.

Optical Imaging with a HER2-targeted Affibody can monitor Hsp90 treatment response in a xenograft mouse model

SM Van de Ven[1,3], SG Elias[5,3], CT Chan[2,3], Z Miao[2,3], Z Cheng[2,3], A De[2,3], SS Gambhir[3,4]
[1]Radiology, [5]Julius Center for Health Sciences and Primary Care, University Medical Center Utrecht, Netherlands; Departments of [2]Radiology, [3]MIPS, [4]Bioengineering, Stanford University, CA

Aim: The goal of this study was to determine if fluorescence imaging with a HER2-targeted affibody can be used for non-invasive and repetitive imaging of HER2 expression and monitoring of the Hsp90 treatment effect on HER2 expression in human breast cancer xenografts in mouse models. Methods: MCF7 parental cells and two clones (A and B) transfected with HER2 were used for characterization by flow cytometry and western blotting, and to establish human breast cancer xenografts in nude mice. Anti-HER2 affibody (ZHER2:342) was labeled with AlexaFluor680 for optical imaging studies. Mice received either 120 mg/kg of the Hsp90 inhibitor 17-DMAG in 4 doses at 12 hour intervals i.p. (n=10), or PBS as a carrier control in a similar dosing scheme (n=5). Time-resolved fluorescence optical images were obtained at 4 different days: pre-treatment at day -1, and post-treatment at day 3, 6, and 9. On each imaging day optical images were acquired pre- and 5 hours post-injection of 500 pmol of Affibody-AlexaFluor680 in a volume of 150 µl via tail vein. Mice were sacrificed at day 9 and tumors were excised to correlate in vivo optical imaging signal with ex vivo HER2 levels by western blot. Results: Cell culture studies showed that HER2 expression was dependent on 17-DMAG dose. In vivo optical imaging signal was reduced by 21% in Clone B tumors ($p=0.016$) and by 13% in MCF7 parental tumors ($p=0.063$) at 3 days after 17-DMAG treatment; optical imaging signal recovered in both tumor types at day 6-9 after 17-DMAG treatment. In the carrier group no significant signal reduction was observed. Pearson correlation coefficient of in vivo optical imaging signal with ex vivo HER2 levels ranged from 0.74 to 0.89. Conclusion: Optical imaging with an affibody can be used to non-invasively monitor changes in HER2 expression in vivo in response to treatment with an Hsp90 inhibitor. This work supports the use of pre-clinical models to monitor drug efficacy in a low-cost high-throughput fashion with optical imaging.

References/Funding Source Presentation Num 0518B Poster 4b: Imaging Molecular and/or Cellular Processes & Drug and/or Radiation Therapy September 11, 2010 / 15:15-16:45

Intravital Microscopy Reveals Surprising Differential Extravasation of Quantum Dots and Nanotubes Across Multiple Tumor Models in Living Subjects

BR Smith[1], S Tabakman[2], H Dai[2], SS Gambhir[1]
Departments of [1]Radiology, MIPS, [2]Chemistry, Stanford University, CA

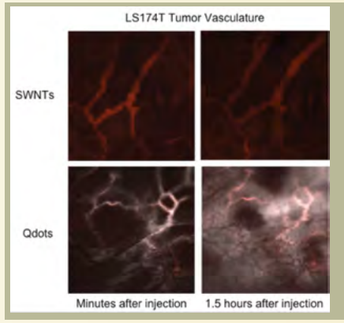

Displays regions of LS174T tumors in mice injected with SWNTs and with Qdots and imaged over time. Tumor signal (fluorescent green) was removed from the emerged images shown above to clarify the extravasation signal. In the top set of images, no SWNTs have extravasated from the vasculature over a period 1.5 hours. On the bottom, Qdots have clearly extravasated from the vasculature within 1.5 hours of injection.

Nanoparticles (nps) comprising various materials, shapes, and sizes are becoming ubiquitous within molecular imaging, particularly for cancer diagnosis/treatment. Because nps are typically introduced via intravenous injection and expected to localize in tumor, a deeper understanding of how and why these nps extravasate from tumor neovasculature into interstitium is critical. It is essential to the field to characterize shape- and size-dependent np behavior across multiple tumor varieties in order to provide researchers with the ability to design the appropriate np for its purpose. This will also help optimize np formulations and decrease the time for clinical translation. We probed the extravasational behavior of two np types with three different tumor types using intravital microscopy (IVM) in 30 living mice. We used nude mice with an ear tumor model. We employed near-infrared (800nm) emitting quantum dots (qdots) (~20 nm diameter) and single-walled carbon nanotubes (SWNTs, 2 nm X 200 nm) conjugated to Cy5.5. Three different tumor cell lines were employed, all transduced with EGFP for visualization: SKOV3, LS174T, and U87MG cells. Long-circulating dye was injected to visualize the vasculature. No extravasation occurred in SKOV-3 with either np. In U87MG tumors, SWNTs extravasated rapidly (35.1% average fluorescence increase in interstitium from 2 to 30 minutes post-injection) while qdots extravasated minimally (12.7% increase from 2 minutes to 1.5 hours). However, intriguingly in LS174T tumors the opposite occurred: qdots extravasated rapidly (294% increase from 2 minutes to 1.5 hours), while SWNTs extravasated minimally. This role reversal reveals unanticipated complexity in np extravasational behavior and we quantified it using a region of interest analysis to better understand the underlying mechanisms. We thus directly visualized np extravasation from tumor blood vessels and demonstrated surprising np- and tumor-dependent differences, which will aid in the design of nps for optimal tumor uptake.

References/Funding Source Presentation Number 0634B Poster Session 3b: Imaging Molecular and/or Cellular Processes & Drug and/or Radiation Therapy September 10, 2010 / 15:15-16:45 / Room: Main Hall Lobby

How Do Nanoparticles Target Cancer? Real-time Microscopic Imaging with Carbon Nanotubes in Mouse Tumor Models

BR Smith[1], C Zavaleta[1], Z Liu[2], J Ramunas[3], J Rosenberg[1], R Tong[4], H Dai[2], SS Gambhir[1,4]

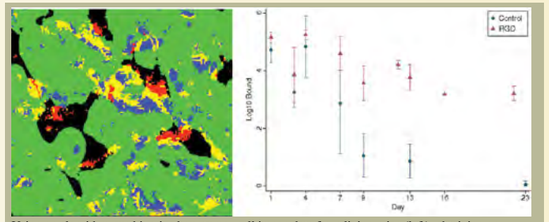

Using an algorithm, we binarized our tumor cell image data from living mice (left), obtaining an image showing cell (green) and bound SWNTs (yellow). On the right, a graph shows the behavior of SWNTs depending on if the ligand is specific (RGD) or non-specific (RAD). Over the first week, SWNT association is similar between the two, but afterward RGD_SWNTs tend to remain bound over 3 weeks post-injection.

While nanoparticles have become invaluable in the molecular imaging toolkit, little is known about the mechanisms by which they target diseased tissues. Single-walled carbon nanotubes (SWNTs) were previously demonstrated to display among the highest tumor uptake across nanoparticle constructs (12-15% ID/g). We thus carefully examined the modes of uptake by directly observing SWNTs entering tumor vasculature, specifically binding luminal targets, extravasating from vessels, and binding to tumor cells over time. To understand the fundamental mechanisms underlying SWNT tumor uptake, we confirmed and correlated our intravital microscopy (IVM) results with macroscopic Raman imaging, which quantifies SWNTs' intrinsic Raman signal. We used RGD peptide-bound SWNTs and controls to study the kinetics and routes of SWNT uptake and the ability of integrin targeting to enhance SWNT uptake and retention. We prepared targeted SWNTs by conjugating RGD (targeting αvβ3-integrins expressed on tumor neovasculature and some tumor cells, ~60/SWNT) and Cy5.5 dye (22/SWNT). Dorsal window chambers were surgically implanted into mice and EGFP-U87MG (expressing αvβ3-integrins) or EGFP-SKOV3 tumor cells were inoculated. 25 mice (U87MG, SKOV-3, no tumor) were imaged with RGD-SWNTs (~60 pmol) and RAD and no peptide controls. Mice were imaged during tail-vein injection and frequently over the following two months with Raman and IVM. Unlike controls, RGD-SWNTs were observed to bind tumor blood vessels. Within hours, all SWNT conjugates extravasated in U87MG tumor beds, but not SKOV-3 as quantified using 10-50 fields-of-view per mouse per time point. RGD-SWNTs were observed associated with tumor cells in U87MG tumors significantly more than RAD-SWNT controls ($P<0.0001$). Furthermore, RGD-SWNTs differentially bound tumor cells over time compared with controls ($P<0.007$) and they persisted in tumor for more than a month. Control SWNTs cleared within ~1 week. In summary, IVM allowed detailed exploration of the mechanisms of SWNT uptake in tumor. This work offers unprecedented understanding of the mechanisms/temporal framework of nanoparticle dynamics in tumors, which should translate into superior properties for pre-clinical and clinical utility.

References/Funding Source Presentation Number 0633B Poster Session 3b: Imaging Molecular and/or Cellular Processes & Drug and/or Radiation Therapy September 10, 2010 / 15:15-16:45 / Room: Main Hall Lobby

Publications

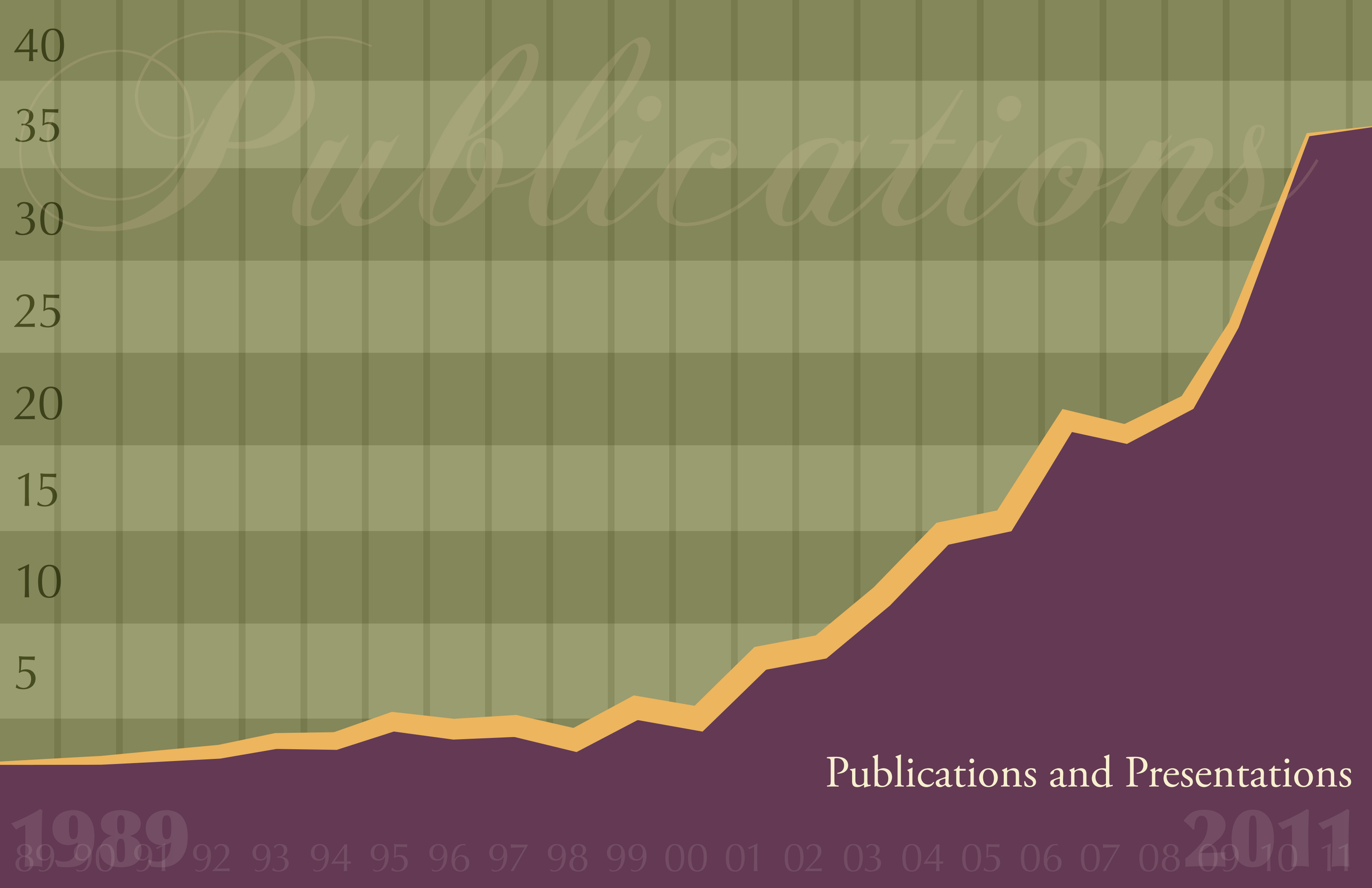

Publications and Presentations

Peer-Reviewed Presentations at Scientific Meetings

ISMRM 2011 (May 7-13, Quebec, Canada)

Luo Q, Glover GH.	Slice-direction SENSE: A Sensitive Acquisition Method for Detecting Neuronal Current MRI Signal Induced by Epilepsy.
Stevens KJ, Worters PW, Gold GE, Rosenberg JK, Hargreaves BA.	MR Imaging after Spinal Fusion using Slice Encoding for Metal Artifact Correction (SEMAC).
Qiu D, Zaharchuk G, Feng S, Christen T, Sung K, Moseley ME.	Quantitative Susceptibility Imaging using L1 regularized reConstruction with Sparsity Promoting Transformation: SILC.
Moran CJ, Nnewihe AN, Daniel BL, Granlund KL, Hargreaves BA.	High-Resolution 3D T2-Weighted Spin-Echo Imaging With a 16-Channel Breast Coil.
Worters P, Butts-Pauly K, Hargreaves BA.	Metal Artifact Reduction using Slice Encoding with Shear Correction.
Vogelsong M, Pappas G, Staroswiecki E, Bangerter NK, Han E, Hargreaves BA, Braun HJ, Safran M, Gold GE.	Are Sports Good for your Knees? An MRI Evaluation of the Effects of Basketball on Knee Health in Division I Collegiate Athletes.
Saranathan M, Hargreaves BA, Moran CJ, Daniel BL.	Variable-Resolution Dynamic Contrast-Enhanced Breast MRI Acquisition.
Khalighi MM, Saranathan M, Grissom W, Kerr AB, Watkins R, Rutt BK.	Parallel Transmit using 3D Spokes RF Pulses for Improved B1+ Homogeneity over 3D Volume.
Christen T, Lemasson B, Pannetier N, Farion R, Remy C, Zaharchuk G, Barbier EL.	Is T2* Enough to Assess Oxygenation? A Quantitative Blood-Oxygen Level Dependent Analysis in Brain Tumors.
Nnewihe AN, Sung KH, Daniel BL, Hargreaves BA.	Novel Variable Voxel Intensity Correction Scheme and Application to Breast Imaging.
Griffin HM, Park DJ, Morrell GR, Kaggie J, Peterson BA, Gold GE, Bangerter NK.	Partial Volume Correction for Quantitative Sodium MRI of the Human Breast.
Josan S, Hurd R, Kerr AB, Yen Y-F, Larson PE, Pfefferbaum A, Spielman D, Mayer D.	Effects of RF Excitation Scheme on Signal-to-Noise-Ratio and Apparent Rate Constant Estimation in Dynamic Volumetric Imaging of Hyperpolarized [1-13C]-pyruvate.
Vasanawala SS, Lai P, Alley MT, Gold GE, Pauly JM, Lustig M.	Impact of Compressed Sensing on Volumetric Knee MRI.
Zeineh M, Kitzler HH, Atlas S, Vogel M, Rutt BK.	Susceptibility Mapping of Alzheimer Plaques at 7T.
Han M, Hargreaves BA, Krug R.	Bilateral Hip MRI using Dual-Band Excitation with Slab-Phase Modulation.
Alley MT, Murphy MJ, Keutzer K, Lustig M, Vasanawala SS.	Improved Time-Resolved, 3D Phase Contrast Imaging through Variable Poisson Sampling and Partial Respiratory Triggering.
Balchandani P, Khalighi MM, Hsieh SS, Setsompop K, Pauly J, Spielman D.	Adiabatic B1 Shimming Algorithm for Multiple Channel Transmit at 7T.
Mayer D, Yen Y-F, Hurd R, Josan S, Park J, Pfefferbaum A, Spielman D.	Hyperpolarized [1-13C]-Lactate as a Tool for the In Vivo Investigation of Cardiac Metabolism.
Monu UD, Worters PW, Sung K, Koch KM, Gold GE, Hargreaves BA.	B1 Mapping Near Metallic Implants.
Park JM, Josan S, Jang T, Merchant M, Yen Y-F, Hurd R, Recht L, Spielman D, Mayer D.	Metabolic Kinetics of a Glioma Model using Hyperpolarized 13C Magnetic Resonance Spectroscopic Imaging.

Peer-Reviewed Presentations at Scientific Meetings

ISMRM 2011 (May 7-13, Quebec, Canada)

Jordan CD, Daniel BL, Koch KM, Yu H, Conolly S, Hargreaves BA.	Validation of Susceptibility-Based Models with Field Map Measurements in the Breast.
Javed A, Park DJ, Morell GR, Kaggie J, Newbould RD, Staroswiecki E, Gold GE, Bangerter NK.	Phase Sensitive B1 Mapping in Sodium with a 3D Cones Trajectory.
Saranathan M, Rettmann D, Brau AS, Hargreaves BA, Vasanawala SS.	Ultra High Spatio-Temporal Resolution Liver Imaging using a New View Ordering Scheme and a 2-point Dixon Acquisition.
Sung K, Nnewihe AN, Daniel BL, Hargreaves BA.	High Frequency Subband Compressed Sensing with ARC Parellel Imaging.
Saranathan M, Worters PW, Vasanawala SS.	Non-contrast Outer Radial Inner Square k-space Scheme (NORISKS)- A Breath-held Balanced SSFP-Dixon Technique for Non-contrast Enhanced Renal MRA.
Chen W, Zhang T, Han ET, Gold GE.	Joint Anatomical and Biochemical Imaging using 3D FSE.
Caverly RJ, Doherty WE, Watkins R.	Time Domain Modeling of MR Linear Balanced Duplexers Switched with Low Magnetic Moment PIN Diodes.
Saranathan M, Khalighi MM, Kerr A, Rutt BK.	Fast 3D B1+ Mapping using an Optimized, Asymmetric Bloch-Siegert Method.
Rutt BK.	B0 and B1 Inhomogeneities: Correction Pipeline.
Su J, Kitzler HH, Zeineh M, Harper-Little C, Leung A, Kremenchutzky M, Deoni SC, Rutt BK.	Sensitive Detection of Myelination Change in Multiple Sclerosis by mcDESPOT.
Vasanawala SS, Grafendorfer T, Calderon P, Scott G, Alley MT, Lustig M, Brau AC, Sonik A, Pai P, Hargreaves BA.	Millimeter Isotropic Resolution Volumetric Pediatric Abdominal MRI with a Dedicated 32 Channel Phased Array Coil.
Hargreaves BA, Gold GE, Pauly JM, Butts-Pauly K, Koch KM.	Metal-Induced Artifacts in MRI.
Granlund KL, Staroswiecki E, Moran CJ, Alley MT, Daniel BL, Hargreaves BA.	Prospective Motion Correction for T2- and Diffusion-Weighted Breast Imaging with FADE.
Rieke V, Holbrook AB, Grissom W, Santos JM, McConnell MV, Butts-Pauly K.	Real-time Hybrid MR Thermometry of Human Ventricular Myocardium With and Without Blood Suppression.
Khalighi MM, Glover GH, Pandit P, Hinks S, Kerr AB, Saranathan M, Rutt BK.	Single-Shot Spiral Based Bloch-Siegert B1 Mapping.
Giannini V, Ghanouni P, Sommer G, Diederich C, Holbrook AB, Salgaonkar VA, Prakash P, Gill H, Bouley DM, Butts-Pauly K.	Assessing Thermal Tissue Damage with Biexponential Diffusion-Weighted MRI.
Keenan KE, Besier T, Smith RL, Beaupre GS, Gold GE.	Estimating the Short-time Elastic Modulus of Cartilage using T1ρ and T2.
Kaggie J, Park D, Newbould RD, Morrell GR, Hargreaves BA, Staroswiecki E, Gold GE, Bangerter NK.	In Vivo Breast Sodium T1 Measurements Using Inversion Recovery 3D Cones.
Braun HJ, Vogelsong MA, Staroswiecki E, Hargreaves BA, Bangerter N, Han E, Fattor J, Friedlander AL, Shah O, Beaubien JM, Gold GE.	T2, T1p, and Sodium MRI of Articular Cartilage in Patients with Osteoarthritis Treated with Arthritis Relief Plus Cream.

Peer-Reviewed Presentations at Scientific Meetings

ISMRM 2011 (May 7-13, Quebec, Canada) (DONE)

Schmiedeskamp H, Straka M, Zaharchuk G, Fischbein NJ, Lansberg MG, Olivot J-M, Albers GW, Moseley ME, Bammer R.	Spin- and Gradient-Echo EPI for Imaging of Brain Perfusion with MRI.
Staroswiecki E, Granlund KL, Alley MT, Gold GE, Hargreaves BA.	Simultaneous Estimation of T2 and ADC in Human Articular Cartilage In Vivo with a Modified 3D DESS Sequence at 3T.
Worters P, Saranathan M, Xu A, Vasanawala SS.	Robust Renal MRA using Breath-hold, IR-prep, Dixon bSSFP at 3T.
Sung K, Daniel BL, Hargreaves BA.	Location Constrained Approximate Message Passing (LCAMP) Algorith for Compressed Sensing.
Qiu D, Moseley ME, Zaharchuk G.	Comparison of Pseudocontinuous and Velocity Selective Arterial Spin Labeling with Gold Standard Xenon CT: a Study in Patients with Moyamoya Disease.
Gu M, Spielman DM, Zahr NM, Pfefferbaum A, Sullivan EV, Mayer D.	CT-PRESS Based Spiral Spectroscopic Imaging with Robust Water and Lipid Suppression using Multiple Dualband Frequency-Selective RF Pulses.
Rieke V, Werner B, McDannold N, Grissom W, Martin E, Butts-Pauly K.	Hybrid Referenceless and Multi-baseline Thermometry for MRgFUS Brain Applications.
Christen T, Zaharchuk G.	Measuring Brain Oxygenation in Humans using a Quantitative BOLD Approach.
Muelly M, Huang W, Chen W, Huo D, Zhao X, Gold GE.	Improved 3D-FSE Isotropic Imaging of the Knee using Enhanced Flip Angle Modulation and Crusher Gradient Optimization.
Bitton RR, Kaye E, Butts-Pauly K.	MR-ARFI and SWI to Detect Calcifications in the Brain in MRgHIFU Treatments.
Khalighi MM, Rutt BK, Saranathan M, Kerr AB.	RF Pulse Optimization for Bloch-Siegert B1+ Mapping.
Sung K, Daniel BL, Hargreaves BA.	Transmit B1 Field Inhomogeneity and T1 Estimation Errors in Breast DCE MRI at 3T.
Skeffington WM, Martinez-Seantiesteban FM, Collick BD, Alejski A, Rutt BK, Garces LJ, Szczesny PM.	Insert Gradient Subsystem Tuning by Direct Impedance Measurements.
Su J, Kitzler HH, Zeineh M, Harper-Little C, Leung A, Kremenchutzky M, Deoni SC, Rutt BK.	mcDESPOT-Derived MWF Improves EDSS Prediction in MS Patients Compared to Only Atrophy Measures.
Chen CA, Chen W, Goodman SB, Hargreaves BA, Koch KM, Lu W, Brau AC, Braun HJ, Gold GE.	Changes in Patient Management due to Correction of Metal Artifact in the Knee.
Christen T, Schmiedeskamp H, Straka M, Bammer R, Zaharchuk G.	Comparison of Different EPI-based Approaches to Measure T2' in Human Brain for the Purpose of Oxygenation Measurements.
Wade T, McKenzie C, Rutt BK.	Theoretical and Experimental Efficiency and Optimization of Flip Angle Mapping Techniques.

Peer-Reviewed Presentations at Scientific Meetings

SNM 2011 (June 4-8, San Antonio, Texas) (DONE)

Miao Z, Ren G, Liu H, Qi S, Wu S, Cheng Z.	An 18F-FBEM Labeled Affibody for PET Imaging of Tumor EGFR Expression.
Hoppmann S, Qi S, Miao Z, Liu H, Jiang H, Cheng Z.	Characterization of 177Lu-Affibody-HSA Bioconjugate for Radionuclide Therapy of EGFR-expressing Head and Neck Carcinomas.
Liu S, Liu H, Miao Z, Jiang H, Cheng Z.	Novel 18F-labeled Aliphatic Probe for Melanoma Imaging.
Liu S, Liu H, Miao Z, Cheng Z.	Development of 18F-labeled Picolinamide Probes for Melanoma PET Imaging.
Liu S, Liu H, Jiang H, Cheng Z.	Development of [18F]AlF-NOTA-RGD2 Probe for MicroPET Imaging in U87MG-tumor Bearing Mice.
Liu S, Liu H, Miao Z, Cheng Z.	A Novel Probe with Dual Targeting Mechanisms for Tumor Imaging using Positron Emission Tomography.
Iagaru A, Mosci C, Mittra E, Shen B, Chin FT, Chen X, Telli M, Gambhir SS.	18F FPPRGD2 in Breast Cancer Subjects: A Novel PET Radiopharmaceutical for Imaging avB3 Integrin Levels.
Iagaru A, Mittra E, Sathekge M, Prakash V, Iyet V, Dick D, Lapa P, Isidoro J, de Lima J, Gambhir SS.	Combined 18F NaF and 18F FDG PET/CT: Initial Results of a Multi-center Trial.
Quon A, Sprinz C, de Abreu MR, Neto JMA, Iagaru A, Hennermann S.	Integrated F18 NaF PET/CT Scanning for the Evaluation of Patients with Chronic Pain after Spinal Surgery.
Natarajan A, Gowrishankar G, Nielsen C, Wang S, Iagaru A, Goris M, Gambhir SS.	Prediction of Human PET Imaging Dose to Monitor NHL Therapy using <64>Cu-DOTA-rituximab and a Transgenic Mouse Model.
Gonzalez E, Olcott P, Levin CS.	Multiplexed Molecular Imaging with PET: Methods to Greatly Enhance the Sensitivity of Simultaneous Imaging of Multiple Positron Emitting Isotopes.
Mittra E. Mosci C, Iagaru A, Fels L, Bacher-Stier C, Chin FT, Gambhir SS.	Studies of the 18F L-glutamate Derivative BAY 94-9392 in Cancer Patients: A Novel Radiopharmaceutical for PET Imaging.
Ren G, Xu Y, MiaoZ, Qi S, Liu H, Cheng Z.	Profiling EGFR in Triple Negative Breast Tumors using PET.
Jiang H, Moore S, Liu S, Liu H, Miao Z, Cochran F, Cochran J, Zhang H, Cheng Z.	An 18F-labeled Agouti-related Protein for PET Imaging of Integrin Positive Tumor.
Chen K, Miao Z, Cheng Z.	In Vivo PET Imaging to Track Mesenchymal Stem Cells Labelled with Copper-64-pyruvaldehyde-bis (N4-methylthiosemicarbazone).
Olcott P, Levin CS, Glover GH.	Characterization of RF-transparent Electro-optically Coupled PET Block Detectors for Simultaneous PET/MR Imaging.
Qi S, Miao Z, Liu H, Feng Y, Cheng Z.	Evaluation of Four Affibody Based Near-infrared Fluorescent Probes for Optical Imaging of Epidermal Growth Factor Receptor Positive Tumors.

Peer-Reviewed Presentations at Scientific Meetings

RSNA 2010 (Nov 29-Dec 3, Chicago, Illinois)

Andre JB, Zaharchuk G, Saritas EU, Chin CT, Nishimura DW, Shankaranarayanan A, Fischbein NJ.	Clinical Evaluation of Reduced Field-of-View Diffusion-weighted Imaging of the Human Spinal Cord.
Barth RA.	MR Imaging of the Fetal Neck and Chest.
Barth RA, Bulas DI.	Pediatric Radiology Series: Fetal Imaging.
Biswal S.	New Development in Imaging for Musculoskeletal Pain.
Blankenberg FG.	Apoptosis Imaging: Oncologic Imaging Applications.
Boas FE, Fleischmann D.	Evaluation of the Metal Deletion Technique (MDT): A New Method for Reducing Metal Streak Artifacts in Computed Tomography Scans.
Chan FP.	MR Imaging.
Deshpande N, Ren Y, Foygel K, Willmann JK.	Noninvasive Assessment of Temporal Tumor Angiogenic Marker Expression Levels with Molecular Ultrasound Imaging.
Do BH, Biswal S, Stevens KJ, Rubin DL.	Toward Best Practice Reporting: A Natural Language Processor to Identify Semantic Content and Automatically Generate Standardized Knee MRI Reports.
Do BH, Biswal S, Stevens KJ, Gold GE, Beaulieu CF, Lutz AM, Rubin DL.	X-Ray Head MSK: A Musculoskeletal Radiology Web Reference Based on RadLex.
Federle MP.	Focal Liver Lesions in the Cirrhotic Liver.
Federle MP.	Lymphoma.
Flesichmann D.	The ABCs of Aortic Dissection.
D'Souza AL, Tseng J, Rosenberg J, Butts-Pauly K, Gambhir SS, Glazer GM.	Low-Frequency Ultrasound Amplifies the Release of Multiple Tumor Biomarkers in Living Subjects.
Hallett RL.	Postprocessing, Work Flow, and Interpretation.
Williamson EE, Catalano C, Hallett RL, Nikolaou K.	Vascular Imaging Series: CT Angiography - Strategies for Technique Optimization.
Thurmond AS, Maubon A, Hovsepian DM, Moore Jr AV, De Lavir JRR, Bass JC, Machan LS, Zagoria RJ.	Fallopian Tube Catheterization - Hands-on Workshop.
Ikeda DM.	When to Follow.
Jordan JE, Jordan YF, Lightfoote JB, Cole KDR.	Reinterpretation of Brain CT Imaging Studies in Stroke Imaging: Quality Improvement Outcomes.
Kamaya A, Maturen KE, Desser TS, Hussain HK.	Evaluation of Hepatocellular Carcinoma in the Preoperative Liver Transplantation Patient: What Transplant Surgeons Want Radiologists to Know.
Kuo WT, Roberts AC.	Acute and Chronic Pulmonary Emboli: Diagnosis and Treatment - An Interactive Session.
Lynch DA, Leung AN, Klein JS.	Case-based Review: Interstitial Lung Disease, Pulmonary Infection, and Solitary Pulmonary Nodule - An Interactive Session.
Leung AN.	STR/ATS Guidelines for Evaluating Pulmonary Embolism in Pregnancy.
Lipson JA, Nwamuo DC, Rubin DL.	The Annotated Breast Map: A Novel Paradigm to Improve Interpretation in Breast Imaging.
Meer A, Basu PA, Baker L, Atlas SW.	Exposure to Ionizing Radiation and Estimate of Secondary Cancers in the Era of High Speed CT Scanning.

Peer-Reviewed Presentations at Scientific Meetings

RSNA 2010 (Nov 29-Dec 3, Chicago, Illinois) (DONE)

Napel S.	Automated Image Retrieval Based on Lesion and Case Similarity.
Panje C, Psyz MA, Wang DS, Ren Y, Schneider M, Willmann JK.	Influence of Microbubble and DNA Doses on in Vivo Ultrasound-mediated Gene Delivery with Cationic vs Neutral Microbubbles.
Poullos PD, Federle MP, Wan W.	Multi-Detector CT Imaging of Traumatic Abdominal Wall Hernias.
Heimbigner JH, Reynolds Jr WW, Alexander S.	Practical Guidance for MDCT Venography of the Body.
Roos JE.	CT Imaging.
Rubin DL, Kleper V, Flanders AE, Channin DS, Mongkolwat P.	An Approach to Structured Reporting in Clinical Research.
Rubin DL.	Background, motivations, and overview of applications.
Rubin DL, Du Vall SL.	Natural Language Processing in Radiology.
Rubin DL, Napel S, Federle MP, Jeffrey RB, Do BH, Beaulieu CF, Harrigal C, Abelson D, Klang K, Ghanouni P.	Reader Variation in CT Imaging Interpretation of Focal Liver Lesions.
Rubin DL, Beaulieu CF, Rodriguez C, Baldassano C, Napel S.	Reinventing Radiology Reporting: Combining Structured Capture and Radiology Image Anotation.
Rubin DL, Korenblum D, Yeluri V, Frederick P, Herfkens RJ.	Semantic Annotation and Image Markup in a Commercial PACS Workstation.
Rubin DL, Channin DS.	The RadLex Playbook: A Nomenclature for Radiological Imaging.
Rubin DL, Fleischmann D, Yeluri V, Frederick P, Herfkens RJ.	Toward Real-time Monitoring for Patient Safety: Recording, Extracting, and Reporting CT Radiation Dose Using New DICOM Standards.
Rubin DL.	What are Standard Terminologies?
Rubin GD, Tall M, Roychoudhury K, Roos JE, Paik DS, Napel S, Ly DL.	Perception of Lesions in the Gaze Cone Periphery: Impact of Lesion Size, Distance, and Local Lung Complexity on Detection.
Rutt BK.	USPIO MR Contrast Agents: Recent Advances and Applications.
Segall GM.	Cardiac.
Segall GM, Graham MM.	Case-based Review of Nuclear Medicine: PET/CT Workshop - Cancers of the Thorax.
Stevens KJ.	Fluid Collections and Inflammatory Change around the Knee.
Takaoka H, Funabashi N, Uehara M, Ueda M, Komuro I, Rubin GD, Daimon M, Murayama T.	Quantitative Measurement of Abnormal Late-enhancement Volume in the Left Ventricular Myocardium in Myocardial Diseases by Multi-Detector Row CT (CT) Compared to Cardiac Magnetic Resonance: Segmental Analysis.
Takaoka H, Funabashi N, Uehara M, Ishibashi I, Komuro I, Rubin GD.	Utility of Non Contrast CT Just after Percutaneous Coronary Intervention in Subjects with De Novo Acute Myocardial Infarction Quantitative Volume Evaluation for Prediction of Infarct Size in Comparison with Conventional Left Ventriculogram.
Vasanawala SS.	MR Imaging of Pediatric Liver Disease
Wang A, Pelc NJ.	Synthetic CT: Generating Images of Arbitrary CT Protocols using a Dual Energy Scan.
Wilson SR, Mattrey RF, Willmann JK.	Ultrasound/Gastrointestinal Series: Contrast-enhanced US - Where Are We in 2010?
Yeom KW, Partap S, Rosenberg J, Telischak N, Minn AY, Barnes PD.	Effect of Patient Age and Radiotherapy Dosage on the Incidence of MRI-detected Microhemmorrhage Following Treatment for Pediatric Medulloblastoma.

Peer-Reviewed Presentations at Scientific Meetings

RSNA 2010 (Nov 29-Dec 3, Chicago, Illinois)

Zaharchuk G, Dake MD, Cooke JP, Herfkens RJ.	Comparison of Magnetic Resonance Imaging and Contrast Venography in the Evaluation of Chronic Cerebrospinal Venous Insufficiency in Multiple Sclerosis Patients.
Zaharchuk G.	Expert Panel Q&A.
Zaharchuk G, Marks MP, Do HM, Rosenberg J, Steinberg GK.	Identifying Collateral Flow using Arterial Spin Labeling MR Imaging in Moyamoya Disease.
Zaharchuk G.	Perfusion Imaging Methods in Practice.
Zissen MH, Kunz P, Fisher G, Quon A.	18F-5-fluorouracil Dynamic PET/CT Reveals Decreased Tracer Uptake after Bevacizumab in Colorectal Metastases.
Castaneda R, Boddington S, Wendland M, Henning T, Mandrussow L, Daldrup-Link HE.	Labeling Human Embryonic Stem Cel Derived Cardiomyocytes for Tracking with MR Imaging: Optimizing for the Clinic.
Castaneda R, Boddington S, Wendland M, Henning T, Mandrussow L, Daldrup-Link HE.	Labeling Human Embryonic Stem Cel Derived Cardiomyocytes for Tracking with MR Imaging: Optimizing for the Clinic.
Don Grasparil A, Jose F, Daldrup-Link HE.	Utility of MR Enterography versus Endoscopy for Assessment of Active Ileal Inflammation in Inflammatory Bowel Disease in the Pediatric Age Group: A Preliminary Study.

WMIC 2010 (Sept 8-11, Kyoto, Japan)

Behera D, Jacobs KE, Behera S, Biswal S.	18F-FDG PET-MRI can be Used to Identify Injured Peripheral Nerves in a Model of Neuropathic Pain.
Behera D, Jacobs KE, Behera S, Biswal S.	Manganese-Enhanced Magnetic Resonance Imaging (MEMRI) Highlights Injured Peripheral Nerves in Neuropathic Pain (Chronic Constrictive Injury).
Chin FT, Hoehne A, Parsons WH, Behera D, Du Bois J, Biswal S.	[18F]Saxitoxin PET-MRI: A New PET-based Method for Imaging Pain in Living Subjects.
Blankenberg FG, Levashova Z, Sarkar SK, Backer M, Backer JM.	Preclinical SPECT Imaging of VEGF Receptors in Tumor Vasculature in the Course of Treatment with Pazopanib, a Small Molecule TKI.
Levashova Z, Krivoshein AV, Backer M, Backer JM, Blankenberg FG.	Therapeutic Effects of Targeted Delivery of Lu-177 to Tumor Vasculature.
Sun X, Yan Y, Liu S, Niu G, Cao Q, Chen X.	18F-FPPRGD2 and 18F-FDG PET Imaging of Abraxane Therapy Response.
Hoppmann S, Miao Z, Liu H, Liu S, Cheng Z.	Chemically Conjugated Affibody-HSA as a Potential Radiotherapeutic Agent for Treatment of HER2-Positive Cancer.
Hoppmann S, Miao Z, Liu S, Liu H, Cheng Z.	Chemically Conjugated Affibody-HSA for PET Imaging of HER2-Expressing Tumors.
Gao J, Chen K, Miao Z, Ren G, Gambhir SS, Cheng Z.	Affibody-based Nanoprobes for HER2-Expressing Cell and Tumor Imaging.
Kimura R, Jones D, Jiang L, Miao Z, Gambhir SS, Cheng Z, Cochran JR.	Development of a Multivalent Dual-RGD Knottin Peptide: Engineering Higher Affinity Translates to Slower Tumor Clearance Rates In Vivo.
Liu S, Liu H, Ren G, Kimura R, Cochran JR, Gambhir SS, Cheng Z.	PET Imaging of Integrin Expression using Fluorine-18 Labeled Knottin Peptides.
Miao Z, Ren G, Jiang L, Liu H, Webster JM, Zhang R, Namavari M, Gambhir SS, Syud FA, Cheng Z.	Small Animal PET Imaging of HER2 Positive Tumors with a Novel 18F-labeled Two-helix Peptide.

Peer-Reviewed Presentations at Scientific Meetings

WMIC 2010 (Sept 8-11, Kyoto, Japan)

Chang E, Liu S, Gowrishankar G, Yaghoubi S, Wedgeworth PJ, Chin FT, Berndorff D, Gekeler V, Gambhir SS, Cheng Z.	Good Reproducibility with the Integrin Tracer 18F-FP-PRGD2 in Human Xenografts.
Chang E, Neofytou E, Liu S, Wedgeworth PJ, Wang X, Beygui RE, Chen X, Wu JC, Gambhir SS, Cheng Z.	18F-FP-PRGD2 Uptake Tracks Effect of Drugs on Murine Ischemic Infarcts.
Chang Y-F, Patel M, H J-J, Gambhir SS.	Monitoring the Dynamics of CD8+ T Cell Responses in the Small Animal Model.
de la Zerda A, Bodapati S, Teed R, Tabakman S, Liu Z, Khuri-Yakub B, Chen X, Dai H, Gambhir SS.	Family of Enhanced Photoacoustic Imaging Agents for High Sensitivity and Multiplexing Studies in Living Mice.
de la Zerda A, Wang J, Perez V, Ruggeri M, Gambhir SS, Awdeh R.	Optical Coherence Molecular Imaging using Gold Nanorods in Living Mice Eyes.
Dragulescu-Andrasi A, Chan CT, De A, Gambhir SS.	Bioluminescence Resonance Energy Transfer (BRET): Marked Enhancement of In Vivo Protein-protein Interaction Imaging Based on Red-light Emitting Proteins.
D'Souza AL, Gambhir SS, Glazer GM.	Localization and Characterization of Tumors by Ultrasound-Induced Release of Multiple Biomarkers.
Hackel BJ, Kimura R, Gambhir SS.	64Cu-Labeled Fibronectin Domain for PET Imaging of EGFR+ Tumors.
Hughes NP, Mehta S, Buffa FM, Adams RF, Gambhir SS, Harris AL.	Uncovering the Molecular Correlates of Dynamic Contrast-Enhanced MRI in Breast Cancer Using 3D Pharmacokinetic Mapping and Gene Expression Profiling.
Ito K, Smith BR, Parashurama N, Miething C, Lowe S, Gambhir SS.	Imaging of Vascular Progression Within a Lymph Node in a Lymphoma Mouse Model.
Jokerst JV, Miao Z, Zavaleta C, Chan CT, Cheng Z, Gambhir SS.	Affibody-Functionalized, Multimodal Raman/Fluorescence Nanoparticles for Biomarker Profiling and Tumor Imaging.
Kimura R, Hackel BJ, Gambhir SS.	Engineering Novel High Affinity Integrin αvβ6 Binders in Different Cystine Knot Scaffolds: MicroPET Imaging Reveals Several Promising Candidates for Clinical Translation.
Kothapalli SR, Ma TJ, Vaithilingam S, Oralkan O, Khuri-Yakub B, Gambhir SS.	Transrectal Photoacoustic Imaging of the Prostate using Capacitive Micromachined Ultrasound Transducers.
Levi J, Kothapalli SR, Ma TJ, Kuri-Yakub B, Gambhir SS.	Dual Wavelength Imaging of a Novel Activatable Photoacoustic Probe.
Mittra E, Fan-Minogue H, Lin FI, Sriram V, Medicherla S, Gambhir SS.	Comparison of 18F-FDG and 18F-FLT Small-animal PET Imaging in an Orthotopic Glioblastoma Mouse Model.
Natarajan A, Gowrishankar G, Nielsen CH, Wang S, van Bruggen N, Gambhir SS.	Evaluation of a PET Antibody Tracer for Monitoring Lymphoma Therapy in a Humanized Transgenic Mouse Model.
Ronald JA, Katzenberg RH, Nielsen CH, Jae HJ, Hofmann LV, Gambhir SS.	A Novel Paradigm to Markedly Enhance the Specificity of Gene Expression in Hepatocellular Carcinoma Using MicroRNAs.
Smith BR, Rallapalli H, Prescher J, Zavaleta C, Rosenberg J, Liu Z, Dai H, Gambhir SS.	Preliminary Intravital Microscopic Analysis Reveals Macrophage Uptake of Circulating Nanotubes and RGD-dependent Delivery into Tumor.
Smith BR, Tabakman S, Dai H, Gambhir SS.	Intravital Microscopy Reveals Surprising Differential Extravasation of Quantum Dots and Nanotubes Across Multiple Tumor Models in Living Subjects.
Smith BR, Zavaleta C, Liu Z, Ramunas J, Rosenberg J, Tong R, Dai H, Gambhir SS.	How Do Nanoparticles Target Cancer? Real-time Microscopic Imaging with Carbon Nanotubes in Mouse Tumor Models.

Peer-Reviewed Presentations at Scientific Meetings

WMIC 2010 (Sept 8-11, Kyoto, Japan) (DONE)

Van de Ven SM, Elias SG, Chan CT, Miao Z, Cheng Z, De A, Gambhir SS.	Optical Imaging with a HER2-targeted Affibody can Monitor Hsp90 Treatment Response in a Xenograft Mouse Model.
Yan X, Ray P, Tong R, Sathirachinda A, Gambhir SS.	The Mighty Mouse: Ubiquitous Expression of a Tri-Fusion (Bioluminescence, Fluorescence, PET) Reporter Gene in a Transgenic Mouse Model.
Zavaleta C, Jokerst JV, Liu JT, Mandella MJ, Garai E, Hardy J, Contag C, Gambhir SS.	Use of Tumor Targeted Raman Nanoparticles for Early Detection of Colon Cancer in Conjunction with a Newly Developed Raman Endoscope.
Habtel F, Doyle T, Paik D.	Reduction of Variability in microPET quantitation using ROImax-based Statistics.
Kode KK, Shachaf C, Elchuri SV, Nolan G, Paik D.	Raman Labeled Nanoparticles for In-vivo Imaging: Characterization of Variability and Improved Method for Unmixing.
Paulmurugan R, Thillai VS.	Imaging Histone Methylation in Living Animals.
Zissen MH, Kunz PL, Fisher G, Quon A.	18F-5-fluorouracil Dynamic PET/CT Reveals Decreased Tracer Uptake After Bevacizumab in Colorectal Metastasis.
Rao J, Rutt BK, Liang G, Ma N, Chen Y, Ye D, Ma ML, Ronald JA.	Controlled Self-assembly of Nanoparticles: A General Template for Developing “Smart” MRI Contrast Agents.
Zhan K, Xie H, Gall J, Rao J.	Fluorescent Real Time Imaging of APP β-secretase (BACE1) Activity in Live Cells.
Darpolor MM, Yen Y-F, Chua M-S, Xing L, Clarke-Katzenberg R, Shi W, Mayer D, Josan S, Hurd RE, Pfefferbaum A, Senadheera L, So S, Hofmann LV, Glazer G, Spielman DM.	In Vivo Metabolic Imaging of Hyperpolarized [1-13C]-Pyruvate in Orthotopic Hepatocellular Carcinoma.
Deshpande N, Ren Y, Foygel K, Rosenberg J, Willmann JK.	Longitudinal Assessment of Expression Levels of Tumor Angiogenic Markers with Molecular Ultrasound Imaging.
Deshpande N, Ren Y, Foygel K, Schneider M, Pasricha PJ, Willmann JK.	Quantification of Inflammation in Inflammatory Bowel Disease by Molecular Ultrasound Imaging.
Panje C, Psyz MA, Wang DS, Ren Y, Schneider M, Willmann JK.	In Vivo Ultrasound-mediated Gene Delivery with Cationic and Neutral Microbubbles: Effect of Varying Microbubble and DNA Doses.
Psyz MA, Guracar I, Foygel K, Willmann JK.	Assessment of a Novel Real-Time Motion Correction Technique for Contrast-enhanced Ultrasound Imaging of Tumor Vascularity.
Lartey FM, Cord KT, Shen B, Chua JY, Tirouvanziam R, Palmer T, Guzman R, Chin FT, Graves E, Loo Jr BW.	In Vivo PET Imaging of STroke in Mice using a Novel Radioligant 18F-PBR06.
Castaneda R, Boddington S, Wendland M, Henning T, Mandrussow L, Liu S, Daldrup-Link HE.	Achieving a Preserved Differentiation Capacity and Significant MR Effect of SPIO-labeled Human Embryonic Stem Cell Derived Cardiomyocytes.
Castaneda R, Boddington S, Golovko D, Zhang D, Wang ZJ, Fu Y, Corot C, Coussens L, Daldrup-Link HE.	HR Imaging with new Folate-Receptor targeted Contrast Agents.
Castaneda R, Boddington S, Hsiao E, Henning TD, Wendland M, Golovko D, Daldrup-Link HE.	Labeling Human iPS Cells with USPIO Nanoparticle Ferumoxytol.

Other Scientific Meeting Presentations

Other Presentations 2010

Atlas SW.	Advances in Brain MRI: High Field and Beyond. 14th Radiology Meeting: Recent Advances in Brain CT and MR; April 22, 2010; Santiago, Chile.
Atlas SW.	Technology and Innovation in Radiology. 67th Annual Honorary Holmes Lecture of the New England Roentgen Ray Society; April 8, 2011; Harvard, MA.
Atlas SW.	Stroke MRI: Trends. Advances in Brain MRI: High Field and Beyond. Annual Russian Radiology National Congress; May 26, 2010; Moscow, Russia.
Atlas SW.	Stroke Imaging: Rationale and Current Status. New Frontiers in MRI: Fetal Imaging. MRI in Cerebrovascular Disease. MRI in Brain Tumors: Fundamentals and Advances. RDO Diagnostic Clinic; August 10, 2010; Sao Paulo, Brazil.
Atlas SW.	Brain Tumors I: Fundamentals of Imaging Mass Lesions. Brain Tumors II: Case Discussion. White Matter Diseases: The Role of Imaging. Vascular Malformations and Aneurysms of the CNS. Imaging Stroke and Hemorrhage I: Current Concepts. Stroke and Hemorrhage II: Case Discussion. Pediatric Brain: What You Need to Know. Essentials of Spine Imaging. Imaging the Eye and Orbit. Pituitary and Parasellar Lesions. Stoller & Atlas: A Case by Case Tutorial in Musculoskeletal and Neuroradiology; January 27-29, 2011; Las Vegas, NV.
Bammer R.	Diffusion-Weighted EPI with Parallel Imaging: Improving Resolution, Reducing Artifacts. Perfusion MRI. 18th Meeting of the International Society for Magnetic Resonance in Medicine; May 4, 2010; Stockholm, Sweden.
Bammer R.	High Field and Parallel Imaging. 20th Annual Current Concepts in MRI; October 27, 2010; Monterey, CA.
Bammer R.	Computer vision-based Real-Time Adaptive Motion-Correction in MRI. 2nd Eurographics Workshop on Visual Computing for Biology and Medicine; July 2010; Leipzig, Germany.
Bammer R.	MR Physics. 8th SPR Symposium on Pediatric Cardiovascular MR/Basic Course; January 18-21, 2011; Stanford, CA.
Bammer R.	Strategies for DTI Data Acquisition. Department of Defense (DoD) Workshop on Diffusion MRI of Traumatic Brain Injury Roadmap Project; June 2010; Chicago, IL.
Barnes P.	Neuroimaging in the Evaluation of pattern and timing of fetal and neonatal brain abnormalities. 27th Annual Conference on Obstetrics, Gynecology, Perinatal Medicine, Neonatology, and the Law; January 2-6, 2011; Maui, HI.
Barnes P.	Imaging of fetal and neonatal brain abnormalities. Birth Injury Group. American Association of Justice; July 11, 2010; Vancouver, BC Canada.
Barnes P.	Child Abuse and the Mimics. Update on Issues & Controversies in the Era of Evidence-based Medicine. Imaging of Pediatric CNS Malformations. Pediatric Head & Neck Imaging I & II. Pediatric Spine Imaging. Department of Radiology at University of British Columbia's Children's Hospital; October 13, 2010; Vancouver, BC Canada.
Beaulieu CF.	Optimization of MDCT for MSK Applications. MRI of the Brachial Plexus - Have no Fear. MRI of the Knee - Beyond the Menisci and Ligaments. Essentials of MSK Procedures. 19th Annual Diagnostic Imaging Update; March 2011; Kauai, HI.
Beaulieu CF.	Technical Aspects of MRI of the Knee. 20th Annual Current Concepts in MRI; October 27, 2010; Monterey, CA.
Biswal S.	New Developments in Imaging for Musculoskeletal Pain. 96th Scientific Assembly and Annual Meeting of the RSNA; November 28 - December 3, 2010; Chicago, IL.
Biswal S.	Sodium Ion Channel-Selective Toxins As Tools For Imaging Pain Generators. Bio-X Interdisciplinary Initiatives Symposium; August 25, 2010; Stanford, CA.
Blankenberg F.	Oxidative Stress in Apoptosis and Mitochondrial Related Disease. 2010 ALS User's Meeting Workshop Infrared Spectromicroscopy: The Berkeley Synchrotron Infrared Structural Biology (BSISB) Program; October 14, 2010; Lawrence Berkeley National Laboratories, CA.
Blankenberg F.	In Vivo Imaging of Cell Death. 7th Annual Training Course on Concepts and Methods in Programmed Cell Death & 18th Euroconference on Apoptosis / ECDO; September 2010; Ghent, Belgium.
Blankenberg F.	Oncologic Imaging in the Era of Molecular Medicine. Imaging of Apoptosis. 96th Scientific Assembly and Annual Meeting of the RSNA; November 28 - December 3, 2010; Chicago, IL.

Other Scientific Meeting Presentations

Other Presentations 2010

Blankenberg F.	Apoptosis – The Target and Challenge. Society of Nuclear Medicine; June 5, 2010; Salt Lake City, UT.
Butts-Pauly K.	Image Guidance of Focused Ultrasound. 52nd Annual Meeting of the American Association of Physicists in Medicine (AAPM); July 2010; Philadelphia, PA.
Chan F.	Imaging Heart Valves in Children: An Open and Shut Case. Imaging Airways in Children: An Inside and Outside Look. Pediatric Chest CT and Radiation Dose – Cost/Benefit. 12th Annual International Symposium on Multidetector-Row CT; May 18-21, 2010; San Francisco, CA.
Chan F.	Normal Cardiac Anatomy for Imaging. How Do I Assess MAPCAs for My Surgeons? 8th SPR Symposium on Pediatric Cardiac MR / 6th Advanced Pediatric Cardiovascular Imaging Course; January 2011; Stanford, CA.
Chan F.	Practical Pediatric Vascular Imaging: MR Imaging. 96th Scientific Assembly and Annual Meeting of the RSNA; November 28 - December 3, 2010; Chicago, IL.
Cheng Z.	18F-labeled Benzamides for Preclinical PET Imaging of Melanoma Metastases. 3rd Annual Scientific Retreat of the Melanoma Research Alliance; February 17, 2011; Washington, DC.
Cheng Z.	Exploring Chemical Space for Development of Novel Molecular Probes for Cancer Imaging. Howard University; February 18, 2011; Washington, DC.
Cheng Z.	Nanoprobes for Cancer Molecular Imaging. Huazhong University of Science and Technology Union Hospital; September 18, 2010; Wuhan, China.
Cheng Z.	Novel Small Proteins for Molecular Probes Discovery. National Institute of Biomedical Imaging and Bioengineering (NIBIB)/National Institutes of Health (NIH); February 18, 2011; Washington, DC.
Cheng Z.	Optical Imaging of Cancer using Bionanotechnology. University of Science and Technology of China; September 24, 2010; Hefei, China.
Daldrup-Link H.	The Future of Breast Cancer Imaging. Breast Cancer Oncology Retreat; Jan 28, 2011; UC San Francisco, CA.
Daldrup-Link H.	Imaging of Pediatric Abdominal Tumors. Children's Hospital of Eastern Ontario Grand Rounds; February 7, 2010; Ottawa, Canada.
Daldrup-Link H.	Cell Tracking with MR Imaging and Optical Imaging. Retreat of the Institute for Stem Cell Biology and Regenerative Medicine; January 24, 2011; Stanford, CA.
Daldrup-Link H.	Pediatric GU Imaging. UCSF Radiology Resident Review Course; March 2, 2010; San Francisco, CA.
Daniel BL.	MRI of the Breast. MRI of the Prostate. Body MR: Upcoming Techniques and Applications. Body MR Cases Workshop. 20th Annual Current Concepts in MRI; October 27, 2010; Monterey, CA.
Daniel BL.	Enhancing Foci Should Be Ignored. MRI of Silicone Breast Augmentation. Breast MRI "Jeopardy" Game - Test Your Wits at Breast MRI Interpretation. To Cut or to Core...When to do Different Kinds of MRI-Guided Interventions. 9th Annual Symposium on Advances in Breast MRI; October 14, 2010; Las Vegas, NV.
Daniel BL.	Breast MRI update: Current Status and Future Directions. Stanford Medicine Imaging Center Forum; September 30, 2010; Palo Alto, CA.
Do H.	Advances in Endovascular Treatment of Stroke. Endovascular Therapy of Intracranial Aneurysms. Spinal Augmentation Procedures: Clinical Innovations and Trials Update. 18th Annual Summer Diagnostic Imaging Update; July 13-16, 2010; Vancouver, BC Canada.
Do H.	State-of-the-Art Vertebral Augmentation. 40th Annual Scientific Meeting of the Western Angiographic and Interventional Society; September 11-15, 2010; Lanai, HI.
Fahrig R.	Cardiac CT Fluoroscopy – A Convergent Technology. 6th Advanced Pediatric Cardiovascular Imaging Course; January 21-23, 2011; Stanford, CA.
Fahrig R.	Expanding Clinical Applications for DynaCT: Challenges and Solutions. COBRA (Community of Bay Area Radionuclide Imagers); March 1, 2011; Stanford, CA.

Other Scientific Meeting Presentations

Other Presentations 2010

Fahrig R.	CT Imaging Technology: Advances for Mummy Scanning. Phoebe A. Hearst Museum of Anthropology; February 23, 2011; Berkeley, CA.
Fischbein N.	Imaging Protocols and Normal Imaging Anatomy. Imaging of the Visual Pathways. Orbital Disease: A Case-Based Discussion. 2010 Bay Area Ophthalmology Course; 2010; Stanford, CA.
Fischbein N.	Advances in Spinal MR Imaging. Imaging of Central Skull Base Tumors. 20th Annual Current Concepts in MRI; October 27, 2010; Monterey, CA.
Fischbein N.	Central Skull Base Neoplasms: Imaging Spectrum. 44th Annual Meeting of the American Society of Head and Neck Radiology; October 6-10, 2010; Houston, TX.
Fischbein N.	Imaging of Nasopharyngeal and Central Skull Base Malignancy. 48th Annual Meeting of the American Society of Neuroradiology; May 15-20, 2010; Boston, MA.
Fischbein N.	Central Nervous System Imaging in the Neuro-Intensive Care Unit. 8th Annual Meeting of the Neurocritical Care Society; September 15-18, 2010; San Francisco, CA.
Fleischmann D.	Acute Aortic Syndrome: Part 1: Aortic Dissection. Acute Aortic Syndrome, Part 2: Intramural Hematoma (IMH) and Penetrating Atherosclerotic Ulcer (PAU). Pre- and Post-operative Imaging of the Aortic Root. CT Technology Update. 18th Annual Summer Diagnostic Imaging Update; July 13-16, 2010; Whistler, BC, Canada.
Fleischmann D.	Scanning and Radiation Dose Parameters in CT. Contrast Medium Induced Nephrotoxicity (CIN) Precautions and policies in patients with decreased renal function. Physiologic Basis of Contrast Medium Injection Strategies for Vascular, Neuro, and Abdominal CT. 2D and 3D Abdominal Vascular Anatomy and Pathology. 4th Stanford Computed Tomography Workshop; Nov 18, 2010; Stanford, CA.
Fleischmann D.	The ABCs of Aortic Dissection. 96th Scientific Assembly and Annual Meeting of the RSNA; November 28 - December 3, 2010; Chicago, IL.
Fleischmann D.	Radiation Dose 101. The Physiologic Basis of Contrast Medium Enhancement. 3D Minisymposium: Live 3D and 4D Rendering of the Aortic Root. Lower Extremity CTA and CTV. Diagnostic Imaging Update at Bachelor Gulch; Jan 3-7, 2011; Beaver Creek, CO.
Fleischmann D.	3D and 4D Imaging of the Aortic Root. Aortic Dissection and its Complications. Society of Computed Body Tomography and MR Summer Practicum; August 8-11, 2010; Grand Teton National Park, WY.
Gambhir SS.	New Approaches for Imaging Dementia with PET. Alternatives to FDG PET-CT for Oncology. Earlier Detection of Cancer. Recent Advances in Cardiac SPECT. 19th Annual Diagnostic Imaging Update; March 2011; Kauai, HI.
Gambhir SS.	Integrating Biomarkers and Imaging. 23rd International Conference on Screening for Lung Cancer (IELCAP); October 2010; New York, NY.
Gambhir SS.	Future of Radiological Imaging in the Context of Diagnostic Medicine. 96th Scientific Assembly and Annual Meeting of the RSNA; November 28 - December 3, 2010; Chicago, IL.
Gambhir SS.	Emerging Strategies for the Merger of In Vitro and In Vivo Diagnostics. NCI Think Tank Mini Workshop Board of Scientific Advisors; February 2011; Bethesda, MD.
Gambhir SS.	Novel Strategies for Early Cancer Detection. Stand Up To Cancer Dream Team Summit Meeting; January 2011; Miami, FL.
Glover G.	Dynamics of Restless State Networks. Resting State Brain Connectivity Conference; September 16-19, 2010; Milwaukee, WI.
Gold GE.	MRI of the Elbow. MRI of the Ankle. MRI of the Shoulder. MRI of the Knee. MSK MRI Technical Considerations. 15th Annual Snowmass Clinical MRI: New Essentials - What You Need to Know; February 17, 2011; Snowmass, CO.
Gold GE.	Biochemical MR Imaging: Does it have a Future in Routine Clinical Practice. 37th Annual International Skeletal Society Musculoskeletal Imaging Update; September 29, 2010; Athens, Greece.
Gold GE.	Advanced MRI of Articular Cartilage and Osteoarthritis. Cornell University Grand Rounds; March 15, 2011; NY, NY.

Other Scientific Meeting Presentations

Other Presentations 2010

Gold GE.	Advanced MRI of Articular Cartilage and Osteoarthritis. Hospital for Special Surgery Grand Rounds; March 16, 2011; New York, NY.
Gold GE.	Advanced MSK Protocols at 3.0T. MRI of the Wrist – TFCC and Ligaments. SCBT/MR Summer Practicum; August 8, 2010; Moran, WY.
Hargreaves B.	Gradient Echo Imaging – Physics for Clinicians. Guess that Artifact. 18th Meeting of the International Society for Magnetic Resonance in Medicine; May 4, 2010; Stockholm, Sweden.
Hargreaves B.	Artifacts in MRI. Body MRI Concepts. Sequences and Contrast. Gradient Echo Family Sequences. What is MRI? 20th Annual Current Concepts in MRI; October 27, 2010; Monterey, CA.
Hargreaves B.	MRI of the Hip. 4th Conference on Quantitative Measures of Osteoarthritis; June 5, 2010; Vancouver, BC Canada.
Hargreaves B.	Physics of Breast MRI at 3T. What's My Artifact? Advanced Techniques for Breast MRI. Top 5 Technical Advances that will Affect your Breast MRI Practice. 9th Annual Symposium on Advances in Breast MRI; October 14, 2010; Las Vegas, NV.
Hargreaves B.	MRI of Articular Cartilage: Human Studies. Orthopaedic Research Society Annual Meeting; January 14, 2011; Long Beach, CA.
Hofmann LV.	Venous Thromboembolic Disease II: Chronic Venous Occlusions. Ground Control to Major Tom: When Systems in the IR Suite Break Down. 36th Annual Scientific Meeting of the Society of Interventional Radiology; March 28-31, 2011; Chicago, IL.
Hofmann LV.	Endovascular Treatment of Acute and Chronic DVT. Oakland Children's Hospital Grand Rounds; September 15, 2010; Oakland, CA.
Hofmann LV.	A New Chronic Venous Disease Initiative. Venous Disease Coalition Conference; September 20, 2010; Washington, DC.
Hovsepian D.	Interventional Radiology in the U.S.: Uterine Fibroid Embolization. Arterial Embolization for Pelvic Trauma. 90th Anniversary Symposium of Yerevan State Medical University; October 2010; Yerevan, Armenia.
Hovsepian D.	Fallopian Tube Recanalization. 96th Scientific Assembly and Annual Meeting of the RSNA; November 28 - December 3, 2010; Chicago, IL.
Hovsepian D.	Uterine Fibroid Embolization for Selected Patients. Association for Radiologic & Imaging Nursing (ARIN); October 23, 2010; Redwood City, CA.
Hovsepian D.	Introduction to Uterine Fibroid Embolization. Evening Seminar for Patient Education; May 2010; Stanford, CA.
Hwang, G	Tips and Tricks for RF Ablation: Liver. Management of Renal Tumors – Transarterial and Percutaneous: The Whole Gamut. Stereotactic Radiotherapy vs. Percutaneous Ablation Techniques: Results in Lung and Liver Tumors. Fiducial Implantation for Stereotactic Radiotherapy: How I Do It. 18th Annual Summer Diagnostic Imaging Update; July 13-16, 2010; Whistler, Canada.
Hwang, G	How to Handle Complications. Glycemic Control in the IR Suite. Liquid Embolics. 36th Annual Scientific Meeting of the Society of Interventional Radiology; March 28-31, 2011; Chicago, IL.
Iagaru A.	Imaging Angiogenesis: What can Different Modalities do? PET/CT in Angiogenesis Imaging. 96th Scientific Assembly and Annual Meeting of the RSNA; November 28 - December 3, 2010; Chicago, IL.
Iagaru A.	Introduction to PET/CT. Hospital Mae de Deus Symposium; April 26, 2010; Porto Alegre, Brazil.
Iagaru A.	Lymphomas: What can Nuclear Medicine do for you? Medical Oncology Grand Rounds; November 16, 2010; Stanford, CA.
Iagaru A.	Updates on PET/CT and Thyroid Cancer. Nuclear Medicine Grand Rounds; April 6, 2010; Stanford, CA.
Ikeda DM.	Benign MRI Findings. 96th Scientific Assembly and Annual Meeting of the RSNA; November 28 - December 3, 2010; Chicago, IL.

Other Scientific Meeting Presentations

Other Presentations 2010

Ikeda DM.	ACR BIRADS MRI Lexicon 2010 Update. Should Enhancing Foci be Ignored? Breast MRI in Neoadjuvant Chemotherapy and Partial Breast Irradiation. Correlating Digital Mammography, Sonography, and MRI. 9th Annual Symposium on Advances in Breast MRI; October 14, 2010; Las Vegas, NV.
Ikeda DM.	MRI Interpretation. Correlating Mammograms/US/MRI. False Negative Breast Imaging. Lesions for Biopsy. Breast 2011; March 26-27, 2011; Sydney, Australia.
Ikeda DM.	A Practical Approach to Image Interpretation. Breast MR with Guided Biopsy; February 7, 2011; Reston, VA.
Ikeda DM.	Correlating Mammography, Ultrasound and MRI. False Negative Mammo, Ultrasound, and MRI. MRI Indications. New Developments in Breast Imaging. Update in Advanced Breast Imaging; September 3-4, 2010; Bruges, Belgium.
Kamaya A.	Thyroid Nodule Evaluation and the Post Thyroidectomy Neck. HCC Imaging: What every Radiologist should know. Pregnancy and Postpartum Related Complications. Acute Gynecologic Emergency Imaging. 19th Annual Diagnostic Imaging Update; March 2011; Kauai, HI.
Komakula S.	Case Presentation: Intradural Intramedulary Lesions. 2nd Intensive Interactive Brain and Spine Imaging Conference; March 28, 2011; Salt Lake City, UT.
Kuo W.	Catheter-Directed Therapy for Acute PE. 36th Annual Scientific Meeting of the Society of Interventional Radiology; March 28-31, 2011; Chicago, IL.
Kuo W.	An Update on Retrievable IVC Filters. Complex Filter Retrieval: Advanced Techniques. Mission Impossible: Managing Filter Disasters. Endovascular Therapy for Massive PE: The Final Frontier. 4th Annual Meeting of the Latest Advances in Interventional Techniques (LAVA); July 2010; Maui, HI.
Kuo W.	Endovascular Therapy for Acute PE. 96th Scientific Assembly and Annual Meeting of the RSNA; November 28 - December 3, 2010; Chicago, IL.
Levin CS.	Strategies to Advance Time-of-Flight Positron Emission Tomography (ToF-PET): Study of Detector, Image Reconstruction and System Attributes for Advancing Sub-nanosecond Timing. New Technologies for Combining PET and MRI without Mutual Interference. 2010 Korean Society of Medical Physics; September 16-17, 2010; Seoul, South Korea.
Levin CS.	Instrumentation and Algorithms for 1 Millimeter Resolution Clinical PET. 2010 Stanford-Catholic University of Korea Joint Symposium; September 7, 2010; Seoul, South Korea.
Levin CS.	Exploiting Coherent Light in Positron Emission Tomography. Beckman Laser Institute's Laser Microbeam and Medical Program Seminar Series; November 16, 2010; UC Irvine, CA.
Levin CS.	Molecular Imaging Instrumentation Research at Stanford. Central Research Laboratory of Hamamatsu Photonics; September 13, 2010; Hamamatsu City, Japan.
Levin CS.	Technologies for Combining PET and MRI without Mutual Interference. Samsung Advanced Institute of Technology (SAIT); September 15, 2010; Gyeonggi-do, South Korea.
Lin M.	MDCT of Cardiac Valve Replacements. Preoperative Imaging of Pectus Excavatum. Volumetric Assessment of Pulmonary Nodules on CT. 12th Annual International Symposium on Multidetector-Row CT; May 18-21, 2010; San Francisco, CA.
Lipson JA.	Targeted Ultrasound after Breast MRI. Anatomy, Physiology, & Pathology of the Breast. 9th Annual Symposium on Advances in Breast MRI; October 14, 2010; Las Vegas, NV.
Lipson JA.	Breast Imaging in Breast Cancer Diagnosis. Cancer Education Seminar Series; October 5, 2010; Stanford, CA.
Louie J.	Chronic Venous Occlusion. 36th Annual Scientific Meeting of the Society of Interventional Radiology; March 28-31, 2011; Chicago, IL.
Lutz A.	Early Detection of Ovarian Cancer Using Targeted Microbubble-Enhanced Ultrasound. 4th Comprehensive Cancer Research Training Program (CCRTP); September 2010; Stanford, CA.
Lutz A.	Novel Diagnostic Tools in Ovarian Cancer Early Detection. Ovarian Cancer Action/ Helene Harris Memorial Trust Meeting; January 2011; Fort Lauderdale, FL.

Other Scientific Meeting Presentations

Other Presentations 2010

Marks M.	Preliminary Analysis of Endovascular Treatment Results for DEFUSE 2 Trial. DEFUSE Investigators Meeting; October 2010; Palo Alto, CA.
Marks M.	Endovascular Treatment of Ischemic Stroke. Stanford University Hospital; September 2010; Stanford, CA.
Marks M.	Intracranial Stenting: Unique Requirements, Novel Technologies, and Present Status. Transcatheter Cardiovascular Therapeutics; September 2010; Washington, DC.
Moseley M.	Debate: Should the Diffusion-Perfusion Study Group be Split? 18th Meeting of the International Society for Magnetic Resonance in Medicine; May 4, 2010; Stockholm, Sweden.
Moseley M.	MR Basic Concepts. MR Advanced Topics. American Society Neuroimaging; January 2011; San Francisco, CA.
Napel S.	Automated Image Retrieval Based on Lesion and Case Similarity. 96th Scientific Assembly and Annual Meeting of the RSNA; November 28 - December 3, 2010; Chicago, IL.
Newman B.	Anomalies of the Great Arteries. Airway Abnormalities Associated with Congenital Heart Disease. 38th Annual Meeting of the North American Society for Cardiovascular Imaging; October 3-5, 2010; Seattle, WA.
Newman B.	Disorders of the Large Airways in the Pediatric Population. 96th Scientific Assembly and Annual Meeting of the RSNA; November 28 - December 3, 2010; Chicago, IL.
Newman B.	Radiation Dose Reduction in Pediatric Cardiac CT. Advanced Pediatric Cardiac Imaging Symposium; January 18-23, 2011; Stanford, CA.
Newman B.	Point Counterpoint – Dose Related Issues in Cardiac CT Imaging. Ultrasound Body Applications in Children. ALARA CT; March 5-6, 2011; Dallas, TX.
Newman B.	Congenital Intra and Extrahepatic Portosystemic Shunts. CT of Congenital Lung Malformations in Children. CT of the Thymus in Children - Normal and Abnormal. 12th Annual International Symposium on Multidetector-Row CT; May 18-21, 2010; San Francisco, CA.
Nino-Murcia M.	Abdomen and Pelvis Cases. CT Review for the Nuclear Medicine Physician - Department of Veterans Affairs Employee Education System and Nuclear Medicine Service Postgraduate Course; August 3, 2010; Palo Alto, CA.
Paik D.	MicroCT Image Analysis. Caliper Life Sciences; May 2010.
Paulmurugan R.	Novel Imaging Assay Technologies to Monitor Fundamental Cellular Events in Living Subjects. 8th World Congress on Trauma, Shock, Inflammation and Sepsis; March 9-13, 2011; Munich, Germany.
Plevritis S.	Modeling the Natural History of Lung Cancer. Canary Foundation Annual Lung Cancer Working Group Meeting; March 28, 2011; Palo Alto, CA.
Plevritis S.	Radiogenomics: Integration of Medical Images and Transcriptomic Data in Non-Small Cell Lung Cancer. National Institute of Biomedical Imaging and Bioengineering; December 17, 2010; Bethesda, MD.
Plevritis S.	Systems Biology of Cancer. Stanford Hematology and Oncology Retreat; October 28, 2010; Asilomar, CA.
Plevritis S.	Modeling the Role of Differentiation in Cancer Progression. UCSF Cancer Center Workshop on Physical and Computational Approaches in Cancer Biology; March 18, 2011; San Francisco, CA.
Poullos P.	Virtual Colonoscopy for the Radiology Nurse. Radiologic Imaging Nurses Symposium; October 23, 2010; Redwood City, CA.
Poullos P.	Virtual Colonoscopy for the Technologist. Stanford CT Technologist In-Service; April 14, 2010; Stanford, CA.
Quon A.	FDG and Physiologic Effects on Medical Devices. Roche Advisory Board Meeting; December 2010.
Quon A.	Molecular Imaging and PET/CT From the Physician's Perspective. GE Molecular Imaging University; March 2011.
Quon A.	PET/CT and Nuclear Medicine in Neuroendocrine Tumors. Stanford Caring for Carcinoid Foundation; September 2010; Stanford, CA.

Other Scientific Meeting Presentations

Other Presentations 2010

Quon A.	PET/CT and the Post-Therapy Evaluation of Head/Neck Cancers. PET/CT Head/Neck Cases. UCSF Radiation Oncology Seminar on Head/Neck Cancers; April 2010; UC San Francisco, CA.
Rao J.	Drug Development: Choosing the Right Imaging Platform for your Drug or Biologic. 2010 National Biotechnology Conference; May 19, 2010; San Francisco, CA.
Rao J.	Novel Approaches to Imaging Protease Activity In Vivo. 2010 WMIC Preconference Satellite Meeting; September 6, 2010; Seoul, South Korea.
Rao J.	Metals in Biology. 240th Fall Annual Conference of the American Chemical Society; August 22-26, 2010; Boston, MA.
Rao J.	Proprotein Processing, Trafficking & Secretion. Gordon Research Conferences at Colby-Sawyer College; July 18-23, 2010; New London, NH.
Rao J.	Building Molecules for In Vivo Imaging of Biology and Diseases. Institute for Bioscience and Biotechnology Research (IBBR); April 25, 2011; University of Maryland College Park, MD.
Reiss AL.	Multi-site Neuroimaging Studies: Studies Preparation, Scan Acquisition, Imaging Processing, Cross-site Calibration and Data Analysis. Diabetes Research in Children Network (DirecNet); April 2010; Tampa, FL.
Reiss AL.	The Neuroscience of Humor. Euroscience Open Forum; July 2010; Torino, Italy.
Reiss AL.	Translational Research in Developmental Disabilities and Clinical Neuroscience. Harvard University & Massachusetts General Hospital; June 2010; Boston, MA.
Rubin D.	Informatics Infrastructure for Quantitative Assessment of Cancer Treatment Response. 52nd Annual Meeting of the American Association of Physicists in Medicine (AAPM); July 2010; Philadelphia, PA.
Rubin D.	Informatics Infrastructure to Standardize and Optimize Quantitative Imaging in Clinical Trials and Drug Development. Joint FDA, SNM, RSNA conference at NIH; April 2010; Bethesda, MD.
Rubin D.	Radiology in the Era of Quantitative Imaging, E-Science, and Biomedical Informatics. Memorial Sloan Kettering Cancer Center; May 2010; New York, NY.
Segall G.	PET/CT in Thoracic Malignancies. 57th Annual Meeting of the Society of Nuclear Medicine; June 5-9, 2010; Salt Lake City, UT.
Segall G.	PET/CT Read with the Experts: Cancers of the Thorax. 96th Scientific Assembly and Annual Meeting of the RSNA; November 28 - December 3, 2010; Chicago, IL.
Sommer FG.	Simplifying MDCT Urography Acquisition. MDCT of Renal Function: Approaches and Applications. 12th Annual International Symposium on Multidetector-Row CT; May 18-21, 2010; San Francisco, CA.
Sommer FG.	Pelvic MR. Renal MRI. Body MRI cases workshop. 20th Annual Current Concepts in MRI; October 27, 2010; Monterey, CA.
Sommer FG.	Renal MDCT including CT Urography. Prostate MRI Update. Emerging Technique of MR-guided HIFU Therapy. The 3D mini-symposium. Female Pelvic MRI. Diagnostic Imaging Update at Bachelor Gulch; Jan 3-7, 2011; Beaver Creek, CO.
Spielman D.	How do we Make an Image. 20th Annual Current Concepts in MRI; October 27, 2010; Monterey, CA.
Stevens K.	Case-based Learning of the Foot and Ankle. 18th Meeting of the International Society for Magnetic Resonance in Medicine; May 4, 2010; Stockholm, Sweden.
Stevens K.	Fluid Collections and Inflammatory Change around the Knee. 96th Scientific Assembly and Annual Meeting of the RSNA; November 28 - December 3, 2010; Chicago, IL.
Stevens K.	Commonly Missed Injuries of the Ankle and Foot. International Skeletal Society; October 2010; Athens, Greece.
Sze D.	Endovascular Repair of High-risk Thoracic Aortic Disease. 18th Annual Tsukiji Conference; October, 2010; Tokyo, Japan.

Other Scientific Meeting Presentations

Other Presentations 2010

Sze D.	Embolization: Basics. Radioembolization: Advanced workshop. Practical Interventional Oncology: Basic Principles. 36th Annual Scientific Meeting of the Society of Interventional Radiology; March 28-31, 2011; Chicago, IL.
Sze D.	Endovascular Repair of Thoracic Aortic Disease. Chiba University; October 2010; Chiba, Japan.
Sze D.	C-arm CT Applications in Radioembolization. Redistribution of Hepatic Arterial Flow. Society of Interventional Radiology Y90 Symposium; February 2011; Scottsdale, AZ.
Sze D.	Treatment of Chronic Total Occlusion. Catheter-based Thrombolysis of Pulmonary Embolism. Mechanical Lysis: Can we get on-table Success for Thrombosis and Embolization. Vascular Interventional Advances (VIVA); October 2010; Las Vegas, NV.
Vasanawala SS.	Approaches to Body MRI. MRCP and Enterography. Pediatric Abdominal MRI. 15th Annual Snowmass Clinical MRI: New Essentials - What You Need to Know; February 17, 2011; Snowmass, CO.
Vasanawala SS.	Advances in Pediatric Body MRI and PET/MR. Controversial Dose Related Issues in Cardiac CT. 2011 SPR ALARA-CT Meeting; March 2011; Dallas, TX.
Vasanawala SS.	Hepatobiliary MRI. Cardiac MRI Concepts. Approaches to MRA. 20th Annual Current Concepts in MRI; October 27, 2010; Monterey, CA.
Vasanawala SS.	Accelerated Imaging and Noise Reduction in MR. 8th SPR Symposium on Pediatric Cardiovascular MR/Basic Course; January 18-21, 2011; Stanford, CA.
Vasanawala SS.	Pediatric Hepatobiliary MRI. 96th Scientific Assembly and Annual Meeting of the RSNA; November 28 - December 3, 2010; Chicago, IL.
Willmann J.	Molecular Imaging: Pancreatic cancer. Canary Foundation Early Detection Symposium; March 29, 2011; Palo Alto, CA.
Willmann J.	Quantification and Monitoring of Inflammation in Inflammatory Bowel Disease using Molecular Imaging. Digestive Disease Center; October 16, 2010; Stanford, CA.
Willmann J.	Multi-modality Molecular Imaging. IEEE International Ultrasonics Symposium; October 12, 2010; San Diego, CA.

Published Papers

Published Papers

Abdelmaksoud MHK, Louie JD, Hwang GL, Kothary N, Hofmann LV, Hovsepian DM, Kuo WT, Sze DY. Development of New Hepaticoenteric Collateral Pathways after Hepatic Arterial Skeletonization in Preparation for Yttrium-90 Radioembolization. J Vasc Interv Radiol. 2010;21(9):1385-95.

Ahn BC, Ronald JA, Kim YI, Katzenberg R, Singh A, Paulmurugan R, Ray S, Hofmann LV, Gambhir SS. Potent, Tumor-Specific Gene Expression in an Orthotopic Hepatoma Rat Model using a Survivin-Targeted, Amplifiable Adenoviral Vector. Gene Ther. 2011 Feb 10 [Epub ahead of print].

Akgul CB, Rubin DL, Napel S, Beaulieu CF, Greenspan H, Acar B. Content Based Image Retrieval in Radiology: Current Status and Future Directions. J Digit Imaging. 2011;24(2):208-22. PMID: 20376525.

Aksoy M, Skare S, Holdsworth S, Bammer R. Effects of Motion and B-Matrix Correction for High-Resolution DTI with Short-Axis PROPELLER-EPI. NMR Biomed. 2010 Aug;23(7):794-802. PMID: 20222149.

Allen SP, Morrell GR, Peterson B, Park D, Gold GE, Kaggie JD, Bangerter NK. Phase-Sensitive Sodium B1 Mapping. Magn Reson Med. 2011 April;65(4):1125-30. PMID: 21413078.

Anderson L, Middleton WD, Teefey SA, Reading CC, Langer JE, Desser T, Szabunio MM, Mandel SJ, Hildebolt CF, Cronan JJ. Hashimoto Thyroiditis: Part 1, Sonographic Analysis of the Nodular Form of Hashimoto Thyroiditis. AJR Am J Roentgenol. 2010 Jul;195(1):208-15.

Anderson L, Middleton WD, Teefey SA, Reading CC, Langer JE, Desser T, Szabunio MM, Mandel SJ, Hildebolt CF, Cronan JJ. Hashimoto Thyroiditis: Part 2, Sonographic Analysis of Benign and Malignant Nodules in Patients with Diffuse Hashimoto Thyroiditis. AJR Am J Roentgenol. 2010 Jul;195(1):216-22.

Published Papers

Published Papers

Atlas SW. Don't Tweak Obamacare, Repeal It. Forbes. December 14, 2010.

Atlas SW. Obamacare Under Attack: Is It Time to Eliminate Government Health Insurance? National Review Online. 2011 Jan 17.

Atlas SW. Poison Pill. Hoover Digest. Winter 2011, Number 1; January 12, 2011.

Atlas SW. The Disregarded Options of American Health Care. Defining Ideas. 2011 February 6.

Atlas SW. The Ignored Facts of American Healthcare. Defining Ideas. 2010 December 13.

Atlas SW. The Worst Study Ever? Commentary Magazine, April, 2011.

Auer VJ, Bucher J, Schremmer-Danninger E, Piontek G, Paulmurugan R, Pierre-Maechler P, Reiser MF, Stangl MJ, Berger F. Non-Invasive Imaging of Ferucarbotran Labeled INS-1E Cells and Rodent Islets In Vitro and in Transplanted Diabetic Rats. Curr Pharm Biotechnol. 2011 Apr;12(4):488-96.

Bailey SL, Sigal BM, Plevritis SK. Impact of Tumor Volume Doubling Time and Mammographic Tumor Detectability on Screening Outcomes in Women 40-49 years Old. J Natl Cancer Inst. 2010;102(16):1263-71.

Baker LC, Afendulis C, Atlas SW. Assessing Cost-Effectiveness and Value as Imaging Grows: The Case of Carotid Artery CT. Health Affairs. 2010;29:2260-67.

Balchandani P, Pauly J, Spielman D. Designing Adiabatic Radio Frequency Pulses using the Shinnar-Le Roux Algorithm. Magn Reson Med. 2010 Sep;64(3):843-51. PMID: 20806378. PMCID: PMC2975518.

Barnea-Goraly N, Lotspeich LJ, Reiss AL. Similar White Matter Aberrations in Children with Autism and their Unaffected Siblings: A Diffusion Tensor Imaging Study using Tract-Based Spatial Statistics. Arch Gen Psychiatry. 2010;67(10):1052-60. PMID: 20921121.

Barnes P, Galaznik J, Gardner H, Shuman M. Infant Acute Life-Threatening Event – Dysphagic Choking Versus Nonaccidental Injury. Sem Ped Neurol. 2010;17:7-11.

Barnes P. Imaging of NAI and the Mimics: Issues and Controversies in the Era of Evidence-Based Medicine. Radiol Clin North Am. 2011;49:205-29.

Basu PA, Ruiz-Wibbelsmann JA, Spielman SB, Van Dalsem VF 3rd, Rosenberg JK, Glazer GM. Creating a Patient-Centered Imaging Service: Determining what Patients want. AJR Am J Roentgenol. 2011 Mar;196(3):605-10. PMID: 21343503.

Bendall SC, Simonds EF, Qiu P, Amir E, Krutzik P, Finck R, Bruggner R, Melamed R, Ornatsky O, Balderas R, Plevritis SK, Sachs K, Pe'er D, Tanner S, Nolan G. Single-Cell Mass Cytometry of Differential Immune and Drug Responses across a Human Hematopoietic Continuum. Science. 2011 May 6:687-96.

Bjorquist OA, Fryer SL, Reiss AL, Mattson SN, Riley EP. Cingulate Gyrus Morphology in Children and Adolescents with Fetal Alcohol Spectrum Disorders. Psychiatry Res. 181(2):101-7, 2010. PMID: 20080394. PMCID: PMC2815126.

Boas FE, Fleischmann D. Evaluation of Two New Iterative Techniques for Reducing Metal Artifacts in Computed Tomography. Radiology. 2011 (Epub ahead of print).

Boddington S, Sutton EJ, Henning TD, Nedopil A, Sennino B, Kim A, Daldrup-Link HE. Labeling Human Mesenchymal Stem Cells with Fluorescent Contrast Agents: The Biological Impact. Mol Imaging Biol. 2011;13(1):3-9.

Boddington SE, Henning TD, Jha P, Schlieve C, Mandrussow L, DeNardo D, Bernstein HS, Ritner C, Golovko D, Zhao S, Daldrup-Link H. Labeling Human Embryonic Stem Cell Derived Cardiomyocytes with Indocyanine Green for Noninvasive tracking with Optical Imaging: An FDA Compatible Alternative to Firefly Luciferase. Cell Transplant. 2010;19(1): 55-65. PMCID: 2939828.

Bray S, Dunkin B, Hong DS, Reiss AL. Reduced Function Connectivity during Working Memory in Turner Syndrome. Cereb Cortex. 2011 March 25 [Epub ahead of print].

Brody JD, Weiyun ZA, Czerwinski DK, Torchia JT, Levy M, Advani RH, Kim YH, Hoppe RT, Knox SJ, Shin LK, Wapnir I, Tibshirani RJ, Levy R. In Situ Vaccination with a TLR9 Agonist Induces Systemic Lymphoma Regression. J Clin Oncol. 2010;28(28):4324-32.

Brown G, Mathalon DH, Stern H, Ford J, Mueller B, Greve D, McCarthy G, Voyvodic J, Glover G, Diaz M, Yetter E, Ozyurt IB, Jorgensen KW, Wible CG, Turner JA, Thompson WK, Potkin S, FBIRN. Multisite Reliability of Cognitive BOLD Data. NeuroImage. 2010;54:2163-75.

Cao F, Xie X, Gollan T, Zhao L, Narsinh K, Lee RJ, Wu JC. Comparison of Gene Transfer Efficiency in Human Embryonic Stem Cells. Mol Imaging Biol. 2010;12:15-24. PMID: 19551446.

Published Papers

Cao Z, Fan-Minogue H, Bellovin DI, Yevtodiyenko A, Arzeno J, Yang Q, Gambhir SS, Felsher DW. MYC Phosphorylation, Activation, and Tumorigenic Potential in Hepatocellular Carcinoma are Regulated by HMG-CoA Reductase. Cancer Res. 2011 [Epub ahead of print].

Carpenter CM, Pogue BW, Jiang S, Wang J, Hargreaves BA, Rakow-Penner R, Daniel BL, Paulsen KD. MR Water Quantitative Priors Improves the Accuracy of Optical Breast Imaging. IEEE Trans Med Imaging. 2011;30(1):159-168.

Carpenter CM, Rakow-Penner R, Jiang S, Daniel BL, Pogue BW, Glover GH, Paulsen KD. Inpired Gas-Induced Vascular Change in Tumors with Magnetic-Resonance-Guided Near-Infrared Imaging: Human Breast Pilot Study. J Biomed Opt. 2010 May-Jun;15(3):036026.

Carpenter CM, Rakow-Penner R, Jiang S, Pogue BW, Glover GH, Paulsen KD. Monitoring of Hemodynamic Changes Induced in the Healthy Breast through Inspired Gas Stimuli with MR-Guided Diffuse Optical Imaging. Med Phys. 2010 Apr;37(4):1638-46. PMID: 20443485.

Carrion VG, Haas BW, Garrett A, Song S, Reiss AL. Reduced Hippocampal Activity in Youth with Post-Traumatic Stress Symptoms: An fMRI Study. J Pediatr Psychol. 35(5):559-69, 2010. PMID: 19995868.

Carrion VG, Weems CF, Reichert K, Hoffman BC, Reiss AL. Decreased Prefrontal Cortical Volume Associated with Increased Bedtime Cortisol in Traumatized Youth. Biol Psychiatry. 2010;68(5):491-3. PMID: 20579974.

Chan KT, Popat RA, Sze DY, Kuo WT, Kothary N, Louie JD, Hovsepian DM, Hwang GL, Hofmann LV. Common Iliac Vein Stenosis and Risk of Pulmonary Embolism: An Inverse Correlation. J Vasc Interv Radiol. 2011 Feb;22(2):133-41.

Chang CE, Glover GH. Time-Frequency Dynamics of Resting-State Brain Connectivity Measured with fMRI. NeuroImage. 2010;50:81-9.

Chang CE, Glover GH. Variable Density Spiral-In/Out fMRI. Magn Reson Med. 2011;65:1287-96.

Chang E, Liu S, Gowrishankar G, Yaghoubi S, Wedgeworth JP, Chin F, Berndorff D, Gekeler V, Gambhir SS, Cheng Z. Reproducibility Study of 18F-FP-PRGD2 Uptake in Murine Models of Human Tumor Xenografts. Eur J Nucl Med Mol imaging. 2011;38(4):722-30. PMID: 21125268.

Chen C, Kijowski R, Shapiro L, Tuite M, Davis K, Klaers J, Block W, Gold GE. Cartilage Morphology at 3.0T: Assessment of Three-dimensional MR Imaging Techniques. J Magn Reson Imaging. 2010 Jul;32(1):173-83. PMID: 20578024.

Chen CA, Chen W, Goodman SB, Hargreaves BA, Koch KM, Lu W, Brau AC, Draper CE, Delp SL, Gold GE. New MR Imaging Methods for Metallic Implants in the Knee: Artifact Correction and Clinical Impact. JMRI. 2011;33(5):1121-7.

Chen H, Li F, Zhao X, Yuan C, Rutt BK, Kerwin WS. Extended Graphical Model for Analysis of Dynamic Contrast-Enhanced MRI. Magn Reson Med. 2011 Mar 9. doi:10.1002/mrm.22819. PMID: 21394770.

Chen IY, Gheysens O, Ray S, Padmanabhan P, Paulmurugan R, Wang Q, Loening AM, Rodriguez-Porcel M, Willmann JK, Sheikh AY, Hoyt G, Contag CH, Robbins RC, Biswal S, Wu JC, Gambhir SS. A Bi-Directional Vector for Indirect Imaging and Amplification of Transgene Expression Mediated by a Weak Cardiac-Specific Promoter. Gene Ther. 2010 Jul;17(7):827-38.

Chen IY, Gheysens O, Ray S, Wang Q, Padmanabhan P, Paulmurugan R, Loening AM, Rodriguez-Porcel M, Willmann JK, Sheikh AY, Nielsen CH, Hoyt G, Contag CH, Robbins RC, Biswal S, Wu JC, Gambhir SS. Indirect Imaging of Cardiac-Specific Transgene Expression Using a Bidirectional Two-Step Transcriptional Amplification Strategy. Gene Ther. 2010;17(7):827-38. PMID: 20237511.

Chen J, Butts-Pauly K. Optimization of Encoding Gradients for MR-ARFI. MRM. 2010 Apr;63(4):1050-8. PMID: 20373406.

Cheng Z, De Jesus OP, Kramer DJ, De A, Webster JM, Gheysens O, Levi J, Namavari M, Wang S, Park JM, Zhang R, Liu H, Lee B, Syud FA, Gambhir SS. 64Cu-labeled Affibody Molecules for Imaging of HER2 Expressing Tumors. Mol Imaging Biol. 2010;12(3):316-24. PMID: 19779897.

Chennupati SK, Quon A, Kamaya A, Pai RK, La T, Krakow TE, Graves E, Koong AC, Chang DT. Positron Emission Tomography for Predicting Pathologic Response After Neoadjuvant Chemoradiotherapy for Locally Advanced Rectal Cancer. Am J Clin Oncol. 2011 Mar 17 [Epub ahead of print].

Chin FT, Shen B, Liu S, Berganos RA, Chang E, Mittra E, Chen X, Gambhir SS. First Experience with Clinical-Grade [(18)F]FPP(RGD)(2): An Automated Multi-step Radiosynthesis for Clinical PET Studies. Mol Imaging Biol. 2011 [Epub ahead of print].

Choudhury KR, Paik DS, Yi CA, Napel S, Roos JE, Rubin GD. Assessing Operating Characteristics of CAD Algorithms in the Absence of a Gold Standard. Med Phys. 2010;37(4):1788-95.

Chua JY, Pendharkar AV, Wang N, Choi R, Andres RH, Gaeta X, Zhang J, Moseley ME, Guzman R. Intra-Arterial Injection of Neural Stem Cells using a Microneedle Technique does not cause Microembolic Strokes. J Cereb Blood Flow Metab. 2011 May;31(5):1263-71. PMID: 21157474.

Published Papers

Cohen DJ, Nichols T, Brignone L, Hall SS, Reiss AL. Insular Volume Reduction in Fragile X Syndrome. Int J Dev Neurosci. 2011 Jan 31. [Epub ahead of print]. PMID: 21291994.

Cohen JD, Mock JR, Nichols T, Zadina J, Corey DM, Lemen L, Bellugi U, Galaburda A, Reiss AL, Foundas AL. Morphometry of Human Insular Cortex and Insular Volume Reduction in Williams Syndrome. J Psychiatr Res. 2010;44(2):81-9. PMID: 19660766. PMCID: PMC2813413.

Collins LK, Levin TL, Berdon WE, Cowles RA, Newman B. Rudhe Syndrome: Reversible Right Middle Lobe Emphysema in Infants with Left-to-Right Shunts – A Historical Review. Pediatr Radiol. 2010; 40(5):762-5. PMID: 20135111.

Convex Reynolds PD, Olcott PD, Pratx G, Lau FWY, Levin CS. Optimization of Coincidence Time Resolution for a High Resolution PET System. IEEE Trans Med Imaging. 2010 Sept;30(2):391-400.

Coogan JS, Chan FP, Taylor CA, Feinstein JA. Computational Fluid Dynamic Simulations of Aortic Coarctation Comparing the Effects of Surgical and Stent Based Treatments on Aortic Compliance and Ventricular Workload. Catheter Cardiovasc Interv. 2011 Apr 1:77(5):680-91.

Cooper L, Kong J, Gutman D, Wang F, Cholleti S, Pan T, Widener P, Sharma A, Mikkelsen T, Flanders A, Rubin DL, Van Meir E, Kurc T, Moreno C, Brat D, Saltz J. An Integrative Approach for In Silico Glioma Research. An Integrative Approach for In Silico Glioma Research. IEEE Trans Biomed Eng. 57(10):2617-21.

Crema MD, Roemer FW, Marra MD, Burstein D, Gold GE, Eckstein F, Baum T, Mosher TJ, Carrino JA, Guermazi A. Articular Cartilage in the Knee: Current MR Imaging Techniques and Applications in Clinical Practice and Research. Radiographics. 2011 Jan-Feb;31(1):37-61. PMID: 21257932.

Cui X, Bray S, Bryant DM, Glover GH, Reiss AL. A Quantitative Comparison of NIRS and fMRI Across Multiple Cognitive Tasks. NeuroImage. 2011;54(4):2808-21. PMID: 21047559. PMCID: PMC3021967.

Cui X, Bray S, Reiss AL. Functional Near Infrared Spectroscopy (NIRS) Signal Improvement based on Negative Correlation between Oxygenated and Deoxygenated Hemoglovin Dynamics. NeuroImage. 2010;49(4):3039-46. PMID: 19945536. PMCID: PMC2815126.

Cui X, Bray S, Reiss AL. Speeded Near-Infrared Spectroscopy (NIRS) Response Detection. PLoS ONE. 2010 Nov 11;5(11):e15474. PMID: 21085607. PMCID: PMC2978722.

Cukur T, Shimakawa A, Yu H, Hargreaves BA, Hu BS, Nishimura DG, Brittain JH. Magnetization-Prepared IDEAL bSSFP: A Flow-Independent Technique for Noncontrast-Enhanced Peripheral Angiography. JMRI. 2010;33(4):931-9.

Daadi MM, Davis AS, Arac A, Li Z, Maag AL, Bhatnagar R, Jiang K, Sun G, Wu JC, Steinberg GK. Human Neural Stem Cell Grafts Modify Microglial Response and Enhance Axonal Sprouting in Neonatal Hypoxic-Ischemic Brain Injury. Stroke. 2010;41(3):516-23. PMID: 20075340.

Daley ME, Le QT, Jain AK, Maxim PG, Hsu A, Loo BW Jr, Kaplan MJ, Fischbein NJ, Colevas AD, Pinto H, Chang DT. Intensity-Modulated Radiotherapy for Locally Advanced Cancers of the Larynx and Hypopharynx. Head Neck. 2011;33(1):103-11.

Daly ME, Le QT, Kozak MM, Maxim PG, Murphy JD, Hsu A, Loo BW, Kaplan MJ, Fischbein NJ, Chang DT. Intensity-Modulated Radiotherapy for Oral Cavity Squamous Cell Carcinoma: Patterns of Failure and Predictors of Local Control. Int J Radiat Oncol Biol Phys. 2010 Jul 31 [Epub ahead of print].

Darpolor MM, Yen YF, Chua MS, Xing L, Clarke-Katzenberg RH, Shi W, Mayer D, Josan S, Hurd RE, Pfefferbaum A, Senadheera L, So S, Hofmann LV, Glazer GM, Spielman DM. In Vivo MRSI of Hyperpolarized [1-(13)C]pyruvate Metabolism in Rat Hepatocellular Carcinoma. NMR Biomed. 2010 Dec 12 [Epub ahead of print]. PMID: 21154868. PMCID: PMC3073155.

de la Zerda A, Bodapati S, Teed R, Schipper M, Keren S, Smith B, Ng J, Gambhir SS. A Comparison between Time Domain and Spectral Imaging Systems for Imaging Quantum Dots in Small Living Animals. Mol Imaging Biol. 2010;12(5):500-8.

de la Zerda A, Liu Z, Bodapati S, Teed R, Vaithilingam S, Khuri-Yakub BT, Chen X, Dai H, Gambhir SS. Ultrahigh Sensitivity Carbon Nanotube Agents for Photoacoustic Molecular Imaging in Living Mice. Nano Letters, 2010;10(6):2168-72.

de la Zerda A, Paulus Y, Teed R, Bodapati S, Dollberg Y, Kuri-Yakub B, Blumenbranz M, Moshfeghi D, Gambhir SS. Photoacoustic Ocular Imaging. Opt Lett. 2010;35(3):270-2.

Dehkharghani S, Dillon WP, Bryant SO, Fischbein NJ. Unilateral Calcification of the Caudate and Putamen: Association with Underlying Developmental Venous Anomaly. AJNR Am J Neuroradiol. 2010;31:1848-52.

Delbeke D, Graham M, Royal H, Segall G, Shulkin BL, Ziessman HA. Conjoint Statement of the SNM, ACNM, and ABNM on Credentialing and Delineation of Privileges for Therapeutic Procedures using Radiopharmaceuticals. J Nucl Med. 2011;52(2):323-6.

Deshmukh SD, Shin DS, Willman JK, Rosenberg J, Shin L, Jeffrey RB. Non-Emergency Small Bowel Obstruction: Assessment of CT Findings that Predict Need for Surgery. Eur Radiol. 2010;21(5):982-6.

Deshmukh SD, Willmann JK, Jeffrey RB. Pathways of Extrapancreatic Perineural Invasion by Pancreatic Adenocarcinoma: Evaluation with 3D Volume-Rendered MDCT Imaging. AJR AM J Roentgenol. 2010;194:668-674.

Deshpande N, Needles A, Willmann JK. Molecular Ultrasound Imaging: Current Status and Future Directions. Clin Radiol. 2010;65:567-81.

Deshpande N, Pysz MA, Willmann JK. Molecular Ultrasound Assessment of Tumor Angiogenesis. Angiogenesis. 2010;13:175-88.

Deshpande N, Ren Y, Foygel K, Rosenberg J, Willmann JK. Tumor Angiogenic Marker Expression Levels during Tumor Growth: Longitudinal Assessment with Molecular Ultrasound Imaging. Radiology. 2011;258:804-11.

Do B, Wu A, Biswal B, Kamaya A, Ruibin DL. Informatics in Radiology: RADTF: A Semantic Search-Enabled, Natural Language Processor-Generated Radiology Teaching File. Radiographics. 2010;30(7):2039-48. PMID 20801868.

Do B, Wu A, Biswal, S, Kamaya A, Rubin D. RadTF: A Semantic Search Enabled, Natural Language Processor (NLP) Generated Radiologic Teaching File. Radiographics. 2010;30(7):2039-48.

Do BH, Mari C, Tseng JR, Quon A, Rosenberg J, Biswal S. Pattern of 18f-Fdg Uptake in the Spinal Cord in Patients with Non-Central Nervous System Malignancy. Spine. (Phila Pa 1976) 2011 Feb 9 [Epub ahead of print].

Draper CE, Besier TF, Fredericson M, Santos JM, Beaupre GS, Delp SL, Gold GE. Differences in Patellofemoral Kinematics Between Weight-Bearing and Non-Weight-Bearing Conditions in Patients with Patellofemoral Pain. J Orthop Res. 2011 Mar;29(3):312-7. PMID: 20949442.

Draper CE, Chew KT, Wang R, Jennings F, Gold GE, Fredericson M. Comparison of Quadriceps Angle Measurements using Short-Arm and Long-Arm Goniometers: Correlation with MRI. PM R. 2011 Feb;3(2):111-6. PMID: 21333949.

Dudukovic NM, Preston AR, Archie JJ, Glover GH, Wagner AD. High-Resolution fMRI Reveals Match Enhancement and Attentional Modulation in the Human Medial Temporal Lobe. J Cogn Neurosci. 2011;23:670-82.

Fan X, Ren P, Dhal S, Bejerano G, Goodman SB, Druzin ML, Gambhir SS, Nayak NR. Noninvasive Monitoring of Placenta-Specific Transgene Expression by Bioluminescence Imaging. PLoS One. 2011;6(1):e16348.

Fan-Minogue H, Cao Z, Paulmurugan R, Chan CT, Massoud TF, Felsher DW, Gambhir SS. Noninvasive Molecular Imaging of c-Myc Activation in Living Mice. Proc Natl Acad Sci USA. 2010 Sep 7;107(36):15892-7.

Fischbein NJ, Wijman CA. Nontraumatic Intracranial Hemorrhage. Neuroimaging Clin N Am. 2010;20:469-92.

Forman C, Aksoy M, Hornegger J, Bammer R. Self-Encoded Marker for Optical Prospective Head Motion Correction in MRI. Med Image Comput Comput Assist Interv. 2010;13(Pt 1):259-66. PMID: 20879239.

Ganguly A, Simons J, Schneider A, Keck B, Bennett R, Coogan S, Herfkens R, Fahrig R. In Vivo Imaging of Femoral Artery Nitinol Stents for Deformation Analysis. JVIR. 2011 Feb;22(2):244-9.

Ganguly A, Simons J, Schneider A, Keck B, Bennett R, Fahrig R. In Vitro Imaging of Femoral Artery Nitinol Stents for Deformation Analysis. JVIR. 2011 Feb;22(2):236-43.

Ganguly A, Yoon S, Fahrig R. Dose and Detectability for a Cone-Beam C-Arm CT System Revisited. Med Phys. 2010 May;37(5):2264-8.

Gao H, Zhu L, Fahrig R. Modulator Design for X-ray Scatter Correction Using Primary Modulation: Material Selection. Med Phys. 2010 Aug;37(8):4029-37.

Gao J, Chen K, Miao Z, Ren G, He X, Chen X, Gambhir SS, Cheng Z. Affibody-Based Nanoprobes for HER2-Expressing Cell and Tumor Imaging. Biomaterials. 2011;32(8):2141-8. PMID 21147502.

Gao J, Chen K, Xie R, Xie J, Lee S, Cheng Z, Peng X, Chen X. Ultrasmall Near-Infrared Non-Cadmium Quantum Dots for In Vivo Tumor Imaging. Small. 2010;6(2):256-61. PMID: 19911392.

Gao J, Chen K, Xie RG, Xie J, Yang YJ, Cheng Z, Peng XG, Chen XY. In Vivo Tumor-Targeted Fluorescence Imaging using Near-Infrared Non-Cadmium Quantum Dots. Bioconjug Chem. 2010;21(4):604-9. PMID:20369817.

Gao J, Chen X, Cheng Z. Near-Infrared Quantum Dots as Optical Probes for Tumor Imaging. Curr Top Med Chem. 2010;10(12):1147-57. PMID: 20388111.

Garrett A, Kelly R, Gomez R, Keller J, Schatzberg AF, Reiss AL. Aberrant Brain Activation During a Working Memory Task in Psychotic Major Depression. Am J Psychiatry. 2011;168(2):173-82. PMID: 21078708.

Gayer G, Petrovitch I, Jeffrey RB. Foreign Objects Encountered in the Abdominal Cavity at CT. Radiographics. 2011 Mar-Apr;31(2):409-28. PMID: 21415187.

Gayer G, Petrovitch I. CT Diagnosis of a Large Peritoneal Loose Body: A Case Report and Review of the Literature. Br J Radiol. 2011 Apr;84(1000):e83-5. PMID: 21415299.

Gean AD, Fischbein NJ, Purcell DD, Aiken A, Manley G, Stiver SI. The Benign Anterior Temporal Epidural Hematoma: An Indolent Lesion with a Characteristic Imaging Appearance Followign Blunt Head Trauma. Radiology. 2010;257:212-8.

Gean AD, Fischbein NJ. Head Trauma. Neuroimaging Clin N Am. 2010;20:527-56.

Geevarghese SK, Geller DA, de Haan H, Horer M, Knoll A, Mescheder A, Nemunaitis J, Reid T, Sze DY, Tanabe KK. Phase I/II Study of an Oncolytic Herpes Simplex Virus, NV1020, in Patients with Heavily Pretreated Refractory Colorectal Cancer Metastatic to the Liver. Hum Gene Ther. 2010 May 20 [Epub ahead of print].

Gentles AJ, Plevritis SK, Majeti R, Alizadeh AA. A Leukemic Stem Cell Gene Expression Signature Predicts Survival in Acute Myeloid Leukemia. JAMA. 2010;304(24):2706-15.

Ghatan CE, Kuo WT, Hofmann LV, Kothary N. Making the Case for Early Medical Student Education in Interventional Radiology: A Survey of 2nd-year Students in a Single U.S. Institution. J Vasc Interv Radiol. 2010 Apr;21(4):549-53.

Gheysens O, Chen IY, Rodriguez-Porcel M, Chan C, Rasooly J, Vaerenberg C, Paulmurugan R, Willmann JK, Deroose C, Wu J, Gambhir SS. Non-Invasive Bioluminescence Imaging of Myoblast-Mediated Hypoxia-Inducible Factor-1 Alpha Gene Transfer. Mol Imaging Biol. 2011 Jan 26 [Epub ahead of print].

Ghole SA, Bakhtary S, Staudenmayer K, Sze DY, Pai RK, Visser BC, Norton JA, Poultsides GA. Ruptured Biliary Cystadenoma Managed by Angiographic Embolization and Interval Partial Hepatectomy. Dig Dis Sci. 2011 Mar 29 [Epub ahead of print].

Ghosh Z, Wilson KD, Wu Y, Hu S, Quertermous T, Wu JC. Persistent Donor Cell Gene Expression among Human Induced Pluripotent Stem Cells Contributes to Differences with Human Embryonic Stem Cells. PLoS One. 2010;5(2):e8975. PMID: 20126639.

Girard E, Al-Ahmad A, Rosenberg J, Luong R, Moore T, Lauritsch G, Boese J, Fahrig R. Contrast-Enhanced Cardiac C-Arm CT Evaluation of Radiofrequency Ablation Lesions in the Left Ventricle. JACC: Cardiovascular Imaging. 2011;4(3):259-68.

Golarai G, Hong S, Haas BW, Galaburda A, Mills DL, Bellugi U, Grill-Spector K, Reiss AL. The Fusiform Face Area is Enlarged in Williams Syndrome. J Neurosci. 2010;30(19):6700-12. PMID: 20463232.

Golovko D, Henning T, Bauer JS, Settles M, Frenzel T, Mayerhofer A, Rummeny E, Daldrup-Link HE. Accelerated Stem Cell Labeling with Ferucarbotran and Protamine. Eur Radiol. 2010;20(3):640-8. PMCID: 2822227.

Gonzalez-Lara LE, Xu X, Hofstetrova K, Pniak A, Chen Y, McFadden CD, Martinez-Santiesteban FM, Rutt BK, Brown A, Foster PJ. The Use of Cellular Magnetic Resonance Imaging to Track the Fate of Iron-Labeled Multipotent Stromal Cells after Direct Transplantation in a Mouse Model of Spinal Cord Injury. Mol Imaging Biol. 2010 Aug;13(4):702-11. PMID: 20686855.

Goodman M, Willmann JK, Jeffrey RB. Incidentially Discovered Solid Pancreatic Masses: Imaging and Clinical Observations. Abdom Imaging. [Epub ahead of print].

Gothelf D, Hoeft F, Ueno T, Sugiura L, Lee AD, Thompson P, Reiss AL. Developmental Changes in Multivariate Neuroanatomical Patterns that Predict Risk for Psychosis in 22q11.2 Deletion Syndrome. J Psychiatr Res. 2011;45(3):322-31. PMID: 20817203. PMCID: PMC3000448.

Greenberg SB, Bhutta S, Braswell L, Chan F. Computed Tomography Angiography in Children with Cardiovascular Disease: Low Dose Techniques and Image Quality. Int J Cardiovasc Imaging. 2011 Jan 7 [Epub ahead of print].

Greve DN, Mueller B, Liu TT, Turner JA, Voyvodic J, Yetter E, Diaz M, McCarthy G, Wallace S, Roach B, Ford JM, Mathalon DA, Calhoun V, Wible C, Glover GH, The FBIRN. A Novel Method for Quantifying Scanner Instability in fMRI. MRM. 2011;65(4):1053-61.

Grissom WA, Lustig M, Holbrook AB, Rieke V, Pauly JM, Butts-Pauly K. Reweighted l(1) Referenceless PRF Shift Thermometry. Magn Reson Med. 2010 Oct;64(4):1068-77. PMID: 20564600.

Grissom WA, Rieke V, Holbrook AB, Medan Y, Lustig M, Santos J, McConnell MV, Butts-Pauly K. Hybrid Referenceless and Multibaseline Subtraction MR Thermometry for Monitoring Thermal Therapies in Moving Organs. Med Phys. 2010 Sep;37(9):5014-26. PMID: 20964221.

Gu Y, Matteson JL, Skelton RT, Deal AC, Stephan F, Duttweiler F,Gasaway TM, Levin CS. Study of a High Resolution, 3-D Positioning Cross-Strip Cadmium Zinc Telluride Detector for PET. Phys Med Biol. 2011;56:1563.

Gu Y, Pratx G, Lau FWY, Levin CS. Effects of Multiple-Interaction Photon Events in a High-Resolution PET System that uses 3-D Positioning Detectors. Med Phys. 2010;37:5494-508.

Gyang E, Yeom K, Hoppe C, Partap S, Jeng M. Effect of Chronic Red Cell Transfusion Therapy on Vasculopathies and Silent Infarcts in Patients with Sickle Cell Disease. Am J Hematology. 2011 Jan;86(1):104-6.

Haas BW, Hoeft F, Searcy YM, Bellugi U, Mills D, Reiss AL. Individual Differences in Social Behavior Predict Amygdala Response to Fearful Facial Expressions in Williams Syndrome. Neuropsychologia. 2010;48(5):1283-8. PMID: 20036269.

Hahn J, Barnes P, Clegg N, Stashinko E. Septopreoptic Holoprosencephaly: A Mild Subtype Associated with Midline Craniofacial Anomalies. AJNR Am J Neuroradiol. 2010;31:1596-1601.

Hall SS, Lightbody AA, Hirt M, Rezvani A, Reiss AL. Autism in Fragile X Syndrome: A Category Mistake? J Am Acad Child Adolesc Psychiatry. 2010;49(9):921-33. PMID: 20732628. PMCID: PMC2943372.

Hamilton JP, Glover GH, Hsu JJ, Johnson RF, Gotlib IH. Modulation of Subgenual Anterior Cingulate Cortex Activity with Real-Time Neurofeedback. Hum Brain Map. 2011;32:22-31.

Hammerick KE, Huang Z, Sun N, Lam MT, Prinz FB, Wu JC, Commons GW, Longaker M. Elastic Properties of Induced Pluripotent Stem Cells. Tissue Eng Part A. 2011;17(3-4):495—502. PMID: 20807017.

Han M, Hargreaves BA. Reduction of Flow Artifacts by Using Partial Saturation in RF-Spoiled Gradient-Echo Imaging. Magn Reson Med. 2011;65(5):1326-34.

Hargreaves BA, Chen W, Lu W, Alley MT, Gold GE, Brau AC, Pauly JM, Butts-Pauly K. Accelerated Slice Encoding for Metal Artifact Correction. J Magn Reson Imaging. 2010 Apr;31(4):987-96. PMID: 20373445.

He X, Gao J, Gambhir SS, Cheng Z. Near-Infrared Fluorescent Nanoprobes for Cancer Molecular Imaging: Current Status and Future Perspectives. Trends Mol Med. 2010;16(12):574-83. PMID: 20870460.

He X, Wang KM, Cheng Z. In Vivo Near-Infrared Fluorescence Imaging of Cancer with Nanoparticles-Based Probes. Wiley Interdiscip Rev Nanomed Nanobiotechnol. 2010;2(4):349-66. PMID: 20564463.

Hiona A, Lee AS, Nagendran J, Xie X, Connolly AJ, Robbins RC, Wu JC. Pretreatment with Angiotensin-Converting Enzyme Inhibitor Attenuates Doxorubicin-Induced Cardiomyopathy via Preservation of Mitochondrial Function. J Thorac Cardiovasc Surg. 2011 Aug;142(2):396-403.e3. PMID: 21094500.

Ho DY, Lin M, Schaenman J, Rosso F, Leung AN, Coutre SE, Sista RR, Montoya JG. Yield of Diagnostic Procedures for Invasive Fungal Infections in Neutropenic Febrile Patients with Chest Computed Tomography Abnormalities. Mycoses. 2011 Jan;54(1):59-70.

Hoeft F, Carter JC, Hazlett H, Lightbody AA, Piven J, Reiss AL. Region-Specific Alterations in Brain Development in One to Three Year-Old Boys with Fragile X Syndrome. Proc Natl Acad Sci USA. 2010;107(20):9335-9. PMID: 20439717. PMCID: PMC2889103.

Hoeft F, McCandliss B, Black J, Gantman A, Zakerani N, Hulme C, Lyytinen H, Whitfield-Gabrieli S, Glover GH, Reiss AL, Gabrieli JDE. Neural Systems Predicting Long-Term Outcome in Dyslexia. Proc Natl Acad Sci USA. 2011;108(1):361-6. PMID: 21173250. PMCID: PMC3017159.

Hoeft F, Walter E, Lightbody AA, Hazlett HC, Chang C, Piven J, Reiss AL. Neuroanatomical Differences in Toddler Boys with Fragile X Syndrome and Idiopathic Autism. Arch Gen Psychiatry. 2011;68(3):295-305. PMID: 21041609.

Hollander SA, Yasnovsky JR, Reinhartz O, Chan F, Sandborg C, Hunt S, Bernstein D, Chin C. Behcet's Disease and Heart Transplantation: A Word of Caution. J Heart Lung Transplant. 2010 Nov;29(11):1306-8.

Hong JC, Yu Y, Rao AK, Dieterich S, Maxim PG, Le QT, Diehn M, Sze DY, Kothary N, Loo BW. High Retention and Safety of Vascular Embolization Coils as Fiducial Markers for Image-Guided Stereotactic Ablative Radiotherapy of Pulmonary Tumors. Int J Radiat Oncol Biol Phys. 2010 Jul 31 [Epub ahead of print].

Hoppmann S, Miao Z, Liu S, Liu H, Bao A, Cheng Z. Radiolabeled Affibody-Human Serum Albumin Bioconjugates for HER2 Positive Cancer Targeting. Bioconjug Chem. 2011;22(3):413-21. PMID 21299201.

Hristov D, Adler J, Gibbs I, Moore T, Dodd R, Marks M, Do HM. Frameless Image Guided Robotic Radiosurgery of Arteriovenous Malformation Localized on Spatially Correlated Digital Subtraction and C-Arm CT Angiography Images. J Neuro Intervent Surg. 2010;2(3):252-4.

Hristov D, Liu L, Adler JR, Gibbs IC, Moore T, Sarmiento M, Chang SD, Dodd R, Marks M, Do HM. Technique for Targeting Arteriovenous Malformations using Frameless Image Guided Robotic Radiosurgery. Int J Radiat Oncol Biol Phys. 2011 Mar 15;79(4):1232-40.

Hristov D, Liu L, Adler JR, Gibbs IC, Moore T, Sarmiento M, Chang SD, Dodd RL, Marks MP, Do HM. Localization Technique for Frameless Image-Guided Robotic Radiosurgery of Arteriovenous Malformations. Int J Radiat Oncol Biol Phys. 2011;79(4):1232-40.

Hsiao A, Alley MT, Massaband P, Herfkens RJ, Chan FP, Vasanawala SS. Improved Cardiovascular Flow Quantification with Time-Resolved Volumetric Phase-Contrast MRI. Pediatr Radiol. 2011 Jan 11 [Epub ahead of print].

Hu S, Huang M, Li Z, Jia F, Ghosh Z, Lijkwan MA, Fasanaro P, Sun N, Wang X, Martelli F, Robbins RC, Wu JC. MicroRNA-210 as a Novel Therapy for Treatment of Ischemic Heart Disease. Circulation. 2010;122:S124-S31. PMID: 20837903.

Huang J, Bu L, Xie J, Chen K, Cheng Z, Li X, Chen X. Effects of Nanoparticle Size on Cellular Uptake and Liver MRI with Polyvinylpyrrolidone-Coated Iron Oxide Nanoparticles. ACS Nano. 2010;4(12):7151-60. PMID: 21043459.

Huang J, Xie J, Chen K, Bu L, Lee S, Chen Z, Li X, Chen X. HSAcoated MnO Nanoparticles with Prominent MRI Contrast for Tumor Imaging. Chem Commun (Camb). 2010;46:6684-6. PMID: 20730157.

Huang NF, Niiyama H, Peter C, De A, Natkunam Y, Fleissner F, Li Z, Rollins MD, Wu JC, Gambhir SS, Cooke JP. Embryonic Stem Cell-Derived Endothelial Cells Engraft Into the Ischemic Hindlimb and Restore Perfusion. Arterioscler Thromb Vasc Biol. 2010;30(5):984-91. PMID: 20167654.

Hurd RE, Yen YF, Mayer D, Chen A, Wilson D, Kohler S, Bok R, Vigneron D, Kurhanewicz J, Tropp J, Spielman D, Pfefferbaum A. Metabolic Imaging in the Anesthetized Rat Brain using Hyperpolarized [1-13C] Pyruvate and [1-13C] Ethylpyruvate. Magn Reson Med. 2010 May;63(5):1137-43. PMID: 20432284. PMCID: PMC2890241.

Hurd RE, Yen YF, Tropp J, Pfefferbaum A, Spielman DM, Mayer D. Cerebral Dynamics and Metabolism of Hyperpolarized [1-(13)C]pyruvate using Time-Resolved MR Spectroscopic Imaging. J Cereb Blood Flow Metab. 2010 Oct;30(10):1734-41. PMID: 20588318.

Iagaru A, Mittra ES, Dick DW, Gambhir SS. Prospective Evaluation of (99m)Tc MDP Scintigraphy, (18)F NaF PET/CT, and (18)F FDG PET/CT for Detection of Skeletal Metastases. Mol Imaging Biol. 2011 [Epub ahead of print].

Iagaru A, Mittra ES, Gambhir SS. FDG-PET/CT in Cancers of the Head and Neck: What is the Definition of Whole Body Scanning? Mol Imaging Biol. 2011;13:362-7.

Iagaru A, Mittra ES, Ganjoo K, Knox SJ, Goris ML. 131I-Tositumomab (Bexxar®) vs. 90Y-Ibritumomab (Zevalin®) Therapy of Refractory/Relapsed Non-Hodgkin Lymphoma. Mol Imaging Biol. 2010 Apr;12(2):198-203.

Illes J, Tairyan K, Federico CA, Tabet A, Glover GH. Reducing Barriers to Ethics in Neuroscience. Front Hum Neurosci. 2010;4:1.

James ML, Shen B, Zavaleta C, Berganos RA, Mesangeau C, Shaikh J, Gambhir SS, Matsumoto RR, McCurdy CR, Chin FT. [18F]FTC-146: A Novel and Highly Selective PET Ligand for Visualizing Sigma-1 Receptors in Living Subjects. NeuroImage. 2010;52(1):S123-4.

Jang ES, Won JH, Kim YW, Cheng Z, Choy JH. Dynamic Transition between Zn-HDS and ZnO: Growth and Dissolving Mechanism of Dumbbell-like ZnO Bipod Crystal. Cryst Eng Comm. 2011;13(2):546-52.

Jang ES, Won JH, Kim YW, Cheng Z, Choy JH. Synthesis of Porous and Noporous ZnO Nanobelt, Multipod, and Hierarchical Nanostructure from Zn-HDS. J Solid State Chem. 2010;183(8):1835-40.

Jarvinen-Pasley A, Adolphs R, Yam A, Hill KJ, Grichanik M, Reilly J, Mills D, Reiss AL, Korenberg JR, Bellugi U. Affiliative Behavior in Williams Syndrome: Social Perception and Real-Life Social Behavior. Neuropsychologia. 2010;48(7):2110-9. PMID: 20385151.

Jarvinen-Pasley A, Pollack S, Yam A, Hill KJ, Grichanick M, Mills D, Reiss AL, Korenberg JR, Bellugi U. Atypical Hemispheric Asymmetry in the Perception of Negative Human Vocalizations in Individuals with Williams Syndrome. Neuropsychologia. 2010;48(4):1047-52. PMID: 20005238. PMCID: PMC2847456.

Jarvinen-Pasley A, Vines BW, Hill KJ, Yam A, Grichanik M, Mills D, Reiss AL, Korenberg JR, Bellugi U. Cross-Modal Influences of Affect across Social and Non-Social Domains in Individuals with Williams Syndrome. Neuropsychologia. 2010;48(2):456-66. PMID: 19822162.

Jha P, Froehlich A, McCarville B, Navarro O, Babyn P, Goldsby R, Daldrup-Link HE. Unusual Association of Alveolar Rhabdomyosarcoma with Pancreatic Metastasis: Emerging Role of PET-CT in Tumor Staging. Pediatr Radiol. 2010;40:1380–6. PMCID: 2895865.

Jia F, Wilson KD, Sun N, Gupta DM, Huang M, Li Z, Robbins RC, Kay MA, Longaker MT, Wu JC. Minicircle DNA Induces Pluripotency in Adult Human Cells. Nat Methods. 2010;7(3):197-9. PMID: 20139967.

Jiang H, Cheng Z, Tian M, Zhang H. In Vivo Imaging of Embryonic Stem Cell Therapy. Eur J Nucl Med Mol imaging. 2011;38(4):774-84. PMID: 21107558.

Published Papers

Jiang L, Kimura RH, Miao Z, Silverman AP, Ren G, Liu HG, Li P, Gambhir SS, Cochran JR, Cheng Z. Evaluation of a 64Cu-Labeled Cystine-Knot Peptide based on Agouti-Related Protein for EPT of Tumors Expressing avB3 Integrin. J Nucl Med. 2010;51(2):251-8. PMID: 20124048.

Jiang L, Miao Z, Kimura RH, Liu HG, Cochran JR, Culter CS, Bao A, Li PY, Cheng Z. Preliminary Evaluatoin of 177Lu-Labeled Knotting Peptides for Integrin Receptors-Targeted Radiotherapy. Eur J Nucl Med Mol imaging. 2011;38(4):613-22. PMID: 21153409.

Jimenez-Requena F, Delgado-Bolton R, Fernandez-Perez C, Gambhir SS, Schwimmer J, Perez-Vazquez J, Carreras-Delgado J. Meta-analysis of the Performance of [18F] FDG-PET in Cutaneous Melanoma. Eur J Nucl Med Mol imaging. 2010;37(2): 284-300.

Jokerst JV, Miao Z, Zavaleta CL, Cheng Z, Gambhir SS. Affibody Functionalized Gold-Silica Nanoparticles for Raman Molecular Imaging of the Epidermal Growth Factor Receptor. Small. 2011;7(5):625-33. PMID: 21302357.

Josan S, Yen YF, Hurd R, Pfefferbaum A, Spielman D, Mayer D. Application of Double Spin Echo Spiral Chemical Shift Imaging to Rapid Metabolic Mapping of Hyperpolarized [1-(13)C]-Pyruvate. J Magn Reson. 2011 Apr;209(2):332-6. PMID: 21316280. PMCID: PMC3072043.

Kahn CE, Langlotz CP, Channin DS, Rubin DL. Informatics in Radiology: An Information Model of the DICOM Standard. Radiographics. 2011 Jan-Feb;31(1):295-304. PMID 20980665.

Kamaya A, Gross M, Akatsu H, Jeffrey RB. Recurrence in the Thyroidectomy Bed: Sonographic Findings. AJR Am J Roentgenol. 2011;196(1):66-70.

Kao D, Witteles R, Quon A, Wu J, Gambhir SS, Fowler M. Rosiglitazone Increases Myocardial Glucose Metabolism in Insulin-Resistant Cardiomyopathy. J Am Coll Cardiol. 2010;55(9):926-7. PMID 20185047.

Kapinos G, Fischbein NJ, Zaharchuk G, Venkatasubramanian C. Migraine-like Headache with Visual Deficit and Perfusion Abnormality on MRI. Neurology. 2010;74:1743-5.

Karamchandani J, Fischbein NJ, Harsh G, Katznelson L, Vogel H. Retrosellar Intracranial Extracerebral Glioneuronal Heterotopion. Clin Neuropathol. 2010 Sep;29(5):297-300.

Kaye EA, Chen J, Butts-Pauly K. Rapid MR-ARFI Method for Focal Spot Localization during Focused Ultrasound Therapy. Magn Reson Med. 2011 Mar;65(3):738-43. PMID: 21337406.

Keenan KE, Besier TF, Pauly JM, Han E, Rosenberg J, Smith RL, Delp SL, Beaupre GS, Gold GE. Prediction of Glycosaminoglycan Content in Human Cartilage by Age, T1ρ, and T2 MRI. Osteoarthritis Cartilage. 2011 Feb;19(2):171-9. PMID: 21112409.

Khan N, Dodd R, Marks MP, Bell-Stephens T, Vavao J, Steinberg GK. Failure of Primary Percutaneous Angioplasty and Stenting in Prevention of Ischemia in Moyamoya Angiopathy. Cerebrovasc Dis. 2011;31(2):147-53.

Kijowski R, Gold GE. Routine 3D Magnetic Resonance Imaging of Joints. J Magn Reson Imaging. 2011 Apr;33(4):758-71. PMID: 21448939.

Kim JE, Newman B. Evaluation of a Radiation Dose Reduction Strategy for Pediatric Chest CT. AJR Am J Roentgenol. 2010;194:1188-93.

Kimura RH, Jones DS, Jiang L, Miao Z, Cheng Z, Cochran JR. Functional Mutation of Multiple Solvent-Exposed Loops of the Ecballium Elaterium Trypsin Inhibitor-II Cystine Knot Miniprotein. PLos One. 2011 Feb 18;6(2):e16112. PMID: 21364742.

Kimura RH, Miao Z, Cheng Z, Gambhir SS, Cochran JR. A Dual-Labeled Knottin Peptide for PET and Near-Infrared Fluorescence Imaging of Integrin Expression in Living Subjects. Bioconjug Chem. 2010;21(3):436-44. PMID: 20131753.

Koch K, Hargreaves B, Butts-Pauly K, Chen W, Gold GE, King K. Magnetic Resonance Imaging near Metal Implants. J Magn Reson Imaging. 2010 Oct;32(4):773-87. PMID: 20882607.

Koch KM, Brau AC, Chen W, Gold GE, Hargreaves BA, Koff M, McKinnon GC, Potter HG, King KF. Imaging Near Metal with a MAVRIC-SEMAC Hybrid. Magn Reson Med. 2011 Jan; 65(1):71-82. PMID: 20981709.

Koch KM, Hargreaves BA, Butts-Pauly K, Chen W, Gold GE, King KF. Using MRI to Image Near Metal Implants. JMRI. 2010 Oct;32(4):773-87.

Komakula ST, Burr RT, Lee JN, Anderson J. Opposite Cerebral Dominance for Reading and Sign Language. Journal of Neuroradiology Case Reports. 2010;4(3):11-4.

Komakula ST, Warmuth-Metz M, Hildenbrand P, Loevner L, Hewlett R, Salzman K, Couldwell W, Lin CT, Osborn A. Pineal Parenchymal Tumor of Intermediate Differentiation: Imaging Spectrum of an Unusual Tumor in 11 Cases. Neuroradiology. 2010 Nov [Epub ahead of print].

Published Papers

Kong Y, Yao H, Ren H, Subbian S, Cirillo SLG, Sacchettini JC, Rao J, Cirillo JD. Imaging Tuberculosis with Endogenous β-Lactamase Reporter Enzyme Fluorescence in Living Mice. Proc Natl Acad Sci USA. 2010;107:12239-44.

Koo S, Hargreaves BA, Gold GE, Dragoo JL. Fabrication of Custom-Shaped Grafts for Cartilage Regeneration. Int J Artif Organs. 2010 Oct;33(10):731-7. PMID: 21058268.

Korenblum D, Rubin DL, Napel S, Rodriguez C, Beaulieu CF. Managing Biomedical Image Metadata for Search and Retrieval of Similar Images. J Digit Imaging. 2011 Aug;24(4):739-48. PMID: 20844917.

Kothary N, Bartos JA, Hwang GL, Dua R, Kuo WT, Hofmann LV. CT-Guided Percutaneous Needle Biopsy of Indeterminate Pulmonary Pathology: Efficacy of Obtaining a Diagnostic Sample in Immunocompetent and Immunocompromised Patients. Clin Lung Cancer. 2010 Jul 1;11(4):251-6.

Kothary N, Ghatan CE, Hwang GL, Kuo WT, Sze DY, Hovsepian DM, Desser TS, Hofmann LV. Renewing Focus on Resident Education: Increased Responsibility and Ownership in Interventional Radiology Rotations Improves the Educational Experience. J Vasc Interv Radiol. 2010 Nov;21(11):1697-702.

Krishnamoorthi R, Ramarajan N, Wang NE, Newman B, Rubesova E, Mueller C, Barth RA. Effectiveness of a Staged Ultrasound & Computed Tomography Protocol for the Diagnosis of Pediatric Appendicitis: Reducing Radiation Exposure in the Age of ALARA. Radiology. 2011;259(1):231-9.

Kuo WT, Cupp JS. The Excimer Laser Sheath Technique for Embedded IVC Filter Removal. J Vasc Interv Radiol. 2010 Dec;21:1896-9.

Kuo WT, Hofmann LV. Optimizing Endovascular Therapy for Acute PE: Primum Non Nocere. J Vasc Interv Radiol. 2010;21:1776-7.

Kurian A, Sigal B, Plevritis SK. A Survival Analysis of Cancer Risk Reduction Strategies for BRCA1/2 Mutation Carriers. J Clin Oncol. 2010;28(2):222-31.

Lau FWY, Vandenbroucke A, Reynolds PD, Olcott PD, Horowitz MA, Levin CS. Analog Signal Multiplexing for PSAPD-Based PET Detectors: Simulation and Experimental Validation. Phys Med Biol. 2010;55:7149-74.

Lazzaro NA, Wright B, Osborn AG, Fischbein NJ, Castillo M, Glastonbury CM, Hildenbrand PG, Wiggins RH. Artery of Percheron Infarction: Imaging Patterns and Clinical Spectrum. AJNR Am J Neuroradiol. 2010;31:1283-9.

Le UN, Kim HS, Kwon JS, Kim MY, Nguyen VH, Jiang SN, Lee BI, Hong Y, Shin MG, Rhee JH, Bom HS, Ahn Y, Gambhir SS, Choy HE, Min JJ. Engineering and Visualization of Bacteria for Targeting Infarcted Myocardium. Molecular Therapy. 2011 [Epub ahead of print].

Lee CI, Tsai EB, Sigal BM, Plevritis SK, Garber AM, Rubin GD. Incidental Extracardiac Findings at Coronary CT: Clinical and Economic Impact. AJR Am J Roentgenol. 2010;194(6):1531-8.

Lee HD, Lord SJ, Iwanaga S, Zhan K, Xie H, Williams JC, Wang H, Bowman GR, Goley ED, Shapiro L, Twieg RJ, Rao J, Moerner WE. Superresolution Imaging of Targeted Proteins in Fixed and Living Cells using Photoactivatable Organic Fluorophores. J Am Chem Soc. 2010;132:15099-101.

Lee J, Albers GW, Marks MP, Lansberg MG. Treatment of Capsular Warning Syndrome TIAs with Intracranial Angioplasty. J Neurol Sci. 2010;296(1-2):115-20.

Lee J, Lee KH, Jeon J, Dragulescu-Andrasi A, Xiao F, Rao J. Combining SELEX Screening and Rational Design to Develop Light-Up Fluorophore-RNA Aptamer Pairs for RNA Tagging. ACS Chem Biol. 2010;5:1065-1074.

Lee M, Sze DY, Bonham CA, Daugherty TJ. Hepatic Arteriovenous Malformations from Hereditary Hemorrhagic Telangiectasia: Treatment with Liver Transplantation. Dig Dis Sci. 2010;55:3059-62.

Lee, GC, Goodwill PW, Phuong K, Inglis BA, Scott GC, Hargreaves BA, Li L, Chen AC, Shah, RN, Conolly SM. Pyrolytic Graphite Foam: A Passive Magnetic Susceptibility Matching Material. JMRI. 2010;32(3):684-91.

Levashova Z, Backer M, Hamby CV, Pizzonia J, Backer JM, Blankenberg FG. Molecular Imaging of Changes in the Prevalence of Vascular Endothelial Growth Factor Receptor in Sunitinib-Treated Murine Mammary Tumors. J Nucl Med. 2010 Jun;51(6):959-66.

Levi J, Kothapalli SR, Ma TJ, Hartman K, Khuri-Yakub BT, Gambhir SS. Design, Synthesis, and Imaging of an Activatable Photoacoustic Probe. J Am Chem Soc. 2010;132(32):11264-9.

Lew C, Alley MT, Spielman DM, Bammer R, Chan FP. Breathheld Autocalibrated Phase-Contrast Imaging. J Magn Reson Imaging. 2010 Apr;31(4):1004-14. PMID: 20373447. PMCID: PMC2903748.

Li Z, Hu S, Ghosh Z, Han Z, Wu JC. Functional Characterization and Expression Profiling of Human Induced Pluripotent Stem Cell- and Embryonic Stem Cell-Derived Endothelial Cells. Stem Cells Dev. 2011 Feb 28 [Epub ahead of print]. PMID 21235328.

Published Papers

Lin F, Iagaru A. Current Concepts and Future Directions in Radioimmunotherapy. Curr Drug Discov Technol. 2010 Dec 1;7(4):253-62.

Liu C, Zhang J, Moseley ME. Auto-Calibrated Parallel Imaging Reconstruction for Arbitrary Trajectories using K-Space Sparse Matrices (kSPA). IEEE Trans Med Imaging. 2010 Mar;29(3):950-9. PMID: 20199928. PMCID: PMC2996098.

Liu H, Patel MR, Prescher JA, Patsialou A, Qian D, Lin J, Wen S, Chang YF, Bachmann MH, Shimono Y, Dalerba P, Adorno M, Lobo N, Bueno J, Dirbas FM, Goswami S, Somio G, Condeelis J, Contag CH, Gambhir SS, Clarke MF. Cancer Stem Cells from Human Breast Tumors are Involved in Spontaneous Metastases in Orthotopic Mouse Models. Proc Natl Acad Sci USA. 2010;107(42):18115-20.

Liu H, Ren G, Zhang X, Chen L, Han P, Cheng Z. Optical Imaging of Reporter Gene Expression Using a Positron-Emission-Tomography Probe. J Biomed Opt. 2010;15(6):060505. PMID: 21198146.

Liu H, Zhang X, Xing B, Han P, Gambhir SS, Cheng Z. Radiation-luminescence-excited Quantum Dots for In Vivo Multiplexed Optical Imaging. Small. 2010;6(10):1087-91. PMID: 20473988.

Liu HG, Ren G, Miao Z, Zhang XF, Tang X, Han PZ, Gambhir SS, Cheng Z. Molecular Optical Imaging with Radioactive Probes. PLoS One. 2010;5(3):e9470. PMID: 20208993.

Liu YI, Brown SS, Elihu A, Bonham CA, Concepcion W, Longacre TA, Kamaya A. Hepatic Epithelioid Hemangioendothelioma. Dig Dis Sci. 2010 Oct 30.

Liu YI, Kamaya A, Desser T, Rubin D. A Bayesian Network for Differentiating Benign versus Malignant Thyroid Nodules Using Sonographic and Demographic Features. AJR Am J Roentgenol. 2011;196(5):W598-W605.

Lock J, Garrett A, Beenhakker J, Reiss AL. Abberrant Brain Activation During a Response Inhibition Task in Adolescent Eating Disorder Subtypes. Am J Psychiatry. 2011;168(1):55-64. PMID: 21123315. PMCID: PMC3016457.

Loening A, Dragulescu-Andrasi A, Gambhir SS. A Red-Shifted Renilla Luciferase for Transient Reporter-Gene Expression. Nat Methods. 2010;7(1):5-6.

Loh Y, Duckwiler GR, Onyx trial investigators. A Prospective, Multi-Center, Randomized Trial of Onyx Liquid Embolic System and N-Butyl Cyanoacrylate Embolization of Cerebral Arteriovenous Malformations. JNS. 2010;113:733-41.

Lu W, Butts-Pauly K, Gold GE, Pauly JM, Hargreaves BA. Slice Encoding for Metal Artifact Correction with Noise Reduction. Magn Reson Med. 2011;65(5):1352-7. PMID: 21287596.

Lutz A, Willmann J, Drescher C, Ray P, Cochran FV, Urban N, Gambhir SS. Early Diagnosis of Ovarian Carcinoma: Is a Solution in Sight? Radiology. 2011;259(2):329-45.

Ma N, Marshall AF, Gambhir SS, Rao J. Facile Synthesis, Silanization, and Biodistribution of Biocompatible Quantum Dots. Small. 2010;6(14):1520-8, 2010.

Mackenzie JD, Yen YF, Mayer D, Tropp JS, Hurd RE, Spielman DM. Detection of Inflammatory Arthritis by Using Hyperpolarized 13C-Pyruvate with MR Imaging and Spectroscopy. Radiology. 2011 May;259(2):414-20. PubMed PMID: 21406626.

Mansouri MA, Iagaru A. 18F FDG PET/CT Demonstration of Lymphohistiocytic Meningitis. Clin Nucl Med. 2010 Aug;35(8):633-4.

Marzelli MJ, Hoeft F, Hong DS, Reiss AL. Neuroanatomical Spatial Patterns in Turner Syndrome. NeuroIage. 2011;55(2):439-47. PMID: 21195197. PMCID: PMC3035734.

Massoud TF, Paulmurugan R, Gambhir SS. A Molecularly Engineered Split Reporter for Imaging Protein-Protein Interactions with Positron Emission Tomography. Nat Med. 2010 Aug:16(8):921-6.

Mayer D, Yen YF, Levin YS, Tropp J, Pfefferbaum A, Hurd RE, Spielman DM. In Vivo Application of Sub-Second Spiral Chemical Shift Imaging (CSI) to Hyperpolarized 13C Metabolic Imaging: Comparison with Phase-Encoded CSI. J Magn Reson. 2010 Jun;204(2):340-5. PMID: 20346717. PMCID: PMC2893149.

Mayer D, Yen YF, Takahashi A, Josan S, Tropp J, Rutt BK, Hurd RE, Spielman DM, Pfefferbaum A. Dynamic and High-Resolution Metabolic Imaging of Hyperpolarized [1-(13)C]-Pyruvate in the Rat Brain using a High-Performance Gradient Insert. Magn Reson Med. 2011 May;65(5):1228-33. doi: 10.1002/mrm.22707. PMID: 21500253.

McAdams T, Fredericson M, Vogelsong M, Gold GE. New Developments in Magnetic Resonance Imaging Techniques for Shoulder Instability In Athletes. Open Access Journal of Sports Medicine. 2010 Aug;1:137-42.

McDougall IR, Iagaru A. Thyroid Stunning: Fact or Fiction? Semin Nucl Med. 2011 Mar;41(2):105-112.

Published Papers

Meer AB, Louie JD, Abdelmaksoud MH, Kothary N, Hovsepian DM, Hofmann LV, Kuo WT, Hwang GL, Sze DY. Intrahepatic Collateral Supply to the Previously Embolized Right Gastric Artery: A Potential Pitfall for Nontarget Radioembolization. J Vasc Interv Radiol. 2011 Apr;22(4):575-7.

Meer AB, Louie JD, Kothary N, Hovsepian DM, Hofmann LV, Kuo WT, Hwang GL, Sze DY. The Accessory Right Gastric Artery: A Potential Pitfall for Nontarget Radioembolization. J Vasc Interv Radiol. 2011;22:575-7.

Meier R, Golovko D, Tavri S, Henning TD, Knopp C, Piontek G, Rudelius M, Heinrich P, Reinhardt V, Heinrich P, Wels W, Daldrup-Link HE. Depicting Adoptive Immunotherapy for Prostate Cancer in an Animal Model with MR Imaging. Magn Res Med. 2011;65(3):756–63, 2011.

Meier R, Henning TD, Boddington S, Tavri S, Arora S, Corot C, Daldrup-Link HE. Breast Cancers: MR Imaging of Folate Receptor Expression with the Folate-Specific Nanoparticle P1133. Radiology. 2010;255(2):527-35.

Meier R, Krug C, Golovko D, Boddington S, Piontek G, Rudelius M, Sutton E, Baur-Melnyk A, Fung-Jones E, Daldrup-Link HE. ICG-Enhanced Imaging of Arthritis with an Integrated Optical Imaging/X-Ray System. Arthritis Rheum. 2010;62(8):2322-7. PMCID: 2921028.

Miao Z, Levi J, Cheng Z. Protein Scaffolds Based Molecular Probes for Cancer Molecular Imaging. Amino acids. 2010 Feb 21 [Epub ahead of print]. PMID: 20174842.

Miao Z, Ren G, Liu H, Jiang L, Cheng Z. Cy5.5 Labeled Affibody Molecule for Near-Infrared Optical Imaging of Epidermal Growth Factor Receptor 1 Expression. J Biomed Opt. 2010;15(3):036007. PMID: 20615009.

Miao Z, Ren G, Liu H, Jiang L, Cheng Z. Small-Animal PET Imaging of Human Epidermal Growth Factor Receptor 1 Positive Tumor with a 64Cu Labeled Affibody Protein. Bioconjug Chem. 2010;21(5):947-54. PMID: 20402512.

Mimura M, Hoeft F, Kato M, Kobayashi N, Sheau K, Mills D, Galaburda AM, Korenberg JR, Bellugi U, Reiss AL. A Preliminary Study of Orbitofrontal Activation and Hypersociability in Williams Syndrome. J Neurodev Disord. 2010;2(2):93-8. PMID: 21304831.

Mitra R, Do H, Alamin T, Cheng I. Facet Pain in Thoracic Compression Fractures. Pain Med. 2010;11:1674-7.

Mitra R, Nguyen A, Stevens KJ. Fluoroscopically Guided Supraglenoid Tubercle Steroid Injection for the Management of Bicipital Tendonitis. Pain practice. 2010 Nov [Epub ahead of print].

Mitsunaga MM, Garrett A, Howe M, Karchemskiy A, Reiss AL, Chang K. Increased Subgenual Cingulate Cortex Volume in Pediatric Bipolar Disorder Associated with Mood Stabilizer Exposure. J Child Adolesc Psychopharmacol. 2011 Apr;21(2):149-55. PMID: 21486168.

Mittra E, Goris M, Kardan A, Burton L, Liu S, Shen B, Chin FT, Chen X, Gambhir SS. Human Pharmacokinetic and Dosimetry Studies of [18F]FPP(RGD)2: A Novel PET Radiopharmaceutical for Imaging Angiogenesis. J Nucl med. 2010;51(1):1433.

Mittra ES, Goris ML, Iagaru AH, Kardan A, Burton L, Berganos R, Chang E, Liu S, Shen B, Chin FT, Chen X, Gambhir SS. Pharmacokinetic and Dosimetry Studies of [18F]FPPRGD2: A PET Radiopharmaceutical for Imaging αvβ3 Integrin Levels. Radiology. [Epub ahead of print].

Mittra ES, Goris ML, Iagaru AH, Kardan A, Burton L, Berganos R, Chang E, Liu S, Shen B, Chin FT, Chen X, Gambhir SS. Pilot Pharmacokinetic and Dosimetric Studies of F-FPPRGD2: A PET Radiopharmaceutical Agent for Imaging {alpha}v{beta}3 Integrin Levels. Radiology. 2011 Jul;260(1):182-91.

Mittra ES, Iagaru A, Leung A. Case 166: Metastatic Left Pulmonary Artery Sarcoma. Radiology. 2011 Feb;258(2):645-8.

Mittra ES, Iagaru A. 18F FDG PET and PET/CT for Evaluating Primary Bone Tumors. PET Clin. 2010 Jul;5(3):327-40.

Mlynash M, Campbell DM, Leproust EM, Fischbein NJ, Bammer R, Eyngorn I, Hsia AW, Moseley M, Wijman CA. Temporal and Spatial Profile of Brain Diffusion-Weighted MRI After Cardiac Arrest. Stroke. 2010 Aug;41(8):1665-72.PMID: 20595666. PMCID: PMC2914620.

Mobley BC, McKenney JK, Bangs CD, Callahan K, Yeom K, Hayden MG, Cherry AM, Edwards MS, Fisher PG, Vogel H. Loss of SMARCB1/INI1 Expression in Poorly Differentiated Chordomas. Acta Neuropathologica. 2010 Dec;120(6):745-53.

Mullen KM, Vohr BR, Katz KH, Seider KC, Lacadie CM, Hampson M, Makuch RW, Reiss AL, Constable T, Ment LR. Preterm Birth Results in Alterations in Neural Connectivity at Age 16 Years. NeuroImage. 2011;54(4):2562-70. PMID: 21073965. PMCID: PMC3020252.

Murphy JD, La TH, Chu K, Quon A, Fischbein NJ, Maxim PG, Graves EE, Loo BW Jr., Le QT. Postradiation Metabolic Tumor Volume Predicts Outcome in Head-and-Neck Cancer. Int J Radiat Oncol Biol Phys. 2011 Jun 1;80(2):514-21.

Nagamine M, Mimura M, Reiss AL, Hoeft F. Investigating the "Social Brain" through Williams Syndrome. Brain and Nerve. 2010;62(8):877-84. PMID: 20714036.

Napel SA, Beaulieu CF, Rodriguez C, Cui J, Xu J, Gupta A, Greenspan H, Ma Y, Rubin DL. Automated Retrieval of CT Images of Liver Lesions Based on Image Similarity: Method and Preliminary Results. Radiology. 2010;256(1):243-52. PMID: 18515044.

Narsinh KH, Jia F, Robbins RC, Kay MA, Longaker MT, Wu JC. Generation of Adult Human Induced Pluripotent Stem Cells using Non-Viral Minicircle DNA Vectors. Nat Protoc. 2011;6(1):78-88. PMID: 21212777.

Narsinh KH, Sun N, Sanchez-Freire V, Lee AS, Almeida P, Hu S, Jan T, Wilson KD, Leong D, Rosenberg J, Yao M, Wu JC. Increased Heterogeneity and Metastability of Human Induced Pluripotent Stem Cells Revealed by Single Cell Transcriptional Profiling. J Clin Invest. 2011;121(3):1217-21.

Narvid J, Do HM, Blevins NH, Fischbein NJ. CT Angiography as a Screening Tool for Dural Arteriovenous Fistula in Patients with Pulsatile Tinnitus: Feasibility and Test Characteristics. AJNR Am J Neuroradiol. 2011;32(3):446-53.

Nedopil A, Klenk C, Kim C, Golovko D, Li S, Wendland M, Daldrup-Link HE. MR Signal Characteristics of Viable and Apoptotic Human Mesenchymal Stem Cells in MASI for Treatment of Osteoarthritis. Invest Radiol. 2010;45(10):634-40. PMCID: 2943569.

Newbould RD, Skare ST, Alley MT, Gold GE, Bammer R. Three Dimensional T1, T2, and Proton Density Mapping with Inversion Recovery Balanced SSFP. Magn Reson Imaging. 2010 Nov;28(9):1374-82. PMID: 20692784.

Newman B, Feinstein JA, Cohen RA, Feingold B, Kreutzer, J, Patel H, Chan FP. Congenital Extrahepatic Portosystemic Shunt Associated with Heterotaxy and Polysplenia. Pediatr Radiol. 2010 Jul;40(7):1222-30. PMID 20069288.

Nielsen CH, Kimura RH, Withofs N, Tran PT, Miao Z, Cochran JR, Cheng Z, Felsher D, Kjaer A, Willmann JK, Gambhir SS. PET Imaging of Tumor Neovascularization in a Transgenic Mouse Model with a Novel 64Cu-DOTA-Knottin Peptide. Cancer Res. 2010;70(22):9022-30. PMID: 21062977.

Niu G, Sun X, Cao Q, Courter D, Koong A, Le QT, Gambhir SS, Chen X. Cetuximab-Based Immunotherapy and Radioimmunotherapy of Head and Neck Squamous Cell Carcinoma. Clin Cancer Res. 2010;16(7):2095-105.

O'Sullivan T, Munro EA, Parashurama N, Conca C, Gambhir SS, Harris JS, Levi O. Implantable Semiconductor Biosensor for Continuous In Vivo Sensing of Far-Red Flourescent Molecules. Opt Express. 2010;18(12):12513-25.

Olivot JM, Mlynash M, Kleinman JT, Straka M, Venkatasubramanian C, Bammer R, Moseley ME, Albers GW, Wijman CA, DASH investigators. MRI Profile of the Perihematomal Region in Acute Intracerebral Hemorrhage. Stroke. 2010 Nov;41(11):2681-3. PMID: 20947849.

Pal S, Draper CE, Fredericson M, Gold GE, Delp SL, Beaupre GS, Besier TF. Patellar Maltracking Correlates with Vastus Medialis Activation Delay in Patellofemoral Pain Patients. Am J Sports Med. 2011;39(3):590-8. PMID: 21076015.

Panula S, Medrano JV, Kee K, Bergstrom R, Nguyen HN, Byers B, Wilson KD, Wu JC, Simon C, Hovatta O, Reijo Pera RA. Human Germ Cell Differentiation from Fetal- and Adult-Derived Induced Pluripotent Stem Cells. Hum Mol Genet. 2011:20(4):752-62. PMID: 21131292.

Park YL, Elayaperumal S, Daniel B, Ryu SC, Shin M, Savall J, Black RJ, Moslehi B, Cutkosky MR. Real-Time Estimation of 3-D Needle Shape and Deflection for MRI-Guided Interventions. IEEE/ASME Transactions on Mechatronics. 2010;15(6):906-15.

Parris D, Fischbein NJ, Mackey S, Carroll I. A Novel CT-Guided Approach to Diagnostic Genitofemoral Nerve Block and Ablation. Pain Med. 2010;11:785-9.

Patel MR, Chang YF, Chen IY, Bachmann MH, Yan X, Contag CH, Gambhir SS. Longitudinal, Noninvasive Imaging of T-cell Effector Function and Proliferation in Living Subjects. Cancer Res. 2010;70(24):10141-9.

Paulmurugan R. Molecular Imaging in Current Pharmaceutical. Curr Pharm Biotechnol. 2011 Apr;12(4):458.

Pearl JI, Lee A, Leveson-Gower DB, Sun N, Ghosh Z, Lan F, Ransohoff J, Negrin RS, Davis MM, Wu JC. Short-Term Blockade of Leukocyte Costimulatory Molecules Promotes Engraftment of Embryonic and Induced Pluripotent Stem Cells. Cell Stem Cell. 2011;8(3):309-17. PMID: 21362570.

Pendharkar AV, Chua JY, Andres RH, Wang N, Gaeta X, Wang H, De A, Choi R, Chen S, Rutt B, Gambhir SS, Guzman R. Biodistribution of Neural Stem Cells After Intravascular Therapy for Hypoxic-Ischemia. Stroke. 2010 Sep;41(9):2064-70. PMID: 20616329.

Peng H, Levin CS. Recent Development in PET Instrumentation. Curr Pharm Biotechnol. 2010;11:555-71.

Peng H, Olcott PD, Levin CS. Design Study of a High-Resolution Breast-Dedicated PET System built from Cadmium Zinc Telluride Detectors. Phys Med Biol. 2010;55:2761-88.

Pratx G, Surti S, Levin CS. Fast List-Mode Reconstruction for Time-of-Flight PET using Graphics Hardware. IEEE Transactions on Nuclear Sciences. 2010 Nov;58(1):105-9.

Pricola KL, Karamchandani J, Vogel H, Dahl GV, Yeom K, Edwards MS, Guzman R. Langerhans Cell Histiocytosis in a 5-month old Presenting with Biparietal Masses. J Neurosurg Pediatr. 2010 Oct;6(4):393-7.

Pu J, Paik DS, Meng X, Roos JE, Rubin GD. Shape Break-and-Repair Strategy and Its Application to Automated Medical Image Segmentation. IEEE Transactions on Visualization and Computer Graphics. 2011;17(1):115-24.

Pysz MA, Foygel K, Panje CM, Needles A, Tian L, Willmann JK. Assessment and Monitoring Tumor Vascularity with Contrast-Enhanced Ultrasound Maximum Intensity Persistence Imaging. Invest Radiol. 2011;46:187-95.

Pysz MA, Foygel K, Rosenberg J, Gambhir SS, Schneider M, Willmann JK. Antiangiogenic Cancer Therapy: Monitoring with Molecular US and a Clinically Translatable Contrast Agent (BR55). Radiology. 2010;256(2):519-27.

Pysz MA, Foygel K, Rosenberg J, Gambhir SS, Schneider M, Willmann JK. Monitoring Anti-Angiogenic Cancer Therapy with Molecular Ultrasound and a New Clinically Translatable Contrast Agent (BR55). Radiology. 2010;256:519-27.

Pysz MA, Gambhir SS, Willmann JK. Molecular imaging: Current Status and Emerging Strategies. Clin Radiol. 2010;65(7):500-16.

Pysz MA, Willmann JK. Molecular Ultrasound: An Emerging Technology for Abdominal and Pelvic Imaging. Gastroenterology. 2011;140:785-90.

Qiu P, Gentles A, Plevritis SK. Discovering Biological Progression Underlying Microarrays Samples. PLoS Comput Biol. 2011 Apr;7(4):e1001123.

Rab H, Gonzalez-Gonzalez E, Smith B, Gambhir SS, Kino GS, Solgaard O, Kaspar RL, Contag C. Assessing Delivery and Quantifying Efficacy of Small Interfering Ribonucleic Acid Therapeutics in the Skin Using a Dual-Axis Confocal Microscope. J Biomed Opt. 2010 May-Jun;1 (3):036027.

Rakow-Penner R, Daniel B, Glover GH. Detecting Blood Oxygen Level-Dependent (BOLD) Contrast in the Breast. J Magn Reson Imaging. 2010 Jul;32(1):120-9.

Rakow-Penner R, Glader B, Yu H, Vasanawala SS. Adrenal and Renal Corticomedullary Junction Iron Deposition in Red Cell Aplasia. Pediatr Radiol. 2010 Dec;40(12):1955-7.

Raman B, Raman R, Napel S, Rubin GD. Automated Quantification of Aortoaortic and Aortoiliac Angulation for CT Angiography (CTA) of Abdominal Aortic Aneurysms (AAA) Prior to Endovascular Repair. J Vasc Interv Radiol. 2010 Nov;21(11):1746-50. PMID: 20932776.

Ren G, Liu S, Liu H, Miao Z, Cheng Z. Radiofluorinated Rhenium Cyclized a-MSH Analogs for PET Imaging of Melanocortin Receptor 1. Bioconjug Chem. 2010;21(12):2355-60. PMID: 21073170.

Ren G, Pan Y, Cheng Z. Molecular Probes for Malignant Melanoma Imaging. Curr Pharm Biotechnol. 2010;11(6):590-602. PMID: 20497118.

Ren P-G, Huang Z, Ma T, Biswal S, Smith RL, Goodman SB. Surveillance of Systemic Trafficking of Macrophages Induced by UHMWPE Particles in Nude Mice by Non-Invasive Imaging. J Biomed Mater Res A. 2010;94(3):706-11.

Ren PG, Irani A, Huang Z, Ma T, Biswal S, Goodman SB. Continuous Infusion of UHMWPE Particles Induces Increased Bone Macrophages and Osteolysis. Clin Orthop Relat Res. 2011;469(1):113-22.

Rodriguez-Porcel M, Gheysens O, Paulmurugan R, Chen IY, Peterson KM, Willmann JK, Wu JC, Zhu X, Lerman LO, Gambhir SS. Antioxidants Improve Early Survival of Cardiomyoblasts after Transplantation to the Myocardium. Mol Imaging Biol. 2010;12(3):325-34. PMID: 20013064.

Rossi MA, Stebbins G, Murphy C, Greene D, Brinker S, Sarcu D, Tenharmsel A, Stoub T, Stein MA, Hoeppner TJ, Byrne RW, Moseley ME, Bammer R, Bild S, Dennis J, Arnett N, Balabanov A, Bergen D, Kanner AM, Smith MC. Predicting White Matter Targets for Direct Neurostimulation Therapy. Epilepsy Res. 2010 Oct;91(2-3):176-86. PMID: 20728313.

Rubin DL, Flanders A, Kim W, Siddiqui KM, Kahn CE. Ontology-Assisted Analysis of Web Queries to Determine the Knowledge Radiologists Seek. J Digit Imaging. 2011 Feb;24(1):160-4. PMID 20354755.

Rubin DL, Napel S. Imaging Informatics: Toward Capturing and Processing Semantic Information in Radiology Images. Yearb Med Inform. 2010:34-42. PMID: 20938568.

Rubin DL, Wang D, Chambers DA, Chambers JG, South BR, Goldstein MK. Natural Language Processing for Lines and Devices in Portable Chest X-Rays. AMIA Annu Symp Proc. 2010 Nov 13;2010:692-6.

Russell HV, Groshen SG, Ara T, DeClerck YA, Hawkins R, Jackson H, Daldrup-Link HE, Marachelian A, Skerjanec A, Park J, Katzenstein H, Matthay KK, Blaney SM, Villablanca JG. A Phase I Study of Zoledronic Acid and Low Dose Cyclophosphamide in Children with Recurrent/Refractory Neuroblastoma: A New Approaches to Neuroblastoma Therapy (NANT) Study. Pediatr Blood Cancer. 2010 Nov 12 [Epub ahead of print].

Published Papers

Sahoo D, Seita J, Bhattacharya D, Inlay MA, Weissman IL, Plevritis SK, Dill DL. MiDReG: A Method of Mining Developmentally Regulated Genes using Boolean Implications. PNAS. 2010;107(13):5732-7.

Salehian S, Fischbein NJ. Association of Venous Malformation of the Head and Neck with Meningocephalocele. AJNR Am J Neuroradiol. 2010 Apr 1 [Epub ahead of print].

Salem R, Lewandowski RJ, Gates VL, Nutting CW, Murthy R, Rose SC, Soulen MC, Geschwind JF, Kulik L, Kim YH, Spreafico C, Maccauro M, Bester L, Brown DB, Ryu RK, Sze DY, Rilling WS, Sato KT, Sangro B, Bilbao JI, Jakobs TF, Ezziddin S, Kulkarni S, Kulkarni A, Liu DM, Valenti D, Hilgard P, Antoch G, Muller SP, Alsuhaibani H, Mulcahy MF, Burrel M, Real MI, Spies S, Esmail AA, Raoul JL, Garin E, Johnson MS, Benson AB 3rd, Sharma RA, Wasan H, Lambert B, Memon K, Kennedy AS, Riaz A. Technology Assessment Committee; Interventional Oncology Task Force of the Society of Interventional Radiology. Research Reporting Standards for Radioembolization of Hepatic Malignancies. J Vasc Interv Radiol. 2011;22:265-78.

Schmiedeskamp H, Newbould RD, Bammer R. Improvements in Parallel Imaging Accelerated Functional MRI using Multiecho Echo-Planar Imaging. Magn Reson Med. 2010;63:959-69. PMID: 20373397.

Segall G, Delbeke D, Stabin MG, Even-E, Fair J, Sajdak R, Smith GT. The SNM Practice Guideline for Sodium 18F-fluoride PET/CT Bone Scans. J Nucl Med. 2010;51(11):1813-20.

Segall G. Therapy Response Evaluation with Positron Emission Tomography-Computed Tomography. Semin Ultrasound CT MRI. 2010;31(6):490-5.

Sekar TV, Dhanabalan A, Paulmurugan R. Imaging Cellular Receptors in Breast Cancers - An Overview. Curr Pharm Biotechnol. 2011 Apr;12(4):508-27.

Shapiro L, Staroswiecki E, Gold GE. Magnetic Resonance Imaging of the Knee: Optimizing 3 Tesla Imaging. Semin Roentgenol. 2010 Oct;45(4):238-49. PMID: 20727453.

Shi ZS, Loh Y, Walker G, Duckwiler GR, MERCI and Multi-MERCI investigators. Clinical Outcomes in Middle Cerebral Artery Trunk Occlusions Versus Secondary Division Occlusions after Mechanical Thrombectomy: Pooled Analysis of the Mechanical Embolus Removal in Cerebral Ischemia (MERCI) and Multi MERCI trials. Stroke. 2010;41(5):953-60.

Shi ZS, Loh Y, Walker G, Duckwiler GR, MERCI and Multi-MERCI investigators. Endovascular Thrombectomy for Acute Ischemic Stroke in Failed Intravenous Tissue Plasminogen Activator Versus Non-Intravenous Tissue Plasminogen Activator Patients: Revascularization and Outcomes Stratified by the Site of Arterial Occlusions. Stroke. 2010;41(6):1185-92.

Shin LK, Jeffrey RB. Sonography and CT of the Mimics of Appendicitis. Ultrasound Q. 2010;26(4):201-10.

Singh M, Chang KD, Mazaika P, Garrett A, Adleman N, Kelley R, Howe M, Reiss AL. Neural Correlates of Response Inhibition in Pediatric Bipolar Disorder. J Child Adolesc Psychopharmacol. 2010;20(1):15-24. PMID: 20166792. PMCID: PMC2835388.

Singh M, Spielman D, Adleman N, Alegria D, Howe M, Reiss A, Chang K. Brain Glutamatergic Characteristics of Pediatric Offspring of Parents with Bipolar Disorder. Psychiatry Res. 2010 May 30;182(2):165-71. PMID: 20413280. PMCID: PMC2866778.

Singh MK, Spielman D, Libby A, Adams E, Acquaye T, Howe M, Kelley R, Reiss AL, Chang KD. Neurochemical Deficits in the Cerebellar Vermis in Child Offspring of Parents with Bipolar Disorder. Bipolar Disord. 2011 Mar;13(2):189-97. doi:10.1111/j.1399-5618.2011.00902.x. PMID: 21443573. PMCID:PMC3066452.

Slater BJ, Chan FP, Davis K, Dutta S. Institutional Experience with Laparoscopic Partial Splenectomy for Hereditary Spherocytosis. J Pediatr Surg. 2010 Aug;45(8):1682-6.

Smith BR, Cheng Z, De A, Rosenberg J, Gambhir SS. Dynamic Visualization of RGD-Quantum Dot Binding to Tumor Neovasculature and Extravasation in Multiple Living Mouse Models Using Intravital Microscopy. Small. 2010;6(20):2222-9. PMID: 20862677.

Smith C, Mehta R, Gibson DF, Levashova Z, Blankenberg FG, Tait JF. Characterization of a Recombinant Form of Annexin VI for Detection of Apoptosis. Bioconjug Chem. 2010 Aug 18;21(8):1554-8.

Soliman F, Glatt CE, Bath KG, Levita L, Jones RM, Pattwell SS, Jing D, Tottenham N, Amso D, Somerville LH, Voss HU, Glover G, Ballon DJ, Liston C, Teslovich T, Van Kempen T, Lee FS, Casey BJ. A Genetic Variant BDNF Polymorphism Alters Extinction Learning in Both Mouse and Human. Science. 2010 Feb 12;327(5967):863-6.

Spanoudaki VC, Lau FWY, Vandenbroucke A, Levin CS. Physical Effects of Mechanical Design Parameters of a Breast-Dedicated PET System on Photon Sensitivity and Spatial Resolution Performance. Med Phys. 2010;37:5838-49.

Spanoudaki VC, Levin CS. Investigating the Temporal Resolution Limits of Scintillation Detection: Comparison between Experiment and Simulation. Phys Med Biol. 2011;56:735-56.

Published Papers

Spanoudaki VC, Levin CS. Photo-Detectors for Time of Flight Positron Emission Tomography (ToF-PET). Sensors. 2010 Nov;10(11):10484-505.

Spanoudaki VC, Levin CS. Scintillation Induced Response in Passively-Quenched Si-Based Single Photon Counting Avalanche Diode Arrays. Opt Express. 2011;19:1665-79.

Starman J, Star-lack J, Virshup G, Shapiro E, Fahrig R. Investigation into the Optimal Linear Time-Invariant Lag Correction for Radar Artifact Removal. Med Phys. 2011;38:2398-411.

Staroswiecki E, Bangerter NK, Gurney PT, Grafendorfer T, Gold BE, Hargreaves BA. In-Vivo Sodium Imaging of Human Patellar Cartilage with a 3D Cones Sequence at 3T and 7T. J Magn Reson Imaging. 2010 Aug;32(2):446-51. PMID: 20677276.

Steele JR, Hovsepian DM, Schomer DF. The Joint Commission Practice Performance Evaluation: A Primer for Radiologists. J Amer Coll Radiol. 2010;7(6):425-30.

Steele JR, Wallace MJ, Hovsepian DM, James BC, Kundu S, Miller DL, Rose SC, Sacks D, Shah SS, Cardella JF. Guidelines for Establishing a Quality Improvement Program in Interventional Radiology. J Vasc Interv Radiol. 2010;21(5):617-625.

Stevens KJ, Crain JM, Akizuki KH, Beaulieu CF. Imaging and Ultrasound-Guided Steroid Injection of Internal Oblique Muscle Strains in Baseball Pitchers. Am J Sports Med. 2010;38(3):581-5.

Stevens KJ, Wallace CG, Chen W, Rosenberg JK, Gold GE. Imaging of the Wrist at 1.5 Tesla using Isotropic Three-Dimensional Fast Spin Echo Cube. J Magn Reson Imaging. 2011 Apr;33(4):908-15. PMID: 21448957.

Stikov N, Keenan KE, Pauly JM, Smith RL, Dougherty RF, Gold GE. Cross-Relaxation Imaging of Human Articular Cartilage. Magn Reson Med. 2011 Mar 17. doi:10.1002/mrm.22865. PMID: 21416504.

Straka M, Albers GW, Bammer R. Real-Time Diffusion-Perfusion Mismatch Analysis in Acute Stroke. J Magn Reson Imaging. 2010 Nov;32(5):1024-37. PMID: 21031505.

Sutton EJ, Henning TD, Boddington S, Demos S, Krug C, Meier R, Kornak J, Zhao S, Baehner R, Sharifi S, Daldrup-Link HE. In Vivo MRI and Optical Imaging Comparison of Viable and Non-Viable Mesenchymal Stem Cells with a Bifunctional Label. Mol Imaging. 2010;9(5):278-90. PMCID: 3060764.

Swijnenburg RJ, Govaert JA, van der Bogt KE, Pearl JI, Huang M, Stein W, Hoyt G, Vogel H, Contag CH, Robbins RC, Wu JC. Timing of Bone Marrow Cell Delivery has Minimal Effects on Cell Viability and Cardiac Recovery Following Myocardial Infarction. Circ Cardiovasc Imaging. 2010;3(1):77-85 PMID: 19920031.

Tan JC, Busque S, Workeneh B, Ho B, Derby G, Blouch KL, Sommer FG, Edwards B, Myers BD. Effects of Aging on Glomerular Function and Number in Living Kidney Donors. Kidney Int. 2010;78(7):686-92.

Tang BT, Fonte TA, Chan FP, Tsao PS, Feinstein JA, Taylor CA. Three-Dimensional Hemodynamics in the Human Pulmonary Arteries under Resting and Exercise Conditions. Ann Biomed Eng. 2011 Jan;39(1):347-58.

Tenenbaum JD, Whetzel PL, Anderson K, Borromeo CD, Dinov ID, Gabriel D, Kirschner B, Mirel B, Morris T, Noy N, Nyulas C, Rubenson D, Saxman PR, Singh H, Whelan N, Wright Z, Athey BD, Becich MJ, Ginsburg GS, Musen MA, Smith KA, Tarantal AF, Rubin DL, Lyster P. The Biomedical Resource Ontology (BRO) to Enable Resource Discovery in Clinical and Translational Research. J Biomed Inform. 2011 Feb;44(1):137-45. PMID: 20955817.

Thakor A, Luong R, Paulmurugan R, Lin F, Kempen P, Zavaleta C, Chu P, Massoud TF, Sinclair R, Gambhir SS. The Fate and Toxicity of Raman-Active Silica-Gold Nanoparticles in Mice. Sci Transl Med. 2011;3(79):79ra33.

Thakor AS, Paulmurugan R, Kempen P, Zavaleta C, Sinclair R, Massoud TF, Gambhir SS. Oxidative Stress Mediates the Effects of Raman Active Gold Nanoparticles in Human Cells. Small. 2011 Jan 3;7(1):126-36.

Thomason ME, Dennis EL, Joshi AA, Joshi SH, Dinov ID, Chang C, Henry ML, Johnson RF, Thompson PM, Toga AM, Glover GH, Van Horn JD, Gotlib IH. Resting-State fMRI can Reliably Map Neural Networks in Children. NeuroImage. 2011;55:165-75.

Tognolini A, Al-Ahmad A, Wang PJ, Hsia HH, Herfkens RJ, Girard E, Moore T, Fahrig R. Intra-procedure Visualization of the Esophagus using Interventional C-arm CT as Guidance for Left Atrial Radiofrequency Ablation. Academic Radiology. 2011 Mar 28 [Epub ahead of print].

Tognolini A, Louie JD, Hwang GL, Hofmann LV, Sze DY, Kothary N. C-arm CT for Hepatic Interventions: A Practical Guide. J Vasc Interv Radiol. 2010 Dec;21(12):1817-23.

Tognolini A, Louie JD, Hwang GL, Kuo WT, Hovsepian DM, Hofmann LV, Sze DY, Kothary N. Utility of C-Arm CT in Patients with Hepatocellular Carcinoma Undergoing Transhepatic Arterial Chemoembolization. J Vasc Interv Radiol. 2010 Mar;21(3):339-47.

Published Papers

Published Papers

Tseng JR, Stuart D, Aardalen K, Kaplan A, Azis N, Hughes NP, Gambhir SS. Use of DNA Microarray and Small Animal Positron Emission Tomography in Preclinical Drug Evaluation of RAF265, a Novel B-Raf/VEGFR-2 Inhibitor. Neoplasia. 2011;13(3):266-75.

Tu SW, Peleg M, Carini S, Bobak M, Ross J, Rubin DL, Sim I. A Practical Method for Transforming Free-Text Eligibility Criteria into Computable Criteria. J Biomed Inform. 2011 Apr;44(2):239-50. PMID: 20851207.

Turner JA, Mejino JLV, Brinkley J, Detwiler LT, Lee HJ, Martone M, Rubin DL. Application of Neuroanatomical Ontologies for Neuroimaging Data Annotation. Front Neuroinform. 2010;4, pii:10. PMID: 20725521.

Ueda T, Fleischmann D, Dake MD, Rubin GD, Sze DY. Incomplete Endograft Apposition to the Aortic Arch: Bird-Beak Configuration Increases Risk of Endoleak Formation after Thoracic Endovascular Aortic Repair. Radiology. 2010;255(2):645-52.

Van de Ven SMWY, Lin MC, Daniel BL, Sareen PK, Lipson JA, Pal S, Dirbas FM, Ikeda DM. Freehand MRI-Guided Preoperative Needle Localization of Breast Lesions after MRI-Guided Vacuum-Assisted Core Needle Biopsy (VACNB) without Marker Placement. J Magn Reson Imaging. 2010 Jul;32(1):101-9.

Van de Ven SMWY, Mincu N, Brunette J, Ma G, Khayat M, Ikeda DM, Gambhir S. Molecular Imaging using Light Absorbing Imaging Agents and a Clinical Optical Breast Imaging System – A Phantom Study. Mol Imaging Biol. 2011 Apr;13(2):232-8.

Vandenbroucke A, Foudray AMK, Olcott PD, Levin CS. Performance Characterization of a New High Resolution PET Scintillation Detector. Phys Med Biol. 2010;55(19):5895-911.

Vandevenne J, Pearle A, Lang P, Butts-Pauly K, Bergman G. Clinical Feasibility of a Magnetic Resonance Tracking System to Guide the Position of the Scan Plane during Physiologic Joint Motion. Radiol Med. 2010 Feb;115(1):133-40. PMID: 20041313.

Vasanawala SS, Jackson E. A Method of Rapid Robust Respiratory Synchronization for MRI. Pediatr Radiol. 2010 Oct;40(10):1690-2.

Vasanawala SS, Lustig M, Hargreaves BA, Alley MT, Pauly JM. Improved Pediatric MRI via Compressed Sensing. Radiology. 2010 Aug;256(2):607-16.

Vasanawala SS, Madhuranthakam AJ, Venkatesan R, Sonik A, Lai P, Brau AC. Volumetric Fat-Water Separated T2-Weighted MRI. Pediatr Radiol. 2011 Jul;41(7):875-83.

Vasanawala SS. MRI of the Liver - How to do it. Pediatr Radiol. 2010 Apr;40(4):431-7.

Virk MS, Sugiyama O, Park SH, Gambhir SS, Adams DJ, Drissi H, Lieberman JR. "Same Day" Ex-vivo Regional Gene Therapy: A Novel Strategy to Enhance Bone Repair. Molecular Therapy. 2011 [Epub ahead of print].

Wang B, Sommer G, Spielman D, Shortliffe LM. Evaluation of Dynamic Contrast-Enhanced MRI in Detecting Renal Scarring in a Rat Injury Model. J Magn Reson Imaging. 2010 May;31(5):1132-6. PMID: 20432348. PMCID: PMC2921162.

Wang C, Stebbins GT, Medina DA, Shah RC, Bammer R, Moseley ME, Detoledo-Morrell L. Atrophy And Dysfunction Of Parahippocampal White Matter In Mild Alzheimer's Disease. Neurobiol Aging. 2010 Mar 30 [Epub ahead of print]. PMID: 20359781. PMCID: PMC2910843.

Wang J, Xie J, Zhou X, Cheng Z, Gu N, Teng G, Hu Q, Zhu F, Chang S, Zhang F, Lu G, Chen X. Ferritin Enhances SPIO Tracking of C6 Rat Glioma Cells by MRI. Mol Imaging Biol. 2011;13(1):87-93. PMID: 20440566.

Whitford TJ, Mathalon DH, Shenton ME, Roach BJ, Bammer R, Adcock RA, Bouix S, Kubicki M, De Siebenthal J, Rausch AC, Schneiderman JS, Ford JM. Electrophysiological and Diffusion Tensor Imaging Evidence of Delayed Corollary Discharges in Patients with Schizophrenia. Psychol Med. 2010;22:1-11. PMID: 20663254.

Wijman CA, Venkatasubramanian C, Bruins S, Fischbein NJ, Schwartz N. Utility of Early MRI in the Diagnosis and Management of Acute Spontaneous Intracerebral Hemorrhage. Cerebrovasc Dis. 2010;30:456-63.

Willmann JK, Kimura RH, Deshpande N, Lutz AM, Cochran JR, Gambhir SS. Targeted Contrast-Enhanced Ultrasound Imaging of Tumor Angiogenesis with Contrast Microbubbles Conjugated to Integrin-Binding Knottin Peptides. J Nucl Med. 2010;51(3):433-40.

Wilson KD, Hu S, Venkatasubrahmanyam S, Fu JD, Sun N, Abilez OJ, Baugh JJA, Jia F, Ghosh Z, Li RA, Butte AJ, Wu JC. Dynamic MicroRNA Expression Programs during Cardiac Differentiation of Human Embryonic Stem Cells: Role for miR-499. Circ Cardiovasc Genet. 2010;3(5):426-35. PMID: 20733065.

Wilson KD, Sun N, Huang M, Zhang WY, Lee AS, Li Z, Wang SX, Wu JC. Effects of Ionizing Radiation on Self-Renewal and Pluripotency of Human Embryonic Stem Cells. Cancer Res. 2010;70(13):5539-48. PMID: 20530673.

Worters PW, Hargreaves BA. Balanced SSFP Transient Imaging using Variable Flip Angles for a Predefined Signal Profile. Magn Reson Med. 2010;64(5):1405-13.

Published Papers

Xia Z, Xing Y, Jeon J, Kim Y-P, Gall J, Dragulescu-Andrasi A, Gambhir SS, Rao J. Immobilizing Reporters for Molecular Imaging of Extracellular Microenvironment in Living Animals. ACS Chem Biol. 2011 Aug 10 [Epub ahead of print].

Xie X, Hiona A, Lee AS, Cao F, Huang M, Li Z, Cherry A, Pei XT, Wu JC. Effects of Long Term Culture on Human Embryonic Stem Cells. Stem Cells Dev. 2011;20(1):127-38. PMID: 20629482.

Ye D, Gao L, Ma ML, Rao J. Controlling Intracellular Macrocyclization for the Imaging of Protease Activity. Angewandte Chemie International Edition. 2011;50:2275-9.

Yen YF, Le Roux P, Mayer D, King R, Spielman D, Tropp J, Butts-Pauly K, Pfefferbaum A, Vasanawala S, Hurd R. T(2) Relaxation Times of (13)C Metabolites in a Rat Hepatocellular Carcinoma Model Measured In Vivo using (13)C-MRS of Hyperpolarized [1-(13)C]pyruvate. NMR Biomed. 2010 May;23(4):414-23.PMID: 20175135. PMCID: PMC2891253.

Yong J, Rasooly J, Dang H, Lu Y, Middleton B, Zhang Z, Hon L, Namavari M, Stout DB, Atkinson MA, Tian J, Gambhir SS, Kaufman DL. Multimodality Imaging of {beta}-Cells in Mouse Models of Type I and II Diabetes. Diabetes. 2011 [Epub ahead of print].

Yoon S, Pineda AR, Fahrig R. Simultaneous Segmentation and Reconstruction: A Level Set Method Approach for Limited View Computed Tomography. Med Phys. 2010 May;37(5):2264-8.

Young P, Brau AC, Iwadate Y, Vasanawala S, Daniel BL, Herfkens RJ. Respiratory Navigated Free Breathing 3D Spoiled Gradient-Recalled Echo Sequence for Contrast-Enhanced Examination of the Liver: Diagnostic Utility and Comparison With Free Breathing and Breath-Hold Conventional Examinations. AJR Am J Roentgenol. 2010 Sep;195(3):687-91.

Yu J, Du KT, Fang Q, Gu Y, Mihardja SS, Sievers RE, Wu JC, Lee RJ. The Use of Human Mesenchymal Stem Cells Encapsulated in RGD Modified Alginate Microspheres in the Repair of Myocardial Infarction in the Rat. Biomaterials. 2010;31(27):7012-20. PMID: 20566215.

Zaharchuk G, Saritas EU, Andre JB, Chin CT, Rosenberg J, Brosnan T, Shankaranarayan A, Nishimura DG, Fischbein NJ. Reduced Field-of-view Diffusion Imaging of the Human Spinal Cord: Comparison with Conventional Single-shot Echo-planar Imaging. AJNR Am J Neuroradiol. 2011 Mar 31 [Epub ahead of print].

Zaharchuk G, Straka M, Marks MP, Albers GW, Moseley ME, Bammer R. Combined Arterial Spin Label and Dynamic Susceptibility Contrast Measurement of Cerebral Blood Flow. Magn Reson Med. 2010 Jun;63(6):1548-56. PMID: 20512858. PMCID: PMC2905651.

Zhao Y, Zhao S, Kuge Y, Strauss WH, Blankenberg FG, Tamaki N. Localization of Deoxyglucose and Annexin A5 in Experimental Atheroma Correlates with Macrophage Infiltration but not Lipid Deposition in the Lesion. Mol Imaging Biol. 2010 Aug 5 [Epub ahead of print].

Zissen M, Wallace G, Stevens KJ, Fredericson M, Beaulieu CF. High Hamstring Tendinopathy: Magnetic Resonance and Ultrasound Imaging and Therapeutic Efficacy of Percutaneous Corticosteroid Injection. AJR Am J Roentgenol. 2010;195:993-8.

Zissen MH, Kunz P, Subbarayan M, Chin FT, Conti PS, Fisher GA, Quon A. 18F-5-Fluorouracil Dynamic Positron Emission Tomography/ Computed Tomography Shows Decreased Tracer Activity after Bevacizumab in Colorectal Metastases. Nucl Med Commun. 2011;32(5):343-7.

Sheikh AY, van der Bogt KE, Doyle TC, Sheikh MK, Ransohoff KJ, Ali ZA, Palmer OP, Robbins RC, Fischbein MP, Wu JC. Micro-CT for characterization of murine CV disease models. JACC Cardiovascular Imaging 2010;3:783-785. PMID 20633858. PMCID 2952324.

Hiona A, Lee AS, Nagendran J, Xie X, Connolly AJ, Robbins RC, Wu JC. Pretreatment with angiotensin-converting enzyme inhibitor attenuates doxorubicin-induced cardiomyopathy via preservation of mitochondrial function. Journal Thoracic & Cardiovascular Surgery 2010; Epub ahead of print. PMID: 21094500. NIHMS 244375

Books and Book Chapters

Books and Book Chapters

Atlas SW. (2011). Access in America: Advanced Medical Technology, Innovative Treatments, Preventive Care and Screening. In Atlas SW (Ed.), Inside America's Health Care: Access to Excellence. Stanford, CA: Hoover Press.

Atlas SW. (2010). American Health Care: Ignored Facts and Disregarded Options. In Atlas SW (Ed.), Reforming America's Health Care System: The Flawed Vision of ObamaCare. Stanford, CA: Hoover Press.

Atlas SW. (2011). Essentials of the US Health Care System. In Atlas SW (Ed.), Inside America's Health Care: Access to Excellence. Stanford, CA: Hoover Press.

Books and Book Chapters

Books and Book Chapters

Atlas SW. (2011). Health System Quality: Why Life Expectancy and Infant Mortality Don't Measure Up. In Atlas SW (Ed.), Inside America's Health Care: Access to Excellence. Stanford, CA: Hoover Press.

Atlas SW. (2011). Innovation from America's Doctors and Medical Scientists. In Atlas SW (Ed.), Inside America's Health Care: Access to Excellence. Stanford, CA: Hoover Press.

Atlas SW. (2011). Inside America's Health Care: Access to Excellence. Atlas SW (Ed.). Stanford, CA: Hoover Press.

Atlas SW. (2011). Maintaining Excellence with Reform. In Atlas SW (Ed.), Inside America's Health Care: Access to Excellence. Stanford, CA: Hoover Press.

Atlas SW. (2010). Reforming America's Health Care System: The Flawed Vision of ObamaCare. Atlas SW (Ed.). Stanford, CA: Hoover Press.

Atlas SW. (2011). The Facts: Medical Care for Serious Disease in the United States. In Atlas SW (Ed.), Inside America's Health Care: Access to Excellence. Stanford, CA: Hoover Press.

Atlas SW. (2011). WHO Rankings: A Critical Appraisal. In Atlas SW (Ed.), Inside America's Health Care: Access to Excellence. Stanford, CA: Hoover Press.

Bammer R, Holdsworth SJ, Aksoy M, Skare ST. (2010). Phase Error and Correction in Diffusion MRI. In Jones D (Ed.), Diffusion MRI (pp. 218-49). Oxford University Press.

Skare ST, Bammer R. (2010). EPI-based Pulse Sequences for Diffusion Tensor MRI. In Jones D (Ed.), Diffusion MRI (pp. 182-202). Oxford University Press.

Daldrup-Link HE, Goldsby R. (2010). Solid Tumors Outside of the CNS. In Daldrup-Link HE, Gooding C (Eds.), Essentials of Pediatric Radiology. New York, NY: Cambridge University Press.

Daldrup-Link HE, Gooding C. (2010). Essentials of Pediatric Radiology. Daldrup-Link HE, Gooding C (Eds.). New York, NY: Cambridge University Press.

Golovko D, Sutton E, Daldrup-Link HE. MR Contrast Media. In Baur A (Ed.), MRI of the Bone Marrow. Heidelberg: Springer.

Desser TS, Hann LE. Ultrasound of the Liver, Biliary Tree, and Pancreas. In Blumgart LH (Ed.), Surgery of the Liver, Biliary Tract, and Pancreas (5th ed.). Philadelphia, PA: Elsevier.

Fischbein NJ, Lee N. (2010). Head and Neck. In Hoppe RT, Phillips TL, Roach M III, (Eds.), Leibel Phillips Textbook of Radiation Oncology (3rd ed., pp. 331-62). Philadelphia, PA: Elsevier.

Fischbein NJ, Ong K. Radiology. In Lalwani A (Ed.), Current Diagnosis and Treatment in Otalaryngology - Head and Neck Surgery (3rd ed.). New York, NY: Lange Medical Publishers.

Lal D, Fischbein N, Harsh GR. Chordomas and Chondrosarcomas. In Sheehan EP, Laws ER Jr (Eds.), Tumors of the Sella and Parasellar Region.

Fleischmann D, Chin AS, Miller DC. (2011). Three- and Four-Dimensional Imaging in Acute Aortic Syndrome. In Hodler J, von Schulthess GK, Zollikofer CL (Eds.), Diseases of the Heart, Chest, & Breast. Milan, Heidelberg, London: Springer.

Hallett R, Fleischmann D. Diagnostic Non-invasive Evaluation: Computed Tomography. In Geschwind J-F, Dake M (Eds.), Abrams Angiography: Interventional Radiology (3rd ed.). Lippincott Williams & Wilkins.

Chan C, Gambhir SS. (2010). Encyclopedic Reference on Imaging. In Ntziachristos V (Ed.), Springer Medicine eBook Collection. New York, NY: Springer.

Figueiredo ML, Gambhir SS, Carey M, Wu L. (2010). Cell-Specific Imaging of Reporter Gene Expression Using a Two-Step Transcriptional Amplification Strategy. In Gambhir SS, Yaghoubi S. (Eds.), Molecular Imaging with Reporter Genes (pp. 127-50). New York, NY: Cambridge University Press.

Gambhir SS, Yaghoubi S. (2010). Molecular Imaging with Reporter Genes. New York, NY: Cambridge University Press.

Gambhir SS. Molecular Imaging: A Primer. Springer-Verlag Publishers.

Massoud TF, Paulmurugan R, Chan C, Fan-Minogue H, Gambhir SS. (2010). Reporter Gene Imaging of Cell Signal Transduction. In Gambhir SS, Yaghoubi S (Eds.), Reporter Gene Imaging of Cell Signal Transduction (pp. 195-226). New York, NY: Cambridge University Press.

Penuelas I, Yaghoubi S, Prosper F, Gambhir SS. (2010). Clinical Applications of Reporter Gene Technology in Living Subjects. In Gambhir SS, Yaghoubi S (Eds.), Molecular Imaging with Reporter Genes (pp. 297-314). New York, NY: Cambridge University Press.

Ray P, Gambhir SS. (2010). Multimodality Imaging of Reporter Genes. In Gambhir SS, Yaghoubi S (Eds.), Molecular Imaging with Reporter Genes (pp. 113-26). New York, NY: Cambridge University Press.

Books and Book Chapters

Books and Book Chapters

Rodriguez-Porcel MG, Gambhir SS. (2010). Imaging of Reporter Genes and Stem Cells. In Gambhir SS, Yaghoubi S (Eds.), Molecular Imaging with Reporter Genes (pp. 275-96). New York, NY: Cambridge University Press.

Weissleder R, Ross B, Rehemtulla A, Gambhir SS. (2010). Molecular Imaging: Principles and Practice. Shelton, CT: People's Medical Publishing House.

Wu J, Gambhir SS. (2010). Molecular Imaging of Gene Expression and Cell Therapy. In Zaret B, Beller G (Eds.), Clinical Nuclear Cardiology: State of the Art and Future Direction (4th ed., pp. 723-37). Mosby, Inc.

Yaghoubi S, Gambhir SS. (2010). Gene Therapy and Imaging of Transgene Expression. In Gambhir SS and Yaghoubi S (Eds.), Living Subjects in Molecular Imaging with Reporter Genes (pp. 227-38). New York, NY: Cambridge University Press.

Besier TF, Draper C, Pal S, Fredericson M, Gold GE, Delp S, Beaupre G. (2011). Imaging and Musculoskeletal Modeling to Investigate the Mechanical Etiology of Patellofemoral Pain. In Sanchis-Alfonso V (Ed.), Anterior Knee Pain and Patellar Instability. Springer-Verlag London Limited.

Goris ML. (2011). Nuclear Medicine Applications and their Mathematical Basis (1st ed.). World Scientific Publishing Co. Inc.

Steele JR, Hovsepian DM. Statistical Process Control in Radiology. In Aubujudeh H, Bruno M (Eds.), Quality and Safety in Radiology. Oxford University Press.

Thurmond AS, Hovsepian DM. (2011). Fallopian Tube Recanalization. In Pelage J-P (Ed.), Gynecological Interventional Radiology. Elsevier.

Yamada K, Hovsepian DM. (2011). Traumatic Arterial Injuries: Abdomen. In Geschwind J-F, Dake M (Eds.), Abrams Angiography: Interventional Radiology (3rd ed.). Lippincott Williams & Wilkins.

Hwang GL. Chronic Lower Extremity Veno-occlusive Disease: Medical Management and Interventional Strategies. In Geschwind J-F, Dake M (Eds.), Abrams Angiography: Interventional Radiology (3rd ed.). Lippincott Williams & Wilkins.

Chandra V, Dirbas FM, Ikeda DM. (2011). Image-guided breast biopsy. In Dirbas FM, Scott-Conner C (Eds.), Breast Surgical Techniques and Interdisciplinary Management (223-46). New York, NY: Springer.

Gutierrez RL, Horst KC, Dirbas FM, Ikeda DM. (2011). Breast Imaging Following Breast Conservation Therapy. In Dirbas FM, Scott-Conner C (Eds.), Breast Surgical Techniques and Interdisciplinary Management (pp. 975-95). New York, NY: Springer.

Kuo WT. (2011). Endovascular Therapy for Acute Pulmonary Embolism. In Geschwind J-F, Dake M (Eds.), Abrams Angiography: Interventional Radiology (3rd ed.). Lippincott Williams & Wilkins.

Spanoudaki V, Levin CS. (2011). Design Considerations of Small-animal PET Scanners. In Zaidi H (Ed.), Multimodality Molecular Imaging of Small-Animals: Instrumentation and Applications. Springer.

Levin CS. (2010). Imaging System Physics, Technology, and Methods for Visualization and Quantification of Reporter Gene Expression in Living Subjects. In Gambhir SS, Yaghoubi S (Eds.), Reporter Gene Imaging. New York, NY: Cambridge University Press.

Levin CS. (2010). Instrumentation and Methods to Combine Small Animal PET with other Imaging Modalities. In Gambhir SS, Weissleder, Ross, Rehemtulla (Eds.), Molecular Imaging: Principles and Practice. BC Decker Inc.

Levin CS. (2011). Molecular Imaging Instrumentation. In Chen S (Ed.), Molecular Imaging Probes for Cancer Research (Ch. 2). World Scientific.

Pratx G, Cui J, Prevrhal S, Levin CS. (2011). 3-D Tomographic Image Reconstruction from Unordered Lines with CUDA. In Zaidi H (Ed.), GPU Gems 3 (Ch. 42). New York, NY: Springer.

Taghibakhsh F, Levin CS. (2011). Recent Advances in Positron Emission Tomography (PET) Technology. In Iniewski K (Ed.), Sensor Technologies: Biological and Medical Sensors. CRC Press.

Marks MP. (2011). Endovascular treatment of Moyamoya Disease. In Khan N, Wanebo JE, Zambramski JM, Spetzler RF (Eds.), Moyamoya Angiopathy: Current Status in Diagnosis and Treatment. New York, NY: Thieme Medical Publishers, Inc.

Moseley ME. (2011). DWI in Cerebral Ischemia: The Early Days. In Jones D (Ed.), Diffusion MRI: Theory, Methods, and Applications. Elsevier.

Ha BY, Newman B. (2011). Pediatric Emergency Imaging. In Wang N, Shandro J, Fassi B, Sohoni A (Eds.), A Practical Guide to Pediatric Emergency Medicine: Caring for Children in the Emergency Department. New York, NY: Cambridge University Press.

Newman B, Kurland G. (2011). Tools for Diagnosis and Management of Respiratory Disease. In Rudolph C, Rudolph A, Lister G, Lewis F, Gershon A (Eds.), Rudolph's Pediatrics (22nd ed.). New York, NY: McGraw Hill Medical.

Books and Book Chapters

Books and Book Chapters

Newman B, Varich LJ. (2010). Neonatal Imaging. In Daldrup-Link HE, Gooding CA (Eds.), Essentials of Pediatric Radiology: A Multimodality Approach. New York, NY: Cambridge University Press.

Massoud TF, Paulmurugan R, Chan C, Fan-Minogue H, Gambhir SS. (2010). Molecular Imaging with Reporter Genes. In Gambhir SS, Yaghoubi S (Eds.), Reporter Gene Imaging of Cell Signal Transduction (pp. 195-226). New York, NY: Cambridge University Press.

Massoud TF, Paulmurugan R, Ray P, De A, Chan C, Fan-Minogue H, Gambhir SS. (2010). Molecular Imaging Principles and Practice. In Weissleder R, Ross BD, Rehemtulla A, Gambhir SS (Eds.), Molecular Imaging of Protein-Protein Interactions (pp. 781-807). Shelton, CT: People's Medical Publishing House.

Paulmurugan R. (2011). Introduction to Cancer Biology. In Chen X (Ed.), Fundamentals of Molecular Imaging, Molecular Imaging Probes for Cancer Imaging. Singapore: World Scientific Publishing.

Plevritis SK. (2010). Mining Genomic Data for Molecular Imaging Targets. In Weissleder R, Gambhir SS, Ross BD, Rehemtulla A (Eds.), Molecular Imaging: Principles and Practice. McGraw Hill Publishers.

Quon A, Graves EE, Loo Jr BW, Xing L. (2010). The Use of Molecular Imaging in Clinical Oncology. In Hoppe R, Phillips T, Roach M (Eds.), Leibel and Phillips Textbook of Radiation Oncology. Saunders.

Chan J, Fisk NM, Lee E SM, Rutt BK, Wang SC. Intracellular Drug Delivery: Fundamentals and Applications. In Prokop A (Ed.), Magnetic Resonance Trackign of Stem Cells with Iron Oxide Particles (pp. 1-35). New York, NY: Springer.

Gazdinski LM, Foster PJ, Lee E SM, Rutt BK. Stem Cell Labeling for Delivery and Tracking Using Non-Invasive Imaging. Kraitchman D, Wu J (Eds.). CRC Press.

Thomas P, Spielman D, Recht L. (2011). The Bevacizumab "Pseudoresponse"in Glioma: Disappointment or Opportunity? In Zgela V (Ed.), Brain Tumor.

Spielman D. (2011). Neurochemical Imaging – MRS. In Spielman D (Ed.), Handbooks of Alzheimer's Disease, Volume 2 - Imaging the Alzheimer's Disease Brain.

Chan JC, Gambhir SS, Willmann JK. (2011). Imaging Techniques in Drug Development and Clinical Practice. In Kratz F, Senter P, Steinhagen H (Eds.), Drug Delivery in Oncology. Weinheim, Germany: Wiley-VCH.

Deshpande N, Willmann JK. (2011). Micro- and Nano-particle based Contrast-enhanced Ultrasound Imaging. In Chen X (Ed.), Nanoplatform-based Molecular Imaging. New York, NY: John Wiley & Sons.

Pysz MA, Willmann JK. (2011). Applications of Molecular Small-animal Imaging in Oncology. In Zaidi H (Ed.), Multimodality Molecular Imaging of Small Animals: Instrumentation and Applications. New York, NY: Springer.

Papers Submitted or In Press

Papers Submitted or In Press

Le TT, Fischbein NJ, Andre JB, Wijman C, Rosenberg J, Zaharchuk G. Identification of Venous Signal on Arterial Spin Labeling Improves Diagnosis of Dural Arteriovenous Fistulae and Small Arteriovenous Malformations. Am J Neurorad (submitted).

Zhan K, Xie H, Gall J, Ma ML, Salehi A, Griesbeck O, Rao J. Real-Time Imaging of Rab5 Activity using a Prequenched Biosensor. ACS Chemical Biology (in-press).

Sun C, Pratx G, Carpenter CM, Liu H Cheng Z, Gambhir SS, Xing L. Synthesis and Radioluminescence of PEGylated Eu3+-doped Nanophosphors as Bioimaging Probes. Advanced materials (in-press).

Carlson AP, Brown AM, Zager E, Uchino K, Marks MP, Robertson C, Sinson GP, Marmarou A, Yonas H. Xenon/CT CBF at 28% Xenon Provides Uniquely Safe Access to Quantitative, Clinically useful CBF Information: A Multicenter Study. AJNR Am J Neuroradiol (in-press).

Pandey P, Steinberg GK, Westbroek EM, Dodd RL, Do HM, Marks MP. Intraoperative Angiography for Cranial Dural AV Fistula. AJNR Am J Neuroradiol (in-press).

Kwon OK, Kim SH, Jacobsen E, Marks MP. Clinical Implications of ICA Flow Impairment caused by Filter Occlusion during Carotid Artery Stenting. AJNR Am J Neuroradiol (submitted).

Christe A, Torrente J, Lin M, Yen A, Hallett R, Roychoudhury R, Schmitzberger F, Vock P, Roos J. Computed-Tomography (CT) Screening and follow-up of Lung Nodules: Effect of CT-Tube Current-Time, Nodule Size and Density on Detectability of Lung Nodules and Impact of Tube Current-Time on the Apparent Nodule Size. AJR Am J Roentgenol (accepted).

Papers Submitted or In Press

Papers Submitted or In Press

Maturen K, Kamaya A, Maheshwary R, Pandya A, Wasnik A, Dillman J, Kaza R. Ultrasound Imaging of Bowel Pathology: Technique and Important Diagnoses in the Acute Abdomen. AJR Am J Roentgenol (accepted).

Blankenberg FG, Norfray J. Multimodality Molecular Imaging of Apoptosis in Oncology. AJR Am J Roentgenol (in-press).

Gayer G, Desser TS, Hertz M, Osadchy A, Daniel BL, Zissin R. Spontaneous Suburothelial Hemorrhage in Coagulopathic Patients - CT diagnosis. AJR Am J Roentgenol (in-press).

Liu YI, Kamaya A, Desser TD, Rubin DL. A Bayesian Network for Differentiating Benign versus Malignant Thyroid Nodules using Sonographic and Demographic Features. AJR Am J Roentgenol (submitted).

Padilla-Thornton AE, Willmann JK, Olcott E, Jeffrey RB. Adenocarcinoma of the Uncinate Process of the Pancreas: Distinctive Clinical and Imaging Features. AJR Am J Roentgenol (submitted).

Newman B, Ganguly A, Robinson T, Kim JE. Comparison of Different Methods of Calculating CT Radiation Effective Dose in Children. AJR Am J Roentgenol (submitted).

Rubesova E, Newman B, Dutta S, Hartman G, Rosengerg J, Barth RA. Management of Bronchopulmonary Malformations: Results of the SPR and ESPR Survey. AJR Am J Roentgenol (submitted).

Liu Y, Shin LK, Jeffrey RB, Kamaya A. Quantitatively Defining Washout in Hepatocellular Carcinoma. AJR Am J Roentgenol (submitted).

Hsiao A, Lustig M, Alley MT, Murphy M, Chan FP, Herfkens RJ, Vasanawala SS. Rapid Pediatric Cardiac MR Assessment of Flow and Ventricular Volume. AJR Am J Roentgenol (submitted).

Sigg D, Levin C, Quon A. Resolution and Sampling Considerations in CT-based Partial Volume Correction applied to SUV Measurements of Discrete Lesions in PET. AJR Am J Roentgenol (submitted).

Yeom K, Holdsworth SJ, Skare ST, Barnes P, Bammer R. Diffusion-Weighted Readout-Segmented EPI in Pediatric Patients. AJR Am J Roentgenol (submitted).

Ganguly A, Fieselmann A, Marks MP, Rosenberg J, Boese J, Deuerling-Zheng M, Straka M, Zaharchuk G, Bammer R, Fahrig R. Cerebral Perfusion CT (PCT) using an Interventional C-Arm Imaging System: Cerebral Blood Flow (CBF) Measurements. Am J Neurorad (in-press).

Holdsworth S, Yeom K, Skare S, Barnes P, Bammer R. Clinical Application of Readout-Segmented (RS)-EPI for Diffusion-Weighted Imaging in Pediatric Brain. Am J Neurorad (in-press).

Zaharchuk G, Fischbein NJ, Rosenberg J, Herfkens RJ, Dake MD. Comparison of Magnetic Resonance and Contrast Venography of the Cervical Venous System in Multiple Sclerosis. Am J Neurorad (in-press).

Chan KT, Tye, GA, Popat RA, Kuo WT, Unver K, Kothary N, Sze DY, Hofmann LV. Common Iliac Vein Stenosis: A Risk Factor for Oral Contraceptive-Induced Deep Vein Thrombosis. Am J Obstetrics Gynecology (in-press).

Behera D, Jacobs KE, Biswal S. Advances in Musculoskeletal Molecular and Functional Imaging: Imaging Pain. Am J Roentgenol (submitted).

Safran MR, Giordano G, Lindsey DP, Gold GE, Rosenberg J, Zaffagnini S, Giori NJ. The Biomechanical Behavior of the Intact Acetabular Labrum: A Clue to its Function and Guide for Protectoin after Labral Repair. Am J Sports Med (submitted).

Hiti C, Stevens K, Jamati M, Garza D, Matheson G. Athletic Osteitis Pubis: A Comprehensive Review with a Focus on Treatment. Am J Sports Med (accepted).

Ren G, Webster JM, Liu Z, Zhang R, Miao Z, Gambhir SS, Syud FA, Cheng Z. In Vivo Targeting of HER2 Positive Tumor using 2-Helix Affibody Molecules. Amino Acids (submitted).

Liang G, Ronald J, Chen Y, Ye D, Pandit P, Ma ML, Rutt B, Rao J. Controlled Self-Assembly of Nanoparticles as Molecular Magnetic Resonance Imaging Contrast Agents. Angewandte Chemie International Edition (in-press).

Aksoy D, Bammer R, Venkatasubramanian C, Gupta SN, Mlynash M, Narayana R, Eyngorn I, Snider RW, Fischbein N, Wijman CA. MRI Profile of Blood-Brain Barrier Injury in Acute Intracerebral Hemorrhage. Annals of Neurology (in-press).

Campbell BCV, Purushotham A, Christensen S, Desmond PM, Nagakane Y, Parsons MW, Lansberg MG, Mlynash M, Straka M, De Silva DA, Olivot J-M, Bammer R, Albers GW, Donnan GA, Davis SM. Sustained Reversal of Diffusion Lesions is Rare after Stroke Thrombolysis. Annals of Neurology (in-press).

Zhang X, Liu H, Miao Z, Kimura R, Fan F, Cheng Z. Macrocyclic Chelator Assembled RGD Multimers for Tumor Targeting. Bioorganic Medicinal Chemistry Letters (in-press).

Papers Submitted or In Press

Papers Submitted or In Press

Gayer G, Ben Ely A, Maymon R, Hertz M. Enlargement of the Spleen as an Incidental Finding on CT in Postpartum Women with Fever. British J Radiology (in-press).

Ren G, Blum G, Gheysens O, Gambhir SS, Bogyo M, Cheng Z. 64Cu-Labeled-Acycloxymethyl Ketone Analog for Imaging Tumor Cathepsin B Activity. Cancer Res (submitted).

Kuo W, Cupp J, Louie J, Kothary N, Hofmann L, Sze D, Hovsepian D. Complex Retrieval of Embedded IVC Filters: Alternative Techniques and Histologic Tissue Analysis. Cardiovasc Interv Radiol (in-press).

Henning TD, Boddington S, Taubert S, Jha P, Tavri S, Golovko D, Ackermann L, Daldrup-Link HE. Somatic Differentiation and MR Imaging of Magnetically Labeled Human Embryonic Stem Cells. Cell Transplantation (in-press).

Campbell BCV, Costello C, Christensen S, Ebinger M, Parsons MW, Desmond PM, Barber PA, Butcher KS, Levi CR, De Silva DA, Lansberg MG, Mlynash M, Olivot J-M, Straka M, Bammer R, Albers GW, Donnan GA, Davis SM. Fluid-Attenuated Inversion Recovery (FLAIR) Hyperintensity in Acute Ischemic Stroke Does Not Predict Hemorrhagic Transformation. Cerebrovasc Dis (in-press).

Razgulin A, Ma N, Rao J. Strategies for In Vivo Imaging of Enzyme Activity: An Overview and Recent Advances. Chemical Society Reviews (in-press).

Xing B, So M-K, Xie H, Yao H, Lartey F, Liu F, Rao J. A Near-Infrared Fluorogenic Cephalosporin Probe for Tomographic Imaging of ß-lactamase Expression In Vivo. Chemistry - A European Journal (submitted).

Yang Y, Aw J, Chen K, Padmanabhan P, Hou Y, Cheng Z, Xing B. Enzyme Responsive Multifunctional Magnetic Nanoparticles for Intracellular Drug Delivery and Tumor Imaging. Chemistry An Asian Journal (in-press).

Kedziorek DA, Hofmann LV, Gilson WD, Stuber M, Cosby K, Huang G, Kohl BD, Barnett BP, Simons B, Walczak P, Bulte JWM, Gabrielson K, Kraitchman DL. X-ray Visible Stem Cell Therapy Activate the Growth of Compensatory Blood Vessels in a Rabbit Model of Peripheral Arterial Disease. Circulation (submitted).

Mosci C, Iagaru A. PET/CT Imaging of Thyroid Cancer. Clin Nucl Med (in-press).

Hsu JL, Kuschner WG, Paik J, Bower N, Kothary N. The Diagnostic Yield of CT-Guided Percutaneous Lung Biopsy in Solid Organ Transplant Recipients. Clin Transplant (accepted).

Daldrup-Link HE, Golovko D, DeNardo D, Ruffell B, Castaneda R, Ansari C, Tikhomirov GA, Rao J, Wendland M, Corot C, Coussens LM. MR Imaging of Tumor Associated Macrophages with Clinically Applicable Iron Oxide Nanoparticles. Clin Cancer Res (accepted).

Van de Ven SMWY, Elias S, Chan CT, Miao Z, Cheng Z, De A, Gambhir SS. Optical Imaging with HER2-Targeted Affibody Molecules can Monitor Hsp90 Treatment Response in a Xenograft Mouse Model. Clin Cancer Res (submitted).

Maclaren J, Schneider F, Herbst M, Hennig J, Bammer R, Zaitsev M, Walrabe U. An Adaptive MR-Compatible Lens and Objective. Concepts in Magn Reson B (submitted).

Liu S, Shen B, Chin F, Cheng Z. Recent Progress in Radiofluorination of Peptides for PET Molecular Imaging. Curr Org Synth (in-press).

Wu S, Chang E, Cheng Z. Molecular Probes for Bioluminescence Imaging. Curr Org Synth (in-press).

Kong Y, Shi Y, Chang M, Akin A, Francis K, Zhang N, Troy TL, Yao H, Rao J, Cirillo SLG, Cirillo JD. Whole Body Imaging of Infection using Bioluminescence. Current Protocols for Microbiology (in-press).

Kong Y, Akin A, Francis K, Zhang N, Troy TL, Xie H, Rao J, CIrrilo SLG, Cirillo JD. Whole Body Imaging of Infection using Fluorescence. Current Protocols for Microbiology (in-press).

Aye T, Reiss AL, Kesler S, Hoang S, Drobny J, Park Y, Schleifer K, Baumgartner H, Wilson D, Buckingham B. The Feasibility of Detecting Neuropsychological and Neuroanatomical Effects of Type 1 Diabetes Mellitus in Young Children. Diabetes Care (in-press).

Christe A, Lin M. CT Patterns: Comparison of Standard-Dose and Simulated Low Dose CT of the Chest in Patients with Fungal Infection. EJR (submitted).

Sims ME, Shin LK, Rosenberg JK, Jeffrey RB. Multidetector CT of Acute Vascular Injury in Blunt Abdominal/ Pelvic Trauma: Imaging Predictors of Treatment. Eur J Trauma Emerg Surg (in-press).

Liu S, Liu H, Jiang H, Zhang H, Cheng Z. One-Step Radiosynthesis of 18F-AIF-NOTA-RGD2 for Tumor Angiogenesis PET Imaging. Eur J Nucl Med Mol imaging (in-press).

Papers Submitted or In Press

Papers Submitted or In Press

Miao Z, Ren G, Jiang L, Liu H, Webster JM, Zhang R, Namavari M, Gambhir SS, Syud F, Cheng Z. A Novel 18F-Labeled 2-Helix Small Protein for PET Imaging of HER2 Positive Tumor. Eur J Nucl Med Mol imaging (in-press).

Srabani S, Sekar TV, Paulmurugan R. Optical Imaging of Nitroreductase Reporter Gene System in Living Mouse. Gene Therapy (submitted).

Chinn G, Levin CS. A Maximum NEC Criterion for Compton Collimation to Accurately Identify True Coincidences in PET. IEEE Transaction on Medical Imaging (in-press).

Fieselmann A, Ganguly A, Deuerling-Zheng Y, Zellerhoff M, Rohkohl C, Boese J, Hornegger J, Fahrig R. Interventional 4-D C-arm CT Perfusion Imaging using Interleaved Scanning and Partial Reconstruction Interpolation. IEEE Transactions on Medical Imaging (submitted).

Chinn G, Levin CS. Maximum Likelihood Compressed Sensing. IEEE Transactions on Signal Processing (submitted).

Won JH, Rosenberg J, Rubin GD, Napel S. A Protein Side-Chain Placement-Based Solution Method for Uncluttered Single-Image Visualization. IEEE Transactions on Visualization and Computer Graphics (submitted).

Levy MA, Rubin DL. Computational Approaches to Assist in the Evaluation of Cancer Treatment Response. Imaging in Medicine (in-press).

Fiselmann A, Kowarschik M, Ganguly A, Fahrig R. Deconvolution-Based CT and MR Perfusion Measurement Theoretical Model Revisited and Practical Implementation Details. International J Biomedical Imaging (in-press).

Ren Y, Fleischmann D, Foygel K, Molvin L, Lutz AM, Koong AC, Jeffrey RB, Tian L, Willmann JK. Antiangiogenic and Radiation Therapy: Early Effects on In Vivo CT Perfusion Parameters in Human Colon Cancer Xenografts in Mice. Invest Radiol (submitted).

Straka M, Albers GW, Lansberg MG, Kemp SM, Marks MP, Wilder M, Weschler LR, Bammer R. Automated Assessment of Acute Stroke Lesions using CT Perfusion: Application to Infarct Core and Critically Hypoperfused Tissue. Invest Radiol (in-press).

Ren Y, Fleischmann D, Foygel K, Molvin L, Lutz AM, Koong AC, Tian L, Willmann JK. Assessment of Early Antiangiogenic and Radiation Therapy Effects on CT Perfusion Parameters in Human Colon Cancer Xenografts in Mice. Invest Radiol (submitted).

Ryu SC, Renaud P, Black RJ, Daniel BL, Cutkosky M. Feasibility Study of an Optically Actuated MR-Compatible Active Needle. IROS (submitted).

Sin J, Beck A, Pai R, Stevens K. Multifocal Epithelioid Hemangioma with Reactive Bone Formation. ISRN Pathology (submitted).

Neofytou E, Chang E, Patlola B, Kimura N, Lijkwan M, Joubert L-M, Rajadas J, Wu J, Chen X, Robbins RC, Gambhir SS, Cheng Z, Beygui RE. Enhanced Vascularization of Tissue-Engineered Dipose Tissue-Derived Stem Cell on Three-Dimensional Scaffolds. J Biomedical Materials Research part A (in-press).

Fraello D, Maller-Kesselman J, Vohr B, Katz K, Kesler S, Schneider K, Reiss AL, Ment L, Spann M. Consequence of Preterm Birth in Early Adolescence: The Role of Language on Auditory Short-Term Memory. J Child Neurology (in-press).

Hong DS, Dunkin B, Reiss AL. Psychosocial Functioning and Social Cognitive Processing in Girls with Turner Syndrome. J Developmental Behavioral Pediatrics (in-press).

Xu J, Faruque JS, Beaulieu CF, Rubin DL, Napel S. A Comprehensive Descriptor of Shape: Method and Application to Content-Based Retrieval of Similar Appearing Lesions in Medical Images. J Digit Imaging (in-press).

Raman B, Raman R, Rubin GD, Napel S. Automated Tracing of the Adventitial Contour of Aortoiliac and Peripheral Arterial Walls in CT Angioraphy (CTA) to allow Calculation of Non-Calcified Plaque Burden. J Digit Imaging (in-press).

Shore M, Rubin DL, Kahn CE. Integration of Imaging Signs into RadLex. J Digit Imaging (in-press).

Bammer R. Echo-Planar Imaging. J Magn Reson Imaging (in-press).

Stevens KJ, Wallace CG, Chen W, Rosenberg JK, Gold GE. Imaging of the Wrist at 1.5T using Isotropic 3D-FSE-Cube. J Magn Reson Imaging (in-press).

Postma E, van Hillergersberg R, Daniel BL, Merckel LG, Verkooijen HM, van den Bosch MAA. Magnetic Resonance Image-guided Ablation of Breast Cancer: Where do we Stand Today? J Magn Reson Imaging (in-press).

Shapiro L, Harish M, Hargreaves B, Starosweicki E, Gold GE. Advances in Musculoskeletal MRI, Technical Considerations. J Magn Reson Imaging (in-press).

Elayaperumal S, Park YL, Worters P, Daniel B, Cutkosky M. Real-Time Three-Dimensional Shape Determination of Interventional Tools and MRI Scan Plane Control with Miniaturized Optical Fiber Bragg Grating Strain Sensors. J Magn Reson Imaging (submitted).

Papers Submitted or In Press

Papers Submitted or In Press

Paulmurugan R, Tamrazi A, Katzenellenbogen JA, Massoud TF, Gambhir SS. Non-Invasive Molecular Imaging of Estrogen Receptor α and β Subtype Assembly. J Molecular Endocrinology (submitted).

Marks MP, Steinberg GK. Cerebral Proliferative Angiopathy. J Neuro Intervent Surg (submitted).

Behera D, Jacobs KE, Behera S, Rosenberg J, Biswal S. 18F-FDG PET-MRI can be Used to Identify Injured Peripheral Nerves in a Model of Neuropathic Pain. J Nucl Med (in-press).

Olcott PD, Pratx G, Johnson D, Mansouri MA, Mitra E, Niederkohr R, Levin CS. Feasibility of Intra-Operative Gamma Camera used in Conjunction with Gamma Detection Probes in Sentinel Lymph Node Biopsy and Radio-Guided Surgery. J Nucl Med (submitted).

Blankenberg FG, Levashova Z, Backer M, Goris ML, Backer JM. Fractionated Systemic Radiotherapy with scVEGF/177Lu Leads to Sustained Disruption of the Tumor Vasculature and Intratumoral Apoptosis. J Nucl Med (submitted).

Quon A, Iagaru A, Abreu M, Hennemann S, Neto J, Sprinz C. Integrated 18F-NaF PET/CT for the Evaluation of Post-Operative Pain in Patients with Prior Spinal Fixation Surgery. J Nucl Med (submitted).

De A, Namavari M, Zhang R, Gourishankar G, Padilla De Jesus O, Lee B, Webster JM, Cheng Z, Ray P, Wang S, Patel M, Levi J, Kovacs E, Grade H, Syud FA, Gambhir SS. MicroPET imaging of Tumor Bearing Mice with HER2 Targeted 18F-Labeled Affibody Tracer for Quantitative Measurement of the Surface Biomarker. J Nucl Med (submitted).

Lin FI, Rao J, Mittra ES, Nallapareddy K, Chengapa A, Dick DW, Gambhir SS, Iagaru A. Prospective Comparison of Combined 18F FDG and 18F NaF PET/CT vs. 18F FDG PET/CT Imaging for Detection of Malignancy. J Nucl Med (submitted).

Vasanawala SS, Barth RA, Ganguly A, Fahrig R, Rosenberg J, Rieke V, Kane P, Daniel B, Kennedy WA. Magnetic Resonance Voiding Cystography at 0.5T and 1.5T Field Strength for the Evaluation of Vesicoureteral Reflux. J Pediatr Urol (submitted).

Kode K, Shachaf C, Elchuri S, Nolan G, Paik DS. Raman Labeled Nanoparticles: Characterization of Variability and Improved Method for Unmixing. J Raman Spectroscopy (submitted).

Shahbaba B, Tibshirani R, Shachaf CM, Plevritis SK. Bayesian Gene Set Analysis for Identifying Significant Biological Pathways. J Royal Statistical Society: Applied Statistics (Series C) (submitted).

Abdelmaksoud MH, Louie JD, Kothary N, Hwang GL, Kuo WT, Hofmann LV, Hovsepian DM, Sze DY. Embolization of Parasitized Extrahepatic Arteries to Reestablish Intrahepatic Arterial Supply to Tumors prior to 90Y Radioembolization. J Vasc Interv Radiol (in-press).

Kothary N, Abdelmaksoud MHK, Tognolini A, Fahrig R, Louie JD, Hwang G, Hofmann LV, Sze DY. Imaging Guidance with C-arm CT: A Prospective, Randomized Study Evaluating the Impact of CACT on Patient Radiation Exposure. J Vasc Interv Radiol (in-press).

Higgins LJ, Hwang GL, Katzenberg RH, Kothary N, Sze DY, Hofmann LV. In Vitro Design and Characterization of the Nonviral Gene Delivery Vector Iopamidol, Protamine, Ethiodized of Reagent (VIPER). J Vasc Interv Radiol (in-press).

Meer AB, Louie JD, Abdelmaksoud MHK, Kothary N, Hovsepian DM, Hofmann LV, Kuo WT, Hwang GL, Sze DY. Intrahepatic Collateral Supply to the Previously Embolized Right Gastric Artery: A Potential Pitfall for Nontarget Radioembolization. J Vasc Interv Radiol (in-press).

Kuo WT, Hovsepian DM, Hofmann LV, Sze D. Photothermal Ablation With the Excimer Laser Sheath Technique for Embedded IVC Filter Removal: Initial Results From a Prospective Study. J Vasc Interv Radiol (in-press).

Stewart JK, Kuo WT, Hovsepian DM, Hofmann LV, Bonham CA, Sze DY. Portal Venous Remodeling after Endovascular Reduction of Pediatric Autogenous Portosystemic Shunts. J Vasc Interv Radiol (in-press).

Abdelmaksoud MHK, Louie JD, Kothary N, Hwang GL, Kuo WT, Hofmann LV, Hovsepian DM, Sze DY. Consolidation of Hepatic Arterial Inflow by Embolization of Variant Hepatic Arteries in Preparation for 90Y Radioembolization. J Vasc Interv Radiol (submitted).

Kothary N, Louie J, Hwang G, Kuo WT, Sze D, Hofmann LV, Hovsepian DM. Prospective Evaluation of the Impact of C-Arm CT on Radiation Exposure During Transhepatic Arterial Chemoembolization. J Vasc Interv Radiol (submitted).

Kothary N, Abdelmaksoud M, Tognolini A, Hwang GL, Sze DY, Hofmann LV, Louie JD. Transarterial Chemoembolization for Hepatocellular Carcinomas in Watershed Segments: Utility of C-arm CT for Treatment Planning. J Vasc Interv Radiol (submitted).

Hathout L, Do HM. Mathematical Modeling of Vascular Tortuosity. J Vasc Res (submitted).

Papers Submitted or In Press

Liu Y, Shin LK, Kamaya A, Jeffrey RB. MDCT Triphasic Evaluation of the Liver Pre-transplantation: Importance of Equilibrium Phase Washout and Morphology for Characterizing Hypervasuclar Lesions. JCAT (submitted).

Draper CE, Fredericson M, Gold GE, Besier TF, Delp SL, Beaupre GS, Quon A. Patients with Patellofemoral Pain Exhibit Elevated Bone Metabolic Activity at the Patellofemoral Joint. Journal of MRI (submitted).

Choi J-A, Gold GE. MR Imaging of Articular Cartilage Physiology. Magn Reson Imaging Clin N Am (in-press).

Barral JK, Santos JM, Damrose EJ, Fischbein NJ, Nishimura DG. Real-Time Motion Correction for High-Resolution Larynx Imaging. Magn Reson Med (accepted).

Aksoy M, Forman C, Straka M, Skare S, Holdsworth S, Hornegger J, Bammer R. Real-time Optical Motion Correction for Diffusion Tensor Imaging. Magn Reson Med (in press).

Nnewihe A, Grafendorfer T, Daniel B, Calderon P, Alley M, Hargreaves B. Custom 16-Channel Bilateral Breast Coil for Multidirectional Parallel Imaging Acceleration. Magn Reson Med (in press).

Vasanawala SS, Yu H, Shimakawa A, Jeng M, Brittain JH. Estimation of Liver T2* in Transfusion Related Iron. Overload Patients with Weighted Least Squares T2* IDEAL. Magn Reson Med (in press).

Aksoy M, Forman C, Straka M, Çukur T, Hornegger J, Bammer R. Hybrid Prospective and Retrospective Head Motion Correction. Magn Reson Med (in press).

Schmiedeskamp HH, Straka M, Bammer R. Compensation of Slice Profile Mismatch in Combined Spin- And Gradient-Echo EPI Pulse Sequences. Magn Reson Med (in press).

Josan S, Spielman D, Yen Y-F, Hurd R, Pfefferbaum A, Mayer D. Dynamic Volumetric Imaging of Ethanol Metabolism in Rat Liver with Hyperpolarized [1-13C]-Pyruvate. Magn Reson Med (submitted).

Sung K, Hargreaves BA. High-Frequency Subband Compressed Sensing MRI with Quadruplet Sampling. Magn Reson Med (submitted).

Christen T, Zaharchuk G, Pannetier N, Serduc R, Joudiou N, Vial JC, Remy C, Barbier EL. Quantitative MR Estimates of Blood Oxygenation based on T2*: A Numerical Study of the Impact of Model Assumptions. Magn Reson Med (submitted).

Balchandani P, Khalighi MM, Glover G, Pauly J, Spielman D. Self-Refocused Adiabatic Pulse for Spin Echo Imaging at 7T. Magn Reson Med (submitted).

Staroswiecki E, Granlund K, Alley M, Gold GE, Hargreaves BA. Simultaneous Estimation of T2 and ADC in Human Articular Cartilage In Vivo with a Modified 3D DESS Sequence at 3T. Magn Reson Med (submitted).

Quist B, Hargreaves B, Cukur T, Morrell G, Gold G, Banberter N. Simultaneous Fat Suppression and Band Reduction with Large-Angle Multiple-Acquisition bSSFP. Magn Reson Med (submitted).

Schmiedeskamp H, Straka M, Newbould RD, Andre JB, Zaharchuk G, Bammer R. Combined Spin- and Gradient-Echo Perfusion-Weighted Imaging. Magn Reson Med (submitted).

Kopeinigg D, Aksoy M, Forman C, Straka M, Hornegger J, Bammer R. Real-time Optical Motion Correction for 3D Time-of-Flight (TOF) Angiograms using a MR Compatible Mono-Vision Camera System with an Extended Field of View Marker. Magn Reson Med (submitted).

Cui J, Pratx G, Prevrhal S, Shao L, Levin CS. Fully 3-D List-Mode Time-of-Flight PET Imaging Reconstruction on GPU using CUDA. Med Phys (submitted).

Forman C, Aksoy M, Hornegger J, Bammer R. Self-Encoded Marker for Optical Prospective Head Motion Correction in MRI. Medical Image Analysis (in-press).

Constantin D, Fahrig R, Keall P. A Study of the Effect of In-line and Perpendicular Magnetic Fields on Beam Characteristics of Medical Linear Accelerator Electron Guns. Medical Physics (accepted).

Peng H, Olcott PD, Spanoudaki V, Levin CS. Can Large-Area Avalanche Photodiodes be used for a PET Detector Insert for an MRI System? Medical Physics (in-press).

Holbrook AB, Ghanouni P, Santos JM, Medan Y, Butts-Pauly K. In Vivo MR Acoustic Radiation Force Imaging in the Porcine Liver. Medical Physics (in-press).

Peng H, Levin CS, Chronik BA. Simulation Study of PET Spatial Resolution and Contrast Recovery Improvement for PET/MRI Dual Modality Systems. Medical Physics (submitted).

Papers Submitted or In Press

Papers Submitted or In Press

Maier A, Wigstrom L, Hofmann H, Zhu L, Strobel N, Hornegger J, Fahrig R. Three-Dimensional Anisotropic Adaptive Filtering of Projection Data for Noise Reduction in Cone Beam CT. Medical Physics (submitted).

Pal S, Besier T, Draper C, Fredericson M, Gold GE, Beaupre G, Delp S. Vasti Activation Ratio Correlates with Delay and Maltracking in PF Pain Subjets. Medicine & Science in Sports & Exercise (submitted).

Henning TD, Khurana A, Gawande R, Tavri S, Golovko D, Sutton EJ, Horvai A, Sennino B, McDonald D, Meier R, Hapfelmeier A, Derugin N, Link TM, Daldrup-Link HE. MR Imaging of Ferumoxides Labeled Mesenchymal Stem Cells in Cartilage Defects: In Vitro and In Vivo Investigations. Molecular Imaging (in-press).

Namavari M, Chang YF, Kusler B, Yaghoubi S, Mitchell BS, Gambhir SS. A Novel Synthesis of 2'-Deoxy-2'-[(18)F]Fluoro-9-?-D: -Arabinofuranosylguanine: a Novel Agent for Imaging T-Cell Activation with PET. Mol Imaging Biol (in-press).

Koo S, Clark D, Andriacchi T, Gold GE, Quon A. A Pilot Study of 18F-Sodium Fluoride PET/CT Imaging of Healthy and Osteoarthritic Knees. Mol Imaging Biol (submitted).

Behera D, Kamaya S, Lee S-W, Graves EA, Yeomans D, Gold GE, Biswal S. Manganese-Enhanced MRI Highlights Injured Nerves in Neuropathic Pain. Molecular Pain (submitted).

Ghanouni P, Behera D, Xie J, Chen X, Biswal S. Minocycline Mitigates Macrophage Recruitment to a Peripheral Nerve Injury. Molecular Pain (submitted).

Bangerter N, Cukur T, Hargreaves BA, HuB, Quist B, Park D, Gold GE, Nishimura D. 3D Fluid-Suppressed T2-Prep Flow-Independent Peripheral Angiography using Balanced SSFP Magnetic Resonance Imaging. MRI (in-press).

Lu A, Daniel BL, Kaye E, Butts-Pauly K. MRI of Frozen Tissue Demonstrates a Phase Shift. MRM (in-press).

Zavaleta CL, Hartman KB, Miao Z, James ML, Kempen P, Thakor A, Nielsen CH, Sinclair R, Cheng Z, Gambhir SS. Preclinical Evaluation of Raman Nanoparticle Biodistribution for their Potential use in Clinical Endoscopy Imaging. Nano Letters (submitted).

Merk DR, Chin JT, Dake BA, Maegdefessel L, Miller M, Clark SJ, Burnett CE, Kimura N, Tsao PS, Blankenberg FG, Levashova Z, Spin JM, Mohr FW, Dietz HC, Robbins RC, Fischbein MP. Apoptosis and miR-29b Participate in Early Aneurysm Development in Marfan Syndrome. Nature (submitted).

Jonquet C, Whetzel P, Youn CH, Thomas DG, Baker NA, Paik DS, Twigger SN, Sarkar IN, Musen MA, Shah NH. Ontology-Based Annotation as a Web Service. Nature Biotechnology (submitted).

Blankenberg F, Perlman SL, Kinsman SL, Spicer KM, Levashova L, Kheifets V, Shrader WD, Thoolen M, Miller G, Enns GM. Brain Tc99m-HMPAO SPECT Imaging of Oxidative Stress in Children with Mitochondrial Disease Treated with a Novel Reversible Two Electron-Redox Cycling Agent. Nature Med (submitted).

Enns GM, Perlman SL, Kinsman SL, Spicer KM, Barnes A, Kheifets V, Shrader WD, Thoolen M, Blankenberg FG, Miller G. Redox Modulation Therapy with α-Tocotrienol Quinone (ATQ3) in Mitochondrial Disease. Nature Med (submitted).

Hoeft F, Gabrieli J, Whitfield-Gabrieli S, Haas B, Bammer R, Menon V, Spiegel D. Neural Basis Of Hypnotizability Revealed By Resting State Functional Connectivity. Nature Neurosci (in-press).

Iagaru A, Gambhir SS. New Methods for Imaging Tumor Angiogenesis. Nature Reviews Cancer (submitted).

Ashford J, Adamson M, Beale T, La D, Hernandez B, Noda A, Rosen A, Spielman D, Yesavage J. MRI Spectroscopy Assessment of Memantine Treatment in Mild to Moderate Alzheimer Dementia. Neurology (submitted).

Kesler SR, Sheu K, Koovakkattu D, Reiss AL. Changes in Frontal-Parietal Activation and Math Skills Perfromance following Adaptive Number Sense Training: Preliminary Results from a Pilot Study. Neuropsychological Rehabilitation (in-press).

Darsaut TE, Darsaut NM, Chang SD, Silverberg GD, Shuer LM, Tian L, Dodd RL, Do HM, Marks MP, Steinberg GK. Predictors of Clinical and Angiographic Outcome Following Surgical or Endovascular Therapy of Very Large and Giant Intracranial Aneurysms. Neurosurgery (in-press)

Darsaut TE, Guzman R, Marcellus ML, Edwards MS, Liu T, Do HM, Chang SD, Levy RP, Adler JR, Marks MP, Steinberg GK. Management of Pediatric Intracranial Arteriovenous Malformations: Experience with Multimodality Therapy. Neurosurgery (in-press)

Karamchandani J, Fischbein NJ, Gibbbs I, Harsh G, Vogel H. Papillary Endothelial Hyperplasia Mimicking Neoplasm Following Radiosurgery. Neurosurgery (in-press)

Papers Submitted or In Press

Papers Submitted or In Press

Pandey P, Steinberg GK, Dodd RL, Do HM, Marks MP. A Simplified Method for Administration of Intra-Arterial Nicardipine for Vasospasm using Guide Catheter Infusion. Neurosurgery (submitted).

Jacobs KE, Behera D, Rosenberg R, Gold GE, Moseley M, Yeomans D, Biswal S. Oral Manganese as an MRI Contrast Agent for the Detection of Nociceptive Activity. NMR in Biomed (accepted).

Xu T, Mayer D, Gu M, Yen YF, Josan S, Johansson E, Tropp J, Hurd RE, Spielman DM. Quantitation of In-Vivo Metabolic Kinetics using Dynamic 13C Magnetic Resonance Spectroscopic Imaging. NMR in Biomed (submitted).

Hunter DJ, Arden N, Conaghan PG, Eckstein F, Gold GE, Grainger A, Guermazi A, Harvey W, Jones G, le Graverand MPH, Laredo JD, Lo G, Losina E, Mosher TJ, Roemer F, Zhang W. Definition of Osteoarthritis on MRI: Results of a Delphi Exercise. Osteoarthritis Cartilage (submitted).

Shapiro L, Gold GE. MRI of Weight-Bearing and Movement. Osteoarthritis Cartilage (submitted).

Carroll IR, Barad M, Fischbein NJ, Mackey S. Human Response to Intrathecal Botulinum Toxin. Pain Med (in-press).

Williams JP, Vasanawala SS. Active Gastrointestinal Hemorrhage Identification by Blood Pool Contrast-Enhanced Magnetic Resonance Angiography. Pediatr Radiol (in-press).

Castaneda R, Boddington S, Wendland M, Henning TD, Mandrussow L, Daldrup-Link HE. MR Imaging of Human Embryonic Stem Cell Derived Cardiomyocytes: Should Iron Oxide Nanoparticle Labeling occur Before or After Differentiation? Pediatr Radiol (in-press).

Tamrazi A, Vasanawala SS. Pediatric Functional Hepatobiliary MR Imaging with GD-EOB-DTPA: Initial Experience. Pediatr Radiol (in-press).

Newman B, Vasanawala SS. Point Counterpoint – Dose Related Issues in Cardiac CT Imaging. Pediatr Radiol (in-press).

Newman B. Ultrasound Body Applications in Children. Pediatr Radiol (in-press).

Vasanawala SS, Chan FP, Newman B, Alley MT. Combined Respiratory and Cardiac Triggered Blood Pool Contrast Agent Enhanced Pediatric Cardiovascular MRI. Pediatr Radiol (submitted).

Lee ES, Loe IM, Yeatman JD, Bammer R, Feldman HM. White Matter Characteristics Associated with Attention, Anxiety, and Executive Function in Preterm and Full-Term Children. Pediatrics (submitted).

Newman B, John S, Goske M, Hernandez-Schulman M. Pause and Pulse: Radiation Dose in Pediatric Fluoroscopy – What the Pediatrician Needs to Know. Pediatrics in Review (in-press).

Fieselmann A, Dennerlein F, Deuerling-Zheng Y, Boese J, Fahrig R, Hornegger J. A Model for Filtered Backprojection Reconstruction Artifacts due to Time-Varying Attenuation Values in Perfusion C-arm CT. Phys Med Biol (in-press).

Pratx G, Levin CS. Online Detector Response Calculations for High-Resolution PET Image Reconstruction. Phys Med Biol (in-press).

Vandenbroucke A, McLaughlin TJ, Levin CS. Performance Evaluation of a Large Area Position Sensitive Avalance Photodiode Coupled to an LSO Crystal as a Function of Temperature and Bias Voltage. Phys Med Biol (submitted).

Rubin DL. Measuring and Improving Quality in Radiology: Meeting the Challenge with Informatics. Radiographics (in-press).

Kamaya A, Federle M, Desser TS. Fat Necrosis: Imaging Spectrum. Radiographics (submitted).

Eslamy H, Newman B. Pneumonia in Normal and Immunocompromised Children: An Overview and Update. Radiol Clin North Am (in-press).

Wang DS, Pysz MA, Panje CM, Paulmurugan R, Gambhir SS, Schneider M, Willmann JK. Cationic Microbubbles Enhance Ultrasound-Mediated Gene Delivery in a Mouse Tumor Model. Radiology (accepted).

Deshpande N, Lutz AM, Ren Y, Foygel K, Tran L, Schneider M, Pasricha PJ, Willmann JK. Quantification and Monitoring Inflammation in Colitis by Targeted Contrast-Enhanced Ultrasound Imaging. Radiology (accepted).

Wang DV, Pysz MA, Panje C, Paulmurugan R, Rosenberg J, Gambhir SS, Schneider M, Willmann JW. Enhanced Ultrasound-Mediated Gene Delivery Using Cationic Microbubbles. Radiology (accepted).

Lutz AM, Willmann JK, Drescher C, Ray P, Cochran F, Urban N, Gambhir SS. Early Diagnosis of Ovarian Cancer: Is a Solution in Sight? Radiology (in-press).

Papers Submitted or In Press

Papers Submitted or In Press

Kircher MF, Willmann JK. Molecular Body Imaging: MRI, CT and US – Applications. Radiology (in-press).

Kircher MF, Willmann JK. Molecular Body Imaging: MRI, CT and US – Techniques. Radiology (in-press).

Larson PE, Gold GE. Science to Practice: Can Inflammatory Arthritis be Monitored by MRI with Injected Hyperpolarized 13C-Pyruvate? Radiology (in-press).

Bu L, Chen K, Cheng Z, Shen B, Chen X. Assessment and Comparison of Magnetic Nanoparticles as MRI Contrast Agents in a Rodent Model of Human Hepaocellular Carcinoma. Radiology (submitted).

Sigg D, Levin CS, Quon A. Axial Sampling Error in CT-Based Partial Volume Correction of SUV Measurements. Radiology (submitted).

Hyun D, Kim SH, Im SA, Han SW, Lee JY, Willmann JK, Eo JS, Paeng JC, Han JK, Choi BI. Comparison Between Whole-Tumor Perfusion CT and 18F-FDG PET-CT in Liver Metastases as an Early Response Predictor after Chemotherapy: Preliminary Study. Radiology (submitted).

Win SS, Do HM. Cost-Effectiveness of Balloon Kyphoplasty versus Vertebroplasty in Symptomatic Vertebral Compression Fractures in the U.S.. Radiology (submitted).

Gawande R, Khurana A, Messing S, Zhang D, Castaneda R, Goldsby R, Hawkins R, Daldrup-Link HE. Differentiation of Normal Thymus from Anterior Mediastinal Lymphoma and Lymphoma Recurrence on Pediatric PET-CT. Radiology (submitted).

Nakatamari H, Ueda T, Ishioka F, Raman B, Suito H, Kurihara K, Paik DS, Rubin GD, Gleischmann D, Dake MD, Ito H, Sze DY. Discriminant Analysis of Native Thoracic Aortic Curvature: Risk Prediction for Endoleak Formation Following Thoracic Endovascular Aortic Repair. Radiology (submitted).

Meer A, Basu P, Baker L, Atlas SW. Exposure to Ionizing Radiation and Estimate of Secondary Cancers in the Era of High Speed CT Scanning. Radiology (submitted).

Vasanawala SS, Lai P, Alley MT, Gold GE, Lustig M. Improved Volumetric Knee MRI via Compressed Sensing. Radiology (submitted).

Hsaio A, Alley M, Massaband P, Alley M, Herfkens R, Chan FP, Vasanawala SS. Quantitative Flow Assessment of Congenital Heart Disease with Time-Resolved Volumetric Phase-Contrast MRI. Radiology (submitted).

Andre J, Zaharchuk G, Fischbein NJ, Augustin M, Albers GW, Bammer R. Yield of Parallel Imaging and Acquisition Matrix Size in Diffusion-Weighted MRI of Stroke. Radiology (submitted).

Lanza GM, Farahani K, Baker JR, Chang E, Cheng Z, Grodzinski P, Ferrara K, Hynynen K, Kelloff G, Lee YE, Patri A, Sept D, Schnitzer JE, Wood B, Zhang M, Zheng G, Moonen C. Image Guided Drug Delivery: Unleashing the Power of Imaging in the Fight Against Cancer. Sci Transl Med (submitted).

Tran PT, Bendapudi PK, Lin HJ, Choi P, Koh S, Chen J, Horng G, Hughes NP, Schwartz LH, Miller VA, Kawashima T, Kitamura T, Paik DS, Felsher DW. Survival and Death Signals can be used to Predict when Oncogene Inactivation will Elicit Oncogene Addiction. Sci Transl Med (submitted).

Thakor AS, Luong R, Paulmurugan R, Lin FI, Kempin P, Zaveleta C, Chu P, Massoud TF, Sinclair R, Gambhir SS. The Fate and Toxicity of Raman Active Silica-Gold-Nanoparticles in Mice. Sci Transl Med (in-press).

Henning TD, Do T, Sutton EJ, Baehner F, Horvai A, Sennino B, McDonald D, Meier R, Misselwitz B, Link TM, Daldrup-Link HE. MR Imaging Features of Gadofluorine labeled Matrix associated Stem Cell Implants in Cartilage Defects. Skeletal Radiology (submitted).

Li P, Fischbein NJ, Do HM, Blevins NH. Dural Arteriovenous Fistula Following Translabyrinthine Resection of Cerebellopontine Angle Tumors: Report of Two Cases. Skull Base (in-press).

Kim B, Dhatt H, Rosenberg J, Mittra E, Do BH, Graves EA, Biswal S. A Difference in the Pattern of 18F-FDG Uptake within the Spinal Canal in Low Back Pain Patients. Spine (submitted).

Purushotham A, Campbell B, Straka M, Mlynash M, Olivot J-M, Bammer R, Kemp SM, Albers GW, Lansberg MG. Apparent Diffusion Coefficient Threshold for Delineation of Ischemic Core. Stroke (in-press).

Zaharchuk G, Straka M, Marks MP, Albers GW, Moseley ME, Bammer R. Arterial Spin Labeling MRI Can Identify Collateral Perfusion in Patients with Moyamoya Disease. Stroke (in-press).

Christensen S, Campbell BC, Perez de la Ossa N, Lansberg M, Straka M, De Silva DA, Nagakane Y, Ogata T, Mlynash M, Olivot J-M, Desmond P, Bammer R, Albers GW, Donnan GA, Davis SM. Optimal Perfusion Thresholds for Prediction of Tissue Destined for Infarction in the Combined EPITHET-DEFUSE Dataset. Stroke (in-press).

Papers Submitted or In Press

Mlynash M, Lansberg MG, De Silva DA, Lee J, Christensen S, Straka M, Campbell BCV, Olivot J-M, Bammer R, Desmond P, Donnan GA, Davis SM, Albers GW. Refining the Definition of the Malignant Profile Insights From the DEFUSE-EPITHET Pooled Data Set. Stroke (in-press).

Ogata T, Christensen S, Nagakane Y, Ma H, Campbell BCV, Churilov L, Lansberg MG, Straka M, De Silva DA, Mlynash M, Olivot JM, Desmond PM, Bammer R, Albers GW, Davis SM, Donnan GA. The Effects of Alteplase 3-6 hrs after Stroke in the EPITHET- DEFUSE Combined Dataset. Stroke (in-press).

Lee J, Lansberg MG, Mlynash M, De Silva DA, Christensen S, Straka M, Campbell BCV, Olivot JM, Desmond P, Bammer R, Donnan GA, Davis SM, Albers GW. Validation of the Malignant Profile in the DEFUSE-EPITHET Pooled Database. Stroke (in-press).

De Silva DA, Churilov L, Olivot JM, Christensen S, Lansberg MG, Mlynash M, Campbell BCV, Desmond P, Straka M, Bammer R, Albers GW, Donnan GA. Greater Effect of Stroke Thrombolysis in the Presence of Arterial Obstruction. Stroke (in-press).

Saad WE, Sze DY. Variations of BRTO: Balloon-Occluded Antegrade Transvenous Obliteration (BATO) and Alternative/Adjunctive Routes for BRTO. Tech Vasc Interv Radiol (in-press).

Kim MJJ, Do Y, Wapnir IL, Daniel BL, Ikeda DM. MRI Enhancement Correlates with High Grade Desmoid Tumor of Breast. The Breast Journal (in-press).

Zeineh M, Holdsworth SJ, Bammer R. Diffusion Tensor MRI of the Hippocampus. Topics of MRI (in-press).

Van AT, Granziera C, Bammer R. Q-space, DSI, and HARDI MRI. Topics of MRI (in-press).

Andre J, Zaharchuk G, Fischbein NJ, Bammer R. Diffusion-Weighted MRI of the Spinal Cord. Topics of MRI (submitted).

Bammer R. The Role of Diffusion Tensor MRI in Forensic Medicine. Topics of MRI (submitted).

Charalel RA, Shin LK, Jeffrey RB. Complicated Cholecystitis: The Complementary Roles of Sonography and CT. Ultrasound Q (in-press).

Chan L, Shin LK, Pai RK, Jeffrey RB. Pathologic Continuum of Acute Appendicitis: Sonographic Findings and Clinical Management Implications. Ultrasound Q (in-press).

Shin DS, Jeffrey RB, Desser TS. Pearls and Pitfalls in Hepatic Ultrasonography. Ultrasound Q (in-press).

Thomas DG, Klaessig F, harper SL, Fritts M, Hoover MD, Gaheen S, Stokes TH, Reznik-Zellen R, Freund Et, Klemm JD, Paik DS, Baker NA. Informatics and Standards for Nanomedicine Technology. WIRES Nanomedicine and Nanobiotechnology (in-press).

Funding

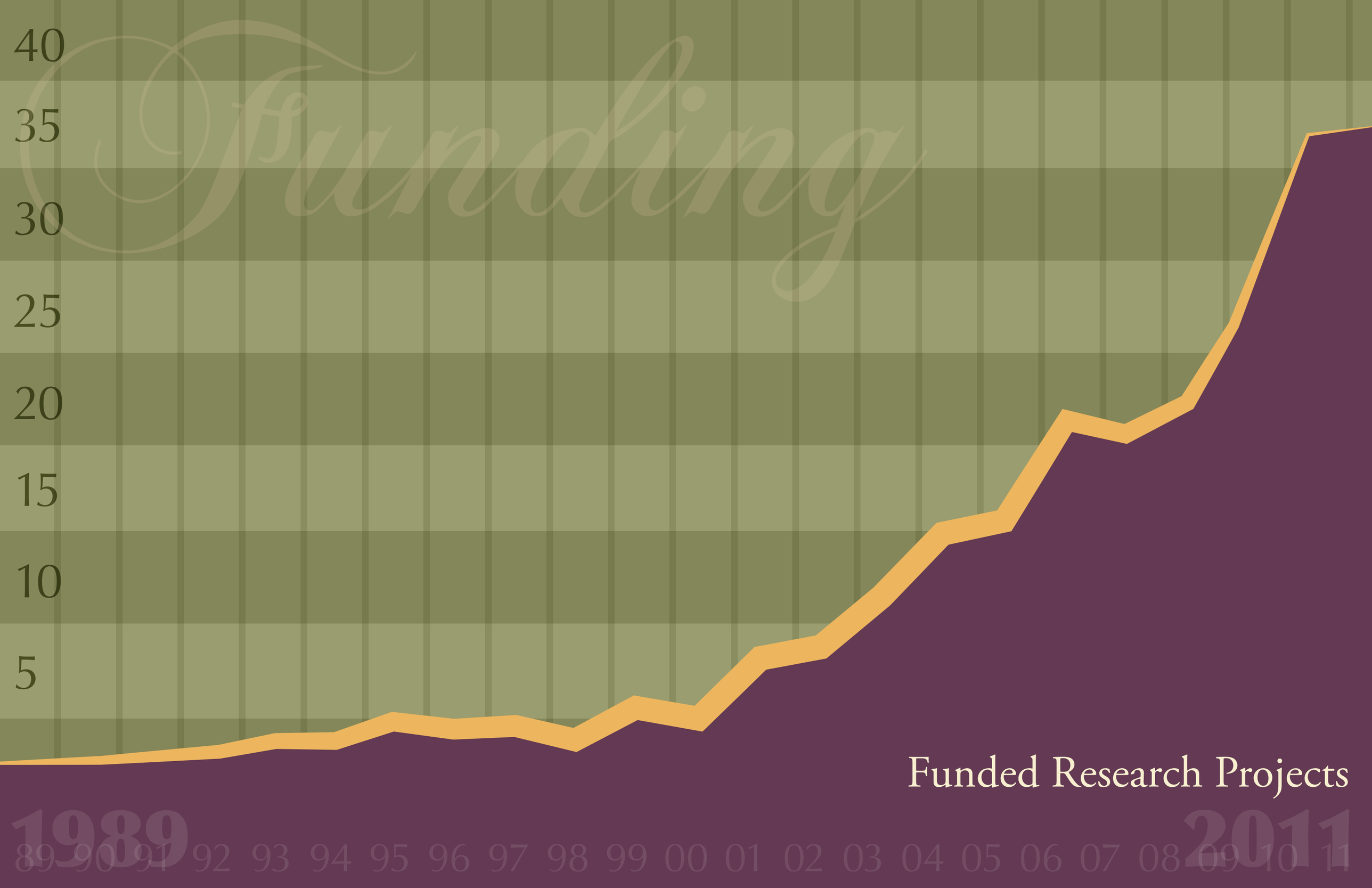
40
35
30
25
20
15
10
5
Funded Research Projects
1989
2011
89 90 91 92 93 94 95 96 97 98 99 00 01 02 03 04 05 06 07 08 09 10 11

NIH Supported Research

For additional awards, see Awards and Honors pages 22 - 25
* New for 2011
**Longstanding project renewed for another 4-5 years

PI	Type	Title
Priti Balchandani, PhD	K99	*High resolution magnetic resonance imaging and spectroscopy of epilepsy at 7T
Roland Bammer, PhD	R01	Novel Acquisition Methods for Diffusion MRI
Roland Bammer, PhD	R01	*Real-Time MRI Motion Correction System
Roland Bammer, PhD	R01	Short Axis EPI for Diffusion Tensor MRI at High Field
Roland Bammer, PhD	R01	Improving SENSE MRI for Spiral and Echo-planar Imaging in Stroke
Kim Butts Pauly, PhD	R01	MR-Image Guided Focused Ultrasound for Treatment of Liver and Renal Cancer
Kim Butts Pauly, PhD	R21	MRI Methods for Guiding Focused Ultrasound in the Brain
Catie Chang, PhD	F31	Temporal Characteristics of Intrinsic Brain Networks using fMRI
Zhen Cheng, PhD	R01	Radiolabeled RGD Peptides for Breast Cancer Imaging and Therapy
Zhen Cheng, PhD	R01	VEGFR-2 Targeted Imaging
Heike Daldrup Link, MD	R21	*Imaging of Tumor-Associated Macrophages with Ferumoxytol
Heike Daldrup Link, MD	R21	Novel Imaging Approach to Monitor Chondrogenic Differentiation of iPS Cells
Heike Daldrup Link, MD	R01	Monitoring of Stem Cell Engraftment in Arthritic Joints with MR Imaging
Heike Daldrup Link, MD	R01-MPI	Improved Drug Delivery to Tumors Using Novel Tissue Perfusion Approaches
Bruce Daniel, MD	R21	*High Resolution 3D Diffusion-weighted Breast MRI
Rebecca Fahrig, PhD	R01	C-Arm CT for Guidance of Cardiac Interventions
Rebecca Fahrig, PhD	R01	MR-Compatible X-ray Tube
Rebecca Fahrig, PhD	S10	*Axiom zeego shared instrument grant
Rebecca Fahrig, PhD	R01	Dual KV/MV Imaging for Metal Artifact Reduction
Rebecca Fahrig, PhD	R21	Ultrafast Tomosynthesis for Transbronchial Biopsy Guidance
Sam Gambhir, MD, PhD	U54	Center for Cancer Nanotechnology Excellence and Translation (CCNE-T)
Sam Gambhir, MD, PhD	P50	In Vivo Cellular and Molecular Imaging Center @ Stanford
Sam Gambhir, MD, PhD	U01	*New Tools for Prostate Cancer Detection and Prognostication
Sam Gambhir, MD, PhD	R25	**Stanford Molecular Imaging Scholars (SMIS)
Sam Gambhir, MD, PhD	R01	Reporter Imaging of Protein-Protein Interactions
Sam Gambhir, MD, PhD	R01	Imaging Cytolytic T Cells in Cancer Patients Using PET Reporter Genes/Reporter Probes
Sam Gambhir, MD, PhD	U54	Center of Cancer Nanotechnology Excellence Focused on Therapy Response (CCNE-TR)
Arun Ganguly, PhD	K99	High Performance CMOS Based X-ray Detector for C-AM CT Imaging
Gary M. Glazer, MD	T32	Advanced Techniques for Cancer Imaging and Detection
Gary Glover, PhD	P41	Center for Advanced Magnet Resonance Technology at Stanford
Garry Gold, MD	R01	MRI for Early Detection of Osteoarthritis

For additional awards, see Awards and Honors pages 22 - 25
* New for 2011
**Longstanding project renewed for another 4-5 years

PI	Type	Title
Brian Hargreaves, PhD	R01	High-Resolution Whole-Breast MRI at 3.0T
Brian Hargreaves, PhD	R21	Magnetic Resonance Imaging Near Metallic Implants
Craig Levin, PhD	R01	Enhancing Molecular Cancer Imaging with Cadmium Zinc Telluride PET
Craig Levin, PhD	R01	*Preclinical Translation of New Scintillation Light Detection Concepts for PET
Craig Levin, PhD	R01	Advanced PET System Dedicated to Breast Cancer Imaging
Michael Moseley, PhD	R01	Microvascular Measures of Perfusion in Stroke Recanalization
Sandy Napel, PhD	R01	Improving Radiologist Detection of Lung Nodules with CAD
Norbert Pelc, ScD	R01	Inverse Geometry CT for Dose-efficient Volumetric Imaging
Norbert Pelc, ScD	T32	*Predoctoral Training in Biomedical Imaging at Stanford University
Sylvia Plevritis, PhD	U01	Breast Cancer Trend Analysis Using Stochastic Simulation
Sylvia Plevritis, PhD	U54	Modeling the Role of Differentiation in Cancer Progression
Andrew Quon, MD	R01	*FLT-PET/CT for Therapy Monitoring of DLBCL
Jianghong Rao, PhD	R01	QD-BRET Nanosensors for Protease Detection and Imaging
Jianghong Rao, PhD	R01-MPI	Actively Contraolled and Targeted Single-Molecule Probes for Cellular Imaging
Viola Rieke, PhD	K99	MRI-guided Cardiac Focused Ultrasound Ablation
Daniel Rubin, MD, MS	U01	Computerized Quantitative Imaging Assessment of Tumor Burden
Brian Rutt, PhD	S10	*Next Generation 7T MRI Platform Upgrade with Parallel Transmit Capabilities
Bryan Smith, PhD	K99	*How do Nanoparticles Target Cancer? An In Vivo Experimental/Mathematical Study
Graham Sommer, MD	R21	MRI-Guided Ultrasonic Ablation of Pancreatic Cancer
Graham Sommer, MD	R01	Precise MRI-directed Sonic Ablation of Prostate Cancer
Daniel Spielman, PhD	R01	Metabolic Imaging of the Cardioprotective Effects of Alcohol and ALDH2 Activators
Daniel Spielman, PhD	R01	1H MRSI of the Human Brain at 7T
Shreyas Vasanawala, MD, PhD	R01	Rapid Robust Pediatric MRI
Juergen Willmann, MD	R21	Early Detection of Pancreatic Cancer with Targeted Contrast-enhanced Ultrasound
Joseph Wu, MD, PhD	DP2	09: Inducing Pluripotency with MiRNAs: New Paradigm Shift in Cell Reprogramming
Joseph Wu, MD, PhD	R21	Biological Insights into Dynamics of Stem Cell Differentiation and Misbehavior
Joseph Wu, MD, PhD	RC1	*Molecular and Cellular Phenotype of Aging and ips Cells
Joseph Wu, MD, PhD	R33	Nanostructuring and Molecular Imaging of Engineered Cardiovascular Tissues
Joseph Wu, MD, PhD	RC	Molecular Imaging of Resident Cardiac Stem Cells
Joseph Wu, MD, PhD	R01	Molecular Imaging of Targeted Cardiac Gene Therapy
Joseph Wu, MD, PhD	R01	Integrated Strategies for Novel Treatment of Myocardial Ischemia

NIH Supported Research

For additional awards, see Awards and Honors pages 22 - 25
* New for 2011
**Longstanding project renewed for another 4-5 years

PI	Type	Title
Joseph Wu, MD, PhD	R01	Re-Education of the Immune System for hES Cell Tolerance
Joseph Wu, MD, PhD	R01	Molecular Imaging of Cardiac Stem Cell Therapy
Greg Zaharchuk, MD, PhD	R01	Quantifying Collateral Perfusion in Cerebrovascular Disease

NIH Collaborations (Sub-Contracts)

PI	Type	Title
Zhen Cheng, PhD	Ocean Nanotech	Iron Oxide Nanoparticle Probes for Target Specific MR Molecular Imaging
Heike Daldrup Link, MD	UCSF	Improved Drug Delivery to Tumors using Novel Tissue Perfusion Approaches
Sam Gambhir, MD, PhD	Fred Hutch	Ovarian Cancer Early Detection Using Microbubble Contrast Enhanced Ultrasound (CEUS) Targeting Tumor Associated Angiogenesis
Sam Gambhir, MD, PhD	USC	Multi-Scale Complex Systems Transdisciplinary Analysis of Response to Therapy (MC-START)
Sam Gambhir, MD, PhD	UCLA	Multimodel Qdot Probes for Bioimaging of Cells and Tumors in Small Animals
Gary Glover, PhD	UC Irvine	Functional Imaging Research in Schizophrenia Testbed
Garry Gold, MD	UCSF	Data Coordinating Center for Osteoarthritis Initiative
Rusty Hofmann, MD	Wash U	Pharmacomechanical Catheter-Directed Thrombolysis for Acute DVT-Attract Trial
Rusty Hofmann, MD	Wash U	ATTRACT: Industry Portion
Sylvia Plevritis, PhD	MGH	*Comparative Modeling of Lung Cancer Control Policies
Sylvia Plevritis, PhD	Georgetown	*Comparative Modeling: Informing Breast Cancer Control Practice & Policy
Daniel Rubin, MD, MS	ACR	American College of Radiology Imaging Network (ACRIN) Committee Agreement Rubin
Daniel Rubin, MD, MS	Emory Univ	In Silico Research Center
Daniel Rubin, MD, MS	Northwestern	Annotations and Image Markup Project - Phase I and II
Daniel Rubin, MD, MS	RSNA	Enriching the RadLex Ontology to Enable Biomedical Imaging Research in Neuroimaging
Daniel Rubin, MD, MS	U Pittsburgh	The ODIE Toolkit - Software for Information Extraction and Biomedical Ontology Development
Daniel Rubin, MD, MS	NCI	Ontology-based Integration of Human Studies Data
Daniel Rubin, MD, MS	Brigham & Women's	Neuroimaging Analysis Center (NAC)
Daniel Spielman, PhD	SRI	Dynamic Metabolic Imaging of Hyperpolarized Substrates
Joseph Wu, MD, PhD	SDSU	Engineering Cardiac Progenitor Cells to Enhance Myocardial Regeneration

California Supported Research

PI	Type	Title
Rachel Bitton, PhD	UCOP	MRI Guided Focused Ultrasound in Breast Cancer Treatment
Frances Lau, PhD	UCOP	Electronics for High Resolution Breast-dedicated PET
Brian Rutt, PhD	CIRM	*Development of single cell MRI Using Genetically-Encoded Iron-based reporters

Professional Society & Foundation Supported Research

PI	Type	Title
Zhen Cheng, PhD	Melanoma Rsch	18F Labeled Benzamides for Pre-Clinical PET Imaging of Melanoma Metastases
Sam Gambhir, MD, PhD	Doris Duke	Molecular Imaging of Cancer with a Voltage Sensor
Sam Gambhir, MD, PhD	Ben & Catherine Ivy Fd	*Next Generation Neuro-Oncological Imaging Strategies
Sam Gambhir, MD, PhD	Ben & Catherine Ivy Fd	18F PPRGD2 PET/CT and MRI Evaluation of Response to Anti-Angiogenesis Therapy in Recurrent Glioblastoma Multiforme (GBM)
Sam Gambhir, MD, PhD	Lung Cancer Rsch Fdn	*Differential Gene Expressions for FDG Avid Normal Tissue and Tumors
Sam Gambhir, MD, PhD	AMI	Study Drug: Sodium Fluoride F18 Injection
Sam Gambhir, MD, PhD	Canary Fd	Center of Excellence in Early Detection of Cancer
Rakhee Gawande, PhD	SPR	*Whole Body Diffusion-weighted MR Scans for Cancer Staging in Pediatric Patients: A Radiation Free Alternative to FDG-PET
Garry Gold, MD	Arthritis Fd	*Sodium MRI of Post-traumatic Arthritis
Benjamin Hackel, PhD	ACS	Novel High Affinity Protein Scaffolds for Molecular Imaging of Tumors
Shijun Hu, PhD	AHA	Transplantation and Imaging of Novel Cardiac Stem Cell Therapy
Aya Kamaya, MD	Society of Uroradiology	*Photoacoustic Imaging of Bladder Cancer
Aya Kamaya, MD	Society of Gastrointestinal Radiologists	*Prognostic Value of Early Perfusion CT changes in colorectal liver metastases
Jianghong Rao, PhD	Gates Fdn - Texas A&M	Development of Fluorgenic Probes for In Vivo Imaging of Tuberculosis
Daniel Rubin, MD, MS	SIIM	Tool Support for Radiologist-Oncologist Workflow in Using Quantitative Methods to Assess Disease Response
Lewis Shin, MD	RSNA	RSNA Research Seed Grant
Daniel Sze, MD, PhD	Cook Fd	The Zilver PTX Drug Eluding Vascular Stent in the Above the Knee Femoralpopliteal Artery
Ruud Vinke, PhD	Netherlands Rsch Org	*A Novel Time-of-Flight Positron Emission Tomography System Based on Monolithic Scintillation Detectors
Joseph Wu, MD, PhD	BWF	Molecular and Cellular Mechanisms of Cardiac Regeneration
Joseph Wu, MD, PhD	Ed Mallinckrodt Fd	Innovative Approach for Reprogramming Stem Cells for Regenerative Medicine
Greg Zaharchuk, MD, PhD	NERF	Optimizing Arterial Spin Label MRI for the Visualization of Collateral Flow in Moyamoya Disease
Keren Ziv, PhD	Life Sciences Rsch Fdn	Non-invasive and Real-time Monitoring of Stem Cells Using Photoacoustic Molecular Imaging in Living Mice

Other Government Supported Research

For additional awards, see Awards and Honors pages 22 - 25
* New for 2011
**Longstanding project renewed for another 4-5 years

PI	Type	Title
Zhen Cheng, PhD	DOD	Mesenchymal Stem Cell as Targeted-delivery Vehicle in Breast Cancer
Zhen Cheng, PhD	DOD	Peptoid-based PET Probes for Prostate Cancer Imaging
Craig Levin, PhD	DOE	*New Strategies for 0.5mm Resolution/High Sensitivity Multi-radionuclide Imaging
Jianghong Rao, PhD	DOD	Enzyme-triggered Polymerization: A New Platform for Breast Cancer Imaging
Daniel Spielman, PhD	DOA	*In Vivo Imaging of Branched Chain Amino Acid Metabolism in Prostate Cancer
Arne Vandenbroucke, PhD	DOD	Commissioning and Characterizing a Dedicated High Resolution Breast PET Camera
Adam de la Zerda, PhD	DOD	Early Assessment of Breast Cancer Therapy Responses Using Photoacoustic Molecular Imaging

Industry Supported Research

PI	Type	Title
Rebecca Fahrig, PhD	Siemens	Pilot Study: A Pancreatic Model for Drug Discovery
Rebecca Fahrig, PhD	Siemens	Cardiac Imaging using C-arm CT: EP registration and perfusion
Rebecca Fahrig, PhD	Siemens	Perfusion Imaging using C-arm CG: Brain and Liver
Sam Gambhir, MD, PhD	Schering AG	Collaborative Research Agreement: Project 1: Tumor Lymphangiogenesis Imaging, Project 2: PET Imaging of Breast Cancer using Fructose Analogues
Sam Gambhir, MD, PhD	Bayer	*Open-label Study for an Exploration of Tumor Accumulation and Safety and Tolerability of the F-labeled PET/CT (Positron Emission Tomography) Tracer BAY 94-9392 Following a Single Intravenous Administration of 300 MBq
Sam Gambhir, MD, PhD	Bayer	Contract Manufacturing Agreement
Sam Gambhir, MD, PhD	Agilent	*Magnetic Nanoparticle Platform for Quantitative Targeted Proteomics
Gary M. Glazer, MD	GE	GE PACS System
Gary M. Glazer, MD	GEMS	Destination Digital Agreement
Garry Gold, MD	GEC	Advanced MR Applications Development
Rusty Hofmann, MD	Pfizer	A Safety and Efficacy Trial Evaluating the Use of Apixaban for The Extended Treatment of Deep Vein Thrombosis and Pulmonary Embolism
Rusty Hofmann, MD	WL Gore	*Evaluation of GORE VIABAHN Endoprosthesis with Heparin Bioactive Surface for the Treatment of Venous Occlusions and Stenoses
Rusty Hofmann, MD	Pfizer	A Safety and Efficacy Trial Evaluating the Use of Apixaban in the Treatment of Symptomatic Deep Vein Thrombosis and Pulmonary Embolism
David Hovsepian, MD	InSightec	*A Pivotal Study to Evaluate the Effectiveness and Safety of ExAblate Treatment of Metastatic Bone Tumors for the Palliation of Pain in patients who are not candidates for radiation therapy
Debra Ikeda, MD	ART INC	SSC-311 Adjunctive Efficacy Study of the SoftScan Optical Breast Imaging System
Nishita Kothary, MD	Siemens	Advanced Applications in Interventions Radiology Addendum ID: SUMC-2010-AX-01
Craig Levin, PhD	Philips	GPU-based 3-D List Mode OSEM for ToF PET

Industry Supported Research

For additional awards, see Awards and Honors pages 22 - 25
* New for 2011
**Longstanding project renewed for another 4-5 years

PI	Type	Title
Michael Marks, MD	ev3 Neurovascular	SWIFT-solitaire FR with the intention for thrombectomy study
Michael Marks, MD	Chestnut Med Tech	*Compassionate Use of the Pipeline Stent for Aneurysm Treatment
Norbert Pelc, ScD	GEMS	Advanced Computed Tomography (CT) Systems and Algorithms
Andrew Quon, MD	NCCN	Evaluating Sunitinib Therapy in Renal Cell Carcinoma
Virginia Spanoudaki, PhD	Axa Group	1mm Resolution Position Emission Tomography for Enhanced Molecular Breast Cancer Imaging
Daniel Sze, MD, PhD	WL Gore	Evaluation of the GORE TAG Thoracic Endoprosthesis - 45 mm for the Primary Treatment of Aneurysm of the Descending Thoracic Aorta
Daniel Sze, MD, PhD	WL Gore	An Evaluation of the GORE Conformable TAG Thoracic Endoprosthesis for the Primary Treatment of Aneurysm of the Descending Thoracic Aorta
Daniel Sze, MD, PhD	WL Gore	Evaluation of the GORE TAG Thoracic Endoprosthesis for the Treatment of Complex Pathology of the Descending Thoracic Aorta
Daniel Sze, MD, PhD	WL Gore	Evaluation of the GORE TAG Thoracic Endoprosthesis for Treatment of Descending Thoracic Aneurysms
Juergen Willmann, MD	BRACCO	Characterization of Focal Liver Lesions with Sonovue-Enhanced Ultrasound Imaging: A Phase III, Intrapatient Comparative Study vs Unenhanced Ultrasound Imaging Using Histology or Combined Imaging/Clinical Data as Truth

CBIS Seed Funding

The mission of the Center for Biomedical Imaging at Stanford (CBIS) is to facilitate the clinical, research, and educational missions of Stanford within the imaging community. Major events supported by CBIS include the annual campus-wide Symposium, mini symposia, seminars, and the Seed Grant Program. New programs in 2011 include the "Q&A at the Scan Centers" program, the CBIS Report, an electronic newsletter with each issue presenting a CBIS faculty member profile. This year's CBIS Seed Grant Recipients are listed here. For more information about the Seed Grant funded projects, please see: http://cbis.stanford.edu/people/2011seedgrants.html.

PI	Department	Title
Michael Lin, MD, PhD	Peds	Chemistry-based engineering of autocatalytic fluorescent proteins for whole-animal imaging in the optical window
Andrew Quon, MD	Radiology	18F-Sodium Flouride PET/CT for the pre-surgical evaluation of back pain
Colin Carpenter, PhD	Rad Onc	Tri-modality Molecular Surgical Guidance Integrated into a Laparoscope
Stephen Smith, PhD	Molecular and Cellular Physiology	New Laboratory Component of MCP 222 - Biological Light Microscopy
Dimitre Hristov, PhD	Radiation Oncology	Magnetic Resonance Imaging of Radiation-Activated Alginate Nanoparticle Drug/Sensitizer Delivery
Geoffrey Kerchner, MD, PhD	Neurology and Neurological Sciences	Microstructural Correlates of Motor Deficits in Parkinson Disease with Ultra-High Field 7-Tesla MRI
Joyce Y. Liao, MD, PhD	Ophthalmology	In Vivo Imaging of the Mouse Optic Nerve in Aging and in Experimental Anterior Ischemic Optic Neuropathy
Manjula Tamura, MD, MPH	Medicine - Nephrology	Relation between chronic kidney disease, hypertension control and brain perfusion

Collaborators Outside of Stanford

We also enjoy many collaborations with foundations, agencies, institutions, and industry for whose support we are indeed thankful. We look forward to continued success in these collaborative endeavors as well.

Academy of Molecular Imaging
Advanced Research Technologies (ART), Inc.
Agilent
American Cancer Society
American College of Radiology
American Heart Association
Angiotech
Arthritis Foundation
Axa Group
Bayer Corporation
Ben and Catherine Ivy Foundation
Biosense, Inc
Booz-Allen & Hamilton, Inc
Bracco Group
Burroughs Wellcome Fund
California Insitute for Regenerative Medicine
Canary Foundation
Chestnut Medical Technologies, Inc
Cook Foundation
Department of Defense
Department of Energy
Department of the Army
Doris Duke Foundation
Edward Mallinckrodt Jr. Foundation
ev3 Neurovascular
FeRx, Inc.
Fred Hutchinson Cancer Research Center
Gates Foundation
GE Healthcare
GE Medical Systems
Genentech
General Electric Company
InSightec
Kai Pharmaceuticals
Kitware, Inc
Life Science Research Foundation
Lucile Packard Foundation
Lung Cancer Research Foundation
Marsha Rivkin Center for Ovarian Cancer
Melanoma Research Foundation
National Comprehensive Cancer Network
National Institutes of Health
Netherlands Research Organization
Neuroradiology Educ & Rsch Foundation
Ocean NanoTech, LLC
Palo Alto Institute for Research & Education (PAIRE)
Palo Alto Veterans Administration
Pfizer Pharmaceuticals
Philips Healthcare
Radiological Society of North America
Richard M. Lucas Cancer Foundation
Schering AG
SibTech, Inc
Siemens Corporate Research
Siemens Medical Solutions
Sir Peter & Lady Michael Foundation
Society for Pediatric Radiology
Society of Gastrointestinal Radiologists
Society of Nuclear Medicine
Society of Uroradiology
SRI International
Triple Ring Technologies, Inc
University of California, Berkeley
University of California, Davis
University of California, Irvine
University of California, Los Angeles
University of California, San Diego
University of California, San Francisco
University of Miami
University of Pittsburgh
University of Southern California
University of Texas, A & M
University of Texas, Austin
University of Washington
Varian Associates
W.L. Gore and Associates

Collaborating Stanford Departments

We work with almost three hundred faculty, postdoctoral fellows, students, and research staff from across the University. We wish to thank you all for the friendly, productive collaborations that we enjoy all year long. Stanford departments with whom we have long-standing research projects include the following:

Aeronautics and Astronautics
Anesthesia
Applied Physics
Biochemistry
Bioengineering
Biology
Bio-X
Cancer Biology
Cancer Center
Cardiothoracic Surgery
Chemical Engineering
Chemistry
Comparative Medicine
Computer Sciences
Developmental Biology
Electrical Engineering
ENT
Freeman Spogli Institute
Genetics
Health Research and Policy
Hematology
Infectious Diseases
Institute for Computational & Mathematical Engineering
Lucile Packard Children's Hospital
Materials Science and Engineering
Mathematics
Mechanical Engineering
Medical Informatics
Medicine
Microbiology and Immunology
Molecular and Cellular Physiology
Neurobiology
Neurology and Neurological Sciences
Neurosurgery
Obstetrics & Gynecology
Oncology
Opthalmology
Orthopedics/Orthopedic Surgery
Otolaryngology
Pathology
Pediatrics
Pediatrics/Neonatology
Physics
Psychiatry and Behavioral Sciences
Psychology
Radiation Oncology
Stanford Center for Biomedical Ethics
Stroke Center
Surgery
Urology